

All Topological Bands of All Nonmagnetic Stoichiometric Materials

Maia G. Vergniory^{†,1,2,3,*} Benjamin J. Wieder^{†,4,5,6,*} Luis Elcoro,⁷ Stuart S. P. Parkin,⁸ Claudia Felser,³ B. Andrei Bernevig,⁶ and Nicolas Regnault^{6,9,†}

¹*Donostia International Physics Center, P. Manuel de Lardizabal 4, 20018 Donostia-San Sebastian, Spain*

²*IKERBASQUE, Basque Foundation for Science, Bilbao, Spain*

³*Max Planck Institute for Chemical Physics of Solids, 01187 Dresden, Germany*

⁴*Department of Physics, Massachusetts Institute of Technology, Cambridge, MA 02139, USA*

⁵*Department of Physics, Northeastern University, Boston, MA 02115, USA*

⁶*Department of Physics, Princeton University, Princeton, New Jersey 08544, USA*

⁷*Department of Condensed Matter Physics, University of the Basque Country UPV/EHU, Apartado 644, 48080 Bilbao, Spain*

⁸*Max Planck Institute of Microstructure Physics, 06120 Halle, Germany*

⁹*Laboratoire de Physique de l'École Normale Supérieure, PSL University, CNRS, Sorbonne Université, Université Paris Diderot, Sorbonne Paris Cité, Paris, France*

(Dated: June 10, 2022)

Topological Quantum Chemistry and Symmetry-Based Indicators have facilitated large-scale searches for materials with topological properties at the Fermi energy (E_F). We report the completion of a publicly accessible catalog of stable and fragile topology in all of the bands both at and away from E_F in the 96,196 processable entries in the Inorganic Crystal Structure Database. Our calculations represent the completion of the symmetry-indicated band topology of known nonmagnetic materials, and enable the discovery of repeat-topological and supertopological materials, which include rhombohedral bismuth and Bi_2Mg_3 . We find that 52.65% of all materials are topological at E_F , roughly 2/3 of bands across all materials exhibit symmetry-indicated stable topology, and that 87.99% of all materials contain at least one stable or fragile topological band.

The field of solid-state physics has over the past 15 years advanced in large part by the discovery of nontrivial electronic band topology in nonmagnetic crystalline solids [1, 2]. Since the conceptual proposal and theoretical prediction of the first 2D [3, 4] and 3D [5] topological insulators (TIs), researchers have predicted solid-state realizations of topological phases of matter at a rapid pace. Notable examples include symmetry-protected topological semimetals (TSMs) [6–10] and topological crystalline insulators (TCIs) [11–17]. Owing to negligible electron-electron interactions, many of the theoretical predictions of TI, TCI, and TSM phases in solid-state materials were shortly afterwards confirmed in spectroscopic and transport experiments [18–27].

Initially, solid-state TIs and TSMs were believed to be rare and esoteric phases of matter. However over the past four years, the theories of Topological Quantum Chemistry (TQC) [28, 29] and symmetry-based indicators (SIs) [16, 17, 30–36] have facilitated high-throughput searches for magnetic [37] and nonmagnetic [38–40] topological materials, revealing solid-state TIs and TSMs to be ubiquitous in nature. For example, Ref. [38] reported high-throughput analyses of the symmetry-indicated stable band topology at the Fermi level (E_F) in $\sim 26,000$ stoichiometric, inorganic, “high-quality” crystal structures obtained from the Inorganic Crystal Structure Database (ICSD) [41]. Of the $\sim 26,000$ ICSD entries, roughly \sim

7,000 were found to be topological at E_F [38].

This result raises two questions. First, the complete ICSD contains 96,196 stoichiometric ICSD entries with processable (non-corrupt) structural data as defined in Section SM 4 of the Supplementary Material (SM), raising the question of whether a high percentage of *all* of the known inorganic materials are topological at E_F . Second, energetically isolated groupings of bands may exhibit nontrivial topology, independent of the electronic filling. Hence, the distribution of topological bands *away from* E_F in real materials is also a major outstanding question in the study of quantum matter. In this work, we answer both questions by performing a complete study of symmetry-indicated band topology in all known, stoichiometric, inorganic crystalline solids without magnetic order. In contrast to the previous high-throughput topological materials searches in Refs. [38–40], our calculations include a complete diagnosis of symmetry-indicated band topology away from E_F . Using TQC and nonmagnetic SIs, we compute the symmetry-indicated, nonmagnetic band topology of all bands in all 96,196 stoichiometric ICSD entries with valid structure files from electronic fillings ranging from the core shell up to at least $2N_e$ above, where N_e is the number of valence electrons. Unlike in Refs. [38–40], the SIs used in this work include both the SIs of stable band topology – which indicate familiar strong and weak TI and TCI phases – as well as the recently introduced SIs of *fragile* band topology [42–45] – which represent more exotic TCI phases with topological corner modes [34] and twisted-boundary edge states [46]. Fragile topological phases have emerged as an area of intense interest after recent theoretical studies indicated that the superconducting and correlated-insulating states

* These authors contributed equally to this work.

† To whom correspondence should be addressed: regnault@princeton.edu (N. R.), maiaqv@gmail.com (M. G. V.), bwieder@mit.edu (B. J. W.)

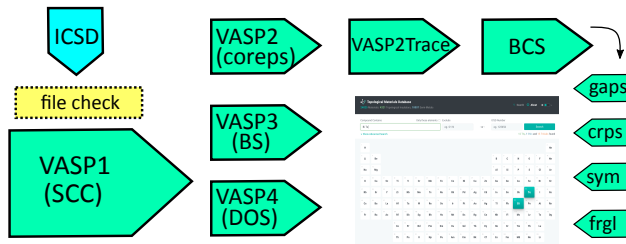


Figure 1. Workflow schematic for generating the [Topological Materials Database](https://www.topologicalquantumchemistry.com/) (<https://www.topologicalquantumchemistry.com/>). For each entry in the Inorganic Crystal Structure Database (ICSD) [41], we first determine if the entry is stoichiometric, contains coordinates for all of the atoms listed in the chemical formula, and lists atomic coordinates compatible with the crystallographic space group (SG) of the material. We then perform self-consistent density functional theory (DFT) calculations, both with and without incorporating the effects of spin-orbit coupling (SOC). Irrespective of whether SOC is taken into account, each DFT calculation consists of four steps (labeled VASP1 – VASP4, see SM 4 for further details) in which we perform a self-consistent calculation (SCC) of the charge density, obtain the symmetry data [small corepresentation (corep) multiplicities] at all integer electronic fillings above the core shell, and compute the electronic band structure (BS) at E_F and the density of states (DOS). Lastly, using the VASP2Trace program [53] previously implemented for Ref. [38] and an updated version of the Check Topological Mat program on the Bilbao Crystallographic Server [54] implemented for this work, we compute for each DFT calculation the stable and fragile topological classifications of all isolated groupings of bands above the core shell as determined by the compatibility relations in Topological Quantum Chemistry (TQC) [28] (see SM 2 and SM 3 for further details).

in magic-angle twisted bilayer graphene may originate from nearly-flat fragile topological bands [47, 48].

Through our calculations, we discover the existence of previously unrecognized classes of topological materials, including enforced TSMs with energetically isolated fragile bands at E_F , *repeat-topological* (RTopo) materials with stable topological insulating gaps at and just below E_F , and *supertopological* (STopo) materials in which *every* energetically isolated set of bands above the core shell is stable topological. We have upgraded the [Topological Materials Database](#) [49] – a publicly available online catalog of topological materials – for accessing and intuitively searching the results of this study. In the SM, we present detailed statistics for our computations, lists of idealized materials in each topological class, and highlight the features of the [Topological Materials Database](#) [49] implemented for this work, which include dynamical zoom options, density-of-states calculations, electronic-structure calculations in the absence of spin-orbit coupling (SOC), and advanced search options (a complete list of added features is provided in SM 7). We find that 52.65% of all materials are topological at E_F , and roughly 2/3 of bands across all materials exhibit the

symmetry-indicated topology of 3D strong TIs, weak TIs, TCIs, and higher-order TIs, which are in this work together classified as topologically *stable*, as they are robust to the addition of trivial or fragile bands (though sensitive to the relaxation of time-reversal and crystal symmetries) [1–5, 11–17, 29, 30]. Most surprisingly, we find that 87.99% of all materials contain at least one stable or fragile topological band in their energy spectrum, even if away from E_F . Our discovery of ubiquitous electronic band topology in solid-state materials motivates the formulation of a new periodic table of chemical compounds in which electronic bands in materials are sorted by a *combination* of common topological features and chemical and structural properties.

Lastly, our characterization of electronic band topology *away from* E_F is immediately useful in numerous experimental settings, including angle-resolved photoemission spectroscopy (ARPES) experiments – which measure states at and below E_F – and pump-probe experiments – in which electrons can be excited to observe bands above E_F . As will be discussed below, our theoretical calculations provides robust explanations for previously puzzling ARPES data. Beyond photoemission experiments, states away from E_F may also be accessed via (electro)chemical doping, electrostatic gating, hydrostatic pressure, and nonequilibrium photoexcitation, and are relevant to Floquet engineering and nonlinear optical experiments [50]. Additionally, even in topologically trivial insulating materials, exotic interaction effects may be accessed by doping or gating the Fermi level into an isolated topological band. For example, independent of the cumulative band topology at higher energies, if a superconducting state is induced from a partially occupied, isolated band, then the nontrivial stable or fragile topology of the isolated band has been shown to provide a lower bound on the superfluid weight [51, 52].

DATA SET GENERATION

In this work, we apply TQC [28, 29] and stable and fragile SIs [16, 17, 30–37, 42–45] to diagnose the symmetry-indicated topology of all isolated bands above the core shell in the stoichiometric materials in the ICSD. To obtain the topological classification of each separated group of bands in the energy spectrum, we employ the methods previously used in the high-throughput material searches in Refs. [37, 38]. Uniquely in this work, after computing the electronic structure using the intrinsic electronic filling $\nu = N_e$, we then vary ν to compute the topological properties above and below E_F . Below, we will summarize the numerical and topological details of our calculations (Fig. 1) – further specific details are provided in SM 2, SM 3, and SM 4.

We begin by selecting one of the 96,196 processable entries in the ICSD with a stoichiometric chemical formula. We next convert the crystal structure listed in the ICSD into an input file for DFT calculations, excluding

cases in which the ICSD structure file is missing atoms listed in the chemical formula or reports atomic positions incompatible with the symmetries of the material space group (SG, see SM 4). We then perform self-consistent, *ab initio* calculations of the electronic band structure and density of states with ν set to charge neutrality ($\nu = N_e$), filtering out cases in which the calculations did not converge or converged to a magnetic (meta)stable state.

Next, as detailed in SM 3, we use the VASP2Trace [53] and Check Topological Mat [54] programs to determine the unitary symmetry eigenvalues of each of the Bloch-state multiplets at each of the maximal (high-symmetry) \mathbf{k} vectors. For each degenerate multiplet of Bloch states, the combination of extracted symmetry eigenvalues establishes a correspondence to an irreducible small corepresentation (corep) of the little group at \mathbf{k} [55]. Then, choosing increasing integer values of the valence electronic filling ν from 0 to at least $2N_e$ (or up to the first filling $\nu > N_e$ at which the electronic band structure is not symmetric and convergent, see SM 3 A), we identify fillings at which all of the Bloch states in each maximal \mathbf{k} vector are fully occupied, such that a gap is present in the energy spectrum at each maximal \mathbf{k} vector (though not necessarily at the same energy, as states are taken to be separately filled up to ν at each \mathbf{k} point). Lastly, at $\nu = N_e$, as well as at each ν at which there is a gap at all maximal \mathbf{k} points, we extract the *symmetry data vector* [29, 37, 38] – defined as the multiplicities of the small coreps corresponding to the filled Bloch-eigenstate multiplets across each of the maximal \mathbf{k} vectors.

Crucially, the symmetry data vector at each ν facilitates the topological classification of filled or energetically isolated groupings of bands. Specifically, in each SG, the *elementary band coreps* (EBRs) correspond to the independent, topologically trivial (*i.e.* Wannierizable [56]) bands [28, 57]. Hence, if a set of bands does not transform in an integer-valued linear combination of EBRs, then the band exhibits nontrivial stable topology. As established in Refs. [37, 38] and detailed in SM 2, a symmetry data vector may be classified into one of five possible topological classes. First, if the symmetry data vector corresponds to a set of Bloch states in which a degenerate multiplet at a maximal \mathbf{k} point is partially filled, then the system is an *enforced semimetal with Fermi degeneracy* (ESFD). As an example, 3D HgTe [ICSD 31845, SG 216 ($F\bar{4}3m$)] is an experimentally-established, ESFD-classified TSM that realizes a 2D TI phase in few-layer quantum-well geometries [4]. Next, if the symmetry data vector corresponds to a set of high-symmetry-point Bloch eigenstates that are implied by the compatibility relations to connect to other states outside of the symmetry data along a high-symmetry line or plane, then the system is an *enforced semimetal* (ES). A well-studied ES material is the archetypal higher-order-topological Dirac semimetal Cd_3As_2 [ICSD 107918, SG 137 ($P4_2/nmc$)] [6, 19, 58, 59]. Conversely, if the symmetry data vector satisfies the compatibility relations along all high-symmetry lines and planes, then the bands

that transform in the symmetry data either correspond to a stable or fragile TI or TCI, a TSM phase, or are topologically trivial. In the case in which the symmetry data vector corresponds to a stable topological set of bands, the bands described by the symmetry data may be classified into two categories. First, if stable topological bands transform in an integer-valued linear combination of pieces of a *disconnected* EBRs, then the bands are classified as a split EBR (SEBR) [28, 57]. Alternatively, if stable topological bands do not transform in an integer-valued linear combination of disconnected EBR pieces, then the bands are classified as “not equal to a linear combination” (NLC). The archetypal symmetry-indicated stable topological material is the experimentally established 3D TI Bi_2Se_3 [ICSD 617079, SG 166 ($R\bar{3}m$)] [18], which is classified as SEBR. Lastly, if the symmetry data of an isolated grouping of bands does correspond to an integer-valued linear combination of EBRs (LCEBR), then the symmetry eigenvalues of the occupied bands are compatible with either fragile or trivial topology (though the bands may also exhibit non-symmetry-indicated stable topology [34]).

In the above cases in which the symmetry data vector satisfies the compatibility relations (SEBR, NLC, and LCEBR), a finer topological classification may be obtained using stable and fragile topological SIs. First, in the presence of non-negligible SOC, nonmagnetic SEBR and NLC bands correspond to stable TIs and TCIs with anomalous surface Dirac cones and helical hinge states [16, 17, 30]. Conversely, as shown in Refs. [29, 31, 34, 36] and detailed in SM 6, in the absence of SOC and magnetism, bands with nontrivial stable SIs correspond to TSM (specifically SEBR-SM and NLC-SM) phases with bulk nodal degeneracies in the Brillouin zone (BZ) interior and topological surface Fermi arcs or flat-band like surface and intrinsic hinge states. Lastly, it was recently discovered that LCEBR bands with or without SOC may in some cases be further classified as fragile topological [42, 43] through the fragile SIs elucidated in Refs. [44, 45]. For all possible classes of symmetry-indicated stable and fragile TI, TCI, and TSM phases in the presence of SOC, we provide in SM 11a detailed enumeration of the most idealized material realizations across all stoichiometric materials in the ICSD. Although we find that there do not exist materials in which the entire valence manifold is fragile topological, we do find numerous examples of experimentally accessible materials with well-isolated fragile bands close to E_F (see SM 11 E).

RESULTS

We will now summarize the symmetry-indicated topological properties of the stoichiometric materials in the ICSD. First, we will discuss statistical trends uncovered across the materials analyzed in this work, including the distribution of topological features at E_F and statistics for SOC-driven topological phase transitions, which are

defined by comparing the stable topology at E_F for each ICSD entry in calculations performed with and without incorporating the effects of SOC. We will then highlight material candidates in which our investigations have uncovered previously unrecognized topological features at experimentally accessible energies.

Material Statistics

At the time of our investigations, the ICSD [41] contained 193,426 entries, of which 96,196 characterized stoichiometric chemical compounds with processable (non-corrupt) CIF structure files. We performed first-principles calculations on all 96,196 processable stoichiometric entries, resulting in convergent electronic structures for 73,234 entries in the presence of SOC, which we grouped into 38,298 unique materials by common chemical formulas and stable topology at E_F (see SM 3 A). In Fig. 2A, we show the distribution of the topology at E_F for the unique materials within each of the 32 crystallographic point groups of the 230 nonmagnetic SGs, and in Fig. 2B, we show the total number of unique materials in each topological class. We find that at intrinsic filling, 6,128 unique materials are symmetry-indicated stable TIs or TCIs, and 14,037 unique materials are TSMs. Our findings represent a doubling of the number of known topological materials from those identified in previous high-throughput calculations [38–40]. Furthermore, we find that 52.65% of unique materials are symmetry-indicated stable TIs, TCIs, or TSMs at E_F , which also represents a doubling from previous estimates of the percentage of 3D topological materials in nature [38, 39]. This percentage is considerably higher than the percentage of topological stoichiometric 2D materials, which has previously been computed to lie within the range of a few to 20% [60, 61].

In SM 5 and SM 8, we respectively provide detailed statistics for the computational resources expended for the calculations performed for this work, and for the topology *at and away* from E_F across the stoichiometric materials in the ICSD. In the presence of SOC, we find that an overwhelming 87.99% of unique materials contain at least one symmetry-indicated stable or fragile topological band [Fig. 2C]. This percentage is all the more surprising, as we have included materials whose SGs have trivial stable SI groups (*e.g.* non-centrosymmetric crystals without high-fold rotoinversion symmetries [16, 17, 29]), such that all isolated bands in the SG are classified by SIs as trivial or fragile. Taking all 38,298 unique materials into consideration – including the materials in SGs with trivial stable SI groups [16, 17, 29] – we find that nearly 2/3 of all energetically isolated bands in nature exhibit symmetry-indicated stable topology. Hence, our investigations reveal that even away from E_F , the *majority* of electronic features in solid-state materials can only be robustly modeled by incorporating topological band theory.

	NLC	SEBR	ES	ESFD	LCEBR
ES	2,104 (35%)	1,585 (26.4%)	944 (15.7%)	38 (0.6%)	1,335 (22.2%)
ESFD	207 (1.5%)	1,089 (7.8%)	2,792 (19.9%)	9,423 (67.3%)	486 (3.5%)
LCEBR	49 (0.3%)	78 (0.5%)	42 (0.3%)	24 (0.2%)	15,672 (98.8%)
NLC-SM	208 (82.9%)	24 (9.6%)	2 (0.8%)	—	17 (6.8%)
SEBR-SM	—	38 (86.4%)	5 (11.4%)	—	1 (2.3%)

Table I. SOC-driven topological phase transitions in the unique stoichiometric materials in the ICSD. We show statistics for the band topology at E_F for the unique stoichiometric materials in the ICSD with and without incorporating the effects of SOC in first-principles calculations. The rows (columns) list the topological classification at E_F in the absence (presence) of SOC. We find that nearly 2/3 of ES-classified unique materials without SOC become stable TIs and TCIs with SOC, whereas most ESFD TSMs without SOC remain semimetallic when SOC is incorporated. Conversely, over 85% of NLC-SM- and SEBR-SM-classified TSMs without SOC (see Refs. [31, 34, 36] and SM 6) become stable TIs and TCIs after incorporating SOC. Complete statistics for the SOC-driven topological phase transitions at E_F in the ICSD are provided in SM 10, and representative materials for each class of TSM-insulator phase transition are provided in SM 11 D.

Lastly, we have also computed detailed statistics for the relative topology of each stoichiometric ICSD entry with and without incorporating the effects of SOC. As discussed above and in SM 10 and demonstrated in Refs. [29, 31, 34, 36], all symmetry-indicated, nonmagnetic stable topological phases without SOC are TSMs. Hence in the absence of SOC, there are both ESFD- and ES-classified TSMs – in which the nodal degeneracies respectively lie at high-symmetry points (ESFD) and along high-symmetry lines and planes (ES) – as well as SEBR-SM- and NLC-SM-classified TSMs – in which the bands along all high-symmetry lines and planes satisfy the insulating compatibility relations [28, 57], and the nodal degeneracies lie in the BZ interior. In Table I we show the number of unique materials in each topological class with and without SOC. Table I indicates that the majority of ES-, NLC-SM-, and SEBR-SM-classified TSMs without SOC become stable TIs and TCIs (NLC- and SEBR-classified) when SOC is introduced, whereas ESFD-classified TSMs without SOC overwhelmingly remain TSMs (ES- and ESFD-classified) when the effects of SOC are incorporated. In SM 10, we provide complete statistics for the SOC-driven topological phase transitions at E_F in the ICSD, and in SM 11 D, we identify representative materials for each class of SOC-driven TSM-insulator transition in Table I.

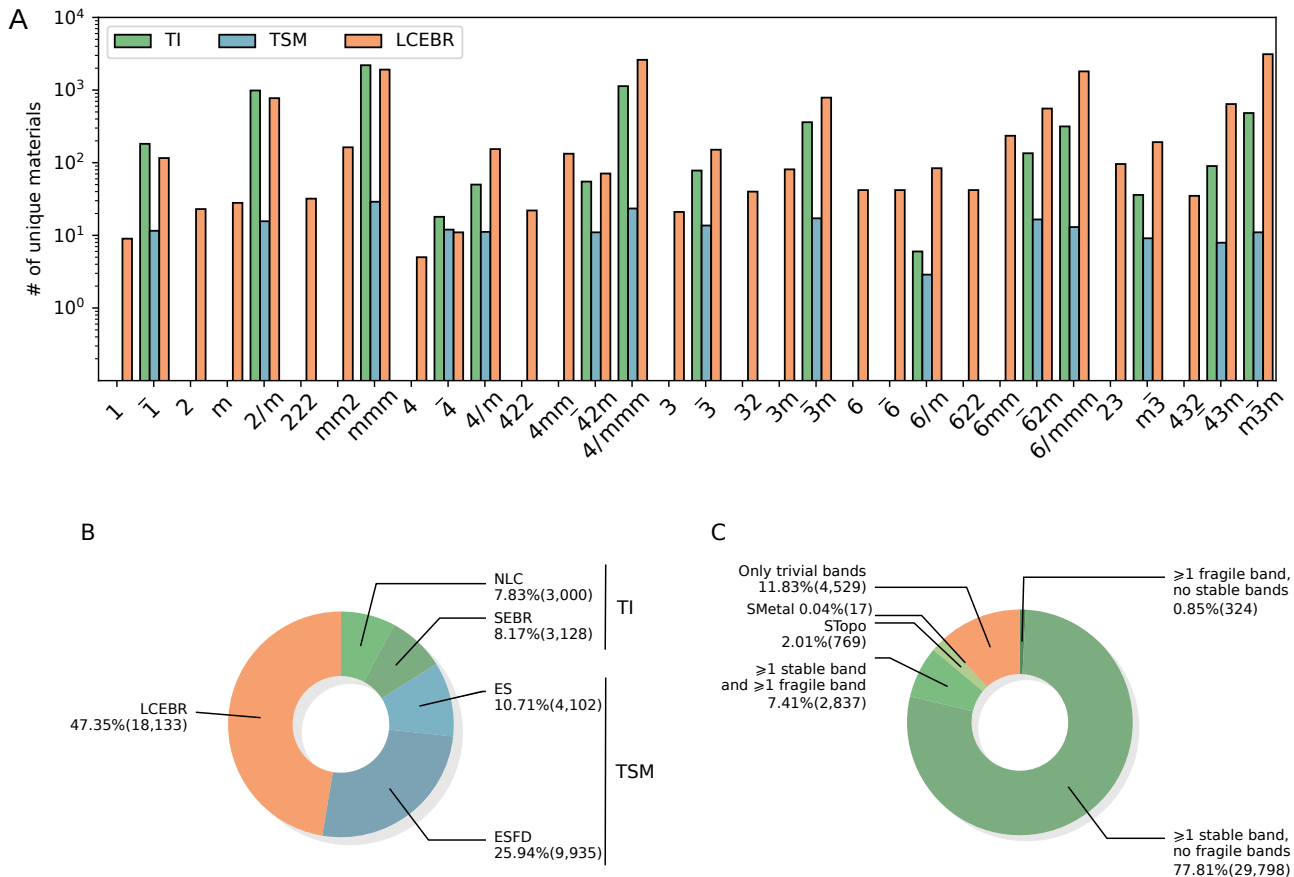


Figure 2. Topology of the stoichiometric materials in the ICSD. (A) Distribution of the topology at E_F with SOC among the 38,298 stoichiometric unique materials in the ICSD as defined in SM 4, subdivided by crystallographic point group (PG). For each of the 32 PGs of the 230 SGs [55], we list the number of symmetry-indicated stable topological (crystalline) insulators (NLC- or SEBR-classified TIs and TCIs), TSMs (ES or ESFD), or unique materials with trivial symmetry-indicated topology (LCEBR). (B) The distribution of the topology at E_F across all PGs and topological classes (see Refs. [37, 38] and SM 2). 16.00% of the unique materials are TIs or TCIs at E_F and 36.65% are TSMs, implying that a remarkable 52.65% of the stoichiometric materials in nature are topological at intrinsic filling. (C) Distribution of the symmetry-indicated band topology away from E_F across the stoichiometric unique materials in the ICSD. An overwhelming 87.99% of materials contain at least one symmetry-indicated stable or fragile topological band across the energy range of our first-principles calculations (see SM 4 for calculation details), which is even more notable when considering that many materials (*e.g.* noncentrosymmetric crystals) have SGs without either stable or fragile SIs (see Refs. [1, 16, 17, 29–36, 44, 45]). Because previous works have demonstrated the existence of *non-symmetry-indicated* TI and TCI phases in materials with trivial stable SIs [1, 3, 13, 14, 34], then the percentage of materials in nature with topological bands at and away from E_F is necessarily *even larger than* 87.99%, suggesting an intriguing direction for future study. In addition to the repeat-topological and supertopological materials (see Fig. 5 and SM 9), we have also discovered the existence of supermetallic (SMetal) materials, in which all of the bands above the core shell are connected up to at least a filling of $2N_e$, where N_e is the number of valence electrons. (see SM 6 and SM 8). Although SMetal materials are relatively rare in the presence of SOC [17 unique materials, see (C)], there are 1,138 unique SMetal materials without SOC, which is consistent with the general trend of increased band connectivity in materials when neglecting the effects of SOC (see Table I and SM 6, SM 8, and SM 10). In SM 8, we provide further detailed statistics for the symmetry-indicated band topology at and away from E_F across all of the stoichiometric materials in the ICSD.

Material Candidates

We next highlight the materials in which our investigations have revealed or provided a different context for topological features within an experimentally accessible range from E_F – an extensive tabulation of the most idealized realizations in nature of all previously-established classes of symmetry-indicated TI, TCI, and TSM phases

in the presence of SOC is further provided in SM 11. To begin, in Fig. 3, we present experimentally favorable material candidates with stable and fragile topology at E_F . First, in Fig. 3A, we show the electronic band structure of MoGe_2 [ICSD 76139, SG 139 ($I4/mmm$)] – a higher-order-topological, centrosymmetric TSM [58] in which the doubly-degenerate valence and conduction bands that meet along ΓM_1 in fourfold Dirac points at

E_F , along with the next-highest doubly-degenerate valence bands, are as a set fragile topological [*i.e.* the two conduction bands and four valence bands closest to E_F in Fig. 3A as a set exhibit nontrivial fragile SIs]. Next, in Fig. 3B, we highlight HgBa₂CuO₄ [ICSD 75720, SG 123 ($P4/mmm$)] – a well-studied high temperature cuprate superconductor [62], which we find to be an ideal ESFD-classified metal with a doubly-degenerate, half-filled band at E_F . Then, in Fig. 3C and D, we respectively show the band structures of the transition-metal chalcogenides (TMCs) TaSe₂ [ICSD 24313, SG 164 ($P\bar{3}m1$)] and TiS₂ [ICSD 72042, SG 227 ($Fd\bar{3}m$)]. Both TaSe₂ and TiS₂ host well-established 2D charge-density-wave phases [63–65]; in this work, we discover that the valence bands extending to ~ 3 eV below (conduction bands extending to ~ 1.5 eV above) E_F in 3D TaSe₂ (TiS₂) are fragile topological.

In Figs. 3E and F, we next respectively show the electronic band structures of the closely-related TMCs Ta₂NiSe₅ [ICSD 61148, SG 15 ($C2/c$)] and Ta₂NiSe₇ [ICSD 61352, SG 12 ($C2/m$)], which show particular promise for experimental investigations owing to their relatively simple normal-state Fermi surfaces. Ta₂NiSe₅ and Ta₂NiSe₇ belong to a larger family of materials previously highlighted for hosting metal-insulator transitions and strongly-correlated phases of matter. Previous investigations have demonstrated that the layered TMC Ta₂NiSe₅ hosts an exotic exciton-insulator phase [66, 67]. By comparing the parity (inversion) eigenvalues of Ta₂NiSe₅ with and without incorporating the effects of SOC [Fig. 4A and B], we find that the narrow-gap semiconducting state of Ta₂NiSe₅ in fact realizes a 3D TI phase originating from weak, SOC-driven band inversion at the Γ point. Unlike Ta₂NiSe₅, Ta₂NiSe₇ [Fig. 3F] is instead a quasi-1D TMC, and has been previously highlighted for exhibiting a charge-density-wave instability [68]. Ta₂NiSe₇ is closely related to the ES-classified, structurally chiral, quasi-1D TMC Weyl semimetal Ta₂ISes₈ [ICSD 35190, SG 97 ($I422$)], see SM 11 C 2], which was shown in recent experimental works to exhibit a topological (axionic) charge-density wave that competes with a superconducting phase under applied pressure [26, 27, 69]. In this work, we find that the room-temperature phase of Ta₂NiSe₇ is a 3D TI originating from a combination of anisotropic orbital coupling and SOC-driven band inversion. Specifically, we find that without SOC, Ta₂NiSe₇ is an ES-classified nodal-line semimetal with band inversions at $k_{x,y} = 0$, $k_z = 0, \pi$ [respectively the Γ and A points in Fig. 4C] driven by orbital coupling in the xy - (ab -) plane [taking the Ta₂NiSe₇ chains to be oriented along the z - (c -axis) direction, see ICSD 61352]. This can be seen by recognizing that Ta₂NiSe₇ without SOC [Fig. 4C] exhibits the same parity eigenvalues as a z -directed weak TI [$(z_{2,1}, z_{2,2}, z_{2,3}, z_4) = (0012)$ when subduced onto SG 2 ($P1$), see SM 6 B and Refs. [5, 30, 31, 36]]. When SOC is reintroduced, the nodal lines at E_F in Ta₂NiSe₇ become gapped, and the band inversion at A is removed,

while the bands at Γ remain inverted [see Fig. 4D].

Finally, in this work, we have additionally performed a high-throughput search for topological bands *away from* E_F . Our calculations have revealed the existence of two additional classes of topological materials: RTopo materials with stable topological insulating gaps at and just below E_F [see Fig. 5A and SM 9 A], and STopo materials in which *every* energetically isolated set of bands above the core shell exhibits symmetry-indicated stable topology [see Fig. 5B and SM 9 B]. From a physical perspective, STopo phases result from a combination of EBR splitting, band backfolding from unit-cell enlargement, and favorable hopping parameters – hence, the identification of an STopo phase in a particular material can be sensitive to sample and calculation details. In SM 9 B, we highlight the example of the experimentally-established higher-order TI rhombohedral bismuth [ICSD 64703, SG 166 ($R\bar{3}m$)] [22], for which some ICSD entries (*e.g.* ICSD 64703) are STopo, whereas others (*e.g.* ICSD 53797) are not. Crucially, Bi (ICSD 64703) and Bi (ICSD 53797) differ only by weak band inversion away from E_F , and both exhibit topologically nontrivial gaps at E_F and just below E_F . This provides a physical motivation for introducing a second topological class – RTopo – for materials like Bi (ICSD 64703). In idealized RTopo materials, there exist two sets of surface or hinge states within consecutive bulk gaps that both lie at energies accessible to ARPES probes without doping (~ 1.5 eV below E_F), a property that is crucially *insensitive* to band inversions at experimentally inaccessible energies far from E_F . The repeated topological surface and hinge states of RTopo materials are analogous to the Fermi-arc “quantum ladder” recently observed in the unconventional chiral semimetal alloy Rh_xNi_ySi [70] (see SM 9 A for further details). Lastly, we emphasize that in principle, the STopo and RTopo classification of materials can be extended from stable topological states to fragile topology – however, we did not in this study encounter any ICSD entries with super- or repeat-fragile topology.

In Fig. 5C and D, we show the bulk and surface states of the RTopo and STopo material Bi₂Mg₃ [ICSD 659569, SG 164 ($P\bar{3}m1$)]. Previous theoretical investigations and spectroscopic experiments have determined Bi₂Mg₃ to be a 3D TI with “surface resonance bands” below E_F at the (0001)-surface Γ point [71]. We find that the surface resonance bands detected in Ref. [71] are in fact the RTopo Dirac-cone surface states of Bi₂Mg₃ in the first gap below E_F [the “0013 RTopo gap” in Fig. 5D]. In SM 11 B and SM 9 C respectively, we provide detailed tabulations of RTopo and STopo materials in the ICSD. Taken together, the large number of experimentally accessible materials in the ICSD with stable topological bands away from E_F (see SM 8), as well as the relative preponderance of RTopo and STopo materials (see SM 11 B and SM 9 C, respectively), suggest that many of the surface resonances detected in previous ARPES investigations may in fact be topological surface states protected by spectral flow below E_F .

DISCUSSION

We have performed a complete calculation of symmetry-indicated stable and fragile band topology at and away from E_F across all known stoichiometric, solid-state, nonmagnetic materials. We have discovered that over half of the materials in nature are stable TIs and TSMs at E_F , and nearly 2/3 of bands across all materials exhibit symmetry-indicated stable topology. Our investigations raise several questions. First, there exist well-established classes of noncentrosymmetric TI and TCI phases that cannot be diagnosed through SIs. For example, depending on experimental or first-principles calculation details, WTe_2 [ICSD 14348, SG 31 ($Pmn2_1$)] can realize an LCEBR-classified TSM phase with tilted Weyl cones [72], or a non-symmetry-indicated twofold-rotation-anomaly TCI phase [34]. Additionally, like stable topological phases with trivial SIs, there also exist non-symmetry-indicated fragile phases that evade the methods employed in this work [58]. It remains an important outstanding question whether computationally-efficient methods beyond TQC and SIs can be formulated for the high-throughput discovery of non-symmetry-indicated topological materials. Several promising studies have recently introduced alternative, scalable methods for high-throughput topological materials identification [73, 74], suggesting a future in which an even larger percentage of materials in nature are recognized as topologically nontrivial. Furthermore, while we have focused our efforts on nonmagnetic topological materials, recent studies have expanded the methods of TQC and SIs to magnetic systems [29, 35], facilitating the high-throughput identification of over 100 magnetic materials with nontrivial topology at E_F [37]. Following the results of this work, future investigations may be directed towards identifying nontrivial electronic band topology away from E_F in magnetic materials, in particular targeting bands in which the topology and magnetism are coupled and experimentally tunable.

Lastly, we note that during the final stages of preparing this work, the 3D TMCs $\text{Ta}_2\text{M}_3\text{Te}_5$ ($\text{M}=\text{Pd},\text{Ni}$) – which are closely related to the TMCs Ta_2NiSe_5 and Ta_2NiSe_7 discovered to be 3D TIs in this work – were theoretically predicted in Ref. [75] to be non-symmetry-indicated mirror TCIs. Experimental evidence of a 2D TI phase in $\text{Ta}_2\text{Pd}_3\text{Te}_5$ monolayers was also reported in Ref. [76].

MATERIALS AND METHODS

The first-principles calculations in this work were performed using the Vienna Ab-initio Simulation Package (VASP) [77–79]. We treated the interaction between the ion cores and the valence electrons using the projector augmented-wave method [80], and we used the generalized gradient approximation (GGA) with the Perdew-Burke-Ernzerhof parameterization for the exchange-correlation potential [81]. For each material

calculation, we used as input the structural parameters reported on the ICSD[41]. For calculations incorporating the effects of SOC, we accounted for the effects of SOC using the second variation method [82]. For the self-consistent calculations (SCC) of the charge density and the density of states, we used a grid of $11 \times 11 \times 11$ k points centered at the Γ point ($k = 0$). For the band structure calculations along high-symmetry lines and planes, we then used the input from the SCC. Each segment of the k path contained 20 k points. At each k point along each path segment, we specifically calculated the energies of at least $2N_e$ Bloch states, where N_e , is the number of valence electrons in the primitive cell; we did not include bands originating from core-shell atomic orbitals. To identify the symmetry-indicated stable and fragile topological bands in each analyzed material, we then used the VASP2Trace [53][83] program and an implementation of the Check Topological Mat [54] program updated for this work (see SM 3 for further details). Lastly, to compute the (0001)-surface spectrum of Bi_2Mg_3 in Fig. 5D, we used WANNIER90 [84] to construct a Wannier-based tight-binding model from the s and p orbitals of Mg and the p orbitals of Bi, which we found to accurately reproduce the bulk electronic band structure of Bi_2Mg_3 (see SM 9 A for further calculation details).

ACKNOWLEDGMENTS

We are grateful to Zhijun Wang for collaboration on previous related works and for writing the VASP2Trace program [83] extensively used in this study (see SM 3). We further acknowledge helpful discussions with Mois I. Aroyo, Barry Bradlyn, Jennifer Cano, Leslie Schoop, Zhida Song, and Yuanfeng Xu. M.G.V. and N.R. additionally thank B.Y. Scarpin for enlightening discussions on VASP and CIF files. We acknowledge the computational resources Cobra/Draco in the Max Planck Computing and Data Facility (MPCDF) and Atlas in the Donostia International Physics Center (DIPC). This research was conducted using the resources of the National Energy Research Scientific Computing Center (NERSC), a U.S. Department of Energy Office of Science User Facility operated under Contract No. DE-AC02-05CH11231. B.J.W., B.A.B., and N.R. were primarily supported by the U.S. Department of Energy (Grant No. DE-SC0016239), and were partially supported by the National Science Foundation (EAGER Grant No. DMR 1643312), a Simons Investigator grant (No. 404513), the Office of Naval Research (ONR Grant No. N00014-20-1-2303), the NSF-MRSEC (Grant No. DMR-142051), the Packard Foundation, the Schmidt Fund for Innovative Research, the BSF Israel US foundation (Grant No. 2018226), the Gordon and Betty Moore Foundation through Grant No. GBMF8685 towards the Princeton theory program, and a Guggenheim Fellowship from the John Simon Guggenheim Memorial Foundation. L.E. was supported by the Government of the Basque Coun-

try (Project IT1301-19) and the Spanish Ministry of Science and Innovation (PID2019-106644GB-I00). M.G.V. acknowledges the Spanish Ministerio de Ciencia e Innovacion (Grant No. PID2019-109905GB-C21). C.F. was supported by the European Research Council (ERC) Advanced Grant No. 742068 “TOP-MAT”, Deutsche Forschungsgemeinschaft (DFG) through SFB 1143, and the Würzburg-Dresden Cluster of Excellence on Complexity and Topology in Quantum Matter-ct.qmat (EXC 2147, Project No. 390858490).

AUTHOR CONTRIBUTIONS

All authors contributed equally to the intellectual content of this work. N.R. and M.G.V. performed the high-throughput first-principles calculations with help from L.E., B.A.B., and B.J.W. The topological analysis of the material calculations was performed by B.J.W. and M.G.V. with help from L.E. and B.A.B. B.J.W., M.G.V., and N.R. proposed the existence of RTopo and STopo phases and identified material candidates. The representative topological materials listed in SM 11 were manually selected by B.J.W. and M.G.V. with help from N.R., and the most experimentally relevant candidates were identified by C.F., S.S.P., M.G.V., and B.J.W. Upgrades to the [Topological Materials Database](#) [49] were implemented by N.R. The main text was written by M.G.V., B.J.W., B.A.B., and N.R. with help from all of the authors. The Supplementary Material was written by B.J.W., M.G.V., and N.R. This study was conceived by B.A.B., M.G.V. and N.R. N.R. was responsible for the overall research direction.

COMPETING INTERESTS:

The authors declare that they have no competing interests.

DATA AND MATERIALS AVAILABILITY

The data supporting the findings of this study are available within the paper and on the [Topological Materials Database](#) [49]. We provide the data of every figure and table within the paper in an open format on Zenodo[85]. Additional information regarding the data generated for this study is available from the corresponding authors upon reasonable request. the Vienna Ab-initio Simulation Package (VASP)[77–79] is a commercial software VASP available at <https://www.vasp.at>.

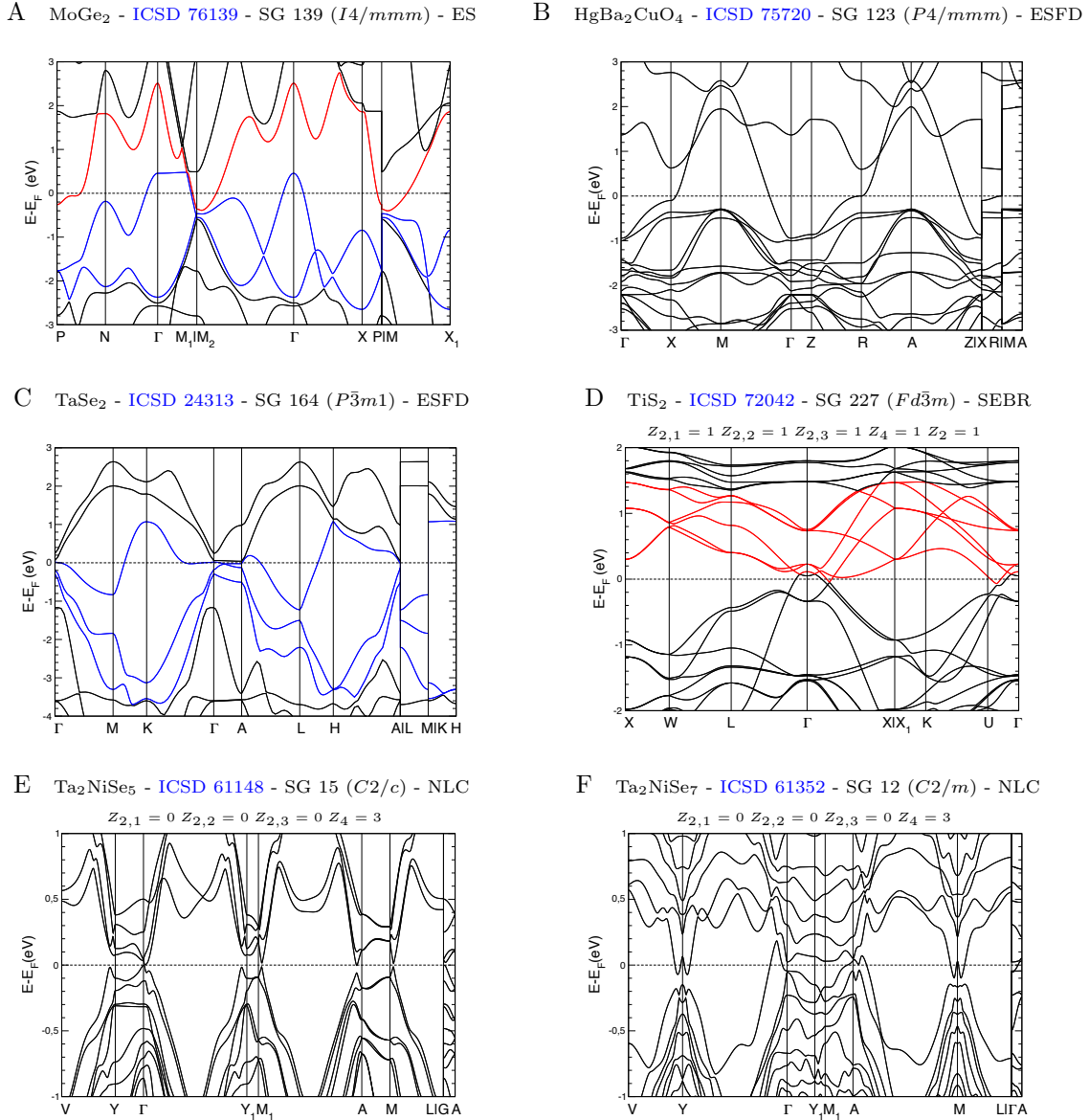


Figure 3. Material candidates with topological features at E_F . We highlight materials with previously unidentified or recontextualized topological features at E_F . In all panels, bands with symmetry-indicated stable and trivial topology are plotted in black, and symmetry-indicated fragile valence (conduction) bands are plotted in blue (red). (A) MoGe₂ [ICSD 76139, SG 139 (*I4/mmm*)] is a higher-order-topological, centrosymmetric Dirac TSM [58] in which the doubly-degenerate valence and conduction bands that meet along ΓM_1 in fourfold Dirac points at E_F , along with the next-highest doubly-degenerate valence bands, are as a set fragile topological. (B) HgBa₂CuO₄ [ICSD 75720, SG 123 (*P4/mmm*)] – an established high- T_C superconductor [62] – is found to be an ideal ESFD-classified metal with a doubly-degenerate, half-filled band at E_F . (C,D) In the transition-metal chalcogenides (TMCs) TaSe₂ [ICSD 24313, SG 164 (*P3m1*)] and TiS₂ [ICSD 72042, SG 227 (*Fd3m*)] – previously determined to host 2D charge-density-wave phases [63–65] – the highest valence and lowest conduction bands are respectively fragile topological. (E) Ta₂NiSe₅ [ICSD 61148, SG 15 (*C2/c*)] is a layered TMC that has been demonstrated to host an exciton-insulator phase [66, 67]; we find that the narrow-gap semiconducting state of Ta₂NiSe₅ is in fact a 3D TI. (F) Conversely, the closely-related quasi-1D TMC Ta₂NiSe₇ [ICSD 61352, SG 12 (*C2/m*)] – which we find to also be a 3D TI – exhibits a charge-density-wave instability [68]. In Fig. 4, we provide further analysis of the band ordering in Ta₂NiSe₅ and Ta₂NiSe₇.

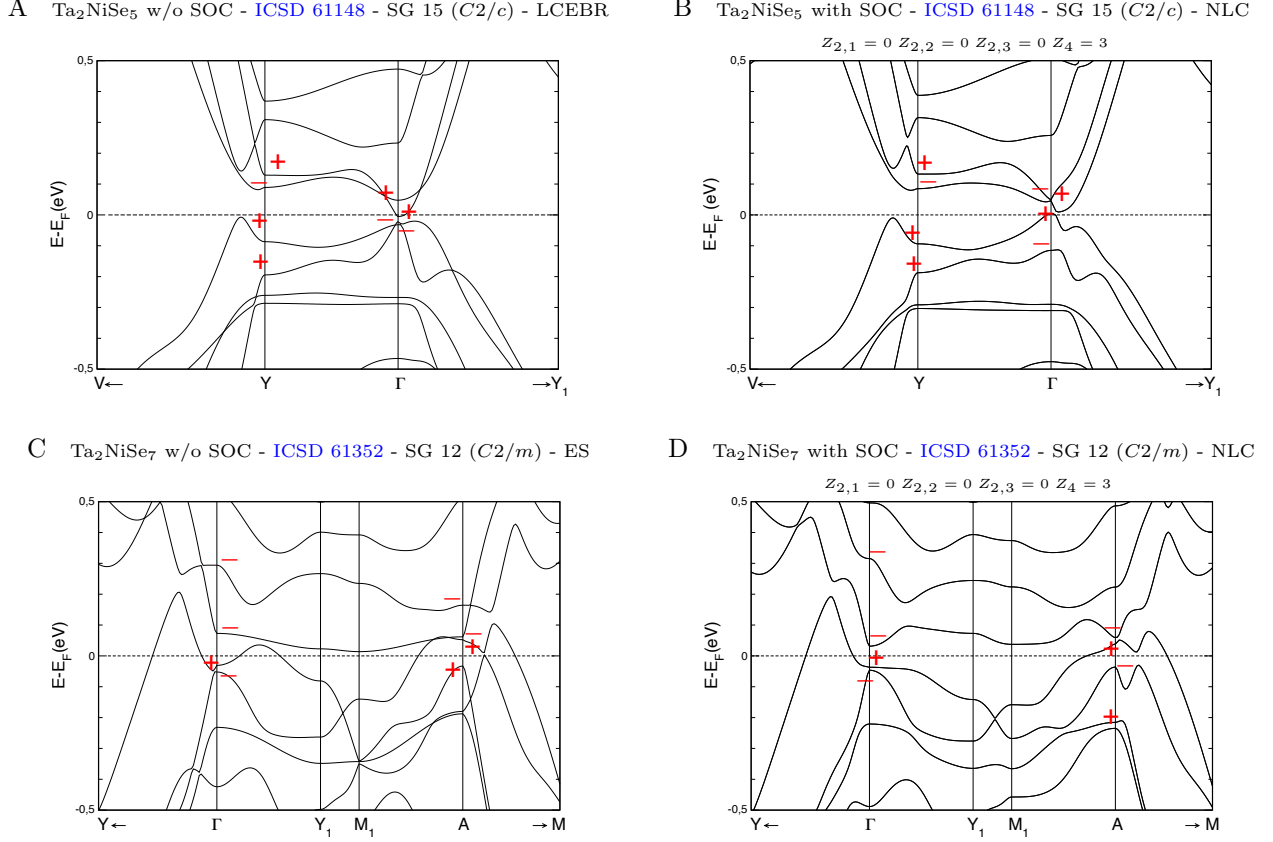


Figure 4. Topological band-inversion transitions in Ta_2NiSe_5 and Ta_2NiSe_7 . We analyze the band ordering of Ta_2NiSe_5 [ICSD 61148, SG 15 ($C2/c$)] and Ta_2NiSe_7 [ICSD 61352, SG 12 ($C2/m$)] with and without SOC. In all panels in this figure, the red \pm symbols respectively indicate Kramers pairs of states with positive and negative parity (inversion) eigenvalues. (A,B) The electronic band structure of Ta_2NiSe_5 respectively neglecting and incorporating the effects of SOC. Without SOC, (A) Ta_2NiSe_5 exhibits trivial symmetry-indicated stable topology at E_F (*i.e.* Ta_2NiSe_5 is LCEBR-classified without SOC). When SOC is reintroduced in (B), it drives a band inversion at Γ , transitioning Ta_2NiSe_5 into a $Z_4 = 3$ 3D TI phase. (C,D) The electronic band structure of Ta_2NiSe_7 respectively neglecting and incorporating the effects of SOC. Unlike in Ta_2NiSe_5 (A), the bands at Γ and A [$k_{x,y} = 0$, $k_z = 0, \pi$, respectively] in Ta_2NiSe_7 (C) are already inverted by orbital coupling in the xy - (ab -) plane, taking the Ta_2NiSe_7 chains to be oriented along the z - (c -axis) direction (see ICSD 61352). Hence without SOC, Ta_2NiSe_7 realizes an ES-classified nodal-line-semimetal phase with the same parity eigenvalues as a z -directed weak TI [$(z_{2,1}, z_{2,2}, z_{2,3}, z_4) = (0012)$] when subduced onto SG 2 ($P\bar{1}$), see SM 6 Band Refs. [5, 30, 31, 36]]. When SOC is reintroduced, the nodal lines at E_F in Ta_2NiSe_7 become gapped, the band inversion at A is removed by SOC, and the bands at Γ remain inverted, overall driving Ta_2NiSe_7 into a $Z_4 = 3$ 3D TI phase.

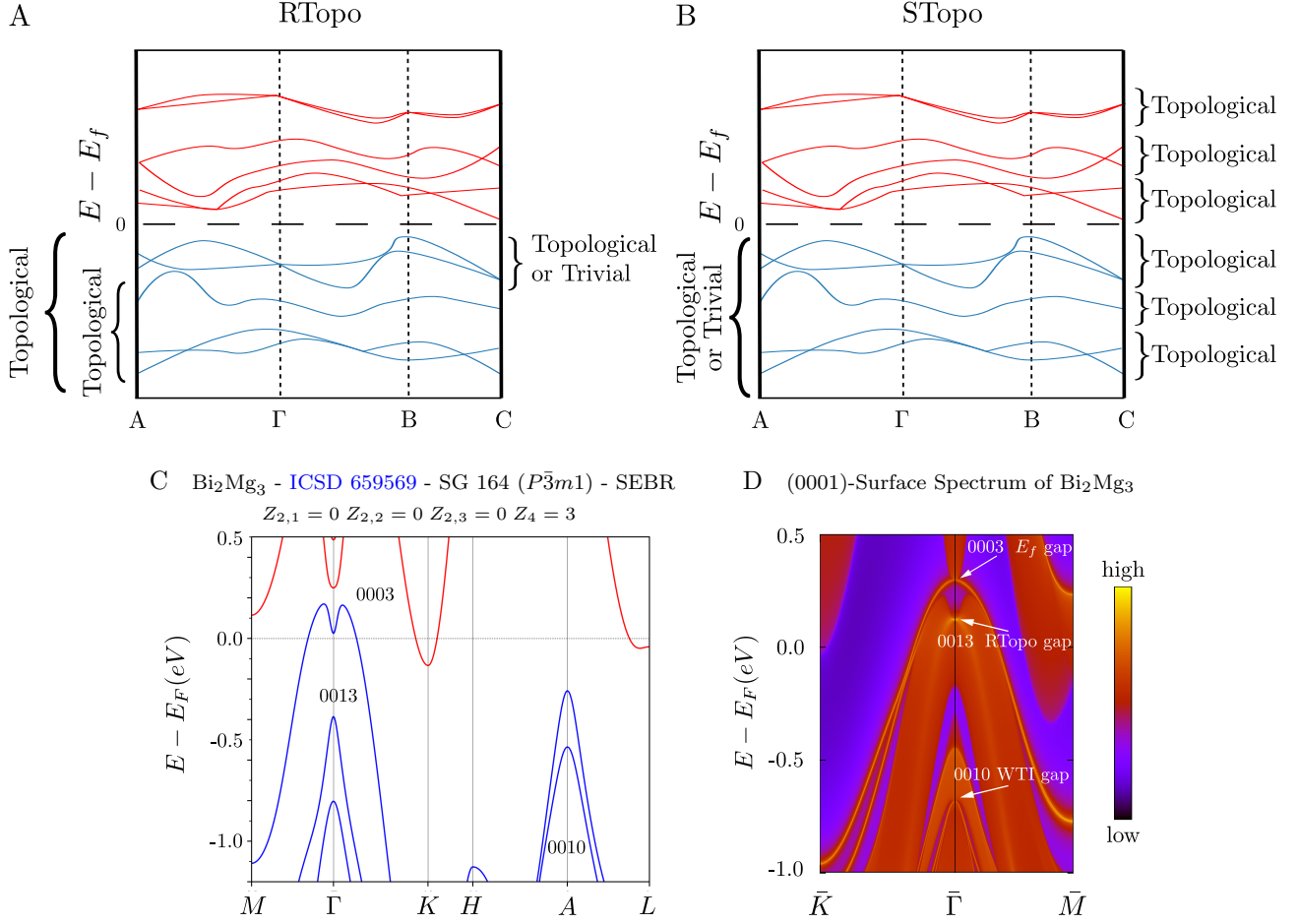


Figure 5. Repeat-topology and supertopology in Bi_2Mg_3 . (A) A schematic depiction of a repeat-topological (RTopo) band structure. In RTopo materials, the gap at the Fermi level, as well as the next gap below E_F as measured by band connectivity through TQC (see SM 2), exhibit cumulative symmetry-indicated stable topology (see SM 9 A). By this definition – which is motivated by the experimental accessibility of topological gaps and boundary states below E_F – we note that it is possible for the isolated bands between E_F and the next-highest gap below E_F to be topologically trivial. (B) A schematic depiction of a supertopological (STopo) band structure. In STopo materials, *every* energetically isolated set of bands in the spectrum exhibits symmetry-indicated stable topology (though the system at E_F is still free to be a TSM or exhibit cumulative trivial topology, see SM 9 B). (C) Bulk band structure of Bi_2Mg_3 [ICSD 659569, SG 164 ($P\bar{3}m1$)], an experimentally-established 3D TI [71] revealed by our investigations to additionally be RTopo and STopo. The numbers between the stable topological bands in (C) indicate the cumulative stable SIs of each band gap in the order $Z_{2w,1}, Z_{2w,2}, Z_{2w,3}, Z_4$ [see Refs. [16, 17, 29, 30, 33, 34] and SM 11 for the physical meaning of the stable SIs in SG 164 ($P\bar{3}m1$)]. (D) (0001)-surface states of Bi_2Mg_3 obtained from surface Green’s functions (see SM 9 A for calculation details). We have labeled the surface states using the cumulative stable SIs of the projected bulk gaps (as determined by band connectivity, see Table S1 in SM 3 for further details). Previous ARPES investigations of Bi_2Mg_3 have revealed the existence of “surface resonance bands” below E_F at the (0001)-surface Γ point [71]. We find that the surface resonance bands in Bi_2Mg_3 are in fact RTopo Dirac-cone surface states in the first gap below E_F [the “0013 RTopo gap”]. The surface Green’s function calculations exhibit additional twofold-Dirac cone surface states within the projected bulk gap ~ 0.8 eV below E_F [the “0010 WTI gap”]. Although the earlier ARPES experiments also observed surface states in the projected 0010 gap in Bi_2Mg_3 [71], we emphasize that the surface states in the 0010 gap in (D) are either trivial or originate from non-symmetry-indicated stable topology, because the cumulative stable SIs (0010) characterize an (obstructed) weak TI phase that does not generically exhibit anomalous twofold Dirac cones on z -normal [(0001)-] surfaces (see SM 11 A 6).

-
- [1] B. J. Wieder, *et al.*, *Nature Reviews Materials* (2021).
- [2] M. Z. Hasan, C. L. Kane, *Rev. Mod. Phys.* **82**, 3045 (2010).
- [3] C. L. Kane, E. J. Mele, *Phys. Rev. Lett.* **95**, 146802 (2005).
- [4] B. A. Bernevig, T. L. Hughes, S.-C. Zhang, *Science* **314**, 1757 (2006).
- [5] L. Fu, C. L. Kane, E. J. Mele, *Phys. Rev. Lett.* **98**, 106803 (2007).
- [6] Z. Wang, H. Weng, Q. Wu, X. Dai, Z. Fang, *Phys. Rev. B* **88**, 125427 (2013).
- [7] B. J. Wieder, Y. Kim, A. M. Rappe, C. L. Kane, *Phys. Rev. Lett.* **116**, 186402 (2016).
- [8] B. Bradlyn, *et al.*, *Science* **353** (2016).
- [9] P. Tang, Q. Zhou, S.-C. Zhang, *Phys. Rev. Lett.* **119**, 206402 (2017).
- [10] N. P. Armitage, E. J. Mele, A. Vishwanath, *Rev. Mod. Phys.* **90**, 015001 (2018).
- [11] L. Fu, *Phys. Rev. Lett.* **106**, 106802 (2011).
- [12] T. H. Hsieh, *et al.*, *Nature Communications* **3**, 982 (2012).
- [13] Z. Wang, A. Alexandradinata, R. J. Cava, B. A. Bernevig, *Nature* **532**, 189 (2016).
- [14] B. J. Wieder, *et al.*, *Science* **361**, 246 (2018).
- [15] W. A. Benalcazar, B. A. Bernevig, T. L. Hughes, *Phys. Rev. B* **96**, 245115 (2017).
- [16] Z. Song, T. Zhang, Z. Fang, C. Fang, *Nature Communications* **9**, 3530 (2018).
- [17] E. Khalaf, H. C. Po, A. Vishwanath, H. Watanabe, *Phys. Rev. X* **8**, 031070 (2018).
- [18] D. Hsieh, *et al.*, *Nature* **460**, 1101 (2009).
- [19] S. Borisenko, *et al.*, *Phys. Rev. Lett.* **113**, 027603 (2014).
- [20] S.-Y. Xu, *et al.*, *Science* **349**, 613 (2015).
- [21] H. Weng, C. Fang, Z. Fang, B. A. Bernevig, X. Dai, *Phys. Rev. X* **5**, 011029 (2015).
- [22] F. Schindler, *et al.*, *Nature Physics* **14**, 918 (2018).
- [23] D. S. Sanchez, *et al.*, *Nature* **567**, 500 (2019).
- [24] Z. Rao, *et al.*, *Nature* **567**, 496 (2019).
- [25] N. B. M. Schröter, *et al.*, *Science* **369**, 179 (2020).
- [26] W. Shi, *et al.*, *Nature Physics* **17**, 381 (2021).
- [27] J. Gooth, *et al.*, *Nature* **575**, 315 (2019).
- [28] B. Bradlyn, *et al.*, *Nature* **547**, 298 (2017).
- [29] L. Elcoro, *et al.*, *Nature Communications* **12**, 5965 (2021).
- [30] L. Fu, C. L. Kane, *Phys. Rev. B* **76**, 045302 (2007).
- [31] Y. Kim, B. J. Wieder, C. L. Kane, A. M. Rappe, *Phys. Rev. Lett.* **115**, 036806 (2015).
- [32] J. Kruthoff, J. de Boer, J. van Wezel, C. L. Kane, R.-J. Slager, *Phys. Rev. X* **7**, 041069 (2017).
- [33] H. C. Po, A. Vishwanath, H. Watanabe, *Nature Communications* **8**, 50 (2017).
- [34] Z. Wang, B. J. Wieder, J. Li, B. Yan, B. A. Bernevig, *Phys. Rev. Lett.* **123**, 186401 (2019).
- [35] H. Watanabe, H. C. Po, A. Vishwanath, *Science Advances* **4** (2018).
- [36] Z. Song, T. Zhang, C. Fang, *Phys. Rev. X* **8**, 031069 (2018).
- [37] Y. Xu, *et al.*, *Nature* **586**, 702 (2020).
- [38] M. G. Vergniory, *et al.*, *Nature* **566**, 480 (2019).
- [39] T. Zhang, *et al.*, *Nature* **566**, 475 (2019).
- [40] F. Tang, H. C. Po, A. Vishwanath, X. Wan, *Nature* **566**, 486 (2019).
- [41] G. Bergerhoff, R. Hundt, R. Sievers, I. D. Brown, *Journal of Chemical Information and Computer Sciences* **23**, 66 (1983).
- [42] J. Cano, *et al.*, *Phys. Rev. Lett.* **120**, 266401 (2018).
- [43] H. C. Po, H. Watanabe, A. Vishwanath, *Phys. Rev. Lett.* **121**, 126402 (2018).
- [44] Z.-D. Song, L. Elcoro, Y.-F. Xu, N. Regnault, B. A. Bernevig, *Phys. Rev. X* **10**, 031001 (2020).
- [45] Y. Hwang, J. Ahn, B.-J. Yang, *Phys. Rev. B* **100**, 205126 (2019).
- [46] Z.-D. Song, L. Elcoro, B. A. Bernevig, *Science* **367**, 794 (2020).
- [47] Z. Song, *et al.*, *Phys. Rev. Lett.* **123**, 036401 (2019).
- [48] H. C. Po, L. Zou, T. Senthil, A. Vishwanath, *Phys. Rev. B* **99**, 195455 (2019).
- [49] [Topological Materials Database](https://www.topologicalquantumchemistry.com/) <https://www.topologicalquantumchemistry.com/>.
- [50] D. N. Basov, R. D. Averitt, D. Hsieh, *Nature Materials* **16**, 1077 (2017).
- [51] S. Peotta, P. Törmä, *Nature Communications* **6**, 8944 (2015).
- [52] F. Xie, Z. Song, B. Lian, B. A. Bernevig, *Phys. Rev. Lett.* **124**, 167002 (2020).
- [53] VASP2Trace <https://github.com/zjwang11/irvsp>.
- [54] Check Topological Mat <https://www.cryst.ehu.es/cryst/checktopologicalmat>.
- [55] C. Bradley, A. Cracknell, *The Mathematical Theory of Symmetry in Solids: Representation Theory for Point Groups and Space Groups* (Clarendon Press, 1972).
- [56] A. A. Soluyanov, D. Vanderbilt, *Phys. Rev. B* **83**, 035108 (2011).
- [57] L. Elcoro, *et al.*, *Journal of Applied Crystallography* **50**, 1457 (2017).
- [58] B. J. Wieder, *et al.*, *Nature Communications* **11**, 627 (2020).
- [59] C.-Z. Li, *et al.*, *Phys. Rev. Lett.* **124**, 156601 (2020).
- [60] A. Marrazzo, M. Gibertini, D. Campi, N. Mounet, N. Marzari, *Nano Letters* **19**, 8431 (2019).

- [61] D. Wang, *et al.*, *Phys. Rev. B* **100**, 195108 (2019).
- [62] Y. Li, *et al.*, *Nature* **455**, 372 (2008).
- [63] J. Zhou, *et al.*, *Nature* **556**, 355 (2018).
- [64] Y. Chen, *et al.*, *Nature Physics* **16**, 218 (2020).
- [65] K. Dolui, S. Sanvito, *EPL (Europhysics Letters)* **115**, 47001 (2016).
- [66] Y. F. Lu, *et al.*, *Nature Communications* **8**, 14408 (2017).
- [67] G. Mazza, *et al.*, *Phys. Rev. Lett.* **124**, 197601 (2020).
- [68] R. M. Fleming, S. A. Sunshine, C. H. Chen, L. F. Schneemeyer, J. V. Waszczak, *Phys. Rev. B* **42**, 4954 (1990).
- [69] Q.-G. Mu, *et al.*, *Phys. Rev. Materials* **5**, 084201 (2021).
- [70] T. A. Cochran, *et al.*, *arXiv e-prints* p. arXiv:2004.11365 (2020).
- [71] T.-R. Chang, *et al.*, *Advanced Science* **6**, 1800897 (2019).
- [72] A. A. Soluyanov, *et al.*, *Nature* **527**, 495 (2015).
- [73] J. Gao, *et al.*, *Science Bulletin* **66**, 667 (2021).
- [74] K. Choudhary, K. F. Garrity, N. J. Ghimire, N. Anand, F. Tavazza, *Phys. Rev. B* **103**, 155131 (2021).
- [75] Z. Guo, *et al.*, *Phys. Rev. B* **103**, 115145 (2021).
- [76] X. Wang, *et al.*, *arXiv e-prints* p. arXiv:2012.07293 (2020).
- [77] G. Kresse, J. Furthmüller, *Computational Materials Science* **6**, 15 (1996).
- [78] G. Kresse, J. Furthmüller, *Phys. Rev. B* **54**, 11169 (1996).
- [79] G. Kresse, J. Hafner, *Phys. Rev. B* **48**, 13115 (1993).
- [80] G. Kresse, D. Joubert, *Phys. Rev. B* **59**, 1758 (1999).
- [81] J. P. Perdew, K. Burke, M. Ernzerhof, *Phys. Rev. Lett.* **77**, 3865 (1996).
- [82] D. Hobbs, G. Kresse, J. Hafner, *Phys. Rev. B* **62**, 11556 (2000).
- [83] J. Gao, Q. Wu, C. Persson, Z. Wang, *Computer Physics Communications* **261**, 107760 (2021).
- [84] G. Pizzi, *et al.*, *Journal of Physics: Condensed Matter* **32**, 165902 (2020).
- [85] Data for "all topological bands of all nonmagnetic stoichiometric materials", 10.5281/zenodo.6123281.
- [86] Z. Song, Z. Fang, C. Fang, *Phys. Rev. Lett.* **119**, 246402 (2017).
- [87] L. Michel, J. Zak, *Phys. Rev. B* **59**, 5998 (1999).
- [88] L. Michel, J. Zak, *Physics Reports* **341**, 377 (2001).
- [89] J. Cano, L. Elcoro, M. I. Aroyo, B. A. Bernevig, B. Bradlyn, *arXiv e-prints* p. arXiv:2107.00647 (2021).
- [90] J. Zak, *Phys. Rev. Lett.* **45**, 1025 (1980).
- [91] M. G. Vergniory, *et al.*, *Phys. Rev. E* **96**, 023310 (2017).
- [92] J. Cano, *et al.*, *Phys. Rev. B* **97**, 035139 (2018).
- [93] M. I. Aroyo, *et al.*, *Zeitschrift für Kristallographie - Crystalline Materials* **221**, 15 (2006).
- [94] M. I. Aroyo, A. Kirov, C. Capillas, J. M. Perez-Mato, H. Wondratschek, *Acta Crystallographica Section A* **62**, 115 (2006).
- [95] S. Liu, A. Vishwanath, E. Khalaf, *Phys. Rev. X* **9**, 031003 (2019).
- [96] B. Bradlyn, Z. Wang, J. Cano, B. A. Bernevig, *Phys. Rev. B* **99**, 045140 (2019).
- [97] A. Bouhon, A. M. Black-Schaffer, R.-J. Slager, *Phys. Rev. B* **100**, 195135 (2019).
- [98] J. Ahn, S. Park, B.-J. Yang, *Phys. Rev. X* **9**, 021013 (2019).
- [99] V. Peri, *et al.*, *Science* **367**, 797 (2020).
- [100] A. Nelson, T. Neupert, T. c. v. Bzdusek, A. Alexandradinata, *Phys. Rev. Lett.* **126**, 216404 (2021).
- [101] B. J. Wieder, B. A. Bernevig, *ArXiv e-prints* (2018).
- [102] A. Kitaev, *AIP Conference Proceedings* **1134**, 22 (2009).
- [103] X.-L. Qi, T. L. Hughes, S.-C. Zhang, *Phys. Rev. B* **78**, 195424 (2008).
- [104] C. Fang, L. Fu, *Science Advances* **5** (2019).
- [105] S.-J. Huang, H. Song, Y.-P. Huang, M. Hermele, *Phys. Rev. B* **96**, 205106 (2017).
- [106] W. A. Benalcazar, T. Li, T. L. Hughes, *Phys. Rev. B* **99**, 245151 (2019).
- [107] L. Fidkowski, T. S. Jackson, I. Klich, *Phys. Rev. Lett.* **107**, 036601 (2011).
- [108] R. Yu, X. L. Qi, A. Bernevig, Z. Fang, X. Dai, *Phys. Rev. B* **84**, 075119 (2011).
- [109] A. Alexandradinata, Z. Wang, B. A. Bernevig, *Phys. Rev. X* **6**, 021008 (2016).
- [110] W. A. Benalcazar, B. A. Bernevig, T. L. Hughes, *Science* **357**, 61 (2017).
- [111] Y. Qian, *et al.*, *Phys. Rev. B* **101**, 155143 (2020).
- [112] VASP2Trace may be accessed to compute the topological classification of a material by selecting the function CHECK-TOPOLOGICAL at <https://cryst.ehu.es/cgi-bin/cryst/programs/topological.pl>.
- [113] L. Elcoro, Z. Song, B. A. Bernevig, *Phys. Rev. B* **102**, 035110 (2020).
- [114] M. N. Ali, *et al.*, *Inorganic Chemistry* **53**, 4062 (2014).
- [115] Z. K. Liu, *et al.*, *Nature Materials* **13**, 677 (2014).
- [116] M. I. Aroyo, ed., *International Tables for Crystallography, Volume A: Space-Group Symmetry*, vol. A (International Union of Crystallography, 2016).
- [117] J. Perez-Mato, *et al.*, *Annual Review of Materials Research* **45**, 217 (2015).
- [118] P. Hohenberg, W. Kohn, *Phys. Rev.* **136**, B864 (1964).
- [119] W. Kohn, L. J. Sham, *Phys. Rev.* **140**, A1133 (1965).
- [120] I. n. Robredo, M. G. Vergniory, B. Bradlyn, *Phys. Rev. Materials* **3**, 041202 (2019).
- [121] A. H. Larsen, *et al.*, *Journal of Physics: Condensed Matter* **29**, 273002 (2017).
- [122] A. Togo, I. Tanaka, *Scripta Materialia* **108**, 1 (2015).

- [123] W. Setyawan, S. Curtarolo, *Computational Materials Science* **49**, 299 (2010).
- [124] Y. Hinuma, G. Pizzi, Y. Kumagai, F. Oba, I. Tanaka, *Computational Materials Science* **128**, 140 (2017).
- [125] A. Jain, *et al.*, *APL Materials* **1**, 011002 (2013).
- [126] C. L. Kane, E. J. Mele, *Phys. Rev. Lett.* **95**, 226801 (2005).
- [127] J. Ma, *et al.*, *Science Advances* **3** (2017).
- [128] S. Liang, *et al.*, *Nature Materials* **18**, 443 (2019).
- [129] B. J. Wieder, C. L. Kane, *Phys. Rev. B* **94**, 155108 (2016).
- [130] G. Chang, *et al.*, *Phys. Rev. Lett.* **119**, 206401 (2017).
- [131] G. Chang, *et al.*, *Nature Materials* **17**, 978 (2018).
- [132] F. Flicker, *et al.*, *Phys. Rev. B* **98**, 155145 (2018).
- [133] M. Nespolo, M. I. Aroyo, B. Souvignier, *Journal of Applied Crystallography* **51**, 1481 (2018).
- [134] D. Takane, *et al.*, *Phys. Rev. Lett.* **122**, 076402 (2019).
- [135] N. B. M. Schröter, *et al.*, *Nature Physics* **15**, 759 (2019).
- [136] R. Yu, H. Weng, Z. Fang, X. Dai, X. Hu, *Phys. Rev. Lett.* **115**, 036807 (2015).
- [137] C. Fang, Y. Chen, H.-Y. Kee, L. Fu, *Phys. Rev. B* **92**, 081201 (2015).
- [138] J. Ahn, D. Kim, Y. Kim, B.-J. Yang, *Phys. Rev. Lett.* **121**, 106403 (2018).
- [139] A. Bouhon, A. M. Black-Schaffer, *ArXiv e-prints* (2017).
- [140] T. c. v. Bzdusek, M. Sigrist, *Phys. Rev. B* **96**, 155105 (2017).
- [141] T. L. Hughes, E. Prodan, B. A. Bernevig, *Phys. Rev. B* **83**, 245132 (2011).
- [142] X. Wan, A. M. Turner, A. Vishwanath, S. Y. Savrasov, *Phys. Rev. B* **83**, 205101 (2011).
- [143] T. Zhang, *et al.*, *Phys. Rev. Research* **2**, 022066 (2020).
- [144] I. Tateishi, *Phys. Rev. Research* **2**, 043112 (2020).
- [145] I. Tateishi, *Phys. Rev. B* **102**, 155111 (2020).
- [146] Z. Ringel, Y. E. Kraus, A. Stern, *Phys. Rev. B* **86**, 045102 (2012).
- [147] J. E. Moore, L. Balents, *Phys. Rev. B* **75**, 121306 (2007).
- [148] B. J. Wieder, K.-S. Lin, B. Bradlyn, *Phys. Rev. Research* **2**, 042010 (2020).
- [149] J. Yu, B. J. Wieder, C.-X. Liu, *Phys. Rev. B* **104**, 174406 (2021).
- [150] H. Watanabe, H. C. Po, A. Vishwanath, M. Zaletel, *Proceedings of the National Academy of Sciences* **112**, 14551 (2015).
- [151] S. M. Young, B. J. Wieder, *Phys. Rev. Lett.* **118**, 186401 (2017).
- [152] H. Yang, *et al.*, *Nature Reviews Materials* **3**, 341 (2018).
- [153] B. Lv, T. Qian, H. Ding, *Nature Reviews Physics* **1**, 609 (2019).
- [154] I. Belopolski, *et al.*, *Nature Communications* **8**, 942 (2017).
- [155] I. Belopolski, *et al.*, *Nature Communications* **7**, 13643 (2016).
- [156] Q. Wu, S. Zhang, H.-F. Song, M. Troyer, A. A. Soluyanov, *Computer Physics Communications* **224**, 405 (2018).
- [157] X. Zhang, L. Jin, X. Dai, G. Liu, *The Journal of Physical Chemistry Letters* **8**, 4814 (2017).
- [158] T. Zhou, *et al.*, *Chinese Physics Letters* **36**, 117303 (2019).
- [159] A. H. Castro Neto, F. Guinea, N. M. R. Peres, K. S. Novoselov, A. K. Geim, *Rev. Mod. Phys.* **81**, 109 (2009).
- [160] J. C. Y. Teo, L. Fu, C. L. Kane, *Phys. Rev. B* **78**, 045426 (2008).
- [161] Y. Tanaka, *et al.*, *Nature Physics* **8**, 800 (2012).
- [162] F. Schindler, *et al.*, *Science Advances* **4** (2018).
- [163] E. Fradkin, E. Dagotto, D. Boyanovsky, *Phys. Rev. Lett.* **57**, 2967 (1986).
- [164] G. Chang, *et al.*, *Science Advances* **2** (2016).
- [165] K. Shiozaki, M. Sato, K. Gomi, *Phys. Rev. B* **91**, 155120 (2015).
- [166] J. Langbehn, Y. Peng, L. Trifunovic, F. von Oppen, P. W. Brouwer, *Phys. Rev. Lett.* **119**, 246401 (2017).
- [167] Z. Wang, *et al.*, *Phys. Rev. B* **85**, 195320 (2012).
- [168] S. M. Young, *et al.*, *Phys. Rev. Lett.* **108**, 140405 (2012).
- [169] J. A. Steinberg, *et al.*, *Phys. Rev. Lett.* **112**, 036403 (2014).
- [170] B.-J. Yang, N. Nagaosa, *Nature Communications* **5**, 4898 (2014).
- [171] Z. K. Liu, *et al.*, *Science* **343**, 864 (2014).
- [172] S.-Y. Xu, *et al.*, *Science* **347**, 294 (2015).
- [173] M. B. de Paz, M. G. Vergniory, D. Bercioux, A. García-Etxarri, B. Bradlyn, *Phys. Rev. Research* **1**, 032005 (2019).
- [174] C. Fang, M. J. Gilbert, B. A. Bernevig, *Phys. Rev. B* **86**, 115112 (2012).
- [175] A. Alexandradinata, X. Dai, B. A. Bernevig, *Phys. Rev. B* **89**, 155114 (2014).
- [176] D. Hsieh, *et al.*, *Nature* **452**, 970 (2008).
- [177] C.-H. Hsu, *et al.*, *Proceedings of the National Academy of Sciences* **116**, 13255 (2019).
- [178] C.-C. Liu, J.-J. Zhou, Y. Yao, F. Zhang, *Phys. Rev. Lett.* **116**, 066801 (2016).
- [179] F. Tang, H. C. Po, A. Vishwanath, X. Wan, *Nature Physics* **15**, 470 (2019).
- [180] C.-H. Hsu, *et al.*, *2D Materials* **6**, 031004 (2019).
- [181] C. Yoon, C.-C. Liu, H. Min, F. Zhang, *arXiv e-prints* p. arXiv:2005.14710 (2020).
- [182] R. Noguchi, *et al.*, *Nature Materials* **20**, 473 (2021).
- [183] A. K. Nayak, *et al.*, *Science Advances* **5** (2019).
- [184] R. Queiroz, I. C. Fulga, N. Avraham, H. Beidenkopf, J. Cano, *Phys. Rev. Lett.* **123**, 266802 (2019).
- [185] F.-T. Huang, *et al.*, *Nature Communications* **10**, 4211 (2019).
- [186] Y.-B. Choi, *et al.*, *Nature Materials* **19**, 974 (2020).

- [187] A. Kononov, *et al.*, *Nano Letters* **20**, 4228 (2020).
- [188] W. Wang, *et al.*, *Science* **368**, 534 (2020).
- [189] R. Noguhi, *et al.*, *Nature* **566**, 518 (2019).
- [190] W. P. Su, J. R. Schrieffer, A. J. Heeger, *Phys. Rev. Lett.* **42**, 1698 (1979).
- [191] C. K. Chiang, *et al.*, *Phys. Rev. Lett.* **39**, 1098 (1977).
- [192] J.-N. Fuchs, F. Piéchon, *Phys. Rev. B* **104**, 235428 (2021).
- [193] Y. Ran, Y. Zhang, A. Vishwanath, *Nature Physics* **5**, 298 (2009).
- [194] Y.-M. Xie, *et al.*, *Nature Communications* **12**, 3064 (2021).
- [195] S. M. Young, C. L. Kane, *Phys. Rev. Lett.* **115**, 126803 (2015).
- [196] N. Kumar, *et al.*, *Advanced Materials* **32**, 1906046 (2020).
- [197] G. Gatti, *et al.*, *Phys. Rev. Lett.* **125**, 216402 (2020).
- [198] F. de Juan, A. G. Grushin, T. Morimoto, J. E. Moore, *Nature Communications* **8**, 15995 (2017).
- [199] D. Rees, *et al.*, *Science Advances* **6** (2020).
- [200] B. Xu, *et al.*, *Proceedings of the National Academy of Sciences* **117**, 27104 (2020).
- [201] Z. Ni, *et al.*, *Nature Communications* **12**, 154 (2021).
- [202] D. J. Rebar, *et al.*, *Phys. Rev. B* **99**, 094517 (2019).
- [203] J. Z. S. Gao, *et al.*, *arXiv e-prints* p. arXiv:2012.11287 (2020).
- [204] E. Emmanouilidou, *et al.*, *Phys. Rev. B* **102**, 235144 (2020).
- [205] G. Sharma, *et al.*, *J. Mater. Chem. A* **4**, 2936 (2016).
- [206] D. Di Sante, *et al.*, *Physical Review B* **96**, 121106 (2017).
- [207] J. F. Khoury, *et al.*, *Journal of the American Chemical Society* **141**, 19130 (2019).
- [208] L. M. Schoop, *et al.*, *Science Advances* **4** (2018).
- [209] C. Fang, M. J. Gilbert, X. Dai, B. A. Bernevig, *Phys. Rev. Lett.* **108**, 266802 (2012).
- [210] G. Xu, H. Weng, Z. Wang, X. Dai, Z. Fang, *Phys. Rev. Lett.* **107**, 186806 (2011).
- [211] S.-M. Huang, *et al.*, *Proceedings of the National Academy of Sciences* **113**, 1180 (2016).
- [212] S. S. Tsirkin, I. Souza, D. Vanderbilt, *Phys. Rev. B* **96**, 045102 (2017).
- [213] W. Wu, Z.-M. Yu, X. Zhou, Y. X. Zhao, S. A. Yang, *Phys. Rev. B* **101**, 205134 (2020).
- [214] H. Weng, C. Fang, Z. Fang, X. Dai, *Phys. Rev. B* **93**, 241202 (2016).
- [215] Z. Zhu, G. W. Winkler, Q. Wu, J. Li, A. A. Soluyanov, *Phys. Rev. X* **6**, 031003 (2016).
- [216] G. Chang, *et al.*, *Scientific Reports* **7**, 1688 (2017).
- [217] B. J. Wieder, *Nature Physics* **14**, 329 (2018).
- [218] B. Q. Lv, *et al.*, *Nature* **546**, 627 (2017).
- [219] J.-Z. Ma, *et al.*, *Nature Physics* **14**, 349 (2018).
- [220] H. Gao, *et al.*, *Phys. Rev. Lett.* **121**, 106404 (2018).
- [221] C. Tournier-Colletta, *et al.*, *Phys. Rev. Lett.* **110**, 236401 (2013).
- [222] Y. Zhang, L.-F. Lin, A. Moreo, S. Dong, E. Dagotto, *Phys. Rev. B* **101**, 174106 (2020).
- [223] H. Yi, *et al.*, *Phys. Rev. Research* **3**, 013271 (2021).
- [224] M. Lin, T. L. Hughes, *Phys. Rev. B* **98**, 241103 (2018).
- [225] D. Călugăru, V. Juričić, B. Roy, *Phys. Rev. B* **99**, 041301 (2019).
- [226] A. L. Szabó, R. Moessner, B. Roy, *Phys. Rev. B* **101**, 121301 (2020).
- [227] A. L. Szabó, B. Roy, *Phys. Rev. Research* **2**, 043197 (2020).
- [228] S. A. A. Ghorashi, T. Li, T. L. Hughes, *Phys. Rev. Lett.* **125**, 266804 (2020).
- [229] H.-X. Wang, Z.-K. Lin, B. Jiang, G.-Y. Guo, J.-H. Jiang, *Phys. Rev. Lett.* **125**, 146401 (2020).
- [230] S. Nie, B. A. Bernevig, Z. Wang, *Phys. Rev. Research* **3**, L012028 (2021).

Supplementary Material for “All Topological Bands of All Non-Magnetic Stoichiometric Materials”

CONTENTS

SM 1. Introduction to the Supplementary Material	19
SM 2. Topological Quantum Chemistry Review	20
A. Elementary Band Representations	20
B. The Compatibility Relations	21
SM 3. Overview of the Previous Functionality of the VASP2Trace Program and New Features of the Check Topological Mat Program	23
A. Overview of the Previous Functionality of the VASP2Trace and Check Topological Mat Programs	23
B. New Features of the Check Topological Mat Program Introduced in this Work	25
SM 4. VASP Calculation Details and Data Set Preparation	27
SM 5. Computation Time and Resources	29
A. Supercomputers and General Computational Resource Usage Statistics	29
B. Computational Resources Expended per SG and per Number of Atoms in the Primitive Cell	30
C. Disk Storage Requirements and Statistics	40
SM 6. Topological Material Classes in the Absence of Spin-Orbit Coupling	45
A. Relative Numbers of Materials in Each Topological Class with and without SOC	48
B. Physical Interpretation of the NLC and SEBR Materials Classes in the Absence of SOC	48
SM 7. Major Updates to the Topological Materials Database	51
SM 8. Statistics for all of the Topological Bands and Band Connectivity in the ICSD	53
A. Topological Classification at the Fermi Level for all of the Stoichiometric Unique Materials in the ICSD with and w/o SOC	56
B. Topological Classification and Connectivity of all of the Bands in all of the Stoichiometric Unique Materials in the ICSD with and w/o SOC	64
SM 9. Repeat-Topology and Supertopology	81
A. Definition of Repeat-Topology	81
B. Definition of Supertopology	84
C. Statistics for Supertopological Materials in the ICSD	84
SM 10. SOC-Driven Topological Phase Transitions	96
SM 11. Lists of Representative Topological Materials	107
A. Symmetry-Indicated TIs, TCIs, and HOTIs	109
1. 3D Strong TIs	109
2. S_4 -Rotoinversion-Indicated Strong TIs and Weyl Semimetals	120
3. Inversion-Symmetry-Protected HOTIs	122
4. Inversion-Symmetry-Indicated Weak TIs and TCIs	131
5. Rotation-Anomaly TCIs and High-Fold-Rotation Mirror TCIs	148
6. Other TCIs with Trivial Z_4 Indices	154
7. TCIs with Threefold Rotation Symmetry	160
B. Repeat-Topological Materials	161

C. Enforced Topological Semimetals	170
1. ESFD-Classified Semimetals	170
2. ES-Classified Semimetals	193
D. Semimetal-Insulator Transitions Driven by Spin-Orbit Coupling	200
E. Materials with Fragile Topological Bands at or Close to E_F	207

LIST OF TABLES

S1. Topology of all of the bands in the RTopo and STopo compound Bi_2Mg_3	26
S2. Number of analyzed compounds.	28
S3. Percentage of unique materials with at least one magnetic ICSD entry and with valence f electrons as determined by VASP (see https://www.smcm.iqfr.csic.es/docs/vasp/node248.html for further details).	28
S4. Total CPU hours expended in each of the four VASP calculation steps, subdivided by calculations performed with and without incorporating the effects of SOC (with SOC and w/o SOC, respectively).	30
S5. Total CPU hours expended for ab-initio calculations with SOC per SG	30
S6. Total CPU hours expended for ab-initio calculations w/o SOC per SG	34
S7. Total CPU hours expended for ab-initio calculations with SOC per number of atoms in the primitive cell	37
S8. Total CPU hours expended for ab-initio calculations w/o SOC per number of atoms in the primitive cell	39
S9. Total disk storage space for ab-initio calculations per SG	40
S10. Total disk storage space for ab-initio calculations per number of atoms in the primitive cell	44
S11. Number of unique materials in each topological class where both SOC and w/o SOC calculations have converged	47
S12. List of all nonmagnetic NLC-SM unique materials without f electrons	50
S13. List of all nonmagnetic SEBR-SM unique materials without f electrons	51
S14. Number of unique materials in each topological class per SG with SOC	56
S15. Number of materials in each topological class per SG w/o SOC	60
S17. Number of topological bands per SG among the unique materials with SOC	64
S18. Number of unique materials per SG with topological bands at any filling with SOC	68
S19. Number of topological bands per SG w/o SOC among the unique materials	72
S20. Number of unique materials per SG with topological bands w/o SOC at any filling	76
S21. High-connectivity nonmagnetic unique materials without f electrons	80
S16. Topology of all of the bands in the ES compound Ni_2SnZr	82
S22. Topology of all of the bands in the RTopo and STopo compound Bi	85
S23. Statistics for supertopological materials with SOC	86
S24. Supertopological nonmagnetic unique materials without f electrons that are NLC at E_F	87
S25. Supertopological nonmagnetic unique materials without f electrons that are SEBR at E_F	88
S26. Supertopological nonmagnetic unique materials without f electrons that are ES at E_F	89
S27. Supertopological nonmagnetic unique materials without f electrons that are ESFD at E_F	91
S28. Supertopological nonmagnetic unique materials without f electrons that are LCEBR at E_F	95
S29. SOC-driven topological phase transition statistics for ES materials w/o SOC	97
S30. SOC-driven topological phase transition statistics for ESFD materials w/o SOC	100
S31. SOC-driven topological phase transition statistics for LCEBR materials w/o SOC	103
S32. SOC-driven topological phase transition statistics for NLC-SM materials w/o SOC	106
S33. SOC-driven topological phase transition statistics for SEBR-SM materials w/o SOC	107

SM 1. INTRODUCTION TO THE SUPPLEMENTARY MATERIAL

In this work, we have introduced a complete catalogue of the symmetry-indicated stable and fragile topology of all of the bands in all of the stoichiometric materials in the Inorganic Crystal Structure Database (ICSD) [41]. Below, we provide Supplementary Material (SM) containing a description of our methodology, as well as detailed statistics for the materials studied in this work. First, in SM 2, we will review the methods employed in this work, which derive from the recently introduced theory of *Topological Quantum Chemistry* (TQC) [28]. Next, in SM 3 and SM 4, we will document the computational machinery that we developed to apply TQC to the ICSD database. Specifically, in SM 3 and SM 4, we will respectively review the **VASP2Trace** program previously implemented for Ref. 38, and will detail updates to the **Check Topological Mat** program implemented for this work – for both programs, we will additionally detail their interface with the density functional theory (DFT) Vienna Ab-initio Simulation Package (VASP) [77, 78]. In SM 5, we will next discuss how we prepared the data used to generate this work, and will detail the CPU time invested per number of atoms in the unit cell of each material, and per each crystallographic space group (SG) [55]. In the following section – SM 6, we will then review the theory of TQC in the absence of spin-orbit coupling (SOC), and will specifically discuss the physical interpretation of symmetry-based indicators of band topology [16, 17, 29, 33, 36, 37, 86] in material calculations performed in the absence of SOC (w/o SOC). In the following section – SM 7 – we will then provide detailed descriptions of the significant **Topological Materials Database** (<https://www.topologicalquantumchemistry.com/>) updates implemented for this work.

In the remaining sections of the Supplementary Material, we will present detailed statistics, tables, and lists supporting the results shown in the main text. First, in SM 8, we will provide extensive statistics for all of the topological bands and band connectivity in the materials studied in this work. Next, in SM 9, we will rigorously define the *repeat-topological* (RTopo) and *supertopological* (STopo) material classes introduced in this work, and will provide a list of all of the symmetry-indicated STopo materials in the ICSD. Then, in SM 10, we will analyze the role of SOC in driving phase transitions between topological (semi)metals w/o SOC and topological (crystalline) insulators with SOC. In SM 10, we will additionally provide detailed statistics for all of the topological phase transitions observed in this work between materials with and w/o SOC. Finally, in SM 11, we will present an extensive list of all of the highest-quality topological (crystalline) insulators and semimetals among all of the stoichiometric materials in the ICSD. Though some of the materials in SM 11 are well known – such as the archetypal 3D topological insulator (TI) Bi_2Se_3 [18] [ICSD 617079, SG 166 ($R\bar{3}m$)] – others are relatively unstudied, and should inspire new experimental investigations as well as provide new context for previously unexplained experimental data.

SM 2. TOPOLOGICAL QUANTUM CHEMISTRY REVIEW

A. Elementary Band Representations

Topological Quantum Chemistry (TQC) [28] is a position-space theory of band topology in crystalline solids. The building blocks of TQC are trivial atomic limits, which transform in elementary band representations (EBRs) [87–89]. Most generally, a band representation (band rep), elementary or otherwise, is a collection of momentum-space states (bands) induced from (exponentially) localized orbitals placed throughout each unit cell of a crystal [88, 90]. If the band rep is induced from a *maximal* Wyckoff position ω and a set of atomic orbitals that transform in an irreducible corepresentation (corep) of the site-symmetry group G_ω [defined in detail in Refs. 28, 57, 91, and 92], then the band rep can be further classified as *elementary* (*i.e.*, as an EBR), provided that the band rep is not an *exceptional case* (see Refs. 28, 29, and 92). Conversely, if the band rep is not elementary, then it can be expressed as a sum of EBRs [92]. In this work and in TQC, we restrict analysis to nonmagnetic (paramagnetic) crystals [*i.e.* Type-II Shubnikov space groups (SGs) [29, 55]], which respect time-reversal (\mathcal{T}) symmetry. The EBRs of the nonmagnetic SGs can be accessed through the BANDREP tool [28, 57] on the Bilbao Crystallographic Server (BCS) [93, 94]. During the preparation of this work, the EBRs of the magnetic SGs were also computed in Ref. 29 (see MBANDREP on the BCS), and were used to perform the first high-throughput search for magnetic topological materials [37].

For the purposes of this work, we are primarily concerned with the small coreps at high-symmetry (maximal) \mathbf{k} points. Specifically, given a set of bands in a first-principles or tight-binding calculation, one can extract the coreps of the occupied bands at the maximal \mathbf{k} points to construct a *symmetry data vector* [38]. Given a symmetry data vector, the first step is to determine if the symmetry data vector is compatible with an insulating gap along all high-symmetry lines and planes – this can be accomplished using the compatibility relations, which are explained in detail in SM 2B. If the symmetry data is incompatible with an insulating gap, then the bulk bands are necessarily (semi)metallic. Semimetals that fail to satisfy the compatibility relations can then be further classified by whether a multiplet of Bloch states (transforming in an irreducible small corep of the little group) at a maximal \mathbf{k} point is partially occupied [enforced semimetal with Fermi degeneracy (ESFD)], or whether the compatibility relations fail along a high-symmetry line or plane [enforced semimetal (ES)]. If the symmetry data vector *is* compatible with an insulating gap (along high-symmetry lines and planes), we then determine if the symmetry data can be re-expressed as a linear combination of EBRs (LCEBR) with integer coefficients. As we will shortly see, in order for a set of bands to be topologically trivial, it is a necessary (but not sufficient) condition that the bands are classified as LCEBR.

The EBRs also provide a means of characterizing the topology of a set of bands obtained from a DFT or tight-binding calculation. Specifically, given an energetically isolated set of bands, the small coreps (symmetry eigenvalues) can imply one of two broad topological classes. First, there are stable topological bands, which characterize strong and weak topological (crystalline) insulators (TIs and TCIs) [5, 16, 17, 30, 33] that cannot be rendered topologically trivial through the addition of bands that are not themselves stable topological. A subset of topological bands, known as *symmetry-indicated* topological bands [5, 16, 17, 30, 33, 86], can be recognized as topologically stable because their symmetry data cannot be expressed as a linear combination of EBRs with integer coefficients. In this work, we follow the nomenclature established in Ref. [38] in which a symmetry-indicated topological band is classified as originating from a split EBR (SEBR) if its symmetry data can be expressed as a linear combination of connected pieces of EBRs that are themselves disconnected (while continuing to not match any linear combination of full EBRs). Continuing to employ the nomenclature of Ref. [38], we classify symmetry-indicated topological bands as NLC if their symmetry data cannot be expressed as an integer-valued linear combination of pieces of EBRs. Additionally, it was recently discovered that there also exist *fragile* topological bands [42–47, 95–100], which, unlike stable topological bands, can characterize a trivial insulator (or an “obstructed” atomic limit [34, 58, 101]) if they are combined with trivial or other fragile bands. TIs and TCIs characterized by stable topological bands can be classified using methods including K-theory [102], surface-state anomalies [14, 16, 17, 29, 103, 104], and layer constructions [16, 29, 105], whereas fragile topological bands can be characterized by corner filling anomalies [34, 45, 58, 95, 98, 101] and quantized twisted-boundary [46, 99] and defect [106] responses. For both stable and fragile TCIs, a complete diagnosis of nontrivial band topology can be obtained by performing (nested) Wilson loop calculations [13, 14, 34, 101, 107–111].

For each SG, symmetry-indicated topological bands labeled NLC or SEBR can be further characterized using symmetry-based indicators (SIs). Specifically, following a prescription detailed in Ref. 32, the authors of Refs. 16, 17, and 33 compared the EBRs, small coreps, and compatibility relations in each SG to determine the linearly independent sets of NLC and SEBR symmetry data [we provide specific details of this calculation in the text below]. In each SG, the calculation prescribed in Ref. 32 returned a set of positive-definite integers – known as the *SI group* (*e.g.* $\{4, 2, 2, 2\}$ in SG 2) – that aligned with the symmetry-indicated classification of strong and weak stable topological (crystalline) insulators in that SG (*e.g.* $\mathbb{Z}_4 \otimes \mathbb{Z}_2^3$). In Refs. 16 and 17, the authors then matched the SI groups (*e.g.* $\mathbb{Z}_4 \otimes \mathbb{Z}_2^3$) to anomalous boundary states and occupied bands with specific combinations of crystal symmetry eigenvalues – known as *SI formulas* (*i.e.* generalized Fu-Kane formulas [30]) – to construct a complete enumeration of all possible

symmetry-indicated stable TIs and TCIs in the nonmagnetic SGs. This method was then expanded in Ref. 36 to the nonmagnetic SGs without SOC to compute the stable SIs for special classes of topological semimetals, which in this work we designate as SEBR-SM and NLC-SM (see SM 6 for further details). Finally, building upon the first demonstration of symmetry-indicated fragile topology in TQC [42], the authors of Refs. 44 and 45 discovered the existence of fragile SIs, specifically showing that if a set of bands is classified as LCEBR, then it can be further classified as fragile if some of the integer coefficients in the linear combination of EBRs are negative.

In summary, TQC provides a unique, deterministic method for diagnosing the topology of any set of energetically isolated bands. Using TQC, we can analyze the full energy spectrum of any material up to any number of bands using the following procedure. First, using VASP2Trace [38, 83, 112] – a program that was implemented by Zhijun Wang to be used in conjunction with VASP [77, 78, 80] – we calculate the characters $\chi(g)$ of all of the unitary symmetries g of the occupied Bloch wavefunctions at all high-symmetry (maximal) \mathbf{k} points, where $\chi(g)$ is equal to the trace of the matrix representative of the symmetry element g in the reducible small corep corresponding to the set of all of the occupied Bloch states at \mathbf{k} . Next, using $\chi(g)$, we compute the multiplicity m_α of the α -th *irreducible* small corep of each little group $G_{\mathbf{k}}$ by systematically applying the so-called *magic formula*:

$$m_\alpha = \frac{1}{\|G_{\mathbf{k}}\|} \sum_{g \in G_{\mathbf{k}}} \chi_\alpha^*(g) \chi(g), \quad (\text{S1})$$

where $\chi_\alpha(g)$ is the character of g in the α -th irreducible small corep of $G_{\mathbf{k}}$, and where $\|G_{\mathbf{k}}\|$ is the order of the little group (*i.e.*, the number of symmetry operations in the little group not including operations related by integer lattice translations). The characters of the irreducible small coreps of the little groups of all \mathbf{k} points in all 230 nonmagnetic SGs can be accessed using the REPRESENTATIONS DSG tool on the BCS implemented for TQC [28, 42, 57, 91, 92, 96]. Next, using an upgraded implementation of the Check Topological Mat [112] tool on the BCS (see SM 3 for a detailed description of new features), we analyze each set of isolated bands. Specifically, we first obtain a symmetry data vector B , defined as:

$$B = (m(\rho_{G_{K_1}}^1), m(\rho_{G_{K_1}}^1), \dots, m(\rho_{G_{K_1}}^2), m(\rho_{G_{K_1}}^2) \dots)^T, \quad (\text{S2})$$

where $m(\rho_{G_{K_i}}^j)$ is the multiplicity of the j -th small corep of the little group G_{K_i} at the maximal momentum K_i . Next, we denote the symmetry data vector of the i -th EBR as EBR_i . Then, for any isolated subset of bands characterized by a symmetry vector that satisfies the compatibility relations, we solve a linear system of equations given by:

$$B = EBR \cdot X, \quad (\text{S3})$$

in which the solution $X = (X_1, X_2 \dots X_N)$ indicates the coefficients of the linear combination of EBRs corresponding to B . The presence of non-integer coefficients in $\{X_1, X_2, \dots, X_N\}$ in Eq. (S3) implies that some or all of the stable SIs are nontrivial for the bands characterized by B . For each SG, the possible existence of non-integer solutions to Eq. (S3), and hence the existence of nontrivial stable SIs, may be predicted through the Smith decomposition of the EBR matrix [32]. Specifically, because an EBR is a non-square matrix with integer coefficients, then its Smith decomposition can be expressed as a product of three matrices with integer coefficients:

$$EBR = L \cdot D \cdot R, \quad (\text{S4})$$

where L and R are unimodular matrices and D is a diagonal matrix. The number of nonzero diagonal elements in D is the rank of the stable SI group, and the matrices L and R can be chosen such that the (diagonal) entries in D are positive integers [29, 113]. If some of diagonal entries $\{n_1, n_2 \dots\}$ are greater than one, then the stable SI group is nontrivial, and is given by $\mathbb{Z}_{n_1} \otimes \mathbb{Z}_{n_2} \otimes \dots$ [*e.g.*, the nonzero elements in D in SG 2 ($P\bar{1}$) are $\{4, 2, 2, 2\}$, corresponding to a stable SI group $\mathbb{Z}_4 \otimes \mathbb{Z}_2^3$]. By then systematically applying VASP2Trace and Check Topological Mat to each isolated set of bands in the electronic structure of each material in the ICSD [41], we obtain the symmetry-indicated stable and fragile band topology of every known stoichiometric, nonmagnetic material.

B. The Compatibility Relations

To determine the connectivity of electronic bands characterized by a given symmetry data vector [Eq. (S3)], one must use the compatibility relations between \mathbf{k} points throughout the BZ. Specifically, in a given SG, the compatibility relations are defined as the dependencies between the multiplicity of the small coreps of the little groups of a \mathbf{k} point in the BZ and the multiplicities of the small coreps of the little groups along a line or plane in which the point sits [91].

The compatibility relations exist because the little group of a line (or a plane) is necessarily a subgroup of the little group of a high-symmetry point along the line (or plane) [55].

A set of bands can be *partially* identified by its decomposition into integer-valued linear combinations of the irreducible small coreps of the little group of each \mathbf{k} point in the BZ. However, in general, it is not necessary to consider the multiplicities of the coreps in the whole BZ to analyze the connectivity of a given symmetry data vector, due to the compatibility relations between the coreps of two connected subsets of \mathbf{k} -vectors. This renders the problem of decomposing bands into the coreps of the little group of the continuous variable \mathbf{k} feasible, because the corep decomposition in the whole BZ is fully fixed by the corep decomposition at only a finite (and in practice very small) number of \mathbf{k} points known as the *maximal* \mathbf{k} vectors [28, 57, 91, 92]. For example, consider a \mathbf{k} point that belongs to a line (l) \mathbf{k}_l for which the little group $\mathcal{G}^{\mathbf{k}}$ of \mathbf{k} is a supergroup of the little group of \mathbf{k}_l , $\mathcal{G}^{\mathbf{k}_l} \leq \mathcal{G}^{\mathbf{k}}$. The matrix representatives of a small corep $\rho_{\mathcal{G}^{\mathbf{k}}}^i$ of the little group $\mathcal{G}^{\mathbf{k}}$ associated with the symmetry operations that belong to $\mathcal{G}^{\mathbf{k}_l}$ transform in a small representation, not necessarily irreducible, of $\mathcal{G}^{\mathbf{k}_l}$. This representation, in general, is equivalent to a direct sum of the irreducible small coreps $\rho_{\mathcal{G}^{\mathbf{k}_l}}^j$ of $\mathcal{G}^{\mathbf{k}_l}$:

$$\rho_{\mathcal{G}^{\mathbf{k}}}^i \downarrow \mathcal{G}^{\mathbf{k}_l} = \bigoplus_{j=1}^s m_{ij}^{\mathbf{k}, \mathbf{k}_l} \rho_{\mathcal{G}^{\mathbf{k}_l}}^j \quad (\text{S5})$$

where s is the number of irreducible small coreps of $\mathcal{G}^{\mathbf{k}_l}$ and $m_{ij}^{\mathbf{k}, \mathbf{k}_l}$ is the (integer) multiplicity of $\rho_{\mathcal{G}^{\mathbf{k}_l}}^j$ in the decomposition of $\rho_{\mathcal{G}^{\mathbf{k}}}^i$. The same arguments can also be employed to calculate the compatibility relations between the multiplicities of the coreps in the symmetry data at a high-symmetry point and the corep multiplicities in a plane containing the high-symmetry point, or between the corep multiplicities along a line and the corep multiplicities in a plane containing the line. For TQC, we previously implemented the program DCOMPREL [28, 42, 57, 91, 92, 96] for obtaining the compatibility relations between each pair of connected \mathbf{k} -vectors in the BZ of each nonmagnetic double (spinful) SG.

The compatibility relations provide a means of analyzing a given symmetry data vector obtained from first-principles or tight-binding calculations. Specifically, as shown in Refs. 37 and 38, there are three cases for the connectivity of a set of Bloch eigenstates characterized by a symmetry data vector, given a specified number of filled Bloch eigenstates (electrons):

1. We observe that a set of small coreps at a maximal point \mathbf{k} corresponds to a set of Bloch states in which a band degeneracy is partially occupied. Numerically using [Check Topological Mat](#), this occurs when the number of bands (small coreps corresponding to the occupied Bloch states) is not the same at every maximal \mathbf{k} -vector (*i.e.*, the sum of the dimensions of the coreps is different from the number of occupied bands in at least at one maximal \mathbf{k} -vector, which can occur because [Check Topological Mat](#) does not output fractional numbers of coreps). In this case, the bands below the Fermi level characterized by the symmetry data vector are necessarily connected to states above the Fermi energy, and therefore fail to satisfy the compatibility relations at a maximal \mathbf{k} point. Following the nomenclature established in Ref. 38, we label a material with a partially filled multiplet of Bloch eigenstates at a maximal \mathbf{k} point as an “enforced semimetal with Fermi degeneracy” (ESFD). A well-known example of an ESFD-classified material is HgTe in SG 216 ($F\bar{4}3m$) [4] (ICSD 31845, see SM 11 C 1).
2. The symmetry data vector corresponds to fully occupied Bloch-state multiplets at all maximal \mathbf{k} points, but the small corep multiplicities in the symmetry data vector do not satisfy the compatibility relations along a line or a plane connecting at least one pair of maximal \mathbf{k} points. Specifically, using [Check Topological Mat](#), this numerically occurs when the number of bands (small coreps corresponding to the occupied Bloch states) at a maximal vector \mathbf{k} is *different than* the corep multiplicities at \mathbf{k} implied through the compatibility relations by the Bloch states that transform in the symmetry data at a different maximal vector \mathbf{k}' . This implies that the bands described by the symmetry data vector necessarily connect along a high-symmetry line or plane to bands above the Fermi energy not included in the symmetry data. In this case, because the symmetry data necessarily characterizes a topological semimetal, then we label the partially occupied connected set of electronic bands characterized by the symmetry data as an “enforced semimetal” (ES). A well-studied example of an ES material is the archetypal Dirac semimetal Cd₃As₂ in SG 137 ($P4_2/nmc$) [6, 19, 114, 115] (ICSD 107918, see SM 11 C 2), which was recently confirmed in theory [58] and experiment [59] to be a *higher-order* topological semimetal.
3. The symmetry data vector corresponds to fully occupied Bloch-state multiplets at all maximal \mathbf{k} points, and the small corep multiplicities in the symmetry data vector *satisfy* the compatibility relations along all lines and planes connecting the maximal \mathbf{k} points. Specifically, using [Check Topological Mat](#), this numerically occurs when the number of bands (small coreps corresponding to the occupied Bloch states) at all maximal \mathbf{k} vectors is *the same* as the corep multiplicities at \mathbf{k} implied through the compatibility relations by the Bloch states that transform in the symmetry data at all other maximal vectors \mathbf{k}' .

The bands described by the symmetry data are therefore compatible with an insulating gap along all high-symmetry lines and planes, and the symmetry data vector is labeled either LCEBR, NLC, or SEBR (see SM 2 A for further details). It is important to emphasize that LCEBR, NLC, and SEBR bands may still be connected to bands at other energies not described by the symmetry data by topological Weyl points or nodal lines in the BZ interior (*i.e.* away from all high-symmetry lines and planes) [29, 31, 36, 111]; NLC- and SEBR-classified topological semimetal phases are discussed in further detail in SM 6 for further details). In particular, as established in Refs. 31 and 36 and discussed in SM 6, *all* NLC and SEBR bands in nonmagnetic crystals w/o SOC characterize topological semimetal phases with nodal degeneracies in the BZ interior (respectively termed NLC-SM and SEBR-SM phases in this work).

Finally, we note that in Check Topological Mat, it is occasionally possible for a set of characters in the symmetry data to appear to violate time-reversal (\mathcal{T}) symmetry. We attribute this situation to numerical error, and in all cases, we have confirmed that the characters match the small irreps of the little groups of the Type-I magnetic (unitary) SG [29, 55] that is a subgroup of the nonmagnetic SG for the symmetry data. In the calculations performed for this work on nonmagnetic materials, we have merged all Bloch states that exhibit \mathcal{T} -breaking splitting on an energy scale of less than 1 meV to ensure that the symmetry data and band structures displayed on <https://www.topologicalquantumchemistry.com/> are \mathcal{T} -symmetric.

SM 3. OVERVIEW OF THE PREVIOUS FUNCTIONALITY OF THE VASP2TRACE PROGRAM AND NEW FEATURES OF THE CHECK TOPOLOGICAL MAT PROGRAM

In a recent previous work [38], the authors introduced the VASP2Trace [83] and Check Topological Mat programs on the BCS to diagnose the topology of materials whose electronic structure has been calculated using VASP [77, 78]. The input files for Check Topological Mat are the output files of VASP2Trace, which calculates the traces (eigenvalues) of the unitary symmetries of the electronic Bloch wavefunctions obtained from VASP [77, 78]. For this work, we have for the first time used VASP2Trace to compute band topology away from E_F , and have introduced new features for Check Topological Mat. In this section, we will first provide in SM 3 A an overview of the previous functionality of the VASP2Trace and Check Topological Mat programs implemented for Ref. 38. We will then in SM 3 B subsequently detail the new features in Check Topological Mat implemented for this work.

A. Overview of the Previous Functionality of the VASP2Trace and Check Topological Mat Programs

In this section, we will briefly summarize the algorithm and output of VASP2Trace and the previous functionality of Check Topological Mat. To begin, in the SG of a crystalline solid, each unitary symmetry operation is defined as $\mathcal{O} = \{R|\mathbf{t}\}$, where R is a point group symmetry operation (rotation or rotoinversion) and \mathbf{t} is a translation vector (which may have a fractional value in the units of the lattice constants) [55]. For each maximal \mathbf{k} point (defined in Refs. 28 and 57), we first obtain the single-particle Bloch wavefunctions $\psi_{n\mathbf{k}}(\vec{r}) \equiv \langle r|\psi_{n\mathbf{k}}\rangle$ using the DFT package VASP [77, 78] and identify a set of orthonormal wavefunctions $\{\psi_{n\mathbf{k}}^1(\vec{r}), \psi_{n\mathbf{k}}^2(\vec{r}), \dots, \psi_{n\mathbf{k}}^m(\vec{r})\}$ with a degeneracy m that each have the same energy eigenvalue $E_n(\mathbf{k})$. If the symmetry operation \mathcal{O} belongs to the little group $G_{\mathbf{k}}$ of \mathbf{k} , then acting on any of the wavefunctions $\psi_{n\mathbf{k}}^i(\vec{r})$ with \mathcal{O} results in a linear combination of all of the m degenerate Bloch states at E_n and \mathbf{k} :

$$\mathcal{O} |\psi_{n\mathbf{k}}^i\rangle = \sum_{j=1}^m O_{ij}^{\mathbf{k}} |\psi_{n\mathbf{k}}^j\rangle, \quad (\text{S6})$$

where $O^{\mathbf{k}}$ is the matrix representative of symmetry operation \mathcal{O} . The ij -th element of $O^{\mathbf{k}}$ is in turn given by:

$$O_{ij}^{\mathbf{k}} = \langle \psi_{n\mathbf{k}}^j | \mathcal{O} | \psi_{n\mathbf{k}}^i \rangle. \quad (\text{S7})$$

The matrix representatives $O^{\mathbf{k}}$ form a (generically reducible) small corep of $G_{\mathbf{k}}$.

It is important to emphasize that in the output of a DFT calculation, numerical precision and symmetry-breaking effects (*e.g.* weak magnetism) may lead to several nondegenerate states appearing as degenerate, or may lead to degenerate states appearing weakly split. Hence, it is necessary to implement a numerical tolerance factor for the energies of states at the same \mathbf{k} point, such that states within the energy range of the tolerance factor are taken to be degenerate. To avoid accidental degeneracies, it is desirable to have as small a tolerance factor as possible up to the

energy scale at which numerical precision issues lead to symmetry-breaking splitting. For this work, we have chosen a tolerance factor of 0.002 eV.

As discussed in [SM 2](#), the multiplicities of the irreducible small coreps in the (generically reducible) representation corresponding to the degenerate states $\{\psi_{n\mathbf{k}}^1(\vec{r}), \psi_{n\mathbf{k}}^2(\vec{r}), \dots, \psi_{n\mathbf{k}}^m(\vec{r})\}$ can be obtained by computing the symmetry characters (traces) of the matrix representatives $O^{\mathbf{k}}$ in Eq. (S7). Hence, it is sufficient to calculate:

$$\chi_{n\mathbf{k}}^O = \sum_{i=1}^m \langle \psi_{n\mathbf{k}}^i | \mathcal{O} | \psi_{n\mathbf{k}}^i \rangle, \quad (\text{S8})$$

for the matrix representative \mathcal{O} of each unitary symmetry operation $g \in G_{\mathbf{k}}$. The traces (characters) $\chi_{n\mathbf{k}}^O$ in Eq. (S8) may straightforwardly be obtained from the WAVECAR output file of VASP, in which the Bloch wavefunctions at each \mathbf{k} point are each expressed as a linear combination of plane waves:

$$\psi_{n\mathbf{k}}^i(\mathbf{r}) = \sum_j C_{j,n\mathbf{k}}^i e^{i(\mathbf{k} + \mathbf{G}_j) \cdot \mathbf{r}}. \quad (\text{S9})$$

In Eq. (S9), each \mathbf{G}_j is a reciprocal lattice vector, and states in different BZs related by reciprocal lattice vectors are orthonormal such that $\langle \mathbf{k} + \mathbf{G}_i | \mathbf{k} + \mathbf{G}_j \rangle = \delta_{ij}$. Although the reciprocal lattice contains an infinite number of BZs related by the vectors \mathbf{G}_j , in practice, VASP only considers the truncated finite set of \mathbf{k} points for which $\frac{\hbar^2}{2m_e}(\mathbf{k} + \mathbf{G}_j)^2 < E_{\text{cutoff}}$, where the energy cutoff E_{cutoff} is an input parameter.

Given $\psi_{n\mathbf{k}}^i(\mathbf{r})$ in the plane-wave basis in Eq. (S9), the action of the symmetry operation O is given by:

$$\begin{aligned} \mathcal{O}\psi_{n\mathbf{k}}^i(\mathbf{r}) &= \{R|\mathbf{t}\}\psi_{n\mathbf{k}}^i(\mathbf{r}) = \psi_{n\mathbf{k}}^i(\{R|\mathbf{t}\}^{-1}\mathbf{r}) = \sum_j C_{j,n\mathbf{k}}^i e^{i(\mathbf{k} + \mathbf{G}_j) \cdot R^{-1}(\mathbf{r} - \mathbf{t})} = \\ &= \sum_j C_{j,n\mathbf{k}}^i e^{iR(\mathbf{k} + \mathbf{G}_j) \cdot (\mathbf{r} - \mathbf{t})} = e^{-i\mathbf{k} \cdot \mathbf{t}} \sum_j C_{j,n\mathbf{k}}^i e^{i(\mathbf{k} + \mathbf{G}_{j'}) \cdot \mathbf{r}} e^{-i\mathbf{G}_{j'} \cdot \mathbf{t}}, \end{aligned} \quad (\text{S10})$$

where $\mathbf{G}_{j'}$ is the reciprocal lattice vector for which:

$$\mathbf{k} + \mathbf{G}_{j'} = R\mathbf{k} + \mathbf{G}_j. \quad (\text{S11})$$

Hence, the i -th element of the diagonal of the matrix representative $O^{\mathbf{k}}$ is given by:

$$\langle \psi_{n\mathbf{k}}^i | \mathcal{O} | \psi_{n\mathbf{k}}^i \rangle = e^{-i\mathbf{k} \cdot \mathbf{t}} \sum_j (C_{j',n\mathbf{k}}^i)^* C_{j,n\mathbf{k}}^i e^{-i\mathbf{G}_{j'} \cdot \mathbf{t}}, \quad (\text{S12})$$

where in each term in the sum over j , the index j' is individually determined through Eq. (S11). The trace of the matrix representative $O^{\mathbf{k}}$ defined in Eq. (S8) is thus given by:

$$\chi_{n,\mathbf{k}}^O = e^{-i\mathbf{k} \cdot \mathbf{t}} \sum_{i=1}^m \sum_j (C_{j',n\mathbf{k}}^i)^* C_{j,n\mathbf{k}}^i e^{-i\mathbf{G}_{j'} \cdot \mathbf{t}}, \quad (\text{S13})$$

such that the trace of the identity operation $\mathcal{O} = \{E|0\}$ is equal to the band degeneracy m at $E_n(\mathbf{k})$.

In summary, [VASP2Trace](#) obtains the plane-wave coefficients $C_{j,n\mathbf{k}}^i$ from the WAVECAR output file generated by VASP for the m degenerate states at an energy E_n and a point \mathbf{k} . [VASP2Trace](#) then produces the following output data:

1. The symmetry operations of the SG (one symmetry operation for each element of the point group of the SG), given in a primitive basis that in general does not correspond to the standard setting of the SG listed in the International Tables for Crystallography [116] or the BCS.
2. The coordinates of the maximal \mathbf{k} vectors of the SG expressed in a reciprocal basis consistent with the (generically non-standard) setting of the outputted symmetry operations.
3. For each maximal \mathbf{k} vector and band n , [VASP2Trace](#) outputs the traces of the symmetry operations of the little group $G_{\mathbf{k}}$ (one trace for each element of the point group of $G_{\mathbf{k}}$).

In Ref. 38, together with the [VASP2Trace](#) program written by Zhijun Wang [83], the authors also introduced the [Check Topological Mat](#) program to diagnose the topology of a material using the output of [VASP2Trace](#). To diagnose

the bulk topology, [Check Topological Mat](#) first compares the symmetry operation traces computed *ab-initio* to the little group character tables on the [BCS](#), allowing the determination of the little group small coreps in the symmetry data at a set of (typically, but not necessarily) maximal \mathbf{k} points.

To identify the multiplicities of the irreducible small coreps in the symmetry data at each maximal \mathbf{k} point, the previous implementation of [Check Topological Mat](#) first converts the data given by [VASP2Trace](#) into the standard setting of the SG used by the programs on the [BCS](#). The conversion between the SG setting in the output of [VASP2Trace](#) and the standard setting of the [BCS](#) is performed using the [IDENTIFY GROUP](#) program on the [BCS](#) [117] to calculate a transformation matrix between the output of [VASP2Trace](#) and the standard setting. The transformation matrix additionally allows the identification of the maximal \mathbf{k} vector labels used by VASP given the output of [VASP2Trace](#). Next, given the characters of the SG symmetry elements in the standard setting [Eq. (S13) after using the [IDENTIFY GROUP](#) program] and the \mathbf{k} vector labels, the small corep multiplicities are obtained through the Schur orthogonality relation (magic formula), as detailed in the text surrounding Eq. (S1) in [SM 2](#). Lastly, the irreducible small corep multiplicities corresponding to the symmetry data are then analyzed using the machinery of TQC to obtain the topological classification of the occupied bands, as detailed in Ref. 38 and [SM 2](#).

However, it is important to emphasize that due to numerical precision issues with bands far above E_F , or symmetry-breaking effects such as magnetism, the Bloch wavefunctions at \mathbf{k} in Eq. (S9) may exhibit unitary symmetry eigenvalues (characters) that are not possible given the symmetry elements in the little group $G_{\mathbf{k}}$. Specifically, for m degenerate Bloch states at a point \mathbf{k} and an energy E_n in the output of a VASP calculation, Eq. (S13) may return impossible combinations of characters for the set of symmetry-operation matrix representatives $\{O^{\mathbf{k}}\}$ if symmetries have become broken, or if the DFT calculations did not converge at E_n and \mathbf{k} . We refer to this situation, in which a group of degenerate states exhibits a set of characters that are together incompatible with the little group $G_{\mathbf{k}}$, as a *bad trace*. At each of the maximal \mathbf{k} vectors, [Check Topological Mat](#) searches in increasing integer electronic fillings for a filling ν at which there is a bad trace at \mathbf{k} . If [Check Topological Mat](#) at any \mathbf{k} vector encounters a bad trace with $\nu \leq N_e$, where N_e is the number of valence electrons, then the topological classification at E_F cannot be determined. In this work, we have discarded the 655 ICSD entries for which VASP calculations converged to a (meta)stable state with bad traces at or below E_F .

B. New Features of the [Check Topological Mat](#) Program Introduced in this Work

In addition to the previous functionality of the [VASP2Trace](#) and [Check Topological Mat](#) programs, we have introduced several new features in this work:

1. The most recent version of [VASP2Trace](#) [83] now allows users to input a number of bands that differs from the number of electrons (*i.e.* a number of bands that differs from the intrinsic electronic filling). In this work, we have used this new feature to perform the first high-throughput analysis of band topology *away from* E_F in nonmagnetic materials, specifically varying the number of electrons used in the input for [VASP2Trace](#) to analyze the topology all of the energetically isolated bands in the electronic structure of each ICSD entry.
2. [Check Topological Mat](#) can now identify small corep multiplicities both with and w/o SOC – the previous iteration of [Check Topological Mat](#) implemented for Ref. 38 could only identify small corep multiplicities in the presence of SOC.
3. [Check Topological Mat](#) now generates a file containing topological data for all energetically isolated sets of bands. For each set of energetically isolated bands (*i.e.* bands that are separated from all other bands at all high-symmetry \mathbf{k} points and along all high-symmetry BZ lines and planes), [Check Topological Mat](#) now indicates if the set of bands is trivial, fragile topological, or stable topological (further differentiating between SEBR or NLC). In the case in which the bands are stable topological, [Check Topological Mat](#) additionally provides the values of the stable SIs using the convention established in Refs. 16 and 36. As an example, we have reproduced in Table S1 the output of [Check Topological Mat](#) for the repeat-topological (RTopo) and supertopological (STopo) compound Bi_2Mg_3 [ICSD 659569, SG 164 ($P\bar{3}m1$)] discussed in the main text (see [SM 9](#) for precise definitions of RTopo and STopo compounds).
4. When [Check Topological Mat](#) diagnoses a partially filled set of bands in a material to be an ES or ESFD semimetal, [Check Topological Mat](#) now provides the compatibility relations along the high-symmetry BZ lines and planes, thus identifying the location(s) of the protected crossing point(s).

For the present work, we have also made the updated version of [Check Topological Mat](#) detailed in this section publicly available on the [BCS](#) at www.cryst.ehu.es/cryst/checktopologicalmat.

A	Γ	H	K	L	M	dim	top. type	ind/band	filling ν	top. type/all	ind/all
-A8(2)	-GM8(2)	-H4-H5(2)	-K4-K5(2)	-L3-L4(2)	-M5-M6(2)	2	SEBR	0 0 0 3	2	SEBR	0 0 0 3
-A9(2)	-GM9(2)	-H6(2)	-K6(2)	-L5-L6(2)	-M3-M4(2)	2	SEBR	0 0 0 1	4	LCEBR	0 0 0 0
-A9(2)	-GM8(2)	-H4-H5(2)	-K6(2)	-L3-L4(2)	-M3-M4(2)	4	SEBR	0 0 0 3	8	SEBR	0 0 0 3
-A8(2)	-GM8(2)	-H6(2)	-K4-K5(2)	-L5-L6(2)	-M5-M6(2)						
-A9(2)	-GM9(2)	-H6(2)	-K6(2)	-L3-L4(2)	-M5-M6(2)	2	SEBR	0 0 1 1	10	SEBR	0 0 1 0
-A8(2)	-GM4-GM5(2)	-H6(2)	-K6(2)	-L5-L6(2)	-M3-M4(2)	4	SEBR	0 0 0 3	14	SEBR	0 0 1 3
-A6-A7(2)	-GM8(2)	-H4-H5(2)	-K4-K5(2)	-L3-L4(2)	-M5-M6(2)						
-A4-A5(2)	-GM6-GM7(2)	-H6(2)	-K6(2)	-L5-L6(2)	-M3-M4(2)	2	SEBR	0 0 1 0	16	SEBR	0 0 0 3
-A8(2)	-GM9(2)	-H4-H5(2)	-K6(2)	-L3-L4(2)	-M3-M4(2)	6	SEBR	0 0 0 2	22	SEBR	0 0 0 1
-A9(2)	-GM9(2)	-H6(2)	-K6(2)	-L5-L6(2)	-M5-M6(2)						
-A6-A7(2)	-GM6-GM7(2)	-H6(2)	-K4-K5(2)	-L5-L6(2)	-M3-M4(2)						
-A9(2)	-GM9(2)	-H6(2)	-K6(2)	-L3-L4(2)	-M5-M6(2)	2	SEBR	0 0 1 1	24	SEBR	0 0 1 2
-A8(2)	-GM8(2)	-H6(2)	-K4-K5(2)	-L3-L4(2)	-M3-M4(2)	8	SEBR	0 0 1 1	32	SEBR	0 0 0 3
-A4-A5(2)	-GM8(2)	-H4-H5(2)	-K6(2)	-L5-L6(2)	-M5-M6(2)						
-A8(2)	-GM4-GM5(2)	-H6(2)	-K4-K5(2)	-L5-L6(2)	-M5-M6(2)						
-A9(2)	-GM8(2)	-H4-H5(2)	-K6(2)	-L3-L4(2)	-M3-M4(2)						

Table S1. A typical table generated by [Check Topological Mat](#). Here, we have used as an example the repeat-topological (RTopo) and supertopological (STopo) compound Bi_2Mg_3 [ICSD 659569, SG 164 ($P\bar{3}m1$)] discussed in the main text (see [SM 9](#) for precise definitions of RTopo and STopo compounds). In this table, the horizontal lines indicate the electronic fillings ν at which the occupied bands satisfy the compatibility relations. Columns A , Γ , H , K , L , and M contain the coreps at each maximal \mathbf{k} point for each energetically isolated set of bands that satisfy the compatibility relations. Column “dim” shows the dimension of each set of bands, Column “top. type” indicates the topology of the isolated bands [which can either be LCEBR, FRAGILE, NLC, or SEBR], and Column “ind/band” contains the stable symmetry-based indicators (SIs) ($Z_{2,1}$ $Z_{2,2}$ $Z_{2,3}$ Z_4) that result from subducing onto SG 2 ($P\bar{1}$). The remaining three columns contain the cumulative information of several combined sets of energetically isolated bands that are filled up to a total number of valence electrons specified by the column “filling ν .” Column “top. type/all” provides the cumulative topology (LCEBR, FRAGILE, NLC, or SEBR) at the gap specified by the electronic filling in the “filling ν ” column, and Column “ind/all” provides the cumulative stable SIs of all of the filled bands up to the same gap. Hence, the values of “ind/all” at each filling ν listed in this table can be obtained by summing the values in the “ind/band” column up to the same filling ν . In Bi_2Mg_3 , the Fermi level lies at a valence filling $\nu = 16$, indicating that the gap at E_F exhibits symmetry-indicated stable (SEBR) topology characterized by the subduced stable SIs (0003).

SM 4. VASP CALCULATION DETAILS AND DATA SET PREPARATION

In this work, we performed ab-initio calculations using Density Functional Theory (DFT) [118, 119] as implemented in the Vienna Ab-initio Simulation Package (VASP) [77, 79]. For each material calculation, we used as input the structural parameters reported on the ICSD [41]. We treated the interaction between the ion cores and the valence electrons using the projector augmented-wave method [80]. For the exchange-correlation potential, we used the generalized gradient approximation (GGA) with the Perdew-Burke-Ernzerhof parameterization for solids [81]. For calculations incorporating the effects of spin-orbit coupling (SOC), we accounted for the effects of SOC using the second variation method [82]. For the plane-wave expansion, we employed a Γ -centered \mathbf{k} -point grid of size $(11 \times 11 \times 11)$ for reciprocal space integration and a 550 eV energy cutoff. Because small changes in the structural parameters of a material with a similarly small gap size can drive a topological phase transition, then for this work, we have analyzed *all* of the entries in the ICSD, including duplicate entries for the same compound that feature only minor variation in the reported parameters. For example in PbTe, there are 42 total entries in the ICSD, of which only 5 have a negative (inverted) gap corresponding to a higher-order topological crystalline insulating (TCI) phase (see Ref. 120 and SM 11 A 5). Therefore, rather than simply report PbTe as a TCI, we provide on <https://www.topologicalquantumchemistry.com/> a complete analysis of all 42 ICSD entries for PbTe, allowing users to choose between entries with and without nontrivial symmetry-indicated topology.

For each material, we prepared input files for VASP using the CIF structure files provided on the ICSD. Specifically, we first used the Atomic Simulation Environment (ASE) [121] to transform the CIF file from the ICSD into a VASP POSCAR structure input file. This step must be performed with caution, because some CIF files on the ICSD are missing atoms that are listed in the chemical formula (typically, but not always, hydrogen atoms), and some unit-cell coordinates are reported in a non-standard basis. To account for the latter issue of differing unit-cell bases, we have employed the PHONOPY [122] package to convert the coordinates of the atoms in the CIF files into positions in a primitive cell chosen in a consistent (standard) basis for each SG. In Table S2, we provide statistics regarding the number of ICSD entries considered in our analysis. In this work, we began by considering the complete list of 193,426 entries in the ICSD. Of the 193,426 ICSD entries, 181,218 contain experimentally-obtained atomic positions, and the remaining 12,208 entries contain theoretically-obtained atomic positions. Separately, of the 193,426 ICSD entries, 96,196 (49.73%) have stoichiometric chemical formulas and processable (non-corrupt) CIF structure files, whereas the remaining 97,230 (50.27%) entries are either not stoichiometric or exhibit corrupted CIF structure files. In general, non-stoichiometric materials cannot be analyzed using TQC without constructing exceedingly large unit cells representing the average structure, and corrupted CIF files can only be processed if repaired using a case-by-case methodology.

Next, having established the primitive cell, we construct the pseudopotential file for each compound and execute VASP. This process is performed in an automated, high-throughput fashion through a script that uses each ICSD CIF file as an input, and then outputs the topological analysis, electronic band structure, and density of states. As shown in Fig. 1 of the main text, our topological analysis is performed by computing the characters of the unitary symmetry operations of the little groups at the maximal \mathbf{k} vectors (see SM 3). For each SG, the list of maximal \mathbf{k} vectors may be obtained by choosing an EBR of the SG using the BANDREP tool on the BCS (www.cryst.ehu.es/cryst/bandrep). The first column in the output of BANDREP contains the maximal \mathbf{k} vectors of the SG.

Beyond the Bloch states at the maximal \mathbf{k} vectors, we also compute for each material the electronic structure (bands) along an SG-dependent \mathbf{k} path to generate band structure plots, and the density of states. For each band structure calculation, we specifically calculate the energies of the Bloch eigenstates at 20 \mathbf{k} points along each \mathbf{k} path segment. At each \mathbf{k} point along each path segment, we calculate the energies of at least $2N_e$ Bloch states, where N_e is the number of valence electrons in the primitive cell; we do not include bands originating from core-shell atomic orbitals. We note that because VASP can be parallelized over bands, the number of bands included in some material calculations is larger than $2N_e$. For completeness and consistency with other previous works [39, 123], we have included in our electronic structure calculations both the minimal paths connecting all \mathbf{k} vectors, as well as additional paths that are not required by band connectivity [28, 91], but are nevertheless commonly employed in earlier works. For each of the 14 Bravais classes and crystallographic point groups, we have constructed \mathbf{k} paths in reduced coordinates (independent of the lattice parameters) using a combination of symmetry considerations and band-structure compatibility relations [113]. We emphasize that this approach differs from other programs, such as the *Seek-path* package [124], which use different criteria to generate \mathbf{k} paths in non-reduced units of the lattice vectors, causing the \mathbf{k} paths to become structure-dependent and vary for materials within the same SG. For example, the high-throughput first-principles calculations performed in Ref. 39 were performed without rescaled \mathbf{k} vectors. Hence, in the *Catalogue of Topological Materials* introduced in Ref. 39, there exist materials with the same SG and different displayed \mathbf{k} paths, whereas the electronic structures of all of the ICSD entries on <https://www.topologicalquantumchemistry.com/> with the same SG are plotted along the same (reduced-coordinate) \mathbf{k} paths. We additionally emphasize that in order to locate all of the band crossings in topological semimetal phases, we found that it was necessary to search for crossing points not just

along the minimal set of high-symmetry lines between pairs of maximal \mathbf{k} vectors, but also along lines connecting the first and second BZs. In some SGs, we also include additional \mathbf{k} paths beyond the first BZ in order to avoid plotting discontinuous band structures. For each ICSD entry on <https://www.topologicalquantumchemistry.com/>, we have made the \mathbf{k} paths and POSCAR files available for users to download directly from the page for each ICSD entry on <https://www.topologicalquantumchemistry.com/>.

As stated in the main text, we define a unique material as the set of ICSD entries that share the same stoichiometric formula, topological subclassification with SOC, SG, and, in the case of a topological semimetal, type of crossing at the Fermi level in the presence of SOC. We emphasize that our definition of a unique material does not account for the topological subclassification of a material w/o SOC, or account for variation in the topology of energetically isolated bands away from E_F . Specifically, for simplicity, two ICSD entries with the same stoichiometric formula, SG, and topological classification (and crossing points if semimetallic) at E_F in the presence of SOC are grouped together as a single unique material, whether or not the topology of the two ICSD entries is different at E_F w/o SOC, or away from E_F with or w/o SOC. Hence as discussed in SM 9, there may exist variation in the topology away from E_F across ICSD entries associated to the same unique material. Additionally, we note that for a fraction of the analyzed ICSD entries, calculations only converged with SOC, and for the same material did not converge w/o SOC. Specifically, calculations performed w/o SOC failed to converge for 3,504 ICSD entries, representing 4.78% of the 73,234 total materials for which calculations converged with SOC. We have further classified our data by tagging materials that are either listed as magnetic on the Materials Project (<https://materialsproject.org/>) [125], or display nonzero magnetic moments in the output of our VASP calculations. Finally, we have also identified the compounds that contain valence f electrons as determined by VASP (*i.e.* the compounds containing atoms with partially filled f orbitals, see <https://www.smcm.iqfr.csic.es/docs/vasp/node248.html> for further details); these materials may exhibit non-negligible electron-electron correlation effects. Throughout this work, we follow the VASP pseudopotential documentation on <https://www.smcm.iqfr.csic.es/docs/vasp/node248.html> in determining whether a material does not carry valence f electrons, which we denote in this work using the shorthand expression “without f electrons.” In Table S3, we list the percentage of unique materials in which any of the associated ICSD entries are magnetic (either as listed on the Materials Project or in our first-principles calculations), and the percentage of unique materials with f electrons at E_F as determined by VASP.

Table S2. Number of analyzed compounds.

	Total	Experimentally-Obtained Atomic Positions	Theoretically-Obtained Atomic Positions
Entries	193,426	181,218	12,208
Stoichiometric and Valid CIF File	96,196	85,701	10,495
Non-Stoichiometric or Corrupted CIF File	97,230	95,517	1,713

Table S3. Percentage of unique materials with at least one magnetic ICSD entry and with valence f electrons as determined by VASP (see <https://www.smcm.iqfr.csic.es/docs/vasp/node248.html> for further details).

Unique Materials with Magnetism	35.82%
Unique Materials with Valence f Electrons	28.69%

Lastly, it is important to emphasize additional issues that arise regarding magnetic ground states in VASP. In this work, all of the calculations were performed with a zero initial magnetic moment on each atom. However for a given compound, there may exist a magnetic ground state that is lower in energy than a metastable non- (para-) magnetic state. Hence in this case, the nonmagnetic solution is a local minimum in the total energy landscape of the system, but may still correspond to the final state in the VASP calculation. Depending on the details of the calculation, then VASP will either remain close to the initialized paramagnetic state, or may find a magnetic state that is lower in energy, but not necessarily the correct magnetic ground state (*i.e.*, there may exist a different magnetic state, or a structurally distorted nonmagnetic state, that is lower in energy). In VASP, the magnetism of a (meta)stable final state is most dependent on the following parameters:

- The total number of bands (NBANDS) in the calculation. Because VASP is parallelized, then the number of bands must be divisible by the number of cores (NPAR) for an accurate and convergent calculation. Hence, VASP adjusts NBANDS to be a multiple of the number of cores. Because NPAR depends on the details of the

VASP configuration and hardware used to perform the calculation, then NPAR may vary for the same VASP calculation performed across two different (super)computers.

- The block size in the blocked Davidson algorithm (NSIM).

In most VASP calculations, NBANDS only affects the rate of convergence, and not the quantitative features (*e.g.* magnetic configuration) of the final state. However, in the presence of multiple nearby local minima in the total energy landscape, NBANDS, NPAR, and NSIM may (uncontrollably) bias the final local minimum of the VASP calculation. In general, when using VASP to perform topological material calculations and to reproduce the calculations performed for this work, we recommend performing several tests with varying NBANDS, NPAR, NSIM, and other parameters, in particular confirming that all calculations converge to the same (ideally global) minimum.

In the high-throughput calculations performed for this work, we found it to be prohibitively difficult to systematically evaluate each ICSD entry for the appearance of metastable (potentially magnetic) final states. However, by manually comparing intermediate self-consistent and band-structure output files in our VASP calculations, we were able to detect only ~ 100 compounds with magnetic and nonmagnetic local minima that were close in energy. Specifically, we compared the magnetization in the self-consistent and band structure output files of each VASP calculation, finding only ~ 100 ICSD entries with large magnetization discrepancies (though we detected slight variations when our tests were performed on different supercomputers, due to varying NPAR, as discussed earlier in this section). This makes us confident that the large majority of our material calculations exhibit reliable (*i.e.* physically realistic) nonmagnetic final states.

SM 5. COMPUTATION TIME AND RESOURCES

In this section, we detail the computational resources used in this work. First, in [SM 5 A](#), we list the supercomputers used to perform the ab-initio calculations in this work, and the number CPU hours expended. Then, in [SM 5 B](#), we provide a more detailed breakdown of our computational resource usage, focusing specifically on the number of CPU hours expended per SG and per number of atoms in the primitive cell. Lastly, in [SM 5 C](#), we detail the disk storage usage requested for the calculations performed in this work, focusing specifically on the disk storage requested per SG and per number of atoms in the primitive cell.

A. Supercomputers and General Computational Resource Usage Statistics

Our calculations were primarily executed on the Draco and Cobra supercomputers of the Max Planck Society (MPG) and on the Cori and Edison supercomputers of the United States Department of Energy (DOE). Below, we provide information about the node architecture, communication network, and peak performance of each supercomputer:

- Draco: HPC system with Intel 'Haswell' Xeon E5-2698 processors (880 nodes with 32 cores @ 2.3 GHz each). 106 of the nodes are equipped with accelerator cards (each with two PNY GTX980 GPUs). Draco also contains 64 Intel 'Broadwell' processors that each have 40 cores and a main memory of 256 GB. In total Draco has 30,688 cores and a total main memory of 128 TB, and provides a peak performance of 1.12 petaflop/s. Beyond the compute nodes used for calculations, Draco has 4 login nodes and 8 I/O nodes, each with 1.5 petabytes of disk storage.
- Cobra: HPC system with 3424 compute nodes, 136,960 CPU cores, 128 Tesla V100-32 GPUs, 240 Quadro RTX 5000 GPUs, 529 TB RAM DDR4, 7.9 TB HBM2, 11.4 petaflop/s peak DP, and 2.64 petaflop/s peak SP.
- Cori: Cray XC40 system with 622,336 Intel processor cores and a theoretical peak performance of 30 petaflop/s (30 quadrillion operations per second).
- Edison: Cray XC30 with 133,824 compute cores for running scientific applications, 357 TB of memory, and 7.56 petabytes of online disk storage with a peak I/O bandwidth of 168 GB/s.

We performed first-principles calculations on a total of 73,234 ICSD entries. As shown in [Fig. 1](#) of the main text and discussed in [SM 4](#), the calculations that we performed can be divided into four steps, which we respectively label as VASP1, VASP2, VASP3, and VASP4:

- VASP1: Self-consistent DFT calculations. The calculations performed in VASP1 generate charge density (CHG-CAR) files, which served as input for the remaining three calculation steps.

- VASP2: Generating the Bloch wavefunctions at the maximal \mathbf{k} vectors, using the input from VASP1. VASP2 generates the output files used to calculate the characters of the unitary symmetry operations of the little groups at the maximal \mathbf{k} points, which we then used to diagnose the material topology, as detailed in SM 3.
- VASP3: Calculating the band structure along high-symmetry lines and planes, using the input from VASP1. Each segment of the \mathbf{k} path contains 20 \mathbf{k} points. At each \mathbf{k} point along each path segment, we calculated the energies of at least $2N_e$ Bloch states, where N_e is the number of valence electrons in the primitive cell; we did not include bands originating from core-shell atomic orbitals. As discussed in SM 4, because VASP is parallelized, then the number of bands must be divisible by the number of cores (NPAR) for an accurate and convergent calculation. Hence, VASP adjusts the number of bands to be a multiple of the number of cores. Because NPAR depends on the details of the VASP configuration and hardware used to perform the calculation, then NPAR may vary for the same VASP calculation performed across two different (super)computers.
- VASP4: Self-consistent calculations of the density of states, using the input from VASP1. To calculate the density of states in VASP4, we employed an $(11 \times 11 \times 11)$ \mathbf{k} -point grid.

In Table S4, we show the number of CPU hours expended in the calculations performed in this work divided into each of the four calculation steps.

Job	CPU h. with SOC	CPU h. w/o SOC
VASP1	9,500,801.70	2,298,583.30
VASP2	170,633.80	56,520.70
VASP3	2,560,882.60	56,520.70
VASP4	5,804,948.80	1,397,550.30
Total Time	18,037,266.90	4,525,673.80

Table S4. Total CPU hours expended in each of the four VASP calculation steps, subdivided by calculations performed with and without incorporating the effects of SOC (with SOC and w/o SOC, respectively).

B. Computational Resources Expended per SG and per Number of Atoms in the Primitive Cell

In this section, we provide tables containing a detailed statistical breakdown of the computational resources expended for this work. First, in Table S5 (Table S6), we list the CPU hours expended to perform ab-initio calculations with SOC (w/o SOC), subdivided by SG. Next, in Table S7 (Table S8), we list the CPU hours expended to perform ab-initio calculations with SOC (w/o SOC), subdivided by the number of atoms in the primitive cell of each material. Most interestingly, we observe that there are vanishingly few stoichiometric materials in the ICSD with greater than 60 atoms in the primitive cell. Specifically, we find that there are 10,835 ICSD entries with greater than 60 in the primitive cell, representing 11.26% of the 96,196 total stoichiometric entries in the ICSD.

Table S5: Total CPU time expended for all of the ab-initio calculations performed in this work incorporating the effects of SOC (with SOC), subdivided by space group (SG). In order, the columns in this table list the SG, the number of ICSDs successfully analyzed in the SG, the CPU hours expended per each of the four calculation steps (VASP1 through VASP4) detailed in SM 5 A, and the total CPU hours expended for materials in the SG.

SG	# ICSDs	VASP1 (CPU hours)	VASP2 (CPU hours)	VASP3 (CPU hours)	VASP4 (CPU hours)	Total (CPU hours)
1	225	67534.5	718.9	4560.6	38488.5	111302.5
2	1885	572989.9	7439.1	81830.9	322951.5	985211.3
3	19	6489.8	26.9	400.9	2675.3	9592.9
4	305	97974.7	576	9153.7	61414.5	169118.9
5	195	73484.8	305.5	4328.2	56460.5	134579
6	39	7746	32.5	429.6	3391.4	11599.5
7	143	52621.6	267.8	4131.8	29000.3	86021.5
8	173	58561.7	188.4	2737.3	36156.2	97643.7
9	278	194291.8	662.5	9442.9	123863.5	328260.7
10	44	7407.7	59.6	938.5	3597	12002.9
11	790	172295.1	1916.7	30243.2	126423.2	330878.2

12	1844	473531.1	3539	46170.5	360788.5	884029.2
13	314	76186.3	801.5	12216.9	39632.1	128836.8
14	3787	1799616	16665.5	259458.6	1067200.4	3142940.5
15	2526	1372458.9	8181.1	124624.6	830990.6	2336255.2
16	2	73	24.3	49.2	70.7	217.1
17	8	909.6	27.1	510.5	618.8	2066
18	42	10938.8	300.9	5175.5	7024	23439.2
19	364	84374.7	2351.3	41287.4	55194.6	183208
20	85	15247.2	134.8	2707	8951.7	27040.7
21	21	1548.9	13.9	244.3	863.6	2670.6
22	17	1404.3	9.9	181.6	775.1	2370.9
23	16	2789.7	17.4	259.2	1087.5	4153.9
24	3	168.2	2.4	28.7	101.3	300.6
25	59	2666.1	58	957.1	1603.2	5284.4
26	85	21846.5	391.8	6848.2	11396.8	40483.4
27	1	89.2	2.2	40.4	67.5	199.3
28	18	1498.6	37.6	635.1	1114.7	3286
29	89	19338.2	522.8	9292.9	14563.9	43717.7
30	6	2866.8	58.1	925.4	1629.4	5479.7
31	247	37185.5	889.3	15277.5	23724.4	77076.7
32	12	3779.4	108.2	1962.8	2783.8	8634.2
33	406	102540.7	2171.8	38634.4	60282.2	203629.2
34	30	8458.9	208.5	3488.3	5763.3	17919.1
35	8	1291	11	213.4	824.7	2340.2
36	412	101801.2	649.6	12947.5	58890.4	174288.7
37	7	1654.4	15.9	338	1094.4	3102.7
38	173	15730.8	118	2542.3	11316.3	29707.4
39	15	3302.6	68.5	887.3	2430	6688.3
40	67	11630.1	122.5	3051.6	10744.8	25549
41	44	14186.7	102	2590	7891	24769.7
42	4	500.1	7.2	96.2	374.8	978.3
43	126	27111.4	224.5	4999.9	21284	53619.8
44	100	10278.7	85.1	1294.8	7763.2	19421.7
45	11	7084.3	52.7	1032.5	3797.5	11967
46	91	23841.1	177.4	3333.6	14095.6	41447.6
47	95	4588.5	161	3059.2	2737.8	10546.5
48	3	153.7	7.4	121.3	110.8	393.2
49	1	98.5	4	65.5	59.1	227.2
50	11	2279.1	79.4	1386.9	1409.5	5154.9
51	147	10885.8	449.7	8318.7	7566.8	27220.9
52	51	9752	378.4	6759.2	6091.3	22981
53	27	1699.2	77.7	1410.5	1275.7	4463.1
54	25	5666.9	261.5	4925.9	4427.9	15282.2
55	548	118860.4	3849.4	67835.6	61494.5	252039.9
56	31	5994.3	212.2	3642.1	3354.3	13202.9
57	208	49081.8	1486.3	27007.4	25043.3	102618.7
58	493	37096.3	1289.4	22742.3	20676.6	81804.6
59	338	37551.5	1166.3	20022.8	18167.1	76907.7
60	252	36258.7	1677.5	31542.6	28260.9	97739.8
61	233	54377.6	2172.4	36147.1	32512.4	125209.5
62	5664	905383.9	28981.3	523829.7	469273.2	1927468.1
63	2188	279088.8	2394.2	43507.4	169019	494009.4
64	435	131710.8	1377.2	26477.8	91983.7	251549.5
65	372	31828	893.7	8655.2	31429.7	72806.6
66	51	7580.5	124.5	2536.3	6356.4	16597.8
67	63	1465.3	25.8	331.3	873.2	2695.6
68	21	5123.5	70.1	1519.6	3280.9	9994
69	75	6718.6	81.2	1652.5	4493.9	12946.1
70	208	30036.8	431.6	10250.5	21787.5	62506.4
71	666	68696.9	797.7	13262.9	44634.7	127392.2
72	240	26125.3	312	5526.8	18592.2	50556.3
73	29	18882.4	222.6	4164.3	8777.1	32046.4
74	370	28410	362.5	6227.7	18657.3	53657.5
75	5	732.2	12.3	234.5	451.8	1430.8

76	12	3354.8	81.1	1256.1	2268.4	6960.4
77	2	42.3	1.4	14.9	28.8	87.4
78	2	942.2	19.3	259.8	523.5	1744.8
79	14	2200.4	19.3	285	1418.3	3923
80	3	1735.2	15	270.9	1017.7	3038.9
81	19	1657.2	48	656.3	1147.8	3509.3
82	275	23777.8	230.4	2910.7	17937	44855.9
83	11	2863.5	59.8	1052.8	1052.8	5029
84	35	2992.7	123	2087.3	2218.5	7421.5
85	54	11358	381.4	6312.3	6706.7	24758.4
86	71	8051.1	262.8	4838.5	5006.1	18158.5
87	298	20912.8	278.2	4524.8	16391.6	42107.3
88	332	30525.1	529.7	8039.4	24842.2	63936.4
90	5	2335.3	65	1021.4	994	4415.7
91	9	534.8	20.6	367.3	368.7	1291.5
92	135	12743	495.2	7427.4	7669.5	28335.1
94	1	22.3	2.3	12.6	14.1	51.4
95	3	196.6	6.2	105.9	106.8	415.6
96	37	1705	94.1	1286.5	1349.4	4435.1
97	2	215.7	3.6	58.2	175.9	453.3
98	7	685.8	10	158.4	547.3	1401.6
99	195	1644.6	74.9	729.8	960.1	3409.3
100	38	6227.6	180.1	2927.2	3610.2	12945.1
102	15	3196.3	73.5	1364.5	1754.2	6388.5
103	9	258.2	15.3	298.5	405.9	977.9
104	4	458.6	17	397.8	521.2	1394.7
105	4	393	16	228	310.3	947.3
106	1	139.3	6.9	54	70.3	270.4
107	159	4325.5	51.9	653.4	3190	8220.7
108	15	2502.9	32.7	551.2	2098.6	5185.4
109	54	2504.3	29.3	408	2427.1	5368.7
110	36	11290.9	117.1	2034.2	6727.7	20169.9
111	27	541.8	22.5	389.6	444.1	1398
112	4	102.9	7	125.2	142.5	377.5
113	167	13435.6	527.2	7351.6	8437.9	29752.3
114	42	5869.9	160.9	2567.3	2881.2	11479.3
115	24	1012.6	39.6	520.7	588.4	2161.3
116	25	1923.3	73.6	1298	1485	4779.8
117	12	2826.3	87.2	1414.2	1608	5935.8
118	12	1583.2	59.4	990.9	1129	3762.4
119	50	2606.9	40.3	595.8	2441.6	5684.5
120	25	3680.8	58.2	953	2724.3	7416.4
121	216	9964.4	182.4	2435.8	9008.1	21590.7
122	515	18306.3	359.9	4071.3	14727.5	37464.9
123	727	9138.4	527	7910.2	6013.3	23589
124	34	3013.3	187.5	3373.3	2539.7	9113.9
125	73	4167.4	193.3	4022.9	2916.9	11300.5
126	12	910.5	58.8	1009	726.2	2704.5
127	574	37869.2	1968.8	32145.3	22982.4	94965.6
128	94	17718.4	723.2	12642.4	9418.7	40502.7
129	1549	19001.8	1879.5	18025.9	13538.8	52446
130	59	8942.4	418.6	7886.6	5681.1	22928.6
131	58	651.5	274.5	676.8	536.3	2139
132	10	341.5	74.1	423	312.5	1151.1
133	5	238.3	14.1	269.8	195.2	717.4
134	9	304.6	24.9	354.4	262.4	946.3
135	91	6534.5	310.8	4810.7	3525.2	15181.1
136	790	29152.5	3660.6	25817.1	18624.4	77254.6
137	160	7048.9	632.4	6872.3	5063.7	19617.3
138	26	5684.8	210.1	3361.3	2476	11732.2
139	3533	107816.6	1729.5	24559.3	86811.5	220916.8
140	959	56603.1	982.3	16694.7	41044.6	115324.6
141	733	44661.2	895.1	14205.8	29961.4	89723.4
142	104	38012.6	655.3	11937.5	21227.4	71832.8

143	19	6765.7	103.9	1502.8	3837.2	12209.5
144	32	9948.2	190.1	2751.8	6470.5	19360.6
145	5	1075.4	20.9	308.2	760.5	2165.1
146	113	25918.6	127.2	1764.4	16159.4	43969.5
147	84	13832.8	382.6	5773.4	7442.1	27430.9
148	822	91747.5	841	12476.9	67723.6	172789
149	15	809.2	76.8	403.9	546.5	1836.4
150	91	10043.7	534.5	3985.8	5418.4	19982.4
151	5	881	29.6	494.5	691.1	2096.1
152	273	6662.8	1740.9	3458.7	4898.2	16760.6
153	2	276.7	12.4	125.3	170.4	584.8
154	140	1804.1	140.6	1111.2	1481	4537
155	70	8848.2	73.4	926.8	5156.8	15005.1
156	255	128759	3557	39738.8	63758.3	235813.1
157	29	1159.6	34.8	509	864.6	2568
158	3	688.1	14.8	306.5	395	1404.3
159	59	6786	438.6	2846	4625.1	14695.6
160	306	44692.4	444.9	6463	35660.1	87260.5
161	252	29282.3	237.9	3457.2	20565.9	53543.3
162	73	1615.2	596.8	1122.7	994.2	4329
163	88	17151.5	1898.2	10981.6	9491.5	39522.8
164	1025	20013.8	5203.1	13803.1	11970.2	50990.2
165	68	6490.7	1406.1	3987	3404.9	15288.7
166	1795	159909.7	1392.2	18670.5	88486.6	268459
167	959	63955.4	925.7	13857.5	43213.4	121952
169	1	90.5	3.5	65.1	86.5	245.7
173	196	37263	1038.7	15754.4	20274.7	74330.8
174	72	12286.9	390.6	4588.3	6398.7	23664.5
175	2	66.1	6.3	62.9	44.6	179.9
176	369	28937.9	1519.5	27429.4	20322.5	78209.3
177	3	242.9	13.7	250.1	171.2	677.9
180	95	740.6	72.6	1000.4	709.4	2522.9
181	15	241	20.9	275.1	186.8	723.9
182	51	1957.6	146.9	2619.7	1891.9	6616.2
183	3	3.7	0.3	1.6	1.6	7.1
185	97	16176.6	429.3	7369.6	7161.5	31137
186	877	45454.6	1691.8	32979.6	32104.5	112230.4
187	251	2258.5	146.1	1794.5	1664.5	5863.6
188	28	2412.5	84	1407.6	1314.6	5218.7
189	871	25895.7	1193.9	21404.6	19445.2	67939.5
190	73	7812.5	442.4	5770.9	5294.1	19319.9
191	1401	21880.5	992.8	15193.9	8156.1	46223.3
192	15	1522.4	134.8	2550.4	1385.5	5593.1
193	498	36772.9	1806.1	39473.2	21158.7	99210.9
194	3433	127489.3	5781.7	101337.4	57052.7	291661.1
195	1	90.5	3.7	62	63.7	219.9
196	1	78.3	0.9	12.1	21.7	112.9
197	36	3709.5	75.2	1465.2	2454.8	7704.8
198	327	17350.1	889.9	13603.1	13919	45762.1
199	41	4559.4	86.5	1664.4	2976.9	9287.2
200	27	1317.3	117.4	1819.9	1197.2	4451.8
201	8	1462.7	82.1	1427.1	970.6	3942.5
202	26	823.7	22.5	397.6	451	1694.9
203	8	828.5	28	591.4	737.5	2185.4
204	331	9737.2	206.2	4302.3	5233.5	19479.2
205	368	8392.1	884.3	12607	8132	30015.4
206	213	72674.7	1026.3	22110.1	30663	126474.2
208	2	11.4	1.5	7	4.2	24
210	1	32.1	1.2	19.1	26.7	79.1
211	1	39.3	2.9	49.7	28.6	120.5
212	29	1946.3	134.8	2104	1203.1	5388.2
213	41	1574.5	167.6	1492	875.9	4110
214	19	2204.1	73.9	1867.9	1419.5	5565.6
215	98	4124.9	248.1	4278.8	3403	12054.8

216	1826	18159.4	415.4	5503	9330	33407.9
217	185	16382.1	354.9	6838.9	7300	30875.9
218	98	8681.2	489.5	8172.1	6399.2	23742.1
219	14	1595.8	34.1	716.4	1094	3440.3
220	299	22985.3	501.7	9567.4	22312.4	55366.7
221	3559	13622.7	2031	13444.2	7459	36556.8
223	578	36140.1	2172.2	38604.6	18647.8	95564.8
224	48	587.7	59.8	618.7	381	1647.1
225	5740	51102.3	1755	26600	27342.9	106800.2
226	110	3272.1	145.4	2975.3	2116.1	8508.9
227	3108	53642.1	1892.3	32005.3	37696.5	125236.2
229	589	7518.1	257.6	5123.9	4291.5	17191.2
230	6	609.8	26.5	704.3	499.2	1839.8
Total	73234	9500790.9	170632.8	2560878.8	5804953.8	18037256.3

Table S6: Total CPU time expended for all of the ab-initio calculations performed in this work without incorporating the effects of SOC (w/o SOC), subdivided by SG. In order, the columns in this table list the SG, the number of ICSDs successfully analyzed in the SG, the CPU hours expended per each of the four calculation steps (VASP1 through VASP4) detailed in SM 5 A, and the total CPU hours expended for materials in the SG.

SG	# ICSDs	VASP1 (CPU hours)	VASP2 (CPU hours)	VASP3 (CPU hours)	VASP4 (CPU hours)	Total (CPU hours)
1	222	16640.5	263.4	2250.8	10564.9	29719.6
2	1755	235667.3	3350.5	33564.7	152953.3	425535.9
3	16	930.1	7	81.8	538.9	1557.8
4	291	17447.8	156	2082.8	11934.1	31620.7
5	186	6913.4	57.2	653.8	4689	12313.4
6	39	1515.9	10.7	124	809.5	2460.1
7	143	8217.1	130.3	1050.1	5396.9	14794.4
8	168	5057.3	41.9	424.9	3167.5	8691.6
9	276	14522.1	112	1485	10613.8	26732.8
10	39	1873.5	14.9	185.8	1110.9	3185.1
11	749	53377.6	554.4	6215.3	33315.3	93462.6
12	1722	87000.4	614.7	7800	50440	145855.1
13	274	19194	170.8	2384.8	12399.9	34149.5
14	3602	391541.5	3358.7	48706.8	272488.3	716095.2
15	2419	177227	1461.2	18799.9	123027.7	320515.8
16	2	16.1	2	14.2	12.1	44.5
17	8	258.1	14.1	213.5	187.3	673
18	42	2809.3	127.5	2381.5	2167.5	7485.8
19	352	21449.7	940.1	17090.4	15336.1	54816.2
20	77	2538.6	36.2	556.2	1810.3	4941.3
21	20	306.5	5	65.1	165.5	542
22	14	312.4	2.9	39.7	134.5	489.6
23	15	510.5	5	58.8	204	778.3
24	3	41.8	0.8	8.6	26.7	77.9
25	58	872.9	42.9	476.7	406	1798.5
26	84	4907.6	169.8	3080.8	2775.5	10933.7
27	1	20.4	1	16.4	14.7	52.5
28	18	403.1	20.4	281.8	255.4	960.7
29	87	4800.4	237.4	4132.5	3720.1	12890.4
30	6	693.3	24.8	465.5	421.4	1605.1
31	245	8475	393.3	6672.2	5951	21491.5
32	12	1042.7	58.7	844	763.6	2709
33	399	22961	912.6	16815.8	15095.1	55784.5
34	30	2285.8	93.4	1827.2	1636.7	5843
35	8	253	16.4	67.5	166.3	503.1
36	392	14360.2	181.5	2621.9	8920	26083.6
37	7	328.9	14.2	99.8	250.9	693.7
38	162	2810.1	193.8	876.2	1508.4	5388.5

39	14	497.3	7.2	134.7	386.3	1025.5
40	64	2449.7	32.1	682.7	2050.8	5215.3
41	44	2926.4	30.2	600.1	1822.1	5378.8
42	4	183.7	2.4	31.6	161.4	379.1
43	125	4866	57.3	1071	3696.1	9690.4
44	93	1896.8	21.7	270.3	878.4	3067.2
45	11	1428.1	12.9	230.8	880.2	2552
46	83	4135.5	40.4	620.8	2283	7079.7
47	86	2117.4	71.1	869.9	787.8	3846.2
48	3	86.4	5.6	64.6	55.3	211.9
50	11	1020	38.6	773.3	700.8	2532.8
51	138	4387.5	181.6	3072.2	2766.1	10407.3
52	48	3899.3	186.1	2798.5	2550.8	9434.7
53	27	798.4	37.4	594.6	557.5	1988
54	23	1833.7	84.6	1722.7	1536.3	5177.3
55	466	37375	1328.4	24747.9	22131.1	85582.4
56	31	1967	89.6	1661.6	1522.9	5241
57	185	21454.5	582.5	11391.2	10321	43749.3
58	481	12890.5	576.2	9232.8	8317.6	31017.1
59	317	14493.3	466	7550.1	6710.8	29220.3
60	247	13852.8	686.1	11583.1	10368.2	36490.2
61	227	17496.1	856.6	15266	13530	47148.7
62	5327	302331.6	10405.5	187244.1	167174.9	667156.1
63	2021	51822.1	601.2	7947.2	23375.5	83745.9
64	421	19419.8	240.5	4187.2	13338.9	37186.4
65	331	11135.8	102.4	1487.7	3952.3	16678.2
66	49	2818.5	33.8	573.4	1907.5	5333.3
67	48	900.2	9.6	108.1	372.4	1390.3
68	21	1599.4	20.6	333.9	1121.1	3075
69	73	2870.6	26.3	413.9	1294.6	4605.5
70	197	7537.8	99.4	1998.5	5604.2	15239.8
71	574	17088	168.7	2306.6	7159	26722.3
72	227	7369.5	83.8	1192.4	3970.2	12615.9
73	21	3113.5	36.8	535.6	2081.5	5767.5
74	342	7896	104.2	1446.9	4571.6	14018.8
75	5	192.3	7.1	112.5	119.3	431.2
76	12	661.9	26.4	487.1	508.3	1683.7
77	2	17.2	1.1	9.9	11	39.2
78	2	289.9	8	148.1	155.6	601.5
79	14	376.5	5.5	69.7	239	690.7
80	3	362.8	3.8	58.2	234	658.8
81	18	373.5	20.3	259.4	289.8	942.9
82	265	3631.4	86.6	708.4	2588	7014.5
83	10	716.2	20.7	345.2	370.8	1452.9
84	35	1121.1	48.9	776.1	802.4	2748.6
85	51	3973.6	130.9	2511	2619.6	9235.2
86	68	2795.4	104.2	1759.5	1788.1	6447.3
87	291	8338	89.3	1091.6	4117.1	13636
88	314	9571.3	128.6	1716.2	6876.7	18292.9
90	5	614.1	23	491.8	363.5	1492.5
91	9	136.1	8.9	130.2	95.1	370.3
92	133	3393.2	182.5	2995.1	2221.3	8792.1
94	1	4.3	0.3	3.7	3	11.2
95	3	44.4	3.2	43.1	31.6	122.3
96	37	350.3	28.3	364.8	291.4	1034.8
97	2	16.6	1.1	12.5	21.8	51.9
98	7	144.1	2.9	37.6	111.9	296.5
99	195	625.5	100.6	527.8	425.9	1679.8
100	38	1376	74	1256.1	897.9	3604
102	15	717.3	34	662.3	473.2	1886.8
103	9	39.2	5.3	43.6	32.8	120.9
104	4	100.9	8.4	127.8	96	333.1
105	4	73.7	4.6	75.3	52.6	206.2
106	1	24	1.7	25.6	18.5	69.8

107	145	789.3	22.7	179.5	450.5	1442
108	14	488.2	8.9	125.7	369.3	992.2
109	50	436.9	12.2	103.3	241.3	793.8
110	36	2058.5	29.2	446.8	1440.3	3974.8
111	26	203.8	18.3	179.9	132.7	534.8
112	4	22.6	2.5	20.4	15.6	61
113	150	2409.9	164.4	2336.3	1741.1	6651.8
114	42	1054.6	67.5	1108.7	791.4	3022.2
115	24	298	19.7	289.5	198.4	805.7
116	25	616.6	40.7	650.1	473.7	1781
117	12	917.1	35.6	684.9	552.7	2190.2
118	12	449.8	28.7	480.6	402.5	1361.6
119	50	631.4	15.4	154.9	413.9	1215.5
120	25	884.6	16.5	220.3	561.1	1682.5
121	205	2258.1	62.4	631.7	1603	4555.2
122	510	3995.8	123.2	1103.7	2803.2	8026
123	699	4342.5	352	2844.7	2142	9681.2
124	33	1119.5	62.1	1194.5	922	3298.1
125	67	1841.9	79.5	1149.6	841.2	3912.1
126	11	372.2	23.8	451.5	321.3	1168.7
127	523	15351.3	591.5	9138.4	6490.3	31571.5
128	89	8301.5	285.2	5630.7	4071.6	18289
129	1506	10738.6	814.4	5929.9	4520.7	22003.5
130	58	4060.1	179.9	3491.2	2537.5	10268.7
131	57	240.7	27.9	179.6	138.2	586.4
132	10	94.2	7.4	87.6	65.6	254.8
133	5	100.6	5.9	104.2	74.5	285.2
134	9	67.8	5.7	62.8	46.3	182.7
135	84	1695.1	107	1590.2	1141.8	4534.1
136	766	9562.1	608.4	8214.9	5921.6	24307
137	158	3107.1	200.6	2993.2	2197.4	8498.4
138	20	1175.6	44.3	776.5	560.3	2556.7
139	3345	30000.9	577	5821.5	14249.1	50648.5
140	916	16784.1	307.6	3577.2	8459.7	29128.5
141	658	12790	221	2852.3	6060.4	21923.7
142	98	8273.9	136.8	2139.7	5064	15614.4
143	18	1468.6	54.8	792.1	1086	3401.5
144	31	3401.4	88.3	1256.7	1685.7	6432
145	5	254.5	10.9	143.7	192.5	601.7
146	108	2882.8	29	293.2	1969.9	5174.9
147	80	3872.6	108.9	1913.7	2397.8	8293
148	794	26005.2	236.8	2812.5	16800	45854.5
149	15	142.5	10.1	100.6	89	342.3
150	88	2728.6	122.8	1604.5	1334.5	5790.4
151	4	199.4	10.1	186.2	154.2	549.9
152	269	1454.2	172	1229.5	1091	3946.7
153	1	35.4	1.9	33.2	28.1	98.5
154	138	617.1	83.1	535.7	460.5	1696.4
155	66	1133	23.4	200.9	729.4	2086.7
156	224	24561.7	714.8	13269.3	11261.8	49807.6
157	27	320.9	27.2	263.3	226.9	838.4
158	3	158.5	7.2	128.9	105.8	400.5
159	57	1159.9	82	985.1	841	3068.1
160	298	5234.3	116.7	1256.6	3419	10026.6
161	251	5052.8	71.6	814.7	3616.4	9555.5
162	70	461.9	43.7	358.9	317.6	1182.1
163	80	4697	193.1	3418.7	2948.8	11257.6
164	996	6051.4	596.2	4239	3709	14595.6
165	66	2066.5	114.8	1803	1511.3	5495.5
166	1679	43048.6	429.4	3973.1	15148.7	62599.9
167	913	34970.4	517.1	4992.7	25149.1	65629.3
169	1	26	2.7	34.2	24.8	87.7
173	176	6442.7	300.5	5379.9	3825.6	15948.7
174	62	1834.8	110.3	1473.5	1136.8	4555.4

175	2	18.4	1.6	19.2	13.7	52.9
176	339	10426.4	599	10057.4	7233.8	28316.6
177	3	83.6	6.6	98.5	54.2	242.9
180	95	302.6	63.2	380.9	220.5	967.3
181	15	65.6	7.7	85.6	48	206.9
182	49	578.1	61.7	816.5	442.3	1898.7
183	3	3.2	1.5	3.8	2.4	10.9
185	84	2742.7	174.9	3049.8	1572.5	7539.9
186	842	8956.8	849.5	10271.5	5688.3	25766.1
187	246	812.3	170.3	771.2	489.3	2243.1
188	27	367	34.1	458.9	250.3	1110.3
189	768	7479.3	674.7	6256.1	3510.8	17920.8
190	67	1486.7	148.8	1859.8	1013.6	4508.9
191	1269	10049.9	680.1	4765	2736.8	18231.8
192	14	627.6	49.3	890.2	482.5	2049.6
193	439	10935.5	515.5	7762.6	4193.8	23407.3
194	3269	42642.6	2690.8	30749.5	16916.5	92999.5
195	1	26.5	1.6	26	16.7	70.7
196	1	12.7	0.4	3.3	4.5	21
197	36	521.6	24.7	355	351.2	1252.6
198	323	4050	333.9	4925.2	3259.5	12568.7
199	40	823.9	22.4	341.6	496.3	1684.2
200	27	526.7	47.7	693.7	452.5	1720.5
201	7	496.5	26.8	473.5	306.3	1303.2
202	26	236.9	7.3	100.6	151	495.8
203	8	285.6	7	133.6	243.8	670.1
204	323	2843.6	73.5	1114.7	1249.5	5281.4
205	364	3012.8	299.7	3650	2415.6	9378.1
206	208	14306.2	184.2	3907.3	6257.4	24655
208	2	2.9	0.9	2.8	1.7	8.4
210	1	10	0.5	4.6	8.1	23.1
211	1	15.9	1.4	22.2	10.5	50.1
212	29	609.5	47.2	738.8	363.7	1759.3
213	41	328.5	36.8	497	244.6	1106.9
214	18	367.9	16.8	373	268.2	1025.9
215	95	1020.6	118	1625.3	810.9	3574.8
216	1798	4916.7	210.6	1411.7	3321.6	9860.6
217	178	2790.9	88	1441.5	1304	5624.4
218	98	1925.3	194.4	3060.3	1496	6676.1
219	13	261.8	8.1	146.6	213.9	630.4
220	295	5456.1	151	2266.3	2167.5	10040.9
221	3493	10189.3	3401	9912.1	6474.7	29977.1
223	568	17296.6	978.4	14360.2	7033.1	39668.4
224	45	271.5	45.9	265.3	142.2	724.8
225	5619	21321.7	842.1	6760.4	12191.7	41116
226	102	984.3	41.3	635.8	757.3	2418.7
227	3012	17366.8	594.4	7540.4	8656.2	34157.8
229	583	3066.4	107	1221.7	1359.9	5755
230	6	219.5	8	159.2	199.3	586
Total	69730	2298583.3	56520.7	773019.5	1397550.3	4525673.8

Table S7: Total CPU time expended for all of the ab-initio calculations performed in this work incorporating the effects of SOC (with SOC), subdivided by the number of atoms in the primitive cell in each material. In order, the columns in this table list the number of atoms, the number of ICSDs successfully analyzed with the same number of atoms, the CPU hours expended per each of the four calculation steps (VASP1 through VASP4) detailed in [SM 5 A](#), and the total CPU hours expended for materials with the listed number of atoms in the primitive cell.

# atoms	# ICSDs	VASP1 (CPU hours)	VASP2 (CPU hours)	VASP3 (CPU hours)	VASP4 (CPU hours)	Total (CPU hours)
1	1178	1692.2	133	455.7	1315.1	3596

2	5838	8707.1	1229	4630.6	5155.7	19722.4
3	2429	8457.2	586.1	2543.2	5180.9	16767.4
4	4851	24909	1465	8512.3	17989.5	52875.8
5	3912	38653.7	1437.9	9362.6	26276.9	75731.1
6	6280	62655.4	3812.2	25308	46531.7	138307.2
7	1169	20558.6	378.2	3953.5	21107.7	45997.9
8	4239	69498.4	1969.7	26406.4	66879.8	164754.4
9	1745	38455.6	1040.8	16788.1	36746.4	93030.9
10	3498	101882.1	3068.6	38573.3	108096.9	251620.9
11	488	37159.7	846.8	8064.9	39050.5	85121.8
12	5023	271212.6	8527.4	131051	280299.7	691090.8
13	748	59115.8	1356.4	12500.1	43733.6	116705.8
14	2462	178253.4	4446.4	48149	209175.9	440024.7
15	429	44783.7	1372.9	9509.1	57785.1	113450.9
16	2980	291702.3	6978.2	101610.2	187394.1	587684.7
17	336	32322.2	607.5	8352.8	25039.6	66322.1
18	1607	187947	5758	57464.4	127823.4	378992.8
19	271	59358.6	475.7	5950.7	24315.9	90100.9
20	3618	480741.1	10167.6	149467.9	299831.8	940208.3
21	199	30273.9	1085.7	6403.3	15711.2	53474.2
22	1613	254127.1	3484	47223.3	131763.9	436598.3
23	148	20209.7	636	4955.5	12606.8	38408
24	2635	452531.4	11618.9	135134.3	232471.7	831756.3
25	65	31170.7	200.7	2461.6	13554.2	47387.2
26	686	151359.6	1566	26140.2	79825.2	258891
27	154	26557.3	325.8	5019.3	15649.1	47551.5
28	2663	520778.7	9095	168200.4	279719.3	977793.3
29	441	64277.5	969.1	18818.8	28707.4	112772.8
30	855	222765	3328.8	51435.4	120702.2	398231.4
31	37	11691.3	96.4	1306.8	7565.8	20660.3
32	1446	529701.1	5729.5	104171.6	335148.4	974750.5
33	76	24907.1	274.1	5145.1	12343.3	42669.6
34	341	171411.2	1259	20640.5	102531.1	295841.7
35	44	34184	188.7	3082.9	21339.5	58795.1
36	1644	674688.5	12436.8	220457.8	371435.6	1279018.7
37	34	23767.8	224	2484.9	8439.8	34916.5
38	494	227118.6	3134.9	53355.6	105738.9	389348.1
39	67	41008.1	654.9	11049.4	16198.3	68910.7
40	1533	590881.7	11528.7	209582.4	338425.5	1150418.3
41	46	32255.1	242.9	4046	17630.1	54174.1
42	495	217781.5	2799.9	47968.9	131825.1	400375.5
43	16	6440.2	87.5	1193.6	3602.1	11323.3
44	791	535425.1	6427.7	111650.2	327926	981429
45	45	23017.7	390.7	6707.1	14180.8	44296.5
46	390	211540.2	2535	43916.8	112491.1	370483
47	10	15904.4	84.5	1334.3	5832.3	23155.4
48	846	523845.7	8847.3	151462.9	312179.8	996335.7
49	33	29334.5	229.2	3864.4	10371.8	43799.9
50	183	121677.3	1375.6	22310.1	68542.9	213905.9
51	12	9202.6	147.6	2251.9	5709.7	17311.7
52	641	574723.4	6738.7	111780.4	280305	973547.6
53	10	10657	54.7	688.1	2446.9	13846.7
54	257	146755.9	2628.7	44400.6	90529.7	284314.9
55	13	10828.9	128.6	2068.7	4207	17233.2
56	552	398960.4	6814.9	116851.8	239838.5	762465.7
57	11	8036.9	158.9	2340.2	3750.3	14286.3
58	161	120980.8	2010.7	29671	57301	209963.4
59	4	6722.4	45.1	706.8	4153.5	11627.8
60	417	351268.4	5045.2	84244.6	208210.1	648768.3
62	2	894.3	21.5	355.4	1717.5	2988.7
64	2	2286.1	35.9	573.9	1571.7	4467.6
68	2	1585.7	22.4	382.6	969	2959.6
70	3	2061.2	28.3	477.9	1953.5	4520.9
72	7	10535.4	119.5	2050	10071.1	22776

74	2	1022.6	21.8	354.5	1834.5	3233.4
76	6	4563.8	81.7	1275.2	4981.3	10902
78	1	1007.7	14.1	227.9	1214.2	2463.9
Total	73234	9500790.9	170632.8	2560878.8	5804953.8	18037256.3

Table S8: Total CPU time expended for all of the ab-initio calculations performed in this work without incorporating the effects of SOC (w/o SOC), subdivided by the number of atoms in the primitive cell in each material. In order, the columns in this table list the number of atoms, the number of ICSDs successfully analyzed with the same number of atoms, the CPU hours expended per each of the four calculation steps (VASP1 through VASP4) detailed in [SM 5 A](#), and the total CPU hours expended for materials with the listed number of atoms in the primitive cell.

# atoms	# ICSDs	VASP1 (CPU hours)	VASP2 (CPU hours)	VASP3 (CPU hours)	VASP4 (CPU hours)	Total (CPU hours)
1	1174	1428.4	150.8	237.9	1464.8	3281.8
2	5757	8494.6	1997.5	4335.5	6970.2	21797.9
3	2375	4654.8	538.7	1930.2	3119.6	10243.2
4	4724	13122.2	1848.2	6104.9	7951.1	29026.4
5	3768	17086.8	1570.1	5693.8	8010.7	32361.4
6	6005	27415.5	1914.6	11614.4	13057.6	54002.1
7	1121	5835.6	302.4	1686	3342.6	11166.6
8	4087	26286.6	1597.5	11208	14378.5	53470.6
9	1634	11539.6	781.9	5615	5671	23607.5
10	3366	29405.9	1002.8	8577.2	16863.4	55849.3
11	442	9348.1	148.4	1500.1	4025.6	15022.2
12	4721	74161.1	2387	25867.7	37434.5	139850.3
13	687	13310.1	255.6	2598	5464.7	21628.4
14	2346	36977.7	811.9	8930.2	19695.8	66415.6
15	404	10900.2	161.3	1705.1	5488.7	18255.3
16	2800	66554.1	1869.7	23967.2	35630.9	128021.8
17	325	8368.3	160.3	1947.3	4687.1	15163
18	1527	43958.1	1050.3	12785.7	21962.3	79756.5
19	235	13056.8	108.7	1274.3	4504.2	18943.9
20	3436	105041.5	2622.5	37317.1	60273.3	205254.4
21	180	6459.4	161.4	2000.5	3555	12176.3
22	1507	54674.8	925	11862.2	31129.2	98591.2
23	143	4653.5	105	1261.1	2887.3	8906.8
24	2445	107421.5	2878.4	44166.6	65128.8	219595.2
25	56	6339.8	50.3	595.5	2730.8	9716.4
26	636	27235.2	577.1	8100.2	15875.6	51788.1
27	144	8156.7	144	1874.2	4699.9	14874.7
28	2484	130370.6	3425.9	56219.6	75007.8	265023.9
29	421	18100.3	276.5	4305.2	7713	30395
30	771	44759.9	1138.5	17363.1	28079.2	91340.7
31	36	2787.1	41.6	430.6	1939.6	5198.9
32	1336	101776.4	2053.3	34289.6	63445.4	201564.7
33	71	7223.7	112.9	1889.5	3001.4	12227.6
34	315	28517.9	359	5176.1	18254	52307
35	42	6647.6	57.5	746.3	3465	10916.3
36	1535	180424.4	4037.4	73477.6	108486.3	366425.8
37	33	5944.5	66.1	823.5	3392.1	10226.2
38	438	58361.8	976.5	16280.2	30233.3	105851.8
39	63	10970.5	200.3	3261.2	5283.2	19715.2
40	1484	164516.7	3821.1	67853.9	103775.8	339967.5
41	39	4761	59.6	888.3	3289	8997.9
42	441	50165.2	858.1	13486.9	33587.9	98098.2
43	14	2472.3	34.2	393.1	1583	4482.6
44	708	115514.9	1865.9	32835.9	80554.8	230771.5
45	38	7729.9	160.7	2177.1	4031.6	14099.4
46	382	48077.9	773.4	12418.4	30508.1	91777.8

47	10	2162	26.9	385.5	1425.3	3999.6
48	815	132027.4	2797.2	51535.4	92872.3	279232.3
49	33	7950.4	65.4	919.6	4103.8	13039.2
50	176	29245.7	426.7	5948.3	19606.6	55227.2
51	10	1858.8	24.8	458	1336.6	3678.3
52	596	112774.2	1755.4	31895.2	73103.5	219528.3
53	10	2535.4	20	249.8	1016.3	3821.5
54	252	42895.2	844.6	14972.5	28809.5	87521.8
55	12	3719.9	39.5	617.8	1600.3	5977.6
56	529	103002.2	2019.1	38861.8	73748.8	217631.9
57	10	1918.4	48.2	717.9	1319.2	4003.8
58	151	28945.3	493.5	9623.3	18075	57137
59	4	1545.6	13.2	182.4	1055.2	2796.4
60	401	86389.7	1441.7	26559.6	61958.9	176349.8
62	2	562.1	3.8	60.9	360.9	987.8
64	2	1124.3	7.9	128.6	701.5	1962.3
68	2	433.1	3.5	49.8	287.9	774.2
70	3	928.2	5.9	95.4	583.8	1613.3
72	7	4042.6	23.3	370.4	2161.8	6598.1
74	2	471.9	3.6	57.1	333.6	866.2
76	6	2508	14.5	222.7	1237.4	3982.6
78	1	533.6	2.2	35.9	218.1	789.7
Total	73234	2298583.3	56520.7	773019.5	1397550.3	4525673.8

C. Disk Storage Requirements and Statistics

In this section, we provide tables detailing the amount of disk storage requested for this work. Overall, we have used 2,037.80Gb of storage for this work, which can be subdivided into 1,694.50Gb (83.15%) for the SOC DFT calculations and 343.30Gb (16.85%) for the DFT calculations performed w/o SOC. To conserve disk space, we have only stored the OUTCAR files outputted by VASP, the CHGCAR files generated during the self-consistent DFT calculations, and the PROCAR files generated during the density of states (DOS) evaluation. All of these files are stored in a compressed BZIP2 format. The majority of the storage is dedicated to the SOC computation output – specifically, the CHGCAR files use 559.30Gb (27.45%), and the PROCAR files use 1,013.80Gb (49.75%). For a more detailed overview, we list in Table S9 the disk storage expended to perform ab-initio calculations subdivided by SG, and in Table S10 we list the disk storage expended to perform ab-initio calculations subdivided by the number of atoms in the primitive cell of each material.

Table S9: Total disk storage space (in Gb) expended for all of the ab-initio calculations performed in this work, subdivided by SG. In order, the columns in this table list the SG, the number of ICSDs successfully analyzed in the SG, the total storage space (in Gb) for the calculations performed with and w/o SOC, the storage for the compressed CHGCAR files generated during the SOC self-consistent DFT calculations, the storage for the compressed PROCAR files generated during the SOC DFT DOS calculations, and the total storage space for the calculations performed w/o SOC.

SG	# ICSDs	Total Storage SOC+w/o SOC (Gb)	CHGCAR SCC Storage (Gb)	PROCAR DOS Storage (Gb)	Total w/o SOC Storage (Gb)
1	225	14	1.54	8.25	2.05
2	1885	119.7	19.8	67.9	27.05
3	19	1.32	0.15	0.95	0.15
4	305	18.92	3.13	11.85	2.9
5	195	9.83	1.83	6.2	1.3
6	39	1.8	0.17	1.32	0.21
7	143	8.53	1.46	5.29	1.36
8	173	5.86	1.15	3.61	0.79
9	278	17.1	3.37	10.42	2.62
10	44	1.76	0.22	1.12	0.25
11	790	39.49	6.18	23.58	6.17
12	1844	70.2	17.18	37	11.06

13	314	16.93	3.31	9.41	2.84
14	3787	244.55	55.26	119.39	51.72
15	2526	135.25	33.73	63.14	25.98
16	2	0.03	0.01	0.02	—
17	8	0.43	0.06	0.29	0.05
18	42	2.15	0.43	1.21	0.39
19	364	20.31	4.55	10.45	3.36
20	85	3.75	0.96	1.96	0.53
21	21	0.51	0.11	0.29	0.07
22	17	0.6	0.14	0.35	0.06
23	16	0.73	0.22	0.38	0.09
24	3	0.11	0.04	0.05	0.02
25	59	1.04	0.12	0.7	0.12
26	85	3.5	0.71	1.99	0.57
27	1	0.05	0.01	0.03	0.01
28	18	0.65	0.07	0.49	0.06
29	89	4.38	0.96	2.44	0.78
30	6	0.36	0.08	0.17	0.09
31	247	11.18	1.73	7.45	1.46
32	12	0.44	0.12	0.14	0.14
33	406	19.5	3.84	11.47	3.27
34	30	1.22	0.27	0.56	0.3
35	8	0.26	0.06	0.12	0.05
36	412	18.25	4.43	10.31	2.32
37	7	0.3	0.09	0.11	0.07
38	173	3.47	0.8	1.86	0.45
39	15	0.81	0.22	0.41	0.11
40	67	2.7	0.67	1.42	0.41
41	44	2.21	0.76	0.81	0.49
42	4	0.2	0.07	0.09	0.03
43	126	6.35	2.4	2.53	1.11
44	100	3.18	0.96	1.64	0.38
45	11	1.01	0.4	0.35	0.21
46	91	5.7	1.71	2.96	0.74
47	95	2.03	0.28	1.21	0.27
48	3	0.09	0.02	0.05	0.01
49	1	0.05	0.01	0.03	—
50	11	0.54	0.07	0.31	0.12
51	147	3.95	0.53	2.51	0.57
52	51	2.92	0.59	1.73	0.46
53	27	0.76	0.2	0.37	0.14
54	25	1.29	0.34	0.63	0.23
55	548	31.89	3.65	20.84	4
56	31	1.58	0.35	0.86	0.3
57	208	11.18	2.23	6.58	1.75
58	493	11.97	2.43	6.69	1.98
59	338	8.63	1.53	4.93	1.39
60	252	11.75	2.22	6.91	2.03
61	233	12.52	2.74	6.99	2.21
62	5664	223.07	40	133.95	34.07
63	2188	53.41	15.98	24.99	7.7
64	435	17.57	4.28	9.16	2.88
65	372	10.18	2.81	5	1.39
66	51	1.81	0.61	0.64	0.39
67	63	0.7	0.16	0.35	0.11
68	21	1.06	0.34	0.42	0.22
69	75	2.77	0.87	1.27	0.43
70	208	9.04	3.09	3.96	1.4
71	666	21.53	8.92	7.59	2.96
72	240	9.68	3.05	4.63	1.4
73	29	2.25	1.31	0.21	0.43
74	370	10.91	3.5	4.92	1.72
75	5	0.33	0.05	0.24	0.03
76	12	0.56	0.18	0.25	0.11

77	2	0.03	0.01	0.01	—
78	2	0.07	0.04	—	0.03
79	14	0.64	0.2	0.32	0.09
80	3	0.43	0.22	0.13	0.07
81	19	0.81	0.14	0.53	0.09
82	275	8.88	2.63	4.57	1.14
83	11	0.46	0.08	0.27	0.06
84	35	1.31	0.24	0.8	0.21
85	54	2.13	0.54	1.03	0.39
86	71	3.63	0.59	2.34	0.48
87	298	7.36	2.69	2.87	1.3
88	332	10.59	4.68	3.15	2.07
90	5	0.19	0.08	0.03	0.06
91	9	0.48	0.09	0.32	0.06
92	135	3.52	0.98	1.79	0.58
94	1	0.02	—	0.01	—
95	3	0.12	0.03	0.07	0.02
96	37	0.93	0.24	0.51	0.13
97	2	0.23	0.04	0.05	0.14
98	7	0.24	0.1	0.09	0.04
99	195	1.23	0.26	0.62	0.18
100	38	1.62	0.29	1.07	0.2
102	15	0.77	0.1	0.56	0.09
103	9	0.13	0.03	0.08	0.02
104	4	0.22	0.04	0.15	0.02
105	4	0.15	0.02	0.1	0.02
106	1	0.06	0.01	0.04	0.01
107	159	2.22	0.79	0.96	0.28
108	15	0.63	0.24	0.26	0.1
109	54	1.37	0.62	0.48	0.2
110	36	2.5	0.71	1.24	0.42
111	27	0.38	0.09	0.21	0.05
112	4	0.07	0.02	0.03	0.01
113	167	5.09	1.1	3.07	0.56
114	42	1.6	0.4	0.89	0.23
115	24	0.34	0.07	0.17	0.05
116	25	1.25	0.14	0.92	0.14
117	12	0.67	0.12	0.41	0.1
118	12	0.57	0.11	0.36	0.07
119	50	1.14	0.52	0.34	0.2
120	25	1.18	0.46	0.47	0.19
121	216	4.82	1.86	1.84	0.7
122	515	10.77	4.49	3.87	1.74
123	727	5.85	1.34	2.59	0.92
124	34	0.62	0.2	0.24	0.13
125	73	1.92	0.48	1.05	0.26
126	12	0.54	0.13	0.31	0.08
127	574	14.47	2.42	8.93	1.73
128	94	4.95	1.05	2.91	0.69
129	1549	13.71	3.68	6.05	2.23
130	59	3	0.58	1.86	0.43
131	58	0.4	0.11	0.17	0.07
132	10	0.22	0.07	0.1	0.03
133	5	0.19	0.01	0.14	0.03
134	9	0.19	0.04	0.11	0.03
135	91	3.28	0.7	1.92	0.47
136	790	11.58	2.43	6.49	1.67
137	160	3.88	0.69	2.36	0.57
138	26	1.41	0.25	0.89	0.13
139	3533	54.9	30.93	10.47	9.08
140	959	21.54	8.14	8.68	3.12
141	733	19.92	8.65	6.91	3.04
142	104	8.49	3.69	3.04	1.33
143	19	1.42	0.28	0.86	0.21

144	32	1.61	0.54	0.63	0.36
145	5	0.38	0.08	0.24	0.05
146	113	5.79	1.28	3.63	0.64
147	84	3.49	0.98	1.62	0.63
148	822	33.51	9.81	16.67	5.36
149	15	0.45	0.14	0.22	0.06
150	91	3.99	0.82	2.48	0.5
151	5	0.27	0.07	0.15	0.04
152	273	4.95	1.38	2.57	0.7
153	2	0.09	0.02	0.05	0.01
154	140	1.81	0.58	0.81	0.28
155	70	2.51	0.86	1.16	0.35
156	255	11.97	3.71	5.41	1.69
157	29	1	0.19	0.66	0.1
158	3	0.14	0.04	0.07	0.02
159	59	2.89	0.55	1.91	0.33
160	306	20.34	14.24	2.56	3.24
161	252	7.86	2.48	3.82	1.21
162	73	1.14	0.35	0.5	0.17
163	88	3.39	1.23	1.34	0.57
164	1025	10.28	3.4	4.07	1.59
165	68	2.87	0.69	1.63	0.43
166	1795	51.92	25.8	14.99	8.24
167	959	25.83	10.4	10.02	4.1
169	1	0.04	0.01	0.02	—
173	196	11.41	2.42	6.14	1.12
174	72	3.58	0.7	2.29	0.39
175	2	0.05	0.01	0.03	0.01
176	369	13.22	3.03	7.23	2.19
177	3	0.12	0.05	0.05	0.02
180	95	0.91	0.3	0.36	0.16
181	15	0.23	0.08	0.09	0.04
182	51	1.25	0.38	0.62	0.18
183	3	0.01	—	—	—
185	97	5.59	1.11	3.69	0.52
186	877	19	5.02	10.71	2.14
187	251	1.52	0.54	0.54	0.24
188	28	1.15	0.35	0.58	0.15
189	871	16.66	4.33	8.77	1.9
190	73	3.06	0.73	1.76	0.38
191	1401	11.26	3.08	4.84	1.72
192	15	0.85	0.26	0.42	0.13
193	498	11.96	4.03	5.47	1.53
194	3433	50.85	15.29	23.62	7.07
195	1	0.04	0.02	0.02	0.01
196	1	0.03	0.01	0.01	—
197	36	1.97	0.65	0.94	0.27
198	327	7.67	2.36	3.84	1.1
199	41	1.64	0.54	0.75	0.23
200	27	0.81	0.21	0.43	0.12
201	8	0.52	0.12	0.3	0.07
202	26	0.69	0.33	0.19	0.12
203	8	0.5	0.23	0.16	0.08
204	331	6.73	2.69	2.3	1.12
205	368	5.8	1.95	2.58	0.93
206	213	13.02	4.11	6.17	1.94
208	2	0.01	0.01	—	—
210	1	0.03	0.01	0.01	0.01
211	1	0.03	0.02	0.01	0.01
212	29	1.02	0.32	0.5	0.16
213	41	1	0.3	0.49	0.15
214	19	0.92	0.41	0.31	0.14
215	98	2.18	0.45	1.35	0.24
216	1826	9.11	3.7	2.52	1.41

217	185	6.53	2.14	3.04	0.82
218	98	4.17	1.4	2.06	0.57
219	14	0.8	0.26	0.39	0.1
220	299	10.02	3.84	4.06	1.43
221	3559	11.29	3.52	3.15	2.19
223	578	11.28	3.19	5.65	1.65
224	48	0.39	0.13	0.15	0.06
225	5740	33.64	14.19	8.95	5.6
226	110	3.17	1.21	1.23	0.46
227	3108	41.14	18.06	12.18	6.54
229	589	4.79	1.79	1.59	0.8
230	6	0.37	0.12	0.17	0.06
Total	73234	2072.48	559.38	1013.81	342.62

Table S10: Total disk storage space (in Gb) expended for all of the ab-initio calculations performed in this work, subdivided by the number of atoms in the primitive cell in each material. In order, the columns in this table list the number of atoms, the number of ICSDs successfully analyzed with the same number of atoms, the total storage space (in Gb) for the calculations performed with and w/o SOC, the storage space used for the compressed CHGCAR files generated during the SOC self-consistent DFT calculations, the storage used for the compressed PROCAR files generated during the SOC DOS DFT calculations, and the total storage space used for the calculations performed w/o SOC.

# atoms	# ICSDs	Total Storage SOC+w/o SOC (Gb)	CHGCAR SCC Storage (Gb)	PROCAR DOS Storage (Gb)	Total w/o SOC Storage (Gb)
1	1178	1.34	0.4	0.08	0.38
2	5838	11.9	4.61	1.48	2.63
3	2429	8.76	3.86	1.6	1.7
4	4851	23.6	9.84	5.7	4.36
5	3912	29.83	13.5	7.48	5.1
6	6280	50.21	19.69	15.6	8.55
7	1169	15.36	7.41	4.05	2.58
8	4239	50.43	17.46	19.92	8.05
9	1745	28.19	10.26	11.35	3.98
10	3498	52.59	17.43	22.76	8.06
11	488	15.25	5.89	6.03	2.21
12	5023	111.11	30.79	56.24	15.91
13	748	20.16	6.82	9.18	2.76
14	2462	62.23	20.79	28.02	8.88
15	429	16.07	4.83	8.12	2.22
16	2980	99.57	24.13	55.9	13.01
17	336	13.85	5.66	5.38	2.06
18	1607	64.96	16.25	34.47	8.18
19	271	13.42	3.58	7.3	1.73
20	3618	152.47	29.56	91.29	20.03
21	199	10.08	1.92	6.4	1.21
22	1613	78.63	19.28	44.71	10.33
23	148	8.11	2.55	4.1	1.05
24	2635	141	26.83	88.31	17.75
25	65	4.93	1.03	3.02	0.62
26	686	45.4	10.52	27.66	5.33
27	154	10.82	2.03	7.03	1.34
28	2663	159.49	33.06	97.87	20.74
29	441	18.63	5.6	8.85	2.69
30	855	60.95	11.88	38.63	7.48
31	37	3.07	0.52	1.89	0.56
32	1446	92.83	19.94	51.6	14.87
33	76	4.35	1.42	1.9	0.74
34	341	21.8	5.94	9.98	4.51
35	44	3.32	1.2	1.13	0.8
36	1644	113.2	25.87	61.42	19.17

37	34	2.13	0.86	0.48	0.66
38	494	34.24	8.51	17.76	5.72
39	67	5.23	1.9	2.04	0.98
40	1533	110.22	25.88	59.04	19.35
41	46	2.93	0.76	1.37	0.6
42	495	37.54	6.64	19.17	6.45
43	16	0.95	0.15	0.45	0.28
44	791	50.33	11.77	21.13	12.38
45	45	2.49	0.84	0.76	0.65
46	390	22.18	8.24	6.98	5.49
47	10	0.45	0.21	—	0.2
48	846	50.64	17.71	14.2	14.46
49	33	2.86	0.84	1.27	0.61
50	183	10.95	3.95	2.87	3.22
51	12	0.51	0.21	0.05	0.17
52	641	37.57	14.32	6.9	11.54
53	10	0.44	0.16	0.08	0.17
54	257	15.03	6.1	3.5	4.36
55	13	0.86	0.25	0.35	0.19
56	552	31.41	13	4.45	10.8
57	11	0.66	0.35	0.04	0.2
58	161	9.55	3.8	2.12	2.73
59	4	0.25	0.1	—	0.12
60	417	23.81	9.86	2.24	9.17
62	2	0.1	0.04	—	0.05
64	2	0.12	0.05	—	0.05
68	2	0.1	0.04	—	0.04
70	3	0.14	0.07	—	0.06
72	7	0.45	0.19	0.06	0.14
74	2	0.1	0.04	—	0.05
76	6	0.29	0.12	—	0.13
78	1	0.06	0.02	—	0.03
Total	73234	2072.48	559.38	1013.81	342.62

SM 6. TOPOLOGICAL MATERIAL CLASSES IN THE ABSENCE OF SPIN-ORBIT COUPLING

In real materials, spin-orbit interaction (SOC) is always present [2, 126]; however, depending on the orbitals at the Fermi energy, the dispersion, and the specific atoms in the material, the effects of SOC can be approximated to be negligible. For each of the materials on <https://www.topologicalquantumchemistry.com/>, we have performed DFT calculations (the details of which are specified in SM 4) both incorporating and neglecting the effects of SOC (though as noted in SM 4, there exist materials on <https://www.topologicalquantumchemistry.com/> for which only calculations incorporating SOC were convergent). As shown in Fig. S1, users on <https://www.topologicalquantumchemistry.com/> can toggle between the results of first-principles calculations performed with and w/o SOC for the same material using the switch on the top-right corner of each material page [light blue box in Fig. S1(A,B)].

In the absence of SOC, the possible stable topological (TQC) classes [28, 38, 42, 57, 91, 92, 96] for each material – NLC, SEBR, ES, ESFD, and LCEBR – are the same as the possible classes in the presence of SOC. However, as we will detail in the text below, the relative number of materials within each topological class, and the physical meaning of the NLC and SEBR classes, strongly differ with and w/o SOC. First, in SM 6 A, we will discuss the relative preponderance of ES-classified materials compared to the relative dearth of NLC- and SEBR-classified compounds in the absence of SOC. Then, in SM 6 B, we will review the physical meaning and expected topological boundary states of each topological class in the absence of SOC. In particular, in SM 6 B, we will focus on the cases of NLC- and SEBR-classified nonmagnetic materials, which were shown in Ref. 36 to be topological semimetals – as opposed to topological (crystalline) insulators – when the effects of SOC are neglected. Throughout this work, we specifically term ICSD entries that are classified as NLC (SEBR) at E_F w/o SOC as NLC-SM (SEBR-SM) topological semimetals. In the language of Refs. 29 and 37, NLC-SM and SEBR-SM phases w/o SOC are *Smith-index semimetals*, as they are characterized by nontrivial values of the SIs of the nonmagnetic (Type-II Shubnikov) single (spinless) SGs [36].

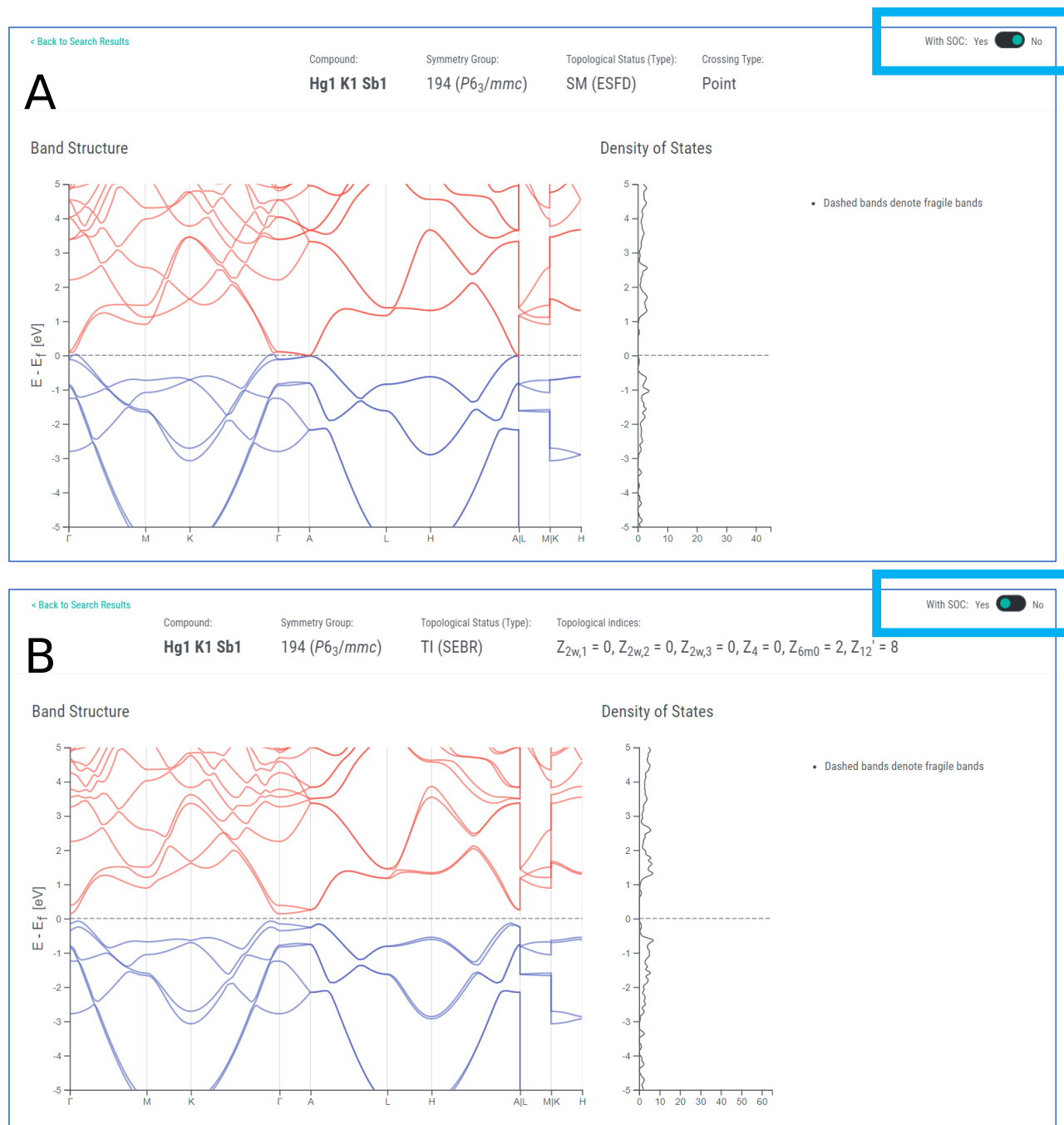


Figure S1. The electronic structure of the candidate hourglass TCI KHgSb (ICSD 56201, see Refs. [13, 14, 109, 127, 128] and SM 11 A 6) without (A) and with (B) the effects of SOC incorporated. Users can toggle between the first-principles analysis and topological data for each material on <https://www.topologicalquantumchemistry.com/> with and without SOC by clicking the switch highlighted in the blue box in the top-right corners of panels A and B.

Number of Unique Materials in Each Stable Topological Class Among the Materials with Convergent Calculations in the Absence of SOC (36,163 Unique Materials)		
Topological Class	Without SOC	With SOC
NLC (-SM)	251 (0.69%)	2,568 (7.10%)
SEBR (-SM)	44 (0.12%)	2,814 (7.78%)
ES	6,006 (16.61%)	3,785 (10.47%)
ESFD	13,997 (38.71%)	9,485 (26.23%)
LCEBR	15,865 (43.87%)	17,511 (48.42%)

Table S11. On <https://www.topologicalquantumchemistry.com/>, there are 36,163 unique materials (as defined in Ref. 38 and in the main text) for which DFT calculations were successfully performed both with and without incorporating the effects of SOC. For each of the stable topological classes, we list the number of materials in the class with and without SOC. As will be discussed in SM 6 B, we have added a parenthetical (-SM) following the NLC and SEBR classes, because NLC- and SEBR-classified nonmagnetic materials are necessarily topological semimetals in the absence of SOC [16, 17, 36]. As discussed in this section, the number of LCEBR compounds is relatively similar whether SOC is incorporated or neglected, whereas there are vanishingly few NLC-SM- and SEBR-SM-classified materials in the absence of SOC. Most specifically, the combined numbers of SEBR- and ESFD-classified materials with SOC ($2,814 + 9,485 = 12,299$) is close to the number of ESFD-classified materials without SOC (13,997), the number of NLC- and ES-classified materials with SOC ($2,568 + 3,785 = 6,353$) is close to the number of NLC-SM- and ES-classified materials without SOC ($251 + 6,006 = 6,257$), and the number of SEBR-SM-classified materials without SOC (44) is small compared to the overall number of calculated materials (0.12% of 36,163). As explained in the text below, the relative absence of NLC-SM and SEBR-SM materials can be understood by recognizing that most NLC- and SEBR-classified materials with SOC become ES-classified when SOC is neglected, because there are significantly many more ways for materials to fail to satisfy the compatibility relations [28, 91, 92] in the absence of SOC [57].

A. Relative Numbers of Materials in Each Topological Class with and without SOC

In Table S11, we show the number (and percentage) of materials in each stable topological class at E_F in the calculations performed with and w/o SOC for the unique materials (defined in Ref. 38 and in the main text) for which DFT calculations (performed as detailed in SM 4) converged both with and without incorporating the effects of SOC. We note that while the number of LCEBR-classified materials are similar with and w/o SOC, there are large differences across the other four stable topological classes. Most notably, in Table S11, the number of NLC- and ES-classified materials with SOC ($2,568 + 3,785 = 6,353$) is close to the number of NLC-SM- and ES-classified materials w/o SOC ($251 + 6,006 = 6,257$), and the number of SEBR-SM-classified materials w/o SOC (44) is small compared to the overall number of calculated materials (0.12% of 36,163). In particular, the number of NLC-SM- and SEBR-SM-classified materials w/o SOC in Table S11 ($251 + 44 = 295$) is smaller by roughly a factor of 20 than the number of NLC- and SEBR-classified materials with SOC ($2,568 + 2,814 = 5,382$). This difference can be understood by recognizing that the matrix representatives of twofold symmetries, such as mirror reflection and twofold rotation, anticommute in the presence of SOC, but *commute* in the absence of SOC, and that twofold crystal symmetries without translations have real-valued (imaginary-valued) eigenvalues in the absence (presence) of SOC [55, 129]. This implies that many more symmetry operations have simultaneously well-defined eigenvalues at each \mathbf{k} point in the absence of SOC than in the presence of SOC in nonmagnetic materials. Consequently, along high-symmetry lines and planes with the same symmetry, there are typically many more small irreducible corepresentation (corep) labels in the absence of SOC than in its presence. For this reason, when bands are inverted in a material w/o SOC, the material is much more likely to become ES-classified (and thus fail to satisfy the compatibility relations) than it is to become NLC-SM-classified, whereas in the presence of SOC, the material has a significantly greater chance of becoming NLC-classified after a bulk band inversion.

As an example, consider a TRIM point \mathbf{k} in a material where the little group $G_{\mathbf{k}}$ contains twofold rotation $\{C_{2z}|000\}$, inversion $\{\mathcal{I}|000\}$, and time-reversal $\{\mathcal{T}|000\}$ symmetries. The combination of inversion and twofold rotation also implies the presence of a mirror symmetry $\{M_z|000\} = \{\mathcal{I}|000\}\{C_{2z}|000\}$. Without SOC, the matrix representatives of inversion, twofold rotation, and mirror symmetries commute, and hence all three symmetries have simultaneously well-defined (real-valued) eigenvalues. There are therefore four one-dimensional (per spin), single-valued coreps at \mathbf{k} , which may be labeled by their $\{C_{2z}|000\}$ and $\{\mathcal{I}|000\}$ eigenvalues. When bands with distinct parity (inversion) eigenvalues are inverted at \mathbf{k} in the absence of SOC, protected crossing points appear along the twofold rotation axis if the bands carry distinct $\{C_{2z}|000\}$ eigenvalues and the same $\{M_z|000\}$ eigenvalues, or appear in the mirror plane if the inverted bands instead carry distinct $\{M_z|000\}$ eigenvalues and the same $\{C_{2z}|000\}$ eigenvalues. Conversely with SOC, the eigenvalues of $\{C_{2z}|000\}$ are imaginary numbers $\pm i$, and states with distinct $\{C_{2z}|000\}$ eigenvalues are paired by $\{\mathcal{T}|000\}$ symmetry at \mathbf{k} , and by $\{\mathcal{I} \times \mathcal{T}|000\}$ symmetry away from \mathbf{k} . Therefore in the presence of SOC, $G_{\mathbf{k}}$ has only two, two-dimensional, double-valued small coreps that may be labeled by their Kramers pairs of distinct parity (inversion) eigenvalues. Hence, when bands with distinct parity eigenvalues are inverted at \mathbf{k} with SOC, protected crossing points do not appear, absent additional symmetries.

Lastly, we note that the general trend of increased band connectivity w/o SOC also extends away from E_F across the stoichiometric materials in the ICSD. We specifically find that 1,047 ICSD entries with SOC (corresponding to 508 unique materials) contain a connected grouping of bands with at least N_e states at each \mathbf{k} point, where N_e is the number of valence electrons. Conversely, 20,899 ICSD entries w/o SOC (corresponding to 10,313 unique materials) contain a connected grouping of bands with at least N_e states at each \mathbf{k} point (taking bands w/o SOC to be spin-degenerate). In SM 8 we will also discuss the extreme case of *supermetallic* (SMetal) materials, in which *all* of the bands included in our VASP calculations are connected (see SM 4 for calculation details). Further supporting the trend of increased band connectivity in the absence of SOC, <https://www.topologicalquantumchemistry.com/> contains 17 unique SMetal materials with SOC, whereas there are 1,138 unique SMetal materials w/o SOC, representing a hundred-fold increase compared to calculations performed with SOC in the number of materials with fully-connected valence bands up to the energy (filling) cutoff of $\sim 2N_e$ imposed in our VASP calculations (see SM 4). Further statistics for materials with highly connected bands on <https://www.topologicalquantumchemistry.com/>, as well as material examples, are provided in SM 8.

B. Physical Interpretation of the NLC and SEBR Materials Classes in the Absence of SOC

To determine the topological class of a material in the absence of SOC, we use the same methods previously employed in Ref. 38. First, we determine if the coreps of the occupied bands at all high-symmetry points satisfy the compatibility relations [28, 91, 92] for an insulating gap to exist at E_F . If the insulating compatibility relations are not satisfied, then the material is classified as either an ESFD semimetal (in which a band degeneracy at a high-symmetry point is partially occupied) or an ES semimetal (in which the compatibility relations fail along a line or plane in the

BZ).

Without SOC, ES and ESFD semimetals exhibit topological boundary states analogous to those of topological semimetals with strong SOC. For ESFD materials, it has been extensively shown [130–132] that if the little group of the \mathbf{k} point of the nodal degeneracy is isomorphic to a chiral SG (defined in this work as an SG without rotoinversion symmetries, more formally referenced as a *Sohncke* SG, see Ref. 133), then the nodal point will carry a topological chiral charge, and will exhibit associated topological surface Fermi arcs. As demonstrated in several recent theoretical and experimental studies [9, 23–25, 130, 134, 135], the surface Fermi arcs are qualitatively the same in dispersion and length in strong- and weak-SOC ESFD semimetals whose nodal degeneracies lie at high-symmetry points with chiral little groups. Specifically, large topological Fermi arcs are typically present in ESFD semimetals in chiral SGs both with and without SOC – in the weak-SOC case, the Fermi arcs are spin-degenerate, whereas in the strong-SOC case, the Fermi arcs are highly-spin-polarized [25, 130], but are typically only weakly split by SOC [23, 24, 134, 135]. In weak-SOC ES semimetals, the nodal degeneracies are typically nodal lines, which are protected by a combination of coreps with different symmetry eigenvalues and weak-SOC topological invariants (*e.g.*, local $\mathcal{I} \times \mathcal{T}$ -symmetry protection, as introduced in Ref. 31). When SOC is negligible, all bulk nodal lines carry associated flat-band-like topological “drumhead” surface states [31, 136], which represent the weak-SOC (nondispersing) limit of the twofold surface Dirac cones of 3D TIs and TCIs. Additionally, it has recently been shown that more exotic, “monopole-charged” variants [137–140] of weak-SOC nodal lines also exhibit flat-band-like hinge states that are representative of a *higher-order* bulk-boundary correspondence, and correspond to the weak-SOC (nondispersing) limit of the helical hinge states of higher-order TIs [34].

In the cases where a material w/o SOC is classified as NLC or SEBR, the differences with the strong-SOC case are more pronounced. First, it was shown in Refs. 16, 17, and 36 that 3D, time-reversal- (\mathcal{T} -) symmetric (*i.e.* nonmagnetic), symmetry-indicated, topological insulating phases are only stable in the presence of non-negligible SOC. However, it was also shown in Refs. 29, 36, 37, 39, and 141 that the valence bands of real materials, when SOC is neglected, are still capable of simultaneously satisfying the insulating compatibility relations while not being equivalent to a linear combination of trivial bands. This presents an apparent contradiction: namely, a set of valence bands in a 3D material without SOC cannot be topologically nontrivial if stable (strong) topological bands do not exist in 3D, \mathcal{T} -symmetric systems without SOC. The resolution – discovered in Ref. 36 – is that in fact *all* NLC- and SEBR-classified materials in the absence of SOC are special cases of topological semimetals that satisfy the compatibility relations for insulators. Specifically, the compatibility relations are only capable of determining if the symmetry eigenvalues (small coreps) of the occupied bands can be smoothly connected to each other along all \mathbf{k} paths with crystal symmetry eigenvalues. However, bulk nodal degeneracies such as Weyl points [142] and nodal lines w/o SOC [137, 138] can also be stabilized by topological invariants evaluated on closed manifolds in momentum space (*e.g.* the Chern number evaluated on a sphere surrounding a Weyl point), *even if the crossing bands have the same corep labels*. In the relatively few materials on <https://www.topologicalquantumchemistry.com/> that are classified as NLC-SM or SEBR-SM in the calculations performed w/o SOC (Tables S12 and S13, respectively), a bulk gap is permitted along all high-symmetry lines and planes, but there is no gap in the BZ interior in the calculations performed w/o SOC.

To classify the NLC-SM and SEBR-SM phases of the materials on <https://www.topologicalquantumchemistry.com/> in the calculations performed w/o SOC, we have employed the SI formulas (topological indices and notation) of Ref. 36. We note that in the notation of Ref. 36, the \mathbb{Z}_2 -valued strong nodal-line-semimetal parity index introduced in Ref. 31 (which is the vanishing-SOC analog of the Fu-Kane parity index [5, 30]), does not appear on <https://www.topologicalquantumchemistry.com/>. Instead, the \mathbb{Z}_2 nodal-line index from Ref. 31 has been subsumed by the \mathbb{Z}_4 -valued parity index z_4 that captures both monopole-charged and uncharged nodal lines, and is the vanishing-SOC (spinless) analog of the \mathbb{Z}_4 -valued index Z_4 for spinful HOTIs discussed in Refs. 16, 17, 29, 33, 34, and 138 and in SM 11 A 3. Specifically, in nonmagnetic materials with inversion symmetry, $z_4 = 1, 2, 3$ phases are all nodal-line semimetals. If the values of all other spinless SIs (*e.g.* weak indices) are trivial, then the nodal lines in a $z_4 = 1, 3$ ($z_4 = 2$) NLC-SM or SEBR-SM carry trivial (nontrivial) monopole charges [34, 138].

To compare the ES nodal-line semimetals that are prevalent throughout <https://www.topologicalquantumchemistry.com/> (SM 6 A) to the nodal-line topological indices previously introduced in Refs. 31 and 36, we have produced subduction tables at the bottom of each material page on <https://www.topologicalquantumchemistry.com/>. Specifically, following the procedure employed in Refs 38, 113, and 143, the most familiar [31, 34, 36] strong \mathbb{Z}_4 and weak \mathbb{Z}_2 parity indices for ES-classified, centrosymmetric, nodal line semimetals w/o SOC (z_4 and $z_{2,i}$ respectively) can be obtained by consulting the subduction table entry for SG 2 ($P\bar{1}$) in calculations performed w/o SOC [noting that, if z_4 and $z_{2,i}$ are trivial for all $i = 1, 2, 3$, then the subduction table will not display an entry for SG 2 ($P\bar{1}$)]. During the preparation of this work, an alternative method for diagnosing the topology of ES-classified nodal-line semimetals in the absence of SOC was also introduced in Refs. 144 and 145, providing additional context for the subduction tables on <https://www.topologicalquantumchemistry.com/> generated for the present work.

Table S12: List of all nonmagnetic unique materials without f electrons that are classified as NLC-SM in calculations performed w/o SOC. In this table, a chemical formula with a * indicates that some (but not all) of the ICSDs associated to the same unique material (defined using its topological class with SOC) are classified as NLC-SM in calculations for the same ICSD entries performed w/o SOC. In this table, the topological indices (spinless SIs) at E_F of the calculations performed w/o SOC are listed in the notation of Ref. 36. Further details and the physical interpretation of each spinless SI in this table are provided in Ref. 36.

Chem. formula	SG #	SG symbol	ICSD	Line/Weyl	no-SOC topological indices
CaAs ₃	2	$P\bar{1}$	193	Line	$z_{2,1} = 1$ $z_{2,2} = 0$ $z_{2,3} = 0$ $z_4 = 1$
CaP ₃	2	$P\bar{1}$	74479	Line	$z_{2,1} = 0$ $z_{2,2} = 1$ $z_{2,3} = 0$ $z_4 = 1$
Ba(Mo ₆ S ₈)	2	$P\bar{1}$	85490	Line	$z_{2,1} = 0$ $z_{2,2} = 0$ $z_{2,3} = 0$ $z_4 = 3$
Bi	2	$P\bar{1}$	426929	Line	$z_{2,1} = 0$ $z_{2,2} = 0$ $z_{2,3} = 1$ $z_4 = 3$
YAsS	14	$P2_1/c$	611344	Line	$z'_2 = 1$ $z_4 = 2$
FeH ₄	11	$P2_1/m$	187148	Line	$z'_2 = 1$ $z_4 = 2$
Al ₂ Fe ₃ Si ₃	2	$P\bar{1}$	422342	Line	$z_{2,1} = 0$ $z_{2,2} = 1$ $z_{2,3} = 0$ $z_4 = 3$
Sr ₂ Co(SeO ₃) ₃	2	$P\bar{1}$	79204	Line	$z_{2,1} = 0$ $z_{2,2} = 1$ $z_{2,3} = 1$ $z_4 = 1$
KH ₂ PO ₃	14	$P2_1/c$	37072	Line	$z'_2 = 1$ $z_4 = 2$
YAsSe	14	$P2_1/c$	611398	Line	$z'_2 = 1$ $z_4 = 2$
Ag(SO ₄)	2	$P\bar{1}$	421341	Line	$z_{2,1} = 1$ $z_{2,2} = 1$ $z_{2,3} = 1$ $z_4 = 1$
SCH ₃	12	$C2/m$	670220	Line	$z'_2 = 1$ $z_{2,2} = 1$ $z_{2,1} = 1$ $z_4 = 2$
Cu ₄ Mo ₆ Se ₈	2	$P\bar{1}$	171431	Line	$z_{2,1} = 1$ $z_{2,2} = 1$ $z_{2,3} = 1$ $z_4 = 1$
K(Os ₂ O ₆)	2	$P\bar{1}$	419880	Line	$z_{2,1} = 1$ $z_{2,2} = 1$ $z_{2,3} = 0$ $z_4 = 3$
Cu(N(CN) ₂) ₂ (NH ₃) ₂	2	$P\bar{1}$	425593	Line	$z_{2,1} = 0$ $z_{2,2} = 1$ $z_{2,3} = 0$ $z_4 = 1$
Rh ₃ Ga ₅	2	$P\bar{1}$	240179	Line	$z_{2,1} = 1$ $z_{2,2} = 0$ $z_{2,3} = 0$ $z_4 = 0$
(PCl ₄) ₂ (Mo ₂ Cl ₁₀)	2	$P\bar{1}$	50441	Line	$z_{2,1} = 1$ $z_{2,2} = 0$ $z_{2,3} = 0$ $z_4 = 3$
PbPt ₂ O ₄	2	$P\bar{1}$	59657	Line	$z_{2,1} = 0$ $z_{2,2} = 1$ $z_{2,3} = 1$ $z_4 = 0$
SrMo ₆ S ₈	2	$P\bar{1}$	65941	Line	$z_{2,1} = 0$ $z_{2,2} = 0$ $z_{2,3} = 0$ $z_4 = 3$
Li ₅ (W ₂ O ₇)	2	$P\bar{1}$	194127	Line	$z_{2,1} = 1$ $z_{2,2} = 1$ $z_{2,3} = 1$ $z_4 = 2$
Ta ₆ S	2	$P\bar{1}$	202564	Line	$z_{2,1} = 0$ $z_{2,2} = 0$ $z_{2,3} = 1$ $z_4 = 2$
CaMo ₆ S ₈	2	$P\bar{1}$	619422	Line	$z_{2,1} = 0$ $z_{2,2} = 0$ $z_{2,3} = 0$ $z_4 = 3$
CaCu(SiO ₄)(H ₂ O)	14	$P2_1/c$	30926	Line	$z'_2 = 1$ $z_4 = 2$
LiCuC ₃ H ₄ PO ₅	15	$C2/c$	243640	Line	$z'_2 = 1$ $z_{2,2} = 1$ $z_{2,1} = 1$ $z_4 = 2$
Tc ₂ P ₃	2	$P\bar{1}$	41017	Line	$z_{2,1} = 0$ $z_{2,2} = 0$ $z_{2,3} = 0$ $z_4 = 1$
HgK	2	$P\bar{1}$	104302	Line	$z_{2,1} = 0$ $z_{2,2} = 1$ $z_{2,3} = 0$ $z_4 = 2$
AgHgO ₂	2	$P\bar{1}$	670059	Line	$z_{2,1} = 0$ $z_{2,2} = 1$ $z_{2,3} = 1$ $z_4 = 2$
CuAuO ₂	12	$C2/m$	670103	Line	$z'_2 = 1$ $z_{2,2} = 1$ $z_{2,1} = 1$ $z_4 = 2$
Cu(WO ₄)*	2	$P\bar{1}$	69759	Line	$z_{2,1} = 0$ $z_{2,2} = 1$ $z_{2,3} = 1$ $z_4 = 3$
Cu(WO ₄)	2	$P\bar{1}$	84558	Line	$z_{2,1} = 0$ $z_{2,2} = 1$ $z_{2,3} = 1$ $z_4 = 1$
FeSe	2	$P\bar{1}$	196300	Line	$z_{2,1} = 0$ $z_{2,2} = 0$ $z_{2,3} = 1$ $z_4 = 1$
FeO ₃	2	$P\bar{1}$	671721	Line	$z_{2,1} = 0$ $z_{2,2} = 1$ $z_{2,3} = 1$ $z_4 = 2$
Li ₄ N ₁	2	$P\bar{1}$	675136	Line	$z_{2,1} = 0$ $z_{2,2} = 0$ $z_{2,3} = 0$ $z_4 = 3$
CLi ₂	12	$C2/m$	670915	Line	$z'_2 = 1$ $z_{2,2} = 1$ $z_{2,1} = 1$ $z_4 = 2$
Ti ₁₁ Ni ₉ Pt ₄	15	$C2/c$	168948	Line	$z'_2 = 1$ $z_{2,2} = 0$ $z_{2,1} = 0$ $z_4 = 2$
VO ₂ *	2	$P\bar{1}$	1502	Line	$z_{2,1} = 0$ $z_{2,2} = 0$ $z_{2,3} = 1$ $z_4 = 1$
Cu(MoO ₄)	2	$P\bar{1}$	39439	Line	$z_{2,1} = 1$ $z_{2,2} = 1$ $z_{2,3} = 0$ $z_4 = 0$
Tc ₂ As ₃	2	$P\bar{1}$	66662	Line	$z_{2,1} = 0$ $z_{2,2} = 0$ $z_{2,3} = 0$ $z_4 = 1$
Mo ₃ S ₄	2	$P\bar{1}$	237587	Line	$z_{2,1} = 0$ $z_{2,2} = 0$ $z_{2,3} = 1$ $z_4 = 3$
(CuCl ₃)(Cu ₂ TeO ₃)	2	$P\bar{1}$	431558	Line	$z_{2,1} = 0$ $z_{2,2} = 0$ $z_{2,3} = 0$ $z_4 = 3$
V ₆ O ₁₃	12	$C2/m$	50409	Line	$z'_2 = 1$ $z_{2,2} = 1$ $z_{2,1} = 1$ $z_4 = 2$
Sc ₅ Cl ₈ N	12	$C2/m$	60856	Line	$z'_2 = 1$ $z_{2,2} = 1$ $z_{2,1} = 1$ $z_4 = 2$
Li ₄ N ₁	2	$P\bar{1}$	675127	Line	$z_{2,1} = 0$ $z_{2,2} = 0$ $z_{2,3} = 1$ $z_4 = 0$
CsHg	2	$P\bar{1}$	62000	Line	$z_{2,1} = 0$ $z_{2,2} = 0$ $z_{2,3} = 1$ $z_4 = 2$
CsHg	2	$P\bar{1}$	150974	Line	$z_{2,1} = 0$ $z_{2,2} = 0$ $z_{2,3} = 1$ $z_4 = 0$
NiOOH	2	$P\bar{1}$	674656	Line	$z_{2,1} = 1$ $z_{2,2} = 0$ $z_{2,3} = 0$ $z_4 = 1$
Ti ₅ O ₅	12	$C2/m$	56694	Line	$z'_2 = 1$ $z_{2,2} = 1$ $z_{2,1} = 1$ $z_4 = 2$
BaBiO ₃	12	$C2/m$	61499	Line	$z'_2 = 1$ $z_{2,2} = 1$ $z_{2,1} = 1$ $z_4 = 2$
Ag(V ₂ P ₂ O ₁₀)	14	$P2_1/c$	73824	Line	$z'_2 = 1$ $z_4 = 2$
Hf ₈ Ni ₂₁	2	$P\bar{1}$	2416	Line	$z_{2,1} = 0$ $z_{2,2} = 0$ $z_{2,3} = 0$ $z_4 = 1$
Ni ₂₁ Zr ₈	2	$P\bar{1}$	402864	Line	$z_{2,1} = 0$ $z_{2,2} = 1$ $z_{2,3} = 0$ $z_4 = 2$
VB ₃	12	$C2/m$	672902	Line	$z'_2 = 0$ $z_{2,2} = 1$ $z_{2,1} = 1$ $z_4 = 0$
Ni ₂₁ Zr ₈	2	$P\bar{1}$	647148	Line	$z_{2,1} = 0$ $z_{2,2} = 1$ $z_{2,3} = 0$ $z_4 = 0$

Ag(SO ₄)	2	$P\bar{1}$	290374	Line	$z_{2,1} = 0$ $z_{2,2} = 0$ $z_{2,3} = 0$ $z_4 = 2$
BaPd ₂ Bi ₂	11	$P2_1/m$	416299	Line	$z'_2 = 1$ $z_4 = 2$
Ni ₁₁ As ₈	15	$C2/c$	164878	Line	$z'_2 = 1$ $z_{2,2} = 1$ $z_{2,1} = 1$ $z_4 = 2$
BC ₅	2	$P\bar{1}$	166556	Line	$z_{2,1} = 0$ $z_{2,2} = 1$ $z_{2,3} = 1$ $z_4 = 3$
Li ₆ P	2	$P\bar{1}$	673928	Line	$z_{2,1} = 0$ $z_{2,2} = 1$ $z_{2,3} = 0$ $z_4 = 3$
NiOOH	58	$Pnmm$	674650	Line	$z'_2 = 1$ $z_4 = 2$ $z_2^- = 1$ $z_2^+ = 1$
Pb ₂ Sr ₂ YCu ₃ O ₈	2	$P\bar{1}$	74154	Line	$z_{2,1} = 1$ $z_{2,2} = 1$ $z_{2,3} = 0$ $z_4 = 1$
Cu(WO ₄)	2	$P\bar{1}$	169004	Line	$z_{2,1} = 1$ $z_{2,2} = 0$ $z_{2,3} = 0$ $z_4 = 3$
Sc ₃ NiSi ₃	12	$C2/m$	48004	Line	$z'_2 = 1$ $z_{2,2} = 0$ $z_{2,1} = 0$ $z_4 = 2$
CLi ₈	2	$P\bar{1}$	670922	Line	$z_{2,1} = 0$ $z_{2,2} = 0$ $z_{2,3} = 1$ $z_4 = 0$
SrPd ₂ Bi ₂	11	$P2_1/m$	416300	Line	$z'_2 = 1$ $z_4 = 2$
Na ₆ Ti ₆ O ₁₃	12	$C2/m$	238302	Line	$z'_2 = 1$ $z_{2,2} = 1$ $z_{2,1} = 1$ $z_4 = 2$
Ag(SO ₄)	15	$C2/c$	290375	Line	$z'_2 = 1$ $z_{2,2} = 0$ $z_{2,1} = 0$ $z_4 = 2$
Au ₂ Ca ₅	15	$C2/c$	58403	Line	$z'_2 = 0$ $z_{2,2} = 1$ $z_{2,1} = 1$ $z_4 = 0$
Pt ₅ P ₂	15	$C2/c$	24327	Line	$z'_2 = 0$ $z_{2,2} = 1$ $z_{2,1} = 1$ $z_4 = 0$
Sb ₂ Te ₃	15	$C2/c$	187497	Line	$z'_2 = 1$ $z_{2,2} = 0$ $z_{2,1} = 0$ $z_4 = 2$
NiS ₂	60	$Pbcn$	169571	Line	$z'_2 = 1$ $z_4 = 2$
Ni ₁₀ Sn ₅ P ₃	2	$P\bar{1}$	59641	Line	$z_{2,1} = 0$ $z_{2,2} = 1$ $z_{2,3} = 1$ $z_4 = 0$
TiNi	2	$P\bar{1}$	150629	Line	$z_{2,1} = 1$ $z_{2,2} = 0$ $z_{2,3} = 1$ $z_4 = 3$
Cu ₇ In ₃	2	$P\bar{1}$	429530	Line	$z_{2,1} = 0$ $z_{2,2} = 0$ $z_{2,3} = 0$ $z_4 = 2$
WNi ₄ P ₁₆	15	$C2/c$	67920	Line	$z'_2 = 1$ $z_{2,2} = 1$ $z_{2,1} = 1$ $z_4 = 2$
Pd ₁₃ Pb ₉	15	$C2/c$	648362	Line	$z'_2 = 1$ $z_{2,2} = 0$ $z_{2,1} = 0$ $z_4 = 2$
Pb ₉ Pd ₁₃	15	$C2/c$	105593	Line	$z'_2 = 1$ $z_{2,2} = 0$ $z_{2,1} = 0$ $z_4 = 2$

Table S13: List of all nonmagnetic unique materials without f electrons that are classified as SEBR-SM in calculations performed w/o SOC. In this table, a chemical formula with a * indicates that some (but not all) of the ICSDs associated to the same unique material (defined using its topological class with SOC) are classified as SEBR-SM in calculations for the same ICSD entries performed w/o SOC. In this table, the topological indices (spinless SIs) at E_F of the calculations performed w/o SOC are listed in the notation of Ref. 36. Further details and the physical interpretation of each spinless SI in this table are provided in Ref. 36.

Chem. formula	SG #	SG symbol	ICSD	Line/Weyl	no-SOC topological indices
Tl ₆ TeO ₁₂	148	$R\bar{3}$	37134	Line	$z_{2,3} = 0$ $z_4 = 3$ $z_{2,1} = 0$ $z_{2,2} = 0$
Mo ₆ Te ₈	148	$R\bar{3}$	59375	Line	$z_{2,3} = 1$ $z_4 = 3$ $z_{2,1} = 1$ $z_{2,2} = 1$
Sc ₇ Cl ₁₂ N	148	$R\bar{3}$	201976	Line	$z_{2,3} = 1$ $z_4 = 3$ $z_{2,1} = 1$ $z_{2,2} = 1$
Mo ₃ Te ₄	148	$R\bar{3}$	644477	Line	$z_{2,3} = 1$ $z_4 = 1$ $z_{2,1} = 1$ $z_{2,2} = 1$
Mo ₃ S ₄	148	$R\bar{3}$	600385	Line	$z_{2,3} = 1$ $z_4 = 2$ $z_{2,1} = 1$ $z_{2,2} = 1$
NiTi ₃ S ₆	148	$R\bar{3}$	26312	Line	$z_{2,3} = 1$ $z_4 = 3$ $z_{2,1} = 1$ $z_{2,2} = 1$
Mo ₃ Se ₄	148	$R\bar{3}$	600386	Line	$z_{2,3} = 1$ $z_4 = 1$ $z_{2,1} = 1$ $z_{2,2} = 1$
Mo ₈ Ga ₄₀ C	148	$R\bar{3}$	617918	Line	$z_{2,3} = 1$ $z_4 = 3$ $z_{2,1} = 1$ $z_{2,2} = 1$
Ni ₃ AsIn	148	$R\bar{3}$	671511	Line	$z_{2,3} = 1$ $z_4 = 3$ $z_{2,1} = 1$ $z_{2,2} = 1$
MoN ₂	166	$R\bar{3}m$	674587	Line	$z'_2 = 1$ $z_4 = 2$
Mo ₆ S ₈	148	$R\bar{3}$	252376	Line	$z_{2,3} = 1$ $z_4 = 2$ $z_{2,1} = 1$ $z_{2,2} = 1$
SiO ₂	162	$P\bar{3}1m$	170552	Line	$z'_2 = 1$ $z_4 = 2$
Ca ₃ Au ₄	148	$R\bar{3}$	54547	Line	$z_{2,3} = 1$ $z_4 = 0$ $z_{2,1} = 1$ $z_{2,2} = 1$
Na ₄ Cl ₃	148	$R\bar{3}$	672989	Line	$z_{2,3} = 1$ $z_4 = 2$ $z_{2,1} = 1$ $z_{2,2} = 1$
Bi ₂ Pt	147	$P\bar{3}$	58847	Line	$z_{2,3} = 1$ $z_4 = 2$
Ni ₄ Ti ₃	148	$R\bar{3}$	105422	Line	$z_{2,3} = 1$ $z_4 = 2$ $z_{2,1} = 1$ $z_{2,2} = 1$
Ge ₉ Pd ₂₅	147	$P\bar{3}$	637543	Line	$z_{2,3} = 1$ $z_4 = 3$

SM 7. MAJOR UPDATES TO THE TOPOLOGICAL MATERIALS DATABASE

In this section, we will briefly overview the most significant changes implemented on the [Topological Materials Database \(https://www.topologicalquantumchemistry.com/\)](https://www.topologicalquantumchemistry.com/) for this work, following its initial introduction in Ref. 38. To begin, in one of the most significant changes implemented on <https://www.topologicalquantumchemistry.com/> for this work, we have processed the complete set of stoichiometric materials in the ICSD, leading to a current total set of 73,234 ICSD entries on <https://www.topologicalquantumchemistry.com/>.

com/ with electronic structures and topological data in the presence of SOC (see SM 4 for first-principles calculation details). This represents an increase of roughly $\sim 50,000$ ICSD entries from the previous content of <https://www.topologicalquantumchemistry.com/> generated for Ref. 38. Beyond the large increase in the number of listed ICSD entries, we have also for this work implemented the following major changes on <https://www.topologicalquantumchemistry.com/>:

- For the large majority of the ICSD entries accessible on <https://www.topologicalquantumchemistry.com/> (69,730 of 73,234 ICSD entries), the electronic structures and topological data are now available with and without the effects of SOC incorporated (see SM 6).
- The electronic band structure and density of states for each entry on <https://www.topologicalquantumchemistry.com/> are displayed with dynamical zoom options. Additionally, by hovering the pointer over a Bloch state in the electronic structure plot or over an energy in the density of states, contextual information can now be accessed, including the energy and the magnitude of the direct gaps above and below a given Bloch state.
- We have for the first time computed the complete set of symmetry-indicated fragile bands above the core shell [42–45] for each stoichiometric ICSD entry. In each band structure plot, the largest sets of bands with cumulative symmetry-indicated fragile topology are labeled with dashed lines. On each entry on <https://www.topologicalquantumchemistry.com/> with fragile topological bands, we have also provided a table summarizing the details of the fragile bands.
- We have introduced a “Topological Data” table for each entry on <https://www.topologicalquantumchemistry.com/> that lists the symmetry-indicated stable and fragile topology of each connected grouping of bands, as well as the cumulative stable and fragile topology of the total set of bands occupied up to each insulating electronic filling as determined by band connectivity (see SM 2 and SM 8).
- For each electronic structure calculation on <https://www.topologicalquantumchemistry.com/>, we have made the VASP input POSCAR files and the \mathbf{k} -path files available for download through links provided below the crystallographic lattice data.

In addition to the basic search options based on chemical composition and ICSD accession codes previously implemented for Ref. 38, we have for this work implemented advanced materials search criteria (see Fig. S2), which include:

- The SG of the ICSD entry.
- The number of atoms in the unit cell (denoted as “No. of elements”).
- The number of valence electrons.
- The direct and indirect band gaps at E_F .
- The dimensionality (point, line, or plane) of the high-symmetry manifold(s) containing the crossing point(s) at E_F if the bulk at E_F is an enforced topological semimetal (ES- or ESFD-classified).
- The number of times that the bands at E_F cross the Fermi level along the plotted \mathbf{k} -path, subdivided by valence and conduction bands.
- The values of the stable SIs [5, 16, 17, 22, 29, 30, 32–34, 86] if the bulk is an NLC- or SEBR-classified topological (crystalline) insulator at E_F when the effects of SOC are incorporated (see SM 2).

Importantly, users may simultaneously specify several advanced search criteria. For example, users may search for weak TIs that contain the element Bi and have z -directed weak-index vectors [5, 16, 30, 146, 147] by entering Bi into the “Compound Contains” bar while specifying the stable SIs $Z_{2w,1} = 0$, $Z_{2w,2} = 0$, and $Z_{2w,3} = 1$ and either $Z_4 = 0$ or $Z_4 = 2$ in the “Topological Insulator Filters” in the “Advanced Search” drop-down menu (see Fig. S2). Further discussions regarding the differences between $Z_4 = 0$ and $Z_4 = 2$ weak TIs are provided in SM 11 A 6.

After performing a basic or advanced search, users are provided a list of matching ICSD entries sorted by the symmetry-indicated stable topological class at E_F in the presence of SOC [“TI” (NLC or SEBR), “SM” (ES or ESFD), or “Trivial” (LCEBR), see Fig. S2]. After choosing an ICSD entry from the search results, users are redirected to the specific page on <https://www.topologicalquantumchemistry.com/> for the ICSD entry; in Fig. S3 we show as an example the material page on <https://www.topologicalquantumchemistry.com/> for the (obstructed) weak TI Bi_3STe_2 [ICSD 107587, SG 164 ($P\bar{3}m1$)] (see SM 11 A 6 and Refs. 5, 16, 26, 30, 146–149). On the page for each ICSD entry on <https://www.topologicalquantumchemistry.com/>, we provide data including:

- The stoichiometric chemical formula, the SG, the crystal lattice parameters, the topological classification at E_F , a dropdown menu of the other ICSD entries associated to the same unique material (see SM 4), the values of the stable SIs [5, 16, 17, 22, 29, 30, 32–34, 86] if the ICSD entry is NLC- or SEBR-classified at E_F , and, if the bulk at E_F is an enforced topological semimetal (ES- or ESFD-classified), whether the crossing point lies at a high-symmetry point or along a high-symmetry line or plane.
- Interactive 3D plots of the real-space crystal structure and the first BZ.
- Interactive plots of the electronic band structure and the density of states.
- The direct gaps at E_F at the high-symmetry \mathbf{k} points, defined both by occupation as determined by VASP and by band index.
- The “Topological Data” table discussed earlier in this section, which contains the individual and cumulative symmetry-indicated topology of each connected set of bands as determined by the compatibility relations (*i.e.* by band connectivity, see SM 2).
- Information for the largest sets of bands with cumulative symmetry-indicated fragile topology in the electronic structure [42–45].
- If the topological classification at E_F is ES, then we provide a table listing the high-symmetry manifolds along which enforced crossing points are required to appear.
- The stable SIs [5, 16, 17, 22, 29, 30, 32–34, 86] of the lowest-symmetry nonmagnetic NLC and SEBR phases that can be realized by breaking crystal symmetries, computed by subduction onto lower-symmetry SGs as detailed in Refs. 29 and 113. There are two cases in which the “Transitions upon symmetry lowering” table is not displayed. First, the “Transitions upon symmetry lowering,” table is not displayed if the bulk cannot be driven by infinitesimal symmetry-breaking into a nonmagnetic NLC or SEBR phase (*i.e.* if the symmetry-indicated stable topology is trivial for all possible group-subgroup subductions). Second, the “Transitions upon symmetry lowering” table is also absent for ESFD materials that are filling-enforced (semi)metals [see Refs. 129, 150, and 151] with accidental degeneracies at E_F [defined in SM 3 A], which prevent the unambiguous identification of subduced small cores.

Finally, many of the ICSD entries listed on <https://www.topologicalquantumchemistry.com/> are also analyzed on the [Materials Project](#) (MP) [125]. While the [Topological Materials Database](#) introduced in Ref. 38 and expanded in this work focuses on the electronic band topology of a given material, the MP provides a general analysis focused on magnetic, structural, and chemical material properties. For materials that are listed both on <https://www.topologicalquantumchemistry.com/> and on the MP, we provide on each ICSD entry page on <https://www.topologicalquantumchemistry.com/> a link to the corresponding MP page. Additionally, for materials that are listed both on <https://www.topologicalquantumchemistry.com/> and on the MP, the MP entry page extracts and reproduces the topological classification at E_F with SOC from the corresponding ICSD entry page on <https://www.topologicalquantumchemistry.com/>.

SM 8. STATISTICS FOR ALL OF THE TOPOLOGICAL BANDS AND BAND CONNECTIVITY IN THE ICSD

The ICSD contains 193,426 entries [41]. In this work, we have analyzed the complete set of 96,196 ICSD entries with stoichiometric chemical formulas and processable (non-corrupt) CIF structure files, achieving convergent electronic-structure calculations for 73,234 ICSD entries with SOC and 69,730 ICSD entries w/o SOC, corresponding to 38,298 unique materials (see SM 4 for calculation details and for the definition of unique materials employed in this work). In this section, we will provide a detailed statistical breakdown of the symmetry-indicated topological classification of all isolated sets of bands in all of the ICSD entries analyzed in this work as determined by band connectivity through TQC (see SM 2). This includes diagnoses of both symmetry-indicated stable [5, 16, 17, 22, 29, 30, 32–34, 86] and fragile [42, 44, 45] topology across all of the bands included in our first-principles calculations, as well as statistics for and examples of materials with large band connectivities. First, in SM 8 A, we will provide detailed statistics for the stable topological classification at E_F with and w/o SOC of all of the stoichiometric materials in the ICSD. Then, in SM 8 B, we will provide detailed statistics for the stable and fragile topological classification of all of the isolated bands (as defined by band connectivity, see SM 2) in the ICSD. We will also in SM 8 B provide statistics for and examples of materials with extremely large band connectivities.

Topological Materials Database

Total Materials 38184
Topological Insulators 6109
Semi-Metals 13985

NAVIGATION
Search
Predict
About

SETTINGS
UI Mode

Compound Contains Only these elements Exclude

Bi Te eg. O1 N - or - eg. 123456 Search

16 TIs, 9 SMs and 30 Trivials found

Advanced Search

Materials Filters

Symmetry Group

No. of Elements 2 35

No. of distinct Elements 2 5

No. of Electrons 11 272

Direct band gap range (eV) 0 0.400

Indirect band gap range (eV) 0 0.400

Semi-metal Filters

Crossing Type

No. of Fermi level crossings 0 60

No. of valence band crossings 0 13

No. of conduction band crossings 0 10

Topological Insulator Filters

Topological Indices

$Z_{2w,1}$ $Z_{2w,2}$

$Z_{2w,3}$ Z_4

Z_2 $Z_{4\pi}$

Z_8 Z_{3m0}

$Z_{3m\pi}$ Z_{6m0}

$Z_{6\pi}$ Z_{12}

Z'_{12}

55 Entries found for Bi, Te, showing:

ALL (55) TI (16) SM (9) Trivial (30)

Compound	Symmetry Group	Topological Indices	Crossing Type	Type
Bi1 Te1	225 ($Fm-3m$)		Point	ESFD
Bi1 Te1	164 ($P-3m1$)	$Z_{2w,1}=0, Z_{2w,2}=0, Z_{2w,3}=1, Z_4=2$		SEBR
Bi1 Te1	164 ($P-3m1$)	$Z_{2w,1}=0, Z_{2w,2}=0, Z_{2w,3}=1, Z_4=0$		SEBR
Bi2 Te3	160 ($R3m$)			LCEBR

Figure S2. A screenshot of the search interface of the updated Topological Materials Database (<https://www.topologicalquantumchemistry.com/>). The top three search bars allow basic search options based on chemical composition and ICSD accession codes. For this work, we have additionally implemented the “Advanced Search” features displayed below the “Back to Periodic Table” button, which are further detailed in this section.

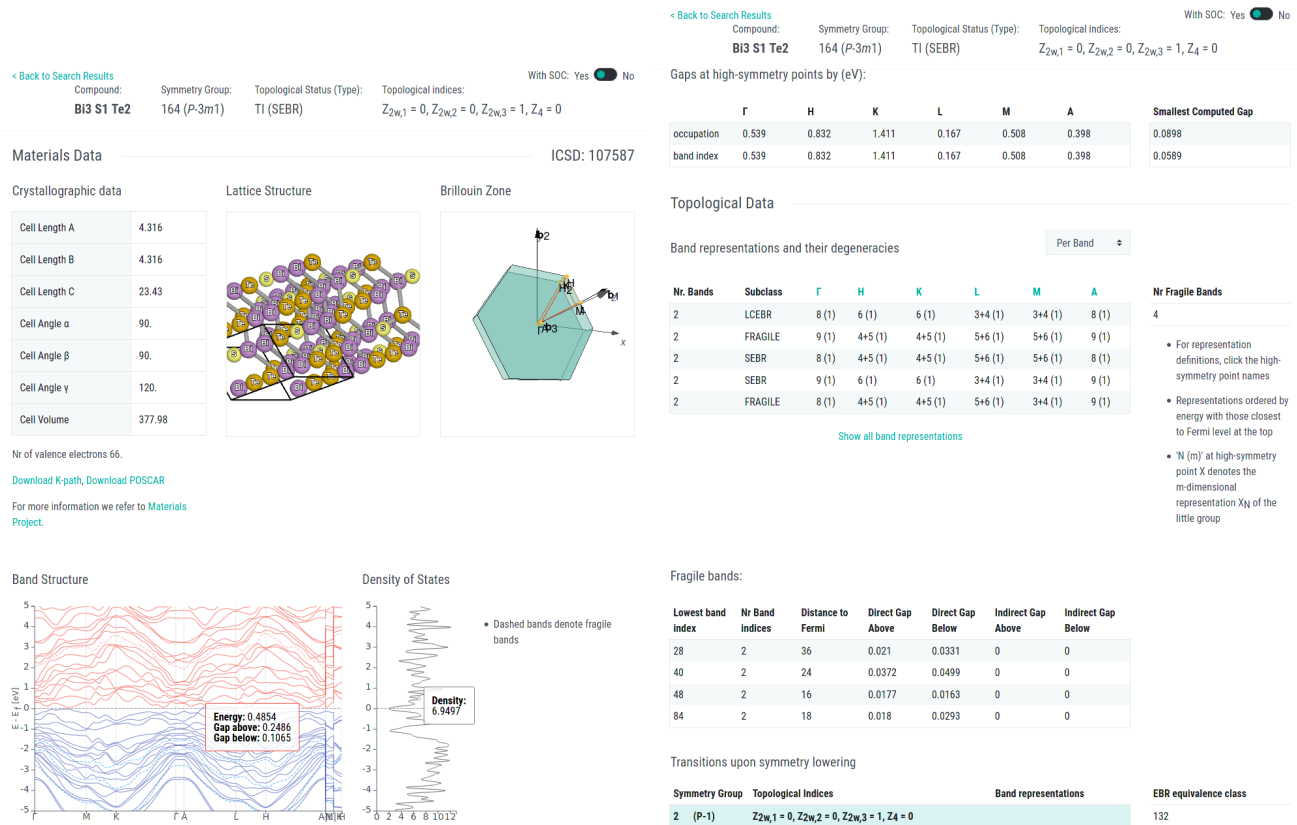


Figure S3. An ICSD entry page on <https://www.topologicalquantumchemistry.com/>. We have chosen as an example the (obstructed) weak TI $\text{Bi}_3\text{S1Te}_2$ [ICSD 107587, SG 164 ($P\bar{3}m1$)] (see SM 11 A 6 and Refs. 5, 16, 26, 30, 146–149). *Left panel* We first list the chemical formula, SG, topological classification at E_F , the stable SIs if the topological classification at E_F is NLC (-SM) or SEBR (-SM) [see SM 2 and SM 6], and, if the bulk at E_F is an enforced topological semimetal (ES- or ESFD-classified), whether the crossing point lies at a high-symmetry point or along a high-symmetry line or plane. On the top-left corner, there is a switch that allows users to toggle between the electronic structures and topological data for the same ICSD entry computed with and without incorporating the effects of SOC. We then display the “Materials Data” for the ICSD entry, which consists of the ICSD accession code, a dropdown list of all other ICSD entries associated to the same unique material (see SM 4), the crystallographic lattice data, interactive plots of the real-space unit cell and the first BZ, and the number of valence electrons. For ICSD entries that are also listed on the [Materials Project](#) (MP) [125], we additionally provide a link to the corresponding page on the MP. Lastly, below the Materials Data, we provide interactive band structure and density-of-states plots. *Right panel* A continuation of the example page on <https://www.topologicalquantumchemistry.com/> shown in the left panel. We first list the direct gaps at E_F at the high-symmetry \mathbf{k} points, defined both by occupation as determined by VASP and by band index. We then list the “Topological Data” table discussed in this section. Next, we list information for the largest sets of bands with cumulative symmetry-indicated fragile topology in the electronic structure [42–45]. Next, if the topological classification at E_F is ES, then we provide a table listing the high-symmetry manifolds along which enforced crossing points are required to appear. Lastly, using subduction onto lower-symmetry SGs as detailed in Refs. 29 and 113, we compute the stable SIs [5, 16, 17, 22, 29, 30, 32–34, 86] of the lowest-symmetry nonmagnetic NLC and SEBR phases that can be realized by breaking crystal symmetries. If the “Transitions upon symmetry lowering” table is not displayed, then the bulk cannot be driven by infinitesimal symmetry-breaking into a nonmagnetic NLC or SEBR phase, or is a filling-enforced, ESFD-classified (semi)metal [see Refs. 129, 150, and 151] with at least one accidental degeneracy at E_F [defined in SM 3 A].

A. Topological Classification at the Fermi Level for all of the Stoichiometric Unique Materials in the ICSD with and w/o SOC

In this section, we will provide statistics for the topological classification at the Fermi level for the unique materials studied in this work (defined in the main text and in SM 4). Specifically, in Table S14 (Table S15), we list the number of materials whose valence bands are in total classified by one of the four stable topological classes introduced in Ref. 38: NLC (-SM), SEBR (-SM), ES, and ESFD. We note that, using the symmetry-based indicators for fragile topology introduced in Refs. 42, 44, and 45, we did not identify any ICSD entries in which the total set of occupied (valence) bands was fragile topological with or w/o SOC (though we did identify energetically-isolated fragile bands near the Fermi energy in many materials, see SM 8 B and SM 11 E).

Table S14: The number of unique materials in each of the topological classes (as defined in the main text and in Ref. 38) in calculations performed with SOC. In this table, the topology of a material is taken to be the total (cumulative) topology of all of the bands occupied up to E_F . In order, the columns in this table list the SG, the number of unique materials in the SG, the number of TIs and TCIs (defined as either NLC or SEBR) in the SG, the number of semimetals (SMs) in the SG (defined as either ES or ESFD), the number of unique materials with trivial symmetry-inducted topology (LCEBR) in the SG, the number of NLC-classified TIs and TCIs in the SG, the number of SEBR-classified TIs and TCIs in the SG, the number of ES-classified SMs in the SG, and the number of ESFD-classified SMs in the SG. For all of the topological classification categories in the table, each number of materials is accompanied by the percentage of materials in the SG in the topological class. When there are no materials in the topological class, the table entry is marked with a dashed horizontal line.

SG	# Mat.	TIs	SMs	Trivial	NLC	SEBR	ES	ESFD
1	151	—	9 (6.0%)	142 (94.0%)	—	—	—	9 (6.0%)
2	1574	182 (11.6%)	116 (7.4%)	1276 (81.1%)	182 (11.6%)	—	—	116 (7.4%)
3	13	—	—	13 (100%)	—	—	—	—
4	228	—	8 (3.5%)	220 (96.5%)	—	—	8 (3.5%)	—
5	156	—	15 (9.6%)	141 (90.4%)	—	—	—	15 (9.6%)
6	28	—	1 (3.6%)	27 (96.4%)	—	—	—	1 (3.6%)
7	85	—	3 (3.5%)	82 (96.5%)	—	—	3 (3.5%)	—
8	144	—	13 (9.0%)	131 (91.0%)	—	—	—	13 (9.0%)
9	199	—	11 (5.5%)	188 (94.5%)	—	—	11 (5.5%)	—
10	38	20 (52.6%)	5 (13.2%)	13 (34.2%)	20 (52.6%)	—	—	5 (13.2%)
11	587	95 (16.2%)	105 (17.9%)	387 (65.9%)	95 (16.2%)	—	—	105 (17.9%)
12	1345	432 (32.1%)	204 (15.2%)	709 (52.7%)	219 (16.3%)	213 (15.8%)	—	204 (15.2%)
13	195	20 (10.3%)	36 (18.5%)	139 (71.3%)	20 (10.3%)	—	—	36 (18.5%)
14	2665	298 (11.2%)	224 (8.4%)	2143 (80.4%)	298 (11.2%)	—	74 (2.8%)	150 (5.6%)
15	1485	122 (8.2%)	200 (13.5%)	1163 (78.3%)	122 (8.2%)	—	—	200 (13.5%)
16	2	—	—	2 (100%)	—	—	—	—
17	8	—	—	8 (100%)	—	—	—	—
18	30	—	2 (6.7%)	28 (93.3%)	—	—	—	2 (6.7%)
19	270	—	20 (7.4%)	250 (92.6%)	—	—	20 (7.4%)	—
20	66	—	2 (3.0%)	64 (97.0%)	—	—	2 (3.0%)	—
21	16	—	6 (37.5%)	10 (62.5%)	—	—	—	6 (37.5%)
22	17	—	—	17 (100%)	—	—	—	—
23	16	—	2 (12.5%)	14 (87.5%)	—	—	—	2 (12.5%)
24	2	—	—	2 (100%)	—	—	—	—
25	45	—	2 (4.4%)	43 (95.6%)	—	—	—	2 (4.4%)
26	60	—	4 (6.7%)	56 (93.3%)	—	—	—	4 (6.7%)
27	1	—	—	1 (100%)	—	—	—	—
28	11	—	2 (18.2%)	9 (81.8%)	—	—	2 (18.2%)	—
29	61	—	1 (1.6%)	60 (98.4%)	—	—	1 (1.6%)	—
30	5	—	1 (20.0%)	4 (80.0%)	—	—	—	1 (20.0%)
31	159	—	14 (8.8%)	145 (91.2%)	—	—	—	14 (8.8%)
32	10	—	—	10 (100%)	—	—	—	—
33	257	—	24 (9.3%)	233 (90.7%)	—	—	24 (9.3%)	—
34	21	—	3 (14.3%)	18 (85.7%)	—	—	—	3 (14.3%)
35	8	—	2 (25.0%)	6 (75.0%)	—	—	—	2 (25.0%)

36	261	—	40 (15.3%)	221 (84.7%)	—	—	—	40 (15.3%)
37	5	—	—	5 (100%)	—	—	—	—
38	104	—	33 (31.7%)	71 (68.3%)	—	—	—	33 (31.7%)
39	13	—	—	13 (100%)	—	—	—	—
40	57	—	5 (8.8%)	52 (91.2%)	—	—	5 (8.8%)	—
41	31	—	1 (3.2%)	30 (96.8%)	—	—	1 (3.2%)	—
42	4	—	—	4 (100%)	—	—	—	—
43	84	—	13 (15.5%)	71 (84.5%)	—	—	—	13 (15.5%)
44	69	—	11 (15.9%)	58 (84.1%)	—	—	—	11 (15.9%)
45	8	—	—	8 (100%)	—	—	—	—
46	57	—	7 (12.3%)	50 (87.7%)	—	—	7 (12.3%)	—
47	51	31 (60.8%)	13 (25.5%)	7 (13.7%)	31 (60.8%)	—	—	13 (25.5%)
48	3	—	—	3 (100%)	—	—	—	—
49	1	—	—	1 (100%)	—	—	—	—
50	7	4 (57.1%)	—	3 (42.9%)	3 (42.9%)	1 (14.3%)	—	—
51	107	47 (43.9%)	36 (33.6%)	24 (22.4%)	47 (43.9%)	—	—	36 (33.6%)
52	39	1 (2.6%)	4 (10.3%)	34 (87.2%)	1 (2.6%)	—	4 (10.3%)	—
53	18	2 (11.1%)	3 (16.7%)	13 (72.2%)	—	2 (11.1%)	—	3 (16.7%)
54	19	4 (21.1%)	2 (10.5%)	13 (68.4%)	4 (21.1%)	—	2 (10.5%)	—
55	394	217 (55.1%)	45 (11.4%)	132 (33.5%)	217 (55.1%)	—	—	45 (11.4%)
56	19	—	4 (21.1%)	15 (79.0%)	—	—	4 (21.1%)	—
57	142	34 (23.9%)	18 (12.7%)	90 (63.4%)	34 (23.9%)	—	18 (12.7%)	—
58	208	41 (19.7%)	47 (22.6%)	120 (57.7%)	41 (19.7%)	—	12 (5.8%)	35 (16.8%)
59	227	70 (30.8%)	72 (31.7%)	85 (37.4%)	32 (14.1%)	38 (16.7%)	—	72 (31.7%)
60	142	14 (9.9%)	11 (7.8%)	117 (82.4%)	14 (9.9%)	—	11 (7.8%)	—
61	122	10 (8.2%)	6 (4.9%)	106 (86.9%)	10 (8.2%)	—	6 (4.9%)	—
62	3006	693 (23.1%)	692 (23.0%)	1621 (53.9%)	693 (23.1%)	—	692 (23.0%)	—
63	1396	466 (33.4%)	490 (35.1%)	440 (31.5%)	271 (19.4%)	195 (14.0%)	—	490 (35.1%)
64	257	59 (23.0%)	46 (17.9%)	152 (59.1%)	—	59 (23.0%)	6 (2.3%)	40 (15.6%)
65	241	135 (56.0%)	73 (30.3%)	33 (13.7%)	77 (31.9%)	58 (24.1%)	—	73 (30.3%)
66	36	6 (16.7%)	9 (25.0%)	21 (58.3%)	6 (16.7%)	—	—	9 (25.0%)
67	30	10 (33.3%)	6 (20.0%)	14 (46.7%)	10 (33.3%)	—	—	6 (20.0%)
68	19	—	4 (21.1%)	15 (79.0%)	—	—	—	4 (21.1%)
69	66	23 (34.9%)	18 (27.3%)	25 (37.9%)	—	23 (34.9%)	—	18 (27.3%)
70	139	32 (23.0%)	11 (7.9%)	96 (69.1%)	—	32 (23.0%)	—	11 (7.9%)
71	452	188 (41.6%)	162 (35.8%)	102 (22.6%)	—	188 (41.6%)	—	162 (35.8%)
72	192	45 (23.4%)	58 (30.2%)	89 (46.4%)	30 (15.6%)	15 (7.8%)	—	58 (30.2%)
73	24	2 (8.3%)	3 (12.5%)	19 (79.2%)	2 (8.3%)	—	3 (12.5%)	—
74	218	64 (29.4%)	80 (36.7%)	74 (33.9%)	64 (29.4%)	—	—	80 (36.7%)
75	5	—	2 (40.0%)	3 (60.0%)	—	—	—	2 (40.0%)
76	12	—	2 (16.7%)	10 (83.3%)	—	—	2 (16.7%)	—
77	2	—	—	2 (100%)	—	—	—	—
78	2	—	—	2 (100%)	—	—	—	—
79	11	—	1 (9.1%)	10 (90.9%)	—	—	1 (9.1%)	—
80	3	—	—	3 (100%)	—	—	—	—
81	14	—	—	14 (100%)	—	—	—	—
82	136	18 (13.2%)	11 (8.1%)	107 (78.7%)	18 (13.2%)	—	1 (0.7%)	10 (7.3%)
83	10	5 (50.0%)	4 (40.0%)	1 (10.0%)	2 (20.0%)	3 (30.0%)	4 (40.0%)	—
84	28	2 (7.1%)	5 (17.9%)	21 (75.0%)	2 (7.1%)	—	3 (10.7%)	2 (7.1%)
85	39	4 (10.3%)	10 (25.6%)	25 (64.1%)	—	4 (10.3%)	2 (5.1%)	8 (20.5%)
86	51	10 (19.6%)	28 (54.9%)	13 (25.5%)	—	10 (19.6%)	17 (33.3%)	11 (21.6%)
87	181	22 (12.2%)	86 (47.5%)	73 (40.3%)	—	22 (12.2%)	23 (12.7%)	63 (34.8%)
88	139	7 (5.0%)	21 (15.1%)	111 (79.9%)	—	7 (5.0%)	4 (2.9%)	17 (12.2%)
89	5	—	2 (40.0%)	3 (60.0%)	—	—	—	2 (40.0%)
90	7	—	1 (14.3%)	6 (85.7%)	—	—	1 (14.3%)	—
91	47	—	16 (34.0%)	31 (66.0%)	—	—	11 (23.4%)	5 (10.6%)
92	1	—	—	1 (100%)	—	—	—	—
93	3	—	1 (33.3%)	2 (66.7%)	—	—	1 (33.3%)	—
94	16	—	1 (6.2%)	15 (93.8%)	—	—	1 (6.2%)	—
95	2	—	1 (50.0%)	1 (50.0%)	—	—	1 (50.0%)	—
96	4	—	—	4 (100%)	—	—	—	—
97	98	—	22 (22.4%)	76 (77.5%)	—	—	7 (7.1%)	15 (15.3%)
98	20	—	12 (60.0%)	8 (40.0%)	—	—	1 (5.0%)	11 (55.0%)
99	12	—	3 (25.0%)	9 (75.0%)	—	—	2 (16.7%)	1 (8.3%)

103	3	—	3 (100%)	—	—	—	—	3 (100%)
104	3	—	1 (33.3%)	2 (66.7%)	—	—	—	1 (33.3%)
105	4	—	—	4 (100%)	—	—	—	—
106	1	—	1 (100%)	—	—	—	1 (100%)	—
107	121	—	68 (56.2%)	53 (43.8%)	—	—	16 (13.2%)	52 (43.0%)
108	15	—	5 (33.3%)	10 (66.7%)	—	—	2 (13.3%)	3 (20.0%)
109	40	—	16 (40.0%)	24 (60.0%)	—	—	1 (2.5%)	15 (37.5%)
110	8	—	2 (25.0%)	6 (75.0%)	—	—	2 (25.0%)	—
111	21	1 (4.8%)	4 (19.1%)	16 (76.2%)	—	1 (4.8%)	—	4 (19.1%)
112	4	—	—	4 (100%)	—	—	—	—
113	84	6 (7.1%)	20 (23.8%)	58 (69.0%)	6 (7.1%)	—	—	20 (23.8%)
114	31	2 (6.5%)	1 (3.2%)	28 (90.3%)	—	2 (6.5%)	1 (3.2%)	—
115	21	4 (19.1%)	6 (28.6%)	11 (52.4%)	—	4 (19.1%)	—	6 (28.6%)
116	17	1 (5.9%)	—	16 (94.1%)	—	1 (5.9%)	—	—
117	11	1 (9.1%)	1 (9.1%)	9 (81.8%)	1 (9.1%)	—	—	1 (9.1%)
118	11	1 (9.1%)	1 (9.1%)	9 (81.8%)	1 (9.1%)	—	—	1 (9.1%)
119	35	2 (5.7%)	6 (17.1%)	27 (77.1%)	2 (5.7%)	—	—	6 (17.1%)
120	15	2 (13.3%)	2 (13.3%)	11 (73.3%)	2 (13.3%)	—	2 (13.3%)	—
121	126	19 (15.1%)	20 (15.9%)	87 (69.0%)	—	19 (15.1%)	—	20 (15.9%)
122	124	16 (12.9%)	10 (8.1%)	98 (79.0%)	—	16 (12.9%)	2 (1.6%)	8 (6.5%)
123	473	90 (19.0%)	313 (66.2%)	70 (14.8%)	52 (11.0%)	38 (8.0%)	98 (20.7%)	215 (45.5%)
124	23	1 (4.3%)	19 (82.6%)	3 (13.0%)	1 (4.3%)	—	7 (30.4%)	12 (52.2%)
125	52	11 (21.1%)	24 (46.1%)	17 (32.7%)	5 (9.6%)	6 (11.5%)	10 (19.2%)	14 (26.9%)
126	12	—	5 (41.7%)	7 (58.3%)	—	—	3 (25.0%)	2 (16.7%)
127	403	71 (17.6%)	282 (70.0%)	50 (12.4%)	71 (17.6%)	—	109 (27.1%)	173 (42.9%)
128	76	15 (19.7%)	34 (44.7%)	27 (35.5%)	—	15 (19.7%)	24 (31.6%)	10 (13.2%)
129	884	230 (26.0%)	435 (49.2%)	219 (24.8%)	108 (12.2%)	122 (13.8%)	102 (11.5%)	333 (37.7%)
130	38	4 (10.5%)	13 (34.2%)	21 (55.3%)	3 (7.9%)	1 (2.6%)	3 (7.9%)	10 (26.3%)
131	44	7 (15.9%)	27 (61.4%)	10 (22.7%)	7 (15.9%)	—	10 (22.7%)	17 (38.6%)
132	10	—	1 (10.0%)	9 (90.0%)	—	—	1 (10.0%)	—
133	3	1 (33.3%)	1 (33.3%)	1 (33.3%)	1 (33.3%)	—	1 (33.3%)	—
134	4	—	3 (75.0%)	1 (25.0%)	—	—	—	3 (75.0%)
135	30	5 (16.7%)	11 (36.7%)	14 (46.7%)	5 (16.7%)	—	8 (26.7%)	3 (10.0%)
136	266	38 (14.3%)	135 (50.8%)	93 (35.0%)	—	38 (14.3%)	76 (28.6%)	59 (22.2%)
137	70	10 (14.3%)	27 (38.6%)	33 (47.1%)	—	10 (14.3%)	10 (14.3%)	17 (24.3%)
138	22	4 (18.2%)	3 (13.6%)	15 (68.2%)	4 (18.2%)	—	3 (13.6%)	—
139	1622	493 (30.4%)	900 (55.5%)	229 (14.1%)	—	493 (30.4%)	307 (18.9%)	593 (36.6%)
140	457	86 (18.8%)	243 (53.2%)	128 (28.0%)	56 (12.2%)	30 (6.6%)	68 (14.9%)	175 (38.3%)
141	267	57 (21.4%)	108 (40.5%)	102 (38.2%)	—	57 (21.4%)	27 (10.1%)	81 (30.3%)
142	77	10 (13.0%)	25 (32.5%)	42 (54.5%)	—	10 (13.0%)	15 (19.5%)	10 (13.0%)
143	18	—	5 (27.8%)	13 (72.2%)	—	—	2 (11.1%)	3 (16.7%)
144	13	—	1 (7.7%)	12 (92.3%)	—	—	—	1 (7.7%)
145	5	—	—	5 (100%)	—	—	—	—
146	87	—	15 (17.2%)	72 (82.8%)	—	—	5 (5.8%)	10 (11.5%)
147	75	8 (10.7%)	9 (12.0%)	58 (77.3%)	—	8 (10.7%)	6 (8.0%)	3 (4.0%)
148	496	70 (14.1%)	142 (28.6%)	284 (57.3%)	—	70 (14.1%)	34 (6.8%)	108 (21.8%)
149	10	—	3 (30.0%)	7 (70.0%)	—	—	1 (10.0%)	2 (20.0%)
150	66	—	11 (16.7%)	55 (83.3%)	—	—	3 (4.5%)	8 (12.1%)
151	5	—	—	5 (100%)	—	—	—	—
152	42	—	12 (28.6%)	30 (71.4%)	—	—	3 (7.1%)	9 (21.4%)
153	2	—	—	2 (100%)	—	—	—	—
154	19	—	2 (10.5%)	17 (89.5%)	—	—	1 (5.3%)	1 (5.3%)
155	54	—	12 (22.2%)	42 (77.8%)	—	—	3 (5.6%)	9 (16.7%)
156	57	—	13 (22.8%)	44 (77.2%)	—	—	7 (12.3%)	6 (10.5%)
157	16	—	3 (18.8%)	13 (81.2%)	—	—	1 (6.2%)	2 (12.5%)
158	3	—	2 (66.7%)	1 (33.3%)	—	—	1 (33.3%)	1 (33.3%)
159	26	—	6 (23.1%)	20 (76.9%)	—	—	4 (15.4%)	2 (7.7%)
160	160	—	42 (26.2%)	118 (73.8%)	—	—	7 (4.4%)	35 (21.9%)
161	87	—	15 (17.2%)	72 (82.8%)	—	—	8 (9.2%)	7 (8.1%)
162	54	7 (13.0%)	20 (37.0%)	27 (50.0%)	—	7 (13.0%)	8 (14.8%)	12 (22.2%)
163	63	5 (7.9%)	21 (33.3%)	37 (58.7%)	—	5 (7.9%)	8 (12.7%)	13 (20.6%)
164	598	113 (18.9%)	207 (34.6%)	278 (46.5%)	—	113 (18.9%)	48 (8.0%)	159 (26.6%)
165	34	4 (11.8%)	16 (47.1%)	14 (41.2%)	—	4 (11.8%)	7 (20.6%)	9 (26.5%)
166	1029	216 (21.0%)	415 (40.3%)	398 (38.7%)	—	216 (21.0%)	112 (10.9%)	303 (29.4%)

167	325	16 (4.9%)	108 (33.2%)	201 (61.9%)	—	16 (4.9%)	32 (9.8%)	76 (23.4%)
169	1	—	—	1 (100%)	—	—	—	—
173	124	—	42 (33.9%)	82 (66.1%)	—	—	39 (31.4%)	3 (2.4%)
174	59	—	42 (71.2%)	17 (28.8%)	—	—	3 (5.1%)	39 (66.1%)
175	2	—	2 (100%)	—	—	—	—	2 (100%)
176	206	6 (2.9%)	82 (39.8%)	118 (57.3%)	—	6 (2.9%)	24 (11.7%)	58 (28.2%)
177	1	—	—	1 (100%)	—	—	—	—
180	28	—	16 (57.1%)	12 (42.9%)	—	—	6 (21.4%)	10 (35.7%)
181	8	—	4 (50.0%)	4 (50.0%)	—	—	1 (12.5%)	3 (37.5%)
182	34	—	22 (64.7%)	12 (35.3%)	—	—	20 (58.8%)	2 (5.9%)
183	1	—	—	1 (100%)	—	—	—	—
185	51	—	29 (56.9%)	22 (43.1%)	—	—	13 (25.5%)	16 (31.4%)
186	392	—	206 (52.5%)	186 (47.5%)	—	—	76 (19.4%)	130 (33.2%)
187	158	13 (8.2%)	111 (70.2%)	34 (21.5%)	13 (8.2%)	—	51 (32.3%)	60 (38.0%)
188	21	—	5 (23.8%)	16 (76.2%)	—	—	2 (9.5%)	3 (14.3%)
189	592	118 (19.9%)	418 (70.6%)	56 (9.5%)	—	118 (19.9%)	138 (23.3%)	280 (47.3%)
190	45	4 (8.9%)	23 (51.1%)	18 (40.0%)	4 (8.9%)	—	5 (11.1%)	18 (40.0%)
191	506	81 (16.0%)	420 (83.0%)	5 (1.0%)	—	81 (16.0%)	194 (38.3%)	226 (44.7%)
192	2	—	—	2 (100%)	—	—	—	—
193	302	15 (5.0%)	268 (88.7%)	19 (6.3%)	—	15 (5.0%)	114 (37.8%)	154 (51.0%)
194	1619	220 (13.6%)	1120 (69.2%)	279 (17.2%)	—	220 (13.6%)	594 (36.7%)	526 (32.5%)
195	1	—	—	1 (100%)	—	—	—	—
196	1	—	1 (100%)	—	—	—	—	1 (100%)
197	20	—	9 (45.0%)	11 (55.0%)	—	—	—	9 (45.0%)
198	173	—	78 (45.1%)	95 (54.9%)	—	—	2 (1.2%)	76 (43.9%)
199	33	—	8 (24.2%)	25 (75.8%)	—	—	1 (3.0%)	7 (21.2%)
200	22	3 (13.6%)	14 (63.6%)	5 (22.7%)	—	3 (13.6%)	—	14 (63.6%)
201	7	1 (14.3%)	3 (42.9%)	3 (42.9%)	—	1 (14.3%)	—	3 (42.9%)
202	18	—	10 (55.6%)	8 (44.4%)	—	—	—	10 (55.6%)
203	6	—	1 (16.7%)	5 (83.3%)	—	—	1 (16.7%)	—
204	151	12 (8.0%)	109 (72.2%)	30 (19.9%)	—	12 (8.0%)	—	109 (72.2%)
205	130	9 (6.9%)	38 (29.2%)	83 (63.9%)	9 (6.9%)	—	4 (3.1%)	34 (26.1%)
206	61	11 (18.0%)	17 (27.9%)	33 (54.1%)	—	11 (18.0%)	2 (3.3%)	15 (24.6%)
208	2	—	—	2 (100%)	—	—	—	—
210	1	—	1 (100%)	—	—	—	—	1 (100%)
211	1	—	1 (100%)	—	—	—	—	1 (100%)
212	14	—	8 (57.1%)	6 (42.9%)	—	—	3 (21.4%)	5 (35.7%)
213	22	—	17 (77.3%)	5 (22.7%)	—	—	3 (13.6%)	14 (63.6%)
214	14	—	8 (57.1%)	6 (42.9%)	—	—	1 (7.1%)	7 (50.0%)
215	54	3 (5.6%)	13 (24.1%)	38 (70.4%)	—	3 (5.6%)	—	13 (24.1%)
216	777	69 (8.9%)	458 (58.9%)	250 (32.2%)	69 (8.9%)	—	24 (3.1%)	434 (55.9%)
217	111	6 (5.4%)	55 (49.5%)	50 (45.0%)	—	6 (5.4%)	1 (0.9%)	54 (48.6%)
218	42	1 (2.4%)	11 (26.2%)	30 (71.4%)	—	1 (2.4%)	6 (14.3%)	5 (11.9%)
219	9	—	3 (33.3%)	6 (66.7%)	—	—	2 (22.2%)	1 (11.1%)
220	143	11 (7.7%)	102 (71.3%)	30 (21.0%)	11 (7.7%)	—	2 (1.4%)	100 (69.9%)
221	1352	133 (9.8%)	1059 (78.3%)	160 (11.8%)	4 (0.3%)	129 (9.5%)	163 (12.1%)	896 (66.3%)
223	222	9 (4.0%)	210 (94.6%)	3 (1.4%)	—	9 (4.0%)	47 (21.2%)	163 (73.4%)
224	17	—	11 (64.7%)	6 (35.3%)	—	—	2 (11.8%)	9 (52.9%)
225	1693	183 (10.8%)	1112 (65.7%)	398 (23.5%)	—	183 (10.8%)	175 (10.3%)	937 (55.4%)
226	46	2 (4.3%)	43 (93.5%)	1 (2.2%)	—	2 (4.3%)	7 (15.2%)	36 (78.3%)
227	841	148 (17.6%)	498 (59.2%)	195 (23.2%)	—	148 (17.6%)	149 (17.7%)	349 (41.5%)
229	210	7 (3.3%)	182 (86.7%)	21 (10.0%)	—	7 (3.3%)	18 (8.6%)	164 (78.1%)
230	6	1 (16.7%)	4 (66.7%)	1 (16.7%)	—	1 (16.7%)	1 (16.7%)	3 (50.0%)
Total	38298	6128 (16.0%)	14037 (36.6%)	18133 (47.4%)	3000 (7.8%)	3128 (8.2%)	4102 (10.7%)	9935 (25.9%)

Table S15: The number of unique materials in each of the topological classes (as defined in the main text and in SM 6) in calculations performed w/o SOC. In this table, the topology of a material is taken to be the total (cumulative) topology of all of the bands occupied up to E_F . In order, the columns in this table list the SG, the number of unique materials in the SG (which we emphasize to be defined using the topological classification with SOC, see SM 4), the number of semimetals (SMs) in the SG (defined as either NLC-SM, SEBR-SM, ES, or ESFD), the number of unique materials with trivial symmetry-inducted topology (LCEBR) in the SG, the number of NLC-SM-classified SMs in the SG, the number of SEBR-SM-classified SMs in the SG, the number of ES-classified SMs in the SG, and the number of ESFD-classified SMs in the SG. For all of the topological classification categories in the table, each number of materials is accompanied by the percentage of materials in the SG in the topological class. When there are no materials in the topological class, the table entry is marked with a dashed horizontal line.

SG	# Mat.	SMs	Trivial	NLC-SM	SEBR-SM	ES	ESFD
1	151	9 (6.0%)	142 (94.0%)	—	—	—	9 (6.0%)
2	1466	277 (18.9%)	1189 (81.1%)	165 (11.3%)	—	—	112 (7.6%)
3	10	7 (70.0%)	3 (30.0%)	—	—	7 (70.0%)	—
4	219	20 (9.1%)	199 (90.9%)	—	—	14 (6.4%)	6 (2.7%)
5	148	31 (20.9%)	117 (79.0%)	—	—	19 (12.8%)	12 (8.1%)
6	28	5 (17.9%)	23 (82.1%)	—	—	4 (14.3%)	1 (3.6%)
7	85	9 (10.6%)	76 (89.4%)	—	—	6 (7.1%)	3 (3.5%)
8	141	26 (18.4%)	115 (81.6%)	—	—	14 (9.9%)	12 (8.5%)
9	197	15 (7.6%)	182 (92.4%)	—	—	4 (2.0%)	11 (5.6%)
10	33	21 (63.6%)	12 (36.4%)	—	—	16 (48.5%)	5 (15.2%)
11	547	197 (36.0%)	350 (64.0%)	4 (0.7%)	—	97 (17.7%)	96 (17.6%)
12	1250	621 (49.7%)	629 (50.3%)	24 (1.9%)	—	406 (32.5%)	191 (15.3%)
13	164	42 (25.6%)	122 (74.4%)	1 (0.6%)	—	21 (12.8%)	20 (12.2%)
14	2520	491 (19.5%)	2029 (80.5%)	24 (0.9%)	—	330 (13.1%)	137 (5.4%)
15	1402	332 (23.7%)	1070 (76.3%)	22 (1.6%)	—	137 (9.8%)	173 (12.3%)
16	2	1 (50.0%)	1 (50.0%)	—	—	1 (50.0%)	—
17	8	3 (37.5%)	5 (62.5%)	—	—	3 (37.5%)	—
18	30	6 (20.0%)	24 (80.0%)	—	—	4 (13.3%)	2 (6.7%)
19	261	28 (10.7%)	233 (89.3%)	—	—	9 (3.5%)	19 (7.3%)
20	58	5 (8.6%)	53 (91.4%)	—	—	3 (5.2%)	2 (3.5%)
21	15	9 (60.0%)	6 (40.0%)	—	—	3 (20.0%)	6 (40.0%)
22	14	11 (78.6%)	3 (21.4%)	—	—	11 (78.6%)	—
23	15	5 (33.3%)	10 (66.7%)	—	—	3 (20.0%)	2 (13.3%)
24	2	—	2 (100%)	—	—	—	—
25	45	14 (31.1%)	31 (68.9%)	—	—	12 (26.7%)	2 (4.4%)
26	59	12 (20.3%)	47 (79.7%)	—	—	8 (13.6%)	4 (6.8%)
27	1	—	1 (100%)	—	—	—	—
28	11	7 (63.6%)	4 (36.4%)	—	—	5 (45.5%)	2 (18.2%)
29	59	2 (3.4%)	57 (96.6%)	—	—	1 (1.7%)	1 (1.7%)
30	5	2 (40.0%)	3 (60.0%)	—	—	1 (20.0%)	1 (20.0%)
31	158	33 (20.9%)	125 (79.1%)	—	—	19 (12.0%)	14 (8.9%)
32	10	—	10 (100%)	—	—	—	—
33	251	43 (17.1%)	208 (82.9%)	—	—	20 (8.0%)	23 (9.2%)
34	21	5 (23.8%)	16 (76.2%)	—	—	2 (9.5%)	3 (14.3%)
35	8	4 (50.0%)	4 (50.0%)	—	—	2 (25.0%)	2 (25.0%)
36	241	53 (22.0%)	188 (78.0%)	—	—	21 (8.7%)	32 (13.3%)
37	5	—	5 (100%)	—	—	—	—
38	95	69 (72.6%)	26 (27.4%)	—	—	38 (40.0%)	31 (32.6%)
39	12	3 (25.0%)	9 (75.0%)	—	—	3 (25.0%)	—
40	54	7 (13.0%)	47 (87.0%)	—	—	3 (5.6%)	4 (7.4%)
41	31	10 (32.3%)	21 (67.7%)	—	—	9 (29.0%)	1 (3.2%)
42	4	—	4 (100%)	—	—	—	—
43	83	21 (25.3%)	62 (74.7%)	—	—	8 (9.6%)	13 (15.7%)
44	62	35 (56.5%)	27 (43.5%)	—	—	24 (38.7%)	11 (17.7%)
45	8	2 (25.0%)	6 (75.0%)	—	—	2 (25.0%)	—

46	55	30 (54.5%)	25 (45.5%)	—	—	23 (41.8%)	7 (12.7%)
47	45	42 (93.3%)	3 (6.7%)	—	—	29 (64.4%)	13 (28.9%)
48	3	1 (33.3%)	2 (66.7%)	—	—	1 (33.3%)	—
50	7	5 (71.4%)	2 (28.6%)	—	—	5 (71.4%)	—
51	100	77 (77.0%)	23 (23.0%)	—	—	42 (42.0%)	35 (35.0%)
52	36	4 (11.1%)	32 (88.9%)	—	—	—	4 (11.1%)
53	18	6 (33.3%)	12 (66.7%)	—	—	3 (16.7%)	3 (16.7%)
54	18	6 (33.3%)	12 (66.7%)	—	—	4 (22.2%)	2 (11.1%)
55	336	252 (75.0%)	84 (25.0%)	—	—	211 (62.8%)	41 (12.2%)
56	19	5 (26.3%)	14 (73.7%)	—	—	1 (5.3%)	4 (21.1%)
57	128	48 (37.5%)	80 (62.5%)	—	—	31 (24.2%)	17 (13.3%)
58	202	98 (48.5%)	104 (51.5%)	1 (0.5%)	—	62 (30.7%)	35 (17.3%)
59	208	143 (68.8%)	65 (31.2%)	—	—	78 (37.5%)	65 (31.2%)
60	139	30 (21.6%)	109 (78.4%)	1 (0.7%)	—	20 (14.4%)	9 (6.5%)
61	119	18 (15.1%)	101 (84.9%)	—	—	16 (13.4%)	2 (1.7%)
62	2800	1451 (51.8%)	1349 (48.2%)	—	—	777 (27.8%)	674 (24.1%)
63	1277	924 (72.4%)	353 (27.6%)	—	—	454 (35.5%)	470 (36.8%)
64	244	111 (45.5%)	133 (54.5%)	—	—	72 (29.5%)	39 (16.0%)
65	213	193 (90.6%)	20 (9.4%)	—	—	123 (57.8%)	70 (32.9%)
66	34	16 (47.1%)	18 (52.9%)	—	—	7 (20.6%)	9 (26.5%)
67	29	17 (58.6%)	12 (41.4%)	—	—	11 (37.9%)	6 (20.7%)
68	19	6 (31.6%)	13 (68.4%)	—	—	2 (10.5%)	4 (21.1%)
69	65	43 (66.2%)	22 (33.9%)	—	—	25 (38.5%)	18 (27.7%)
70	130	47 (36.1%)	83 (63.9%)	—	—	36 (27.7%)	11 (8.5%)
71	385	315 (81.8%)	70 (18.2%)	—	—	162 (42.1%)	153 (39.7%)
72	182	109 (59.9%)	73 (40.1%)	—	—	51 (28.0%)	58 (31.9%)
73	16	1 (6.2%)	15 (93.8%)	—	—	—	1 (6.2%)
74	202	152 (75.2%)	50 (24.8%)	—	—	75 (37.1%)	77 (38.1%)
75	5	2 (40.0%)	3 (60.0%)	—	—	—	2 (40.0%)
76	12	2 (16.7%)	10 (83.3%)	—	—	1 (8.3%)	1 (8.3%)
77	2	—	2 (100%)	—	—	—	—
78	2	—	2 (100%)	—	—	—	—
79	11	1 (9.1%)	10 (90.9%)	—	—	—	1 (9.1%)
80	3	—	3 (100%)	—	—	—	—
81	13	4 (30.8%)	9 (69.2%)	1 (7.7%)	—	—	3 (23.1%)
82	130	37 (28.5%)	93 (71.5%)	2 (1.5%)	—	10 (7.7%)	25 (19.2%)
83	9	8 (88.9%)	1 (11.1%)	—	—	2 (22.2%)	6 (66.7%)
84	28	7 (25.0%)	21 (75.0%)	—	—	4 (14.3%)	3 (10.7%)
85	36	14 (38.9%)	22 (61.1%)	2 (5.6%)	—	3 (8.3%)	9 (25.0%)
86	49	38 (77.5%)	11 (22.4%)	—	—	9 (18.4%)	29 (59.2%)
87	175	106 (60.6%)	69 (39.4%)	2 (1.1%)	—	15 (8.6%)	89 (50.9%)
88	129	27 (20.9%)	102 (79.1%)	—	—	12 (9.3%)	15 (11.6%)
90	5	4 (80.0%)	1 (20.0%)	—	—	2 (40.0%)	2 (40.0%)
91	7	3 (42.9%)	4 (57.1%)	—	—	1 (14.3%)	2 (28.6%)
92	47	18 (38.3%)	29 (61.7%)	—	—	6 (12.8%)	12 (25.5%)
94	1	1 (100%)	—	—	—	1 (100%)	—
95	3	1 (33.3%)	2 (66.7%)	—	—	1 (33.3%)	—
96	16	1 (6.2%)	15 (93.8%)	—	—	—	1 (6.2%)
97	2	1 (50.0%)	1 (50.0%)	—	—	—	1 (50.0%)
98	4	1 (25.0%)	3 (75.0%)	—	—	—	1 (25.0%)
99	98	27 (27.6%)	71 (72.5%)	—	—	1 (1.0%)	26 (26.5%)
100	20	14 (70.0%)	6 (30.0%)	—	—	1 (5.0%)	13 (65.0%)
102	12	6 (50.0%)	6 (50.0%)	—	—	3 (25.0%)	3 (25.0%)
103	3	3 (100%)	—	—	—	—	3 (100%)
104	3	1 (33.3%)	2 (66.7%)	—	—	—	1 (33.3%)
105	4	1 (25.0%)	3 (75.0%)	—	—	1 (25.0%)	—
106	1	1 (100%)	—	—	—	—	1 (100%)
107	112	101 (90.2%)	11 (9.8%)	—	—	13 (11.6%)	88 (78.6%)
108	14	7 (50.0%)	7 (50.0%)	—	—	2 (14.3%)	5 (35.7%)
109	37	23 (62.2%)	14 (37.8%)	—	—	7 (18.9%)	16 (43.2%)
110	8	3 (37.5%)	5 (62.5%)	—	—	2 (25.0%)	1 (12.5%)
111	20	7 (35.0%)	13 (65.0%)	—	—	1 (5.0%)	6 (30.0%)
112	4	—	4 (100%)	—	—	—	—
113	71	26 (36.6%)	45 (63.4%)	—	—	5 (7.0%)	21 (29.6%)

114	31	6 (19.4%)	25 (80.7%)	—	—	3 (9.7%)	3 (9.7%)
115	21	15 (71.4%)	6 (28.6%)	—	—	1 (4.8%)	14 (66.7%)
116	17	3 (17.6%)	14 (82.3%)	—	—	3 (17.6%)	—
117	11	6 (54.5%)	5 (45.5%)	—	—	3 (27.3%)	3 (27.3%)
118	11	3 (27.3%)	8 (72.7%)	—	—	2 (18.2%)	1 (9.1%)
119	35	17 (48.6%)	18 (51.4%)	—	—	8 (22.9%)	9 (25.7%)
120	15	6 (40.0%)	9 (60.0%)	—	—	3 (20.0%)	3 (20.0%)
121	123	56 (45.5%)	67 (54.5%)	—	—	17 (13.8%)	39 (31.7%)
122	124	23 (18.6%)	101 (81.5%)	—	—	11 (8.9%)	12 (9.7%)
123	450	391 (86.9%)	59 (13.1%)	—	—	66 (14.7%)	325 (72.2%)
124	22	19 (86.4%)	3 (13.6%)	—	—	4 (18.2%)	15 (68.2%)
125	49	32 (65.3%)	17 (34.7%)	—	—	7 (14.3%)	25 (51.0%)
126	11	4 (36.4%)	7 (63.6%)	—	—	2 (18.2%)	2 (18.2%)
127	368	326 (88.6%)	42 (11.4%)	—	—	78 (21.2%)	248 (67.4%)
128	71	45 (63.4%)	26 (36.6%)	—	—	12 (16.9%)	33 (46.5%)
129	861	691 (80.3%)	170 (19.7%)	—	—	213 (24.7%)	478 (55.5%)
130	37	23 (62.2%)	14 (37.8%)	—	—	10 (27.0%)	13 (35.1%)
131	43	36 (83.7%)	7 (16.3%)	—	—	11 (25.6%)	25 (58.1%)
132	10	1 (10.0%)	9 (90.0%)	—	—	1 (10.0%)	—
133	3	2 (66.7%)	1 (33.3%)	—	—	—	2 (66.7%)
134	4	3 (75.0%)	1 (25.0%)	—	—	—	3 (75.0%)
135	26	15 (57.7%)	11 (42.3%)	—	—	9 (34.6%)	6 (23.1%)
136	251	188 (74.9%)	63 (25.1%)	—	—	95 (37.9%)	93 (37.0%)
137	68	37 (54.4%)	31 (45.6%)	—	—	10 (14.7%)	27 (39.7%)
138	16	7 (43.8%)	9 (56.2%)	—	—	4 (25.0%)	3 (18.8%)
139	1543	1384 (89.7%)	159 (10.3%)	—	—	332 (21.5%)	1052 (68.2%)
140	431	319 (74.0%)	112 (26.0%)	—	—	100 (23.2%)	219 (50.8%)
141	246	169 (68.7%)	77 (31.3%)	—	—	77 (31.3%)	92 (37.4%)
142	73	35 (48.0%)	38 (52.0%)	—	—	11 (15.1%)	24 (32.9%)
143	17	5 (29.4%)	12 (70.6%)	—	—	—	5 (29.4%)
144	13	2 (15.4%)	11 (84.6%)	—	—	—	2 (15.4%)
145	5	—	5 (100%)	—	—	—	—
146	83	20 (24.1%)	63 (75.9%)	—	—	—	20 (24.1%)
147	71	19 (26.8%)	52 (73.2%)	—	3 (4.2%)	1 (1.4%)	15 (21.1%)
148	479	224 (46.8%)	255 (53.2%)	—	35 (7.3%)	5 (1.0%)	184 (38.4%)
149	10	5 (50.0%)	5 (50.0%)	—	—	—	5 (50.0%)
150	64	15 (23.4%)	49 (76.6%)	—	—	4 (6.2%)	11 (17.2%)
151	4	—	4 (100%)	—	—	—	—
152	40	9 (22.5%)	31 (77.5%)	—	—	2 (5.0%)	7 (17.5%)
153	1	1 (100%)	—	—	—	1 (100%)	—
154	17	2 (11.8%)	15 (88.2%)	—	—	1 (5.9%)	1 (5.9%)
155	50	19 (38.0%)	31 (62.0%)	—	—	2 (4.0%)	17 (34.0%)
156	57	16 (28.1%)	41 (71.9%)	—	—	7 (12.3%)	9 (15.8%)
157	14	5 (35.7%)	9 (64.3%)	—	—	2 (14.3%)	3 (21.4%)
158	3	3 (100%)	—	—	—	1 (33.3%)	2 (66.7%)
159	24	6 (25.0%)	18 (75.0%)	—	—	—	6 (25.0%)
160	158	58 (36.7%)	100 (63.3%)	—	—	6 (3.8%)	52 (32.9%)
161	87	18 (20.7%)	69 (79.3%)	—	—	3 (3.5%)	15 (17.2%)
162	52	27 (51.9%)	25 (48.1%)	—	1 (1.9%)	5 (9.6%)	21 (40.4%)
163	57	25 (43.9%)	32 (56.1%)	—	—	3 (5.3%)	22 (38.6%)
164	574	320 (55.8%)	254 (44.2%)	—	2 (0.3%)	47 (8.2%)	271 (47.2%)
165	33	24 (72.7%)	9 (27.3%)	—	—	6 (18.2%)	18 (54.5%)
166	957	620 (64.8%)	337 (35.2%)	2 (0.2%)	2 (0.2%)	153 (16.0%)	463 (48.4%)
167	301	122 (40.5%)	179 (59.5%)	—	1 (0.3%)	21 (7.0%)	100 (33.2%)
169	1	—	1 (100%)	—	—	—	—
173	113	39 (34.5%)	74 (65.5%)	—	—	11 (9.7%)	28 (24.8%)
174	50	33 (66.0%)	17 (34.0%)	—	—	—	33 (66.0%)
175	2	2 (100%)	—	—	—	—	2 (100%)
176	189	82 (43.4%)	107 (56.6%)	—	—	5 (2.6%)	77 (40.7%)
177	1	—	1 (100%)	—	—	—	—
180	28	18 (64.3%)	10 (35.7%)	—	—	2 (7.1%)	16 (57.1%)
181	8	5 (62.5%)	3 (37.5%)	—	—	1 (12.5%)	4 (50.0%)
182	33	24 (72.7%)	9 (27.3%)	—	—	5 (15.2%)	19 (57.6%)
183	1	—	1 (100%)	—	—	—	—

185	49	29 (59.2%)	20 (40.8%)	—	—	10 (20.4%)	19 (38.8%)
186	370	203 (54.9%)	167 (45.1%)	—	—	40 (10.8%)	163 (44.0%)
187	154	123 (79.9%)	31 (20.1%)	—	—	31 (20.1%)	92 (59.7%)
188	20	4 (20.0%)	16 (80.0%)	—	—	—	4 (20.0%)
189	537	483 (89.9%)	54 (10.1%)	—	—	94 (17.5%)	389 (72.4%)
190	41	25 (61.0%)	16 (39.0%)	—	—	3 (7.3%)	22 (53.7%)
191	452	447 (98.9%)	5 (1.1%)	—	—	63 (13.9%)	384 (85.0%)
192	2	—	2 (100%)	—	—	—	—
193	270	257 (95.2%)	13 (4.8%)	—	—	24 (8.9%)	233 (86.3%)
194	1530	1278 (83.5%)	252 (16.5%)	—	—	235 (15.4%)	1043 (68.2%)
195	1	—	1 (100%)	—	—	—	—
196	1	1 (100%)	—	—	—	—	1 (100%)
197	20	10 (50.0%)	10 (50.0%)	—	—	—	10 (50.0%)
198	170	77 (45.3%)	93 (54.7%)	—	—	1 (0.6%)	76 (44.7%)
199	32	9 (28.1%)	23 (71.9%)	—	—	1 (3.1%)	8 (25.0%)
200	22	17 (77.3%)	5 (22.7%)	—	—	2 (9.1%)	15 (68.2%)
201	6	4 (66.7%)	2 (33.3%)	—	—	—	4 (66.7%)
202	18	10 (55.6%)	8 (44.4%)	—	—	—	10 (55.6%)
203	6	1 (16.7%)	5 (83.3%)	—	—	—	1 (16.7%)
204	145	123 (84.8%)	22 (15.2%)	—	—	4 (2.8%)	119 (82.1%)
205	130	49 (37.7%)	81 (62.3%)	—	—	9 (6.9%)	40 (30.8%)
206	60	30 (50.0%)	30 (50.0%)	—	—	1 (1.7%)	29 (48.3%)
208	2	2 (100%)	—	—	—	2 (100%)	—
210	1	1 (100%)	—	—	—	—	1 (100%)
211	1	1 (100%)	—	—	—	—	1 (100%)
212	14	8 (57.1%)	6 (42.9%)	—	—	2 (14.3%)	6 (42.9%)
213	22	17 (77.3%)	5 (22.7%)	—	—	1 (4.5%)	16 (72.7%)
214	13	7 (53.9%)	6 (46.1%)	—	—	1 (7.7%)	6 (46.1%)
215	53	23 (43.4%)	30 (56.6%)	—	—	—	23 (43.4%)
216	751	517 (68.8%)	234 (31.2%)	—	—	21 (2.8%)	496 (66.0%)
217	108	66 (61.1%)	42 (38.9%)	—	—	6 (5.6%)	60 (55.6%)
218	42	12 (28.6%)	30 (71.4%)	—	—	—	12 (28.6%)
219	8	5 (62.5%)	3 (37.5%)	—	—	2 (25.0%)	3 (37.5%)
220	142	115 (81.0%)	27 (19.0%)	—	—	15 (10.6%)	100 (70.4%)
221	1334	1170 (87.7%)	164 (12.3%)	—	—	107 (8.0%)	1063 (79.7%)
223	217	214 (98.6%)	3 (1.4%)	—	—	13 (6.0%)	201 (92.6%)
224	16	9 (56.2%)	7 (43.8%)	—	—	—	9 (56.2%)
225	1651	1277 (77.3%)	374 (22.6%)	—	—	74 (4.5%)	1203 (72.9%)
226	43	42 (97.7%)	1 (2.3%)	—	—	3 (7.0%)	39 (90.7%)
227	816	673 (82.5%)	143 (17.5%)	—	—	131 (16.1%)	542 (66.4%)
229	205	185 (90.2%)	20 (9.8%)	—	—	8 (3.9%)	177 (86.3%)
230	6	5 (83.3%)	1 (16.7%)	—	—	1 (16.7%)	4 (66.7%)
Total	36163	20298 (56.1%)	15865 (43.9%)	251 (0.7%)	44 (0.1%)	6006 (16.6%)	13997 (38.7%)

B. Topological Classification and Connectivity of all of the Bands in all of the Stoichiometric Unique Materials in the ICSD with and w/o SOC

In this section, we will provide statistics on the symmetry-indicated stable [5, 16, 17, 22, 30, 32–34, 86] and fragile [42, 44, 45] topology of *all* of the isolated bands in all of the stoichiometric unique materials in the ICSD, where in the calculations performed for this work, we have taken the conduction manifold to contain at least as many states as the valence manifold (*i.e.* there are $\geq 2N_e$ total bands, see SM 4 for further calculation details). We have also compiled statistics for materials with large or complete band connectivities [defined as *supermetallic* (SMetal) materials in the text below]. For the statistics compiled in this section for symmetry-indicated insulating topology at varying electronic fillings, we emphasize that the isolated bands (as determined by band connectivity through the compatibility relations in TQC, see SM 2) can never be classified as ESFD- or ES-classified semimetals, which by definition require a connected group of bands to be partially occupied at a high-symmetry point or along a high-symmetry line or plane [38]. Consequently, all of the isolated topological bands analyzed in this section are labeled as either NLC, SEBR, LCEBR, or FRAGILE. We emphasize that in the absence of SOC, all symmetry-indicated topological (NLC-SM- and SEBR-SM-classified) bands in nonmagnetic materials correspond to topological semimetal phases, and are thus connected to other bands at higher or lower energies by nodal points in the BZ interior. However, NLC-SM and SEBR-SM bands are still considered to be isolated by band connectivity, as they satisfy the insulating compatibility relations, which are only defined along high-symmetry BZ lines and planes (see SM 6 and Ref. 36).

To begin, in this work, we are uniquely able to analyze the symmetry-indicated topology of bands away from the Fermi level by using new features of the [Check Topological Mat](#) program, which we have detailed in SM 3. In Table S16, we show the output of [Check Topological Mat](#) for the candidate ES compound Ni_2SnZr [ICSD 105383, SG 225 ($Fm\bar{3}m$)]. Though Ni_2SnZr is an ES-classified SM at E_F with SOC, none of the entries in Table S16 are labeled as “ES,” because the symmetry-indicated topology of energetically isolated groups of bands can only be meaningfully defined by taking the connected bands to be fully occupied (whereas partial occupancy is required to realize an ES-classified semimetal).

Next, in Table S17, we list the number of isolated sets of bands in each topological class per SG with SOC as determined by band connectivity. Remarkably, we find that nearly 2/3 of all of the bands in all of the stoichiometric unique materials in the ICSD exhibit symmetry-indicated stable (NLC or SEBR) topology when incorporating the effects of SOC. Then, in Table S18, we list the number of unique materials in each SG with at least one symmetry-indicated stable or fragile topological set of bands with SOC. We further find that an overwhelming 87.99% of the stoichiometric unique materials in the ICSD have at least one stable or fragile topological band when the effects of SOC are incorporated. For completeness, we next respectively provide in Tables S19 and S20 the number of isolated sets of bands in each topological class per SG w/o SOC as determined by band connectivity, and the number of unique materials in each SG with at least one symmetry-indicated stable or fragile topological set of bands w/o SOC.

Lastly, in this work we have discovered the existence of SMetal materials, which realize an extreme limit of band connectivity in which *all* of the bands included our VASP calculations are connected (*i.e.* materials in which there does not exist an LCEBR-, NLC-, or SEBR-classified gap at any integer electronic filling, including filling the complete set of $\sim 2N_e$ bands in the VASP calculation, see SM 4 for calculation details). As previously discussed in SM 6, <https://www.topologicalquantumchemistry.com/> contains 17 unique SMetal materials with SOC (Table S18), whereas there are 1,138 unique SMetal materials w/o SOC (Table S20), representing a hundred-fold increase w/o SOC in the number of materials with fully-connected valence bands up to the energy (filling) cutoff of $\sim 2N_e$ imposed in our VASP calculations (see SM 4). We have in this work also discovered the existence of materials in which a very large number of bands (≥ 130) are connected, even in the presence of SOC. In Table S21, we list the nonmagnetic unique materials without f electrons that exhibit connected groupings of bands with total dimension greater than or equal to 130 in the calculations performed with SOC.

Table S17: In this table, we list the number of isolated sets of bands with SOC as determined by band connectivity (see SM 2) in unique materials in each SG in each topological class. In order, the columns in this table list the SG, the number of unique materials in the SG, the number of NLC-classified sets of bands, the number of SEBR-classified sets of bands, the number of LCEBR-classified sets of bands, the number of sets of connected fragile bands, and the total number of sets of isolated (connected) bands. For all of the topological classification categories in the table, each number of bands is accompanied by the percentage of bands in the SG in the topological class. When there are no bands in the topological class, the table entry is marked with a dashed horizontal line.

SG	# Mat.	# NLC bands	# SEBR bands	# LCEBR bands	# Fragile bands	Total # isolated bands
----	--------	-------------	--------------	---------------	-----------------	------------------------

1	151	—	—	13263 (100%)	—	13263
2	1574	191942 (81.2%)	—	44364 (18.8%)	—	236306
3	13	—	—	1708 (100%)	—	1708
4	228	—	—	15934 (100%)	—	15934
5	156	—	—	16121 (100%)	—	16121
6	28	—	—	2232 (100%)	—	2232
7	85	—	—	6211 (100%)	—	6211
8	144	—	—	10382 (100%)	—	10382
9	199	—	—	12836 (100%)	—	12836
10	38	3426 (86.0%)	—	556 (14.0%)	—	3982
11	587	25889 (64.1%)	—	14479 (35.9%)	—	40368
12	1345	74986 (54.5%)	33987 (24.7%)	28550 (20.8%)	—	137523
13	195	10984 (68.5%)	—	5058 (31.5%)	—	16042
14	2665	194380 (81.2%)	—	45057 (18.8%)	—	239437
15	1485	75378 (62.2%)	—	45743 (37.8%)	—	121121
16	2	—	—	125 (100%)	—	125
17	8	—	—	563 (100%)	—	563
18	30	—	—	2825 (100%)	—	2825
19	270	—	—	12867 (100%)	—	12867
20	66	—	—	5007 (100%)	—	5007
21	16	—	—	1102 (100%)	—	1102
22	17	—	—	1371 (100%)	—	1371
23	16	—	—	1486 (100%)	—	1486
24	2	—	—	88 (100%)	—	88
25	45	—	—	2184 (100%)	—	2184
26	60	—	—	4400 (100%)	—	4400
27	1	—	—	54 (100%)	—	54
28	11	—	—	500 (100%)	—	500
29	61	—	—	2651 (100%)	—	2651
30	5	—	—	558 (100%)	—	558
31	159	—	—	10121 (100%)	—	10121
32	10	—	—	1129 (100%)	—	1129
33	257	—	—	11039 (100%)	—	11039
34	21	—	—	1695 (100%)	—	1695
35	8	—	—	878 (100%)	—	878
36	261	—	—	16116 (100%)	—	16116
37	5	—	—	415 (100%)	—	415
38	104	—	—	6817 (100%)	—	6817
39	13	—	—	859 (100%)	—	859
40	57	—	—	3548 (100%)	—	3548
41	31	—	—	2464 (100%)	—	2464
42	4	—	—	321 (100%)	—	321
43	84	—	—	5305 (100%)	—	5305
44	69	—	—	4843 (100%)	—	4843
45	8	—	—	917 (100%)	—	917
46	57	—	—	3774 (100%)	—	3774
47	51	3820 (80.8%)	—	907 (19.2%)	—	4727
48	3	65 (40.4%)	47 (29.2%)	49 (30.4%)	—	161
49	1	56 (69.1%)	—	25 (30.9%)	—	81
50	7	258 (40.8%)	128 (20.2%)	246 (38.9%)	—	632
51	107	4669 (75.5%)	—	1513 (24.5%)	—	6182
52	39	870 (48.7%)	—	918 (51.3%)	—	1788
53	18	—	821 (79.3%)	214 (20.7%)	—	1035
54	19	521 (56.8%)	—	397 (43.2%)	—	918
55	394	30767 (86.8%)	—	4699 (13.2%)	—	35466
56	19	592 (59.3%)	—	407 (40.7%)	—	999
57	142	4217 (61.1%)	—	2681 (38.9%)	—	6898
58	208	7453 (67.6%)	—	3577 (32.4%)	—	11030
59	227	5527 (40.3%)	2537 (18.5%)	5664 (41.3%)	—	13728
60	142	3238 (51.1%)	—	3100 (48.9%)	—	6338
61	122	4948 (83.9%)	—	949 (16.1%)	—	5897
62	3006	62367 (52.4%)	—	56672 (47.6%)	—	119039
63	1396	34318 (55.8%)	5070 (8.2%)	22069 (35.9%)	—	61457

64	257	—	15714 (81.5%)	3559 (18.5%)	—	19273
65	241	9201 (55.2%)	4432 (26.6%)	3046 (18.3%)	—	16679
66	36	1430 (68.3%)	—	663 (31.7%)	—	2093
67	30	680 (68.8%)	—	308 (31.2%)	—	988
68	19	—	1039 (61.7%)	644 (38.3%)	—	1683
69	66	—	5218 (78.8%)	1406 (21.2%)	—	6624
70	139	898 (10.6%)	3632 (42.8%)	3965 (46.7%)	—	8495
71	452	8741 (22.2%)	18476 (47.0%)	12128 (30.8%)	—	39345
72	192	6264 (57.1%)	1068 (9.7%)	3628 (33.1%)	—	10960
73	24	993 (60.0%)	—	663 (40.0%)	—	1656
74	218	7724 (72.5%)	—	2928 (27.5%)	—	10652
75	5	—	—	396 (100%)	—	396
76	12	—	—	380 (100%)	—	380
77	2	—	—	20 (100%)	—	20
78	2	—	—	108 (100%)	—	108
79	11	—	—	841 (100%)	—	841
80	3	—	—	214 (100%)	—	214
81	14	—	816 (48.0%)	885 (52.0%)	—	1701
82	136	5741 (46.7%)	—	6550 (53.3%)	1 (0.0%)	12292
83	10	206 (47.9%)	151 (35.1%)	73 (17.0%)	—	430
84	28	821 (65.1%)	—	440 (34.9%)	—	1261
85	39	730 (33.1%)	718 (32.6%)	755 (34.3%)	—	2203
86	51	—	1266 (70.7%)	525 (29.3%)	—	1791
87	181	1369 (12.7%)	6836 (63.4%)	2563 (23.8%)	11 (0.1%)	10779
88	139	253 (4.1%)	3586 (58.7%)	2263 (37.1%)	3 (0.1%)	6105
90	5	—	—	569 (100%)	—	569
91	7	—	—	173 (100%)	—	173
92	47	—	—	1156 (100%)	—	1156
94	1	—	—	37 (100%)	—	37
95	3	—	—	66 (100%)	—	66
96	16	—	—	386 (100%)	—	386
97	2	—	—	138 (100%)	—	138
98	4	—	—	103 (100%)	—	103
99	98	—	—	2228 (100%)	—	2228
100	20	—	—	1175 (100%)	—	1175
102	12	—	—	461 (100%)	—	461
103	3	—	—	29 (100%)	—	29
104	3	—	—	118 (100%)	—	118
105	4	—	—	139 (100%)	—	139
106	1	—	—	29 (100%)	—	29
107	121	—	—	3497 (100%)	—	3497
108	15	—	—	653 (100%)	—	653
109	40	—	—	1117 (100%)	—	1117
110	8	—	—	350 (100%)	—	350
111	21	—	678 (49.8%)	683 (50.2%)	—	1361
112	4	57 (39.0%)	—	89 (61.0%)	—	146
113	84	2055 (35.3%)	—	3767 (64.7%)	—	5822
114	31	—	1524 (64.9%)	823 (35.1%)	—	2347
115	21	—	669 (45.4%)	806 (54.6%)	—	1475
116	17	—	504 (40.4%)	743 (59.6%)	—	1247
117	11	517 (40.8%)	—	749 (59.2%)	—	1266
118	11	364 (43.0%)	—	482 (57.0%)	—	846
119	35	1067 (46.7%)	—	1218 (53.3%)	—	2285
120	15	565 (39.1%)	—	880 (60.9%)	—	1445
121	126	—	4553 (45.6%)	5441 (54.4%)	—	9994
122	124	—	3323 (66.4%)	1684 (33.6%)	—	5007
123	473	8145 (58.1%)	3494 (24.9%)	2385 (17.0%)	2 (0.0%)	14026
124	23	72 (23.8%)	80 (26.4%)	151 (49.8%)	—	303
125	52	659 (32.7%)	696 (34.5%)	662 (32.8%)	1 (0.1%)	2018
126	12	—	210 (46.5%)	242 (53.5%)	—	452
127	403	10069 (80.6%)	—	2412 (19.3%)	7 (0.1%)	12488
128	76	113 (3.4%)	2320 (70.6%)	836 (25.4%)	16 (0.5%)	3285
129	884	6683 (32.6%)	5794 (28.2%)	8029 (39.1%)	6 (0.0%)	20512
130	38	330 (30.6%)	134 (12.4%)	613 (56.9%)	—	1077

131	44	429 (63.5%)	—	247 (36.5%)	—	676
132	10	—	249 (62.9%)	147 (37.1%)	—	396
133	3	29 (43.3%)	11 (16.4%)	27 (40.3%)	—	67
134	4	—	51 (78.5%)	14 (21.5%)	—	65
135	30	560 (59.3%)	—	384 (40.7%)	—	944
136	266	—	5570 (57.4%)	4098 (42.3%)	29 (0.3%)	9697
137	70	—	1827 (59.4%)	1249 (40.6%)	—	3076
138	22	517 (60.0%)	—	344 (40.0%)	—	861
139	1622	7320 (13.0%)	37938 (67.4%)	10985 (19.5%)	68 (0.1%)	56311
140	457	7845 (57.6%)	2501 (18.4%)	3264 (24.0%)	4 (0.0%)	13614
141	267	611 (6.5%)	5800 (62.1%)	2907 (31.1%)	26 (0.3%)	9344
142	77	—	1352 (48.7%)	1425 (51.3%)	—	2777
143	18	2 (0.1%)	—	1393 (89.1%)	168 (10.8%)	1563
144	13	—	—	502 (100%)	—	502
145	5	—	—	203 (100%)	—	203
146	87	—	—	7694 (100%)	—	7694
147	75	—	4625 (73.0%)	1481 (23.4%)	232 (3.7%)	6338
148	496	—	29625 (68.3%)	13720 (31.6%)	57 (0.1%)	43402
149	10	—	—	435 (86.1%)	70 (13.9%)	505
150	66	—	—	3456 (89.2%)	419 (10.8%)	3875
151	5	—	—	165 (100%)	—	165
152	42	—	—	892 (100%)	—	892
153	2	—	—	44 (100%)	—	44
154	19	—	—	423 (100%)	—	423
155	54	—	—	4560 (100%)	—	4560
156	57	—	—	1146 (89.5%)	134 (10.5%)	1280
157	16	—	—	696 (86.9%)	105 (13.1%)	801
158	3	—	—	82 (97.6%)	2 (2.4%)	84
159	26	—	—	904 (98.7%)	12 (1.3%)	916
160	160	—	—	6273 (100%)	—	6273
161	87	—	—	3311 (100%)	—	3311
162	54	—	1617 (72.4%)	482 (21.6%)	135 (6.0%)	2234
163	63	309 (11.0%)	897 (32.0%)	1466 (52.4%)	127 (4.5%)	2799
164	598	—	14976 (68.5%)	5093 (23.3%)	1810 (8.3%)	21879
165	34	1 (0.1%)	432 (48.9%)	419 (47.4%)	32 (3.6%)	884
166	1029	—	39673 (68.7%)	17908 (31.0%)	144 (0.2%)	57725
167	325	1717 (14.2%)	3830 (31.8%)	6501 (54.0%)	1 (0.0%)	12049
169	1	—	—	6 (100%)	—	6
173	124	—	—	2898 (98.4%)	47 (1.6%)	2945
174	59	1403 (64.2%)	—	783 (35.8%)	—	2186
175	2	—	39 (60.9%)	25 (39.1%)	—	64
176	206	671 (12.5%)	2483 (46.2%)	2199 (40.9%)	22 (0.4%)	5375
177	1	—	—	33 (100%)	—	33
180	28	—	—	276 (100%)	—	276
181	8	—	—	62 (100%)	—	62
182	34	—	—	668 (96.2%)	26 (3.8%)	694
183	1	—	—	9 (75.0%)	3 (25.0%)	12
185	51	—	—	975 (94.2%)	60 (5.8%)	1035
186	392	—	—	6973 (97.8%)	160 (2.2%)	7133
187	158	1193 (58.9%)	—	828 (40.9%)	4 (0.2%)	2025
188	21	147 (32.7%)	—	297 (66.0%)	6 (1.3%)	450
189	592	2850 (12.6%)	14666 (64.7%)	5125 (22.6%)	25 (0.1%)	22666
190	45	741 (49.2%)	—	749 (49.7%)	17 (1.1%)	1507
191	506	—	6987 (78.2%)	1929 (21.6%)	17 (0.2%)	8933
192	2	—	17 (68.0%)	8 (32.0%)	—	25
193	302	13 (0.4%)	1705 (54.9%)	1368 (44.0%)	21 (0.7%)	3107
194	1619	5224 (18.7%)	14644 (52.3%)	7725 (27.6%)	393 (1.4%)	27986
195	1	—	—	91 (100%)	—	91
196	1	—	—	83 (100%)	—	83
197	20	—	—	966 (100%)	—	966
198	173	—	—	3771 (100%)	—	3771
199	33	—	—	679 (85.2%)	118 (14.8%)	797
200	22	113 (8.3%)	951 (69.6%)	290 (21.2%)	12 (0.9%)	1366
201	7	117 (23.0%)	299 (58.9%)	92 (18.1%)	—	508

202	18	—	598 (47.5%)	648 (51.4%)	14 (1.1%)	1260
203	6	7 (1.7%)	314 (76.8%)	82 (20.1%)	6 (1.5%)	409
204	151	—	4138 (74.2%)	1353 (24.3%)	83 (1.5%)	5574
205	130	1196 (52.9%)	—	1066 (47.1%)	—	2262
206	61	—	1045 (72.7%)	350 (24.3%)	43 (3.0%)	1438
208	2	—	—	10 (83.3%)	2 (16.7%)	12
210	1	—	—	16 (64.0%)	9 (36.0%)	25
211	1	—	—	22 (100%)	—	22
212	14	—	—	282 (100%)	—	282
213	22	—	—	243 (100%)	—	243
214	14	—	—	233 (90.0%)	26 (10.0%)	259
215	54	178 (7.2%)	909 (36.8%)	1239 (50.1%)	146 (5.9%)	2472
216	777	6971 (44.8%)	—	7464 (48.0%)	1110 (7.1%)	15545
217	111	—	1584 (34.5%)	2843 (61.9%)	163 (3.5%)	4590
218	42	—	547 (41.8%)	755 (57.7%)	6 (0.5%)	1308
219	9	6 (1.6%)	173 (44.6%)	206 (53.1%)	3 (0.8%)	388
220	143	795 (37.8%)	—	1187 (56.4%)	124 (5.9%)	2106
221	1352	1836 (15.8%)	5688 (49.0%)	4070 (35.1%)	7 (0.1%)	11601
223	222	—	1343 (57.4%)	903 (38.6%)	93 (4.0%)	2339
224	17	—	206 (81.1%)	48 (18.9%)	—	254
225	1693	—	23368 (64.0%)	12701 (34.8%)	421 (1.1%)	36490
226	46	38 (6.0%)	342 (54.3%)	243 (38.6%)	7 (1.1%)	630
227	841	285 (1.5%)	14032 (75.5%)	3786 (20.4%)	473 (2.5%)	18576
229	210	42 (1.2%)	2740 (76.1%)	813 (22.6%)	7 (0.2%)	3602
230	6	22 (43.1%)	8 (15.7%)	20 (39.2%)	1 (2.0%)	51
Total	38298	859606 (43.0%)	379321 (19.0%)	750504 (37.6%)	7297 (0.4%)	1996728

Table S18: In this table, we list the number of unique materials that contain at least some topological features with SOC in each SG. In order, the columns in this table list the SG, the number of unique materials in the SG, the number of unique materials with either at least one stable or fragile band in the spectrum or symmetry-enforced crossing points at E_F (*i.e.* materials that are either ES- or ESFD-classified semimetals or exhibit stable or fragile topological bands at any filling). From left to right, in the following columns we list, per SG, the number of unique materials with at least one stable or fragile topological connected set of bands at any filling, at least one fragile topological set of bands at any filling, at least one NLC-classified stable topological band at any filling, at least one SEBR-classified stable topological band at any filling, and at least one stable topological set of bands at any filling. In the remaining three columns, we list the number of materials that do not contain *any* symmetry-indicated stable or fragile topological bands (STriv), the number of supermetallic (SMetal) materials in which *all* of the bands in at least one of the ICSDs associated to the unique material are *fully* connected, and the number of unique materials in which all bands are stable topological [*i.e.* supertopological (STopo) materials, see SM 9]. For all of the topological classification categories in the table, each number of materials is accompanied by the percentage of materials in the SG in the topological class. When there are no materials in the topological class, the table entry is marked with a dashed horizontal line.

SG	# Mat.	Topology	≥ 1 topo. band	≥ 1 frag. band	≥ 1 NLC band	≥ 1 SEBR band	≥ 1 NLC or SEBR band	STriv	SMetal	STopo
1	151	9 (6.0%)	—	—	—	—	—	151 (100%)	—	—
2	1574	1574 (100%)	1574 (100%)	—	1574 (100%)	—	1574 (100%)	—	—	7 (0.4%)
3	13	—	—	—	—	—	—	13 (100%)	—	—
4	228	8 (3.5%)	—	—	—	—	—	228 (100%)	—	—
5	156	15 (9.6%)	—	—	—	—	—	156 (100%)	—	—
6	28	1 (3.6%)	—	—	—	—	—	28 (100%)	—	—
7	85	3 (3.5%)	—	—	—	—	—	85 (100%)	—	—
8	144	13 (9.0%)	—	—	—	—	—	144 (100%)	—	—
9	199	11 (5.5%)	—	—	—	—	—	199 (100%)	—	—

10	38	38 (100%)	38 (100%)	—	38 (100%)	—	38 (100%)	—	—	1 (2.6%)
11	587	587 (100%)	587 (100%)	—	587 (100%)	—	587 (100%)	—	—	1 (0.2%)
12	1345	1345 (100%)	1345 (100%)	—	1345 (100%)	1341 (99.7%)	1345 (100%)	—	—	9 (0.7%)
13	195	195 (100%)	195 (100%)	—	195 (100%)	—	195 (100%)	—	—	1 (0.5%)
14	2665	2665 (100%)	2665 (100%)	—	2665 (100%)	—	2665 (100%)	—	—	24 (0.9%)
15	1485	1485 (100%)	1485 (100%)	—	1485 (100%)	—	1485 (100%)	—	—	—
16	2	—	—	—	—	—	—	2 (100%)	—	—
17	8	—	—	—	—	—	—	8 (100%)	—	—
18	30	2 (6.7%)	—	—	—	—	—	30 (100%)	—	—
19	270	20 (7.4%)	—	—	—	—	—	270 (100%)	—	—
20	66	2 (3.0%)	—	—	—	—	—	66 (100%)	—	—
21	16	6 (37.5%)	—	—	—	—	—	16 (100%)	—	—
22	17	—	—	—	—	—	—	17 (100%)	—	—
23	16	2 (12.5%)	—	—	—	—	—	16 (100%)	—	—
24	2	—	—	—	—	—	—	2 (100%)	—	—
25	45	2 (4.4%)	—	—	—	—	—	45 (100%)	—	—
26	60	4 (6.7%)	—	—	—	—	—	60 (100%)	—	—
27	1	—	—	—	—	—	—	1 (100%)	—	—
28	11	2 (18.2%)	—	—	—	—	—	11 (100%)	—	—
29	61	1 (1.6%)	—	—	—	—	—	61 (100%)	—	—
30	5	1 (20.0%)	—	—	—	—	—	5 (100%)	—	—
31	159	14 (8.8%)	—	—	—	—	—	159 (100%)	—	—
32	10	—	—	—	—	—	—	10 (100%)	—	—
33	257	24 (9.3%)	—	—	—	—	—	257 (100%)	—	—
34	21	3 (14.3%)	—	—	—	—	—	21 (100%)	—	—
35	8	2 (25.0%)	—	—	—	—	—	8 (100%)	—	—
36	261	40 (15.3%)	—	—	—	—	—	261 (100%)	—	—
37	5	—	—	—	—	—	—	5 (100%)	—	—
38	104	33 (31.7%)	—	—	—	—	—	104 (100%)	—	—
39	13	—	—	—	—	—	—	13 (100%)	—	—
40	57	5 (8.8%)	—	—	—	—	—	57 (100%)	—	—
41	31	1 (3.2%)	—	—	—	—	—	31 (100%)	—	—
42	4	—	—	—	—	—	—	4 (100%)	—	—
43	84	13 (15.5%)	—	—	—	—	—	84 (100%)	—	—
44	69	11 (15.9%)	—	—	—	—	—	69 (100%)	—	—
45	8	—	—	—	—	—	—	8 (100%)	—	—
46	57	7 (12.3%)	—	—	—	—	—	57 (100%)	—	—
47	51	51 (100%)	51 (100%)	—	51 (100%)	—	51 (100%)	—	—	—
48	3	3 (100%)	3 (100%)	—	3 (100%)	3 (100%)	3 (100%)	—	—	—
49	1	1 (100%)	1 (100%)	—	1 (100%)	—	1 (100%)	—	—	—
50	7	7 (100%)	7 (100%)	—	7 (100%)	7 (100%)	7 (100%)	—	—	—
51	107	107 (100%)	107 (100%)	—	107 (100%)	—	107 (100%)	—	—	2 (1.9%)
52	39	39 (100%)	39 (100%)	—	39 (100%)	—	39 (100%)	—	—	—
53	18	18 (100%)	18 (100%)	—	—	18 (100%)	18 (100%)	—	—	—
54	19	19 (100%)	19 (100%)	—	19 (100%)	—	19 (100%)	—	—	—
55	394	394 (100%)	394 (100%)	—	394 (100%)	—	394 (100%)	—	—	5 (1.3%)
56	19	19 (100%)	19 (100%)	—	19 (100%)	—	19 (100%)	—	—	—
57	142	142 (100%)	142 (100%)	—	142 (100%)	—	142 (100%)	—	—	—
58	208	208 (100%)	208 (100%)	—	208 (100%)	—	208 (100%)	—	—	1 (0.5%)
59	227	227 (100%)	227 (100%)	—	226 (99.6%)	225 (99.1%)	227 (100%)	—	—	—
60	142	142 (100%)	142 (100%)	—	142 (100%)	—	142 (100%)	—	—	—
61	122	122 (100%)	122 (100%)	—	122 (100%)	—	122 (100%)	—	—	9 (7.4%)
62	3006	3002 (99.9%)	3002 (99.9%)	—	3002 (99.9%)	—	3002 (99.9%)	5 (0.2%)	—	3 (0.1%)
63	1396	1396 (100%)	1396 (100%)	—	1396 (100%)	1187 (85.0%)	1396 (100%)	—	—	6 (0.4%)
64	257	257 (100%)	257 (100%)	—	—	257 (100%)	257 (100%)	—	—	5 (1.9%)
65	241	241 (100%)	241 (100%)	—	241 (100%)	238 (98.8%)	241 (100%)	—	—	2 (0.8%)
66	36	36 (100%)	36 (100%)	—	36 (100%)	—	36 (100%)	—	—	—
67	30	30 (100%)	30 (100%)	—	30 (100%)	—	30 (100%)	—	—	—
68	19	19 (100%)	19 (100%)	—	—	19 (100%)	19 (100%)	—	—	—
69	66	66 (100%)	66 (100%)	—	—	66 (100%)	66 (100%)	—	—	—
70	139	139 (100%)	139 (100%)	—	133 (95.7%)	139 (100%)	139 (100%)	—	—	—
71	452	452 (100%)	451 (99.8%)	—	449 (99.3%)	450 (99.6%)	451 (99.8%)	1 (0.2%)	—	—
72	192	192 (100%)	192 (100%)	—	192 (100%)	173 (90.1%)	192 (100%)	—	—	—
73	24	24 (100%)	24 (100%)	—	24 (100%)	—	24 (100%)	—	—	—

74	218	218 (100%)	218 (100%)	—	218 (100%)	—	218 (100%)	—	—	2 (0.9%)
75	5	2 (40.0%)	—	—	—	—	—	5 (100%)	—	—
76	12	2 (16.7%)	—	—	—	—	—	12 (100%)	—	—
77	2	—	—	—	—	—	—	2 (100%)	—	—
78	2	—	—	—	—	—	—	2 (100%)	—	—
79	11	1 (9.1%)	—	—	—	—	—	11 (100%)	—	—
80	3	—	—	—	—	—	—	3 (100%)	—	—
81	14	14 (100%)	14 (100%)	—	—	14 (100%)	14 (100%)	—	—	—
82	136	136 (100%)	136 (100%)	1 (0.7%)	136 (100%)	—	136 (100%)	—	—	—
83	10	10 (100%)	10 (100%)	—	10 (100%)	10 (100%)	10 (100%)	—	—	1 (10.0%)
84	28	28 (100%)	28 (100%)	—	28 (100%)	—	28 (100%)	—	—	—
85	39	39 (100%)	39 (100%)	—	39 (100%)	39 (100%)	39 (100%)	—	—	—
86	51	51 (100%)	51 (100%)	—	—	51 (100%)	51 (100%)	—	—	—
87	181	181 (100%)	181 (100%)	11 (6.1%)	177 (97.8%)	181 (100%)	181 (100%)	—	—	1 (0.6%)
88	139	139 (100%)	139 (100%)	3 (2.2%)	93 (66.9%)	139 (100%)	139 (100%)	—	—	1 (0.7%)
90	5	2 (40.0%)	—	—	—	—	—	5 (100%)	—	—
91	7	1 (14.3%)	—	—	—	—	—	7 (100%)	—	—
92	47	16 (34.0%)	—	—	—	—	—	47 (100%)	—	—
94	1	—	—	—	—	—	—	1 (100%)	—	—
95	3	1 (33.3%)	—	—	—	—	—	3 (100%)	—	—
96	16	1 (6.2%)	—	—	—	—	—	16 (100%)	—	—
97	2	1 (50.0%)	—	—	—	—	—	2 (100%)	—	—
98	4	—	—	—	—	—	—	4 (100%)	—	—
99	98	22 (22.4%)	—	—	—	—	—	98 (100%)	—	—
100	20	12 (60.0%)	—	—	—	—	—	20 (100%)	—	—
102	12	3 (25.0%)	—	—	—	—	—	12 (100%)	—	—
103	3	3 (100%)	—	—	—	—	—	3 (100%)	—	—
104	3	1 (33.3%)	—	—	—	—	—	3 (100%)	—	—
105	4	—	—	—	—	—	—	4 (100%)	—	—
106	1	1 (100%)	—	—	—	—	—	1 (100%)	—	—
107	121	68 (56.2%)	—	—	—	—	—	121 (100%)	—	—
108	15	5 (33.3%)	—	—	—	—	—	15 (100%)	—	—
109	40	16 (40.0%)	—	—	—	—	—	40 (100%)	—	—
110	8	2 (25.0%)	—	—	—	—	—	8 (100%)	—	—
111	21	21 (100%)	21 (100%)	—	—	21 (100%)	21 (100%)	—	—	—
112	4	4 (100%)	4 (100%)	—	4 (100%)	—	4 (100%)	—	—	—
113	84	84 (100%)	84 (100%)	—	84 (100%)	—	84 (100%)	—	—	—
114	31	31 (100%)	31 (100%)	—	—	31 (100%)	31 (100%)	—	—	—
115	21	21 (100%)	21 (100%)	—	—	21 (100%)	21 (100%)	—	—	—
116	17	17 (100%)	17 (100%)	—	—	17 (100%)	17 (100%)	—	—	—
117	11	11 (100%)	11 (100%)	—	11 (100%)	—	11 (100%)	—	—	—
118	11	11 (100%)	11 (100%)	—	11 (100%)	—	11 (100%)	—	—	—
119	35	35 (100%)	35 (100%)	—	35 (100%)	—	35 (100%)	—	—	—
120	15	15 (100%)	15 (100%)	—	15 (100%)	—	15 (100%)	—	—	—
121	126	126 (100%)	126 (100%)	—	—	126 (100%)	126 (100%)	—	—	—
122	124	124 (100%)	124 (100%)	—	—	124 (100%)	124 (100%)	—	—	4 (3.2%)
123	473	473 (100%)	472 (99.8%)	3 (0.6%)	469 (99.2%)	429 (90.7%)	472 (99.8%)	—	—	41 (8.7%)
124	23	23 (100%)	23 (100%)	—	18 (78.3%)	22 (95.7%)	23 (100%)	—	—	—
125	52	52 (100%)	52 (100%)	1 (1.9%)	52 (100%)	52 (100%)	52 (100%)	—	—	—
126	12	12 (100%)	12 (100%)	—	—	12 (100%)	12 (100%)	—	—	—
127	403	403 (100%)	403 (100%)	7 (1.7%)	403 (100%)	—	403 (100%)	—	—	6 (1.5%)
128	76	76 (100%)	76 (100%)	14 (18.4%)	56 (73.7%)	76 (100%)	76 (100%)	—	—	—
129	884	884 (100%)	884 (100%)	6 (0.7%)	852 (96.4%)	874 (98.9%)	884 (100%)	—	—	1 (0.1%)
130	38	38 (100%)	38 (100%)	—	38 (100%)	35 (92.1%)	38 (100%)	—	—	—
131	44	44 (100%)	44 (100%)	—	44 (100%)	—	44 (100%)	—	—	—
132	10	10 (100%)	10 (100%)	—	—	10 (100%)	10 (100%)	—	—	—
133	3	3 (100%)	3 (100%)	—	3 (100%)	3 (100%)	3 (100%)	—	—	—
134	4	4 (100%)	4 (100%)	—	—	4 (100%)	4 (100%)	—	—	—
135	30	30 (100%)	30 (100%)	—	30 (100%)	—	30 (100%)	—	—	—
136	266	264 (99.2%)	264 (99.2%)	28 (10.5%)	—	264 (99.2%)	264 (99.2%)	2 (0.8%)	—	—
137	70	70 (100%)	70 (100%)	—	—	70 (100%)	70 (100%)	—	—	—
138	22	22 (100%)	22 (100%)	—	22 (100%)	—	22 (100%)	—	—	—
139	1622	1622 (100%)	1622 (100%)	69 (4.2%)	1508 (93.0%)	1618 (99.8%)	1622 (100%)	—	—	43 (2.6%)
140	457	457 (100%)	457 (100%)	4 (0.9%)	457 (100%)	432 (94.5%)	457 (100%)	—	—	45 (9.8%)

141	267	267 (100%)	267 (100%)	23 (8.6%)	203 (76.0%)	267 (100%)	267 (100%)	—	—	2 (0.8%)
142	77	77 (100%)	77 (100%)	—	—	77 (100%)	77 (100%)	—	—	—
143	18	16 (88.9%)	15 (83.3%)	15 (83.3%)	1 (5.6%)	—	1 (5.6%)	—	—	—
144	13	1 (7.7%)	—	—	—	—	—	13 (100%)	—	—
145	5	—	—	—	—	—	—	5 (100%)	—	—
146	87	15 (17.2%)	—	—	—	—	—	87 (100%)	—	—
147	75	75 (100%)	75 (100%)	46 (61.3%)	—	75 (100%)	75 (100%)	—	—	—
148	496	496 (100%)	496 (100%)	52 (10.5%)	—	496 (100%)	496 (100%)	—	—	—
149	10	8 (80.0%)	8 (80.0%)	8 (80.0%)	—	—	—	—	—	—
150	66	48 (72.7%)	46 (69.7%)	46 (69.7%)	—	—	—	1 (1.5%)	—	—
151	5	—	—	—	—	—	—	5 (100%)	—	—
152	42	12 (28.6%)	—	—	—	—	—	42 (100%)	—	—
153	2	—	—	—	—	—	—	2 (100%)	—	—
154	19	2 (10.5%)	—	—	—	—	—	19 (100%)	—	—
155	54	12 (22.2%)	—	—	—	—	—	54 (100%)	—	—
156	57	42 (73.7%)	37 (64.9%)	37 (64.9%)	—	—	—	11 (19.3%)	—	—
157	16	14 (87.5%)	13 (81.2%)	13 (81.2%)	—	—	—	—	—	—
158	3	3 (100%)	2 (66.7%)	2 (66.7%)	—	—	—	1 (33.3%)	—	—
159	26	12 (46.1%)	7 (26.9%)	7 (26.9%)	—	—	—	20 (76.9%)	—	—
160	160	42 (26.2%)	—	—	—	—	—	160 (100%)	—	—
161	87	15 (17.2%)	—	—	—	—	—	87 (100%)	—	—
162	54	54 (100%)	54 (100%)	40 (74.1%)	—	54 (100%)	54 (100%)	—	—	—
163	63	63 (100%)	63 (100%)	46 (73.0%)	62 (98.4%)	63 (100%)	63 (100%)	—	—	—
164	598	598 (100%)	598 (100%)	459 (76.8%)	—	598 (100%)	598 (100%)	—	—	13 (2.2%)
165	34	34 (100%)	33 (97.1%)	13 (38.2%)	1 (2.9%)	33 (97.1%)	33 (97.1%)	1 (2.9%)	—	—
166	1029	1029 (100%)	1029 (100%)	129 (12.5%)	—	1029 (100%)	1029 (100%)	—	—	6 (0.6%)
167	325	324 (99.7%)	324 (99.7%)	1 (0.3%)	303 (93.2%)	323 (99.4%)	324 (99.7%)	3 (0.9%)	—	—
169	1	—	—	—	—	—	—	1 (100%)	—	—
173	124	63 (50.8%)	28 (22.6%)	28 (22.6%)	—	—	—	92 (74.2%)	—	—
174	59	59 (100%)	59 (100%)	—	59 (100%)	—	59 (100%)	—	—	—
175	2	2 (100%)	2 (100%)	—	—	2 (100%)	2 (100%)	—	—	—
176	206	206 (100%)	205 (99.5%)	12 (5.8%)	162 (78.6%)	203 (98.5%)	205 (99.5%)	—	—	5 (2.4%)
177	1	—	—	—	—	—	—	—	—	—
180	28	16 (57.1%)	—	—	—	—	—	28 (100%)	—	—
181	8	4 (50.0%)	—	—	—	—	—	8 (100%)	—	—
182	34	28 (82.3%)	15 (44.1%)	15 (44.1%)	—	—	—	19 (55.9%)	—	—
183	1	1 (100%)	1 (100%)	1 (100%)	—	—	—	—	—	—
185	51	38 (74.5%)	21 (41.2%)	21 (41.2%)	—	—	—	24 (47.1%)	—	—
186	392	255 (65.0%)	80 (20.4%)	80 (20.4%)	—	—	—	288 (73.5%)	—	—
187	158	155 (98.1%)	155 (98.1%)	2 (1.3%)	155 (98.1%)	—	155 (98.1%)	3 (1.9%)	—	1 (0.6%)
188	21	20 (95.2%)	18 (85.7%)	5 (23.8%)	18 (85.7%)	—	18 (85.7%)	3 (14.3%)	—	—
189	592	592 (100%)	592 (100%)	23 (3.9%)	577 (97.5%)	592 (100%)	592 (100%)	—	—	10 (1.7%)
190	45	45 (100%)	45 (100%)	10 (22.2%)	45 (100%)	—	45 (100%)	—	—	—
191	506	506 (100%)	501 (99.0%)	20 (4.0%)	—	501 (99.0%)	501 (99.0%)	—	4 (0.8%)	63 (12.4%)
192	2	2 (100%)	2 (100%)	—	—	2 (100%)	2 (100%)	—	—	—
193	302	302 (100%)	300 (99.3%)	13 (4.3%)	11 (3.6%)	299 (99.0%)	300 (99.3%)	3 (1.0%)	—	3 (1.0%)
194	1619	1607 (99.3%)	1571 (97.0%)	240 (14.8%)	1246 (77.0%)	1542 (95.2%)	1571 (97.0%)	27 (1.7%)	5 (0.3%)	130 (8.0%)
195	1	—	—	—	—	—	—	1 (100%)	—	—
196	1	1 (100%)	—	—	—	—	—	1 (100%)	—	—
197	20	9 (45.0%)	—	—	—	—	—	20 (100%)	—	—
198	173	78 (45.1%)	—	—	—	—	—	173 (100%)	—	—
199	33	29 (87.9%)	28 (84.8%)	28 (84.8%)	—	—	—	2 (6.1%)	—	—
200	22	22 (100%)	22 (100%)	8 (36.4%)	22 (100%)	22 (100%)	22 (100%)	—	—	—
201	7	7 (100%)	7 (100%)	—	7 (100%)	7 (100%)	7 (100%)	—	—	—
202	18	18 (100%)	18 (100%)	7 (38.9%)	—	18 (100%)	18 (100%)	—	—	—
203	6	6 (100%)	6 (100%)	3 (50.0%)	5 (83.3%)	6 (100%)	6 (100%)	—	—	—
204	151	151 (100%)	151 (100%)	57 (37.8%)	—	151 (100%)	151 (100%)	—	—	1 (0.7%)
205	130	129 (99.2%)	129 (99.2%)	—	129 (99.2%)	—	129 (99.2%)	1 (0.8%)	—	2 (1.5%)
206	61	61 (100%)	59 (96.7%)	25 (41.0%)	—	59 (96.7%)	59 (96.7%)	—	—	4 (6.6%)
208	2	2 (100%)	2 (100%)	2 (100%)	—	—	—	—	—	—
210	1	1 (100%)	1 (100%)	1 (100%)	—	—	—	—	—	—
211	1	1 (100%)	—	—	—	—	—	—	—	—
212	14	8 (57.1%)	—	—	—	—	—	14 (100%)	—	—
213	22	17 (77.3%)	—	—	—	—	—	22 (100%)	—	—

214	14	13 (92.9%)	10 (71.4%)	10 (71.4%)	—	—	—	1 (7.1%)	—	—
215	54	54 (100%)	54 (100%)	36 (66.7%)	47 (87.0%)	53 (98.2%)	54 (100%)	—	—	—
216	777	774 (99.6%)	772 (99.4%)	502 (64.6%)	768 (98.8%)	—	768 (98.8%)	5 (0.6%)	—	1 (0.1%)
217	111	111 (100%)	111 (100%)	72 (64.9%)	—	111 (100%)	111 (100%)	—	—	—
218	42	42 (100%)	42 (100%)	5 (11.9%)	—	42 (100%)	42 (100%)	—	—	—
219	9	9 (100%)	9 (100%)	2 (22.2%)	4 (44.4%)	9 (100%)	9 (100%)	—	—	—
220	143	143 (100%)	142 (99.3%)	95 (66.4%)	142 (99.3%)	—	142 (99.3%)	2 (1.4%)	—	—
221	1352	1338 (99.0%)	1299 (96.1%)	7 (0.5%)	899 (66.5%)	1273 (94.2%)	1299 (96.1%)	30 (2.2%)	2 (0.1%)	196 (14.5%)
223	222	222 (100%)	218 (98.2%)	74 (33.3%)	—	218 (98.2%)	218 (98.2%)	2 (0.9%)	—	9 (4.0%)
224	17	17 (100%)	17 (100%)	—	—	17 (100%)	17 (100%)	—	—	1 (5.9%)
225	1693	1679 (99.2%)	1671 (98.7%)	337 (19.9%)	—	1664 (98.3%)	1664 (98.3%)	25 (1.5%)	—	37 (2.2%)
226	46	46 (100%)	44 (95.7%)	7 (15.2%)	22 (47.8%)	44 (95.7%)	44 (95.7%)	1 (2.2%)	—	—
227	841	841 (100%)	840 (99.9%)	322 (38.3%)	231 (27.5%)	840 (99.9%)	840 (99.9%)	1 (0.1%)	1 (0.1%)	33 (3.9%)
229	210	209 (99.5%)	196 (93.3%)	7 (3.3%)	31 (14.8%)	196 (93.3%)	196 (93.3%)	6 (2.9%)	5 (2.4%)	31 (14.8%)
230	6	6 (100%)	6 (100%)	1 (16.7%)	6 (100%)	4 (66.7%)	6 (100%)	—	—	—
Total	38298	34664 (90.5%)	33636 (87.8%)	3162 (8.3%)	24841 (64.9%)	19688 (51.4%)	33312 (87.0%)	4529 (11.8%)	17 (0.0%)	769 (2.0%)

Table S19: In this table, we list the number of isolated sets of bands w/o SOC as determined by band connectivity (see SM 2) in unique materials in each SG in each topological class. In order, the columns in this table list the SG, the number of unique materials in the SG, the number of NLC-classified sets of bands, the number of SEBR-classified sets of bands, the number of LCEBR-classified sets of bands, the number of sets of connected fragile bands, and the total number of sets of isolated (connected) bands. For all of the topological classification categories in the table, each number of bands is accompanied by the percentage of bands in the SG in the topological class. When there are no bands in the topological class, the table entry is marked with a dashed horizontal line.

SG	# Mat.	# NLC bands	# SEBR bands	# LCEBR bands	# Fragile bands	Total # isolated bands
1	151	—	—	13271 (100%)	—	13271
2	1466	181126 (81.7%)	—	40496 (18.3%)	—	221622
3	10	89 (29.0%)	—	218 (71.0%)	—	307
4	219	—	—	9057 (100%)	—	9057
5	148	—	—	7054 (100%)	—	7054
6	28	—	—	692 (100%)	—	692
7	85	—	—	3498 (100%)	—	3498
8	141	—	—	4171 (100%)	—	4171
9	197	—	—	8834 (100%)	—	8834
10	33	40 (14.0%)	—	245 (85.7%)	1 (0.3%)	286
11	547	411 (3.9%)	—	10218 (96.1%)	—	10629
12	1250	7793 (26.8%)	—	21273 (73.0%)	56 (0.2%)	29122
13	164	721 (21.4%)	—	2648 (78.6%)	—	3369
14	2520	14220 (18.0%)	—	64657 (82.0%)	2 (0.0%)	78879
15	1402	14168 (34.3%)	—	27162 (65.7%)	—	41330
16	2	—	—	9 (100%)	—	9
17	8	—	—	61 (100%)	—	61
18	30	—	—	820 (100%)	—	820
19	261	—	—	7018 (100%)	—	7018
20	58	—	—	1463 (100%)	—	1463
21	15	—	—	147 (100%)	—	147
22	14	—	—	184 (100%)	—	184
23	15	—	—	427 (100%)	—	427
24	2	—	—	23 (100%)	—	23
25	45	—	—	280 (100%)	—	280
26	59	—	—	838 (100%)	—	838
27	1	—	—	4 (100%)	—	4
28	11	—	—	91 (100%)	—	91
29	59	—	—	1124 (100%)	—	1124
30	5	—	—	107 (100%)	—	107
31	158	—	—	3384 (100%)	—	3384
32	10	—	—	268 (100%)	—	268

33	251	—	—	5382 (100%)	—	5382
34	21	—	—	504 (100%)	—	504
35	8	—	—	131 (100%)	—	131
36	241	—	—	4848 (100%)	—	4848
37	5	9 (15.2%)	—	50 (84.8%)	—	59
38	95	—	—	1057 (100%)	—	1057
39	12	—	—	120 (100%)	—	120
40	54	—	—	998 (100%)	—	998
41	31	—	—	591 (100%)	—	591
42	4	—	—	96 (100%)	—	96
43	83	—	—	2409 (100%)	—	2409
44	62	—	—	933 (100%)	—	933
45	8	—	—	121 (100%)	—	121
46	55	—	—	667 (100%)	—	667
47	45	—	—	299 (100%)	—	299
48	3	—	—	21 (100%)	—	21
50	7	7 (11.5%)	—	54 (88.5%)	—	61
51	100	—	—	638 (100%)	—	638
52	36	27 (8.1%)	—	307 (91.9%)	—	334
53	18	23 (12.4%)	—	162 (87.6%)	—	185
54	18	1 (0.5%)	—	201 (99.5%)	—	202
55	336	—	—	2814 (100%)	—	2814
56	19	28 (11.3%)	—	220 (88.7%)	—	248
57	128	—	—	1161 (100%)	—	1161
58	202	351 (14.8%)	—	2012 (85.1%)	1 (0.0%)	2364
59	208	—	—	1754 (100%)	—	1754
60	139	151 (10.2%)	—	1330 (89.8%)	—	1481
61	119	—	—	1359 (100%)	—	1359
62	2800	—	—	28024 (100%)	—	28024
63	1277	—	—	8619 (100%)	1 (0.0%)	8620
64	244	—	—	2488 (99.9%)	2 (0.1%)	2490
65	213	—	—	1209 (99.8%)	2 (0.2%)	1211
66	34	17 (6.7%)	—	237 (92.9%)	1 (0.4%)	255
67	29	—	—	170 (100%)	—	170
68	19	8 (4.3%)	—	178 (95.7%)	—	186
69	65	—	—	841 (99.5%)	4 (0.5%)	845
70	130	222 (15.4%)	—	1218 (84.6%)	—	1440
71	385	—	—	2847 (99.9%)	3 (0.1%)	2850
72	182	—	—	1031 (100%)	—	1031
73	16	—	—	186 (100%)	—	186
74	202	—	—	1121 (99.9%)	1 (0.1%)	1122
75	5	24 (16.0%)	—	126 (84.0%)	—	150
76	12	—	—	337 (100%)	—	337
77	2	1 (7.7%)	—	12 (92.3%)	—	13
78	2	—	—	89 (100%)	—	89
79	11	—	—	294 (99.7%)	1 (0.3%)	295
80	3	—	—	137 (100%)	—	137
81	13	196 (46.9%)	—	221 (52.9%)	1 (0.2%)	418
82	130	1936 (40.6%)	—	2762 (58.0%)	65 (1.4%)	4763
83	9	4 (5.6%)	—	67 (94.4%)	—	71
84	28	36 (9.6%)	—	341 (90.5%)	—	377
85	36	111 (20.4%)	—	433 (79.6%)	—	544
86	49	28 (7.3%)	—	353 (92.7%)	—	381
87	175	567 (22.8%)	—	1917 (77.1%)	2 (0.1%)	2486
88	129	350 (17.3%)	—	1655 (82.0%)	13 (0.6%)	2018
90	5	—	—	122 (97.6%)	3 (2.4%)	125
91	7	—	—	59 (100%)	—	59
92	47	—	—	611 (100%)	—	611
94	1	—	—	10 (100%)	—	10
95	3	—	—	21 (100%)	—	21
96	16	—	—	207 (100%)	—	207
97	2	—	—	25 (96.2%)	1 (3.9%)	26
98	4	—	—	32 (100%)	—	32
99	98	—	—	544 (99.5%)	3 (0.6%)	547

100	20	—	—	419 (98.1%)	8 (1.9%)	427
102	12	—	—	132 (100%)	—	132
103	3	—	—	9 (100%)	—	9
104	3	—	—	32 (100%)	—	32
105	4	—	—	39 (100%)	—	39
106	1	—	—	7 (100%)	—	7
107	112	—	—	735 (100%)	—	735
108	14	—	—	174 (100%)	—	174
109	37	—	—	486 (100%)	—	486
110	8	—	—	138 (100%)	—	138
111	20	—	—	119 (100%)	—	119
112	4	—	—	33 (100%)	—	33
113	71	—	—	1092 (99.5%)	6 (0.6%)	1098
114	31	—	—	420 (100%)	—	420
115	21	—	—	166 (100%)	—	166
116	17	—	—	91 (98.9%)	1 (1.1%)	92
117	11	—	—	155 (100%)	—	155
118	11	—	—	117 (100%)	—	117
119	35	—	—	379 (98.4%)	6 (1.6%)	385
120	15	—	—	194 (99.5%)	1 (0.5%)	195
121	123	—	—	1509 (99.5%)	7 (0.5%)	1516
122	124	—	—	1373 (96.5%)	49 (3.5%)	1422
123	450	—	—	1646 (99.6%)	7 (0.4%)	1653
124	22	—	—	98 (100%)	—	98
125	49	—	—	370 (100%)	—	370
126	11	—	—	86 (100%)	—	86
127	368	—	—	2074 (100%)	—	2074
128	71	64 (9.2%)	—	623 (90.0%)	5 (0.7%)	692
129	861	—	—	3736 (99.8%)	8 (0.2%)	3744
130	37	5 (1.6%)	21 (6.8%)	281 (91.5%)	—	307
131	43	—	—	132 (100%)	—	132
132	10	—	—	100 (100%)	—	100
133	3	—	—	8 (100%)	—	8
134	4	—	—	6 (100%)	—	6
135	26	—	—	160 (100%)	—	160
136	251	—	—	1707 (99.9%)	1 (0.1%)	1708
137	68	—	—	541 (99.5%)	3 (0.6%)	544
138	16	—	—	117 (100%)	—	117
139	1543	—	—	6983 (99.8%)	16 (0.2%)	6999
140	431	—	—	2133 (100%)	1 (0.1%)	2134
141	246	—	—	1659 (99.3%)	11 (0.7%)	1670
142	73	—	—	468 (100%)	—	468
143	17	—	—	954 (97.3%)	26 (2.6%)	980
144	13	—	—	439 (100%)	—	439
145	5	—	—	182 (100%)	—	182
146	83	—	—	4154 (100%)	—	4154
147	71	47 (1.9%)	1351 (55.5%)	1015 (41.7%)	22 (0.9%)	2435
148	479	1857 (7.2%)	16880 (65.0%)	7035 (27.1%)	199 (0.8%)	25971
149	10	—	—	237 (97.5%)	6 (2.5%)	243
150	64	—	—	1298 (98.3%)	22 (1.7%)	1320
151	4	—	—	78 (100%)	—	78
152	40	—	—	333 (100%)	—	333
153	1	—	—	6 (100%)	—	6
154	17	—	—	171 (100%)	—	171
155	50	—	—	1351 (100%)	—	1351
156	57	—	—	750 (99.5%)	4 (0.5%)	754
157	14	—	—	238 (97.9%)	5 (2.1%)	243
158	3	—	—	61 (100%)	—	61
159	24	—	—	439 (100%)	—	439
160	158	—	—	2593 (100%)	—	2593
161	87	—	—	1691 (100%)	—	1691
162	52	—	22 (6.0%)	337 (92.3%)	6 (1.6%)	365
163	57	5 (0.5%)	100 (10.3%)	841 (87.0%)	21 (2.2%)	967
164	574	2 (0.1%)	218 (4.9%)	4060 (92.0%)	132 (3.0%)	4412

165	33	—	16 (6.5%)	230 (93.5%)	—	246
166	957	828 (7.9%)	52 (0.5%)	9314 (88.8%)	290 (2.8%)	10484
167	301	37 (1.0%)	448 (12.1%)	3202 (86.8%)	3 (0.1%)	3690
169	1	—	—	5 (100%)	—	5
173	113	—	—	2121 (100%)	1 (0.1%)	2122
174	50	—	—	655 (99.8%)	1 (0.1%)	656
175	2	—	—	16 (100%)	—	16
176	189	14 (0.6%)	62 (2.8%)	2156 (96.5%)	1 (0.0%)	2233
177	1	—	—	9 (100%)	—	9
180	28	—	—	87 (100%)	—	87
181	8	—	—	24 (100%)	—	24
182	33	—	—	263 (98.9%)	3 (1.1%)	266
183	1	—	—	3 (100%)	—	3
185	49	—	—	465 (99.4%)	3 (0.6%)	468
186	370	—	—	3674 (100%)	—	3674
187	154	—	—	737 (99.9%)	1 (0.1%)	738
188	20	—	—	247 (100%)	—	247
189	537	—	—	2614 (99.8%)	4 (0.1%)	2618
190	41	—	—	439 (99.3%)	3 (0.7%)	442
191	452	—	—	1214 (99.6%)	5 (0.4%)	1219
192	2	—	—	8 (100%)	—	8
193	270	—	—	916 (99.8%)	2 (0.2%)	918
194	1530	—	—	6630 (99.3%)	44 (0.7%)	6674
195	1	—	—	28 (100%)	—	28
196	1	—	—	36 (100%)	—	36
197	20	—	—	324 (100%)	—	324
198	170	—	—	2866 (100%)	—	2866
199	32	—	—	426 (100%)	—	426
200	22	—	—	161 (99.4%)	1 (0.6%)	162
201	6	14 (14.6%)	—	82 (85.4%)	—	96
202	18	—	—	324 (97.6%)	8 (2.4%)	332
203	6	23 (18.1%)	—	101 (79.5%)	3 (2.4%)	127
204	145	—	—	833 (100%)	—	833
205	130	—	—	1134 (97.2%)	33 (2.8%)	1167
206	60	—	—	415 (100%)	—	415
208	2	—	—	6 (100%)	—	6
210	1	—	—	9 (60.0%)	6 (40.0%)	15
211	1	—	—	5 (100%)	—	5
212	14	—	—	165 (100%)	—	165
213	22	—	—	154 (100%)	—	154
214	13	—	—	105 (100%)	—	105
215	53	—	—	412 (99.0%)	4 (1.0%)	416
216	751	—	—	4815 (92.3%)	404 (7.7%)	5219
217	108	—	—	924 (99.9%)	1 (0.1%)	925
218	42	—	—	418 (99.8%)	1 (0.2%)	419
219	8	—	—	104 (100%)	—	104
220	142	—	—	819 (99.4%)	5 (0.6%)	824
221	1334	—	—	3387 (99.8%)	8 (0.2%)	3395
223	217	—	—	690 (100%)	—	690
224	16	—	—	59 (100%)	—	59
225	1651	—	—	8290 (97.3%)	232 (2.7%)	8522
226	43	—	—	131 (100%)	—	131
227	816	—	—	3640 (98.0%)	76 (2.0%)	3716
229	205	—	—	755 (99.6%)	3 (0.4%)	758
230	6	—	—	9 (100%)	—	9
Total	36163	225561 (32.6%)	19170 (2.8%)	444191 (64.3%)	1882 (0.3%)	690804

Table S20: In this table, we list the number of unique materials that contain at least some topological features w/o SOC in each SG. In order, the columns in this table list the SG, the number of unique materials in the SG, the number of unique materials with either at least one stable or fragile band in the spectrum or symmetry-enforced crossing points at E_F (*i.e.* materials that are either ES-, ESFD-, NLC-SM- or SEBR-SM-classified semimetals at E_F or exhibit NLC, SEBR, or fragile topological bands at any filling at which the compatibility relations are satisfied). From left to right, in the following columns we list, per SG, the number of unique materials with at least one stable or fragile topological connected set of bands at any filling, at least one fragile topological set of bands at any filling, at least one NLC-classified stable topological band at any filling, at least one SEBR-classified stable topological band at any filling, and at least one stable topological set of bands at any filling. In the remaining three columns, we list the number of materials that do not contain *any* symmetry-indicated stable or fragile topological bands (STriv), the number of supermetallic (SMetal) materials in which *all* of the bands in at least one of the ICSDs associated to the unique material are *fully* connected, and the number of unique materials in which all bands are stable topological [*i.e.* supertopological (STopo) materials, see SM 9]. For all of the topological classification categories in the table, each number of materials is accompanied by the percentage of materials in the SG in the topological class. When there are no materials in the topological class, the table entry is marked with a dashed horizontal line.

SG	# Mat.	Topology	≥ 1 topo. band	≥ 1 frag. band	≥ 1 NLC band	≥ 1 SEBR band	≥ 1 NLC or SEBR band	STriv	SMetal	STopo
1	151	9 (6.0%)	—	—	—	—	—	151 (100%)	—	—
2	1466	1466 (100%)	1466 (100%)	—	1466 (100%)	—	1466 (100%)	—	—	6 (0.4%)
3	10	10 (100%)	9 (90.0%)	—	9 (90.0%)	—	9 (90.0%)	1 (10.0%)	—	—
4	219	20 (9.1%)	—	—	—	—	—	218 (99.5%)	—	—
5	148	31 (20.9%)	—	—	—	—	—	148 (100%)	—	—
6	28	5 (17.9%)	—	—	—	—	—	28 (100%)	—	—
7	85	9 (10.6%)	—	—	—	—	—	85 (100%)	—	—
8	141	26 (18.4%)	—	—	—	—	—	138 (97.9%)	—	—
9	197	15 (7.6%)	—	—	—	—	—	197 (100%)	—	—
10	33	27 (81.8%)	22 (66.7%)	1 (3.0%)	22 (66.7%)	—	22 (66.7%)	10 (30.3%)	—	—
11	547	308 (56.3%)	182 (33.3%)	—	182 (33.3%)	—	182 (33.3%)	349 (63.8%)	3 (0.6%)	—
12	1250	1203 (96.2%)	1151 (92.1%)	46 (3.7%)	1144 (91.5%)	—	1144 (91.5%)	90 (7.2%)	1 (0.1%)	3 (0.2%)
13	164	144 (87.8%)	141 (86.0%)	—	141 (86.0%)	—	141 (86.0%)	26 (15.8%)	—	—
14	2520	2353 (93.4%)	2325 (92.3%)	2 (0.1%)	2325 (92.3%)	—	2325 (92.3%)	216 (8.6%)	—	—
15	1402	1376 (98.2%)	1366 (97.4%)	—	1366 (97.4%)	—	1366 (97.4%)	46 (3.3%)	1 (0.1%)	—
16	2	1 (50.0%)	—	—	—	—	—	1 (50.0%)	—	—
17	8	3 (37.5%)	—	—	—	—	—	7 (87.5%)	—	—
18	30	6 (20.0%)	—	—	—	—	—	30 (100%)	—	—
19	261	28 (10.7%)	—	—	—	—	—	261 (100%)	—	—
20	58	5 (8.6%)	—	—	—	—	—	58 (100%)	—	—
21	15	9 (60.0%)	—	—	—	—	—	12 (80.0%)	—	—
22	14	11 (78.6%)	—	—	—	—	—	14 (100%)	—	—
23	15	5 (33.3%)	—	—	—	—	—	15 (100%)	—	—
24	2	—	—	—	—	—	—	2 (100%)	—	—
25	45	14 (31.1%)	—	—	—	—	—	39 (86.7%)	—	—
26	59	12 (20.3%)	—	—	—	—	—	57 (96.6%)	—	—
27	1	—	—	—	—	—	—	1 (100%)	—	—
28	11	7 (63.6%)	—	—	—	—	—	8 (72.7%)	1 (9.1%)	—
29	59	2 (3.4%)	—	—	—	—	—	59 (100%)	—	—
30	5	2 (40.0%)	—	—	—	—	—	5 (100%)	—	—
31	158	33 (20.9%)	—	—	—	—	—	158 (100%)	—	—
32	10	—	—	—	—	—	—	10 (100%)	—	—
33	251	43 (17.1%)	—	—	—	—	—	251 (100%)	—	—
34	21	5 (23.8%)	—	—	—	—	—	20 (95.2%)	—	—
35	8	4 (50.0%)	—	—	—	—	—	7 (87.5%)	—	—

36	241	53 (22.0%)	—	—	—	—	—	238 (98.8%)	—	—
37	5	5 (100%)	5 (100%)	—	5 (100%)	—	5 (100%)	—	—	—
38	95	69 (72.6%)	—	—	—	—	—	78 (82.1%)	3 (3.2%)	—
39	12	3 (25.0%)	—	—	—	—	—	11 (91.7%)	—	—
40	54	7 (13.0%)	—	—	—	—	—	53 (98.2%)	—	—
41	31	10 (32.3%)	—	—	—	—	—	28 (90.3%)	—	—
42	4	—	—	—	—	—	—	4 (100%)	—	—
43	83	21 (25.3%)	—	—	—	—	—	83 (100%)	—	—
44	62	35 (56.5%)	—	—	—	—	—	58 (93.5%)	—	—
45	8	2 (25.0%)	—	—	—	—	—	8 (100%)	—	—
46	55	30 (54.5%)	—	—	—	—	—	51 (92.7%)	—	—
47	45	42 (93.3%)	—	—	—	—	—	32 (71.1%)	2 (4.4%)	—
48	3	1 (33.3%)	—	—	—	—	—	3 (100%)	—	—
50	7	6 (85.7%)	2 (28.6%)	—	2 (28.6%)	—	2 (28.6%)	4 (57.1%)	1 (14.3%)	—
51	100	77 (77.0%)	—	—	—	—	—	36 (36.0%)	20 (20.0%)	—
52	36	17 (47.2%)	14 (38.9%)	—	14 (38.9%)	—	14 (38.9%)	22 (61.1%)	—	—
53	18	12 (66.7%)	8 (44.4%)	—	8 (44.4%)	—	8 (44.4%)	12 (66.7%)	—	—
54	18	7 (38.9%)	1 (5.6%)	—	1 (5.6%)	—	1 (5.6%)	16 (88.9%)	—	—
55	336	252 (75.0%)	—	—	—	—	—	172 (51.2%)	8 (2.4%)	—
56	19	12 (63.2%)	11 (57.9%)	—	11 (57.9%)	—	11 (57.9%)	10 (52.6%)	—	—
57	128	48 (37.5%)	—	—	—	—	—	98 (76.6%)	—	—
58	202	163 (80.7%)	129 (63.9%)	1 (0.5%)	129 (63.9%)	—	129 (63.9%)	69 (34.2%)	—	—
59	208	143 (68.8%)	—	—	—	—	—	136 (65.4%)	8 (3.9%)	—
60	139	76 (54.7%)	54 (38.9%)	—	54 (38.9%)	—	54 (38.9%)	84 (60.4%)	1 (0.7%)	—
61	119	18 (15.1%)	—	—	—	—	—	116 (97.5%)	—	—
62	2800	1451 (51.8%)	—	—	—	—	—	2257 (80.6%)	10 (0.4%)	—
63	1277	924 (72.4%)	—	—	—	—	—	735 (57.6%)	25 (2.0%)	—
64	244	113 (46.3%)	2 (0.8%)	2 (0.8%)	—	—	—	182 (74.6%)	13 (5.3%)	—
65	213	193 (90.6%)	2 (0.9%)	2 (0.9%)	—	—	—	57 (26.8%)	13 (6.1%)	—
66	34	22 (64.7%)	10 (29.4%)	1 (2.9%)	9 (26.5%)	—	9 (26.5%)	17 (50.0%)	—	—
67	29	17 (58.6%)	—	—	—	—	—	25 (86.2%)	1 (3.5%)	—
68	19	8 (42.1%)	4 (21.1%)	—	4 (21.1%)	—	4 (21.1%)	12 (63.2%)	1 (5.3%)	—
69	65	46 (70.8%)	3 (4.6%)	3 (4.6%)	—	—	—	44 (67.7%)	3 (4.6%)	—
70	130	105 (80.8%)	88 (67.7%)	—	88 (67.7%)	—	88 (67.7%)	40 (30.8%)	—	—
71	385	316 (82.1%)	2 (0.5%)	2 (0.5%)	—	—	—	144 (37.4%)	19 (4.9%)	—
72	182	109 (59.9%)	—	—	—	—	—	112 (61.5%)	7 (3.9%)	—
73	16	1 (6.2%)	—	—	—	—	—	16 (100%)	—	—
74	202	153 (75.7%)	1 (0.5%)	1 (0.5%)	—	—	—	105 (52.0%)	8 (4.0%)	—
75	5	5 (100%)	5 (100%)	—	5 (100%)	—	5 (100%)	—	—	—
76	12	2 (16.7%)	—	—	—	—	—	12 (100%)	—	—
77	2	1 (50.0%)	1 (50.0%)	—	1 (50.0%)	—	1 (50.0%)	1 (50.0%)	—	—
78	2	—	—	—	—	—	—	2 (100%)	—	—
79	11	2 (18.2%)	1 (9.1%)	1 (9.1%)	—	—	—	11 (100%)	—	—
80	3	—	—	—	—	—	—	3 (100%)	—	—
81	13	13 (100%)	13 (100%)	1 (7.7%)	13 (100%)	—	13 (100%)	—	—	—
82	130	130 (100%)	130 (100%)	40 (30.8%)	130 (100%)	—	130 (100%)	—	—	—
83	9	8 (88.9%)	2 (22.2%)	—	2 (22.2%)	—	2 (22.2%)	1 (11.1%)	1 (11.1%)	—
84	28	18 (64.3%)	15 (53.6%)	—	15 (53.6%)	—	15 (53.6%)	13 (46.4%)	—	—
85	36	32 (88.9%)	30 (83.3%)	—	30 (83.3%)	—	30 (83.3%)	7 (19.4%)	—	—
86	49	43 (87.8%)	21 (42.9%)	—	21 (42.9%)	—	21 (42.9%)	19 (38.8%)	—	—
87	175	166 (94.9%)	146 (83.4%)	2 (1.1%)	146 (83.4%)	—	146 (83.4%)	20 (11.4%)	3 (1.7%)	7 (4.0%)
88	129	91 (70.5%)	85 (65.9%)	9 (7.0%)	84 (65.1%)	—	84 (65.1%)	49 (38.0%)	—	—
90	5	5 (100%)	2 (40.0%)	2 (40.0%)	—	—	—	3 (60.0%)	—	—
91	7	3 (42.9%)	—	—	—	—	—	6 (85.7%)	—	—
92	47	18 (38.3%)	—	—	—	—	—	46 (97.9%)	1 (2.1%)	—
94	1	1 (100%)	—	—	—	—	—	1 (100%)	—	—
95	3	1 (33.3%)	—	—	—	—	—	3 (100%)	—	—
96	16	1 (6.2%)	—	—	—	—	—	16 (100%)	—	—
97	2	1 (50.0%)	1 (50.0%)	1 (50.0%)	—	—	—	1 (50.0%)	—	—
98	4	1 (25.0%)	—	—	—	—	—	4 (100%)	—	—
99	98	28 (28.6%)	3 (3.1%)	3 (3.1%)	—	—	—	87 (88.8%)	1 (1.0%)	—
100	20	15 (75.0%)	8 (40.0%)	8 (40.0%)	—	—	—	15 (75.0%)	—	—
102	12	6 (50.0%)	—	—	—	—	—	10 (83.3%)	—	—
103	3	3 (100%)	—	—	—	—	—	1 (33.3%)	—	—

104	3	1 (33.3%)	—	—	—	—	—	—	2 (66.7%)	—	—
105	4	1 (25.0%)	—	—	—	—	—	—	4 (100%)	—	—
106	1	1 (100%)	—	—	—	—	—	—	1 (100%)	—	—
107	112	101 (90.2%)	—	—	—	—	—	—	97 (86.6%)	—	—
108	14	7 (50.0%)	—	—	—	—	—	—	11 (78.6%)	—	—
109	37	23 (62.2%)	—	—	—	—	—	—	37 (100%)	—	—
110	8	3 (37.5%)	—	—	—	—	—	—	8 (100%)	—	—
111	20	7 (35.0%)	—	—	—	—	—	—	19 (95.0%)	—	—
112	4	—	—	—	—	—	—	—	4 (100%)	—	—
113	71	29 (40.9%)	5 (7.0%)	5 (7.0%)	—	—	—	—	62 (87.3%)	—	—
114	31	6 (19.4%)	—	—	—	—	—	—	30 (96.8%)	—	—
115	21	15 (71.4%)	—	—	—	—	—	—	16 (76.2%)	1 (4.8%)	—
116	17	4 (23.5%)	1 (5.9%)	1 (5.9%)	—	—	—	—	15 (88.2%)	—	—
117	11	6 (54.5%)	—	—	—	—	—	—	10 (90.9%)	—	—
118	11	3 (27.3%)	—	—	—	—	—	—	10 (90.9%)	—	—
119	35	20 (57.1%)	5 (14.3%)	5 (14.3%)	—	—	—	—	30 (85.7%)	—	—
120	15	7 (46.7%)	1 (6.7%)	1 (6.7%)	—	—	—	—	10 (66.7%)	—	—
121	123	60 (48.8%)	5 (4.1%)	5 (4.1%)	—	—	—	—	112 (91.1%)	1 (0.8%)	—
122	124	45 (36.3%)	30 (24.2%)	30 (24.2%)	—	—	—	—	92 (74.2%)	—	—
123	450	395 (87.8%)	5 (1.1%)	5 (1.1%)	—	—	—	—	122 (27.1%)	76 (16.9%)	—
124	22	19 (86.4%)	—	—	—	—	—	—	6 (27.3%)	—	—
125	49	32 (65.3%)	—	—	—	—	—	—	30 (61.2%)	—	—
126	11	4 (36.4%)	—	—	—	—	—	—	10 (90.9%)	—	—
127	368	326 (88.6%)	—	—	—	—	—	—	74 (20.1%)	18 (4.9%)	—
128	71	55 (77.5%)	30 (42.2%)	5 (7.0%)	29 (40.9%)	—	29 (40.9%)	—	27 (38.0%)	1 (1.4%)	—
129	861	697 (81.0%)	8 (0.9%)	8 (0.9%)	—	—	—	—	422 (49.0%)	18 (2.1%)	—
130	37	28 (75.7%)	9 (24.3%)	—	2 (5.4%)	8 (21.6%)	9 (24.3%)	—	13 (35.1%)	—	—
131	43	36 (83.7%)	—	—	—	—	—	—	10 (23.3%)	—	—
132	10	1 (10.0%)	—	—	—	—	—	—	10 (100%)	—	—
133	3	2 (66.7%)	—	—	—	—	—	—	1 (33.3%)	—	—
134	4	3 (75.0%)	—	—	—	—	—	—	2 (50.0%)	1 (25.0%)	—
135	26	15 (57.7%)	—	—	—	—	—	—	18 (69.2%)	—	—
136	251	188 (74.9%)	1 (0.4%)	1 (0.4%)	—	—	—	—	131 (52.2%)	26 (10.4%)	—
137	68	38 (55.9%)	3 (4.4%)	3 (4.4%)	—	—	—	—	47 (69.1%)	—	—
138	16	7 (43.8%)	—	—	—	—	—	—	14 (87.5%)	—	—
139	1543	1388 (90.0%)	15 (1.0%)	15 (1.0%)	—	—	—	—	437 (28.3%)	122 (7.9%)	—
140	431	319 (74.0%)	1 (0.2%)	1 (0.2%)	—	—	—	—	163 (37.8%)	58 (13.5%)	—
141	246	175 (71.1%)	10 (4.1%)	10 (4.1%)	—	—	—	—	160 (65.0%)	3 (1.2%)	—
142	73	35 (48.0%)	—	—	—	—	—	—	55 (75.3%)	2 (2.7%)	—
143	17	10 (58.8%)	7 (41.2%)	7 (41.2%)	—	—	—	—	10 (58.8%)	—	—
144	13	2 (15.4%)	—	—	—	—	—	—	13 (100%)	—	—
145	5	—	—	—	—	—	—	—	5 (100%)	—	—
146	83	20 (24.1%)	—	—	—	—	—	—	83 (100%)	—	—
147	71	71 (100%)	71 (100%)	17 (23.9%)	34 (47.9%)	71 (100%)	71 (100%)	—	—	—	—
148	479	479 (100%)	479 (100%)	116 (24.2%)	429 (89.6%)	479 (100%)	479 (100%)	—	—	3 (0.6%)	—
149	10	8 (80.0%)	3 (30.0%)	3 (30.0%)	—	—	—	—	6 (60.0%)	—	—
150	64	24 (37.5%)	12 (18.8%)	12 (18.8%)	—	—	—	—	49 (76.6%)	—	—
151	4	—	—	—	—	—	—	—	4 (100%)	—	—
152	40	9 (22.5%)	—	—	—	—	—	—	39 (97.5%)	—	—
153	1	1 (100%)	—	—	—	—	—	—	1 (100%)	—	—
154	17	2 (11.8%)	—	—	—	—	—	—	17 (100%)	—	—
155	50	19 (38.0%)	—	—	—	—	—	—	50 (100%)	—	—
156	57	18 (31.6%)	3 (5.3%)	3 (5.3%)	—	—	—	—	54 (94.7%)	—	—
157	14	8 (57.1%)	3 (21.4%)	3 (21.4%)	—	—	—	—	9 (64.3%)	—	—
158	3	3 (100%)	—	—	—	—	—	—	3 (100%)	—	—
159	24	6 (25.0%)	—	—	—	—	—	—	24 (100%)	—	—
160	158	58 (36.7%)	—	—	—	—	—	—	156 (98.7%)	—	—
161	87	18 (20.7%)	—	—	—	—	—	—	87 (100%)	—	—
162	52	37 (71.2%)	18 (34.6%)	4 (7.7%)	—	15 (28.9%)	15 (28.9%)	—	29 (55.8%)	1 (1.9%)	—
163	57	47 (82.5%)	38 (66.7%)	14 (24.6%)	5 (8.8%)	34 (59.6%)	35 (61.4%)	—	18 (31.6%)	—	—
164	574	404 (70.4%)	196 (34.1%)	88 (15.3%)	2 (0.3%)	127 (22.1%)	127 (22.1%)	—	302 (52.6%)	7 (1.2%)	7 (1.2%)
165	33	24 (72.7%)	9 (27.3%)	—	—	9 (27.3%)	9 (27.3%)	—	14 (42.4%)	—	—
166	957	792 (82.8%)	499 (52.1%)	159 (16.6%)	412 (43.0%)	33 (3.5%)	436 (45.6%)	—	365 (38.1%)	7 (0.7%)	1 (0.1%)
167	301	234 (77.7%)	177 (58.8%)	—	26 (8.6%)	174 (57.8%)	177 (58.8%)	—	131 (43.5%)	—	1 (0.3%)

169	1	—	—	—	—	—	—	—	1 (100%)	—	—
173	113	40 (35.4%)	1 (0.9%)	1 (0.9%)	—	—	—	—	111 (98.2%)	—	—
174	50	33 (66.0%)	1 (2.0%)	1 (2.0%)	—	—	—	—	37 (74.0%)	—	—
175	2	2 (100%)	—	—	—	—	—	—	—	—	—
176	189	110 (58.2%)	33 (17.5%)	1 (0.5%)	11 (5.8%)	32 (16.9%)	32 (16.9%)	128 (67.7%)	3 (1.6%)	—	—
177	1	—	—	—	—	—	—	1 (100%)	—	—	—
180	28	18 (64.3%)	—	—	—	—	—	19 (67.9%)	5 (17.9%)	—	—
181	8	5 (62.5%)	—	—	—	—	—	8 (100%)	—	—	—
182	33	26 (78.8%)	2 (6.1%)	2 (6.1%)	—	—	—	23 (69.7%)	—	—	—
183	1	—	—	—	—	—	—	1 (100%)	—	—	—
185	49	31 (63.3%)	2 (4.1%)	2 (4.1%)	—	—	—	36 (73.5%)	3 (6.1%)	—	—
186	370	203 (54.9%)	—	—	—	—	—	314 (84.9%)	—	—	—
187	154	123 (79.9%)	1 (0.7%)	1 (0.7%)	—	—	—	77 (50.0%)	3 (1.9%)	—	—
188	20	4 (20.0%)	—	—	—	—	—	19 (95.0%)	—	—	—
189	537	483 (89.9%)	2 (0.4%)	2 (0.4%)	—	—	—	121 (22.5%)	3 (0.6%)	—	—
190	41	25 (61.0%)	2 (4.9%)	2 (4.9%)	—	—	—	29 (70.7%)	—	—	—
191	452	449 (99.3%)	4 (0.9%)	4 (0.9%)	—	—	—	8 (1.8%)	69 (15.3%)	—	—
192	2	—	—	—	—	—	—	2 (100%)	—	—	—
193	270	258 (95.6%)	2 (0.7%)	2 (0.7%)	—	—	—	43 (15.9%)	10 (3.7%)	—	—
194	1530	1285 (84.0%)	31 (2.0%)	31 (2.0%)	—	—	—	532 (34.8%)	142 (9.3%)	—	—
195	1	—	—	—	—	—	—	1 (100%)	—	—	—
196	1	1 (100%)	—	—	—	—	—	1 (100%)	—	—	—
197	20	10 (50.0%)	—	—	—	—	—	20 (100%)	—	—	—
198	170	77 (45.3%)	—	—	—	—	—	168 (98.8%)	—	—	—
199	32	9 (28.1%)	—	—	—	—	—	32 (100%)	—	—	—
200	22	17 (77.3%)	1 (4.5%)	1 (4.5%)	—	—	—	12 (54.5%)	—	—	—
201	6	6 (100%)	5 (83.3%)	—	5 (83.3%)	—	5 (83.3%)	1 (16.7%)	—	—	—
202	18	13 (72.2%)	7 (38.9%)	7 (38.9%)	—	—	—	13 (72.2%)	—	—	—
203	6	5 (83.3%)	5 (83.3%)	2 (33.3%)	5 (83.3%)	—	5 (83.3%)	1 (16.7%)	—	—	—
204	145	123 (84.8%)	—	—	—	—	—	120 (82.8%)	5 (3.5%)	—	—
205	130	62 (47.7%)	24 (18.5%)	24 (18.5%)	—	—	—	111 (85.4%)	—	—	—
206	60	30 (50.0%)	—	—	—	—	—	58 (96.7%)	2 (3.3%)	—	—
208	2	2 (100%)	—	—	—	—	—	2 (100%)	—	—	—
210	1	1 (100%)	1 (100%)	1 (100%)	—	—	—	—	—	—	—
211	1	1 (100%)	—	—	—	—	—	—	—	—	—
212	14	8 (57.1%)	—	—	—	—	—	14 (100%)	—	—	—
213	22	17 (77.3%)	—	—	—	—	—	22 (100%)	—	—	—
214	13	7 (53.9%)	—	—	—	—	—	13 (100%)	—	—	—
215	53	25 (47.2%)	3 (5.7%)	3 (5.7%)	—	—	—	39 (73.6%)	—	—	—
216	751	600 (79.9%)	301 (40.1%)	301 (40.1%)	—	—	—	440 (58.6%)	—	—	—
217	108	66 (61.1%)	1 (0.9%)	1 (0.9%)	—	—	—	82 (75.9%)	3 (2.8%)	—	—
218	42	13 (30.9%)	1 (2.4%)	1 (2.4%)	—	—	—	41 (97.6%)	—	—	—
219	8	5 (62.5%)	—	—	—	—	—	8 (100%)	—	—	—
220	142	115 (81.0%)	5 (3.5%)	5 (3.5%)	—	—	—	119 (83.8%)	—	—	—
221	1334	1171 (87.8%)	8 (0.6%)	8 (0.6%)	—	—	—	278 (20.8%)	237 (17.8%)	—	—
223	217	214 (98.6%)	—	—	—	—	—	34 (15.7%)	24 (11.1%)	—	—
224	16	9 (56.2%)	—	—	—	—	—	11 (68.8%)	—	—	—
225	1651	1293 (78.3%)	168 (10.2%)	168 (10.2%)	—	—	—	959 (58.1%)	78 (4.7%)	—	—
226	43	42 (97.7%)	—	—	—	—	—	4 (9.3%)	1 (2.3%)	—	—
227	816	684 (83.8%)	71 (8.7%)	71 (8.7%)	—	—	—	539 (66.0%)	21 (2.6%)	—	—
229	205	185 (90.2%)	2 (1.0%)	2 (1.0%)	—	—	—	61 (29.8%)	30 (14.6%)	—	—
230	6	5 (83.3%)	—	—	—	—	—	3 (50.0%)	2 (33.3%)	—	—
Total	36163	26660 (73.7%)	9789 (27.1%)	1293 (3.6%)	8387 (23.2%)	982 (2.7%)	8856 (24.5%)	16725 (46.2%)	1138 (3.1%)	28 (0.1%)	—

Table S21: Nonmagnetic unique materials without f electrons in which one or more associated ICSD entries exhibit a connected grouping of bands with dimension ≥ 130 in the presence of SOC. In order, for each unique material containing a grouping of bands with connectivity ≥ 130 with SOC, the columns in this table list the chemical formula, the SG number, the SG symbol, the ICSD number, the stable topological classification at E_F , the number of valence electrons (num e^-), and the largest number of connected bands across the electronic band structures of all of the ICSDs associated to the unique material (noting that the VASP calculations performed in this work have been truncated at fillings of $\sim 2N_e$, see SM 4 for further calculation details). In the right-most column of this table, we also list in parentheses a percentage corresponding to the ratio of the maximum band connectivity with SOC in the unique material relative to $2N_e$, which is the approximate total number of bands in each VASP calculation performed with SOC. A chemical formula with a * indicates that only some (but not all) of the ICSDs associated to the same unique material (defined using its topological class with SOC) contain a connected grouping of bands with dimension ≥ 130 in the presence of SOC.

Chem. formula	SG #	SG symbol	ICSD	Top. subclass.	num e^-	nbr connected bands
Cu ₃ P*	165	$P\bar{3}c1$	628626	ES	228	144 (31.58%)
AgCd ₃ Hf ₃ F ₂₀	176	$P6_3/m$	78893	ESFD	398	136 (17.09%)
Cu ₃ P	185	$P6_3cm$	15056	ES	228	164 (35.96%)
Hf ₅ ZnSb ₃	193	$P6_3/mcm$	42913	ESFD	94	145 (77.13%)
Nb ₅ Ge ₃	193	$P6_3/mcm$	637215	ESFD	154	157 (50.97%)
K ₆ (BiCl ₆)Cl ₂ (H ₃ F ₄)	194	$P6_3/mmc$	68226	LCEBR	292	156 (26.71%)
Ga ₅ V ₆	194	$P6_3/mmc$	108499	ESFD	90	164 (91.11%)
Mg ₁₇ Sr ₂	194	$P6_3/mmc$	150736	ES	108	145 (67.13%)
Hf ₉ (HfMo ₃)Si	194	$P6_3/mmc$	603654	ES	124	136 (54.84%)
W ₁₀ Co ₃ C ₄	194	$P6_3/mmc$	617464	ESFD	206	136 (33.01%)
Hf ₉ Mo ₄ Si*	194	$P6_3/mmc$	638632	ES	128	132 (51.56%)
Cu ₅ Zn ₈	217	$I\bar{4}3m$	2092	ESFD	302	156 (25.83%)
CaHg ₁₁	221	$Pm\bar{3}m$	58902	ES	402	150 (18.66%)
BaHg ₁₁ *	221	$Pm\bar{3}m$	107486	SEBR	426	172 (20.19%)
KHg ₁₁	221	$Pm\bar{3}m$	410566	ESFD	423	130 (15.37%)
Ba ₈ Au ₆ Si ₄ *	223	$Pm\bar{3}n$	40567	ESFD	306	132 (21.57%)
Ru ₄ Y ₃ Ge ₁₃	223	$Pm\bar{3}n$	53900	ESFD	234	216 (46.15%)
Ni ₃ Ba ₄ Ge ₂₀	223	$Pm\bar{3}n$	57034	ESFD	300	136 (22.67%)
Pd ₃ Ba ₄ Ge ₂₀	223	$Pm\bar{3}n$	57035	ESFD	300	136 (22.67%)
Au ₃ Ba ₄ Ge ₂₀	223	$Pm\bar{3}n$	57037	ESFD	306	136 (22.22%)
AuZn ₃	223	$Pm\bar{3}n$	58626	ES	376	132 (17.55%)
Ca ₃ Rh ₄ Sn ₁₃	223	$Pm\bar{3}n$	58930	ESFD	188	168 (44.68%)
Cs ₈ Sn ₄₆	223	$Pm\bar{3}n$	62352	ES	256	177 (34.57%)
Ba ₆ Si ₄₆	223	$Pm\bar{3}n$	94263	ESFD	244	212 (43.44%)
Si ₄₆	223	$Pm\bar{3}n$	186544	LCEBR	184	173 (47.01%)
Si	223	$Pm\bar{3}n$	189393	LCEBR	184	157 (42.66%)
Na ₂ Ba ₆ Si ₄₆	223	$Pm\bar{3}n$	409912	ESFD	246	152 (30.89%)
Ca ₃ Ir ₄ Ge ₁₃	223	$Pm\bar{3}n$	619308	ES	188	216 (57.45%)
Y ₃ Co ₄ Ge ₁₃	223	$Pm\bar{3}n$	623663	ESFD	242	132 (27.27%)
Cs ₄ Sn ₂₃	223	$Pm\bar{3}n$	627107	ESFD	256	177 (34.57%)
Cs ₄ Sn ₂₃	223	$Pm\bar{3}n$	627108	ES	256	177 (34.57%)
Y ₃ Ir ₄ Ge ₁₃	223	$Pm\bar{3}n$	636763	ESFD	242	160 (33.06%)
Y ₃ Os ₄ Ge ₁₃	223	$Pm\bar{3}n$	637488	ESFD	234	216 (46.15%)
Y ₃ Rh ₄ Ge ₁₃	223	$Pm\bar{3}n$	637724	ESFD	242	192 (39.67%)
Cd ₁₃ K*	226	$Fm\bar{3}c$	102002	ESFD	330	184 (27.88%)
BaCu ₁₃	226	$Fm\bar{3}c$	108093	ESFD	306	176 (28.76%)
Ag ₁₃ OsO ₆	226	$Fm\bar{3}c$	413193	ESFD	374	172 (22.99%)
YRu ₂ Zn ₂₀	227	$Fd\bar{3}m$	152110	ESFD	534	156 (14.61%)
Ag ₁₆ Ca ₆ N	229	$Im\bar{3}m$	78395	ESFD	193	188 (48.7%)
Ag ₈ Ca ₃	229	$Im\bar{3}m$	107145	ESFD	188	184 (48.94%)
Al ₄ Ni ₃	230	$Ia\bar{3}d$	58042	SEBR	336	192 (28.57%)
Bi ₄ Rh	230	$Ia\bar{3}d$	58854	ESFD	348	249 (35.78%)
Ga ₄ Ni ₃	230	$Ia\bar{3}d$	103864	ES	336	256 (38.1%)

Ga ₃ Ni ₃ Zn	230	<i>Ia</i> $\bar{3}d$	103898	ESFD	408	184 (22.55%)
------------------------------------	-----	----------------------	--------	------	-----	--------------

SM 9. REPEAT-TOPOLOGY AND SUPERTOPOLOGY

In this work, we introduce the concept of a *repeat-topological* (RTopo) material – a material in which the gap at the Fermi level, as well as the next gap below the Fermi level as measured by band connectivity, exhibit cumulative symmetry-indicated stable topology [see Fig. S4A]. We additionally introduce the concept of a *supertopological* (STopo) material – a material in which *every* energetically isolated set of bands in the spectrum obtained from our first-principles calculations (see SM 4) exhibits symmetry-indicated stable topology [see Fig. S4B]. In this section, we will first rigorously define repeat-topology in SM 9 A. Then, in SM 9 B, we will further define supertopology. Lastly, in SM 9 C, we will provide a detailed statistical breakdown of the STopo unique materials with SOC in the ICSD.

A. Definition of Repeat-Topology

In this section, we introduce and rigorously define *repeat-topological* (RTopo) materials. In this work, to define RTopo materials, we first restrict to ICSD entries in which the entire valence manifold exhibits cumulative stable (NLC or SEBR) topology (*i.e.* the summed stable topological indices of all of the occupied bands are nontrivial). Next, using the compatibility relations (see SM 2 and Refs. [28, 42, 57, 91, 92]), we determine the next-highest electronic filling at which an insulating gap is permitted. If the valence manifold in an ICSD entry when filled up to the next-highest gap below E_F is also stable topological [see Fig. S4A], then we define the ICSD entry to be RTopo. We emphasize that by this definition, it is possible for the isolated bands between E_F and the next-highest gap below E_F to be topologically trivial [see Fig. S4C]. Crucially however, the definition of repeat-topology employed in this work is motivated from an experimental perspective. Specifically, we have in this work defined RTopo materials as exhibiting consecutive stable topological gaps at E_F and just below E_F because topological boundary states below E_F can straightforwardly be observed through ARPES, whereas states above E_F can only be observed by doping or by performing more complicated pump-probe experiments [152–155], and because topological response effects and boundary states in solid-state materials occur as a consequence of *gaps* with nontrivial cumulative band topology, as opposed to isolated topological *bands*. From a physical perspective, idealized RTopo materials will exhibit two sets of surface or hinge states within consecutive bulk gaps that both lie at energies accessible to ARPES probes without doping (~ 1.5 eV below E_F). Hence, the repeated topological surface and hinge states of RTopo ICSD entries in consecutive bulk band gaps are analogous to the Fermi-arc “quantum ladder” recently observed in the unconventional chiral semimetal alloy Rh_{*x*}Ni_{*y*}Si [70]. Specifically, while Rh_{*x*}Ni_{*y*}Si is gapless at E_F and below E_F , Rh_{*x*}Ni_{*y*}Si nevertheless exhibits topological Fermi-arc surface states at E_F and at a filling of two electrons below E_F , representing a closely-related semimetallic analog of the topological (crystalline) insulating RTopo materials discovered in this work.

Next, we extend the definition of RTopo beyond individual ICSD entries to groups of ICSD entries associated to unique materials. In this work, we define a unique material as a material that exhibits the same topological features (*i.e.* topological class or nodal crossing points) with SOC at the Fermi level (see SM 4). Therefore, away from E_F , it is possible for two ICSD entries grouped into the same unique material to have isolated sets of bands with different topology. Because we wish to define RTopo materials in a manner that is robust to numerical uncertainty, we define a unique material to be RTopo if *any* of the ICSD entries associated to the unique material are themselves RTopo. In SM 11 B, we list the RTopo TIs and TCIs on <https://www.topologicalquantumchemistry.com/> with the fewest number of bulk Fermi pockets when the Fermi level is set to 0, or set to the next highest filling at which an insulating gap is permitted by band connectivity.

Lastly, in the main text, we have highlighted Bi₂Mg₃ [ICSD 659569, SG 164 ($P\bar{3}m1$)] as a prototypical RTopo (and STopo, see SM 9 B) material. In Table S1 of SM 3, we previously computed the symmetry-indicated stable and fragile topology of all of the isolated sets of bands in Bi₂Mg₃ using the updated version of the [Check Topological Mat](#) program on the BCS implemented for this work. Next, in Fig. 5D of the main text, we have plotted the (0001)-surface states of Bi₂Mg₃ obtained from surface Green’s functions. To compute the (0001)-surface spectrum shown in Fig. 5D of the main text, we first used WANNIER90 [84] to construct a Wannier-based tight-binding model from the *s* and *p* orbitals of Mg and the *p* orbitals of Bi, which we found to accurately reproduce the bulk electronic band structure of Bi₂Mg₃ obtained from *ab initio* calculations (see ICSD 659569 on <https://www.topologicalquantumchemistry.com/>). We next placed the Wannier-based tight-binding model in a *z*- (*c*-axis) directed slab geometry with 100 layers (slab unit cells) in the stacking (*c*-axis) direction, and then computed the *z*-normal [(0001)-] surface states using the iterative Green’s function method as implemented in WANNIERTOOLS [156]. In the (0001)-surface spectrum of Bi₂Mg₃ shown

Γ	X	L	W	dim	top. type	ind/band	filling ν	top. type/all	ind/all
-GM6(2)	-X6(2)	-L8(2)	-W7(2)	2	TRIVIAL	0 0 0	2	TRIVIAL	0 0 0
-GM8(2)	-X8(2)	-L9(2)	-W6(2)	2	TRIVIAL	0 0 0	4	TRIVIAL	0 0 0
-GM11(4)	-X7(2)	-L9(2)	-W7(2)	4	SEBR	2 0 6	8	SEBR	2 0 6
	-X6(2)	-L6-L7(2)	-W6(2)						
-GM10(4)	-X8(2)	-L9(2)	-W6(2)	4	SEBR	2 0 2	12	TRIVIAL	0 0 0
	-X9(2)	-L6-L7(2)	-W7(2)						
-GM10(4)	-X9(2)	-L9(2)	-W6(2)	6	SEBR	3 1 7	18	SEBR	3 1 7
-GM7(2)	-X7(2)	-L4-L5(2)	-W7(2)						
	-X6(2)	-L8(2)	-W6(2)						
-GM11(4)	-X9(2)	-L8(2)	-W7(2)	4	TRIVIAL	0 0 0	22	SEBR	3 1 7
	-X8(2)	-L4-L5(2)	-W6(2)						
-GM10(4)	-X9(2)	-L8(2)	-W7(2)	4	SEBR	3 1 3	26	SEBR	2 0 2
	-X6(2)	-L6-L7(2)	-W7(2)						
-GM7(2)	-X8(2)	-L9(2)	-W6(2)	14	SEBR	2 0 6	40	TRIVIAL	0 0 0
-GM10(4)	-X7(2)	-L9(2)	-W6(2)						
-GM8(2)	-X7(2)	-L8(2)	-W7(2)						
-GM11(4)	-X6(2)	-L9(2)	-W6(2)						
-GM6(2)	-X7(2)	-L6-L7(2)	-W7(2)						
	-X6(2)	-L8(2)	-W7(2)						
	-X6(2)	-L4-L5(2)	-W7(2)						
-GM9(2)	-X7(2)	-L9(2)	-W6(2)	2	SEBR	1 1 1	42	SEBR	1 1 1
-GM8(2)	-X8(2)	-L6-L7(2)	-W7(2)	6	SEBR	0 0 4	48	SEBR	1 1 5
-GM11(4)	-X9(2)	-L9(2)	-W6(2)						
	-X8(2)	-L8(2)	-W6(2)						
-GM10(4)	-X6(2)	-L4-L5(2)	-W7(2)	4	TRIVIAL	0 0 0	52	SEBR	1 1 5
	-X7(2)	-L8(2)	-W6(2)						

Table S16. A typical table generated by [Check Topological Mat](#) (see [SM 3](#)). Here, we have used as an example the ES-classified compound Ni_2SnZr [[ICSD 105383](#), SG 225 ($Fm\bar{3}m$)]. In this table, the horizontal lines indicate the electronic fillings ν at which the occupied bands satisfy the compatibility relations. Columns Γ , X , L , and W contain the coreps at each maximal \mathbf{k} point for each energetically isolated set of bands that satisfy the compatibility relations. Column “dim” shows the dimension of each set of bands, Column “top. type” indicates the topology of the isolated bands [which can either be LCEBR, FRAGILE, NLC, or SEBR], and Column “ind/band” contains the minimal (Z_8) and non-minimal ($Z_4 = Z_8 \bmod 4$, $Z_2 = Z_8 \bmod 2$) stable SIs [[16](#), [29](#)] of SG 225 ($Fm\bar{3}m$), given in the order (Z_4, Z_2, Z_8). The remaining three columns contain the cumulative information of several combined sets of energetically isolated bands that are filled up to a total number of valence electrons specified by the column “filling ν .” Column “top. type/all” provides the cumulative topology (LCEBR, FRAGILE, NLC, or SEBR) at the gap specified by the electronic filling in the “filling ν ” column, and Column “ind/all” provides the cumulative stable SIs of all of the filled bands up to the same gap. Hence, the values of “ind/all” at each filling ν listed in this table can be obtained by summing the values in the “ind/band” column up to the same filling ν . We emphasize that even though Ni_2SnZr is ES-classified at the Fermi level (there are 28 valence electrons in Ni_2SnZr), none of the entries in this table are labeled as “ES,” because the symmetry-indicated topology of energetically isolated groups of bands can only be meaningfully defined by taking the connected bands to be fully occupied (whereas partial occupancy is required to realize an ES-classified semimetal).

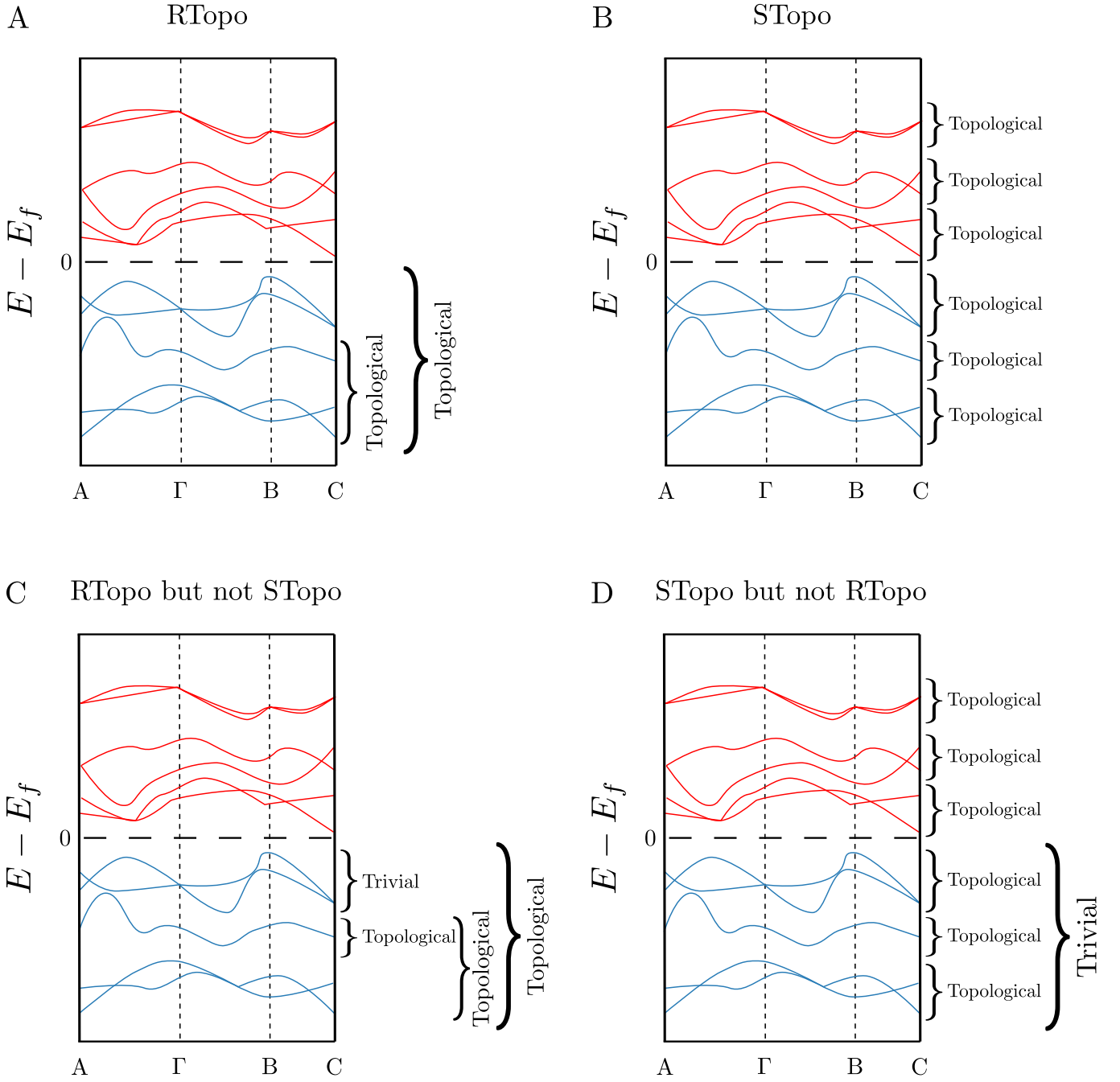


Figure S4. Repeat-topological and supertopological materials. A: A schematic depiction of a repeat-topological (RTopo) band structure. In RTopo materials, the gap at E_F , as well as the next gap below E_F as measured by band connectivity (see SM 2), exhibit cumulative symmetry-indicated stable topology (*i.e.* the *summed* stable topological indices of all of the bands up to E_F and up to the next gap below E_F are nontrivial, see SM 9 A). B: A schematic depiction of a supertopological (STopo) band structure. In STopo materials, *every* energetically isolated set of bands in the spectrum exhibits symmetry-indicated stable topology (see SM 9 B). It is important to emphasize that because repeat-topology is focused on cumulative topology (*i.e.* topological *gaps*), whereas supertopology is defined by the appearance of topological *bands* that may together exhibit cumulative *trivial* topology, then not all RTopo materials are STopo, and not all STopo materials are RTopo. In panel C, we show a schematic example of a band structure that is RTopo, but not STopo. Similarly, in panel D, we show a schematic example of a band structure that is STopo, but not RTopo.

in Fig. 5D of the main text, we observe topological twofold Dirac-cone surface states in both the projected gap at E_F [labeled the “0003 E_F gap” in Fig. 5D of the main text], and just below E_F [labeled the “0013 RTopo gap” in Fig. 5D of the main text]. Most interesting, previous ARPES experiments on Bi_2Mg_3 samples have also detected surface states below the Fermi level, which were labeled as “surface resonance bands” in the earlier works [71, 157, 158]. Hence in this work, we recognize the surface resonance bands detected in Refs. [71, 157, 158] to in fact be the RTopo surface states of Bi_2Mg_3 in the first gap below E_F as determined by band connectivity (see SM 2).

B. Definition of Supertopology

In this section, we introduce and define *supertopological* (STopo) materials. Similar to the definition of RTopo materials introduced in SM 9 A, in this work, we first define an ICSD entry to be STopo if all of the energetically isolated, connected sets of bands with SOC included in our calculations (see SM 4) exhibit symmetry-indicated stable (NLC or SEBR) topology [see Fig. S4B]. We note that by this definition, semimetals (ES or ESFD) and trivial insulators (LCEBR) are also capable of being STopo materials, because the definition of supertopology is independent of the Fermi level (*i.e.* supertopology is independent of the electronic filling). We additionally emphasize that the electronic band structures calculated for this work only contain bands originating from valence atomic orbitals and at least the same number of bands originating from conduction atomic orbitals; we do not consider the topology of bands originating from core-shell atomic orbitals, which are free to be topologically trivial in an STopo material (which is physically motivated, because core-shell atomic orbitals typically lie at energies that are inaccessible in experimental probes). We additionally emphasize that STopo materials are not necessarily also RTopo. For example in an STopo material, it is possible for the isolated bands just below E_F to exhibit stable topological indices that combine with the stable topological indices of the other sets of bands below E_F to sum to trivial values [see Fig. S4D].

As previously with RTopo materials in SM 9 A, we next extend the definition of STopo beyond individual ICSD entries to groups of ICSD entries associated to unique materials. Specifically, in this work, we define a unique material to be STopo if *any* of the ICSD entries associated to the unique material are themselves STopo, thus providing a definition that is less sensitive to numerical uncertainty in materials with small band gaps away from E_F . We find that bismuth (Bi) crystals in SG 166 ($R\bar{3}m$) – recently discovered to be higher-order TIs (HOTIs) [22] – represent a prototypical example of both repeat-topology and supertopology. In Table S22, we show the output of the [Check Topological Mat](#) program (see SM 3) applied to two different ICSD entries for Bi [(ICSD 64703) and (ICSD 53797)] that are associated to the same unique material. Notably, we find that, while both Bi (ICSD 64703) and Bi (ICSD 53797) exhibit the cumulative stable indices of a HOTI at the Fermi level [($Z_{2,1}, Z_{2,2}, Z_{2,3}, Z_4$) = (0, 0, 0, 2) at valence filling $\nu = 10$, see SM 11 A 3], Bi (ICSD 64703) is STopo and RTopo, whereas Bi (ICSD 53797) is RTopo, but not STopo. Crucially, from a physical perspective, Bi (ICSD 64703) and Bi (ICSD 53797) only differ by weak band inversion away from the Fermi level, and both Bi (ICSD 64703) and Bi (ICSD 53797) exhibit topologically nontrivial (SEBR) gaps with the indices ($Z_{2,1}, Z_{2,2}, Z_{2,3}, Z_4$) = (0, 0, 0, 3) just below the Fermi level (see Fig. S5). This indicates that, whether a particular bismuth crystal sample is more closely characterized by the ICSD entry Bi (ICSD 64703) or by Bi (ICSD 53797), ARPES investigations of band gaps below the Fermi level may still reveal fully filled topological surface states (specifically, twofold Dirac cones). In general, when using [Check Topological Mat](#), topological surface and hinge states away from E_F can be predicted by searching the “top. type/all” column (labeled in violet in Table S22) for NLC and SEBR entries at experimentally accessible gaps away from E_F .

C. Statistics for Supertopological Materials in the ICSD

In this section, we provide detailed statistics and lists for all of the STopo unique materials in the ICSD with SOC. As previously discussed in SM 9 B, because the STopo classification is insensitive to the Fermi level, then materials in all of the topological classes (NLC, SEBR, ES, ESFD, and LCEBR) may be STopo. First, in Table S23, we list statistics for all of the STopo unique materials in the ICSD with SOC subdivided by the topology at E_F and by SG. Then, in Tables S24, S25, S26 and S27, we respectively list all of the stoichiometric, nonmagnetic unique STopo materials in the ICSD without f electrons that are classified as NLC, SEBR, ES, ESFD, and LCEBR at E_F .

A Bi SG 166 ($R\bar{3}m$) ICSD 64703

Γ	T	F	L	dim	top. type	ind/band	filling ν	top. type/all	ind/all
-GM8(2)	-T9(2)	-F5-F6(2)	-L3-L4(2)	2	SEBR	1 1 1 0	2	SEBR	1 1 1 0
-GM9(2)	-T8(2)	-F3-F4(2)	-L5-L6(2)	2	SEBR	1 1 1 0	4	LCEBR	0 0 0 0
-GM8(2)	-T9(2)	-F3-F4(2)	-L3-L4(2)	2	SEBR	1 1 1 1	6	SEBR	1 1 1 1
-GM8(2)	-T8(2)	-F5-F6(2)	-L5-L6(2)	2	SEBR	1 1 1 2	8	SEBR	0 0 0 3
-GM4-GM5(2)	-T6-T7(2)	-F5-F6(2)	-L5-L6(2)	2	SEBR	0 0 0 3	10	SEBR	0 0 0 2
-GM9(2)	-T8(2)	-F3-F4(2)	-L3-L4(2)	2	SEBR	0 0 0 1	12	SEBR	0 0 0 3
-GM9(2)	-T9(2)	-F3-F4(2)	-L3-L4(2)	2	SEBR	1 1 1 2	14	SEBR	1 1 1 1
-GM6-GM7(2)	-T4-T5(2)	-F3-F4(2)	-L5-L6(2)	2	SEBR	1 1 1 0	16	SEBR	0 0 0 1
-GM9(2)	-T9(2)	-F5-F6(2)	-L3-L4(2)	2	SEBR	1 1 1 1	18	SEBR	1 1 1 2

B Bi SG 166 ($R\bar{3}m$) ICSD 53797

Γ	T	F	L	dim	top. type	ind/band	filling ν	top. type/all	ind/all
-GM8(2)	-T9(2)	-F5-F6(2)	-L3-L4(2)	2	SEBR	1 1 1 0	2	SEBR	1 1 1 0
-GM9(2)	-T8(2)	-F3-F4(2)	-L5-L6(2)	2	SEBR	1 1 1 0	4	LCEBR	0 0 0 0
-GM8(2)	-T9(2)	-F3-F4(2)	-L5-L6(2)	2	LCEBR	0 0 0 0	6	LCEBR	0 0 0 0
-GM8(2)	-T8(2)	-F5-F6(2)	-L3-L4(2)	2	SEBR	0 0 0 3	8	SEBR	0 0 0 3
-GM4-GM5(2)	-T6-T7(2)	-F5-F6(2)	-L5-L6(2)	2	SEBR	0 0 0 3	10	SEBR	0 0 0 2
-GM9(2)	-T8(2)	-F3-F4(2)	-L3-L4(2)	2	SEBR	0 0 0 1	12	SEBR	0 0 0 3
-GM9(2)	-T9(2)	-F3-F4(2)	-L3-L4(2)	2	SEBR	1 1 1 2	14	SEBR	1 1 1 1
-GM6-GM7(2)	-T4-T5(2)	-F3-F4(2)	-L5-L6(2)	2	SEBR	1 1 1 0	16	SEBR	0 0 0 1
-GM9(2)	-T9(2)	-F5-F6(2)	-L3-L4(2)	2	SEBR	1 1 1 1	18	SEBR	1 1 1 2

Table S22. A typical table generated by [Check Topological Mat](#). Here, we have used as examples two different ICSD entries A: Bi ([ICSD 64703](#)) and B: Bi ([ICSD 53797](#)) for the repeat-topological (RTopo) and supertopological (STopo) unique material Bi. In this table, the horizontal lines indicate the electronic fillings ν at which the occupied bands satisfy the compatibility relations. Columns Γ , T , F , and L contain the coreps at each maximal \mathbf{k} point for each energetically isolated set of bands that satisfy the compatibility relations. Column “dim” shows the dimension of each set of bands, Column “top. type” indicates the topology of the isolated bands [which can either be LCEBR, FRAGILE, NLC, or SEBR], and Column “ind/band” contains the stable SIs ($Z_{2,1}$ $Z_{2,2}$ $Z_{2,3}$ Z_4) that result from subducing onto SG 2 ($P\bar{1}$). The remaining three columns contain the cumulative information of several combined sets of energetically isolated bands that are filled up to a total number of valence electrons specified by the column “filling ν .” Column “top. type/all” provides the cumulative topology (LCEBR, FRAGILE, NLC, or SEBR) at the gap specified by the electronic filling in the “filling ν ” column, and Column “ind/all” provides the cumulative stable SIs of all of the filled bands up to the same gap. Hence, the values of “ind/all” at each filling ν listed in this table can be obtained by summing the values in the “ind/band” column up to the same filling ν . In both A: Bi ([ICSD 64703](#)) and B: Bi ([ICSD 53797](#)), the Fermi level lies at the valence filling $\nu = 10$, indicating that the gap at the Fermi level exhibits the subduced stable SIs (0002). However away from E_F , the bands at valence filling $\nu = 6$ exhibit trivial symmetry-indicated (LCEBR) topology in B, whereas all of the energetically isolated bands in A are classified as stable topological (SEBR). Therefore, A: Bi ([ICSD 64703](#)) is an STopo ICSD entry, whereas B: Bi ([ICSD 53797](#)) is not; however, because A and B are associated to the same unique material, then as a whole, we consider Bi in SG 166 ($R\bar{3}m$) with (0002) SEBR topology at the Fermi level to be an STopo unique material.

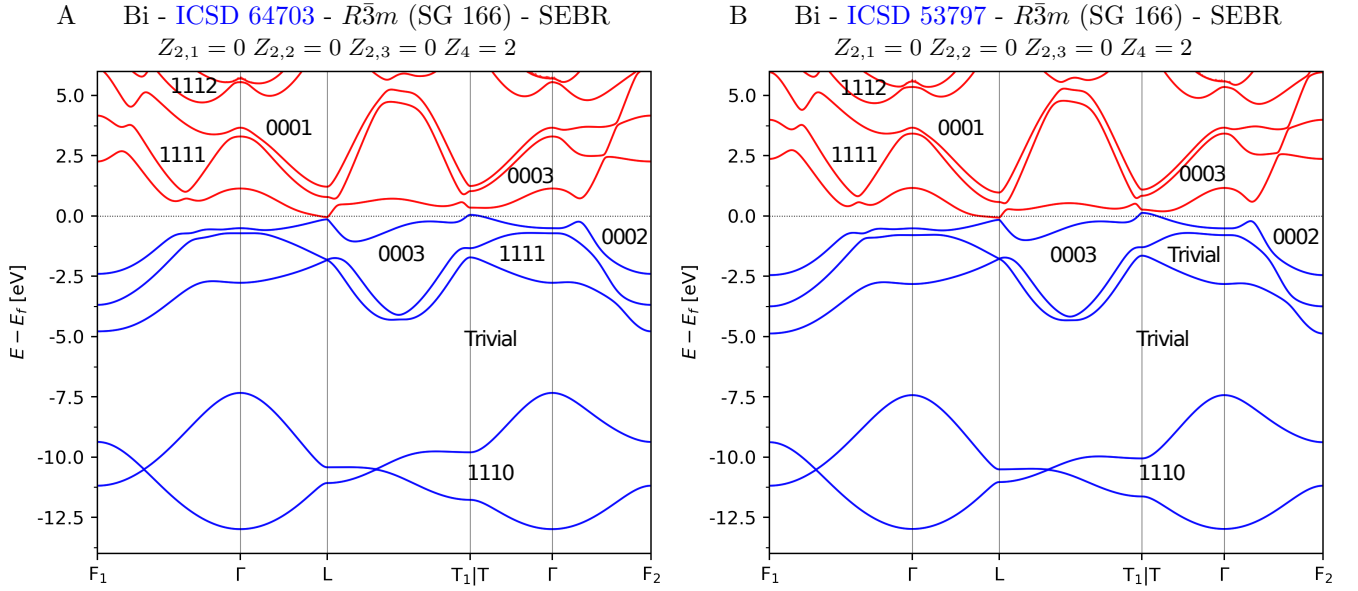


Figure S5. Bulk bands and topology for two ICSD entries associated to the same unique material Bi. Blue (red) colors are used to indicate valence (conduction) bands, and the four numbers listed in each gap indicate the cumulative stable SIs that result from subducing onto SG 2 ($P\bar{1}$): $Z_{2,1}$, $Z_{2,2}$, $Z_{2,3}$, Z_4 , reproduced from the “ind/all” column in Table S22. In both panels A and B, the word “Trivial” indicates a gap in which the cumulative values ($Z_{2,1}$, $Z_{2,2}$, $Z_{2,3}$, Z_4) = (0, 0, 0, 0). In A [B], we show the bulk bands and cumulative stable SIs of A: Bi (ICSD 64703) [B: Bi (ICSD 53797)], which is [not] STopo. Conversely, because the gap at E_F [(0002)] and the next gap below E_F [(0003)] exhibit cumulative symmetry-indicated stable topology, then Bi (ICSD 64703) in A and Bi (ICSD 53797) in B are both RTopo ICSD entries (see SM 9 A). Crucially, though the topological classifications of A and B differ away from E_F , both A and B exhibit the characteristic stable SIs of a HOTI [22] at E_F [($Z_{2,1}$, $Z_{2,2}$, $Z_{2,3}$, Z_4) = (0, 0, 0, 2), see SM 11 A 3].

Table S23: Statistics for supertopological (STopo) materials. The first and second columns respectively list the SG and the number of unique materials in the SG. In order, the next columns list the number of unique materials in the SG that are STopo (defined in SM 9 B), the number that are STopo in which all of the bands are NLC (STopo-NLC), and the number that are STopo in which all of the bands are SEBR (STopo-SEBR). In the final five columns, we respectively list the number of unique STopo materials in the SG that are classified as NLC, SEBR, ES, ESFD, and LCEBR at E_F . For all of the STopo material subclassifications listed in this table, each number of materials is accompanied by the percentage of unique materials in the SG with the STopo subclassification. When there are no unique materials with the STopo subclassification, the table entry is marked with a dashed horizontal line.

SG	# Mat.	STopo	STopo-NLC	STopo-SEBR	STopo and NLC	STopo and SEBR	STopo and ES	STopo and ESFD	STopo and LCEBR
2	1574	7 (0.4%)	7 (0.4%)	—	—	—	—	—	7 (0.4%)
10	38	1 (2.6%)	1 (2.6%)	—	—	—	—	—	1 (2.6%)
11	587	1 (0.2%)	1 (0.2%)	—	1 (0.2%)	—	—	—	—
12	1345	9 (0.7%)	—	—	5 (0.4%)	3 (0.2%)	—	—	1 (0.1%)
13	195	1 (0.5%)	1 (0.5%)	—	—	—	—	—	1 (0.5%)
14	2665	24 (0.9%)	24 (0.9%)	—	5 (0.2%)	—	1 (0.0%)	—	18 (0.7%)
51	107	2 (1.9%)	2 (1.9%)	—	—	—	—	2 (1.9%)	—
55	394	5 (1.3%)	5 (1.3%)	—	—	—	—	—	5 (1.3%)
58	208	1 (0.5%)	1 (0.5%)	—	—	—	—	—	1 (0.5%)
61	122	9 (7.4%)	9 (7.4%)	—	—	—	—	—	9 (7.4%)
62	3006	3 (0.1%)	3 (0.1%)	—	1 (0.0%)	—	—	—	2 (0.1%)
63	1396	6 (0.4%)	2 (0.1%)	—	3 (0.2%)	1 (0.1%)	—	1 (0.1%)	1 (0.1%)
64	257	5 (1.9%)	—	5 (1.9%)	—	4 (1.6%)	—	—	1 (0.4%)
65	241	2 (0.8%)	—	—	2 (0.8%)	—	—	—	—
74	218	2 (0.9%)	2 (0.9%)	—	2 (0.9%)	—	—	—	—

83	10	1 (10.0%)	—	—	1 (10.0%)	—	—	—	—
87	181	1 (0.6%)	—	—	—	1 (0.6%)	—	—	—
88	139	1 (0.7%)	—	1 (0.7%)	—	—	—	—	1 (0.7%)
122	124	4 (3.2%)	—	4 (3.2%)	—	—	—	—	4 (3.2%)
123	473	41 (8.7%)	14 (3.0%)	—	5 (1.1%)	1 (0.2%)	14 (3.0%)	20 (4.2%)	1 (0.2%)
127	403	6 (1.5%)	6 (1.5%)	—	1 (0.2%)	—	—	4 (1.0%)	1 (0.2%)
129	884	1 (0.1%)	—	—	1 (0.1%)	—	—	—	—
139	1622	43 (2.6%)	—	15 (0.9%)	—	14 (0.9%)	11 (0.7%)	12 (0.7%)	6 (0.4%)
140	457	45 (9.8%)	2 (0.4%)	—	9 (2.0%)	2 (0.4%)	10 (2.2%)	21 (4.6%)	3 (0.7%)
141	267	2 (0.8%)	—	1 (0.4%)	—	1 (0.4%)	—	—	1 (0.4%)
164	598	13 (2.2%)	—	12 (2.0%)	—	3 (0.5%)	—	1 (0.2%)	9 (1.5%)
166	1029	6 (0.6%)	—	6 (0.6%)	—	6 (0.6%)	—	—	—
176	206	5 (2.4%)	—	2 (1.0%)	—	—	2 (1.0%)	2 (1.0%)	1 (0.5%)
187	158	1 (0.6%)	1 (0.6%)	—	—	—	—	1 (0.6%)	—
189	592	10 (1.7%)	—	—	—	—	5 (0.8%)	5 (0.8%)	—
191	506	63 (12.4%)	—	63 (12.4%)	—	11 (2.2%)	20 (4.0%)	32 (6.3%)	—
193	302	3 (1.0%)	—	3 (1.0%)	—	—	2 (0.7%)	1 (0.3%)	—
194	1619	130 (8.0%)	2 (0.1%)	38 (2.4%)	—	15 (0.9%)	71 (4.4%)	33 (2.0%)	11 (0.7%)
204	151	1 (0.7%)	—	1 (0.7%)	—	—	—	1 (0.7%)	—
205	130	2 (1.5%)	2 (1.5%)	—	—	—	—	1 (0.8%)	1 (0.8%)
206	61	4 (6.6%)	—	4 (6.6%)	—	—	—	2 (3.3%)	2 (3.3%)
216	777	1 (0.1%)	1 (0.1%)	—	—	—	—	1 (0.1%)	—
221	1352	196 (14.5%)	—	55 (4.1%)	1 (0.1%)	36 (2.7%)	24 (1.8%)	129 (9.5%)	6 (0.4%)
223	222	9 (4.0%)	—	9 (4.0%)	—	—	1 (0.5%)	7 (3.1%)	1 (0.5%)
224	17	1 (5.9%)	—	1 (5.9%)	—	—	—	1 (5.9%)	—
225	1693	37 (2.2%)	—	37 (2.2%)	—	5 (0.3%)	5 (0.3%)	25 (1.5%)	2 (0.1%)
227	841	33 (3.9%)	—	25 (3.0%)	—	4 (0.5%)	10 (1.2%)	12 (1.4%)	7 (0.8%)
229	210	31 (14.8%)	—	29 (13.8%)	—	2 (0.9%)	2 (0.9%)	25 (11.9%)	2 (0.9%)
Total	38298	769 (2.0%)	86 (0.2%)	311 (0.8%)	37 (0.1%)	109 (0.3%)	178 (0.5%)	339 (0.9%)	106 (0.3%)

Table S24: Supertopological (STopo) nonmagnetic unique materials without f electrons that are also NLC-classified at E_F with SOC. In order, the columns list the chemical formula, the SG number, the SG symbol, the ICSD number, whether all of the bands in the STopo material are NLC, whether all of the bands in the STopo material are SEBR, the number of valence electrons, and the cumulative stable SIs at E_F (see SM 11). A chemical formula with a * indicates that only some (but not all) of the ICSDs associated to the same unique material (defined using its topological class with SOC) are STopo.

Chem. formula	SG #	SG symbol	ICSD	All NLC	All SEBR	num e^-	Topological Indices
GeH ₄	11	$P2_1/m$	183082	Yes	No	16	$Z_{2,1} = 0$ $Z_{2,2} = 0$ $Z_{2,3} = 1$ $Z_4 = 3$
WH ₆ *	12	$C2/m$	247613	No	No	24	$Z_{2,1} = 0$ $Z_{2,2} = 0$ $Z_{2,3} = 0$ $Z_4 = 1$
SN*	14	$P2_1/c$	41966	Yes	No	44	$Z_{2,1} = 1$ $Z_{2,2} = 0$ $Z_{2,3} = 0$ $Z_4 = 2$
ZrGe ₂ *	63	$Cmcm$	56054	No	No	24	$Z_{2,1} = 1$ $Z_{2,2} = 1$ $Z_{2,3} = 0$ $Z_4 = 1$
ZrSi ₂ *	63	$Cmcm$	95179	Yes	No	24	$Z_{2,1} = 1$ $Z_{2,2} = 1$ $Z_{2,3} = 0$ $Z_4 = 1$
Ga ₂ Sc	65	$Cmmm$	103956	No	No	18	$Z_{2,1} = 0$ $Z_{2,2} = 0$ $Z_{2,3} = 1$ $Z_4 = 1$
Ga ₃ Ti ₂	83	$P4/m$	103995	No	No	34	$Z_{2,1} = 1$ $Z_{2,2} = 1$ $Z_{2,3} = 1$ $Z_4 = 1$ $Z_{4m,\pi} = 1$ $Z_2 = 1$ $Z_8 = 1$
MoPt ₃	123	$P4/mmm$	161108	No	No	36	$Z_{2,1} = 1$ $Z_{2,2} = 1$ $Z_{2,3} = 1$ $Z_4 = 3$ $Z_{4m,\pi} = 1$ $Z_2 = 1$ $Z_8 = 7$
Cu ₂ NiZn	123	$P4/mmm$	103079	No	No	44	$Z_{2,1} = 0$ $Z_{2,2} = 0$ $Z_{2,3} = 0$ $Z_4 = 1$ $Z_{4m,\pi} = 2$ $Z_2 = 1$ $Z_8 = 1$
Pd ₅ Ti ₃	123	$P4/mmm$	105726	No	No	62	$Z_{2,1} = 0$ $Z_{2,2} = 0$ $Z_{2,3} = 1$ $Z_4 = 3$ $Z_{4m,\pi} = 1$ $Z_2 = 1$ $Z_8 = 3$
Sc	129	$P4/nmm$	52412	No	No	12	$Z_{2,1} = 0$ $Z_{2,2} = 0$ $Z_{2,3} = 0$ $Z_4 = 3$ $Z_2 = 1$
Sc	140	$I4/mcm$	246445	No	No	12	$Z_{2,1} = 1$ $Z_{2,2} = 1$ $Z_{2,3} = 1$ $Z_4 = 3$ $Z_2 = 1$ $Z_8 = 7$
PtTi ₂	140	$I4/mcm$	102797	Yes	No	32	$Z_{2,1} = 0$ $Z_{2,2} = 0$ $Z_{2,3} = 0$ $Z_4 = 3$ $Z_2 = 1$ $Z_8 = 7$
FeZr ₂	140	$I4/mcm$	103712	No	No	32	$Z_{2,1} = 0$ $Z_{2,2} = 0$ $Z_{2,3} = 0$ $Z_4 = 1$ $Z_2 = 1$ $Z_8 = 5$
Pb ₂ Pt	140	$I4/mcm$	54316	No	No	36	$Z_{2,1} = 1$ $Z_{2,2} = 1$ $Z_{2,3} = 1$ $Z_4 = 1$ $Z_2 = 1$ $Z_8 = 1$
NiHf ₂	140	$I4/mcm$	102808	No	No	36	$Z_{2,1} = 1$ $Z_{2,2} = 1$ $Z_{2,3} = 1$ $Z_4 = 1$ $Z_2 = 1$ $Z_8 = 1$
HfRu	221	$Pm\bar{3}m$	104268	No	No	12	$Z_{2,1} = 0$ $Z_{2,2} = 0$ $Z_{2,3} = 0$ $Z_4 = 2$ $Z_{4m,\pi} = 0$ $Z_2 = 0$ $Z_8 = 6$

Table S25: Supertopological (STopo) nonmagnetic unique materials without f electrons that are also SEBR-classified at E_F with SOC. In order, the columns list the chemical formula, the SG number, the SG symbol, the ICSD number, whether all of the bands in the STopo material are NLC, whether all of the bands in the STopo material are SEBR, the number of valence electrons, and the cumulative stable SIs at E_F (see SM 11). A chemical formula with a * indicates that only some (but not all) of the ICSDs associated to the same unique material (defined using its topological class with SOC) are STopo.

Chem. formula	SG #	SG symbol	ICSD	All NLC	All SEBR	num e^-	Topological Indices
Bi	12	$C2/m$	409752	No	No	10	$Z_{2,1} = 0$ $Z_{2,2} = 0$ $Z_{2,3} = 1$ $Z_4 = 2$
TaSb ₂ *	12	$C2/m$	651600	No	No	30	$Z_{2,1} = 1$ $Z_{2,2} = 1$ $Z_{2,3} = 1$ $Z_4 = 2$
Si ₂ Ti*	63	$Cmcm$	168418	No	No	24	$Z_{2,1} = 1$ $Z_{2,2} = 1$ $Z_{2,3} = 0$ $Z_4 = 0$
Ca	64	$Cmce$	107510	No	Yes	8	$Z_{2,1} = 0$ $Z_{2,2} = 0$ $Z_{2,3} = 0$ $Z_4 = 3$
Ga	64	$Cmce$	43388	No	Yes	12	$Z_{2,1} = 1$ $Z_{2,2} = 1$ $Z_{2,3} = 0$ $Z_4 = 1$
MoNi ₄	87	$I4/m$	105047	No	No	46	$Z_{2,1} = 0$ $Z_{2,2} = 0$ $Z_{2,3} = 0$ $Z_4 = 3$ $Z_2 = 1$ $Z_8 = 7$
TiH ₂	139	$I4/mmm$	56184	No	No	6	$Z_{2,1} = 0$ $Z_{2,2} = 0$ $Z_{2,3} = 0$ $Z_4 = 3$ $Z_2 = 1$ $Z_8 = 7$
Hf ₃ Te ₂	139	$I4/mmm$	75936	No	No	24	$Z_{2,1} = 0$ $Z_{2,2} = 0$ $Z_{2,3} = 0$ $Z_4 = 0$ $Z_2 = 0$ $Z_8 = 4$
Al ₃ Zr*	139	$I4/mmm$	107903	No	No	26	$Z_{2,1} = 0$ $Z_{2,2} = 0$ $Z_{2,3} = 0$ $Z_4 = 3$ $Z_2 = 1$ $Z_8 = 7$
HfAl ₃	139	$I4/mmm$	608102	No	No	26	$Z_{2,1} = 1$ $Z_{2,2} = 1$ $Z_{2,3} = 1$ $Z_4 = 2$ $Z_2 = 0$ $Z_8 = 6$
CaCo ₂ Ge ₂	139	$I4/mmm$	406	No	Yes	28	$Z_{2,1} = 1$ $Z_{2,2} = 1$ $Z_{2,3} = 1$ $Z_4 = 3$ $Z_2 = 1$ $Z_8 = 3$
CaCo ₂ Si ₂	139	$I4/mmm$	420974	No	Yes	28	$Z_{2,1} = 1$ $Z_{2,2} = 1$ $Z_{2,3} = 1$ $Z_4 = 3$ $Z_2 = 1$ $Z_8 = 3$
CaNi ₂ Ge ₂	139	$I4/mmm$	408	No	No	30	$Z_{2,1} = 1$ $Z_{2,2} = 1$ $Z_{2,3} = 1$ $Z_4 = 0$ $Z_2 = 0$ $Z_8 = 4$
MoBe ₁₂	139	$I4/mmm$	616334	No	No	30	$Z_{2,1} = 0$ $Z_{2,2} = 0$ $Z_{2,3} = 0$ $Z_4 = 3$ $Z_2 = 1$ $Z_8 = 7$
Ba ₂ Bi	139	$I4/mmm$	2141	No	No	50	$Z_{2,1} = 0$ $Z_{2,2} = 0$ $Z_{2,3} = 0$ $Z_4 = 1$ $Z_2 = 1$ $Z_8 = 5$
Bi*	140	$I4/mcm$	51674	No	No	20	$Z_{2,1} = 1$ $Z_{2,2} = 1$ $Z_{2,3} = 1$ $Z_4 = 0$ $Z_2 = 0$ $Z_8 = 0$
Ga ₂ Sc ₃	140	$I4/mcm$	103957	No	No	120	$Z_{2,1} = 0$ $Z_{2,2} = 0$ $Z_{2,3} = 0$ $Z_4 = 2$ $Z_2 = 0$ $Z_8 = 6$
Si	141	$I4_1/amd$	52460	No	No	8	$Z_{2,1} = 0$ $Z_{2,2} = 0$ $Z_{2,3} = 0$ $Z_4 = 1$ $Z_2 = 1$
Bi ₂ Mg ₃ *	164	$P\bar{3}m1$	659569	No	Yes	16	$Z_{2,1} = 0$ $Z_{2,2} = 0$ $Z_{2,3} = 0$ $Z_4 = 3$
PtTe ₂	164	$P\bar{3}m1$	41385	No	Yes	22	$Z_{2,1} = 0$ $Z_{2,2} = 0$ $Z_{2,3} = 0$ $Z_4 = 3$
PdTe ₂ *	164	$P\bar{3}m1$	83642	No	Yes	22	$Z_{2,1} = 0$ $Z_{2,2} = 0$ $Z_{2,3} = 0$ $Z_4 = 3$
As*	166	$R\bar{3}m$	16516	No	Yes	10	$Z_{2,1} = 1$ $Z_{2,2} = 1$ $Z_{2,3} = 1$ $Z_4 = 3$
P	166	$R\bar{3}m$	53301	No	Yes	10	$Z_{2,1} = 0$ $Z_{2,2} = 0$ $Z_{2,3} = 0$ $Z_4 = 2$
Sb	166	$R\bar{3}m$	55402	No	Yes	10	$Z_{2,1} = 1$ $Z_{2,2} = 1$ $Z_{2,3} = 1$ $Z_4 = 1$
Sb*	166	$R\bar{3}m$	64695	No	Yes	10	$Z_{2,1} = 1$ $Z_{2,2} = 1$ $Z_{2,3} = 1$ $Z_4 = 3$
Bi*	166	$R\bar{3}m$	64703	No	Yes	10	$Z_{2,1} = 0$ $Z_{2,2} = 0$ $Z_{2,3} = 0$ $Z_4 = 2$
CaGe ₂ *	166	$R\bar{3}m$	110107	No	Yes	20	$Z_{2,1} = 0$ $Z_{2,2} = 0$ $Z_{2,3} = 0$ $Z_4 = 1$
Si	191	$P6/mmm$	52456	No	Yes	4	$Z_{2,1} = 0$ $Z_{2,2} = 0$ $Z_{2,3} = 1$ $Z_4 = 2$ $Z_{6m,0} = 5$ $Z_{6m,\pi} = 5$ $Z_{12} = 10$
ZrB ₂	191	$P6/mmm$	30327	No	Yes	10	$Z_{2,1} = 0$ $Z_{2,2} = 0$ $Z_{2,3} = 1$ $Z_4 = 0$ $Z_{6m,0} = 5$ $Z_{6m,\pi} = 3$ $Z_{12} = 8$
TiB ₂	191	$P6/mmm$	30330	No	Yes	10	$Z_{2,1} = 0$ $Z_{2,2} = 0$ $Z_{2,3} = 1$ $Z_4 = 0$ $Z_{6m,0} = 5$ $Z_{6m,\pi} = 3$ $Z_{12} = 8$
HfB ₂	191	$P6/mmm$	30422	No	Yes	10	$Z_{2,1} = 0$ $Z_{2,2} = 0$ $Z_{2,3} = 1$ $Z_4 = 0$ $Z_{6m,0} = 5$ $Z_{6m,\pi} = 3$ $Z_{12} = 8$
CaSi ₂	191	$P6/mmm$	154433	No	Yes	10	$Z_{2,1} = 0$ $Z_{2,2} = 0$ $Z_{2,3} = 1$ $Z_4 = 1$ $Z_{6m,0} = 2$ $Z_{6m,\pi} = 1$ $Z_{12} = 9$
Ti	191	$P6/mmm$	52521	No	Yes	12	$Z_{2,1} = 0$ $Z_{2,2} = 0$ $Z_{2,3} = 0$ $Z_4 = 1$ $Z_{6m,0} = 3$ $Z_{6m,\pi} = 0$ $Z_{12} = 9$
Ti ₂ Zr	191	$P6/mmm$	247962	No	Yes	12	$Z_{2,1} = 0$ $Z_{2,2} = 0$ $Z_{2,3} = 0$ $Z_4 = 1$ $Z_{6m,0} = 3$ $Z_{6m,\pi} = 0$ $Z_{12} = 9$
CaNi ₄ B	191	$P6/mmm$	36504	No	Yes	90	$Z_{2,1} = 0$ $Z_{2,2} = 0$ $Z_{2,3} = 0$ $Z_4 = 3$ $Z_{6m,0} = 3$ $Z_{6m,\pi} = 0$ $Z_{12} = 3$
Mg	194	$P6_3/mmc$	52260	No	Yes	4	$Z_{2,1} = 0$ $Z_{2,2} = 0$ $Z_{2,3} = 0$ $Z_4 = 3$ $Z_{6m,0} = 5$ $Z'_{12} = 11$
Mg	194	$P6_3/mmc$	170902	No	Yes	4	$Z_{2,1} = 0$ $Z_{2,2} = 0$ $Z_{2,3} = 0$ $Z_4 = 3$ $Z_{6m,0} = 1$ $Z'_{12} = 7$
Zn	194	$P6_3/mmc$	52259	No	Yes	24	$Z_{2,1} = 0$ $Z_{2,2} = 0$ $Z_{2,3} = 0$ $Z_4 = 3$ $Z_{6m,0} = 1$ $Z'_{12} = 7$
Ti ₂ PbC	194	$P6_3/mmc$	42926	No	No	32	$Z_{2,1} = 0$ $Z_{2,2} = 0$ $Z_{2,3} = 0$ $Z_4 = 3$ $Z_{6m,0} = 5$ $Z'_{12} = 11$
Ti ₂ SnC*	194	$P6_3/mmc$	161064	No	No	32	$Z_{2,1} = 0$ $Z_{2,2} = 0$ $Z_{2,3} = 0$ $Z_4 = 3$ $Z_{6m,0} = 5$ $Z'_{12} = 11$
HfAl ₂ *	194	$P6_3/mmc$	109245	No	Yes	40	$Z_{2,1} = 0$ $Z_{2,2} = 0$ $Z_{2,3} = 0$ $Z_4 = 3$ $Z_{6m,0} = 5$ $Z'_{12} = 11$
WBe ₂ *	194	$P6_3/mmc$	616501	No	No	40	$Z_{2,1} = 0$ $Z_{2,2} = 0$ $Z_{2,3} = 0$ $Z_4 = 3$ $Z_{6m,0} = 5$ $Z'_{12} = 11$
WB _{2.0}	194	$P6_3/mmc$	23716	No	No	48	$Z_{2,1} = 0$ $Z_{2,2} = 0$ $Z_{2,3} = 0$ $Z_4 = 0$ $Z_{6m,0} = 2$ $Z'_{12} = 8$
HfCr ₂	194	$P6_3/mmc$	109213	No	No	64	$Z_{2,1} = 0$ $Z_{2,2} = 0$ $Z_{2,3} = 0$ $Z_4 = 1$ $Z_{6m,0} = 1$ $Z'_{12} = 1$
AlSc	221	$Pm\bar{3}m$	58098	No	No	6	$Z_{2,1} = 1$ $Z_{2,2} = 1$ $Z_{2,3} = 1$ $Z_4 = 3$ $Z_{4m,\pi} = 1$ $Z_2 = 1$ $Z_8 = 3$
BeTi	221	$Pm\bar{3}m$	58743	No	No	6	$Z_{2,1} = 1$ $Z_{2,2} = 1$ $Z_{2,3} = 1$ $Z_4 = 3$ $Z_{4m,\pi} = 1$ $Z_2 = 1$ $Z_8 = 3$
AlCo	221	$Pm\bar{3}m$	57596	No	Yes	12	$Z_{2,1} = 0$ $Z_{2,2} = 0$ $Z_{2,3} = 0$ $Z_4 = 2$ $Z_{4m,\pi} = 2$ $Z_2 = 0$ $Z_8 = 6$
Allr	221	$Pm\bar{3}m$	57928	No	No	12	$Z_{2,1} = 0$ $Z_{2,2} = 0$ $Z_{2,3} = 0$ $Z_4 = 2$ $Z_{4m,\pi} = 2$ $Z_2 = 0$ $Z_8 = 6$
AgLi	221	$Pm\bar{3}m$	58310	No	Yes	12	$Z_{2,1} = 1$ $Z_{2,2} = 1$ $Z_{2,3} = 1$ $Z_4 = 0$ $Z_{4m,\pi} = 3$ $Z_2 = 0$ $Z_8 = 0$
CaPd	221	$Pm\bar{3}m$	58926	No	Yes	12	$Z_{2,1} = 0$ $Z_{2,2} = 0$ $Z_{2,3} = 0$ $Z_4 = 0$ $Z_{4m,\pi} = 2$ $Z_2 = 0$ $Z_8 = 4$
HfOs	221	$Pm\bar{3}m$	104252	No	Yes	12	$Z_{2,1} = 1$ $Z_{2,2} = 1$ $Z_{2,3} = 1$ $Z_4 = 2$ $Z_{4m,\pi} = 1$ $Z_2 = 0$ $Z_8 = 6$
MgPd	221	$Pm\bar{3}m$	104847	No	No	12	$Z_{2,1} = 0$ $Z_{2,2} = 0$ $Z_{2,3} = 0$ $Z_4 = 3$ $Z_{4m,\pi} = 0$ $Z_2 = 1$ $Z_8 = 7$
MnV	221	$Pm\bar{3}m$	104998	No	No	12	$Z_{2,1} = 1$ $Z_{2,2} = 1$ $Z_{2,3} = 1$ $Z_4 = 1$ $Z_{4m,\pi} = 1$ $Z_2 = 1$ $Z_8 = 1$

OsZr	221	$Pm\bar{3}m$	105580	No	No	12	$Z_{2,1} = 1$ $Z_{2,2} = 1$ $Z_{2,3} = 1$ $Z_4 = 1$ $Z_{4m,\pi} = 1$ $Z_2 = 1$ $Z_8 = 1$
RuTi	221	$Pm\bar{3}m$	106004	No	No	12	$Z_{2,1} = 1$ $Z_{2,2} = 1$ $Z_{2,3} = 1$ $Z_4 = 1$ $Z_{4m,\pi} = 1$ $Z_2 = 1$ $Z_8 = 1$
RuZr	221	$Pm\bar{3}m$	106022	No	No	12	$Z_{2,1} = 1$ $Z_{2,2} = 1$ $Z_{2,3} = 1$ $Z_4 = 1$ $Z_{4m,\pi} = 1$ $Z_2 = 1$ $Z_8 = 1$
TiRu	221	$Pm\bar{3}m$	150936	No	No	12	$Z_{2,1} = 1$ $Z_{2,2} = 1$ $Z_{2,3} = 1$ $Z_4 = 3$ $Z_{4m,\pi} = 3$ $Z_2 = 1$ $Z_8 = 3$
ZrRu	221	$Pm\bar{3}m$	181289	No	No	12	$Z_{2,1} = 1$ $Z_{2,2} = 1$ $Z_{2,3} = 1$ $Z_4 = 3$ $Z_{4m,\pi} = 3$ $Z_2 = 1$ $Z_8 = 3$
MgNi	221	$Pm\bar{3}m$	187256	No	No	12	$Z_{2,1} = 0$ $Z_{2,2} = 0$ $Z_{2,3} = 0$ $Z_4 = 3$ $Z_{4m,\pi} = 0$ $Z_2 = 1$ $Z_8 = 7$
TiFe*	221	$Pm\bar{3}m$	189112	No	No	12	$Z_{2,1} = 1$ $Z_{2,2} = 1$ $Z_{2,3} = 1$ $Z_4 = 3$ $Z_{4m,\pi} = 3$ $Z_2 = 1$ $Z_8 = 3$
FeTi*	221	$Pm\bar{3}m$	190972	No	No	12	$Z_{2,1} = 1$ $Z_{2,2} = 1$ $Z_{2,3} = 1$ $Z_4 = 1$ $Z_{4m,\pi} = 1$ $Z_2 = 1$ $Z_8 = 1$
OsHf	221	$Pm\bar{3}m$	290935	No	No	12	$Z_{2,1} = 1$ $Z_{2,2} = 1$ $Z_{2,3} = 1$ $Z_4 = 0$ $Z_{4m,\pi} = 3$ $Z_2 = 0$ $Z_8 = 0$
AlAu	221	$Pm\bar{3}m$	57495	No	No	14	$Z_{2,1} = 1$ $Z_{2,2} = 1$ $Z_{2,3} = 1$ $Z_4 = 2$ $Z_{4m,\pi} = 3$ $Z_2 = 0$ $Z_8 = 6$
AgGa	221	$Pm\bar{3}m$	104466	No	No	14	$Z_{2,1} = 1$ $Z_{2,2} = 1$ $Z_{2,3} = 1$ $Z_4 = 0$ $Z_{4m,\pi} = 1$ $Z_2 = 0$ $Z_8 = 4$
AgIn	221	$Pm\bar{3}m$	605384	No	No	14	$Z_{2,1} = 1$ $Z_{2,2} = 1$ $Z_{2,3} = 1$ $Z_4 = 0$ $Z_{4m,\pi} = 1$ $Z_2 = 0$ $Z_8 = 4$
CoMn	221	$Pm\bar{3}m$	187981	No	No	16	$Z_{2,1} = 0$ $Z_{2,2} = 0$ $Z_{2,3} = 0$ $Z_4 = 3$ $Z_{4m,\pi} = 0$ $Z_2 = 1$ $Z_8 = 7$
Co ₃ V	221	$Pm\bar{3}m$	187965	No	No	32	$Z_{2,1} = 1$ $Z_{2,2} = 1$ $Z_{2,3} = 1$ $Z_4 = 2$ $Z_{4m,\pi} = 1$ $Z_2 = 0$ $Z_8 = 2$
TlPd ₃ H	221	$Pm\bar{3}m$	247273	No	No	34	$Z_{2,1} = 1$ $Z_{2,2} = 1$ $Z_{2,3} = 1$ $Z_4 = 0$ $Z_{4m,\pi} = 3$ $Z_2 = 0$ $Z_8 = 0$
HfRh ₃ B	221	$Pm\bar{3}m$	614447	No	Yes	34	$Z_{2,1} = 1$ $Z_{2,2} = 1$ $Z_{2,3} = 1$ $Z_4 = 0$ $Z_{4m,\pi} = 1$ $Z_2 = 0$ $Z_8 = 0$
ZrRh ₃ B	221	$Pm\bar{3}m$	615353	No	Yes	34	$Z_{2,1} = 1$ $Z_{2,2} = 1$ $Z_{2,3} = 1$ $Z_4 = 0$ $Z_{4m,\pi} = 1$ $Z_2 = 0$ $Z_8 = 0$
Ni ₃ Cr	221	$Pm\bar{3}m$	188231	No	No	36	$Z_{2,1} = 1$ $Z_{2,2} = 1$ $Z_{2,3} = 1$ $Z_4 = 3$ $Z_{4m,\pi} = 1$ $Z_2 = 1$ $Z_8 = 7$
Pt ₃ Zn	221	$Pm\bar{3}m$	105853	No	No	42	$Z_{2,1} = 0$ $Z_{2,2} = 0$ $Z_{2,3} = 0$ $Z_4 = 2$ $Z_{4m,\pi} = 2$ $Z_2 = 0$ $Z_8 = 6$
AuCu ₃	221	$Pm\bar{3}m$	40351	No	No	44	$Z_{2,1} = 1$ $Z_{2,2} = 1$ $Z_{2,3} = 1$ $Z_4 = 0$ $Z_{4m,\pi} = 1$ $Z_2 = 0$ $Z_8 = 4$
Ca	225	$Fm\bar{3}m$	44348	No	Yes	2	$Z_{2,1} = 0$ $Z_{2,2} = 0$ $Z_{2,3} = 0$ $Z_4 = 0$ $Z_2 = 0$ $Z_8 = 4$
Mg	225	$Fm\bar{3}m$	180453	No	Yes	2	$Z_{2,1} = 0$ $Z_{2,2} = 0$ $Z_{2,3} = 0$ $Z_4 = 0$ $Z_2 = 0$ $Z_8 = 4$
TiH ₂	225	$Fm\bar{3}m$	56182	No	Yes	6	$Z_{2,1} = 0$ $Z_{2,2} = 0$ $Z_{2,3} = 0$ $Z_4 = 3$ $Z_2 = 1$ $Z_8 = 7$
In ₂ LiRh	225	$Fm\bar{3}m$	106806	No	Yes	16	$Z_{2,1} = 0$ $Z_{2,2} = 0$ $Z_{2,3} = 0$ $Z_4 = 3$ $Z_2 = 1$ $Z_8 = 7$
MgIn ₂	227	$Fd\bar{3}m$	423608	No	Yes	16	$Z_{2,1} = 0$ $Z_{2,2} = 0$ $Z_{2,3} = 0$ $Z_4 = 3$ $Z_2 = 1$
Ti ₂ C	227	$Fd\bar{3}m$	77473	No	Yes	48	$Z_{2,1} = 0$ $Z_{2,2} = 0$ $Z_{2,3} = 0$ $Z_4 = 1$ $Z_2 = 1$
Hf ₂ Pd	227	$Fd\bar{3}m$	638772	No	No	144	$Z_{2,1} = 0$ $Z_{2,2} = 0$ $Z_{2,3} = 0$ $Z_4 = 1$ $Z_2 = 1$

Table S26: Supertopological (STopo) nonmagnetic unique materials without f electrons that are also ES-classified at E_F with SOC. In order, the columns list the chemical formula, the SG number, the SG symbol, the ICSD number, whether all of the bands in the STopo material are NLC, whether all of the bands in the STopo material are SEBR, and the number of valence electrons. A chemical formula with a * indicates that only some (but not all) of the ICSDs associated to the same unique material (defined using its topological class with SOC) are STopo.

Chem. formula	SG #	SG symbol	ICSD	All NLC	All SEBR	num e^-
IrV	123	$P4/mmm$	104589	Yes	No	14
RhV*	123	$P4/mmm$	169385	Yes	No	14
MgNiH ₂	123	$P4/mmm$	187258	No	No	14
RuSi ₂	123	$P4/mmm$	154013	No	No	16
AuCu	123	$P4/mmm$	42574	Yes	No	22
NiZn	123	$P4/mmm$	105469	No	No	22
PdZn	123	$P4/mmm$	105752	Yes	No	22
Sn	139	$I4/mmm$	108748	No	No	4
Ge ₂ W	139	$I4/mmm$	9978	No	Yes	14
WSi ₂	139	$I4/mmm$	26869	No	No	14
CaGa ₄	139	$I4/mmm$	58892	No	Yes	14
CrSi ₂	139	$I4/mmm$	71499	No	No	14
Al ₄ Ca	139	$I4/mmm$	151189	No	Yes	14
TiS ₂	139	$I4/mmm$	181504	No	No	16
Au ₂ Hf	139	$I4/mmm$	611956	No	Yes	26
Be ₁₂ Pd	139	$I4/mmm$	109314	No	Yes	34
Ga ₅ Mg ₂	139	$I4/mmm$	23227	No	No	38
Zr ₂ Si	140	$I4/mcm$	652615	No	No	24
RuSn ₂	140	$I4/mcm$	105993	No	No	32
FeZr ₂	140	$I4/mcm$	634145	No	No	32
Hf ₂ Ni	140	$I4/mcm$	151466	No	No	36
V ₄ SiSb ₂	140	$I4/mcm$	82564	No	No	68
TlTe*	140	$I4/mcm$	69027	No	No	72
Ti ₅ FeSb ₂	140	$I4/mcm$	96143	No	No	76
Mo ₅ Si ₃ *	140	$I4/mcm$	35756	No	No	84

W ₅ Zr ₃	140	<i>I4/mcm</i>	653434	No	No	84
ScIr ₃ B ₄	176	<i>P6₃/m</i>	44424	No	Yes	84
Sn ₄ Ir ₇ B ₃	176	<i>P6₃/m</i>	78985	No	Yes	176
MoB ₂ *	191	<i>P6/mmm</i>	614799	No	Yes	12
Ti ₂ TaN ₃	191	<i>P6/mmm</i>	186418	No	Yes	28
ScCo ₃ B ₂	191	<i>P6/mmm</i>	44179	No	Yes	36
CaPt ₅	191	<i>P6/mmm</i>	58929	No	Yes	52
NaPt ₃ B	191	<i>P6/mmm</i>	68092	No	Yes	68
MgFe ₆ Ge ₆	191	<i>P6/mmm</i>	188716	No	Yes	74
TiFe ₆ Ge ₆ *	191	<i>P6/mmm</i>	92173	No	Yes	76
CaNi ₄ B	191	<i>P6/mmm</i>	612693	No	Yes	90
Zr ₅ AgIn ₃	193	<i>P6₃/mcm</i>	190116	No	Yes	80
Ti*	194	<i>P6₃/mmc</i>	168830	No	Yes	8
Ge*	194	<i>P6₃/mmc</i>	189805	No	Yes	8
Cr*	194	<i>P6₃/mmc</i>	151375	No	Yes	12
Ru	194	<i>P6₃/mmc</i>	40354	No	No	16
Fe	194	<i>P6₃/mmc</i>	53450	No	No	16
CaIn ₂	194	<i>P6₃/mmc</i>	58686	No	Yes	16
CaGa ₂	194	<i>P6₃/mmc</i>	58891	No	Yes	16
Ga ₂ Mg	194	<i>P6₃/mmc</i>	103792	No	Yes	16
CaLi ₂	194	<i>P6₃/mmc</i>	106349	No	Yes	16
TcB	194	<i>P6₃/mmc</i>	168897	No	No	20
CaMg ₂	194	<i>P6₃/mmc</i>	58912	No	Yes	24
RhB	194	<i>P6₃/mmc</i>	193833	No	Yes	24
ReB ₃	194	<i>P6₃/mmc</i>	24361	No	Yes	32
AlAuTi	194	<i>P6₃/mmc</i>	57506	No	No	36
Be ₂ Re	194	<i>P6₃/mmc</i>	58732	No	No	44
Ag	194	<i>P6₃/mmc</i>	64707	No	No	44
FeWN ₂	194	<i>P6₃/mmc</i>	81488	No	No	48
BaN ₂	194	<i>P6₃/mmc</i>	106313	No	No	48
MoC*	194	<i>P6₃/mmc</i>	44987	No	No	60
Mg ₂ Y*	194	<i>P6₃/mmc</i>	642901	No	Yes	60
Cr ₂ Ti*	194	<i>P6₃/mmc</i>	102854	No	No	64
Re ₂ Sc	194	<i>P6₃/mmc</i>	105890	No	No	68
Mn ₂ Sc	194	<i>P6₃/mmc</i>	108596	No	No	68
ScMn ₂ *	194	<i>P6₃/mmc</i>	109246	No	No	68
TaB ₄	194	<i>P6₃/mmc</i>	182094	No	No	68
Cr ₂ Ta*	194	<i>P6₃/mmc</i>	626859	No	No	68
WB ₄ *	194	<i>P6₃/mmc</i>	43193	No	No	72
HfRe ₂	194	<i>P6₃/mmc</i>	150512	No	No	72
MoB ₄	194	<i>P6₃/mmc</i>	182095	No	No	72
Re ₂ Zr*	194	<i>P6₃/mmc</i>	650208	No	No	72
ScRu ₂	194	<i>P6₃/mmc</i>	150514	No	No	76
CaHg ₃	194	<i>P6₃/mmc</i>	619356	No	Yes	76
Os ₂ Sc	194	<i>P6₃/mmc</i>	647766	No	No	76
TiOs ₂	194	<i>P6₃/mmc</i>	290936	No	No	80
ZrOs ₂	194	<i>P6₃/mmc</i>	290937	No	No	80
Re ₂ W	194	<i>P6₃/mmc</i>	650203	No	No	80
Ru ₂ Zr*	194	<i>P6₃/mmc</i>	650790	No	No	80
MoN*	194	<i>P6₃/mmc</i>	106926	No	Yes	88
WFe ₂ *	194	<i>P6₃/mmc</i>	600061	No	Yes	88
MoFe ₂ *	194	<i>P6₃/mmc</i>	601488	No	No	88
Mg ₅ Rh ₂	194	<i>P6₃/mmc</i>	104860	No	No	112
Mg ₅ Pd ₂ *	194	<i>P6₃/mmc</i>	246978	No	No	120
KAg ₂	194	<i>P6₃/mmc</i>	150142	No	No	124
HfMo ₂ *	194	<i>P6₃/mmc</i>	638615	No	No	128
Al ₅ Rh ₂ *	194	<i>P6₃/mmc</i>	58153	No	No	132
SrZn ₂	194	<i>P6₃/mmc</i>	246194	No	No	136
Pd ₃ Ti*	194	<i>P6₃/mmc</i>	649037	No	No	136
YZn ₂	194	<i>P6₃/mmc</i>	290900	No	No	140
AlRe	221	<i>Pm$\bar{3}$m</i>	58146	No	No	10
RuSi	221	<i>Pm$\bar{3}$m</i>	44616	No	Yes	12
AlRh	221	<i>Pm$\bar{3}$m</i>	58151	No	No	12
BePd	221	<i>Pm$\bar{3}$m</i>	58728	No	Yes	12

InRh	221	$Pm\bar{3}m$	59515	No	No	12
GaIr	221	$Pm\bar{3}m$	103760	No	No	12
GaRh	221	$Pm\bar{3}m$	103948	No	Yes	12
OsTi	221	$Pm\bar{3}m$	105572	No	No	12
TcV	221	$Pm\bar{3}m$	106143	No	No	12
OsC	221	$Pm\bar{3}m$	185989	No	Yes	12
ZnZr	221	$Pm\bar{3}m$	106235	No	No	16
NiZn	221	$Pm\bar{3}m$	105470	No	No	22
ZrRu ₃	221	$Pm\bar{3}m$	185641	No	No	28
Cd(TiO ₃)	221	$Pm\bar{3}m$	33667	No	No	34
Fe ₃ Pd	221	$Pm\bar{3}m$	103586	No	No	34
ScPd ₃ B	221	$Pm\bar{3}m$	190796	No	Yes	36
Cr	223	$Pm\bar{3}n$	108326	No	Yes	48
Mo	225	$Fm\bar{3}m$	41513	No	Yes	6
PtIn ₂	225	$Fm\bar{3}m$	56259	No	Yes	16
Al ₂ Pd	225	$Fm\bar{3}m$	58116	No	Yes	16
RuSi ₂	225	$Fm\bar{3}m$	154014	No	Yes	16
CdGeP ₂	225	$Fm\bar{3}m$	52804	No	Yes	26
CaPt ₂	227	$Fd\bar{3}m$	108147	No	Yes	44
Cr ₂ Ni	227	$Fd\bar{3}m$	188278	No	No	44
Ni ₂ Zr	227	$Fd\bar{3}m$	105480	No	Yes	48
PbAu ₂	227	$Fd\bar{3}m$	56261	No	No	52
Be ₂₂ Mo*	227	$Fd\bar{3}m$	58718	No	Yes	100
Pb ₂ Sn ₂ O ₆	227	$Fd\bar{3}m$	15308	No	No	104
Sc ₄ Ru ₇ Ge ₆	229	$Im\bar{3}m$	637747	No	Yes	92

Table S27: Supertopological (STopo) nonmagnetic unique materials without f electrons that are also ESFD-classified at E_F with SOC. In order, the columns list the chemical formula, the SG number, the SG symbol, the ICSD number, whether all of the bands in the STopo material are NLC, whether all of the bands in the STopo material are SEBR, and the number of valence electrons. A chemical formula with a * indicates that only some (but not all) of the ICSDs associated to the same unique material (defined using its topological class with SOC) are STopo.

Chem. formula	SG #	SG symbol	ICSD	All NLC	All SEBR	num e^-
MoRh	51	$Pmma$	108608	Yes	No	30
CaRhIn ₄	51	$Pmma$	410891	Yes	No	46
Ga	63	$Cmcm$	43539	Yes	No	6
AlTi*	123	$P4/mmm$	58187	Yes	No	7
GaTi	123	$P4/mmm$	103989	No	No	7
RhTi	123	$P4/mmm$	105951	No	No	13
RuTa	123	$P4/mmm$	105995	No	No	13
PtV	123	$P4/mmm$	105835	Yes	No	15
ReC ₂	123	$P4/mmm$	184664	No	No	15
CuGa ₂	123	$P4/mmm$	102906	No	No	17
HfNiGa ₅	123	$P4/mmm$	634319	No	No	29
Pt ₃ Al	123	$P4/mmm$	109235	No	No	33
Cu ₃ Pd*	123	$P4/mmm$	103083	No	No	43
ReO ₃	127	$P4/mbm$	77680	Yes	No	50
Sc ₂ SiIr ₅ B ₂	127	$P4/mbm$	85629	Yes	No	122
Sc ₅ Rh ₄ Si ₁₀ *	127	$P4/mbm$	602226	Yes	No	182
Sc ₅ Co ₄ Si ₁₀ *	127	$P4/mbm$	624958	Yes	No	182
Sc*	139	$I4/mmm$	52410	No	No	3
In*	139	$I4/mmm$	639813	No	Yes	3
TiGa ₃	139	$I4/mmm$	98937	No	No	13
Ga ₄ Na	139	$I4/mmm$	103822	No	No	13
CuTi ₂ *	139	$I4/mmm$	629388	No	No	19
ScNi ₂ Si ₂	139	$I4/mmm$	106839	No	No	31
Be ₁₂ Ag	139	$I4/mmm$	109313	No	No	35
GaHf ₂	140	$I4/mcm$	102809	No	No	22
Hf ₂ Al	140	$I4/mcm$	150773	No	No	22

Zr ₂ Al	140	<i>I4/mcm</i>	150774	No	No	22
Ti ₂ B	140	<i>I4/mcm</i>	189385	No	No	22
Ta ₂ B	140	<i>I4/mcm</i>	42525	No	No	26
Mo ₂ B	140	<i>I4/mcm</i>	24278	No	No	30
W ₂ B	140	<i>I4/mcm</i>	24279	No	No	30
Cr ₂ B	140	<i>I4/mcm</i>	76127	No	No	30
Al ₂ Cu*	140	<i>I4/mcm</i>	42517	No	No	34
Mn ₂ B	140	<i>I4/mcm</i>	42529	No	No	34
CoZr ₂	140	<i>I4/mcm</i>	102740	No	No	34
RhPb ₂ *	140	<i>I4/mcm</i>	102802	No	No	34
RhZr ₂	140	<i>I4/mcm</i>	102807	No	No	34
IrZr ₂	140	<i>I4/mcm</i>	641204	No	No	34
CoTa ₂ *	140	<i>I4/mcm</i>	102815	Yes	No	38
Tc ₂ Al ₃	164	<i>P3m1</i>	609482	No	Yes	23
HfIr ₃ B ₄	176	<i>P6₃/m</i>	1518	No	No	86
ZrIr ₃ B ₄	176	<i>P6₃/m</i>	614583	No	No	86
AlB ₂	191	<i>P6/mmm</i>	43851	No	Yes	9
ScB ₂	191	<i>P6/mmm</i>	44491	No	Yes	9
TaB ₂ *	191	<i>P6/mmm</i>	30420	No	Yes	11
VB ₂ *	191	<i>P6/mmm</i>	165125	No	Yes	11
AgB ₂	191	<i>P6/mmm</i>	43821	No	Yes	17
AuB ₂	191	<i>P6/mmm</i>	52699	No	Yes	17
Hg ₂ Na	191	<i>P6/mmm</i>	104327	No	Yes	25
Zr ₄ Al ₃ *	191	<i>P6/mmm</i>	603486	No	Yes	25
Hf ₄ Al ₃	191	<i>P6/mmm</i>	608072	No	Yes	25
CaRh ₃ B ₂	191	<i>P6/mmm</i>	66767	No	Yes	35
Co ₃ HfB ₂	191	<i>P6/mmm</i>	23550	No	Yes	37
CoSn*	191	<i>P6/mmm</i>	55564	No	Yes	39
PbRh	191	<i>P6/mmm</i>	105607	No	Yes	39
NiIn*	191	<i>P6/mmm</i>	161111	No	Yes	39
Al ₉ CaCo ₂	191	<i>P6/mmm</i>	57535	No	Yes	47
CaCu ₅	191	<i>P6/mmm</i>	58882	No	Yes	57
LiNi ₆ Ge ₆	191	<i>P6/mmm</i>	41463	No	Yes	255
Ta ₅ N ₆ *	193	<i>P6₃/mcm</i>	29329	No	Yes	110
Na	194	<i>P6₃/mmc</i>	44758	No	Yes	2
Li	194	<i>P6₃/mmc</i>	44760	No	Yes	2
Tc	194	<i>P6₃/mmc</i>	52498	No	No	14
WH	194	<i>P6₃/mmc</i>	247586	Yes	No	14
Re*	194	<i>P6₃/mmc</i>	650069	No	No	14
Ag	194	<i>P6₃/mmc</i>	56269	No	No	22
ReB ₂ *	194	<i>P6₃/mmc</i>	23871	No	No	26
AuSn	194	<i>P6₃/mmc</i>	56262	No	No	30
ReC ₂ *	194	<i>P6₃/mmc</i>	184660	No	No	30
AuMg ₃ *	194	<i>P6₃/mmc</i>	58541	No	No	34
V ₂ CP*	194	<i>P6₃/mmc</i>	29284	No	No	38
V ₂ AsC	194	<i>P6₃/mmc</i>	43874	No	No	38
MnMoN ₂	194	<i>P6₃/mmc</i>	81489	No	No	46
MoCoP ₂	194	<i>P6₃/mmc</i>	624219	No	Yes	50
AlPt ₂ Zr	194	<i>P6₃/mmc</i>	58139	No	No	54
HfAlPt ₂	194	<i>P6₃/mmc</i>	608138	No	Yes	54
W ₂ B ₅	194	<i>P6₃/mmc</i>	615696	No	No	54
Ir ₃ Mo	194	<i>P6₃/mmc</i>	104506	No	No	66
Ir ₃ W	194	<i>P6₃/mmc</i>	104598	No	No	66
MoRh ₃	194	<i>P6₃/mmc</i>	105085	No	No	66
Nb ₂ AsC*	194	<i>P6₃/mmc</i>	43011	No	No	70
CaNiAl ₉	194	<i>P6₃/mmc</i>	63626	No	Yes	78
Hg ₃ Sc	194	<i>P6₃/mmc</i>	104343	No	Yes	78
V ₆ Ga ₅ *	194	<i>P6₃/mmc</i>	635613	No	No	90
Al ₁₀ Mn ₃	194	<i>P6₃/mmc</i>	57974	No	No	102
Hf ₉ W ₄ Co	194	<i>P6₃/mmc</i>	623810	No	No	138
Zr ₉ Mo ₄ Co	194	<i>P6₃/mmc</i>	624247	No	No	138
Al ₂₃ V ₄	194	<i>P6₃/mmc</i>	58203	No	No	178
ReO ₃ *	204	<i>Im$\bar{3}$</i>	77721	No	Yes	100
AlSb	205	<i>Pa$\bar{3}$</i>	41994	Yes	No	64

C	206	$Ia\bar{3}$	5390	No	Yes	32
C ₈	206	$Ia\bar{3}$	74655	No	Yes	32
MgSc	221	$Pm\bar{3}m$	108583	No	No	5
As*	221	$Pm\bar{3}m$	162842	No	Yes	5
TcB	221	$Pm\bar{3}m$	168900	No	Yes	10
AlOs	221	$Pm\bar{3}m$	58107	No	No	11
BeRh	221	$Pm\bar{3}m$	58734	No	Yes	11
CaTl ₃	221	$Pm\bar{3}m$	58942	No	No	11
HfTc	221	$Pm\bar{3}m$	104277	No	No	11
MgRh	221	$Pm\bar{3}m$	104859	No	Yes	11
ReTi	221	$Pm\bar{3}m$	105896	No	No	11
TcTi	221	$Pm\bar{3}m$	106142	No	No	11
OsSi	221	$Pm\bar{3}m$	43417	No	No	12
RhSi	221	$Pm\bar{3}m$	44385	No	Yes	13
AlNi	221	$Pm\bar{3}m$	58037	No	No	13
AlPd	221	$Pm\bar{3}m$	58113	No	No	13
AlPt	221	$Pm\bar{3}m$	58128	No	No	13
AgMg	221	$Pm\bar{3}m$	58322	No	Yes	13
BeCu	221	$Pm\bar{3}m$	58700	No	No	13
InNi*	221	$Pm\bar{3}m$	59432	No	No	13
InPd	221	$Pm\bar{3}m$	59473	No	No	13
GaNi	221	$Pm\bar{3}m$	103853	No	No	13
HfRh	221	$Pm\bar{3}m$	104265	No	No	13
IrZr	221	$Pm\bar{3}m$	104606	No	No	13
PtSc	221	$Pm\bar{3}m$	105784	No	Yes	13
RhTi	221	$Pm\bar{3}m$	105953	No	No	13
HfIr	221	$Pm\bar{3}m$	185632	No	No	13
IrC	221	$Pm\bar{3}m$	185990	No	Yes	13
ZrAl ₃ *	221	$Pm\bar{3}m$	192029	No	Yes	13
HfAl ₃	221	$Pm\bar{3}m$	248537	No	Yes	13
AuSc	221	$Pm\bar{3}m$	58582	No	Yes	14
CuSc	221	$Pm\bar{3}m$	103095	No	No	14
HfPt	221	$Pm\bar{3}m$	104257	No	No	14
PtZr	221	$Pm\bar{3}m$	105857	No	No	14
HfPd	221	$Pm\bar{3}m$	185630	No	No	14
CoTa	221	$Pm\bar{3}m$	187978	No	No	14
ScZn	221	$Pm\bar{3}m$	106041	No	No	15
RhZn	221	$Pm\bar{3}m$	107574	No	Yes	21
CuZn	221	$Pm\bar{3}m$	56276	No	No	23
AgZn	221	$Pm\bar{3}m$	58384	No	No	23
AuCd*	221	$Pm\bar{3}m$	58410	No	No	23
AuTi ₃	221	$Pm\bar{3}m$	58604	No	Yes	23
AuZn*	221	$Pm\bar{3}m$	58625	No	No	23
TiRu ₃	221	$Pm\bar{3}m$	185635	No	No	28
ZrOs ₃	221	$Pm\bar{3}m$	185644	No	Yes	28
Mn ₃ Rh	221	$Pm\bar{3}m$	104961	No	Yes	30
Rh ₃ Sc	221	$Pm\bar{3}m$	105920	No	No	30
Ir ₃ Sc	221	$Pm\bar{3}m$	108568	No	No	30
HfIr ₃ *	221	$Pm\bar{3}m$	104212	No	Yes	31
Ir ₃ Zr	221	$Pm\bar{3}m$	104610	No	No	31
Rh ₃ Ti	221	$Pm\bar{3}m$	105955	No	No	31
ScIr ₃ B	221	$Pm\bar{3}m$	44423	No	No	33
Rh ₃ ScB	221	$Pm\bar{3}m$	44561	No	Yes	33
AlPt ₃	221	$Pm\bar{3}m$	58131	No	No	33
Pd ₃ Sc*	221	$Pm\bar{3}m$	105674	No	No	33
Au ₃ Li	221	$Pm\bar{3}m$	58525	No	Yes	34
Fe ₃ Pt	221	$Pm\bar{3}m$	103598	No	Yes	34
Pt ₃ Zr	221	$Pm\bar{3}m$	105858	No	Yes	34
TiPt ₃	221	$Pm\bar{3}m$	185640	No	No	34
ZrPd ₃	221	$Pm\bar{3}m$	185643	No	No	34
Ag ₃ Mg	221	$Pm\bar{3}m$	58323	No	Yes	35
ScPt ₃ B	221	$Pm\bar{3}m$	190790	No	Yes	36
TiZn ₃	221	$Pm\bar{3}m$	106185	No	No	40
AgPt ₃	221	$Pm\bar{3}m$	58347	No	No	41

VZn ₃	221	$Pm\bar{3}m$	106240	No	No	41
AuPd ₃	221	$Pm\bar{3}m$	180876	No	No	41
HgPt ₃	221	$Pm\bar{3}m$	639147	No	No	42
Cu ₃ Pd	221	$Pm\bar{3}m$	103084	No	Yes	43
Au ₃ Pd	221	$Pm\bar{3}m$	180872	No	Yes	43
Cu ₃ Pt	221	$Pm\bar{3}m$	628749	No	No	43
Au ₃ Cu*	221	$Pm\bar{3}m$	56266	No	No	44
Tl ₃ Au	223	$Pm\bar{3}n$	186643	No	Yes	40
Mo ₃ Zr	223	$Pm\bar{3}n$	105118	No	Yes	44
V ₃ Fe	223	$Pm\bar{3}n$	634028	No	Yes	46
Mo ₃ Os	223	$Pm\bar{3}n$	105054	No	Yes	52
IrMo ₃	223	$Pm\bar{3}n$	640816	No	Yes	54
Na ₄ Si ₂₃	223	$Pm\bar{3}n$	194245	No	Yes	192
PtO ₂	224	$Pn\bar{3}m$	77654	No	Yes	44
Sc	225	$Fm\bar{3}m$	41502	No	Yes	3
Tl*	225	$Fm\bar{3}m$	104199	No	Yes	3
Al*	225	$Fm\bar{3}m$	191766	No	Yes	3
Ti	225	$Fm\bar{3}m$	41503	No	Yes	4
Hf	225	$Fm\bar{3}m$	41519	No	Yes	4
ZrB*	225	$Fm\bar{3}m$	44605	No	Yes	7
VH ₂	225	$Fm\bar{3}m$	56191	No	Yes	7
HfB*	225	$Fm\bar{3}m$	76128	No	Yes	7
Rh*	225	$Fm\bar{3}m$	41516	No	Yes	9
Pd	225	$Fm\bar{3}m$	41517	No	Yes	10
Pt*	225	$Fm\bar{3}m$	64921	No	Yes	10
TcB	225	$Fm\bar{3}m$	168899	No	Yes	10
Cu	225	$Fm\bar{3}m$	43493	No	Yes	11
Au	225	$Fm\bar{3}m$	44362	No	Yes	11
Ag	225	$Fm\bar{3}m$	44387	No	Yes	11
ReC*	225	$Fm\bar{3}m$	77350	No	Yes	11
In ₂ LiRu	225	$Fm\bar{3}m$	639896	No	Yes	15
Al ₂ Au	225	$Fm\bar{3}m$	57501	No	Yes	17
AuIn ₂	225	$Fm\bar{3}m$	58489	No	Yes	17
Be ₂ Ta	227	$Fd\bar{3}m$	58739	No	Yes	18
NaAs ₂	227	$Fd\bar{3}m$	182161	No	Yes	22
CdLi	227	$Fd\bar{3}m$	102008	No	Yes	26
Cr ₂ Ti	227	$Fd\bar{3}m$	102851	No	No	32
Cr ₂ Zr	227	$Fd\bar{3}m$	102860	No	Yes	32
Mo ₂ Zr	227	$Fd\bar{3}m$	105115	No	No	32
Ir ₂ Sc	227	$Fd\bar{3}m$	104558	No	Yes	42
LiPt ₂	227	$Fd\bar{3}m$	104778	No	No	42
CaPd ₂	227	$Fd\bar{3}m$	58927	No	Yes	44
Ag ₂ Na	227	$Fd\bar{3}m$	58337	No	Yes	46
Li	229	$Im\bar{3}m$	44367	No	Yes	1
Ca*	229	$Im\bar{3}m$	44349	No	Yes	2
Zr	229	$Im\bar{3}m$	52544	No	Yes	4
Hf	229	$Im\bar{3}m$	53023	No	Yes	4
V	229	$Im\bar{3}m$	43420	No	Yes	5
Ta	229	$Im\bar{3}m$	53793	No	Yes	5
W	229	$Im\bar{3}m$	43421	No	Yes	6
Mo	229	$Im\bar{3}m$	52267	No	Yes	6
Cu	229	$Im\bar{3}m$	183263	No	Yes	11
CrGa ₄	229	$Im\bar{3}m$	626026	No	Yes	18
Mg ₄ Rh ₇ As ₆	229	$Im\bar{3}m$	94391	No	Yes	101
Pt ₃ Ga ₇ *	229	$Im\bar{3}m$	635137	No	Yes	102
Ag ₈ Ca ₃	229	$Im\bar{3}m$	107145	No	No	188

Table S28: Supertopological (STopo) nonmagnetic unique materials without f electrons that are LCEBR-classified at E_F with SOC. In order, the columns list the chemical formula, the SG number, the SG symbol, the ICSD number, whether all of the bands in the STopo material are NLC, whether all of the bands in the STopo material are SEBR, and the number of valence electrons. A chemical formula with a * indicates that only some (but not all) of the ICSDs associated to the same unique material (defined using its topological class with SOC) are STopo.

Chem. formula	SG #	SG symbol	ICSD	All NLC	All SEBR	num e^-
NaCaH ₃	2	$P\bar{1}$	168714	Yes	No	12
LiBeH ₃	2	$P\bar{1}$	162771	Yes	No	36
NaSbS ₂	2	$P\bar{1}$	200597	Yes	No	36
MnP ₄ *	2	$P\bar{1}$	100786	Yes	No	54
Mg(SiO ₄ H ₂)*	10	$P2/m$	190936	Yes	No	32
BaPbO ₃ *	12	$C2/m$	67811	No	No	64
Al ₂ O ₃	13	$P2/c$	169723	Yes	No	96
Li(AlH ₄)	14	$P2_1/c$	22247	Yes	No	32
SiH ₄	14	$P2_1/c$	159307	Yes	No	32
GeH ₄	14	$P2_1/c$	183080	Yes	No	32
LiNH ₂	14	$P2_1/c$	237209	Yes	No	32
RhSi*	14	$P2_1/c$	79235	Yes	No	52
SiH ₃ I	14	$P2_1/c$	65044	Yes	No	56
ZrO ₂ *	14	$P2_1/c$	57158	Yes	No	64
HfO ₂ *	14	$P2_1/c$	173158	Yes	No	64
(NH ₃ (OH))Cl*	14	$P2_1/c$	14204	Yes	No	88
Tl(BS ₃)	14	$P2_1/c$	73085	Yes	No	96
As ₂ Se ₃ *	14	$P2_1/c$	43226	Yes	No	112
(NH ₄)(H ₂ PO ₃)	14	$P2_1/c$	49544	Yes	No	136
Ca(TiSiO ₅)*	14	$P2_1/c$	158653	Yes	No	160
LiSc(Si ₂ O ₆)*	14	$P2_1/c$	152076	Yes	No	192
Pb ₃ O ₄ *	55	$Pbam$	9754	Yes	No	144
SnPb ₂ O ₄ *	55	$Pbam$	31484	Yes	No	144
Pb ₂ PtO ₄	55	$Pbam$	202214	Yes	No	168
SiO ₂	55	$Pbam$	170516	Yes	No	256
MgH ₂	61	$Pbca$	155811	Yes	No	32
TiO ₂ *	61	$Pbca$	15409	Yes	No	128
(NH ₂)(CN)	61	$Pbca$	40446	Yes	No	128
SnO ₂ *	61	$Pbca$	181280	Yes	No	128
CoAsSe	61	$Pbca$	41731	Yes	No	160
CoPSe*	61	$Pbca$	53060	Yes	No	160
CoSbS*	61	$Pbca$	624859	Yes	No	160
CaH ₂ *	62	$Pnma$	23870	Yes	No	16
NaMgH ₃ *	62	$Pnma$	91795	Yes	No	24
Na(NbO ₃)*	63	$Cmcm$	280098	No	No	128
Ca	64	$Cmce$	162255	No	Yes	8
Na(AlH ₄)*	88	$I4_1/a$	8022	No	Yes	16
LiPN ₂ *	122	$I\bar{4}2d$	32713	No	Yes	32
MgCN ₂	122	$I\bar{4}2d$	44110	No	Yes	32
BeSiN ₂	122	$I\bar{4}2d$	44112	No	Yes	32
Bi ₂ ZnTiO ₆	123	$P4/mmm$	186800	No	No	62
Na(TaO ₃)	127	$P4/mbm$	23322	Yes	No	48
Sn*	139	$I4/mmm$	236686	No	No	4
CaAl ₂ Ga ₂	139	$I4/mmm$	300209	No	Yes	14
Si	139	$I4/mmm$	181908	No	Yes	16
C*	139	$I4/mmm$	190716	No	Yes	16
K ₂ MgF ₄	139	$I4/mmm$	33519	No	No	48
TlGaTe ₂ *	140	$I4/mcm$	635524	No	No	36
InSn ₂ I ₅ *	140	$I4/mcm$	151995	No	No	92
InPb ₂ I ₅ *	140	$I4/mcm$	151998	No	No	92
LiAl	141	$I4_1/amd$	240114	No	Yes	8
CaB ₂ H ₂	164	$P\bar{3}m1$	183134	No	Yes	10
Mg ₃ Sb ₂ *	164	$P\bar{3}m1$	2142	No	Yes	16
CaMg ₂ Sb ₂	164	$P\bar{3}m1$	100045	No	Yes	16

CaAl ₂ Ge ₂	164	$P\bar{3}m1$	409570	No	Yes	16
CaBe ₂ As ₂	164	$P\bar{3}m1$	609867	No	Yes	16
MgBe ₂ As ₂	164	$P\bar{3}m1$	609872	No	Yes	16
Ba ₂ H ₃ I	164	$P\bar{3}m1$	423520	No	Yes	30
C*	194	$P6_3/mmc$	27422	No	Yes	16
TlInS ₂	194	$P6_3/mmc$	25355	No	No	36
KTI	194	$P6_3/mmc$	262071	No	No	48
CuScO ₂ *	194	$P6_3/mmc$	60847	No	No	52
Ni ₃ Zr	194	$P6_3/mmc$	105482	No	No	68
HfMn ₂ *	194	$P6_3/mmc$	104214	No	No	72
ZrMn ₂	194	$P6_3/mmc$	109269	No	No	72
ZrTc ₂	194	$P6_3/mmc$	423221	No	No	72
HfTc ₂ *	194	$P6_3/mmc$	638955	No	Yes	72
MgH ₂	205	$Pa\bar{3}$	168832	Yes	No	16
Ca ₃ N ₂ *	206	$Ia\bar{3}$	34678	No	Yes	128
Li ₃ (ScN ₂)	206	$Ia\bar{3}$	98140	No	Yes	128
Ca(SiO ₃)*	221	$Pm\bar{3}m$	40658	No	No	24
Ca(SnO ₃)	221	$Pm\bar{3}m$	56095	No	Yes	24
Pb(GeO ₃)	221	$Pm\bar{3}m$	185693	No	No	26
Sn(TiO ₃)	221	$Pm\bar{3}m$	186724	No	No	26
C ₃ N ₂	221	$Pm\bar{3}m$	185974	No	No	88
Si ₁₄₆	223	$Pm\bar{3}n$	186544	No	Yes	184
MgH ₂	225	$Fm\bar{3}m$	166234	No	Yes	4
LiAl*	227	$Fd\bar{3}m$	1924	No	Yes	8
Si*	227	$Fd\bar{3}m$	29287	No	Yes	8
Ge	227	$Fd\bar{3}m$	41980	No	Yes	8
GaLi	227	$Fd\bar{3}m$	103775	No	Yes	8
AlH ₃	227	$Fd\bar{3}m$	182535	No	Yes	24
SiO ₂ *	227	$Fd\bar{3}m$	35536	No	Yes	32
Zn ₂ Zr*	227	$Fd\bar{3}m$	653507	No	No	56
Si	229	$Im\bar{3}m$	189392	No	Yes	24

SM 10. SOC-DRIVEN TOPOLOGICAL PHASE TRANSITIONS

In this section, we provide statistics for the SOC-driven topological phase transitions in the materials studied in this work. To begin, there are two broad mechanisms by which a material can be driven into a topological (crystalline) insulating phase. The first mechanism occurs when a semimetal w/o SOC gaps directly into a TI or TCI under the introduction of SOC; in this case, the TI or TCI phase originates from *splitting* bands that were previously connected in the absence of SOC (and possibly in the presence of additional crystal symmetries that are subsequently broken by Rashba- or Dresselhaus-like SOC). The prototypical example of SOC-driven topological splitting occurs in the Kane-Mele model of graphene, which is an ESFD semimetal in the absence of SOC [28, 31, 159], and an SEBR 2D TI when the (weak) effects of SOC are taken into consideration [3, 126]. The second mechanism for realizing a TI or TCI is SOC-driven *band inversion*. In the case of band inversion, a narrow-gap, topologically trivial semiconductor w/o SOC becomes a TI or TCI when introducing SOC changes the band ordering at a small number of \mathbf{k} points in the BZ. In real materials, band inversion arises due to the interplay of SOC and other interactions, which are typically controlled by doping and chemical substitution. A prototypical of example of SOC- and dopant-driven band inversion occurs in the family of (higher-order) topological crystalline and trivial insulators $\text{Pb}_{1-x}\text{Sn}_x\text{Te}$ (see Refs. 12, 16, 30, 104, 120, 160–163 and SM 11 A 5).

In SM 6, we reviewed the previously established result that all 3D, symmetry-indicated topological phases w/o SOC are topological semimetals (either NLC-SM, SEBR-SM, ES, or ESFD). In the case of ES and ESFD semimetals w/o SOC, introducing SOC may split bands and open a topological gap, as occurs in the hourglass insulator KHgSb (ICSD 56201, see Refs. 13, 14, 109, 127, and 128 and SM 11 A 6), or the bulk may remain gapless, as occurs in B20 compounds in the CoSi family of chiral crystals (ICSD 189221, see Refs. 9, 23–25, 130, 134, and 135 and SM 11 C 1). However, in the case of NLC-SM- and SEBR-SM-classified semimetals w/o SOC, infinitesimal SOC will always open a direct gap if the bulk is a centrosymmetric nodal-line semimetal [31, 34, 36], but will conversely not open a gap if the bulk is a noncentrosymmetric spinless (spin-degenerate) Weyl semimetal in the absence of SOC [164]. Specifically, if the bulk is a spinless Weyl semimetal when the effects of SOC are neglected, then introducing infinitesimal SOC will *not* generically open a bulk gap – whether or not the spinless SIs in the absence of SOC are nontrivial – as the

two Weyl points within each spin-degenerate pair carry the same chiral charges (Chern numbers), and hence cannot pairwise annihilate [36, 111, 164].

In the tables below, we provide detailed statistics comparing the topology of all of the stoichiometric unique materials in the ICSD at the Fermi level with and w/o SOC (we emphasize that in this work, a unique material is defined by the topological classification or crossing points at E_F with SOC, see SM 4 for further details). Specifically, in Tables S29, S30, S31, S32, and S33, we respectively list the number of unique materials in each SG that are classified w/o SOC as ES, ESFD, LCEBR, NLC-SM, and SEBR-SM, which we then further divide by the topological classification of the same material in the presence of SOC. Notably, there are relatively few materials in the ICSD that are classified as NLC-SM (Table S32) or SEBR-SM (Table S33 [see SM 6 A for a more detailed discussion of NLC-SM and SEBR-SM materials in the ICSD]).

Table S29: SOC-driven topological phase transition statistics for ES-classified semimetals w/o SOC. In order, the first two columns in this table list the SG and the number of ES-classified unique materials in the SG w/o SOC. If an SG is not listed in the first column, then there are no ES-classified unique materials in the SG w/o SOC. In the remaining five columns, restricting to the same unique materials listed in the second column, we respectively list the number of unique materials that become classified as NLC, SEBR, ES, ESFD, and LCEBR when the effects of SOC are incorporated. For all of the topological classification categories in the table, each number of materials is accompanied by the percentage of materials in the SG in the topological class. When there are no materials in the topological class, the table entry is marked with a dashed horizontal line.

SG	# Mat.	NLC	SEBR	ES	ESFD	LCEBR
3	7	—	—	—	—	7 (100.00%)
4	14	—	—	—	—	14 (100.00%)
5	19	—	—	—	—	19 (100.00%)
6	4	—	—	—	—	4 (100.00%)
7	6	—	—	—	—	6 (100.00%)
8	14	—	—	—	—	14 (100.00%)
9	4	—	—	—	—	4 (100.00%)
10	16	15 (93.75%)	—	—	—	1 (6.25%)
11	97	74 (76.29%)	—	—	—	23 (23.71%)
12	406	177 (43.60%)	160 (39.41%)	—	—	69 (17.00%)
13	21	12 (57.14%)	—	—	—	9 (42.86%)
14	330	227 (68.79%)	—	41 (12.42%)	—	62 (18.79%)
15	137	78 (56.93%)	—	—	—	59 (43.07%)
16	1	—	—	—	—	1 (100.00%)
17	3	—	—	—	—	3 (100.00%)
18	4	—	—	—	—	4 (100.00%)
19	9	—	—	—	—	9 (100.00%)
20	3	—	—	—	—	3 (100.00%)
21	3	—	—	—	—	3 (100.00%)
22	11	—	—	—	—	11 (100.00%)
23	3	—	—	—	—	3 (100.00%)
25	12	—	—	—	—	12 (100.00%)
26	8	—	—	—	—	8 (100.00%)
28	5	—	—	—	—	5 (100.00%)
29	1	—	—	—	—	1 (100.00%)
30	1	—	—	—	—	1 (100.00%)
31	19	—	—	—	—	19 (100.00%)
33	20	—	—	—	—	20 (100.00%)
34	2	—	—	—	—	2 (100.00%)
35	2	—	—	—	—	2 (100.00%)
36	21	—	—	—	—	21 (100.00%)
38	38	—	—	—	—	38 (100.00%)
39	3	—	—	—	—	3 (100.00%)
40	3	—	—	—	—	3 (100.00%)
41	9	—	—	—	—	9 (100.00%)
43	8	—	—	—	—	8 (100.00%)
44	24	—	—	—	—	24 (100.00%)

45	2	—	—	—	—	2 (100.00%)
46	23	—	—	—	—	23 (100.00%)
47	29	25 (86.21%)	—	—	—	4 (13.79%)
48	1	—	—	—	—	1 (100.00%)
50	5	3 (60.00%)	1 (20.00%)	—	—	1 (20.00%)
51	42	40 (95.24%)	—	—	—	2 (4.76%)
53	3	—	2 (66.67%)	—	—	1 (33.33%)
54	4	3 (75.00%)	—	—	—	1 (25.00%)
55	211	173 (81.99%)	—	—	—	38 (18.01%)
56	1	—	—	—	—	1 (100.00%)
57	31	25 (80.65%)	—	—	—	6 (19.35%)
58	62	37 (59.68%)	—	8 (12.90%)	—	17 (27.42%)
59	78	27 (34.62%)	33 (42.31%)	—	—	18 (23.08%)
60	20	13 (65.00%)	—	—	—	7 (35.00%)
61	16	8 (50.00%)	—	4 (25.00%)	—	4 (25.00%)
62	777	572 (73.62%)	—	—	—	205 (26.38%)
63	454	236 (51.98%)	153 (33.70%)	—	—	65 (14.32%)
64	72	—	50 (69.44%)	6 (8.33%)	—	16 (22.22%)
65	123	68 (55.28%)	44 (35.77%)	—	—	11 (8.94%)
66	7	4 (57.14%)	—	—	—	3 (42.86%)
67	11	9 (81.82%)	—	—	—	2 (18.18%)
68	2	—	—	—	—	2 (100.00%)
69	25	—	22 (88.00%)	—	—	3 (12.00%)
70	36	—	28 (77.78%)	—	—	8 (22.22%)
71	162	—	134 (82.72%)	—	—	28 (17.28%)
72	51	25 (49.02%)	13 (25.49%)	—	—	13 (25.49%)
74	75	51 (68.00%)	—	—	—	24 (32.00%)
76	1	—	—	1 (100.00%)	—	—
82	10	8 (80.00%)	—	—	—	2 (20.00%)
83	2	—	1 (50.00%)	1 (50.00%)	—	—
84	4	2 (50.00%)	—	2 (50.00%)	—	—
85	3	—	3 (100.00%)	—	—	—
86	9	—	1 (11.11%)	6 (66.67%)	—	2 (22.22%)
87	15	—	6 (40.00%)	9 (60.00%)	—	—
88	12	—	2 (16.67%)	4 (33.33%)	—	6 (50.00%)
90	2	—	—	—	—	2 (100.00%)
91	1	—	—	—	—	1 (100.00%)
92	6	—	—	4 (66.67%)	—	2 (33.33%)
94	1	—	—	—	—	1 (100.00%)
95	1	—	—	1 (100.00%)	—	—
99	1	—	—	—	—	1 (100.00%)
100	1	—	—	—	—	1 (100.00%)
102	3	—	—	1 (33.33%)	—	2 (66.67%)
105	1	—	—	—	—	1 (100.00%)
107	13	—	—	10 (76.92%)	—	3 (23.08%)
108	2	—	—	1 (50.00%)	—	1 (50.00%)
109	7	—	—	—	—	7 (100.00%)
110	2	—	—	1 (50.00%)	—	1 (50.00%)
111	1	—	—	—	—	1 (100.00%)
113	5	2 (40.00%)	—	—	—	3 (60.00%)
114	3	—	2 (66.67%)	1 (33.33%)	—	—
115	1	—	—	—	—	1 (100.00%)
116	3	—	1 (33.33%)	—	—	2 (66.67%)
117	3	—	—	—	—	3 (100.00%)
118	2	1 (50.00%)	—	—	—	1 (50.00%)
119	8	—	—	—	—	8 (100.00%)
120	3	2 (66.67%)	—	—	—	1 (33.33%)
121	17	—	14 (82.35%)	—	—	3 (17.65%)
122	11	—	10 (90.91%)	—	—	1 (9.09%)
123	66	22 (33.33%)	17 (25.76%)	25 (37.88%)	—	2 (3.03%)
124	4	—	—	4 (100.00%)	—	—
125	7	1 (14.29%)	3 (42.86%)	3 (42.86%)	—	—
126	2	—	—	2 (100.00%)	—	—
127	78	30 (38.46%)	—	42 (53.85%)	—	6 (7.69%)

128	12	—	5 (41.67%)	7 (58.33%)	—	—
129	213	50 (23.47%)	83 (38.97%)	43 (20.19%)	—	37 (17.37%)
130	10	2 (20.00%)	1 (10.00%)	1 (10.00%)	—	6 (60.00%)
131	11	4 (36.36%)	—	4 (36.36%)	—	3 (27.27%)
132	1	—	—	1 (100.00%)	—	—
135	9	2 (22.22%)	—	6 (66.67%)	—	1 (11.11%)
136	95	—	24 (25.26%)	49 (51.58%)	—	22 (23.16%)
137	10	—	6 (60.00%)	3 (30.00%)	—	1 (10.00%)
138	4	—	—	1 (25.00%)	—	3 (75.00%)
139	332	—	203 (61.14%)	100 (30.12%)	—	29 (8.73%)
140	100	32 (32.00%)	16 (16.00%)	39 (39.00%)	—	13 (13.00%)
141	77	—	43 (55.84%)	19 (24.68%)	—	15 (19.48%)
142	11	—	5 (45.45%)	2 (18.18%)	—	4 (36.36%)
147	1	—	—	—	—	1 (100.00%)
148	5	—	—	5 (100.00%)	—	—
150	4	—	—	1 (25.00%)	—	3 (75.00%)
152	2	—	—	1 (50.00%)	—	1 (50.00%)
153	1	—	—	—	—	1 (100.00%)
154	1	—	—	—	—	1 (100.00%)
155	2	—	—	1 (50.00%)	—	1 (50.00%)
156	7	—	—	4 (57.14%)	—	3 (42.86%)
157	2	—	—	—	—	2 (100.00%)
158	1	—	—	—	—	1 (100.00%)
160	6	—	—	—	—	6 (100.00%)
161	3	—	—	2 (66.67%)	—	1 (33.33%)
162	5	—	3 (60.00%)	2 (40.00%)	—	—
163	3	—	3 (100.00%)	—	—	—
164	47	—	33 (70.21%)	7 (14.89%)	—	7 (14.89%)
165	6	—	3 (50.00%)	1 (16.67%)	—	2 (33.33%)
166	153	—	96 (62.75%)	30 (19.61%)	—	27 (17.65%)
167	21	—	6 (28.57%)	11 (52.38%)	—	4 (19.05%)
173	11	—	—	10 (90.91%)	—	1 (9.09%)
176	5	—	3 (60.00%)	2 (40.00%)	—	—
180	2	—	—	—	1 (50.00%)	1 (50.00%)
181	1	—	—	—	—	1 (100.00%)
182	5	—	—	4 (80.00%)	—	1 (20.00%)
185	10	—	—	6 (60.00%)	—	4 (40.00%)
186	40	—	—	30 (75.00%)	2 (5.00%)	8 (20.00%)
187	31	9 (29.03%)	—	19 (61.29%)	—	3 (9.68%)
189	94	—	53 (56.38%)	40 (42.55%)	—	1 (1.06%)
190	3	2 (66.67%)	—	1 (33.33%)	—	—
191	63	—	22 (34.92%)	41 (65.08%)	—	—
193	24	—	10 (41.67%)	14 (58.33%)	—	—
194	235	—	98 (41.70%)	124 (52.77%)	—	13 (5.53%)
198	1	—	—	—	—	1 (100.00%)
199	1	—	—	—	—	1 (100.00%)
200	2	—	2 (100.00%)	—	—	—
204	4	—	4 (100.00%)	—	—	—
205	9	6 (66.67%)	—	1 (11.11%)	—	2 (22.22%)
206	1	—	1 (100.00%)	—	—	—
208	2	—	—	—	—	2 (100.00%)
212	2	—	—	2 (100.00%)	—	—
213	1	—	—	1 (100.00%)	—	—
214	1	—	—	—	1 (100.00%)	—
216	21	13 (61.90%)	—	2 (9.52%)	1 (4.76%)	5 (23.81%)
217	6	—	1 (16.67%)	—	2 (33.33%)	3 (50.00%)
219	2	—	—	—	—	2 (100.00%)
220	15	10 (66.67%)	—	—	4 (26.67%)	1 (6.67%)
221	107	4 (3.74%)	50 (46.73%)	46 (42.99%)	6 (5.61%)	1 (0.93%)
223	13	—	3 (23.08%)	9 (69.23%)	1 (7.69%)	—
225	74	—	34 (45.95%)	33 (44.59%)	3 (4.05%)	4 (5.41%)
226	3	—	1 (33.33%)	1 (33.33%)	1 (33.33%)	—
227	131	—	71 (54.20%)	37 (28.24%)	13 (9.92%)	10 (7.63%)
229	8	—	2 (25.00%)	3 (37.50%)	3 (37.50%)	—

230	1	—	—	1 (100.00%)	—	—
Total	6006	2,104 (35.03%)	1,585 (26.39%)	944 (15.72%)	38 (0.63%)	1,335 (22.23%)

Table S30: SOC-driven topological phase transition statistics for ESFD-classified semimetals w/o SOC. In order, the first two columns in this table list the SG and the number of ESFD-classified unique materials in the SG w/o SOC. If an SG is not listed in the first column, then there are no ESFD-classified unique materials in the SG w/o SOC. In the remaining five columns, restricting to the same unique materials listed in the second column, we respectively list the number of unique materials that become classified as NLC, SEBR, ES, ESFD, and LCEBR when the effects of SOC are incorporated. For all of the topological classification categories in the table, each number of materials is accompanied by the percentage of materials in the SG in the topological class. When there are no materials in the topological class, the table entry is marked with a dashed horizontal line.

SG	# Mat.	NLC	SEBR	ES	ESFD	LCEBR
1	9	—	—	—	9 (100.00%)	—
2	112	1 (0.89%)	—	—	111 (99.11%)	—
4	6	—	—	6 (100.00%)	—	—
5	12	—	—	—	12 (100.00%)	—
6	1	—	—	—	1 (100.00%)	—
7	3	—	—	3 (100.00%)	—	—
8	12	—	—	—	12 (100.00%)	—
9	11	—	—	11 (100.00%)	—	—
10	5	—	—	—	5 (100.00%)	—
11	96	—	—	—	95 (98.96%)	1 (1.04%)
12	191	—	—	—	191 (100.00%)	—
13	20	—	—	—	20 (100.00%)	—
14	137	—	—	—	137 (100.00%)	—
15	173	—	—	—	173 (100.00%)	—
18	2	—	—	—	2 (100.00%)	—
19	19	—	—	19 (100.00%)	—	—
20	2	—	—	2 (100.00%)	—	—
21	6	—	—	—	6 (100.00%)	—
23	2	—	—	—	2 (100.00%)	—
25	2	—	—	—	2 (100.00%)	—
26	4	—	—	—	4 (100.00%)	—
28	2	—	—	2 (100.00%)	—	—
29	1	—	—	1 (100.00%)	—	—
30	1	—	—	—	1 (100.00%)	—
31	14	—	—	—	14 (100.00%)	—
33	23	—	—	23 (100.00%)	—	—
34	3	—	—	—	3 (100.00%)	—
35	2	—	—	—	2 (100.00%)	—
36	32	—	—	—	32 (100.00%)	—
38	31	—	—	—	31 (100.00%)	—
40	4	—	—	4 (100.00%)	—	—
41	1	—	—	1 (100.00%)	—	—
43	13	—	—	—	13 (100.00%)	—
44	11	—	—	—	11 (100.00%)	—
46	7	—	—	7 (100.00%)	—	—
47	13	—	—	—	13 (100.00%)	—
51	35	—	—	—	35 (100.00%)	—
52	4	—	—	4 (100.00%)	—	—
53	3	—	—	—	3 (100.00%)	—
54	2	—	—	2 (100.00%)	—	—
55	41	—	—	—	41 (100.00%)	—
56	4	—	—	4 (100.00%)	—	—
57	17	—	—	17 (100.00%)	—	—
58	35	—	—	—	35 (100.00%)	—
59	65	—	—	—	65 (100.00%)	—

60	9	—	—	9 (100.00%)	—	—
61	2	—	—	2 (100.00%)	—	—
62	674	—	—	674 (100.00%)	—	—
63	470	—	—	—	470 (100.00%)	—
64	39	—	—	—	39 (100.00%)	—
65	70	—	—	—	70 (100.00%)	—
66	9	—	—	—	9 (100.00%)	—
67	6	—	—	—	6 (100.00%)	—
68	4	—	—	—	4 (100.00%)	—
69	18	—	—	—	18 (100.00%)	—
70	11	—	—	—	11 (100.00%)	—
71	153	—	—	—	153 (100.00%)	—
72	58	—	—	—	58 (100.00%)	—
73	1	—	—	1 (100.00%)	—	—
74	77	—	—	—	77 (100.00%)	—
75	2	—	—	—	2 (100.00%)	—
76	1	—	—	1 (100.00%)	—	—
79	1	—	—	1 (100.00%)	—	—
81	3	—	—	—	—	3 (100.00%)
82	25	7 (28.00%)	—	—	10 (40.00%)	8 (32.00%)
83	6	2 (33.33%)	2 (33.33%)	2 (33.33%)	—	—
84	3	—	—	1 (33.33%)	2 (66.67%)	—
85	9	—	—	1 (11.11%)	8 (88.89%)	—
86	29	—	8 (27.59%)	10 (34.48%)	11 (37.93%)	—
87	89	—	14 (15.73%)	13 (14.61%)	59 (66.29%)	3 (3.37%)
88	15	—	2 (13.33%)	—	12 (80.00%)	1 (6.67%)
90	2	—	—	—	2 (100.00%)	—
91	2	—	—	1 (50.00%)	—	1 (50.00%)
92	12	—	—	7 (58.33%)	5 (41.67%)	—
96	1	—	—	1 (100.00%)	—	—
97	1	—	—	1 (100.00%)	—	—
98	1	—	—	—	—	1 (100.00%)
99	26	—	—	7 (26.92%)	15 (57.69%)	4 (15.38%)
100	13	—	—	1 (7.69%)	11 (84.62%)	1 (7.69%)
102	3	—	—	1 (33.33%)	1 (33.33%)	1 (33.33%)
103	3	—	—	—	3 (100.00%)	—
104	1	—	—	—	1 (100.00%)	—
106	1	—	—	1 (100.00%)	—	—
107	88	—	—	6 (6.82%)	51 (57.95%)	31 (35.23%)
108	5	—	—	1 (20.00%)	3 (60.00%)	1 (20.00%)
109	16	—	—	—	13 (81.25%)	3 (18.75%)
110	1	—	—	1 (100.00%)	—	—
111	6	—	1 (16.67%)	—	4 (66.67%)	1 (16.67%)
113	21	—	—	—	19 (90.48%)	2 (9.52%)
114	3	—	—	—	—	3 (100.00%)
115	14	—	4 (28.57%)	—	6 (42.86%)	4 (28.57%)
117	3	1 (33.33%)	—	—	1 (33.33%)	1 (33.33%)
118	1	—	—	—	1 (100.00%)	—
119	9	2 (22.22%)	—	—	6 (66.67%)	1 (11.11%)
120	3	—	—	2 (66.67%)	—	1 (33.33%)
121	39	—	4 (10.26%)	—	20 (51.28%)	15 (38.46%)
122	12	—	3 (25.00%)	1 (8.33%)	8 (66.67%)	—
123	325	28 (8.62%)	18 (5.54%)	64 (19.69%)	210 (64.62%)	5 (1.54%)
124	15	1 (6.67%)	—	3 (20.00%)	11 (73.33%)	—
125	25	3 (12.00%)	3 (12.00%)	5 (20.00%)	14 (56.00%)	—
126	2	—	—	—	2 (100.00%)	—
127	248	32 (12.90%)	—	46 (18.55%)	167 (67.34%)	3 (1.21%)
128	33	—	8 (24.24%)	14 (42.42%)	10 (30.30%)	1 (3.03%)
129	478	51 (10.67%)	34 (7.11%)	48 (10.04%)	330 (69.04%)	15 (3.14%)
130	13	1 (7.69%)	—	2 (15.38%)	9 (69.23%)	1 (7.69%)
131	25	3 (12.00%)	—	5 (20.00%)	17 (68.00%)	—
133	2	1 (50.00%)	—	1 (50.00%)	—	—
134	3	—	—	—	3 (100.00%)	—
135	6	2 (33.33%)	—	1 (16.67%)	3 (50.00%)	—

136	93	—	9 (9.68%)	21 (22.58%)	58 (62.37%)	5 (5.38%)
137	27	—	2 (7.41%)	7 (25.93%)	17 (62.96%)	1 (3.70%)
138	3	1 (33.33%)	—	1 (33.33%)	—	1 (33.33%)
139	1052	—	251 (23.86%)	180 (17.11%)	582 (55.32%)	39 (3.71%)
140	219	18 (8.22%)	8 (3.65%)	22 (10.05%)	167 (76.26%)	4 (1.83%)
141	92	—	8 (8.70%)	4 (4.35%)	73 (79.35%)	7 (7.61%)
142	24	—	4 (16.67%)	10 (41.67%)	10 (41.67%)	—
143	5	—	—	1 (20.00%)	3 (60.00%)	1 (20.00%)
144	2	—	—	—	1 (50.00%)	1 (50.00%)
146	20	—	—	5 (25.00%)	9 (45.00%)	6 (30.00%)
147	15	—	5 (33.33%)	5 (33.33%)	3 (20.00%)	2 (13.33%)
148	184	—	37 (20.11%)	22 (11.96%)	102 (55.43%)	23 (12.50%)
149	5	—	—	1 (20.00%)	2 (40.00%)	2 (40.00%)
150	11	—	—	2 (18.18%)	8 (72.73%)	1 (9.09%)
152	7	—	—	1 (14.29%)	6 (85.71%)	—
154	1	—	—	1 (100.00%)	—	—
155	17	—	—	2 (11.76%)	7 (41.18%)	8 (47.06%)
156	9	—	—	2 (22.22%)	6 (66.67%)	1 (11.11%)
157	3	—	—	1 (33.33%)	2 (66.67%)	—
158	2	—	—	1 (50.00%)	1 (50.00%)	—
159	6	—	—	3 (50.00%)	2 (33.33%)	1 (16.67%)
160	52	—	—	7 (13.46%)	33 (63.46%)	12 (23.08%)
161	15	—	—	6 (40.00%)	7 (46.67%)	2 (13.33%)
162	21	—	2 (9.52%)	6 (28.57%)	11 (52.38%)	2 (9.52%)
163	22	—	1 (4.55%)	8 (36.36%)	10 (45.45%)	3 (13.64%)
164	271	—	58 (21.40%)	37 (13.65%)	150 (55.35%)	26 (9.59%)
165	18	—	1 (5.56%)	6 (33.33%)	8 (44.44%)	3 (16.67%)
166	463	—	84 (18.14%)	68 (14.69%)	281 (60.69%)	30 (6.48%)
167	100	—	5 (5.00%)	16 (16.00%)	66 (66.00%)	13 (13.00%)
173	28	—	—	24 (85.71%)	2 (7.14%)	2 (7.14%)
174	33	—	—	2 (6.06%)	31 (93.94%)	—
175	2	—	—	—	2 (100.00%)	—
176	77	—	3 (3.90%)	16 (20.78%)	52 (67.53%)	6 (7.79%)
180	16	—	—	6 (37.50%)	9 (56.25%)	1 (6.25%)
181	4	—	—	1 (25.00%)	3 (75.00%)	—
182	19	—	—	16 (84.21%)	2 (10.53%)	1 (5.26%)
185	19	—	—	4 (21.05%)	15 (78.95%)	—
186	163	—	—	38 (23.31%)	116 (71.17%)	9 (5.52%)
187	92	3 (3.26%)	—	31 (33.70%)	58 (63.04%)	—
188	4	—	—	2 (50.00%)	2 (50.00%)	—
189	389	—	47 (12.08%)	81 (20.82%)	260 (66.84%)	1 (0.26%)
190	22	2 (9.09%)	—	4 (18.18%)	16 (72.73%)	—
191	384	—	51 (13.28%)	130 (33.85%)	203 (52.86%)	—
193	233	—	5 (2.15%)	84 (36.05%)	140 (60.09%)	4 (1.72%)
194	1043	—	107 (10.26%)	414 (39.69%)	505 (48.42%)	17 (1.63%)
196	1	—	—	—	1 (100.00%)	—
197	10	—	—	—	9 (90.00%)	1 (10.00%)
198	76	—	—	2 (2.63%)	74 (97.37%)	—
199	8	—	—	1 (12.50%)	7 (87.50%)	—
200	15	—	1 (6.67%)	—	13 (86.67%)	1 (6.67%)
201	4	—	1 (25.00%)	—	3 (75.00%)	—
202	10	—	—	—	10 (100.00%)	—
203	1	—	—	1 (100.00%)	—	—
204	119	—	7 (5.88%)	—	104 (87.39%)	8 (6.72%)
205	40	2 (5.00%)	—	2 (5.00%)	34 (85.00%)	2 (5.00%)
206	29	—	9 (31.03%)	2 (6.90%)	13 (44.83%)	5 (17.24%)
210	1	—	—	—	1 (100.00%)	—
211	1	—	—	—	1 (100.00%)	—
212	6	—	—	1 (16.67%)	5 (83.33%)	—
213	16	—	—	2 (12.50%)	14 (87.50%)	—
214	6	—	—	1 (16.67%)	5 (83.33%)	—
215	23	—	3 (13.04%)	—	13 (56.52%)	7 (30.43%)
216	496	45 (9.07%)	—	15 (3.02%)	412 (83.06%)	24 (4.84%)
217	60	—	5 (8.33%)	1 (1.67%)	50 (83.33%)	4 (6.67%)

218	12	—	1 (8.33%)	6 (50.00%)	5 (41.67%)	—
219	3	—	—	2 (66.67%)	1 (33.33%)	—
220	100	1 (1.00%)	—	2 (2.00%)	95 (95.00%)	2 (2.00%)
221	1063	—	63 (5.93%)	114 (10.72%)	878 (82.60%)	8 (0.75%)
223	201	—	6 (2.99%)	37 (18.41%)	158 (78.61%)	—
224	9	—	—	1 (11.11%)	8 (88.89%)	—
225	1203	—	128 (10.64%)	135 (11.22%)	904 (75.15%)	36 (2.99%)
226	39	—	1 (2.56%)	4 (10.26%)	34 (87.18%)	—
227	542	—	69 (12.73%)	108 (19.93%)	325 (59.96%)	40 (7.38%)
229	177	—	5 (2.82%)	15 (8.47%)	156 (88.14%)	1 (0.56%)
230	4	—	1 (25.00%)	—	3 (75.00%)	—
Total	13997	207 (1.48%)	1,089 (7.78%)	2,792 (19.95%)	9,423 (67.32%)	486 (3.47%)

Table S31: SOC-driven topological phase transition statistics for LCEBR-classified materials w/o SOC. In order, the first two columns in this table list the SG and the number of LCEBR-classified unique materials in the SG w/o SOC. If an SG is not listed in the first column, then there are no LCEBR-classified unique materials in the SG w/o SOC. In the remaining five columns, restricting to the same unique materials listed in the second column, we respectively list the number of unique materials that become classified as NLC, SEBR, ES, ESFD, and LCEBR when the effects of SOC are incorporated. For all of the topological classification categories in the table, each number of materials is accompanied by the percentage of materials in the SG in the topological class. When there are no materials in the topological class, the table entry is marked with a dashed horizontal line.

SG	# Mat.	NLC	SEBR	ES	ESFD	LCEBR
1	142	—	—	—	—	142 (100.00%)
2	1189	—	—	—	—	1,189 (100.00%)
3	3	—	—	—	—	3 (100.00%)
4	199	—	—	—	—	199 (100.00%)
5	117	—	—	—	—	117 (100.00%)
6	23	—	—	—	—	23 (100.00%)
7	76	—	—	—	—	76 (100.00%)
8	115	—	—	—	—	115 (100.00%)
9	182	—	—	—	—	182 (100.00%)
10	12	—	—	—	—	12 (100.00%)
11	350	2 (0.57%)	—	—	—	348 (99.43%)
12	629	7 (1.11%)	3 (0.48%)	—	—	619 (98.41%)
13	122	—	—	—	—	122 (100.00%)
14	2029	6 (0.30%)	—	1 (0.05%)	—	2,022 (99.66%)
15	1070	2 (0.19%)	—	—	—	1,068 (99.81%)
16	1	—	—	—	—	1 (100.00%)
17	5	—	—	—	—	5 (100.00%)
18	24	—	—	—	—	24 (100.00%)
19	233	—	—	—	—	233 (100.00%)
20	53	—	—	—	—	53 (100.00%)
21	6	—	—	—	—	6 (100.00%)
22	3	—	—	—	—	3 (100.00%)
23	10	—	—	—	—	10 (100.00%)
24	2	—	—	—	—	2 (100.00%)
25	31	—	—	—	—	31 (100.00%)
26	47	—	—	—	—	47 (100.00%)
27	1	—	—	—	—	1 (100.00%)
28	4	—	—	—	—	4 (100.00%)
29	57	—	—	—	—	57 (100.00%)
30	3	—	—	—	—	3 (100.00%)
31	125	—	—	—	—	125 (100.00%)
32	10	—	—	—	—	10 (100.00%)
33	208	—	—	—	—	208 (100.00%)
34	16	—	—	—	—	16 (100.00%)
35	4	—	—	—	—	4 (100.00%)

36	188	—	—	—	—	188 (100.00%)
37	5	—	—	—	—	5 (100.00%)
38	26	—	—	—	—	26 (100.00%)
39	9	—	—	—	—	9 (100.00%)
40	47	—	—	—	—	47 (100.00%)
41	21	—	—	—	—	21 (100.00%)
42	4	—	—	—	—	4 (100.00%)
43	62	—	—	—	—	62 (100.00%)
44	27	—	—	—	—	27 (100.00%)
45	6	—	—	—	—	6 (100.00%)
46	25	—	—	—	—	25 (100.00%)
47	3	—	—	—	—	3 (100.00%)
48	2	—	—	—	—	2 (100.00%)
50	2	—	—	—	—	2 (100.00%)
51	23	1 (4.35%)	—	—	—	22 (95.65%)
52	32	—	—	—	—	32 (100.00%)
53	12	—	—	—	—	12 (100.00%)
54	12	—	—	—	—	12 (100.00%)
55	84	—	—	—	—	84 (100.00%)
56	14	—	—	—	—	14 (100.00%)
57	80	—	—	—	—	80 (100.00%)
58	104	1 (0.96%)	—	—	—	103 (99.04%)
59	65	—	—	—	—	65 (100.00%)
60	109	—	—	—	—	109 (100.00%)
61	101	—	—	—	—	101 (100.00%)
62	1349	17 (1.26%)	—	—	—	1,332 (98.74%)
63	353	2 (0.57%)	3 (0.85%)	—	—	348 (98.58%)
64	133	—	—	—	—	133 (100.00%)
65	20	—	—	—	—	20 (100.00%)
66	18	1 (5.56%)	—	—	—	17 (94.44%)
67	12	—	—	—	—	12 (100.00%)
68	13	—	—	—	—	13 (100.00%)
69	22	—	—	—	—	22 (100.00%)
70	83	—	—	—	—	83 (100.00%)
71	70	—	—	—	—	70 (100.00%)
72	73	—	—	—	—	73 (100.00%)
73	15	—	—	—	—	15 (100.00%)
74	50	1 (2.00%)	—	—	—	49 (98.00%)
75	3	—	—	—	—	3 (100.00%)
76	10	—	—	—	—	10 (100.00%)
77	2	—	—	—	—	2 (100.00%)
78	2	—	—	—	—	2 (100.00%)
79	10	—	—	—	—	10 (100.00%)
80	3	—	—	—	—	3 (100.00%)
81	9	—	—	—	—	9 (100.00%)
82	93	2 (2.15%)	—	—	—	91 (97.85%)
83	1	—	—	—	—	1 (100.00%)
84	21	—	—	—	—	21 (100.00%)
85	22	—	—	—	—	22 (100.00%)
86	11	—	1 (9.09%)	—	—	10 (90.91%)
87	69	—	—	—	—	69 (100.00%)
88	102	—	—	—	—	102 (100.00%)
90	1	—	—	—	—	1 (100.00%)
91	4	—	—	—	—	4 (100.00%)
92	29	—	—	—	—	29 (100.00%)
95	2	—	—	—	—	2 (100.00%)
96	15	—	—	—	—	15 (100.00%)
97	1	—	—	—	—	1 (100.00%)
98	3	—	—	—	—	3 (100.00%)
99	71	—	—	—	—	71 (100.00%)
100	6	—	—	—	—	6 (100.00%)
102	6	—	—	—	—	6 (100.00%)
104	2	—	—	—	—	2 (100.00%)
105	3	—	—	—	—	3 (100.00%)

107	11	—	—	—	—	11 (100.00%)
108	7	—	—	—	—	7 (100.00%)
109	14	—	—	1 (7.14%)	—	13 (92.86%)
110	5	—	—	—	—	5 (100.00%)
111	13	—	—	—	—	13 (100.00%)
112	4	—	—	—	—	4 (100.00%)
113	45	—	—	—	—	45 (100.00%)
114	25	—	—	—	—	25 (100.00%)
115	6	—	—	—	—	6 (100.00%)
116	14	—	—	—	—	14 (100.00%)
117	5	—	—	—	—	5 (100.00%)
118	8	—	—	—	—	8 (100.00%)
119	18	—	—	—	—	18 (100.00%)
120	9	—	—	—	—	9 (100.00%)
121	67	—	—	—	—	67 (100.00%)
122	101	—	3 (2.97%)	1 (0.99%)	—	97 (96.04%)
123	59	—	—	—	—	59 (100.00%)
124	3	—	—	—	—	3 (100.00%)
125	17	—	—	—	—	17 (100.00%)
126	7	—	—	1 (14.29%)	—	6 (85.71%)
127	42	1 (2.38%)	—	—	—	41 (97.62%)
128	26	—	—	—	—	26 (100.00%)
129	170	1 (0.59%)	—	5 (2.94%)	—	164 (96.47%)
130	14	—	—	—	—	14 (100.00%)
131	7	—	—	—	—	7 (100.00%)
132	9	—	—	—	—	9 (100.00%)
133	1	—	—	—	—	1 (100.00%)
134	1	—	—	—	—	1 (100.00%)
135	11	—	—	—	—	11 (100.00%)
136	63	—	1 (1.59%)	—	—	62 (98.41%)
137	31	—	—	—	—	31 (100.00%)
138	9	—	—	—	—	9 (100.00%)
139	159	—	2 (1.26%)	3 (1.89%)	—	154 (96.86%)
140	112	1 (0.89%)	—	—	—	111 (99.11%)
141	77	—	1 (1.30%)	1 (1.30%)	—	75 (97.40%)
142	38	—	—	—	—	38 (100.00%)
143	12	—	—	1 (8.33%)	—	11 (91.67%)
144	11	—	—	—	—	11 (100.00%)
145	5	—	—	—	—	5 (100.00%)
146	63	—	—	—	1 (1.59%)	62 (98.41%)
147	52	—	—	1 (1.92%)	—	51 (98.08%)
148	255	—	1 (0.39%)	—	—	254 (99.61%)
149	5	—	—	—	—	5 (100.00%)
150	49	—	—	—	—	49 (100.00%)
151	4	—	—	—	—	4 (100.00%)
152	31	—	—	1 (3.23%)	2 (6.45%)	28 (90.32%)
154	15	—	—	—	1 (6.67%)	14 (93.33%)
155	31	—	—	—	—	31 (100.00%)
156	41	—	—	1 (2.44%)	—	40 (97.56%)
157	9	—	—	—	—	9 (100.00%)
159	18	—	—	—	—	18 (100.00%)
160	100	—	—	—	—	100 (100.00%)
161	69	—	—	—	—	69 (100.00%)
162	25	—	—	—	—	25 (100.00%)
163	32	—	1 (3.12%)	—	—	31 (96.88%)
164	254	—	13 (5.12%)	2 (0.79%)	—	239 (94.09%)
165	9	—	—	—	—	9 (100.00%)
166	337	—	15 (4.45%)	3 (0.89%)	—	319 (94.66%)
167	179	—	—	—	—	179 (100.00%)
169	1	—	—	—	—	1 (100.00%)
173	74	—	—	—	—	74 (100.00%)
174	17	—	—	—	—	17 (100.00%)
176	107	—	—	—	—	107 (100.00%)
177	1	—	—	—	—	1 (100.00%)

180	10	—	—	—	—	10 (100.00%)
181	3	—	—	—	—	3 (100.00%)
182	9	—	—	—	—	9 (100.00%)
183	1	—	—	—	—	1 (100.00%)
185	20	—	—	2 (10.00%)	—	18 (90.00%)
186	167	—	—	3 (1.80%)	—	164 (98.20%)
187	31	—	—	—	—	31 (100.00%)
188	16	—	—	—	—	16 (100.00%)
189	54	—	2 (3.70%)	—	—	52 (96.30%)
190	16	—	—	—	—	16 (100.00%)
191	5	—	—	—	—	5 (100.00%)
192	2	—	—	—	—	2 (100.00%)
193	13	—	—	—	—	13 (100.00%)
194	252	—	4 (1.59%)	6 (2.38%)	—	242 (96.03%)
195	1	—	—	—	—	1 (100.00%)
197	10	—	—	—	—	10 (100.00%)
198	93	—	—	—	1 (1.08%)	92 (98.92%)
199	23	—	—	—	—	23 (100.00%)
200	5	—	—	—	1 (20.00%)	4 (80.00%)
201	2	—	—	—	—	2 (100.00%)
202	8	—	—	—	—	8 (100.00%)
203	5	—	—	—	—	5 (100.00%)
204	22	—	—	—	1 (4.55%)	21 (95.45%)
205	81	1 (1.23%)	—	1 (1.23%)	—	79 (97.53%)
206	30	—	1 (3.33%)	—	1 (3.33%)	28 (93.33%)
212	6	—	—	—	—	6 (100.00%)
213	5	—	—	—	—	5 (100.00%)
214	6	—	—	—	—	6 (100.00%)
215	30	—	—	—	—	30 (100.00%)
216	234	3 (1.28%)	—	6 (2.56%)	8 (3.42%)	217 (92.74%)
217	42	—	—	—	—	42 (100.00%)
218	30	—	—	—	—	30 (100.00%)
219	3	—	—	—	—	3 (100.00%)
220	27	—	—	—	—	27 (100.00%)
221	164	—	12 (7.32%)	1 (0.61%)	—	151 (92.07%)
223	3	—	—	—	—	3 (100.00%)
224	7	—	—	1 (14.29%)	—	6 (85.71%)
225	374	—	14 (3.74%)	—	6 (1.60%)	354 (94.65%)
226	1	—	—	—	—	1 (100.00%)
227	143	—	1 (0.70%)	—	2 (1.40%)	140 (97.90%)
229	20	—	—	—	—	20 (100.00%)
230	1	—	—	—	—	1 (100.00%)
Total	15865	49 (0.31%)	78 (0.49%)	42 (0.26%)	24 (0.15%)	15,672 (98.78%)

Table S32: SOC-driven topological phase transition statistics for NLC-SM-classified semimetals w/o SOC. In order, the first two columns in this table list the SG and the number of NLC-SM-classified unique materials in the SG w/o SOC. If an SG is not listed in the first column, then there are no NLC-SM-classified unique materials in the SG w/o SOC. In the remaining five columns, restricting to the same unique materials listed in the second column, we respectively list the number of unique materials that become classified as NLC, SEBR, ES, ESFD, and LCEBR when the effects of SOC are incorporated. For all of the topological classification categories in the table, each number of materials is accompanied by the percentage of materials in the SG in the topological class. When there are no materials in the topological class, the table entry is marked with a dashed horizontal line.

SG	# Mat.	NLC	SEBR	ES	ESFD	LCEBR
2	165	158 (95.76%)	—	—	—	7 (4.24%)
11	4	4 (100.00%)	—	—	—	—
12	24	2 (8.33%)	20 (83.33%)	—	—	2 (8.33%)
13	1	1 (100.00%)	—	—	—	—

14	24	23 (95.83%)	—	—	—	1 (4.17%)
15	22	18 (81.82%)	—	—	—	4 (18.18%)
58	1	—	—	1 (100.00%)	—	—
60	1	1 (100.00%)	—	—	—	—
81	1	—	—	—	—	1 (100.00%)
82	2	1 (50.00%)	—	1 (50.00%)	—	—
85	2	—	—	—	—	2 (100.00%)
87	2	—	2 (100.00%)	—	—	—
166	2	—	2 (100.00%)	—	—	—
Total	251	208 (82.87%)	24 (9.56%)	2 (0.8%)	—	17 (6.77%)

Table S33: SOC-driven topological phase transition statistics for SEBR-SM-classified semimetals w/o SOC. In order, the first two columns in this table list the SG and the number of SEBR-SM-classified unique materials in the SG w/o SOC. If an SG is not listed in the first column, then there are no SEBR-SM-classified unique materials in the SG w/o SOC. In the remaining five columns, restricting to the same unique materials listed in the second column, we respectively list the number of unique materials that become classified as NLC, SEBR, ES, ESFD, and LCEBR when the effects of SOC are incorporated. For all of the topological classification categories in the table, each number of materials is accompanied by the percentage of materials in the SG in the topological class. When there are no materials in the topological class, the table entry is marked with a dashed horizontal line.

SG	# Mat.	NLC	SEBR	ES	ESFD	LCEBR
147	3	—	3 (100.00%)	—	—	—
148	35	—	29 (82.86%)	5 (14.29%)	—	1 (2.86%)
162	1	—	1 (100.00%)	—	—	—
164	2	—	2 (100.00%)	—	—	—
166	2	—	2 (100.00%)	—	—	—
167	1	—	1 (100.00%)	—	—	—
Total	44	—	38 (86.36%)	5 (11.36%)	—	1 (2.27%)

SM 11. LISTS OF REPRESENTATIVE TOPOLOGICAL MATERIALS

In this section, we will provide representative examples of materials on <https://www.topologicalquantumchemistry.com/> with nontrivial bulk topology that can be identified from symmetry eigenvalues and band connectivity (TQC) [28, 42, 57, 91, 92]. Though many of the materials listed in this section have been identified in previous theoretical and experimental works, most of the materials listed in this section were not previously recognized as hosting nontrivial electronic band topology. In each part of this section, we will highlight the most well-studied examples of known topological materials. First, in SM 11 A, we will enumerate the 3D topological insulators (TIs) [5, 30, 141], topological crystalline insulators (TCIs) [11–14, 109, 160, 165], and higher-order TIs (HOTIs) [15–17, 22, 33, 34, 86, 101, 104, 110, 162, 166] with the fewest electron and hole pockets at the Fermi energy (E_F). Next, in SM 11 C, we will list the topological semimetals with the simplest bulk Fermi surfaces, including examples of both conventional Dirac [6, 19, 58, 114, 115, 167–172] as well as unconventional fermion [7–9, 23–25, 130, 131, 134, 135] semimetals. Then, in SM 11 D, we will provide representative examples of spin-orbit-coupling- (SOC-) driven semimetal-to-insulator transitions that result in topological (crystalline) insulators with large gaps at E_F . Finally, in SM 11 E, we will show the materials with the cleanest insulating or semimetallic Fermi surfaces that host fragile topological bands [42–47, 95–100, 173] at or near E_F . We note that in this section, we only display electronic structures and topological data calculated in the presence of SOC; for each material, the electronic structure and topological data calculated in the absence of SOC can be accessed by clicking on the ICSD number listed above each plot. In Fig. S6, we provide an example detailing the labeling scheme and information contained within each of the band-structure plots shown in this section.

We additionally emphasize that for the materials highlighted in this section, we cannot preclude the existence of non-symmetry-indicated topological (crystalline) insulating (*e.g.* hourglass insulating [13, 14, 109, 165] or high-fold mirror-Chern TCI [160, 174]) or Weyl semimetal [20, 21, 142] phases. These non-symmetry-indicated phases cannot be identified through TQC alone, and must instead be diagnosed by performing additional (nested) Wilson-loop calculations [13, 14, 34, 101, 107–111, 175].

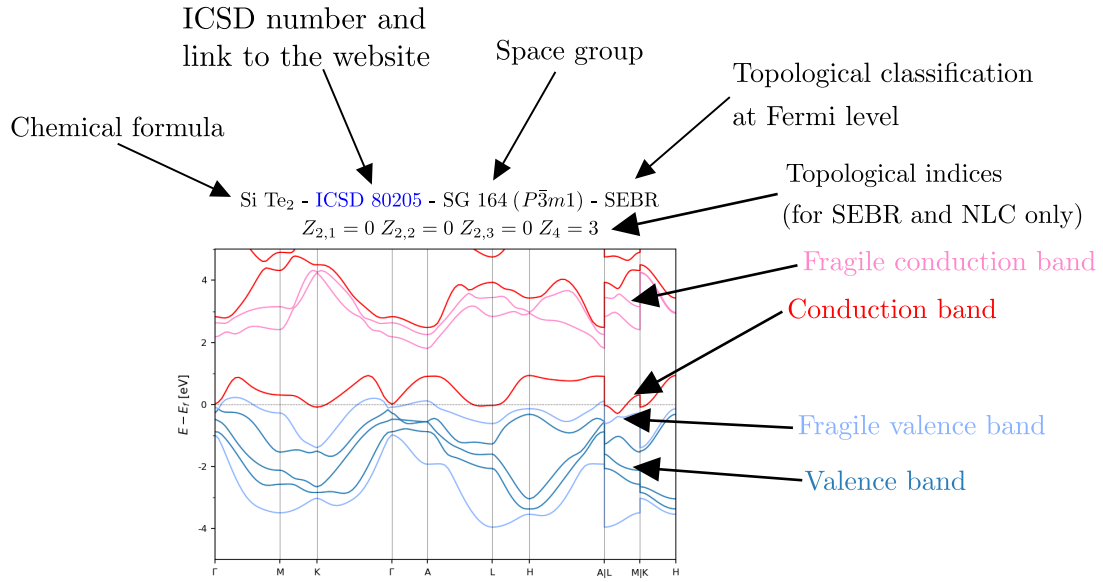


Figure S6. Example band-structure plot. In this figure, we show the band structure and topological indices of SiTe₂ [[ICSD 80205](https://www.topologicalquantumchemistry.com/), SG 164 ($P\bar{3}m1$)] as an example of the labeling scheme and information contained within each of the band-structure plots shown in this section. First, at the top of each band-structure plot, we provide the chemical formula, the ICSD number with a hyperlink to <https://www.topologicalquantumchemistry.com/>, the space group symbol and number, and the topological classification at the Fermi level (*e.g.* NLC, SEBR, ES, or ESFD). If the ICSD entry is classified as SEBR or NLC at E_F , then we further list the cumulative symmetry-based topological indices (stable SIs) at E_F in the notation established in Ref. 16. In the band-structure plot, trivial and stable topological conduction (valence) bands are labeled in red (blue), and fragile conduction (valence) bands are labeled in pink (light blue).

A. Symmetry-Indicated TIs, TCIs, and HOTIs

In this section, we will list the 3D TIs, TCIs, and HOTIs that can be diagnosed from their symmetry eigenvalues through the topological-index formulas established in Refs. 5, 16, 17, 30, and 86. First, in SM 11 A 1, we will list the 3D strong TIs indicated through the Fu-Kane parity criterion [5, 30]. Next, in SM 11 A 2, we will list the S_{4z} rotoinversion-indicated 3D TIs and Weyl semimetals [16, 17, 111]. Then, in SM 11 A 3, SM 11 A 4, SM 11 A 5, SM 11 A 6, and SM 11 A 7, we will list the TCIs and HOTIs diagnosed through the symmetry-based indicators (stable SIs) more recently introduced in Refs. 16, 17, 22, 33, 34, 86, and 162. Lastly, in SM 11 B, we will list the repeat-topological (RTopo) TIs and TCIs (rigorously defined in SM 9 A), which exhibit symmetry-indicated stable topology at the Fermi level and at the next gap below E_F as determined by band connectivity (see SM 2).

1. 3D Strong TIs

In this section, we list the symmetry-indicated 3D strong TIs with the largest band gaps or the fewest and smallest bulk Fermi pockets. First, in Figs. S7, S8, S9, S10, and S11, we list the 3D TIs classified as NLC, and then, in Figs. S12, S13, S14, S15, and S16, we list the 3D TIs classified as SEBR. 3D TIs characteristically exhibit odd numbers of twofold Dirac-cone surface states [5, 18, 30, 176] that are protected by time-reversal (\mathcal{T}) symmetry. Though it was originally recognized that 3D TIs could be identified through a \mathbb{Z}_2 -valued (Fu-Kane) index based on parity [inversion (\mathcal{I})] eigenvalues [5, 30], a more exhaustive consideration of eigenvalue indicators (stable SIs, see Refs. 16, 17, 22, 33, 34, 86, and 162 and SM 2) has revealed that the Fu-Kane parity index is in fact subsumed by a \mathbb{Z}_4 -valued index Z_4 that includes both HOTIs and strong TIs. In the notation of Ref. 16, which we use throughout this work, 3D TIs are indicated either by $Z_4 = 1, 3$ (which coincide with the Fu-Kane parity criterion). The most well known example of a 3D TI [18] – Bi₂Se₃ [ICSD 617079, SG 166 ($R\bar{3}m$)] – is classified as SEBR, and accordingly appears in Fig. S14.

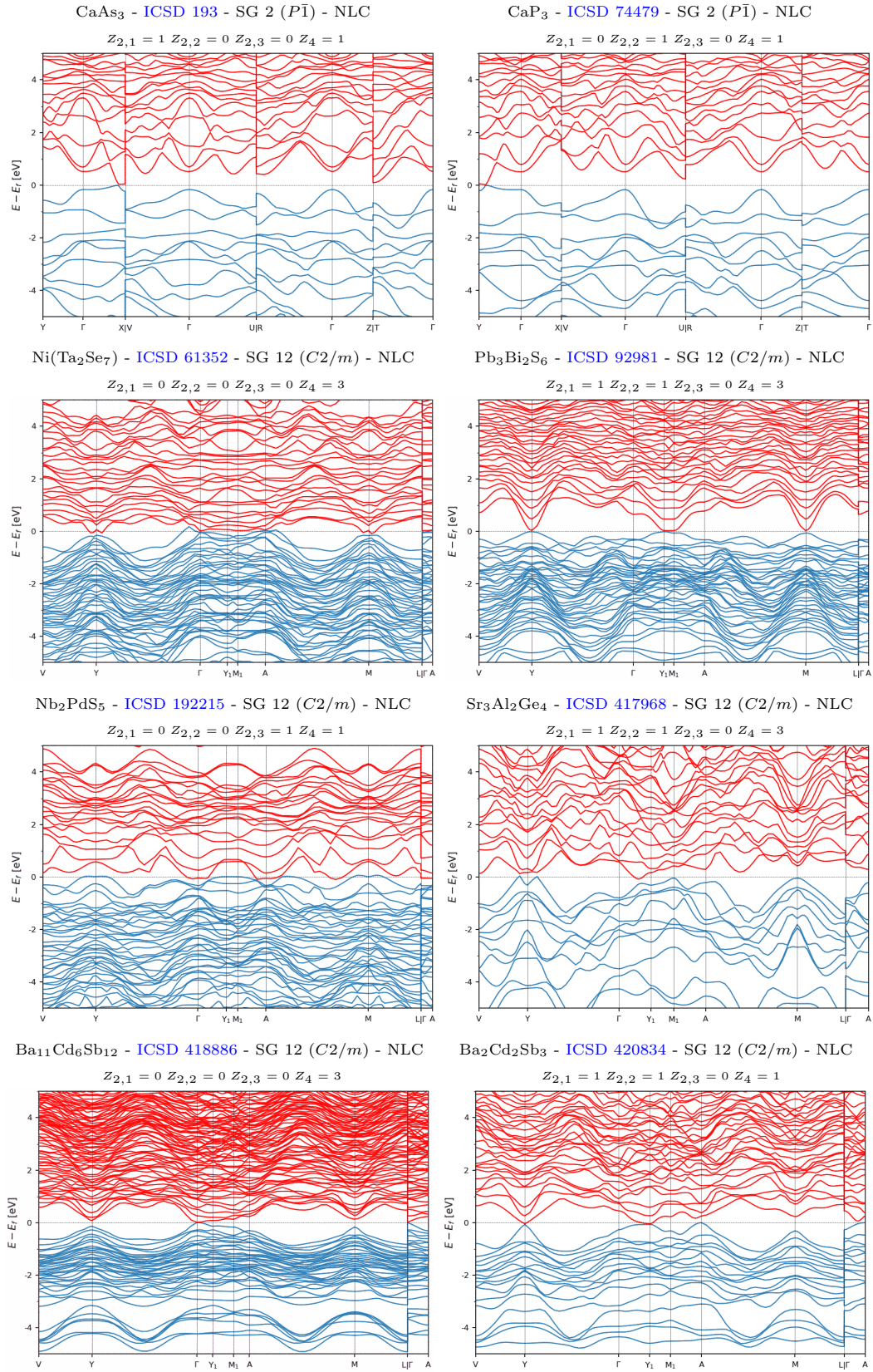


Figure S7. The NLC-classified 3D strong TIs with the largest band gaps or the fewest and smallest bulk Fermi pockets. (part 1/5)

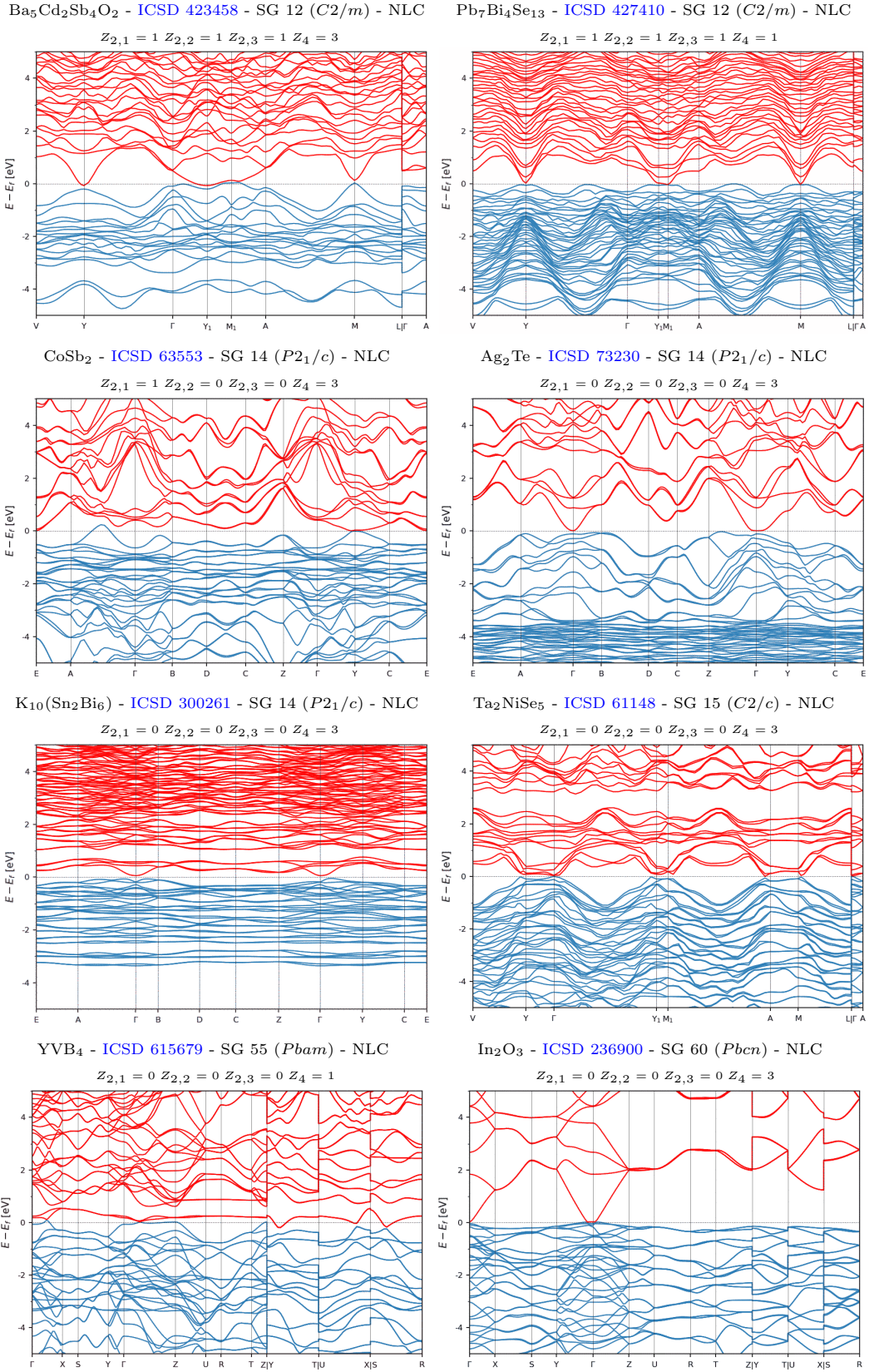


Figure S8. The NLC-classified 3D strong TIs with the largest band gaps or the fewest and smallest bulk Fermi pockets. (part 2/5)

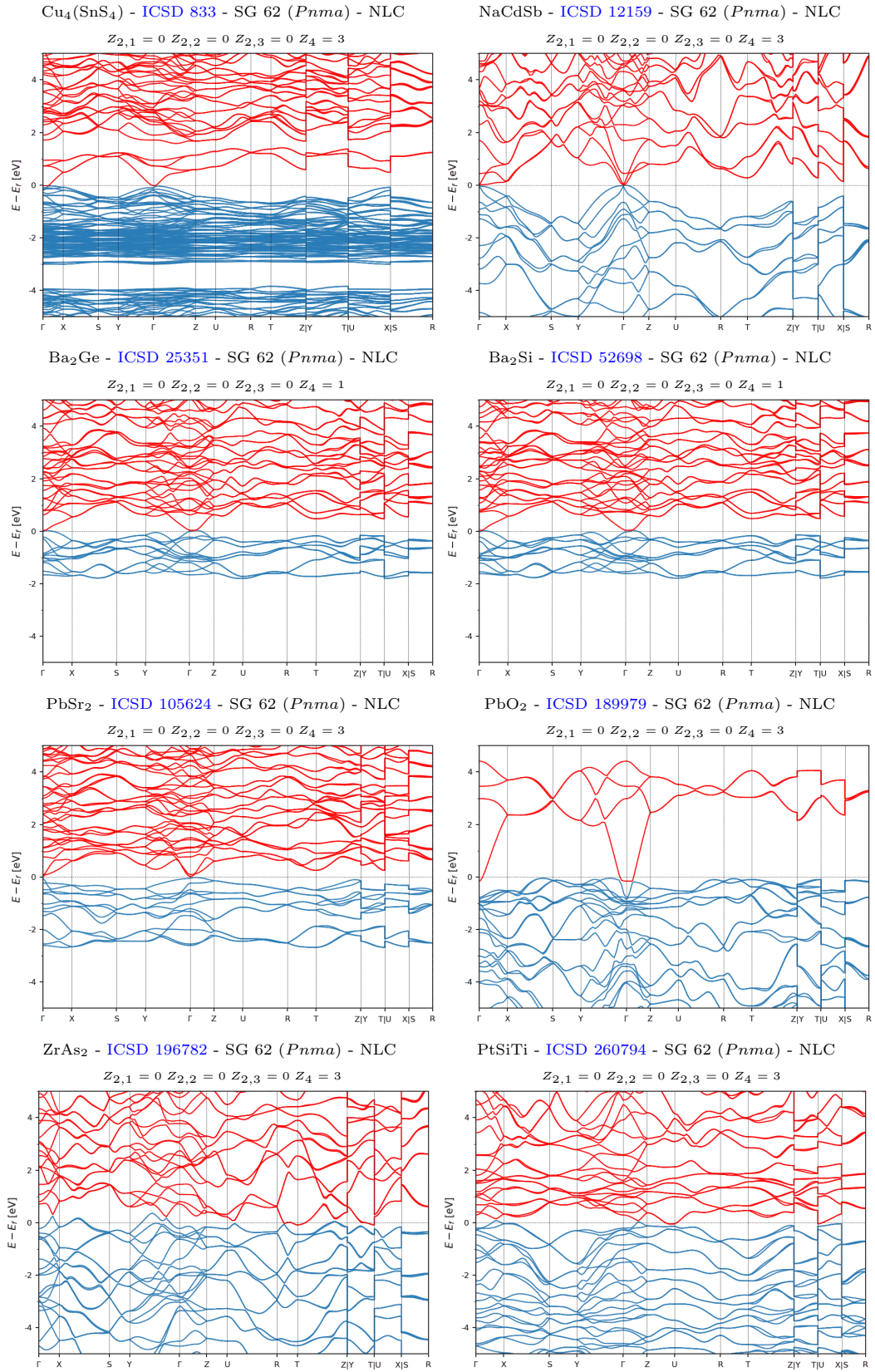


Figure S9. The NLC-classified 3D strong TIs with the largest band gaps or the fewest and smallest bulk Fermi pockets. (part 3/5)

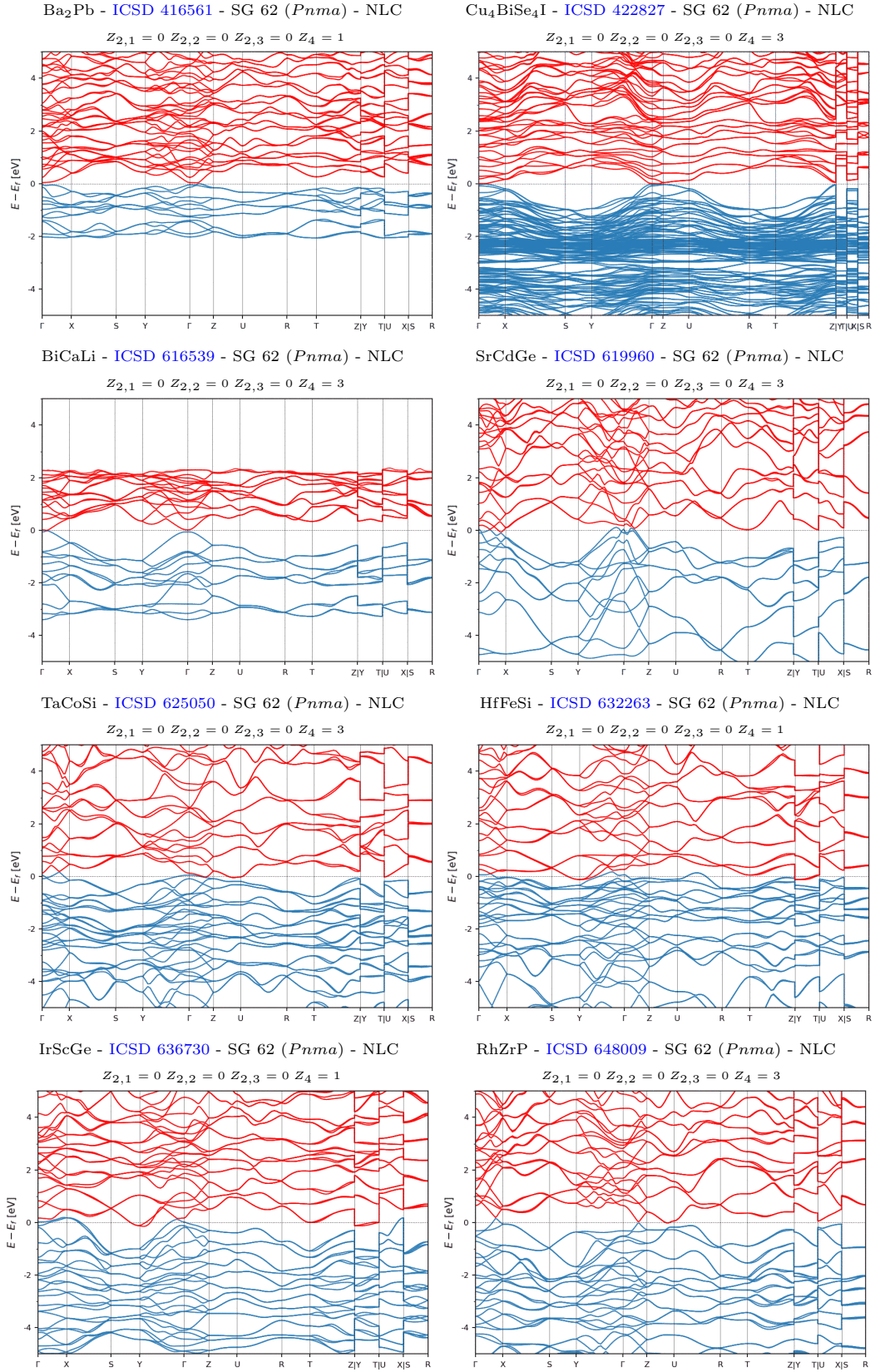


Figure S10. The NLC-classified 3D strong TIs with the largest band gaps or the fewest and smallest bulk Fermi pockets. (part 4/5)

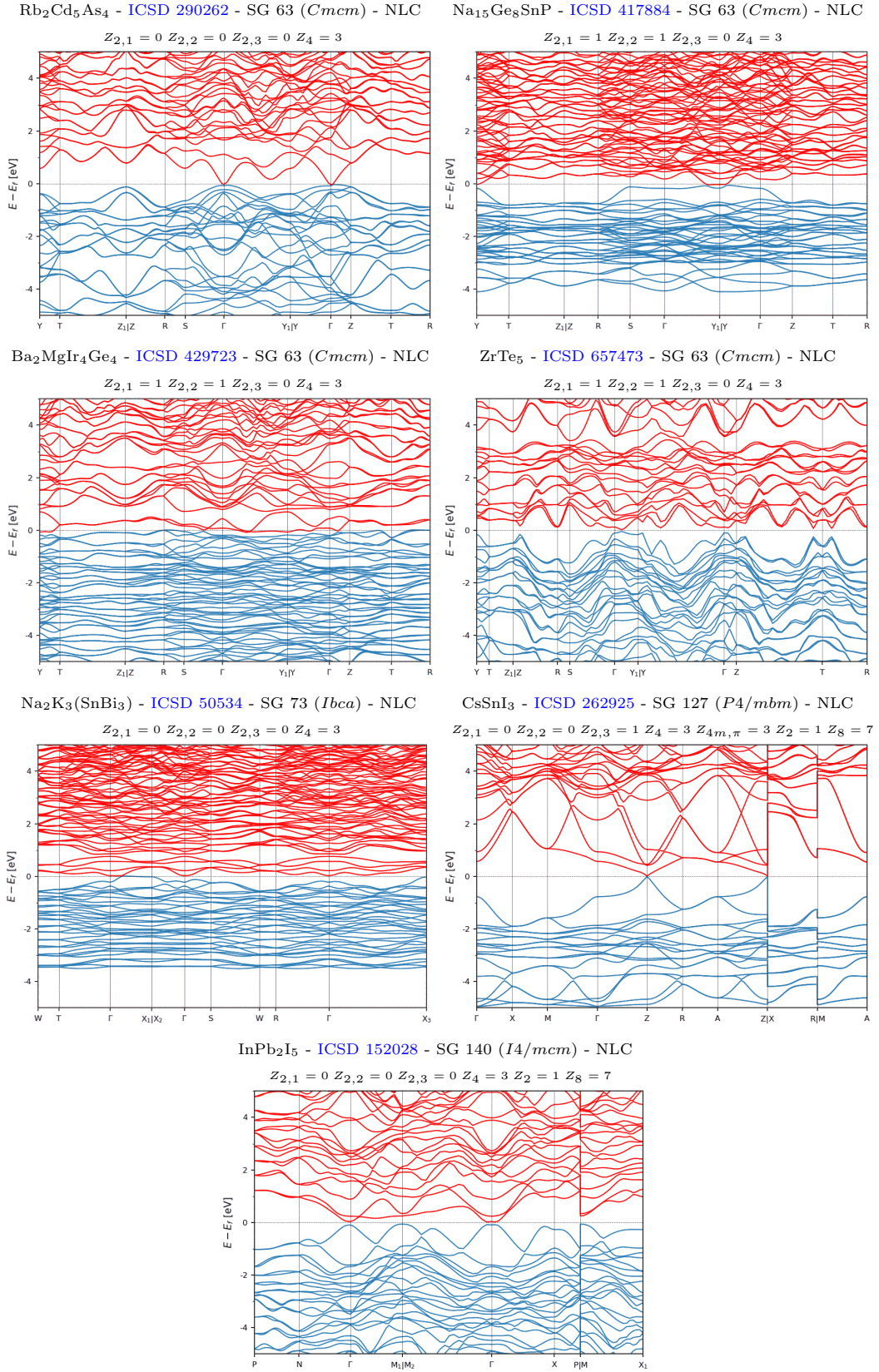


Figure S11. The NLC-classified 3D strong TIs with the largest band gaps or the fewest and smallest bulk Fermi pockets. (part 5/5)

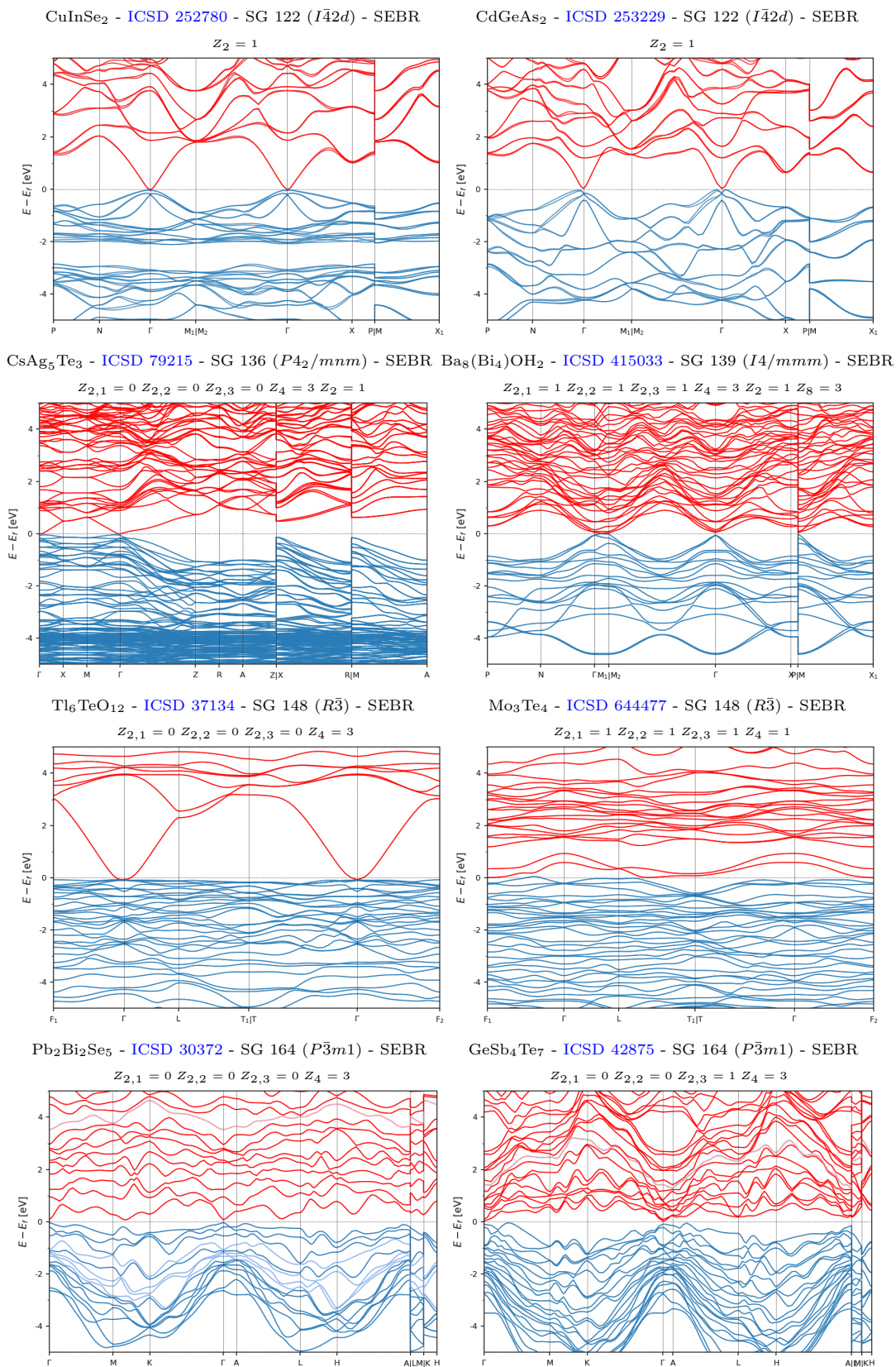


Figure S12. The SEBR-classified 3D strong TIs with the largest band gaps or the fewest and smallest bulk Fermi pockets. (part 1/5)

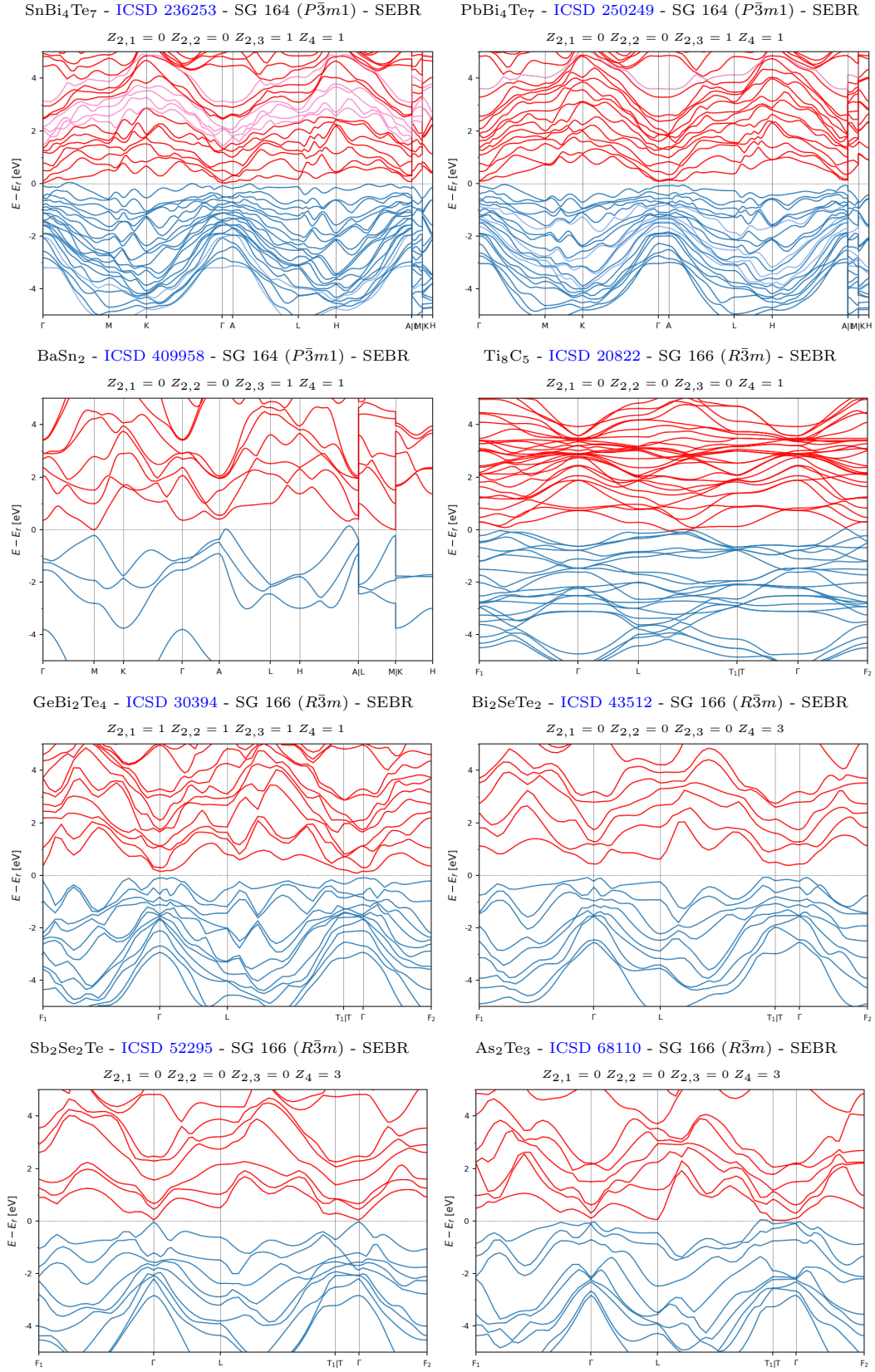


Figure S13. The SEBR-classified 3D strong TIs with the largest band gaps or the fewest and smallest bulk Fermi pockets. (part 2/5)

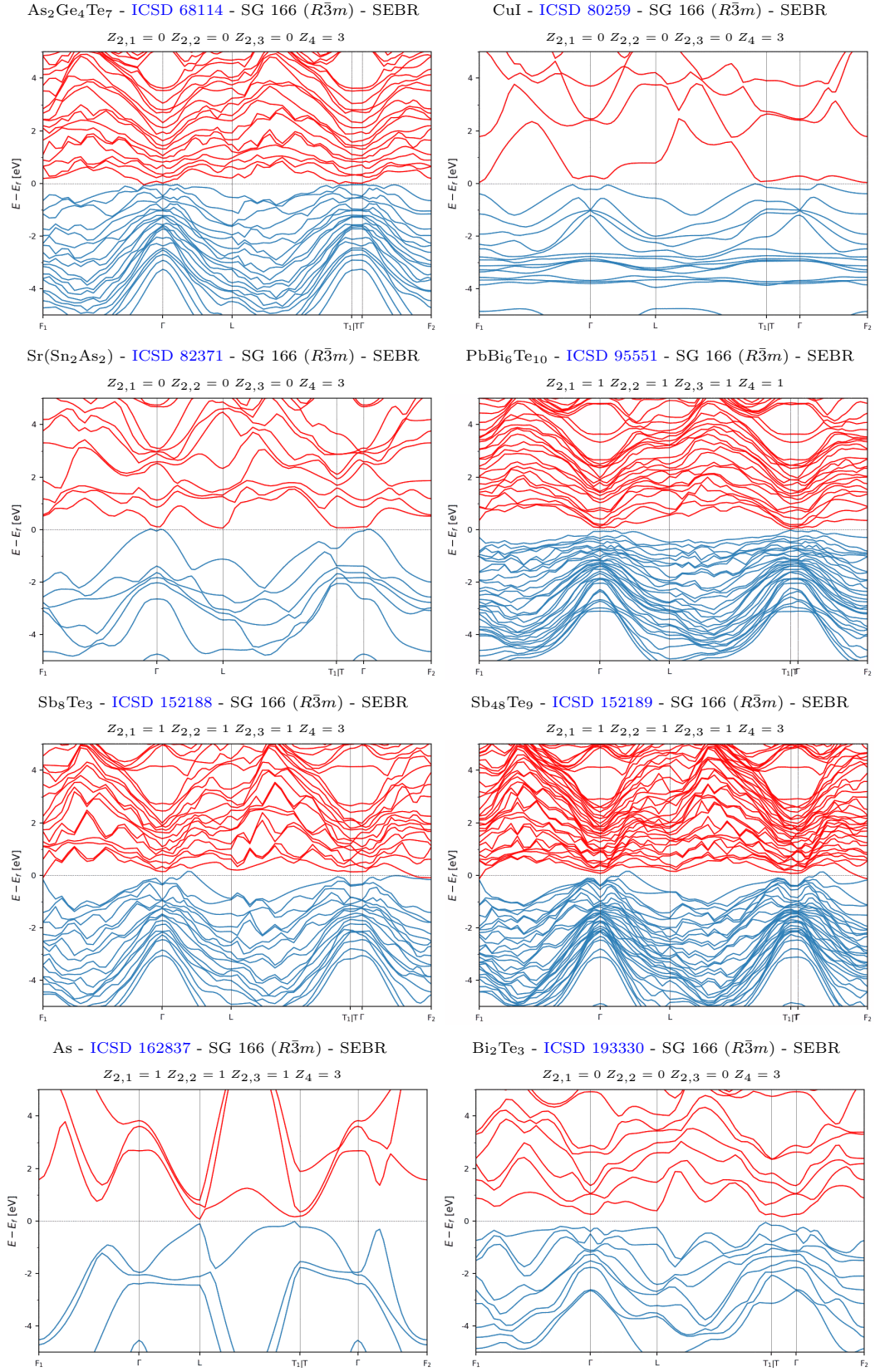


Figure S14. The SEBR-classified 3D strong TIs with the largest band gaps or the fewest and smallest bulk Fermi pockets. (part 3/5)

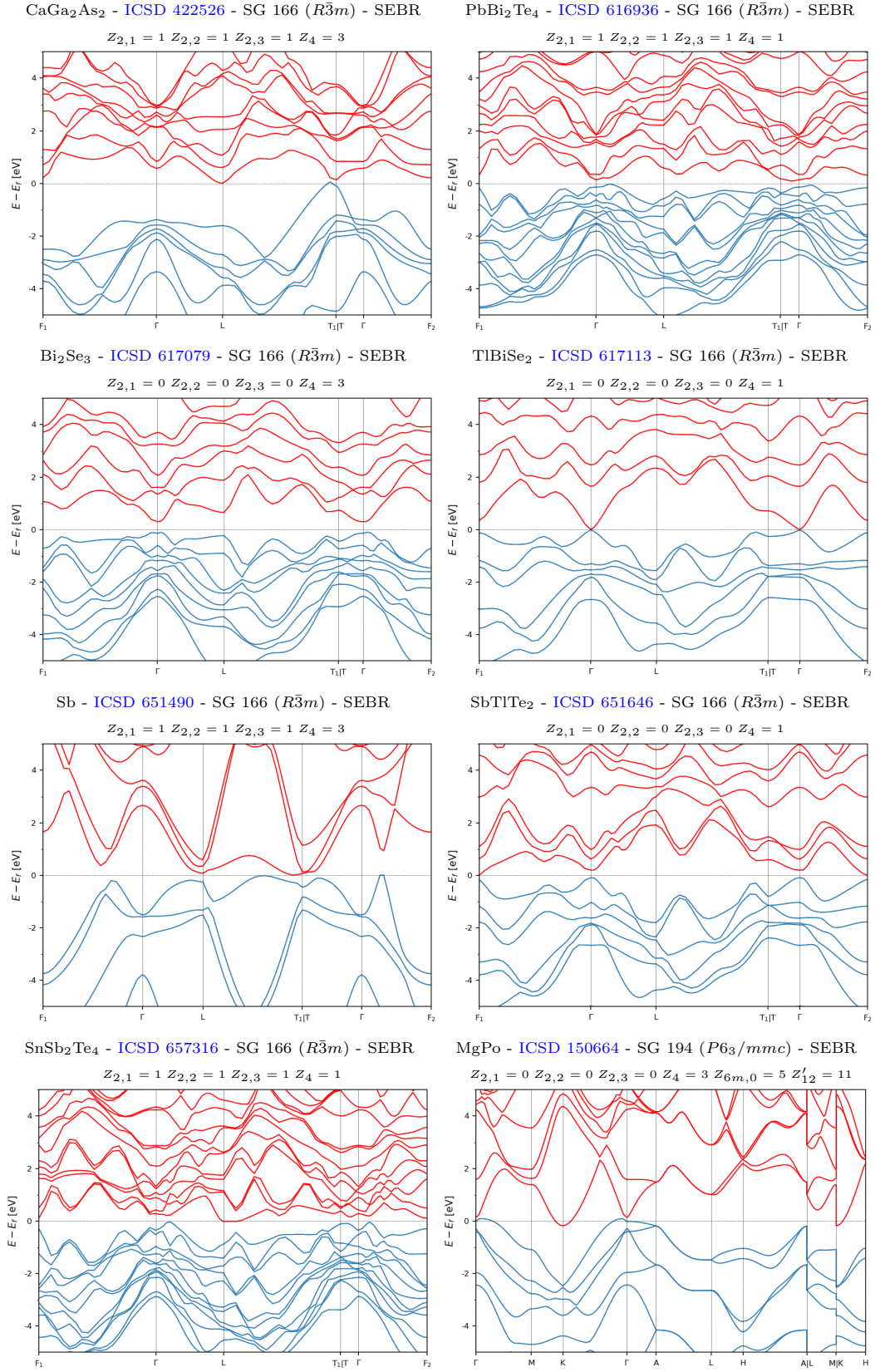


Figure S15. The SEBR-classified 3D strong TIs with the largest band gaps or the fewest and smallest bulk Fermi pockets. (part 4/5)

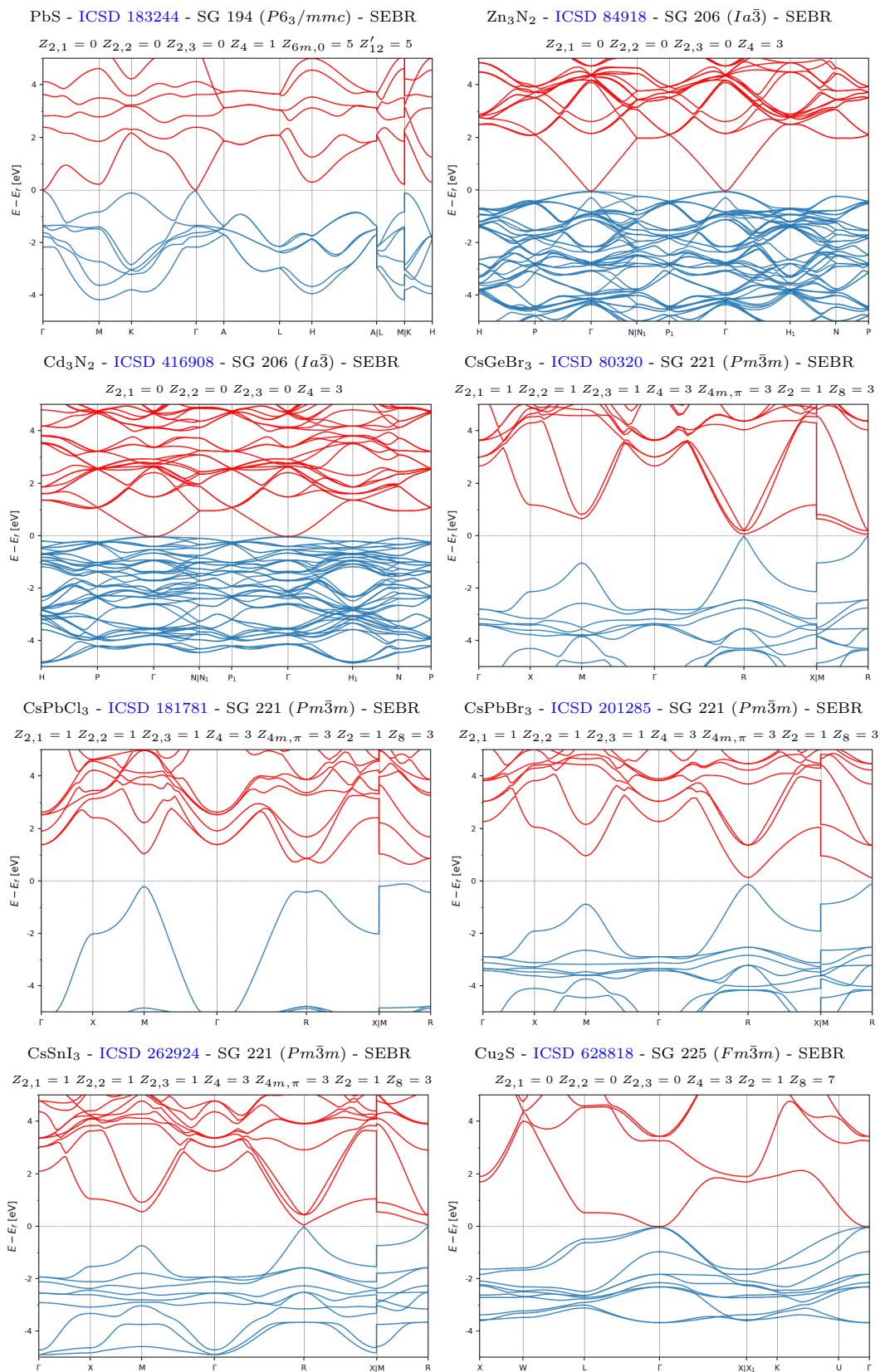


Figure S16. The SEBR-classified 3D strong TIs with the largest band gaps or the fewest and smallest bulk Fermi pockets. (part 5/5)

2. S_4 -Rotoinversion-Indicated Strong TIs and Weyl Semimetals

In this section, we list the noncentrosymmetric stable topological materials with fourfold rotoinversion $S_4 = C_4 \times \mathcal{I}$ symmetry and with the largest gaps or the fewest Fermi pockets along all high-symmetry BZ lines. As shown in Ref. 16, these materials can either be strong 3D TIs or Weyl semimetals, and can only be further distinguished by performing an additional calculation beyond symmetry-based indicators [111]. In terms of the indices introduced in Ref. 16, the materials listed in this section exhibit $Z_2 = 1$ (which is not to be confused with the Fu-Kane parity criterion [5, 30], see SM 11 A 1 for further details), and do not have a well-defined Z_4 index, because they are noncentrosymmetric. First, in Fig. S17, we list the S_4 TIs and Weyl semimetals classified as NLC, and then, in Fig. S18, we list the S_4 TIs and Weyl semimetals classified as SEBR. Among the stoichiometric materials in the ICSD, we find that there are relatively few examples of noncentrosymmetric S_4 -symmetry-indicated TIs and Weyl semimetals that either have SGs in which the only stable SI is Z_2 , or which have trivial values for all stable SIs aside from Z_2 .

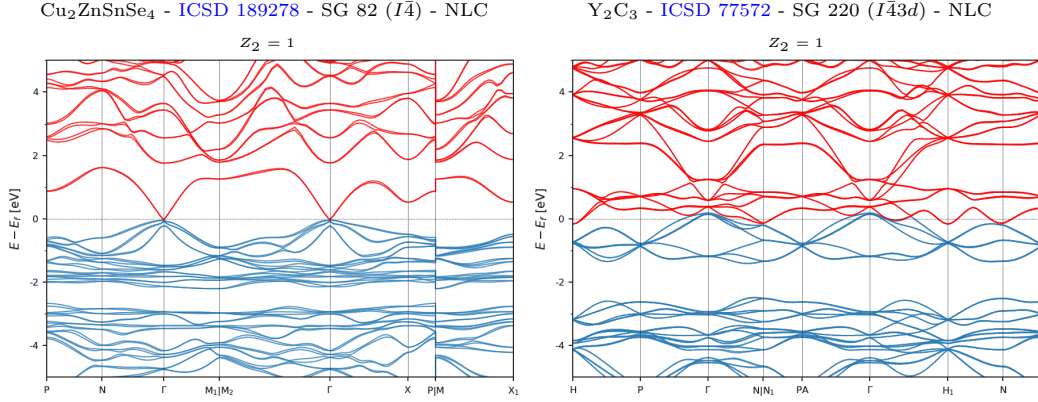


Figure S17. The NLC-classified, S_4 -rotoinversion-indicated, noncentrosymmetric 3D strong TIs and Weyl semimetals with the largest band gaps along high-symmetry lines or the fewest and smallest bulk Fermi pockets.

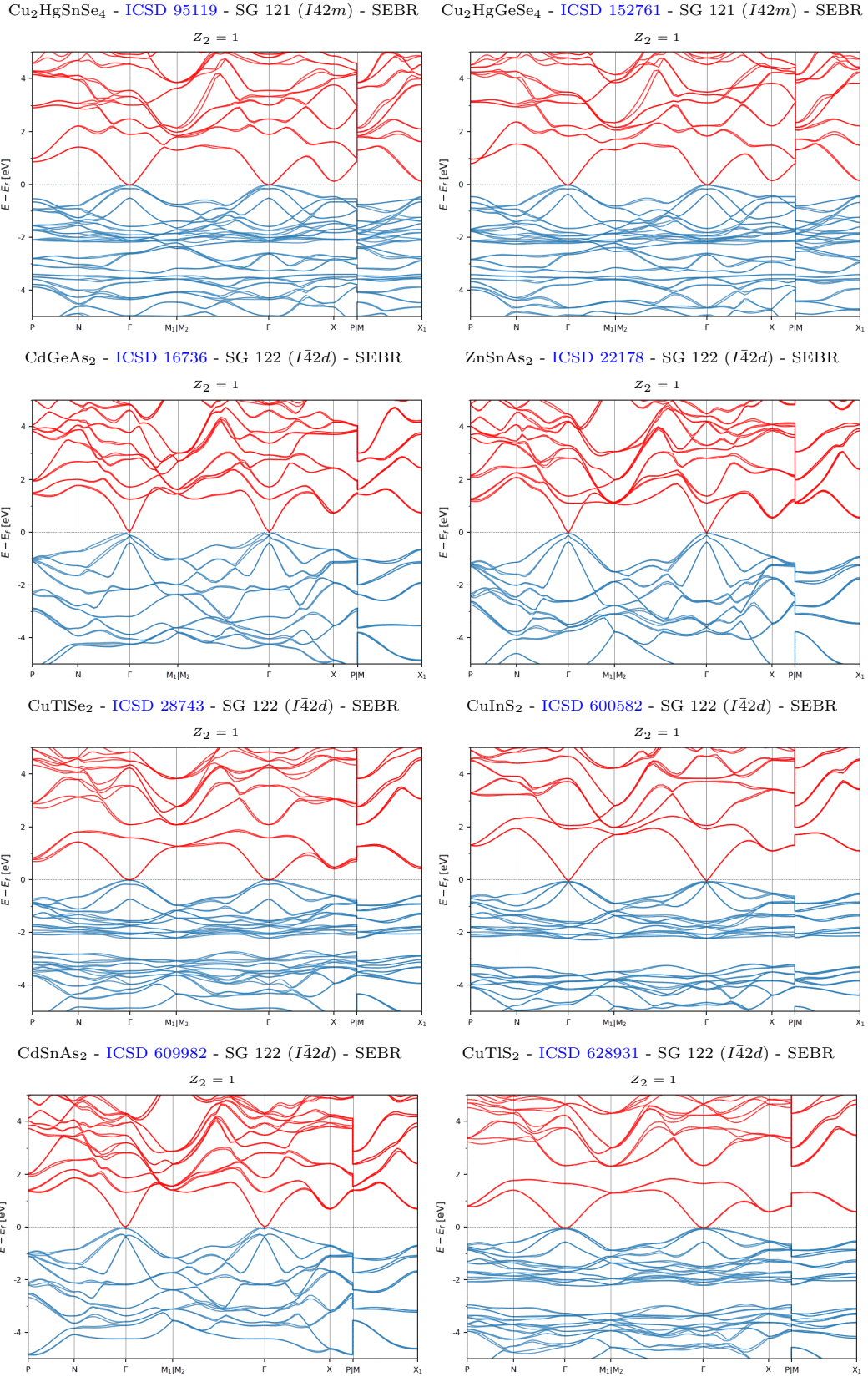


Figure S18. The SEBR-classified, S_4 -rotoinversion-indicated, noncentrosymmetric 3D strong TIs and Weyl semimetals with the largest band gaps along high-symmetry lines or the fewest and smallest bulk Fermi pockets.

3. Inversion-Symmetry-Protected HOTIs

In this section, we list the inversion-symmetry-indicated HOTIs with the largest bulk gaps or the fewest and smallest bulk Fermi pockets. In ideal models of inversion-symmetry-indicated HOTIs, when symmetries other than \mathcal{I} and \mathcal{T} are relaxed, finite samples exhibit gapped 2D surfaces and gapless 1D hinges with anomalous helical modes [16, 17, 22, 33, 34, 104]. In the presence of additional symmetries, such as mirror reflection and twofold rotation (C_2), inversion-symmetry-indicated HOTIs may also exhibit $2+4n$ twofold Dirac cones on specific, high-symmetry surfaces [14, 16, 17, 104]. In terms of the indices introduced in Ref. [16], the materials listed in this section are characterized by $Z_4 = 2$, and exhibit trivial values for all other independent stable SIs. First, in Figs. S19, S20, S21, S22, S23, and S24, we list the HOTIs classified as NLC, and then, in Figs. S25 and S26, we list the HOTIs classified as SEBR. The materials listed in this section include the recently identified HOTIs bismuth [ICSD 64705, SG 166 ($R\bar{3}m$)] [22, 177] and BiBr [ICSD 1560, SG 12 ($C2/m$)] [178–182], which are classified as SEBR, and MoTe₂ [ICSD 14349, SG 11 ($P2_1/m$)] [34, 179], which is classified as NLC. Bismuth, BiBr, and MoTe₂, as well as members of closely-related material families have been the subject of recent intense theoretical and experimental investigations seeking to distinguish \mathcal{I} - and \mathcal{T} -symmetric HOTIs from weak TIs and other TI and TCI phases [29, 183–188]. Notably, \mathcal{I} - and \mathcal{T} -symmetric HOTIs exhibit trivial axion angles $\theta \bmod 2\pi = 0$, and it remains an open and urgent question whether there exist quantized electromagnetic response effects beyond the axionic magnetoelectric effect that can distinguish \mathcal{I} - and \mathcal{T} -symmetric HOTI phases from other TCIs and from trivial insulators [29, 101, 148].

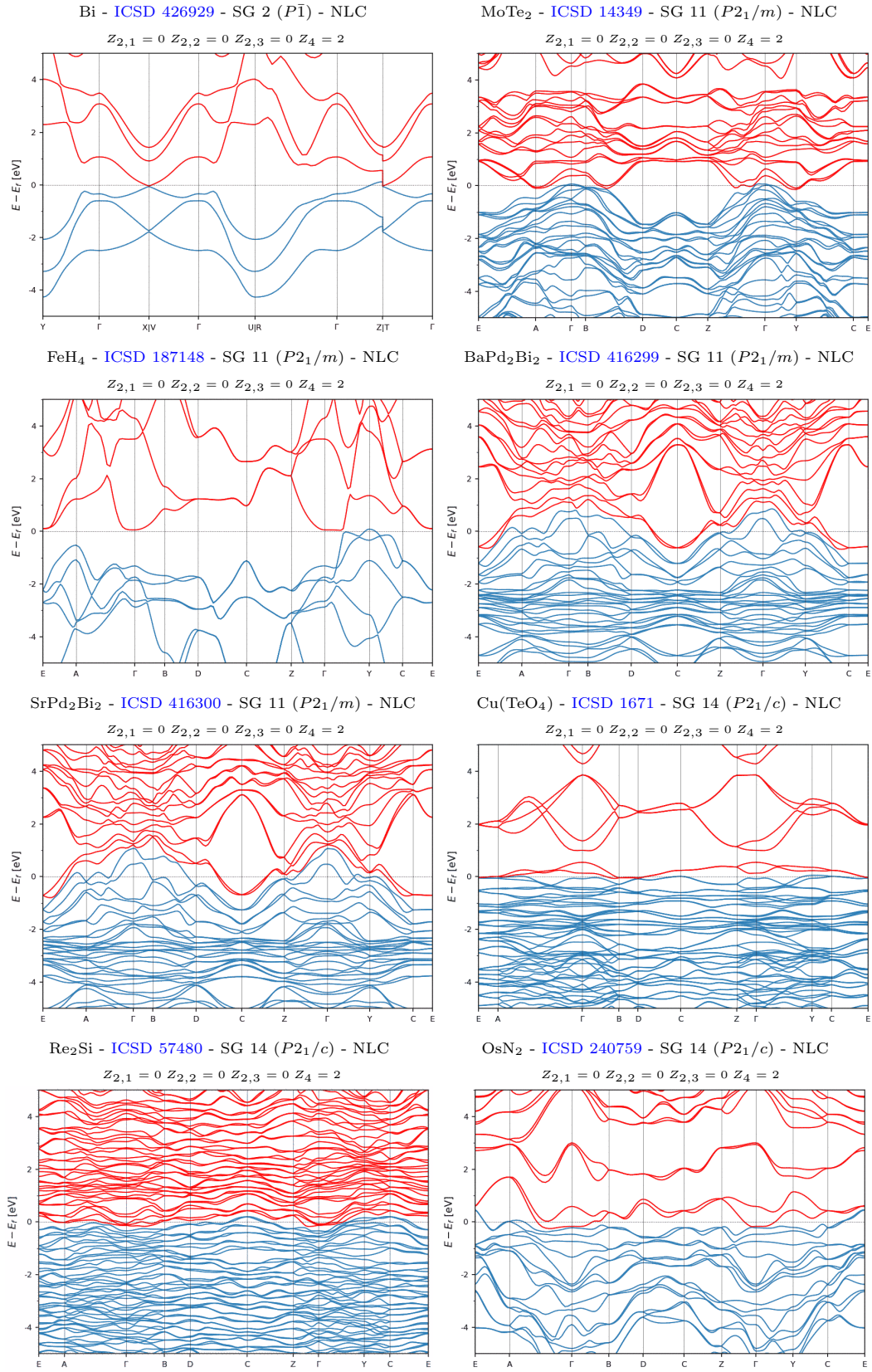


Figure S19. The NLC-classified, inversion-symmetry-indicated HOTIs with the largest band gaps or the fewest and smallest bulk Fermi pockets. (part 1/6)

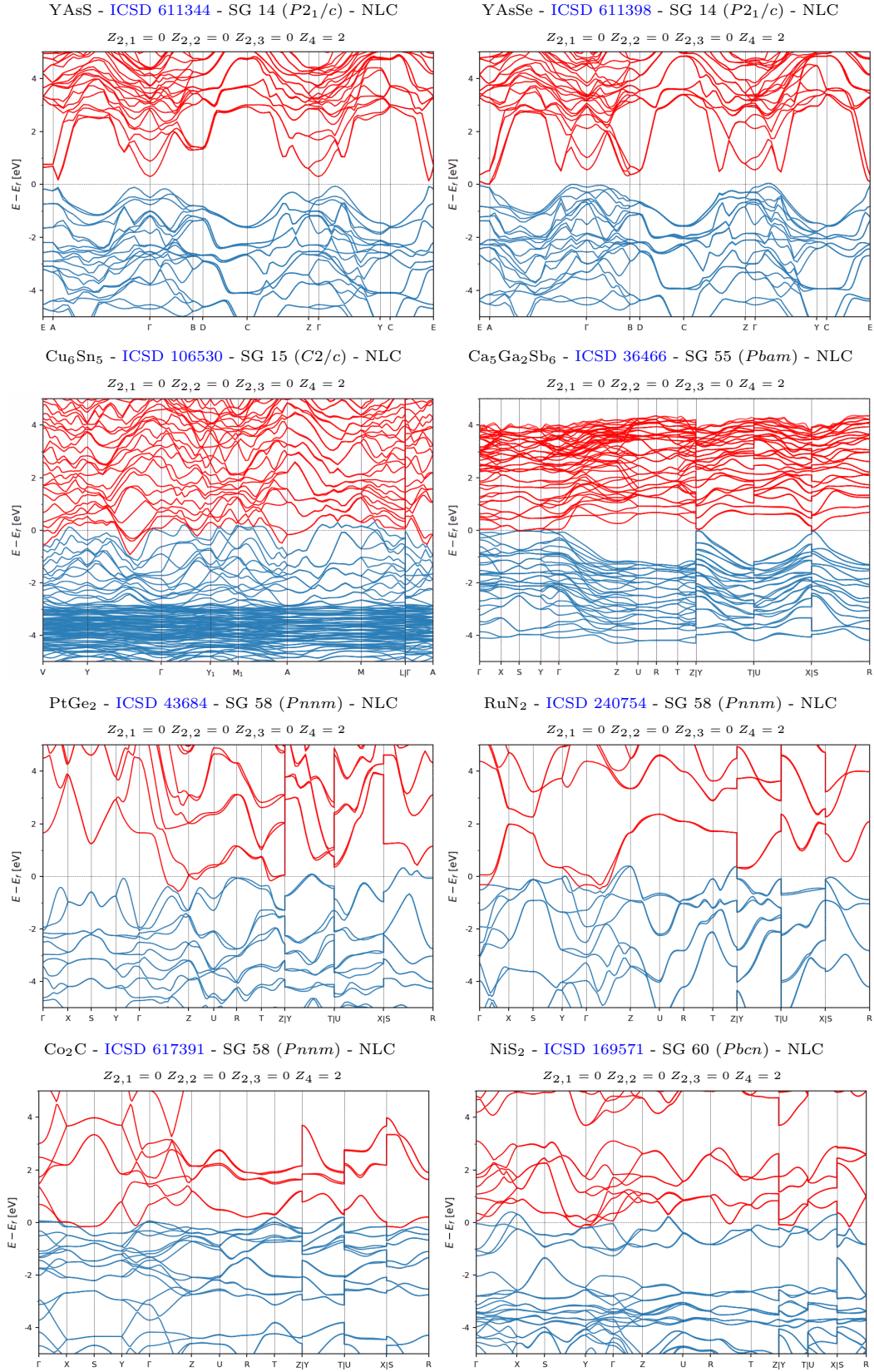


Figure S20. The NLC-classified, inversion-symmetry-indicated HOTIs with the largest band gaps or the fewest and smallest bulk Fermi pockets. (part 2/6)

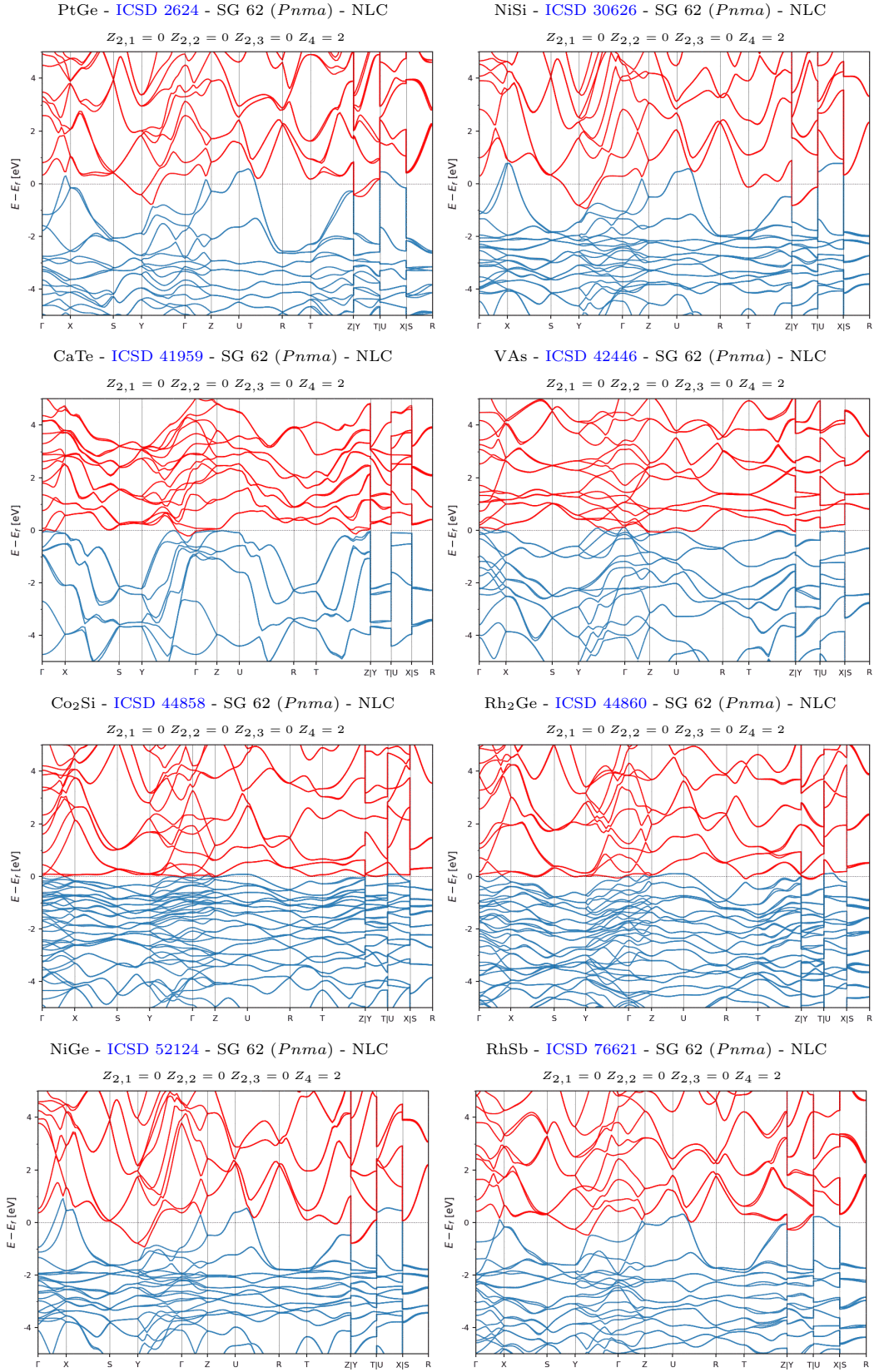


Figure S21. The NLC-classified, inversion-symmetry-indicated HOTIs with the largest band gaps or the fewest and smallest bulk Fermi pockets. (part 3/6)

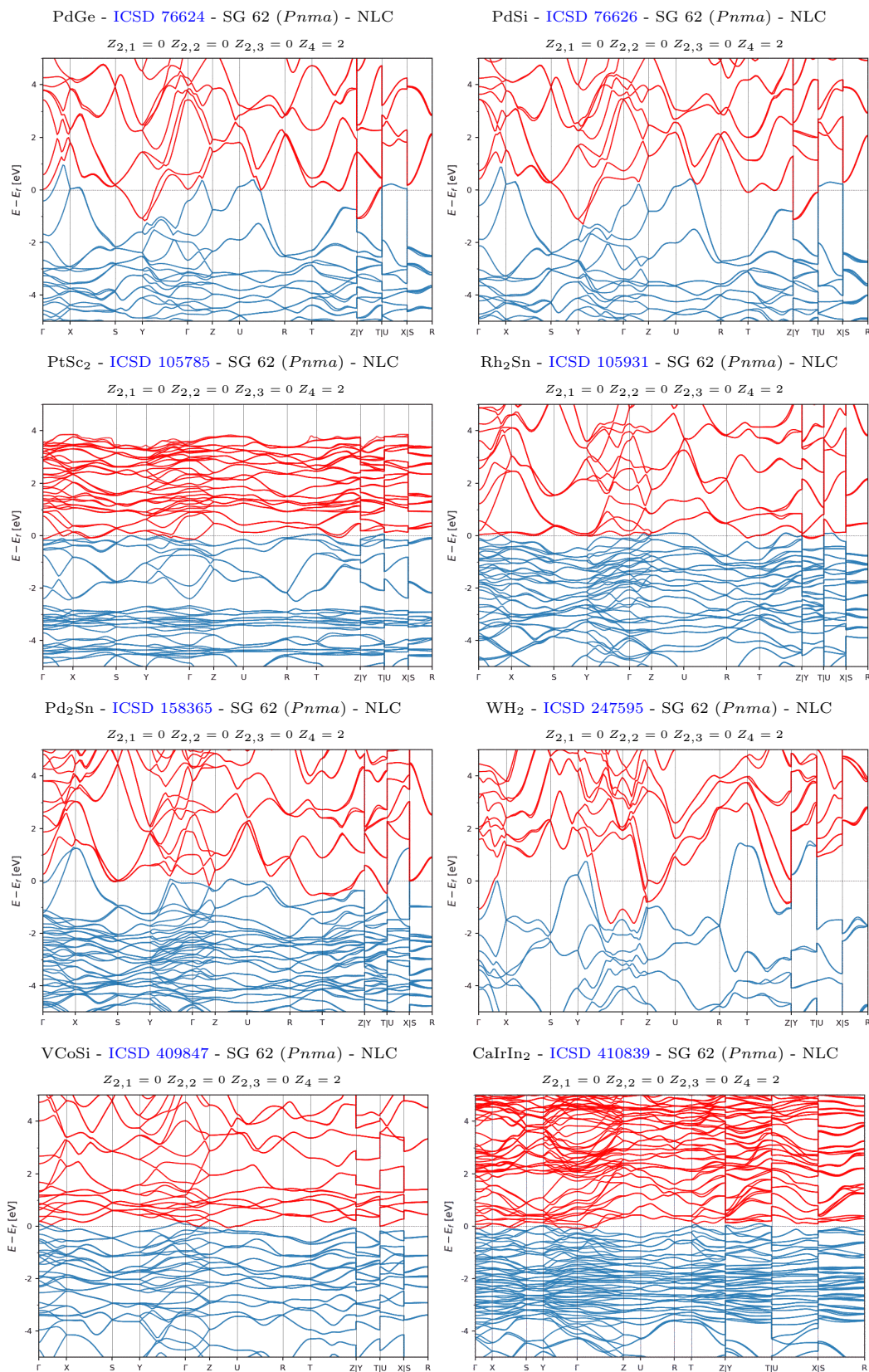


Figure S22. The NLC-classified, inversion-symmetry-indicated HOTIs with the largest band gaps or the fewest and smallest bulk Fermi pockets. (part 4/6)

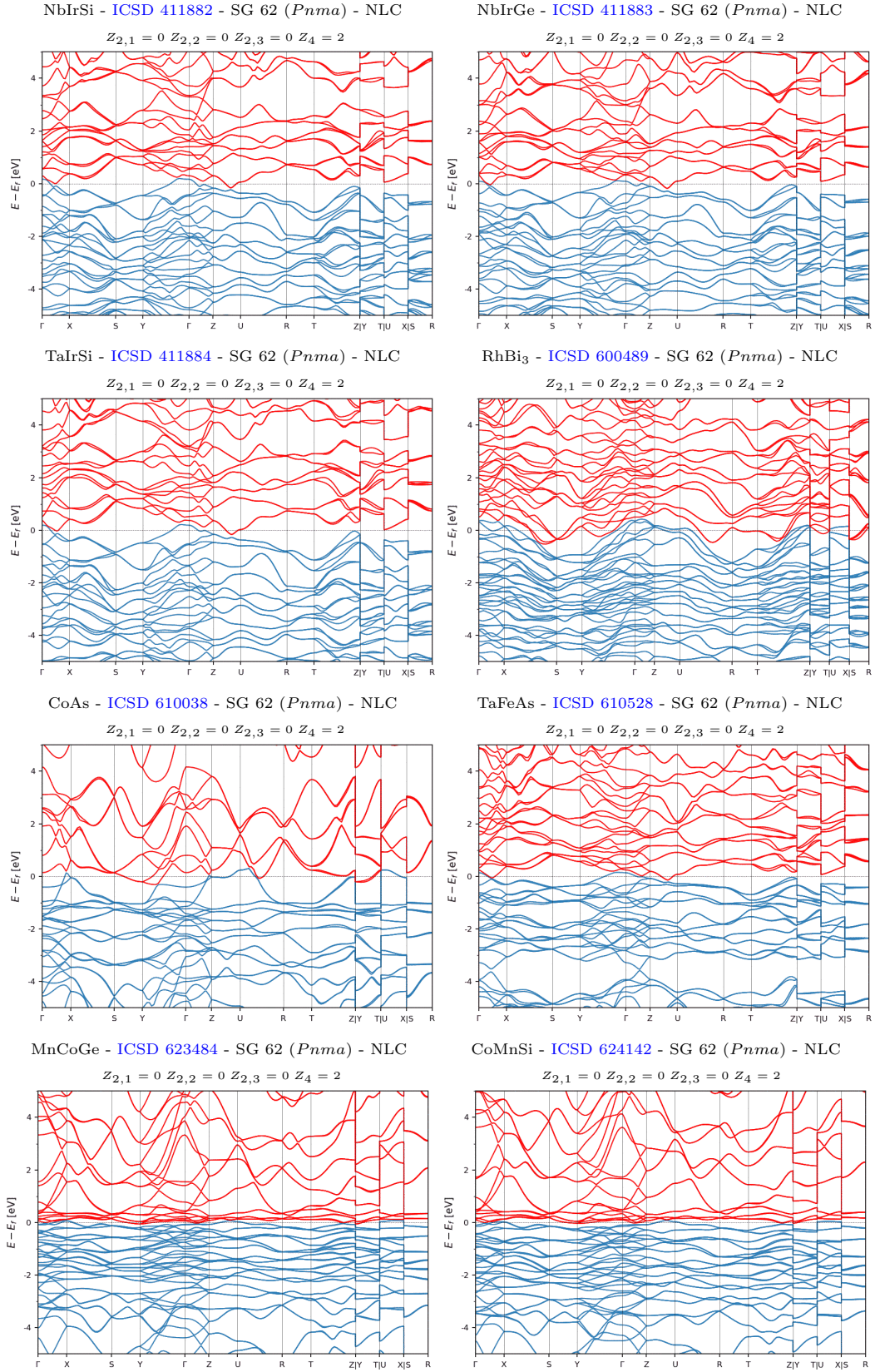


Figure S23. The NLC-classified, inversion-symmetry-indicated HOTIs with the largest band gaps or the fewest and smallest bulk Fermi pockets. (part 5/6)

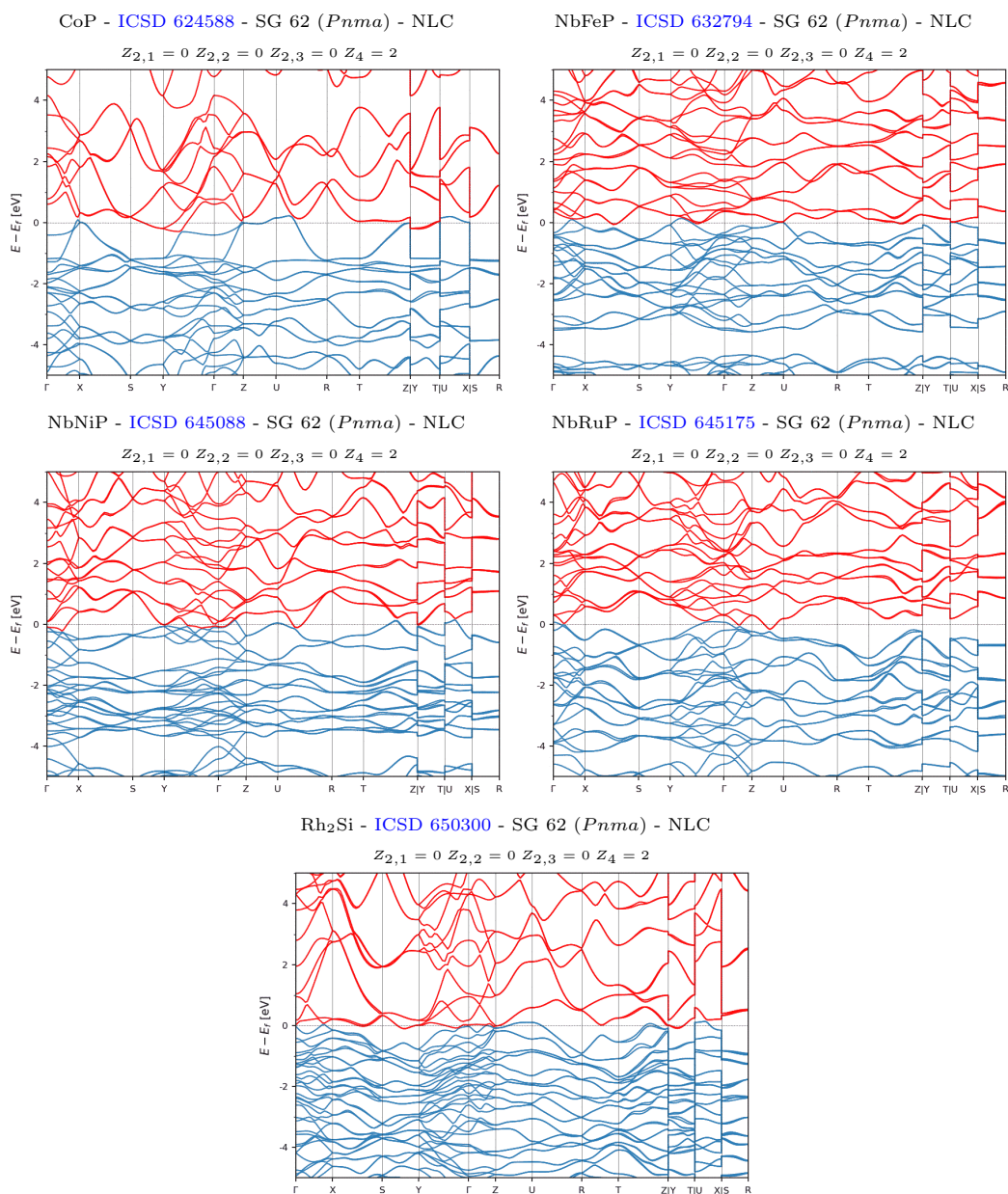


Figure S24. The NLC-classified, inversion-symmetry-indicated HOTIs with the largest band gaps or the fewest and smallest bulk Fermi pockets. (part 6/6)

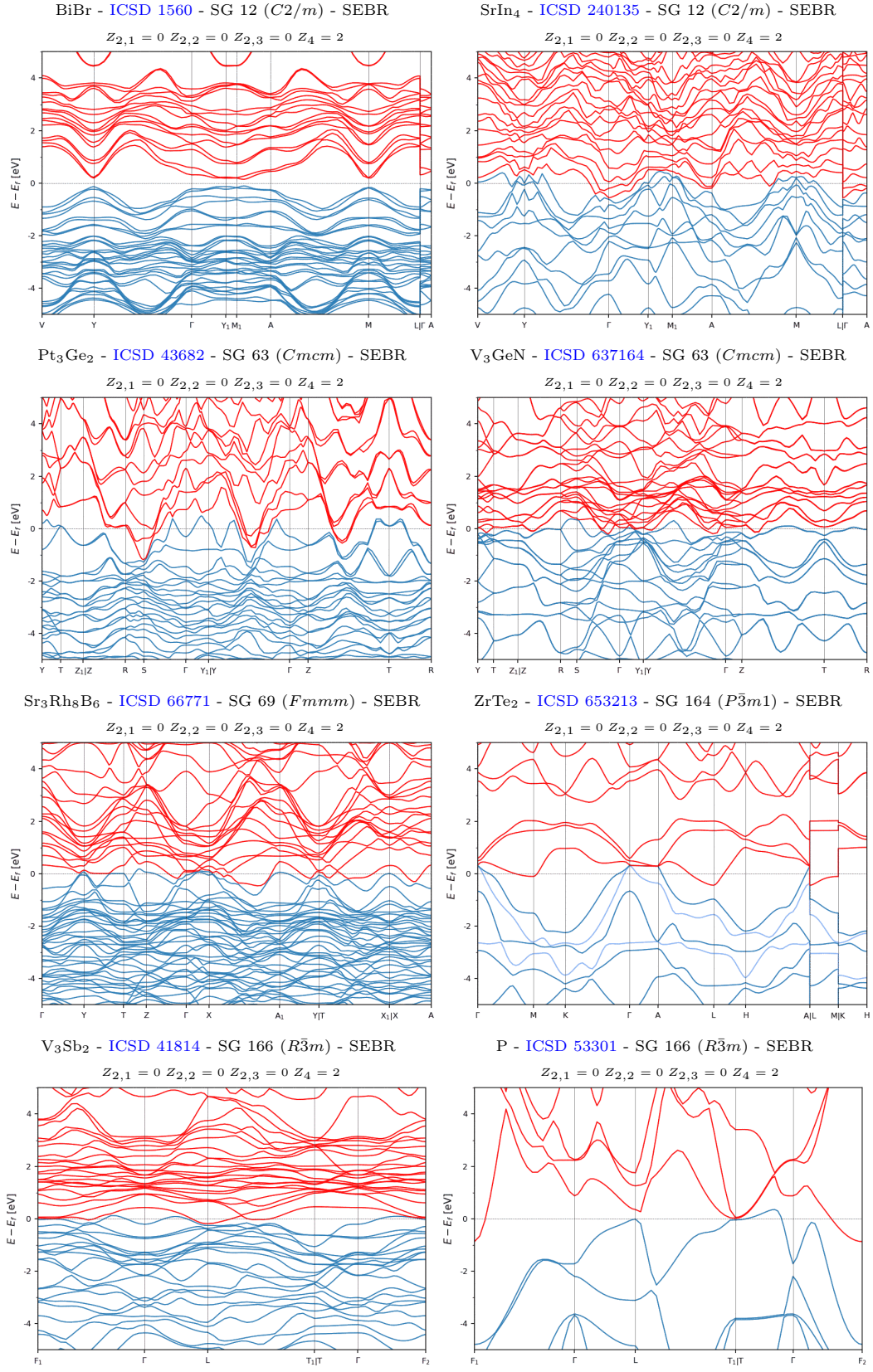


Figure S25. The SEBR-classified, inversion-symmetry-indicated HOTIs with the largest band gaps or the fewest and smallest bulk Fermi pockets. (part 1/2)

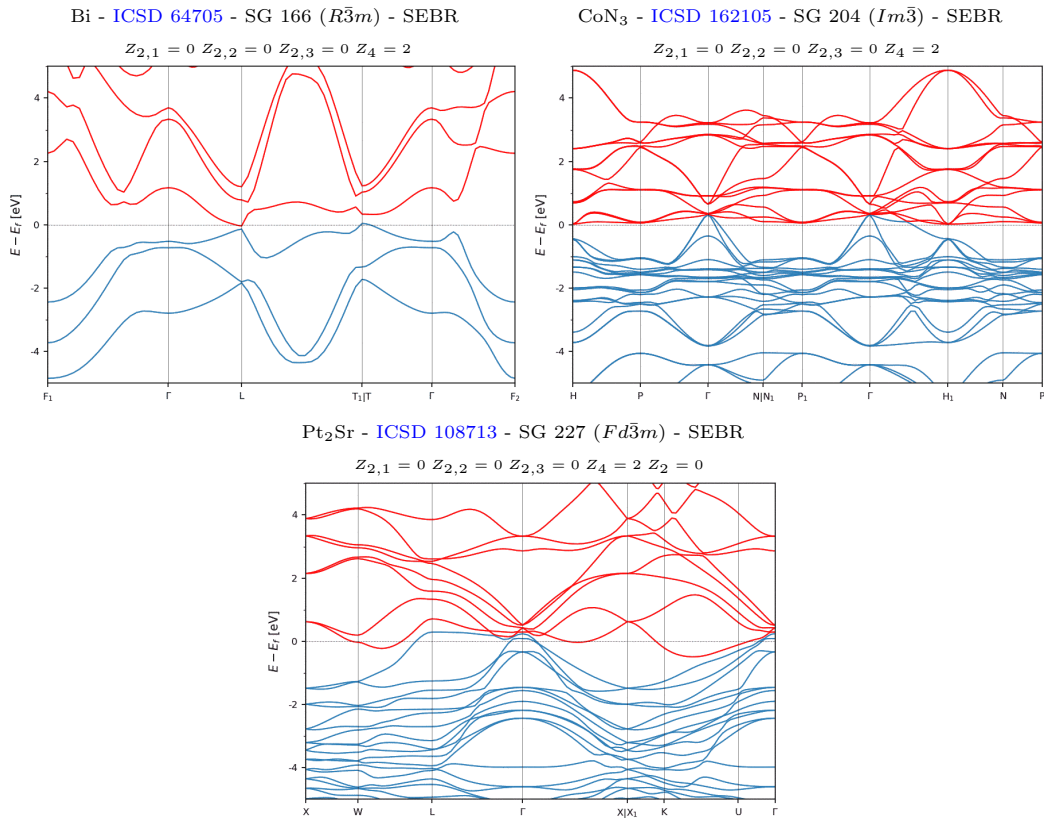


Figure S26. The SEBR-classified, inversion-symmetry-indicated HOTIs with the largest band gaps or the fewest and smallest bulk Fermi pockets. (part 2/2)

4. Inversion-Symmetry-Indicated Weak TIs and TCIs

In this section, we list the inversion-symmetry-indicated weak TIs and TCIs with the largest bulk gaps or the fewest and smallest bulk Fermi pockets. Like the HOTIs previously listed in [SM 11 A 3](#), the weak TIs and TCIs listed in this section have 2D surfaces with even numbers of massless or massive twofold Dirac cones, depending on the Miller indices of the surfaces [[5](#), [30](#), [146](#), [147](#)]. In terms of the indices introduced in [Ref. 16](#), the materials in this section are characterized by $Z_4 = 2$, and exhibit nontrivial values for some or all other independent stable SIs. First, in [Figs. S27](#) and [S28](#), we list the weak TIs and TCIs classified as NLC, and then, in [Figs. S29, S30, S31, S32, S33, S34, S35, S36, S37, S38, S39, S40, S41, and S42](#), we list the weak TIs and TCIs classified as SEBR. The materials listed in this section include the experimentally confirmed weak TI BiI [[ICSD 1559](#), SG 12 ($C2/m$)] [[178](#), [181](#), [182](#), [189](#)], which is classified as SEBR.

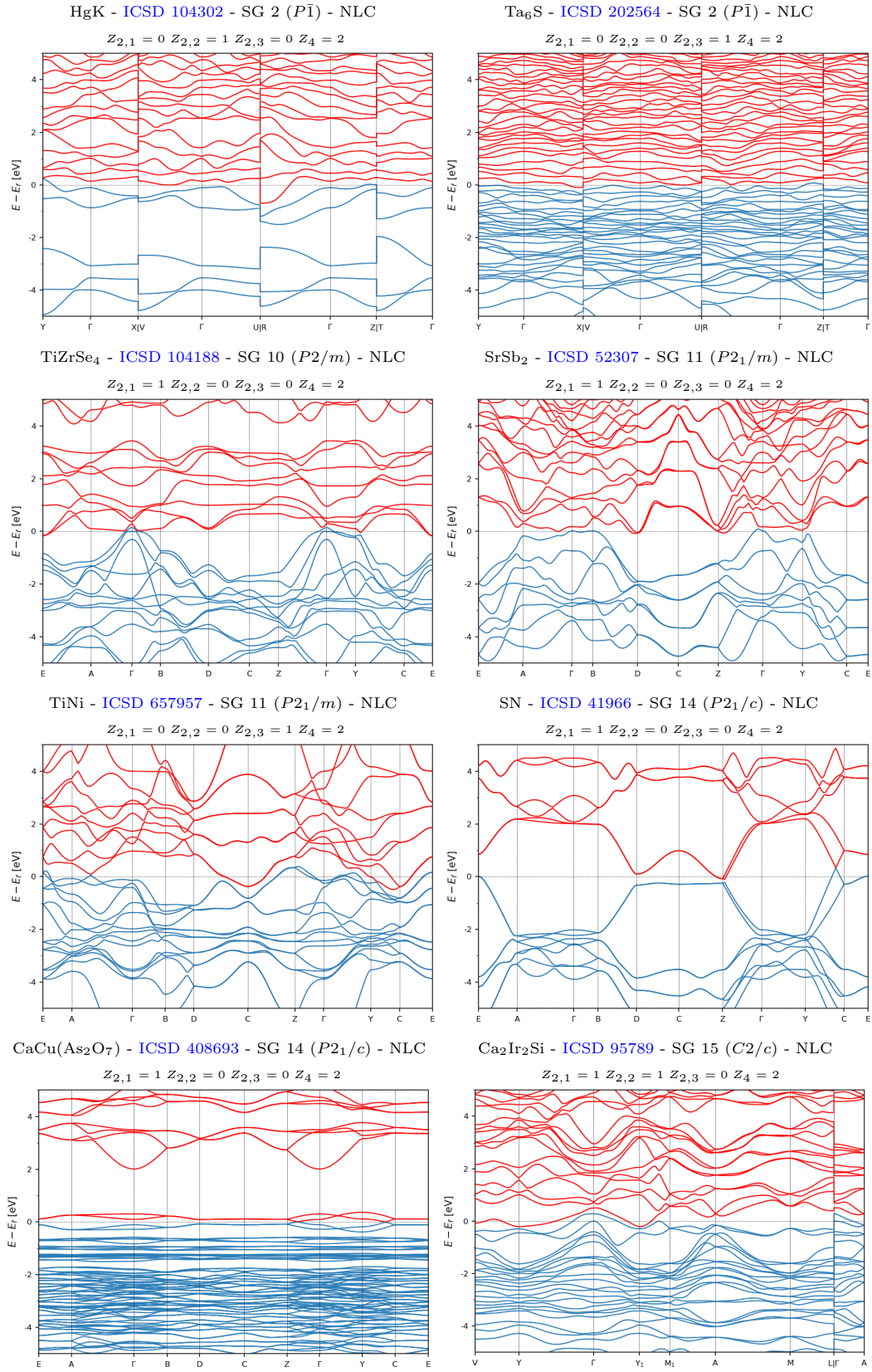


Figure S27. The NLC-classified, inversion-symmetry-indicated weak TIs and TCIs with the largest band gaps or the fewest and smallest bulk Fermi pockets. (part 1/2)

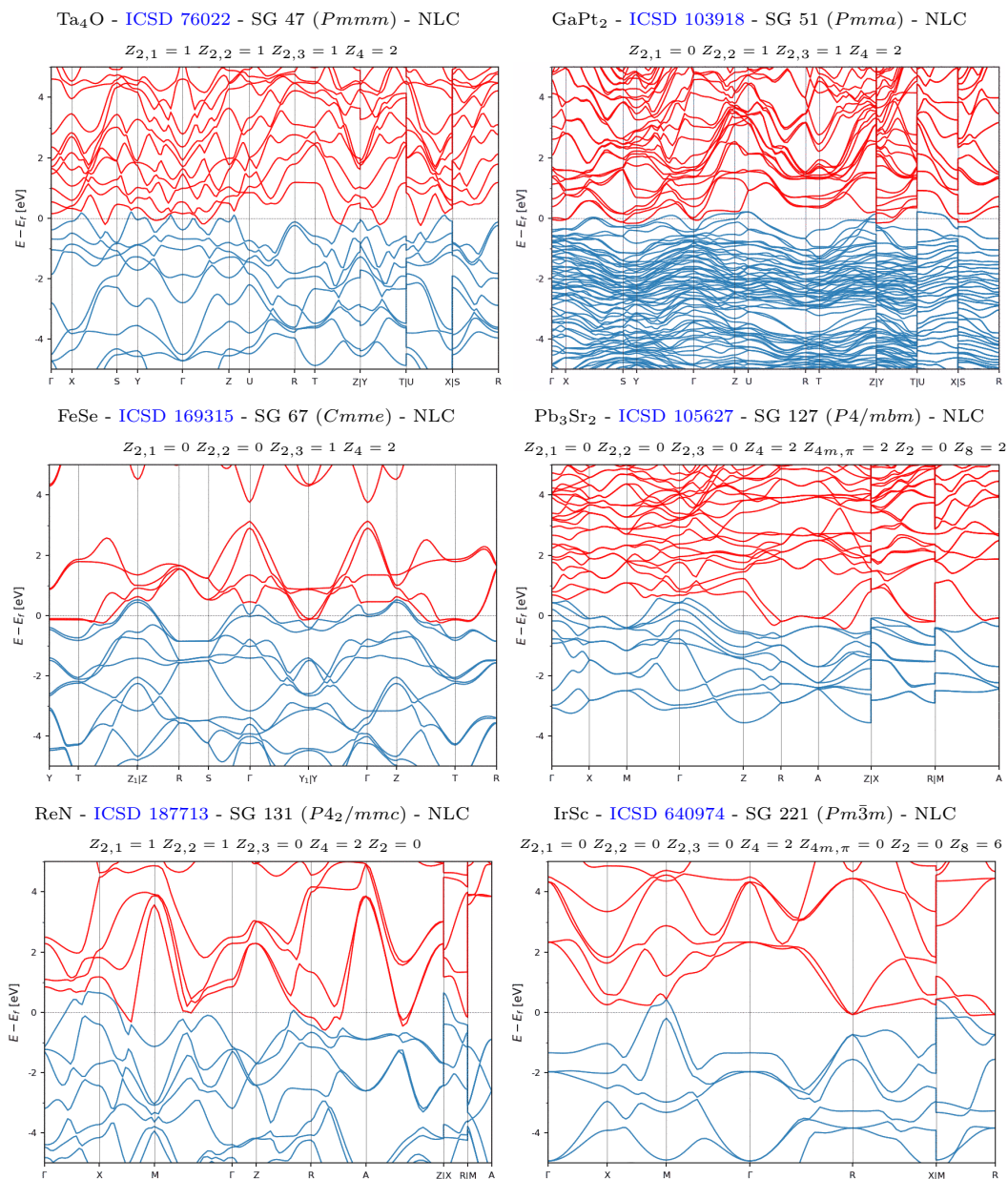


Figure S28. The NLC-classified, inversion-symmetry-indicated weak TIs and TCIs with the largest band gaps or the fewest and smallest bulk Fermi pockets. (part 2/2)

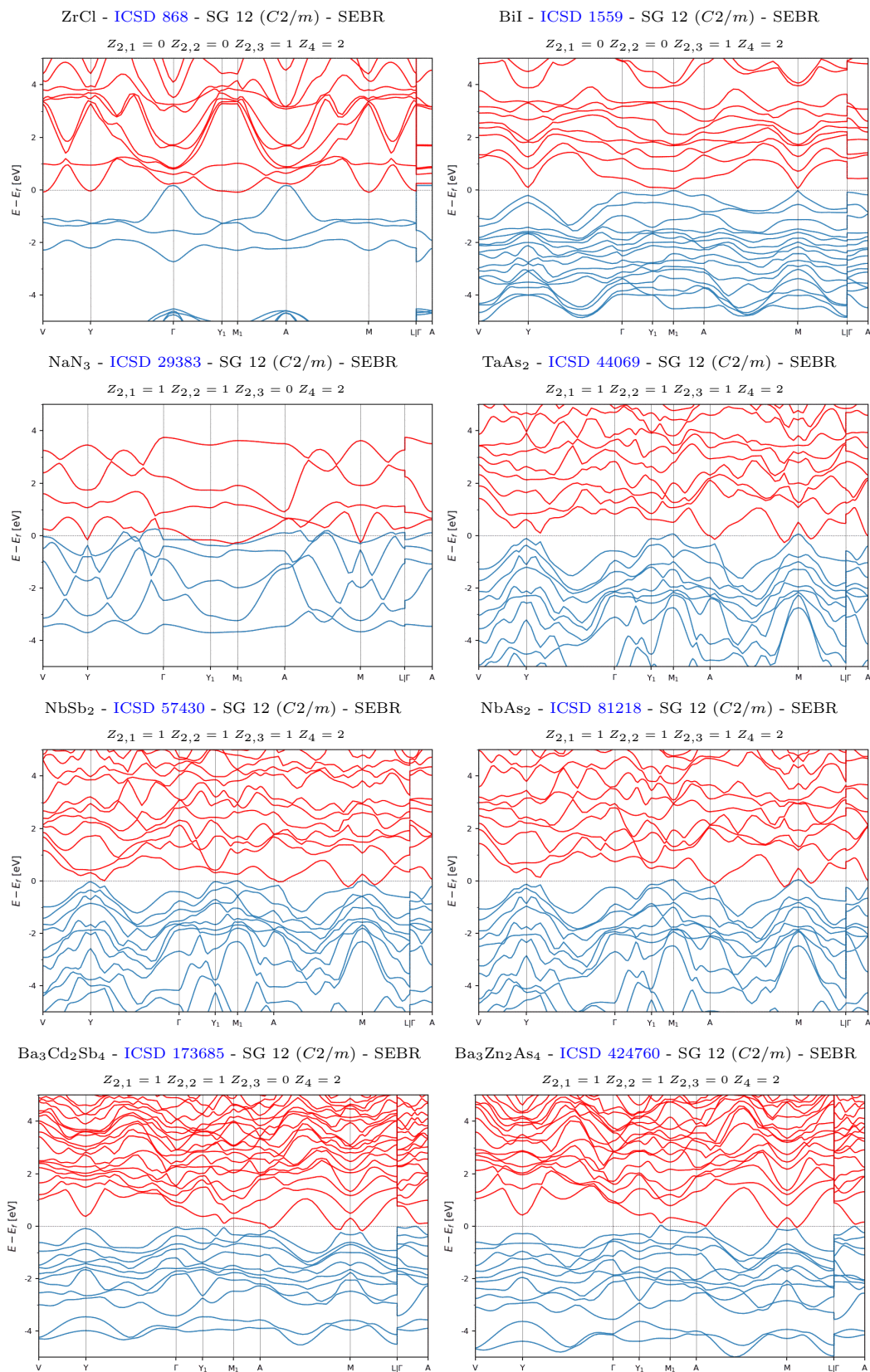


Figure S29. The SEBR-classified, inversion-symmetry-indicated weak TIs and TCIs with the largest band gaps or the fewest and smallest bulk Fermi pockets. (part 1/14)

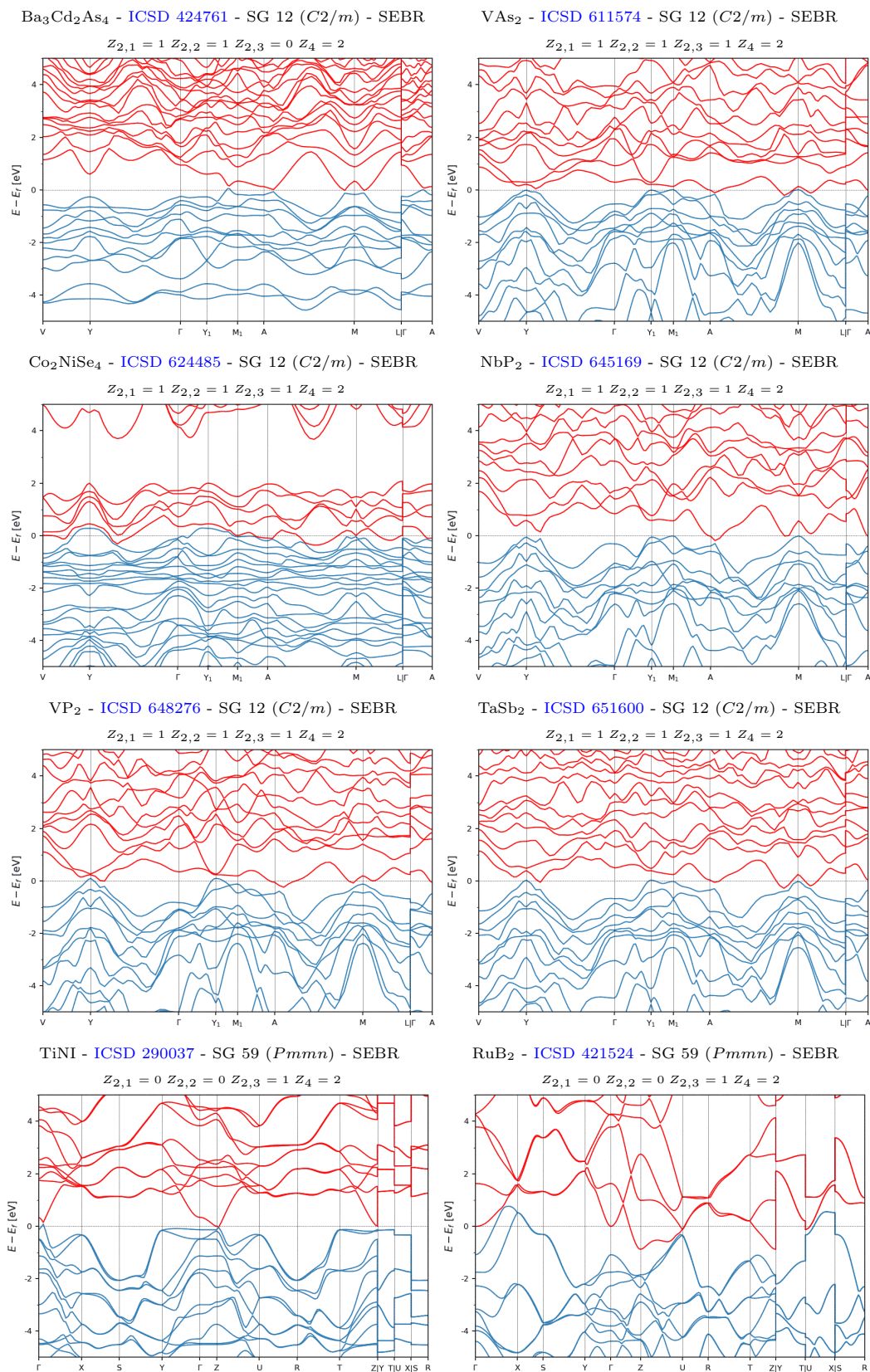


Figure S30. The SEBR-classified, inversion-symmetry-indicated weak TIs and TCIs with the largest band gaps or the fewest and smallest bulk Fermi pockets. (part 2/14)

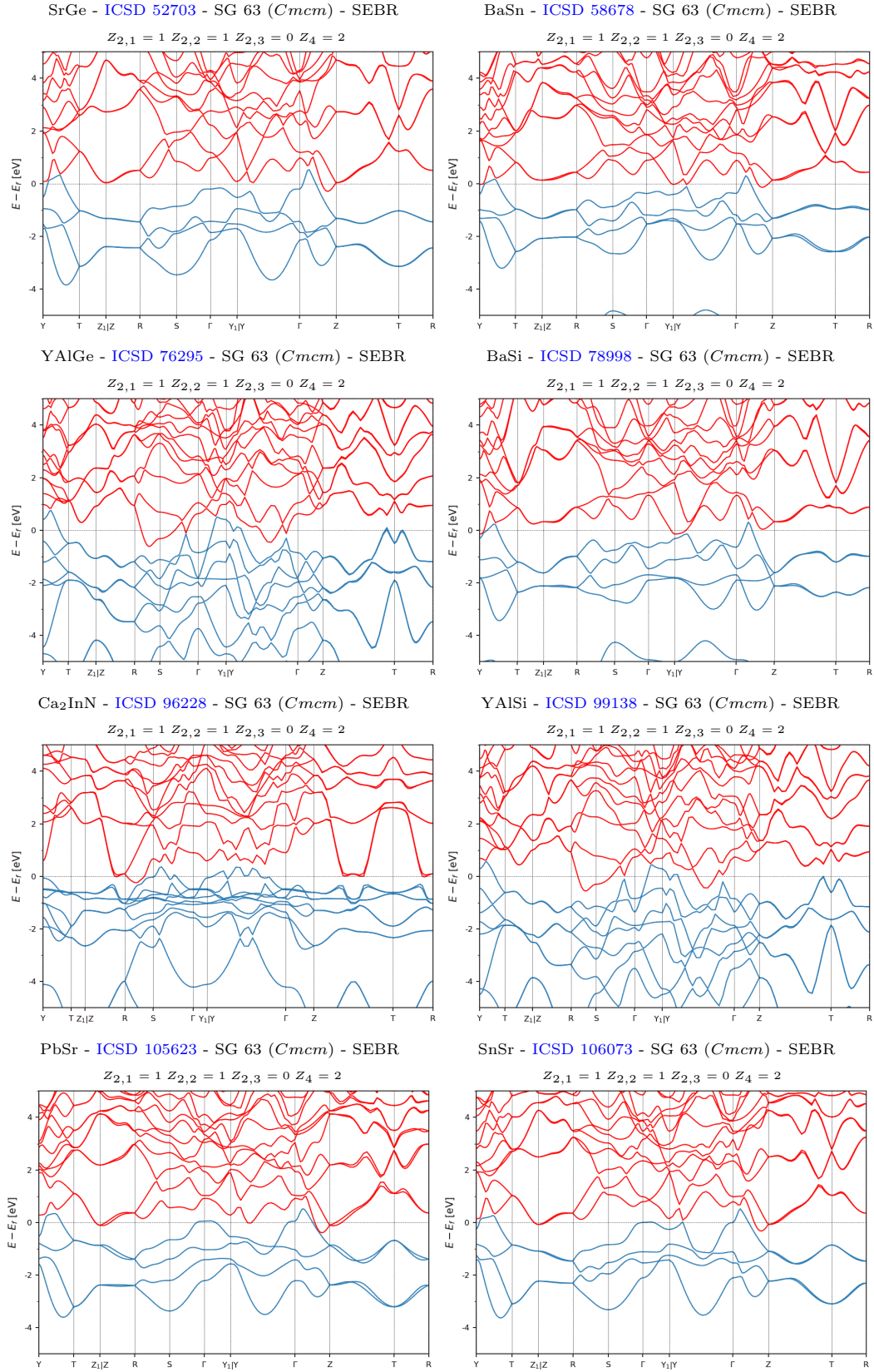


Figure S31. The SEBR-classified, inversion-symmetry-indicated weak TIs and TCIs with the largest band gaps or the fewest and smallest bulk Fermi pockets. (part 3/14)

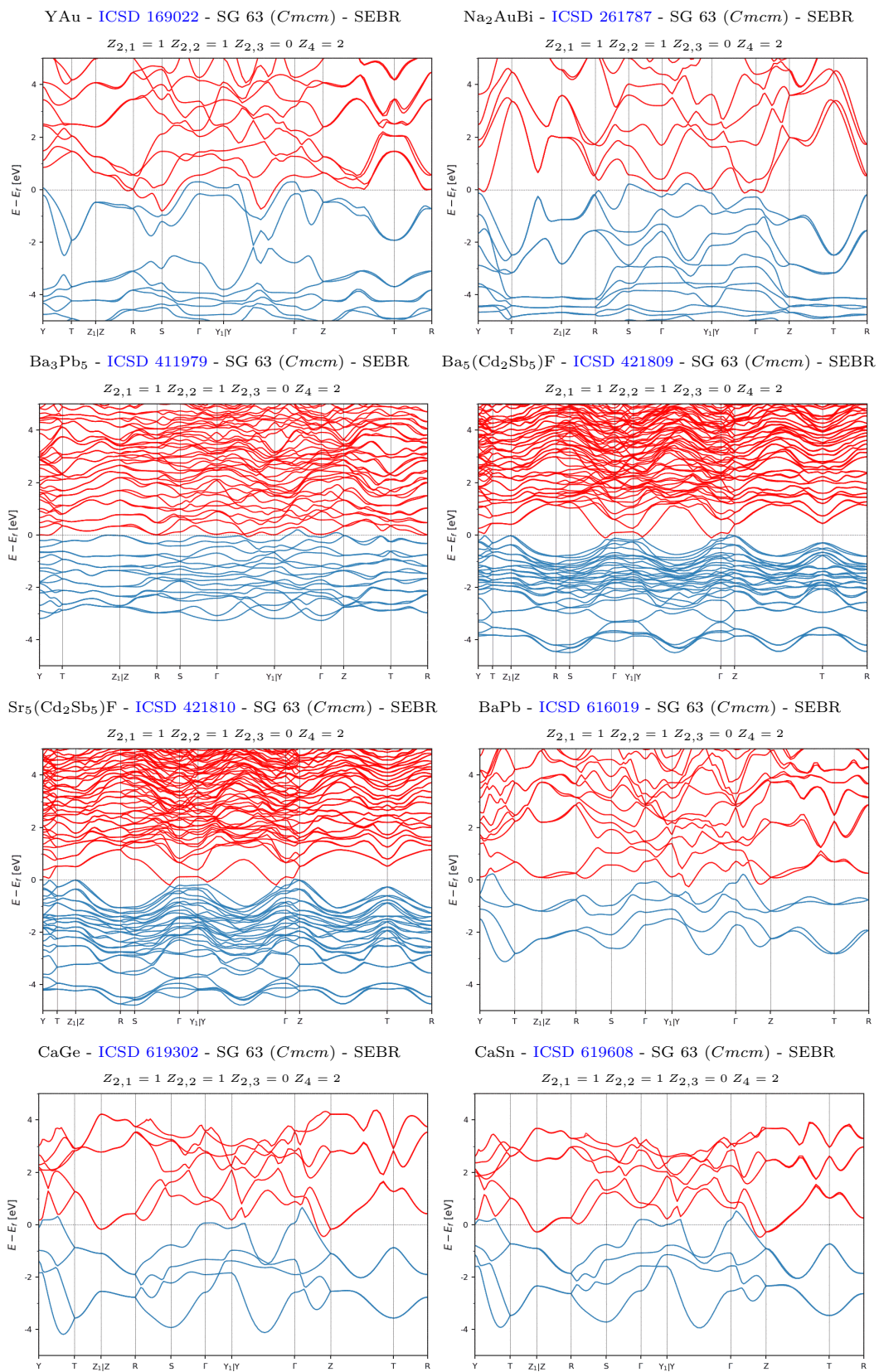


Figure S32. The SEBR-classified, inversion-symmetry-indicated weak TIs and TCIs with the largest band gaps or the fewest and smallest bulk Fermi pockets. (part 4/14)

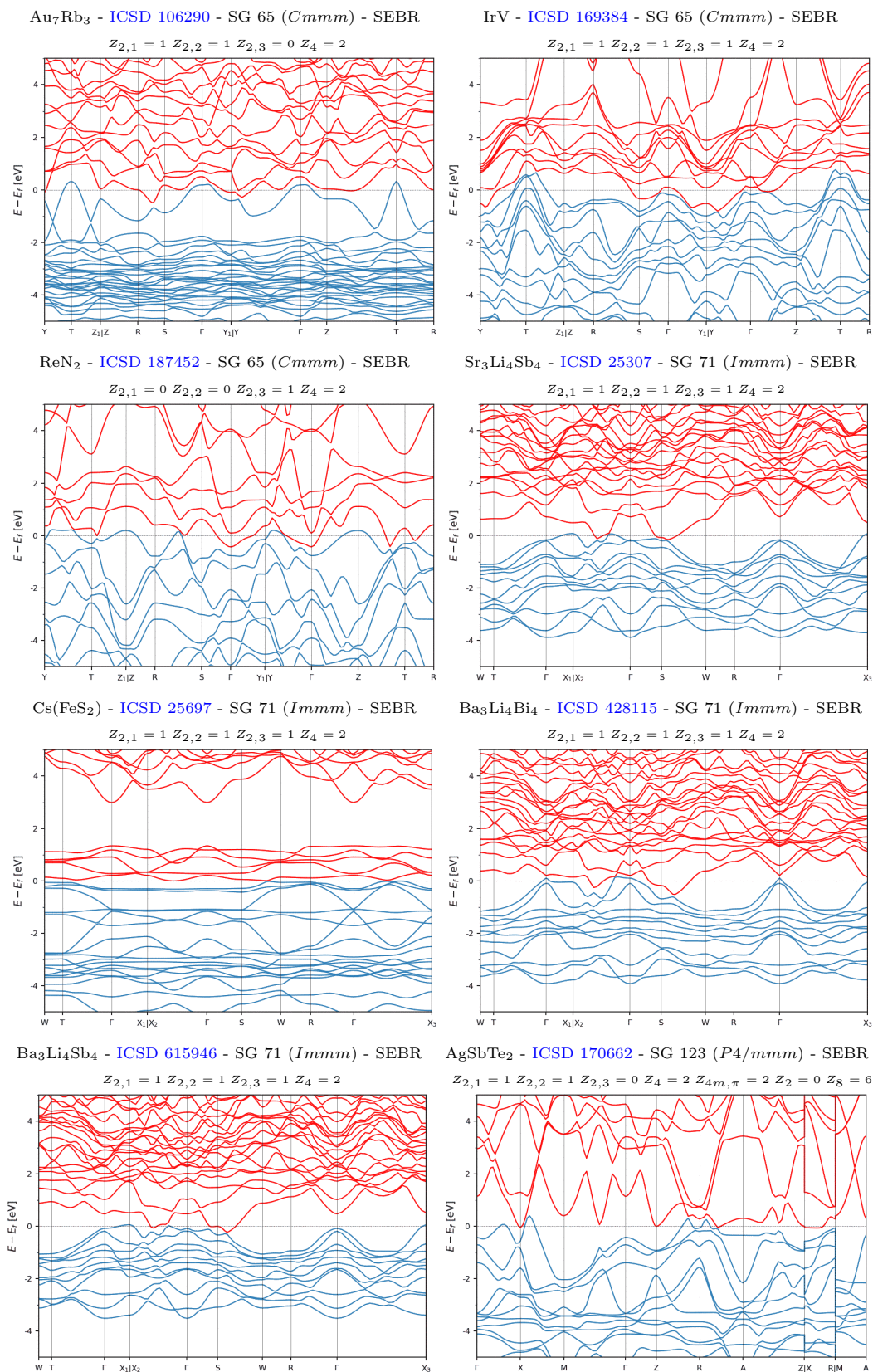


Figure S33. The SEBR-classified, inversion-symmetry-indicated weak TIs and TCIs with the largest band gaps or the fewest and smallest bulk Fermi pockets. (part 5/14)

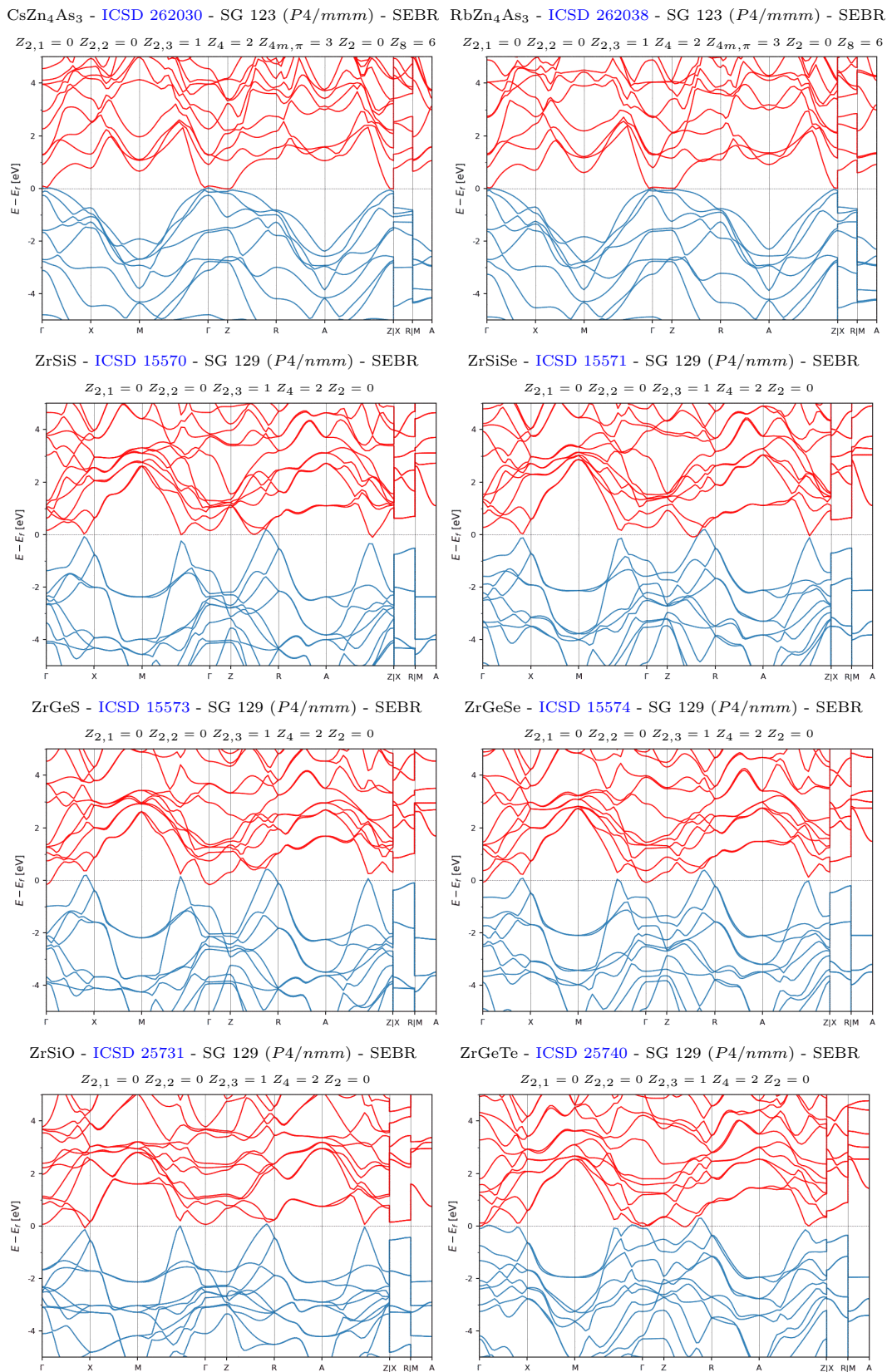


Figure S34. The SEBR-classified, inversion-symmetry-indicated weak TIs and TCIs with the largest band gaps or the fewest and smallest bulk Fermi pockets. (part 6/14)

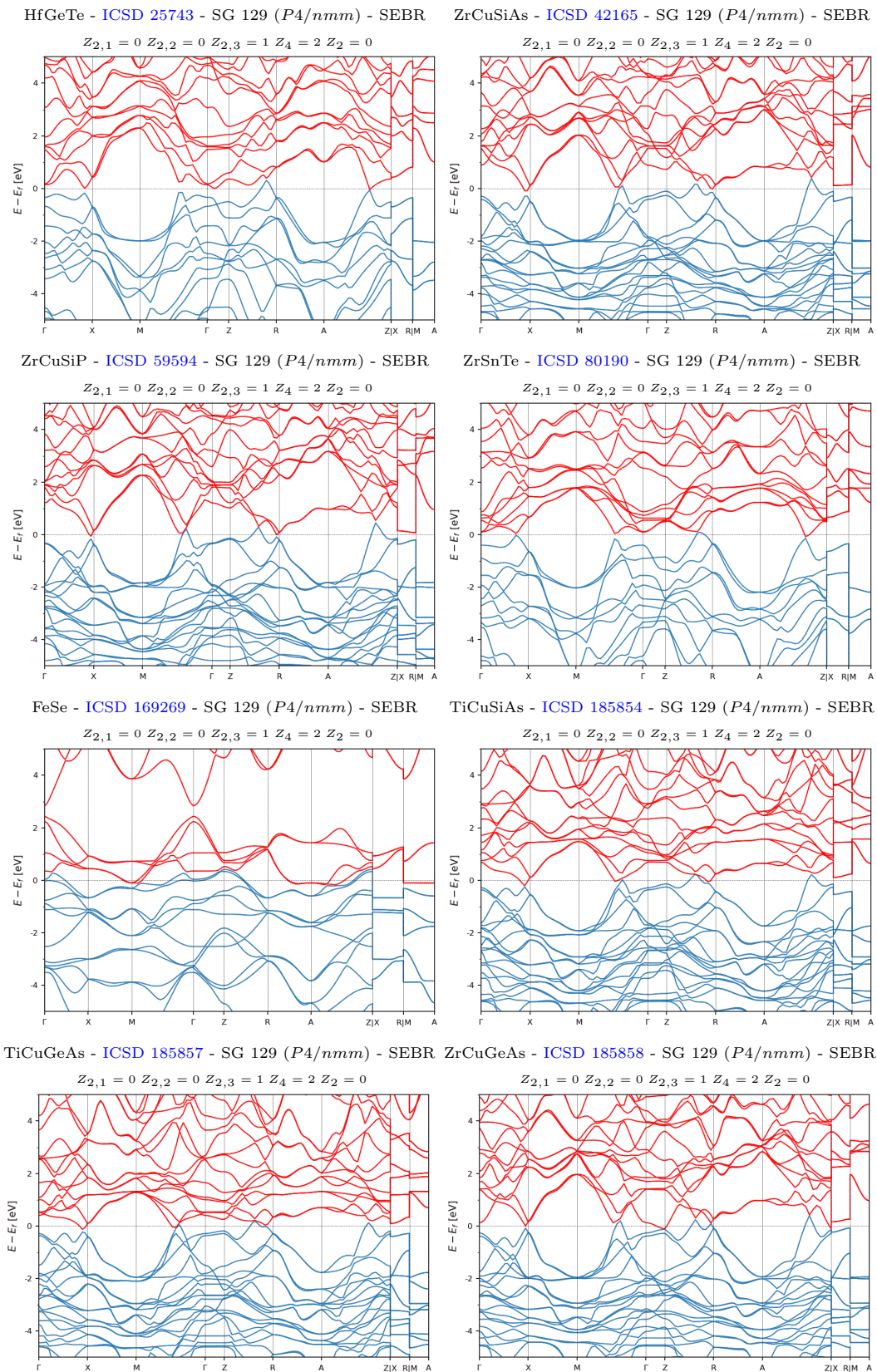


Figure S35. The SEBR-classified, inversion-symmetry-indicated weak TIs and TCIs with the largest band gaps or the fewest and smallest bulk Fermi pockets. (part 7/14)

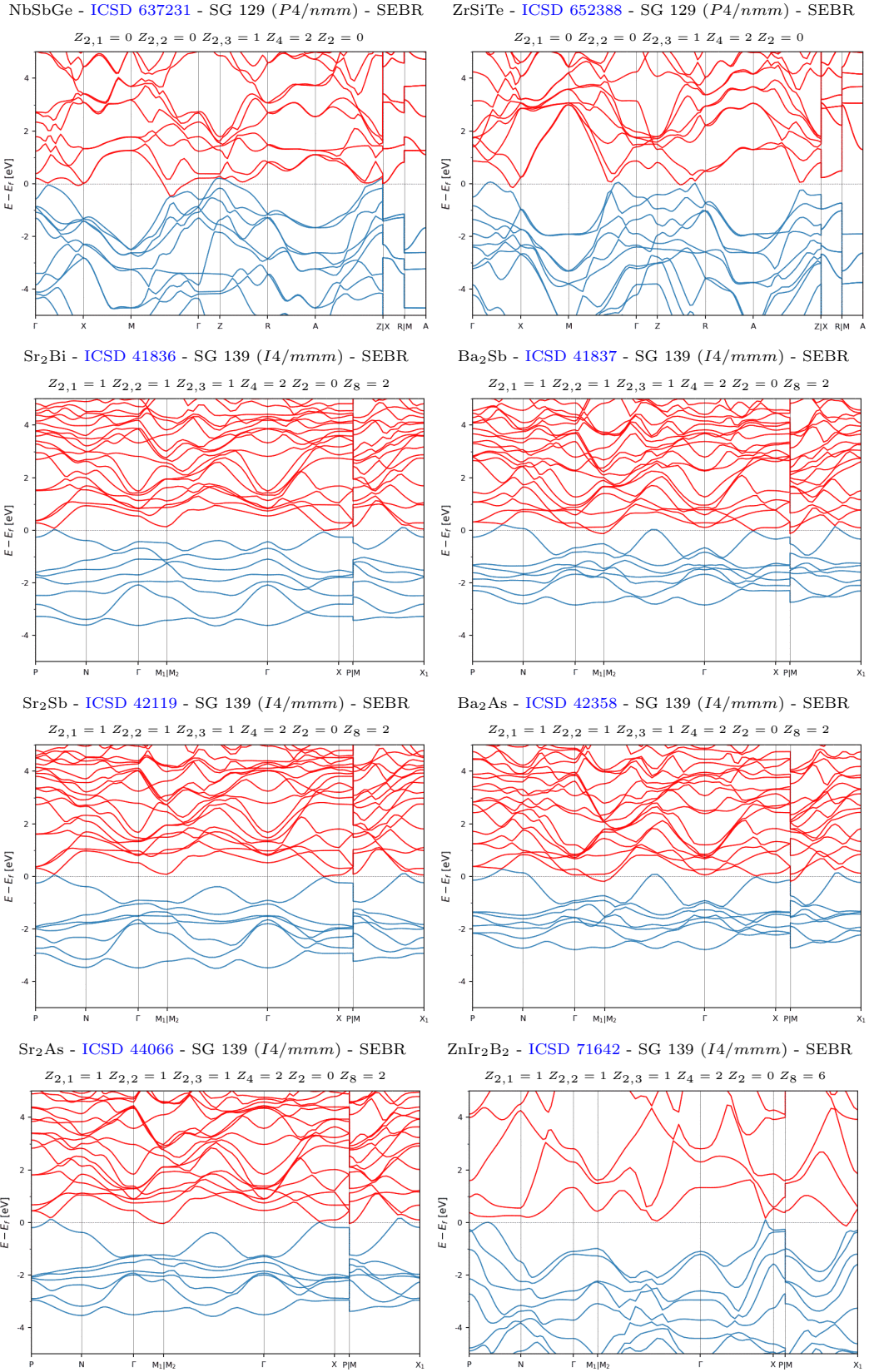


Figure S36. The SEBR-classified, inversion-symmetry-indicated weak TIs and TCIs with the largest band gaps or the fewest and smallest bulk Fermi pockets. (part 8/14)

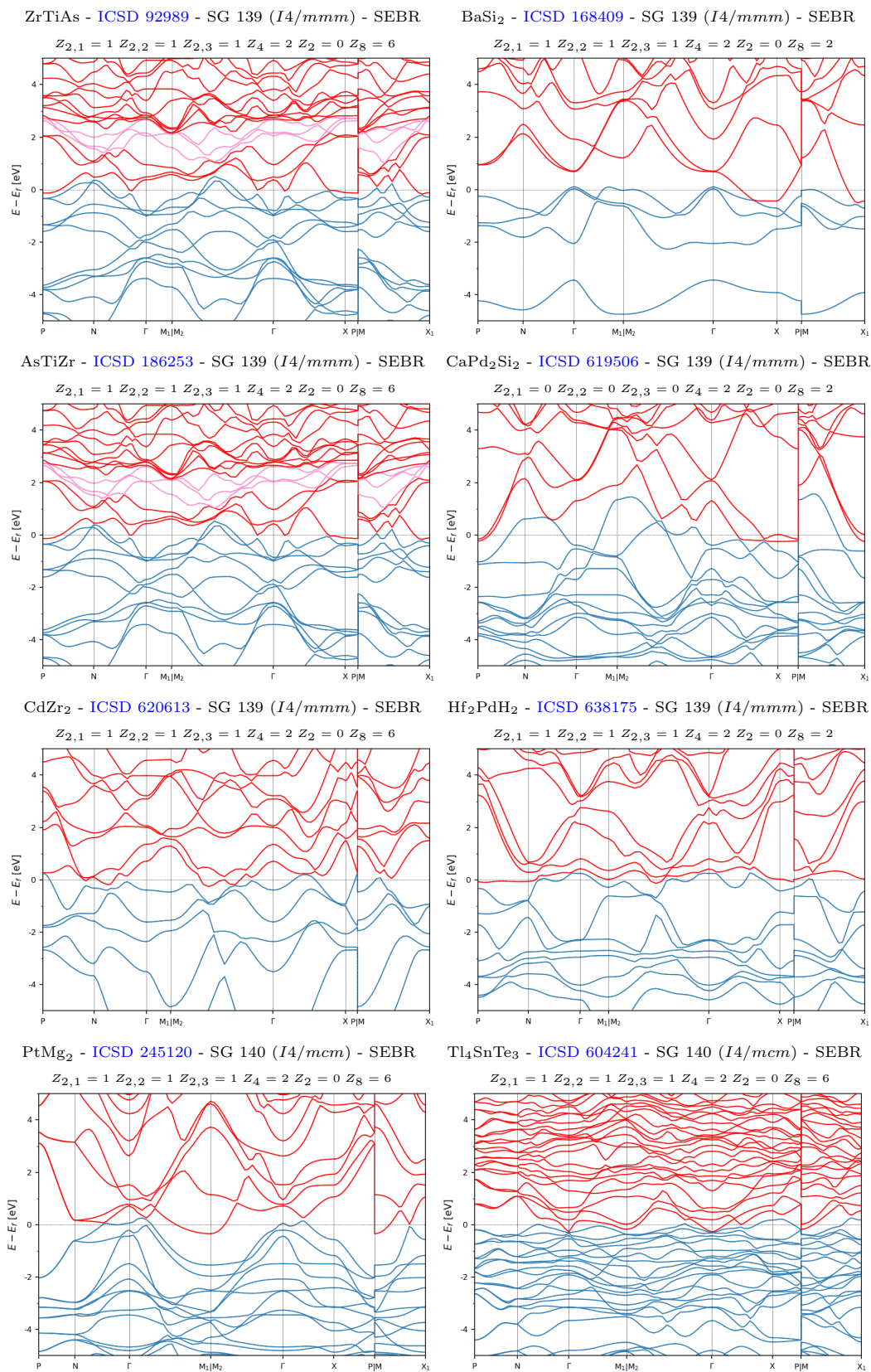


Figure S37. The SEBR-classified, inversion-symmetry-indicated weak TIs and TCIs with the largest band gaps or the fewest and smallest bulk Fermi pockets. (part 9/14)

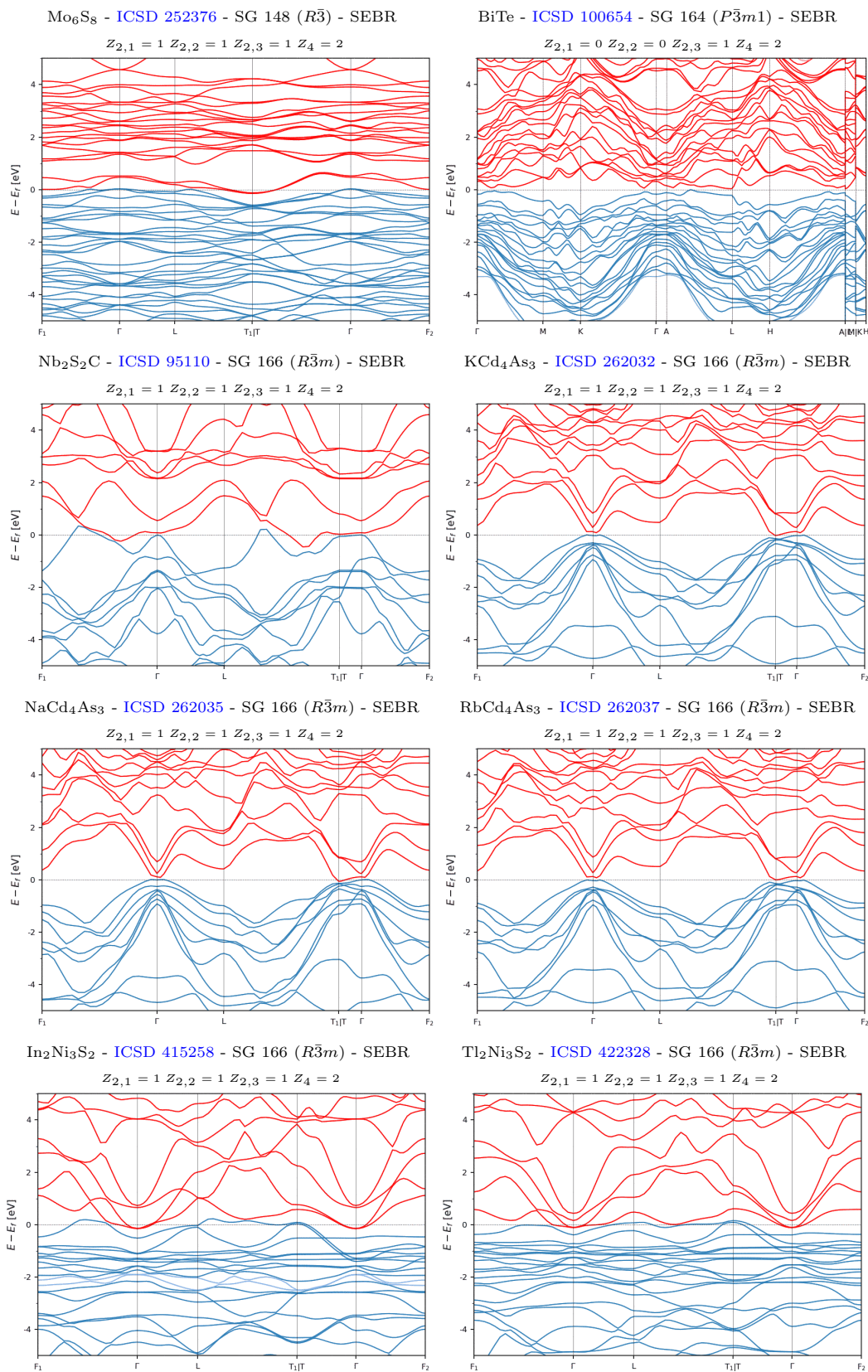


Figure S38. The SEBR-classified, inversion-symmetry-indicated weak TIs and TCIs with the largest band gaps or the fewest and smallest bulk Fermi pockets. (part 10/14)

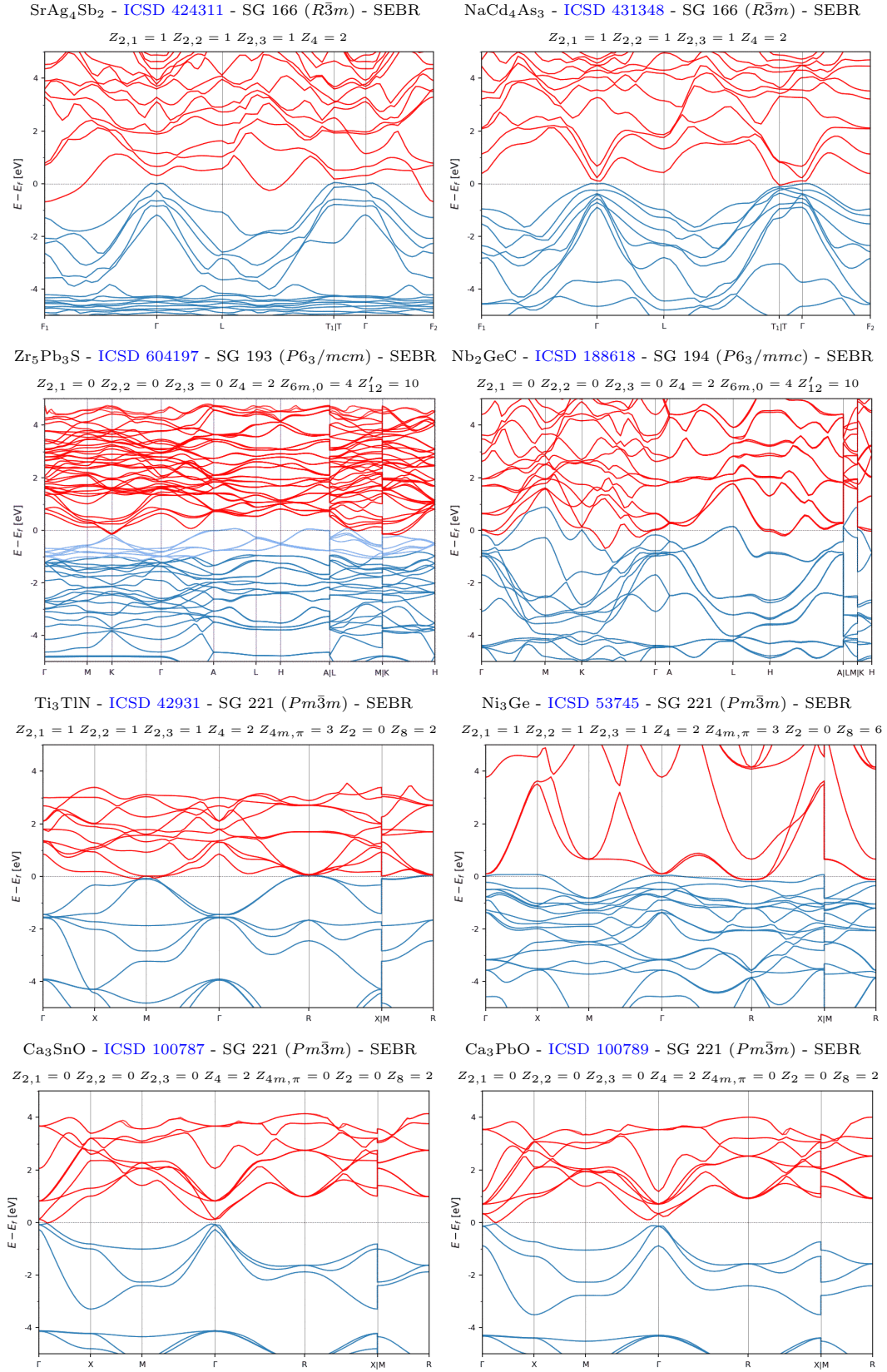


Figure S39. The SEBR-classified, inversion-symmetry-indicated weak TIs and TCIs with the largest band gaps or the fewest and smallest bulk Fermi pockets. (part 11/14)

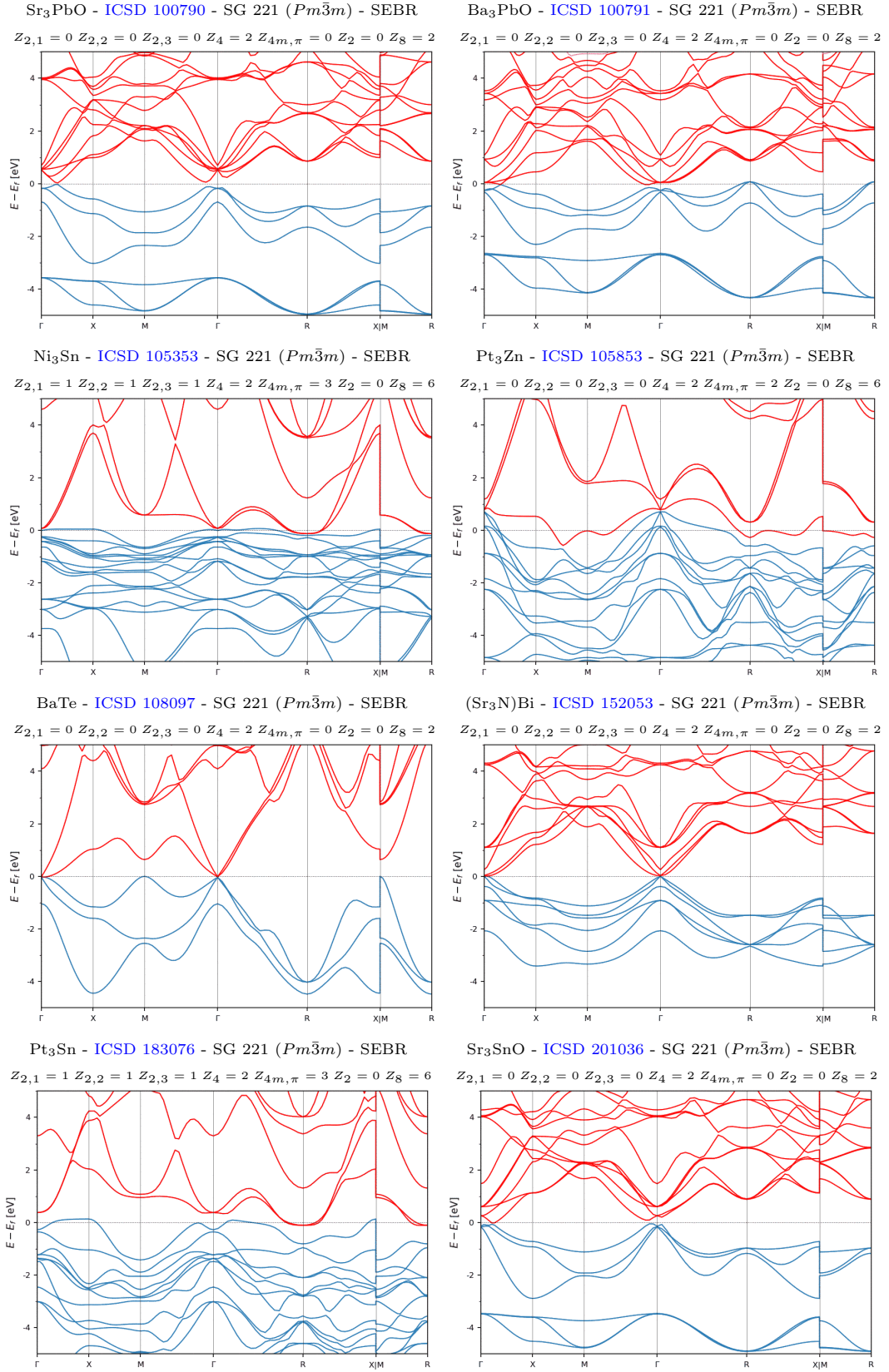


Figure S40. The SEBR-classified, inversion-symmetry-indicated weak TIs and TCIs with the largest band gaps or the fewest and smallest bulk Fermi pockets. (part 12/14)

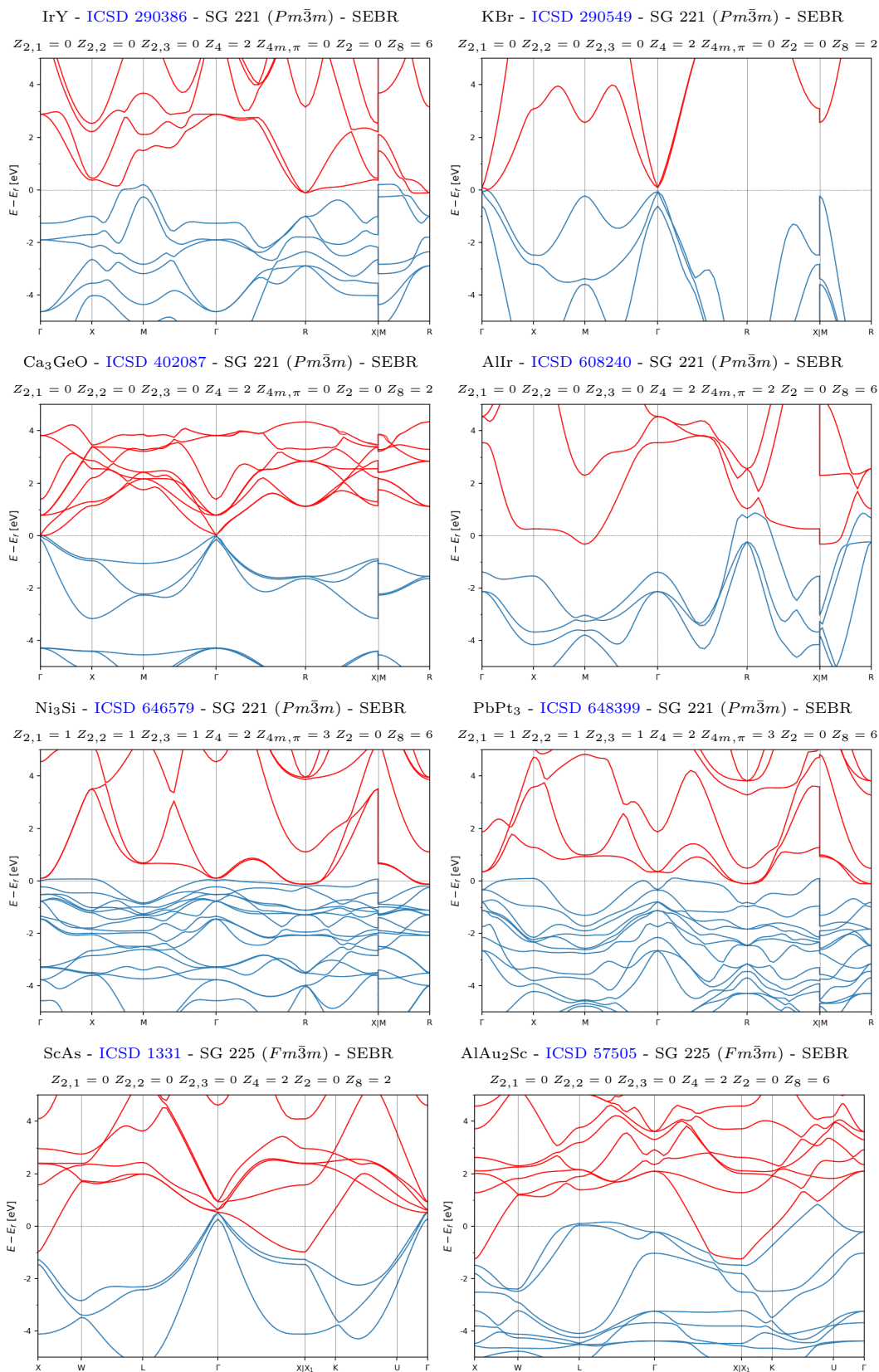


Figure S41. The SEBR-classified, inversion-symmetry-indicated weak TIs and TCIs with the largest band gaps or the fewest and smallest bulk Fermi pockets. (part 13/14)

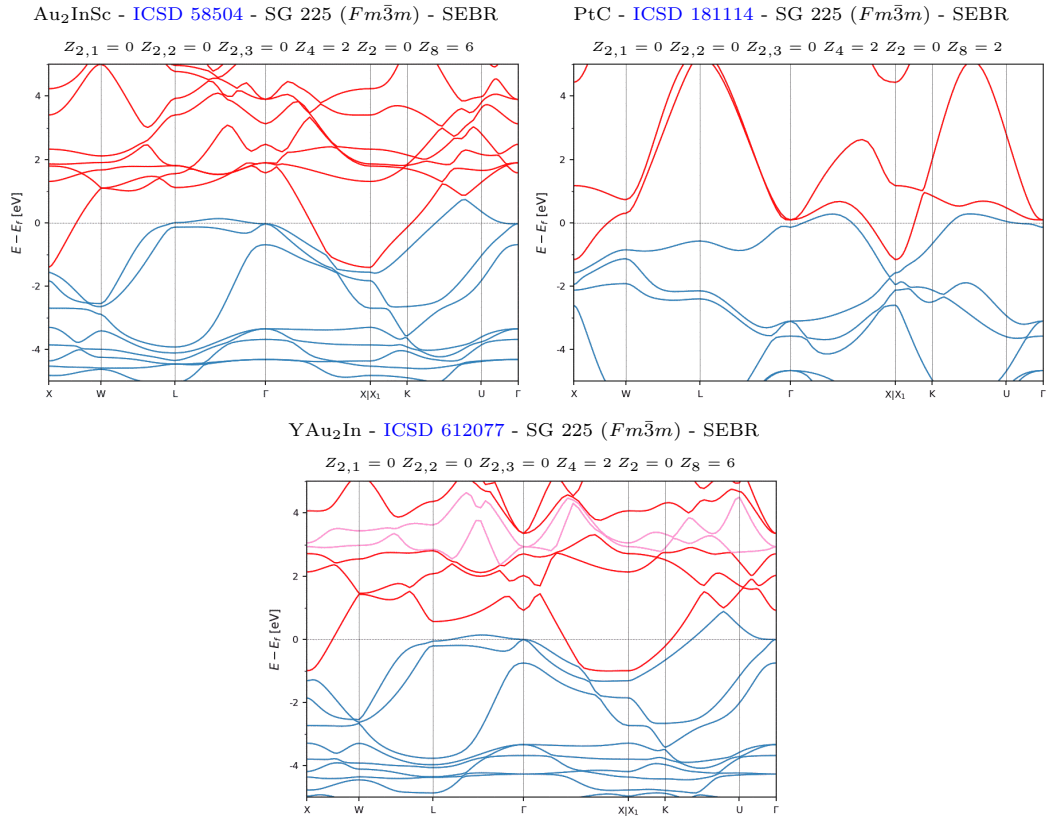


Figure S42. The SEBR-classified, inversion-symmetry-indicated weak TIs and TCIs with the largest band gaps or the fewest and smallest bulk Fermi pockets. (part 14/14)

5. Rotation-Anomaly TCIs and High-Fold-Rotation Mirror TCIs

In this section, we list the symmetry-indicated rotation-anomaly and high-fold-rotation mirror TCIs [16, 17, 86, 101, 104, 174] with the largest bulk gaps or the fewest and smallest bulk Fermi pockets. The TCIs listed in this section exhibit varying, even numbers of massless or massive twofold surface Dirac cones, depending on the Miller indices of the surfaces [16, 17, 86, 101, 104]. On the edges between gapped surfaces, helical hinge modes may also be present, depending on the crystallographic (Miller) indices of the hinges. In terms of the stable SIs introduced in Ref. 16, the materials in this section either exhibit $Z_8 = 4$ or $Z'_{12} = 6$; we do not find any examples of band insulators with $Z_{12} = 6$ and few bulk Fermi pockets. First, in Fig. S43, we list the few sixfold-rotation-anomaly TCIs with $Z'_{12} = 6$, all of which are classified as SEBR. In Fig. S44, we then show the only TCI with $Z_8 = 4$ and a relatively clean Fermi surface that is classified as NLC. Finally, in Figs. S45, S46, S47, and S48, we list the TCIs with $Z_8 = 4$ that are classified as SEBR. The materials identified in this section include members of the well-studied SnTe family, including SnTe [ICSD 652759, SG 225 ($Fm\bar{3}m$)] [12, 16, 104, 160–162] – a prototypical fourfold rotation-anomaly TCI – and PbTe [ICSD 648615, SG 225 ($Fm\bar{3}m$)] [120, 163], which also appears as a fourfold-rotation anomaly TCI, depending on the choice of lattice parameters and DFT functionals. SnTe and PbTe are both classified as SEBR and thus appear in Figs. S47 and S48, respectively.

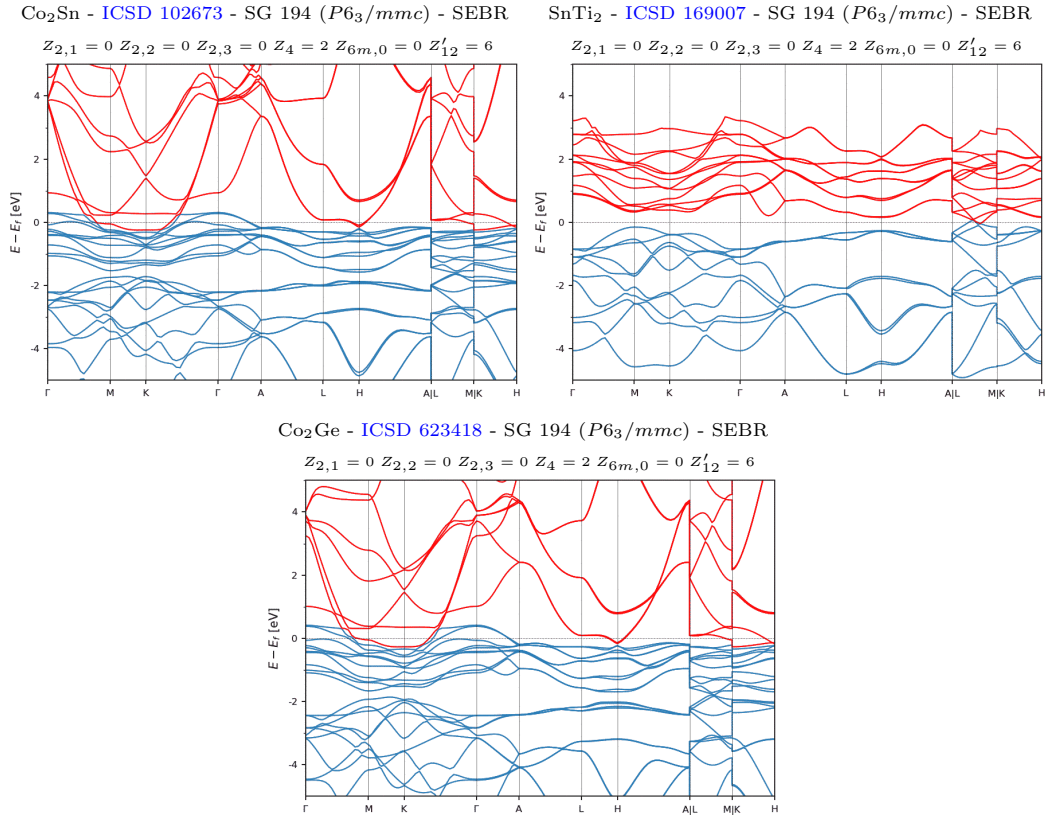


Figure S43. The sixfold-rotation-anomaly TCIs with the largest band gaps or the fewest and smallest bulk Fermi pockets. All of these materials exhibit $Z'_{12} = 6$, and are classified as SEBR.

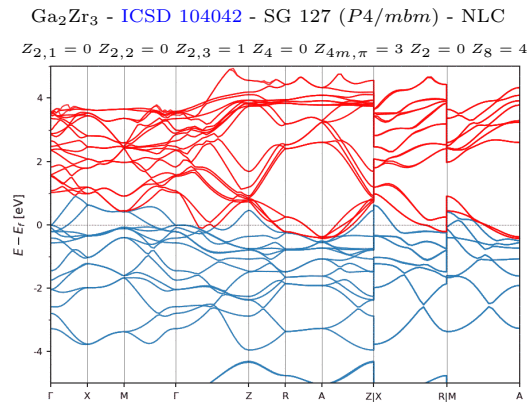


Figure S44. The NLC-classified, fourfold-rotation-anomaly weak TI characterized by $Z_8 = 4$ with the fewest and smallest bulk Fermi pockets.

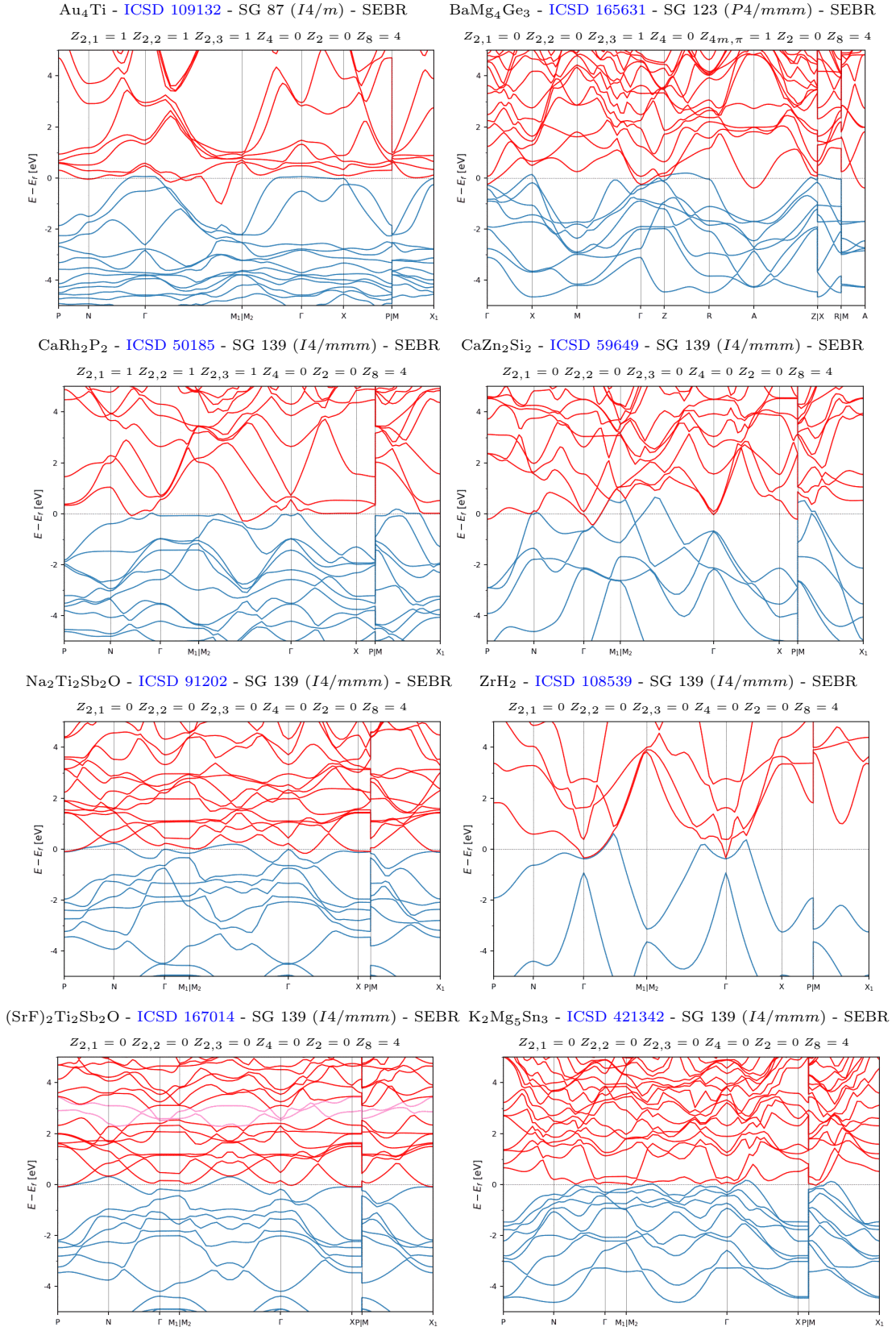
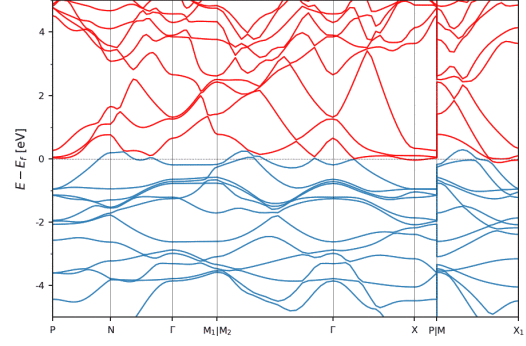
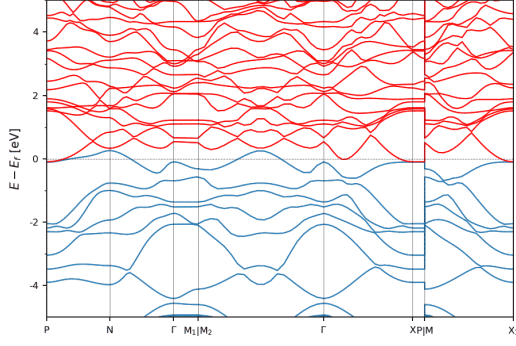
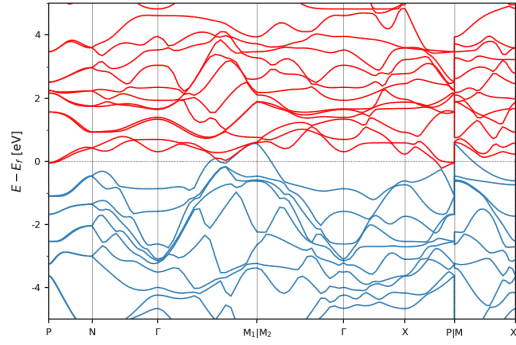


Figure S45. The SEBR-classified, fourfold-rotation-anomaly and mirror TCIs characterized by $Z_8 = 4$ with the largest band gaps or the fewest and smallest bulk Fermi pockets. (part 1/4)

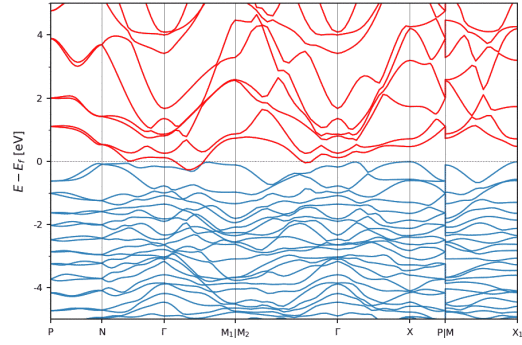
(SrF)₂Ti₂Bi₂O - ICSD 430064 - SG 139 (*I4/mmm*) - SEBR $Z_{2,1} = 0$ $Z_{2,2} = 0$ $Z_{2,3} = 0$ $Z_4 = 0$ $Z_2 = 0$ $Z_8 = 4$ CaCo₂As₂ - ICSD 609899 - SG 139 (*I4/mmm*) - SEBR $Z_{2,1} = 1$ $Z_{2,2} = 1$ $Z_{2,3} = 1$ $Z_4 = 0$ $Z_2 = 0$ $Z_8 = 4$



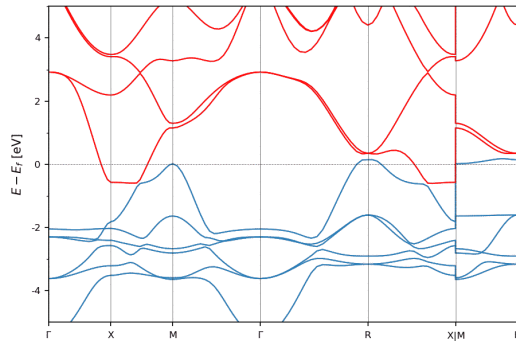
TiSb₂ - ICSD 52322 - SG 140 (*I4/mcm*) - SEBR $Z_{2,1} = 1$ $Z_{2,2} = 1$ $Z_{2,3} = 1$ $Z_4 = 0$ $Z_2 = 0$ $Z_8 = 4$



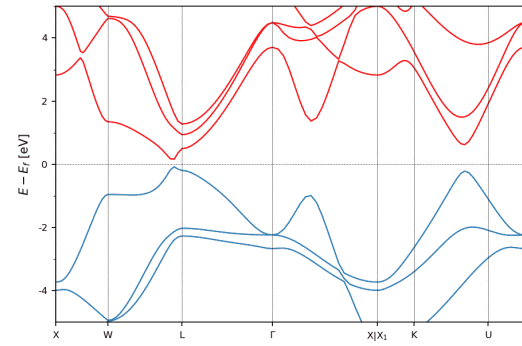
Pt₃Ge - ICSD 77962 - SG 140 (*I4/mcm*) - SEBR $Z_{2,1} = 0$ $Z_{2,2} = 0$ $Z_{2,3} = 0$ $Z_4 = 0$ $Z_2 = 0$ $Z_8 = 4$



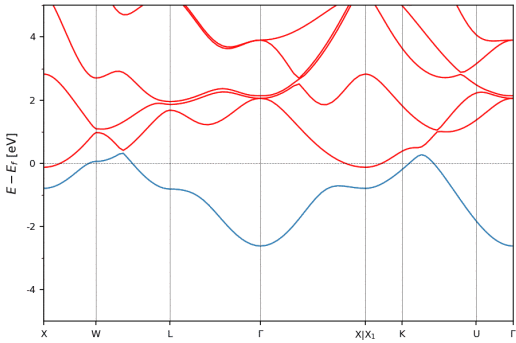
CaPd - ICSD 619498 - SG 221 (*Pm-3m*) - SEBR $Z_{2,1} = 0$ $Z_{2,2} = 0$ $Z_{2,3} = 0$ $Z_4 = 0$ $Z_{4m,\pi} = 2$ $Z_2 = 0$ $Z_8 = 4$



SnSe - ICSD 52424 - SG 225 (*Fm-3m*) - SEBR $Z_{2,1} = 0$ $Z_{2,2} = 0$ $Z_{2,3} = 0$ $Z_4 = 0$ $Z_2 = 0$ $Z_8 = 4$



Ba - ICSD 52679 - SG 225 (*Fm-3m*) - SEBR $Z_{2,1} = 0$ $Z_{2,2} = 0$ $Z_{2,3} = 0$ $Z_4 = 0$ $Z_2 = 0$ $Z_8 = 4$



PbPo - ICSD 105598 - SG 225 (*Fm-3m*) - SEBR $Z_{2,1} = 0$ $Z_{2,2} = 0$ $Z_{2,3} = 0$ $Z_4 = 0$ $Z_2 = 0$ $Z_8 = 4$

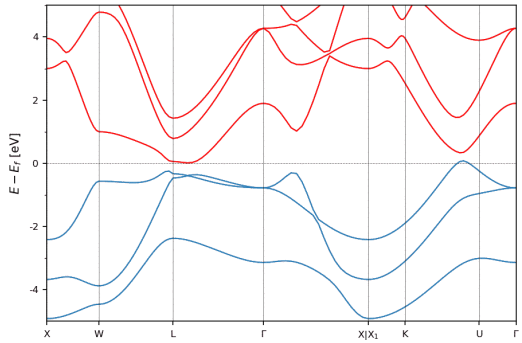


Figure S46. The SEBR-classified, fourfold-rotation-anomaly and mirror TCIs characterized by $Z_8 = 4$ with the largest band gaps or the fewest and smallest bulk Fermi pockets. (part 2/4)

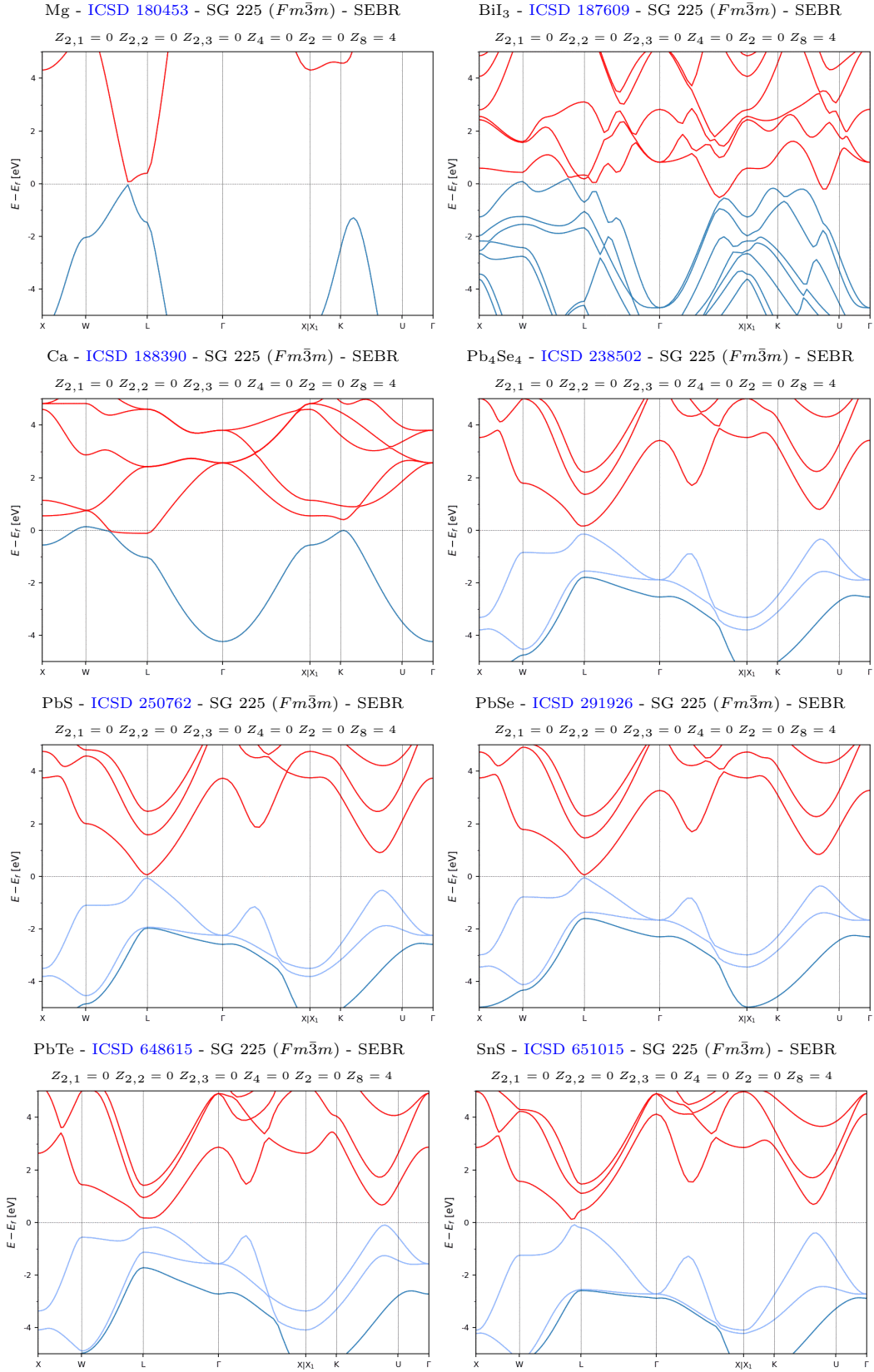


Figure S47. The SEBR-classified, fourfold-rotation-anomaly and mirror TCIs characterized by $Z_8 = 4$ with the largest band gaps or the fewest and smallest bulk Fermi pockets. (part 3/4)

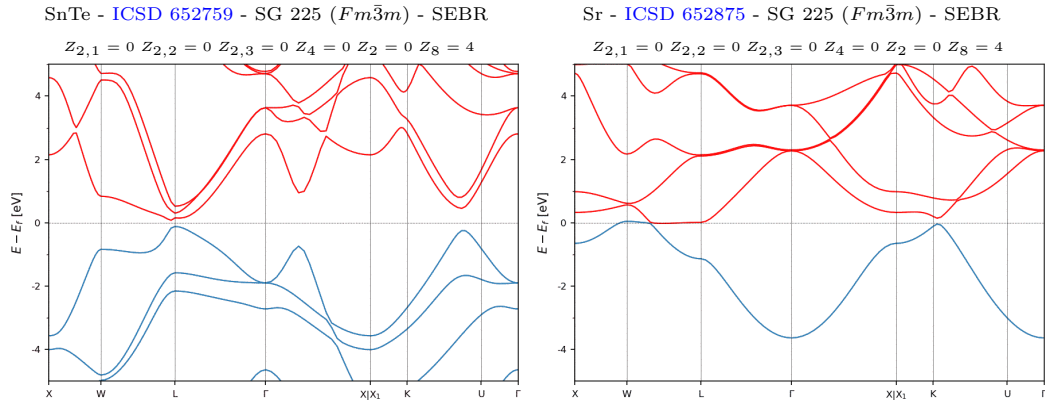


Figure S48. The SEBR-classified, fourfold-rotation-anomaly and mirror TCIs characterized by $Z_8 = 4$ with the largest band gaps or the fewest and smallest bulk Fermi pockets. (part 4/4)

6. Other TCIs with Trivial Z_4 Indices

In this section, we list the remaining TCIs with trivial strong Z_4 indices and nontrivial values for at least one other stable SI, and which have simple bulk Fermi surfaces or insulating gaps. In terms of the stable SIs introduced in Ref. 16, the materials listed in this section specifically exhibit $Z_4 = 0$ and nontrivial values for at least one other stable SI, excluding the cases of $Z_8 = 4$ or $Z'_{12} = 6$, which were previously addressed in SM 11 A 5. The TCIs listed in this section exhibit differing numbers of twofold surface Dirac cones, whose presence is indicated through a combination of weak indices and mirror and rotation-anomaly TCI indices.

Notably, a subset of the TCIs listed in this section exhibit completely trivial strong indices (*i.e.* $Z_4 = 0$ without any other nontrivial strong indices). As shown in Refs. [16, 26, 148, 149], materials with $Z_4 = 0$ and nontrivial weak indices realize “obstructed” weak-TI phases that differ from weak-TI phases by fractional lattice translation. Specifically, when the weak indices $Z_{2,i}$ are nontrivial, the value of the strong index Z_4 can be advanced by 2 (mod 4) by shifting the origin of the unit cell by half of a lattice translation along the direction of the weak-index vector. In an obstructed weak-TI phase, the bulk is topologically equivalent to a stack of 2D TIs oriented along the weak-index vector, but crucially a stack in which the 2D TI layers in each stack unit cell are displaced from the origin by half of a lattice translation along the stacking direction, analogous to the obstructed-atomic-limit phase of the Su-Schrieffer-Heeger model of polyacetylene [89, 148, 149, 190–192]. Like weak TIs, obstructed weak TIs exhibit twofold Dirac-cone surface states and topological defect bound states [148, 149, 184, 193].

Below, in Fig. S49, we first list the $Z_4 = 0$ TCIs that are classified as NLC, and then, in Figs. S50, S51, S52, and S53, we list the $Z_4 = 0$ TCIs that are classified as SEBR. In addition to obstructed weak-TI phases, the materials listed in this section include members of the KHgSb family [ICSD 56201, SG 194 ($P6_3/mmc$)], which have been shown theoretically and experimentally [13, 14, 109, 127, 128] to exhibit a combination of symmetry-indicated mirror-TCI surface states and non-symmetry-indicated glide-protected surface states. In particular, KHgSb itself is classified as SEBR, and thus appears in Fig. S52 under the alternative chemical formula HgKSb.

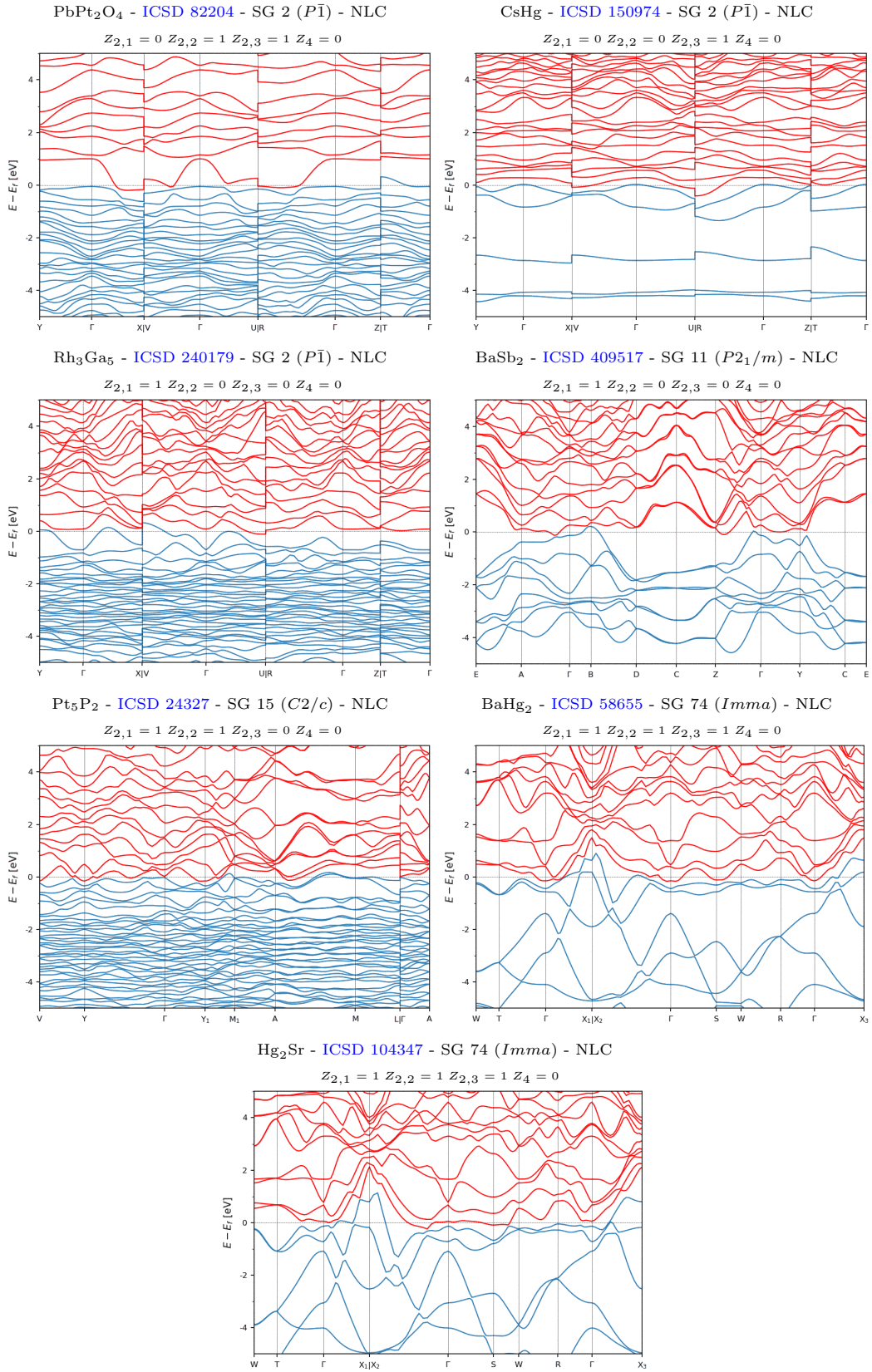


Figure S49. The NLC-classified TCIs with the largest band gaps or the fewest and smallest bulk Fermi pockets whose topology is characterized by $Z_4 = 0$ and undefined or trivial values of Z_8 .

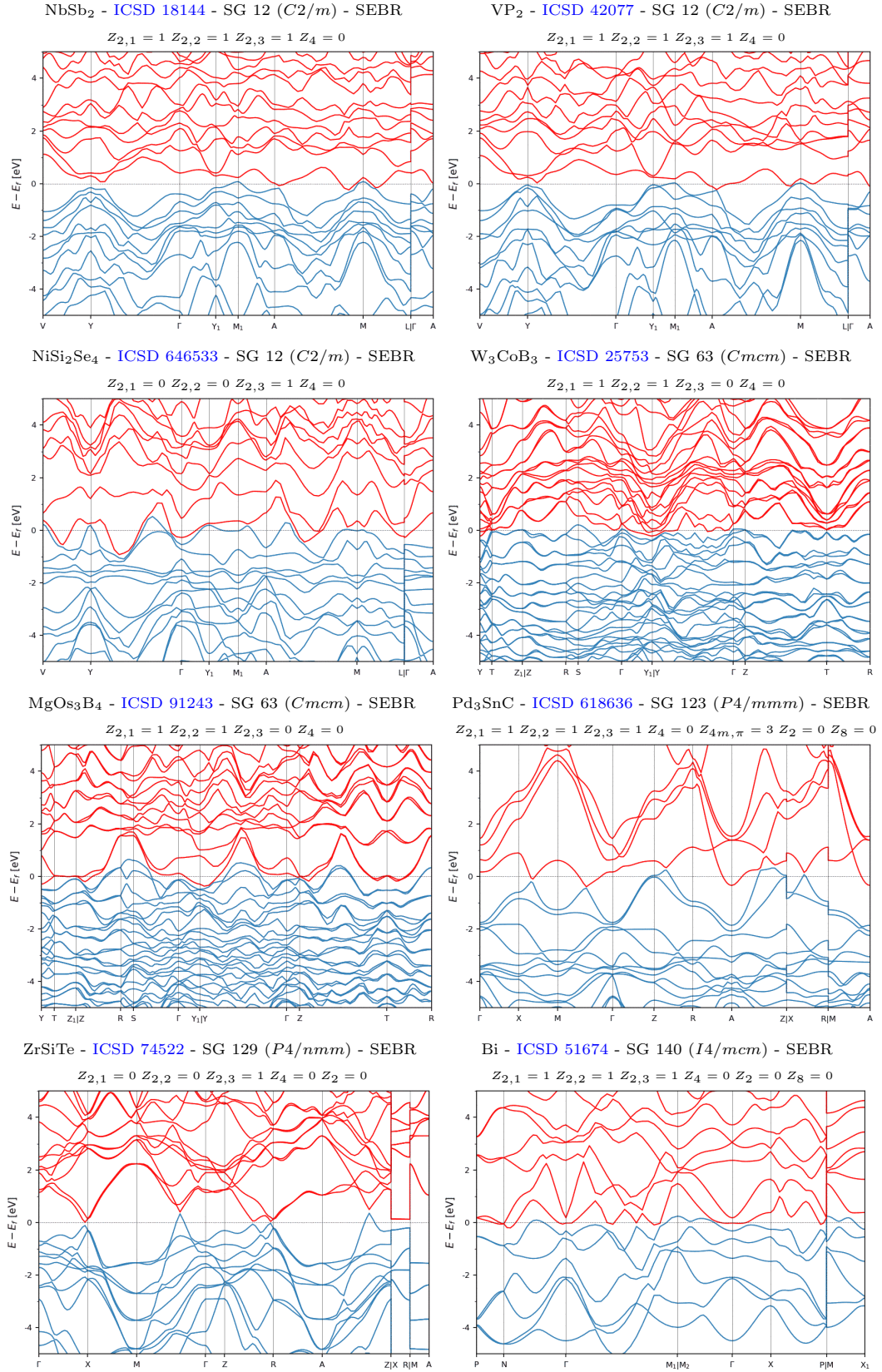


Figure S50. The SEBR-classified TCIs with the largest band gaps or the fewest and smallest bulk Fermi pockets whose topology is characterized by $Z_4 = 0$ and undefined or trivial values of Z_8 . (part 1/4)

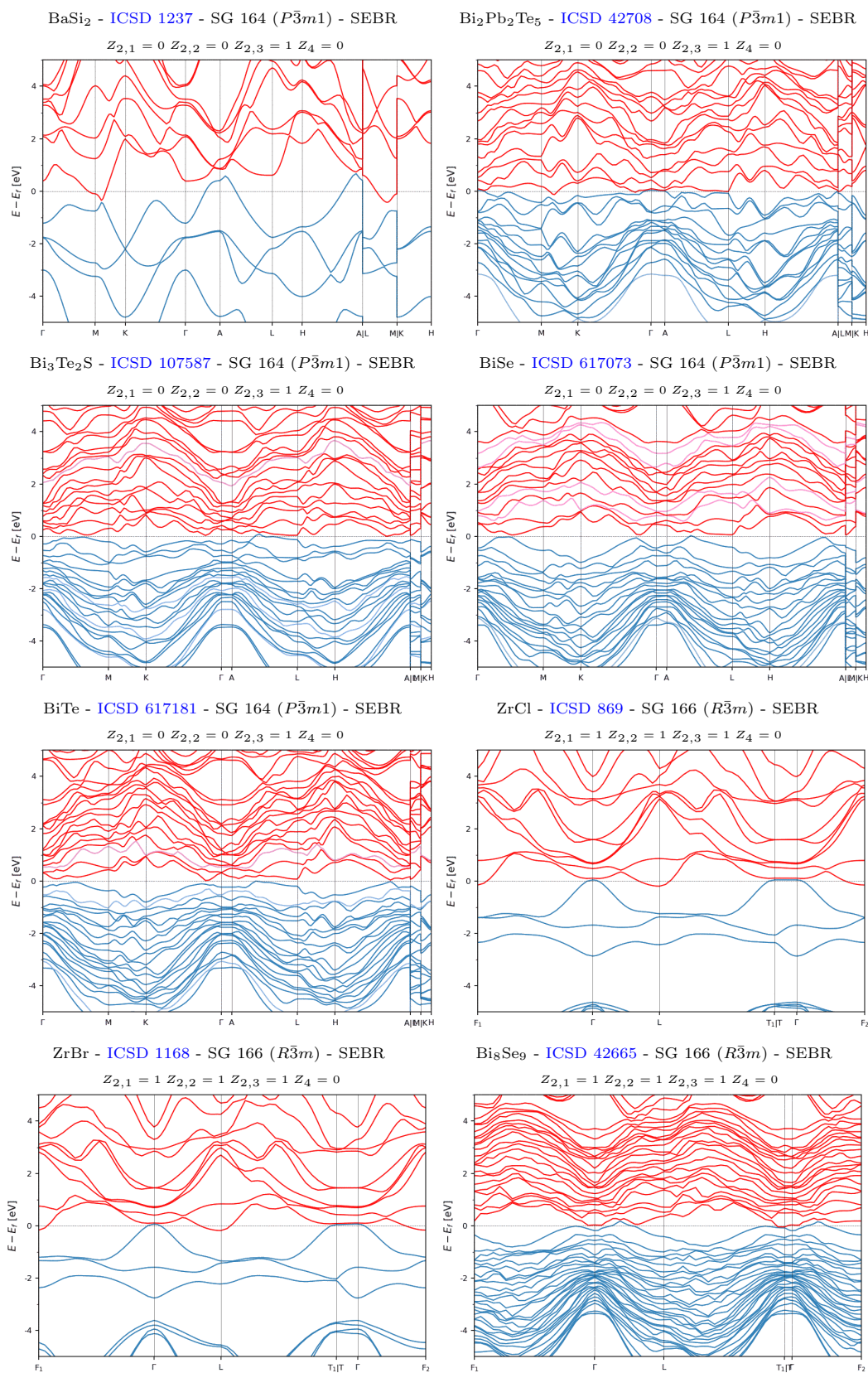


Figure S51. The SEBR-classified TCIs with the largest band gaps or the fewest and smallest bulk Fermi pockets whose topology is characterized by $Z_4 = 0$ and undefined or trivial values of Z_8 . (part 2/4)

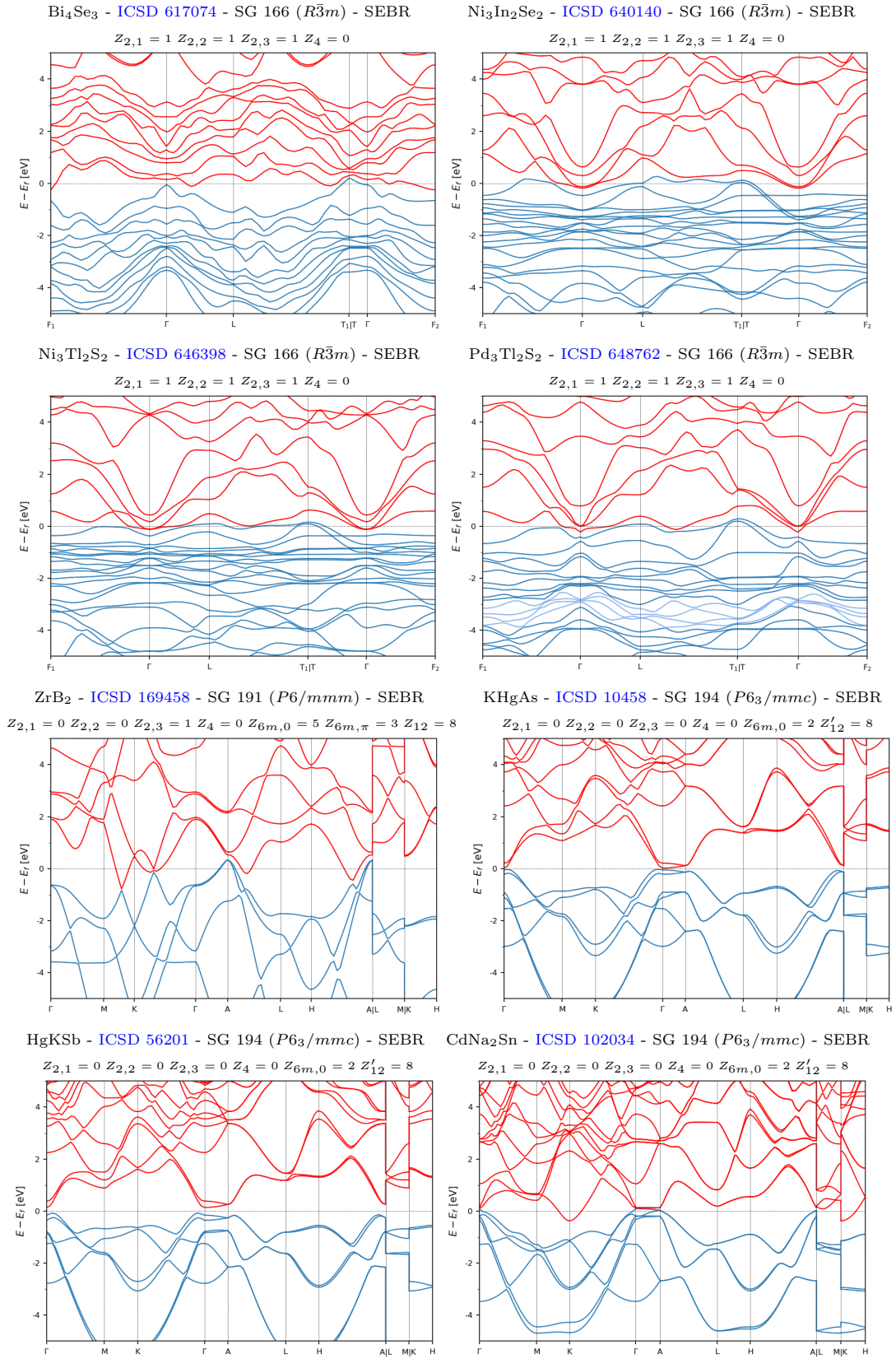


Figure S52. The SEBR-classified TCIs with the largest band gaps or the fewest and smallest bulk Fermi pockets whose topology is characterized by $Z_4 = 0$ and undefined or trivial values of Z_8 . (part 3/4)

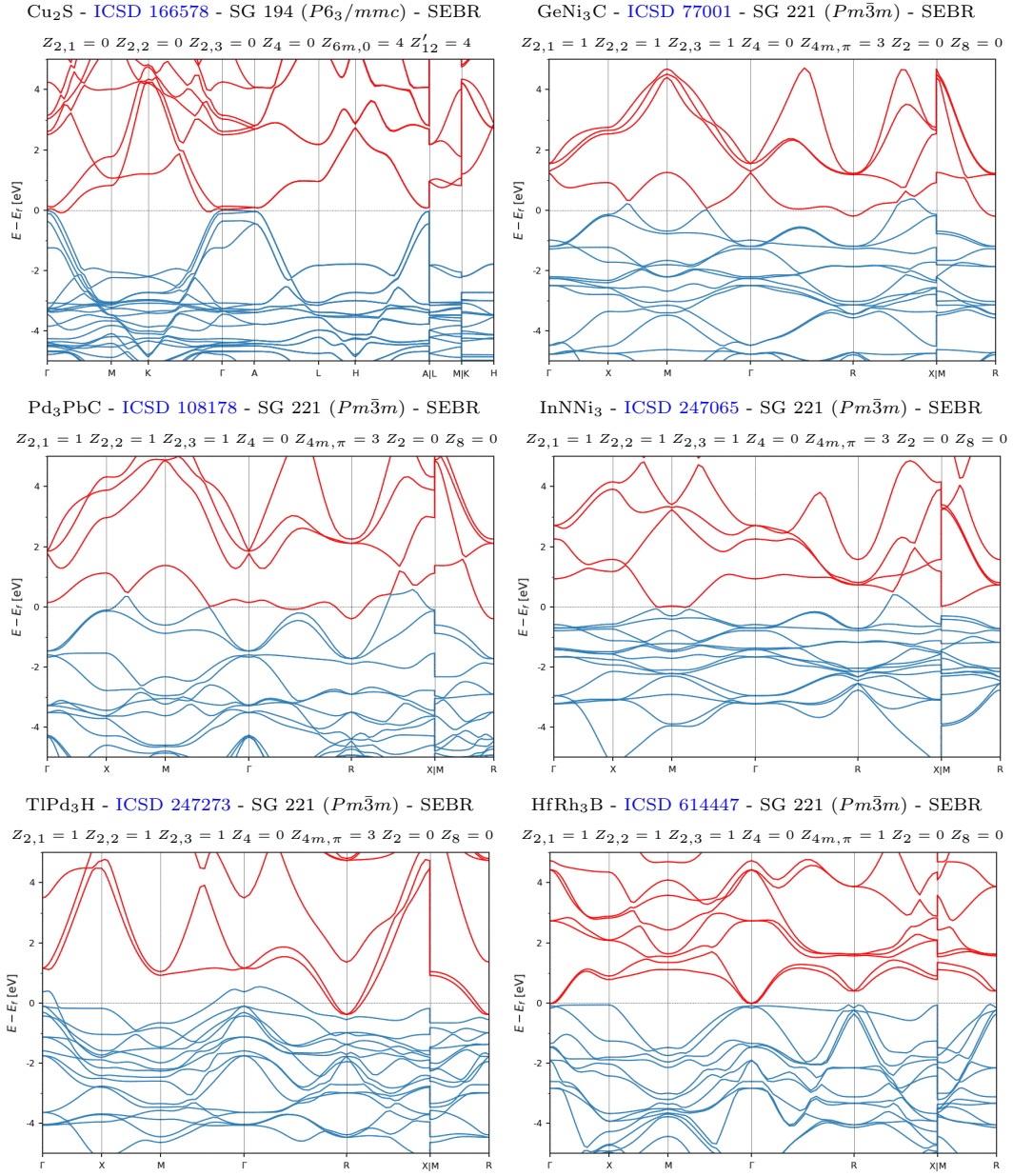


Figure S53. The SEBR-classified TCIs with the largest band gaps or the fewest and smallest bulk Fermi pockets whose topology is characterized by $Z_4 = 0$ and undefined or trivial values of Z_8 . (part 4/4)

7. TCIs with Threefold Rotation Symmetry

In this section, we list the TCIs with threefold rotation symmetry and nontrivial $Z_{3m0,\pi}$ indices. As discussed in Refs. 16, 17, and 29, TCIs with nontrivial $Z_{3m0,\pi}$ indices may also be 3D TIs. Specifically, $Z_{3m0,\pi}$ respectively indicate the mirror Chern numbers in the $k_z = 0, \pi$ planes modulo 3. Insulators with net-odd momentum-space mirror Chern numbers C_{M_z} are 3D TIs – however, because insulators with $C_{M_z} = 2$ and $C_{M_z} = -1$ exhibit the same mirror Chern numbers modulo 3, then further Wilson-loop [13, 14, 107–109, 175] or surface-state calculations must be performed to determine whether insulators with nontrivial $Z_{3m0,\pi}$ are additionally 3D TIs.

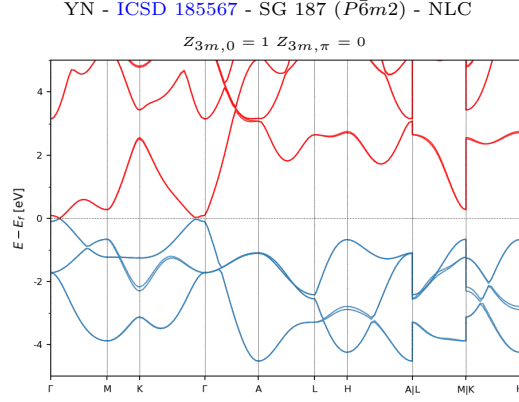


Figure S54. The NLC-classified, threefold-rotation-indicated TCI with the fewest and smallest bulk Fermi pockets.

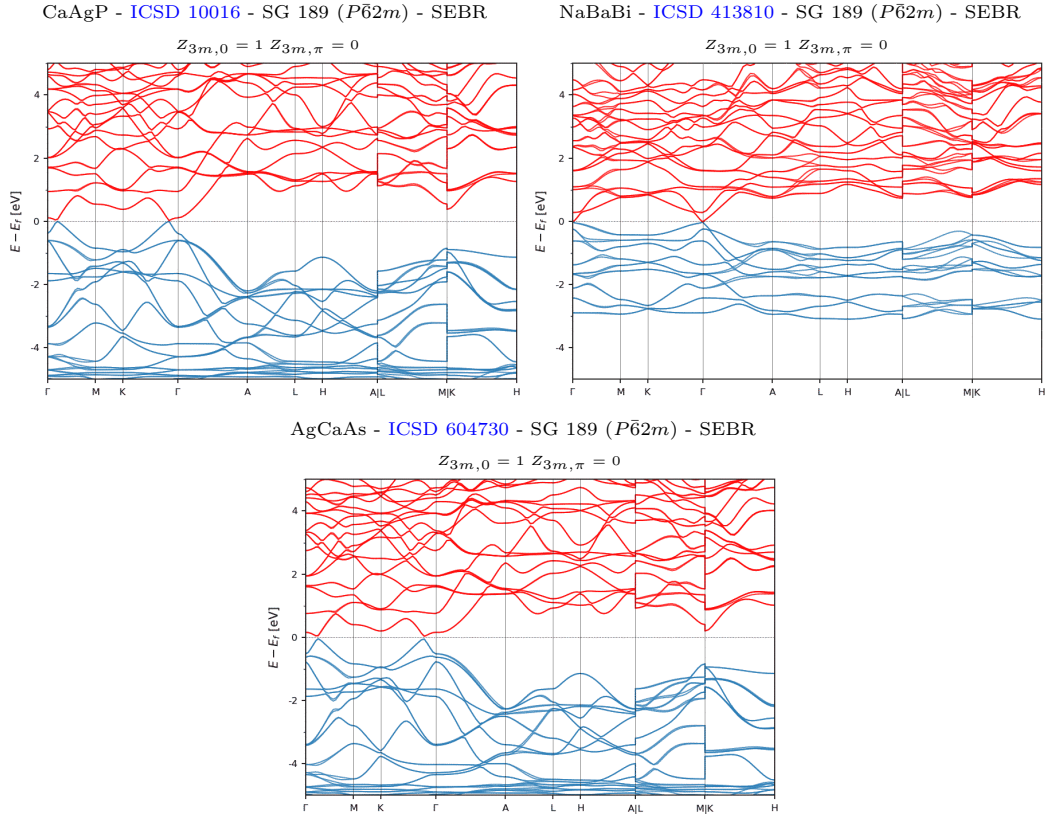


Figure S55. The SEBR-classified, threefold-rotation-indicated TIs and TCIs with the largest band gaps or the fewest and smallest bulk Fermi pockets.

B. Repeat-Topological Materials

In this section, we list the RTopo TIs and TCIs with the largest band gaps or the fewest and smallest bulk Fermi pockets when the Fermi level is set to 0, and when the Fermi level is set to the next highest filling below E_F at which an insulating gap is permitted by band connectivity (see [SM 9 A](#) for further details and a rigorous definition of RTopo materials). As introduced in this work, RTopo materials specifically exhibit stable topological gaps at E_F , and at the next-highest gap below E_F as determined by band connectivity through TQC (see [SM 2](#) and [SM 9 A](#)). First in Figs. [S56](#) and [S57](#), we list the RTopo materials that are classified as NLC at E_F , and then, in Figs. [S58](#), [S59](#), [S60](#), [S61](#), [S62](#), and [S63](#), we list the RTopo materials that are classified as SEBR at E_F .

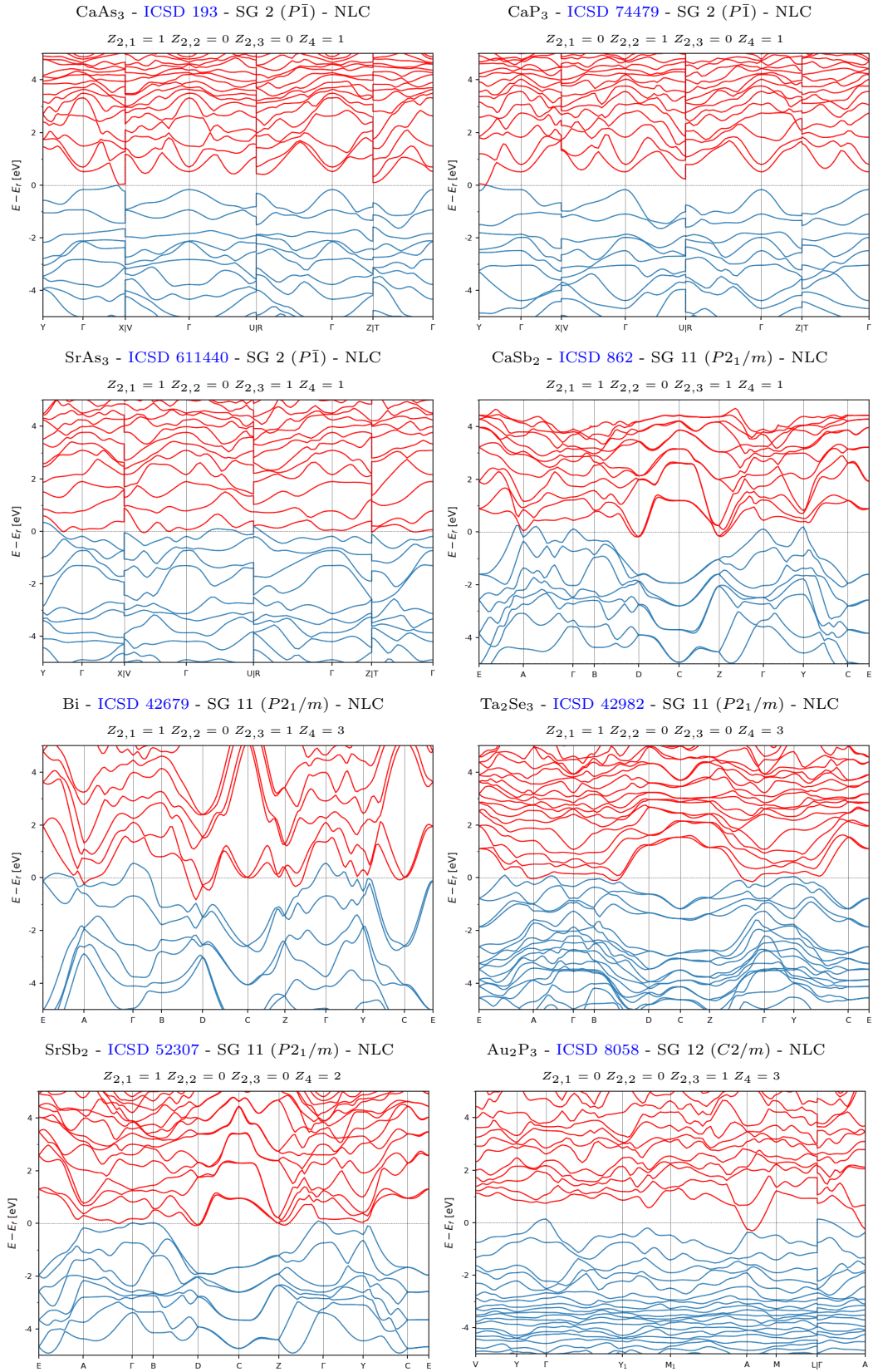


Figure S56. The RTopo TIs and TCIs that are NLC-classified at the Fermi level and have the fewest and smallest bulk Fermi pockets when the Fermi level is set to 0, or set to the next highest filling at which an insulating gap is permitted by band connectivity. (part 1/2)

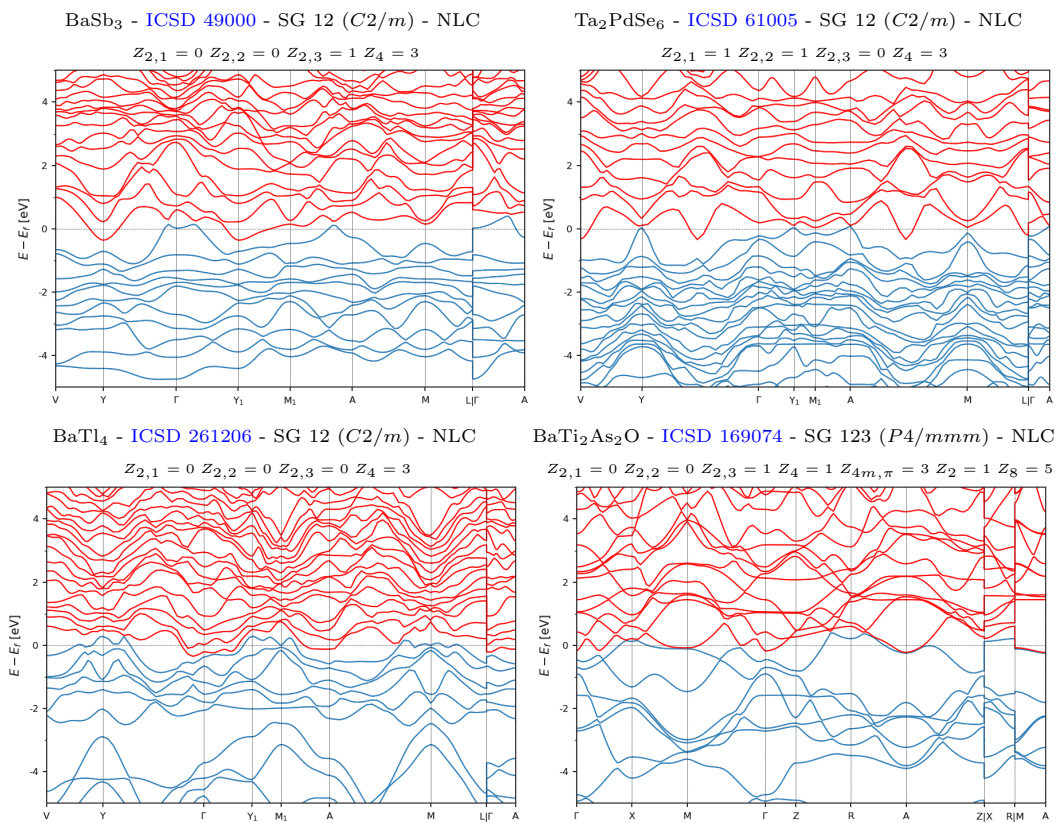


Figure S57. The RTopo TIs and TCIs that are NLC-classified at the Fermi level and have the fewest and smallest bulk Fermi pockets when the Fermi level is set to 0, or set to the next highest filling at which an insulating gap is permitted by band connectivity. (part 2/2)

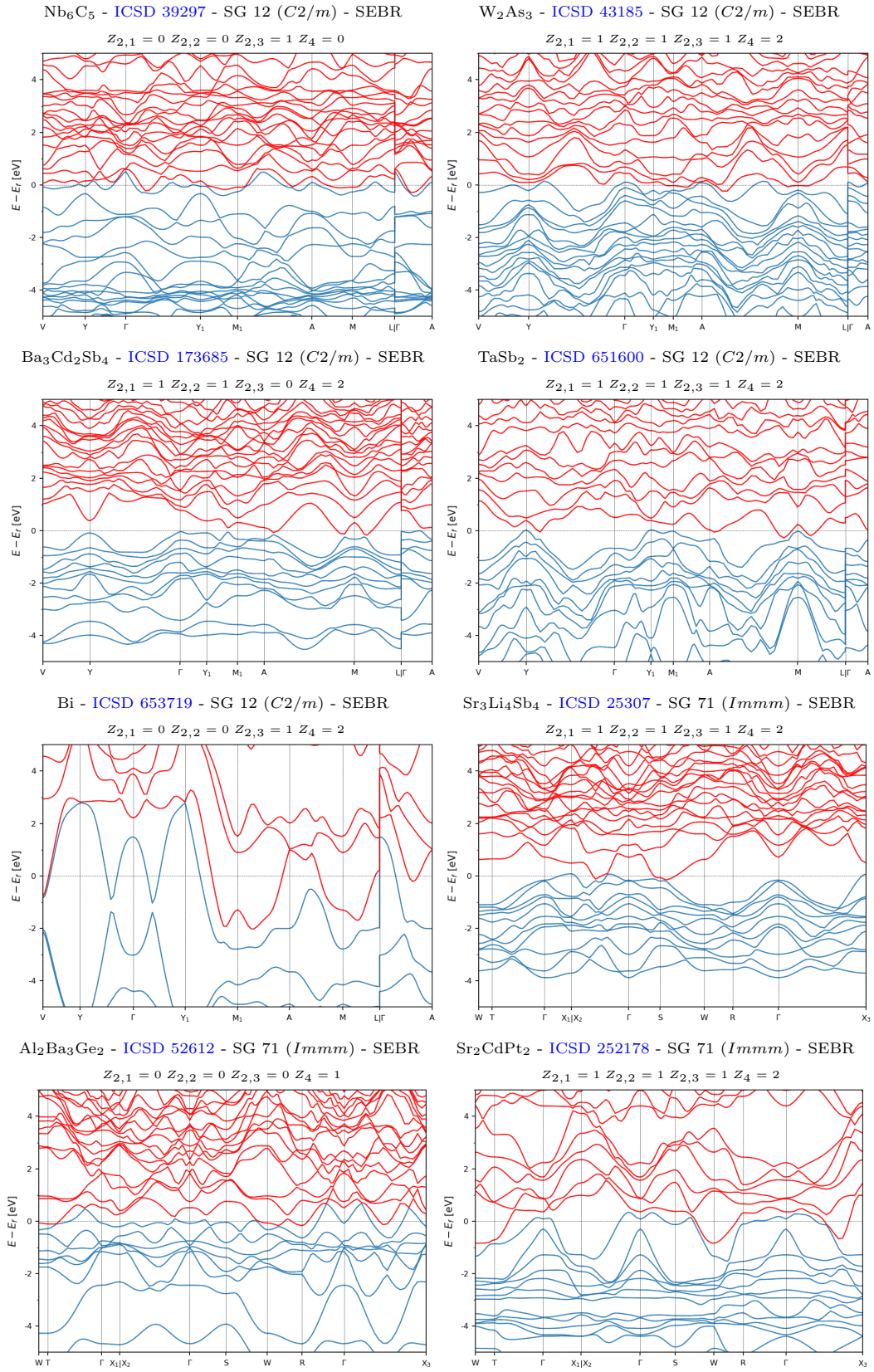


Figure S58. The RTopo TIs and TCIs that are SEBR-classified at the Fermi level and have the fewest and smallest bulk Fermi pockets when the Fermi level is set to 0, or set to the next highest filling at which an insulating gap is permitted by band connectivity. (part 1/6)

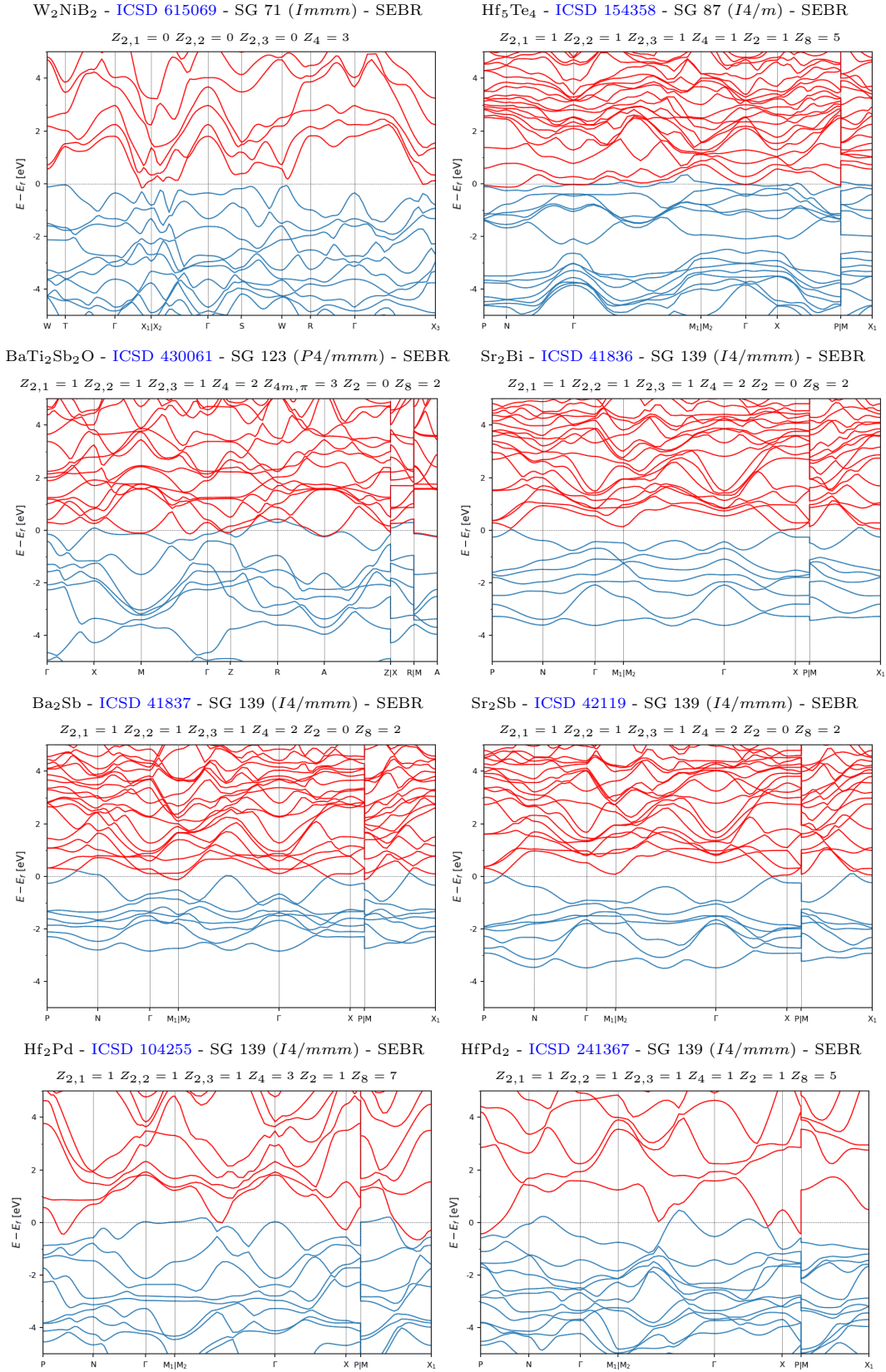


Figure S59. The RTopo TIs and TCIs that are SEBR-classified at the Fermi level and have the fewest and smallest bulk Fermi pockets when the Fermi level is set to 0, or set to the next highest filling at which an insulating gap is permitted by band connectivity. (part 2/6)

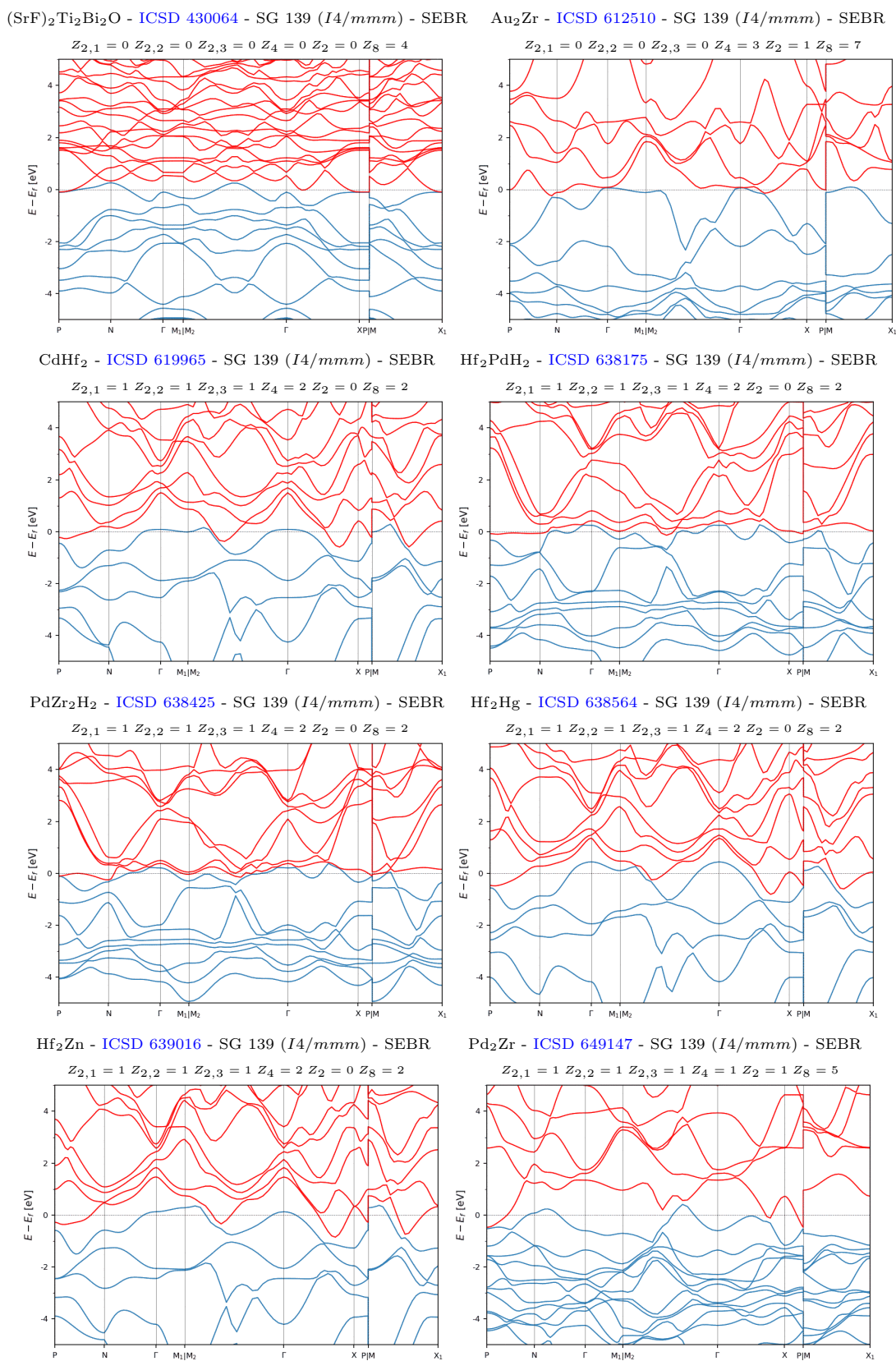


Figure S60. The RTopo TIs and TCIs that are SEBR-classified at the Fermi level and have the fewest and smallest bulk Fermi pockets when the Fermi level is set to 0, or set to the next highest filling at which an insulating gap is permitted by band connectivity. (part 3/6)

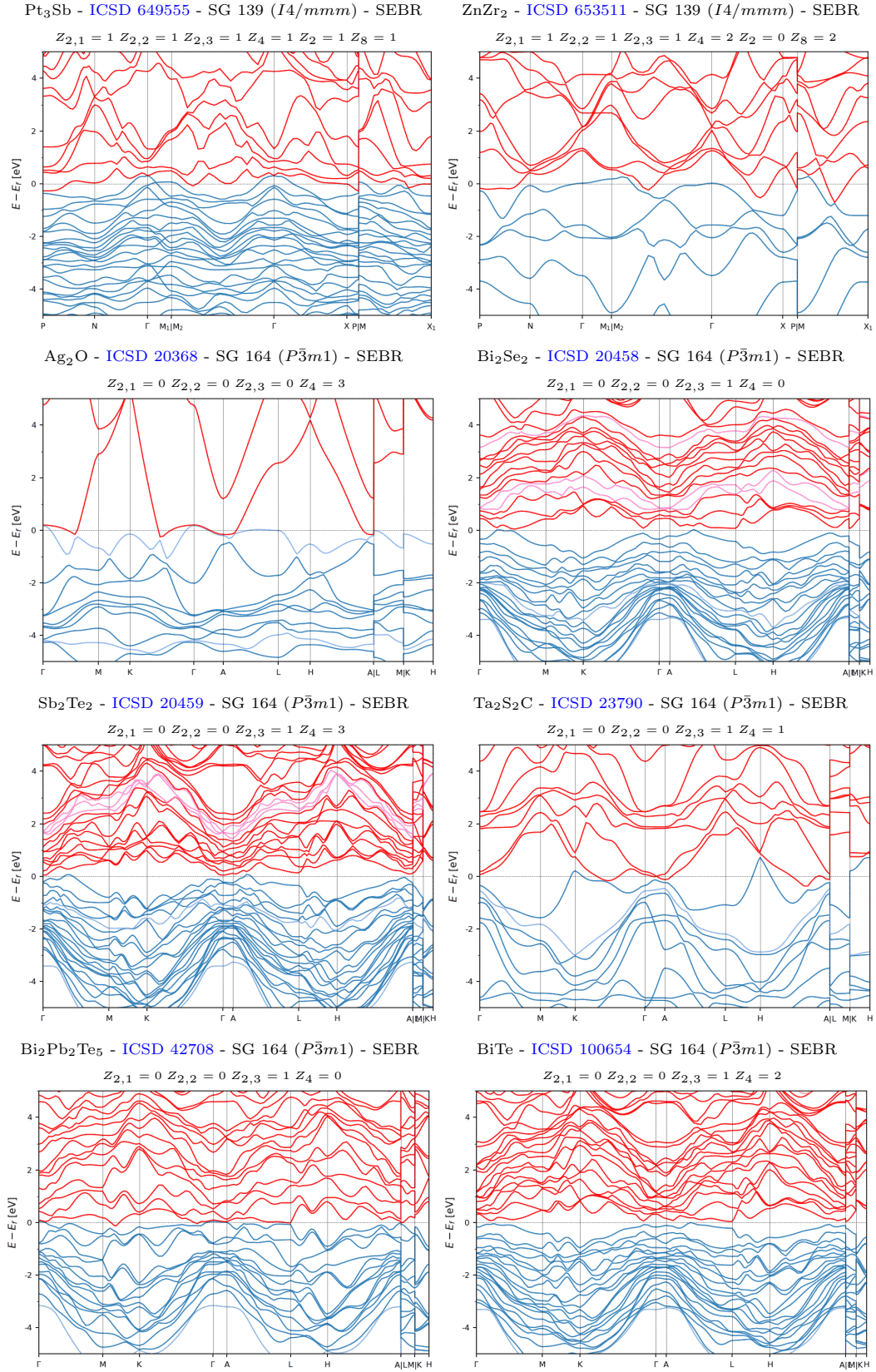


Figure S61. The RTopo TIs and TCIs that are SEBR-classified at the Fermi level and have the fewest and smallest bulk Fermi pockets when the Fermi level is set to 0, or set to the next highest filling at which an insulating gap is permitted by band connectivity. (part 4/6)

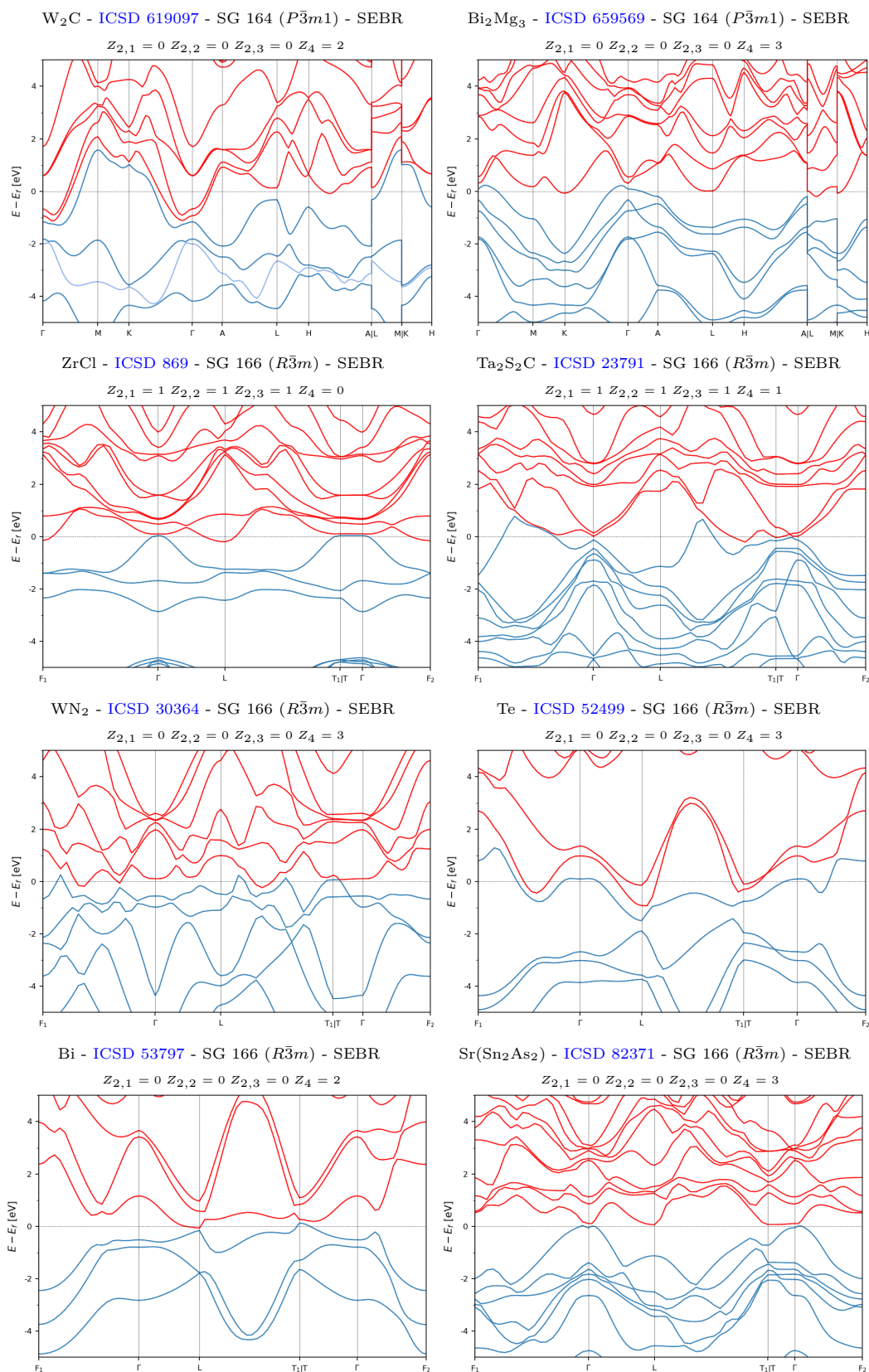


Figure S62. The RTopo TIs and TCIs that are SEBR-classified at the Fermi level and have the fewest and smallest bulk Fermi pockets when the Fermi level is set to 0, or set to the next highest filling at which an insulating gap is permitted by band connectivity. (part 5/6)

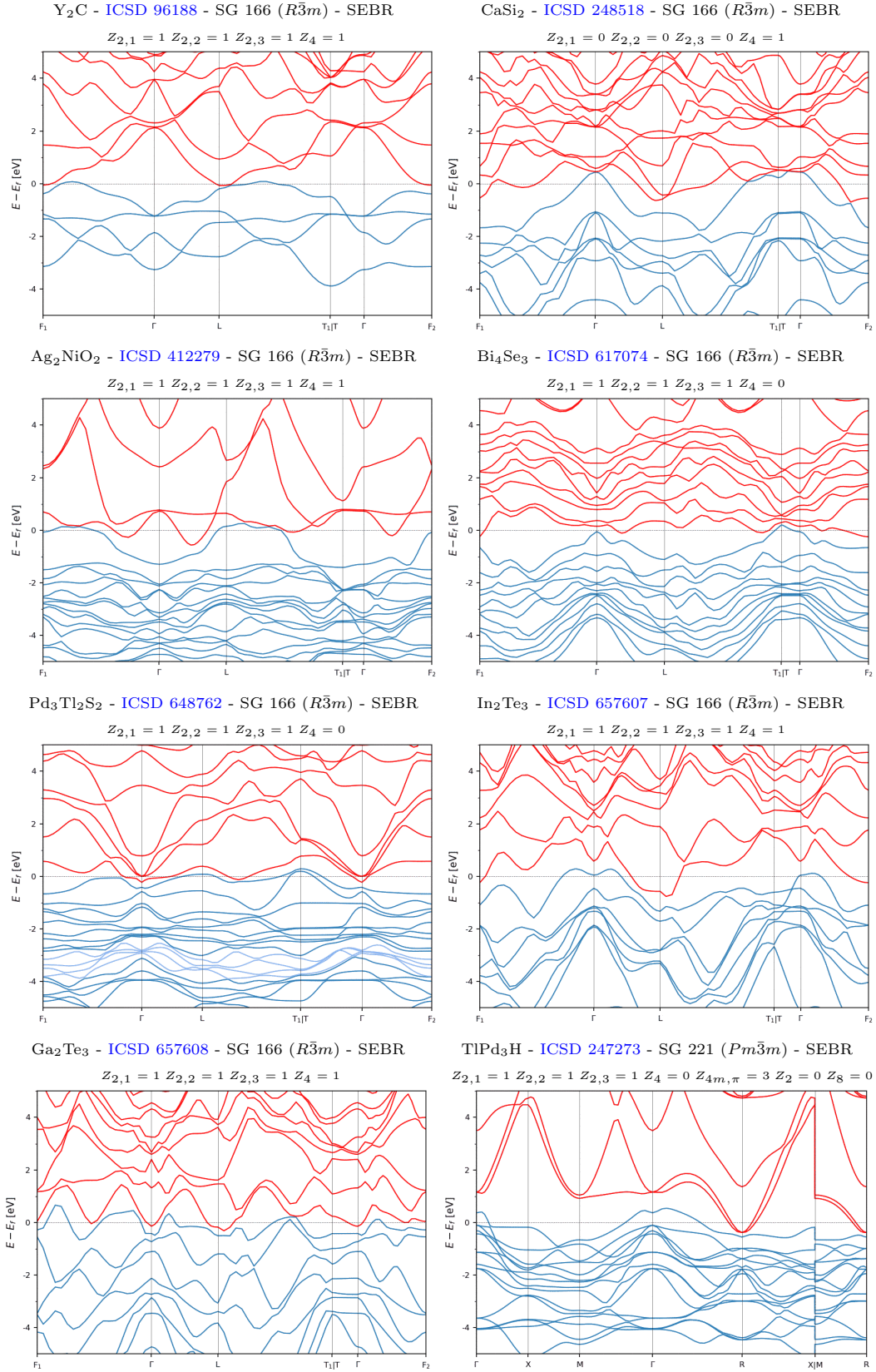


Figure S63. The RTopo TIs and TCIs that are SEBR-classified at the Fermi level and have the fewest and smallest bulk Fermi pockets when the Fermi level is set to 0, or set to the next highest filling at which an insulating gap is permitted by band connectivity. (part 6/6)

C. Enforced Topological Semimetals

In this section, we will list the enforced semimetals with the smallest bulk Fermi pockets. First, in [SM 11 C 1](#), we will list the enforced semimetals whose nodal degeneracies are pinned to high-symmetry BZ points (ESFD), and then, in [SM 11 C 2](#), we will list the enforced semimetals whose nodal degeneracies lie along high-symmetry BZ lines (ES).

1. ESFD-Classified Semimetals

In this section, we list the enforced semimetals whose nodal degeneracies are pinned to high-symmetry BZ points (ESFD in the nomenclature established in Ref. [38](#)). Most generally, ESFD phases can include both conventional (filling-) [[129](#), [150](#), [194](#)] enforced Dirac [[151](#), [168](#), [169](#), [195](#)] and Weyl [[131](#)] semimetals, as well as unconventional (multifold) fermion [[7–9](#), [130](#), [131](#), [196](#)] semimetals. Depending on whether or not the little groups of the \mathbf{k} points of the enforced nodal degeneracies (as well as the full space group) contain rotoinversion symmetries, the ESFD semimetals identified in this section may further be classified as topologically chiral or achiral [[130](#), [131](#)]. ESFD phases in structurally chiral crystals have in particular been highlighted for hosting monopole-like spin textures [[131](#), [197](#)], exhibiting photoresponse signatures of topological chirality [[132](#), [198–201](#)], and as possible venues for realizing topological superconductivity [[202–204](#)].

First, in Fig. [S64](#), we list the ESFD materials with the simplest bulk Fermi surfaces and threefold-degenerate spin-1 fermions [[8](#)] close to E_F . Because the spin-1 fermions in the materials in Fig. [S64](#) all lie at high-symmetry \mathbf{k} points with rotoinversion (specifically S_4) symmetry, then the threefold degeneracies carry net-zero chiral charges, and do not exhibit associated topological surface Fermi arcs [[130](#), [131](#)]. Next, in Figs. [S65](#), [S66](#), [S67](#), [S68](#), [S69](#), [S70](#), [S71](#), [S72](#), [S73](#), and [S74](#), we list the materials with well-isolated achiral fourfold-degenerate spin-3/2 fermions [[8](#)] close to E_F . Then, in Figs. [S75](#), [S76](#), [S77](#), [S78](#), [S79](#), and [S80](#), we list the cubic ESFD materials with chiral crystal structures and enforced chiral fermions [[8](#), [9](#), [130](#), [131](#)] close to E_F , which in most cases include chiral fourfold-degenerate spin-3/2 fermions and chiral sixfold-degenerate double-spin-1 fermions. The materials in Figs. [S75](#), [S76](#), [S77](#), [S78](#), [S79](#), and [S80](#) notably include members of the B20 chiral crystal family, such as CoSi [[ICSD 189221](#), SG 198 ($P2_13$)], which have been shown in recent theoretical and experimental investigations to exhibit large topological surface Fermi arcs [[9](#), [23–25](#), [130](#), [134](#), [135](#)]. In the following figures – Figs. [S81](#), [S82](#), and [S83](#) – we then show the ESFD materials with eightfold-degenerate double Dirac fermions [[7](#), [8](#)] close to E_F that do not exhibit clear magnetic instabilities in DFT. Specifically, in a number of ESFD compounds – most notably candidate double Dirac semimetals such as CuBi₂O₄ [[ICSD 15865](#), SG 130 ($P4/ncc$)] [[8](#), [205](#), [206](#)] – experimental investigations have revealed that the nodal degeneracies become gapped by electron-electron interactions, leading to correlated Mott – or possibly more exotic – insulating phases, even above the transition temperature for magnetic ordering. The candidate double Dirac semimetals shown in Figs. [S81](#), [S82](#), and [S83](#) exhibit less sharply peaked densities of states at E_F than CuBi₂O₄, and may therefore be less susceptible to interaction-driven (semi)metal-insulator transitions. Finally, in Figs. [S84](#) and [S85](#), we list the ESFD materials with other forms of nodal fermions at E_F , such as fourfold degeneracies with quadratic dispersion.

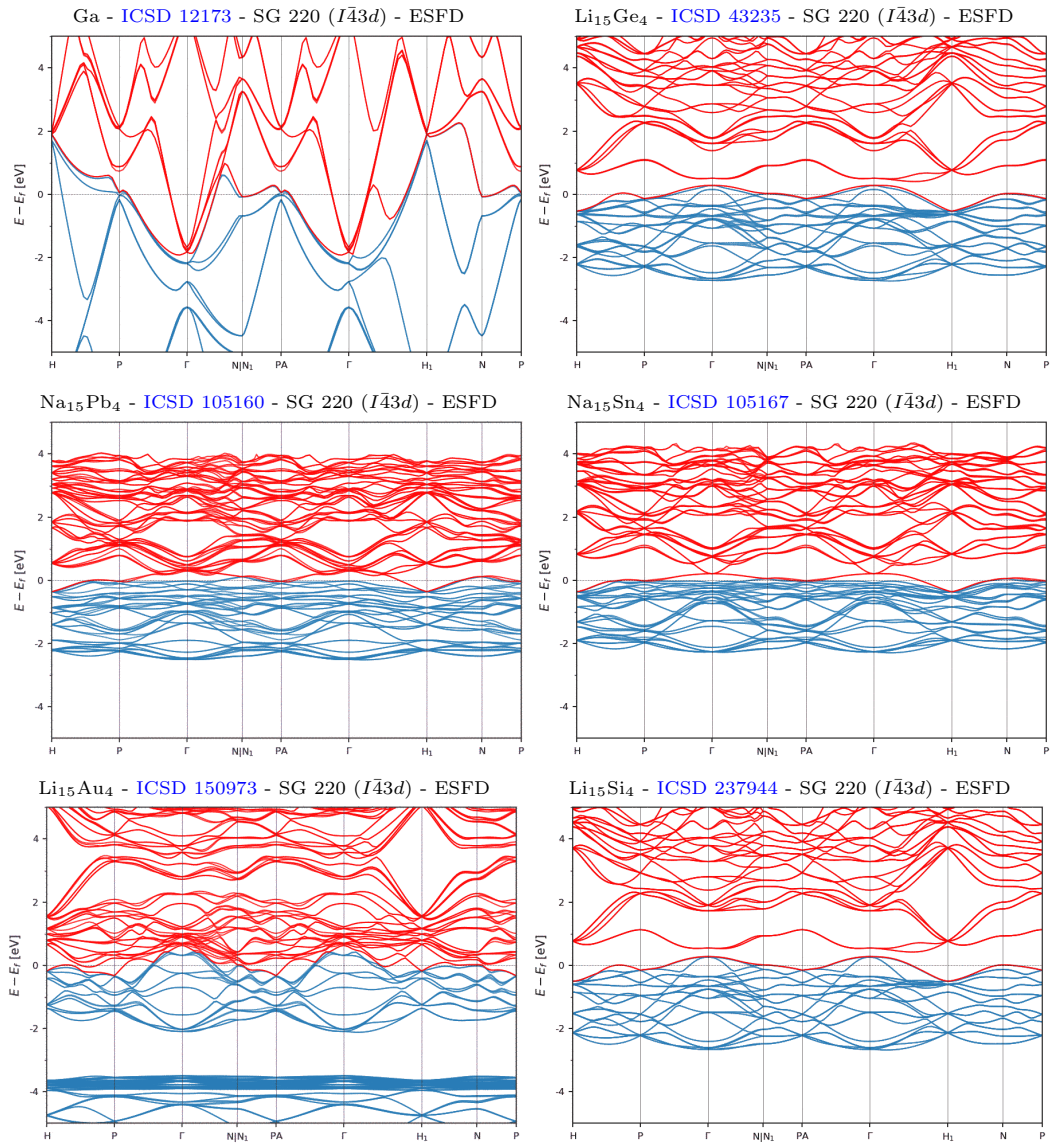


Figure S64. The ESFD-classified topological semimetals with the simplest bulk Fermi surfaces and threefold-degenerate spin-1 fermions close to E_F .

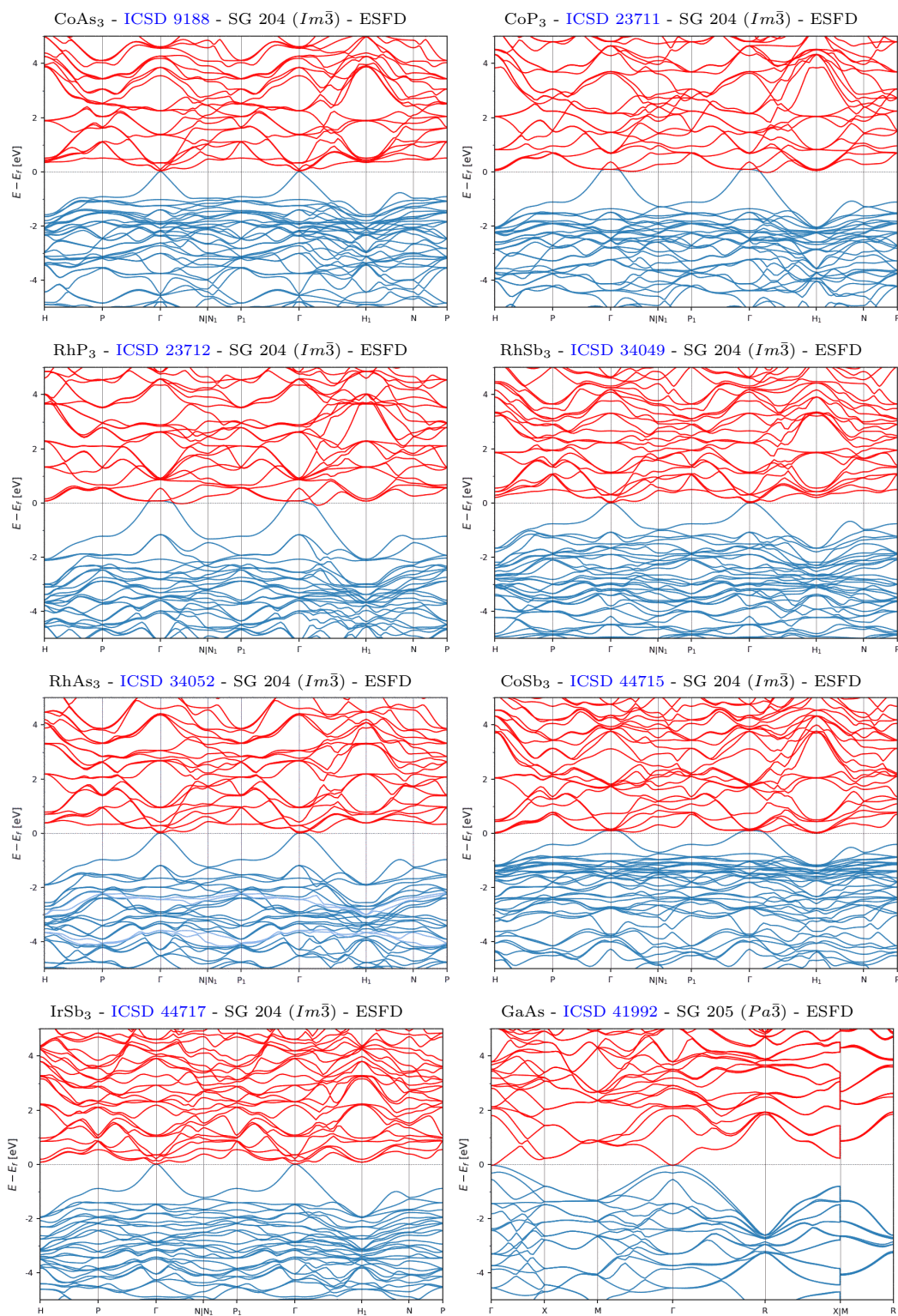


Figure S65. The ESFD-classified topological semimetals with the simplest bulk Fermi surfaces and fourfold-degenerate, achiral spin-3/2 fermions close to E_F . (part 1/10)

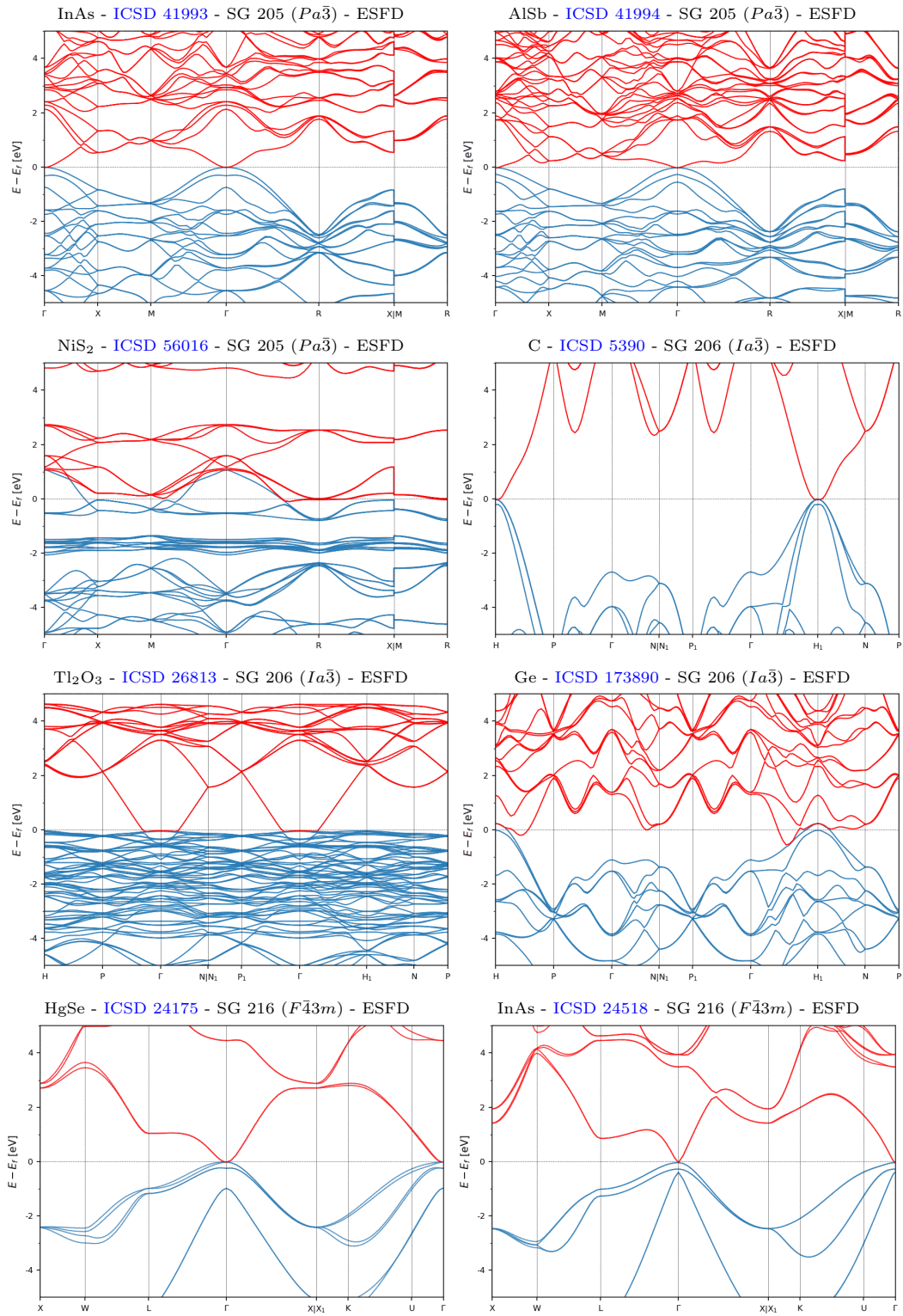


Figure S66. The ESFD-classified topological semimetals with the simplest bulk Fermi surfaces and fourfold-degenerate, achiral spin-3/2 fermions close to E_F . (part 2/10)

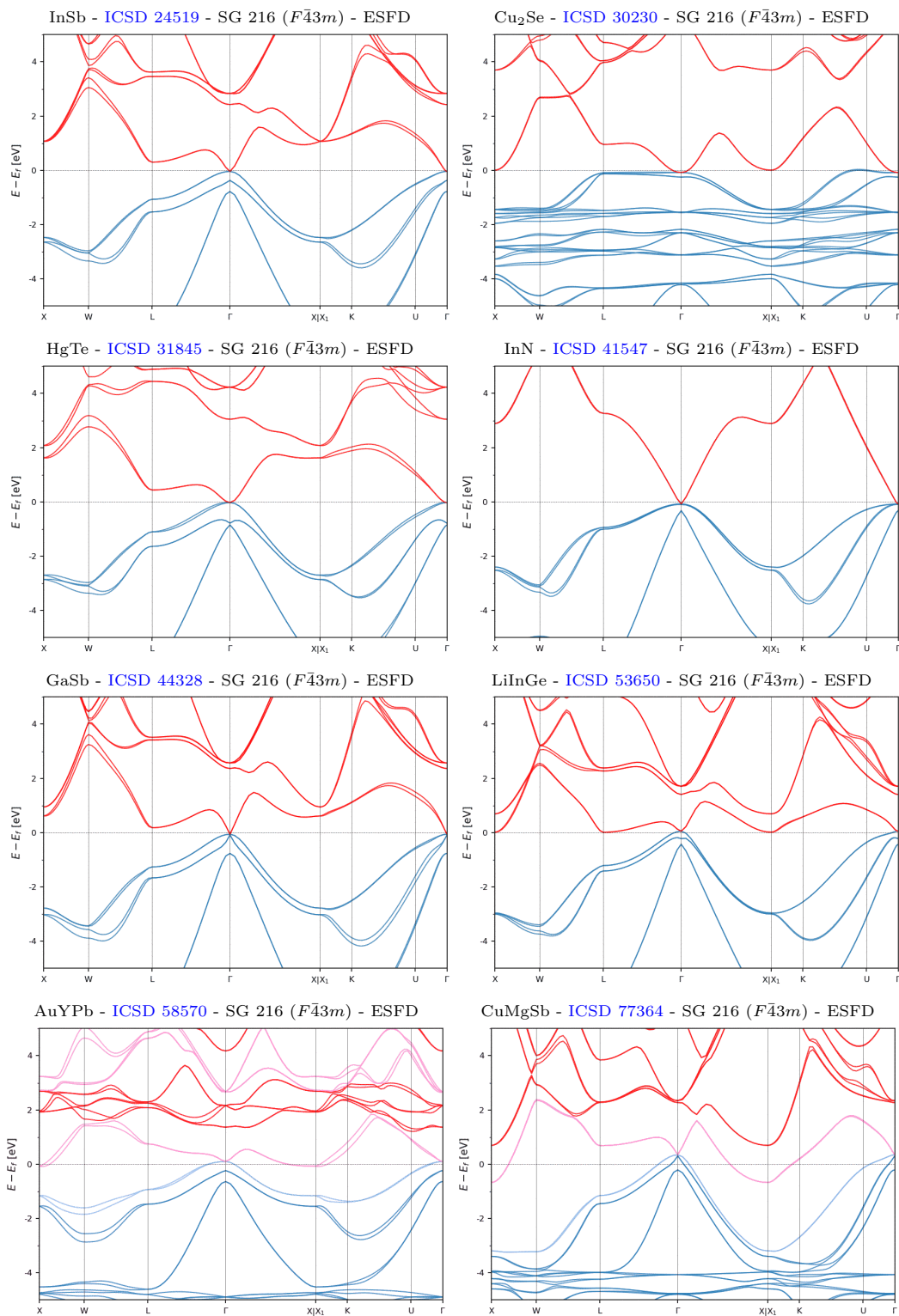


Figure S67. The ESFD-classified topological semimetals with the simplest bulk Fermi surfaces and fourfold-degenerate, achiral spin-3/2 fermions close to E_F . (part 3/10)

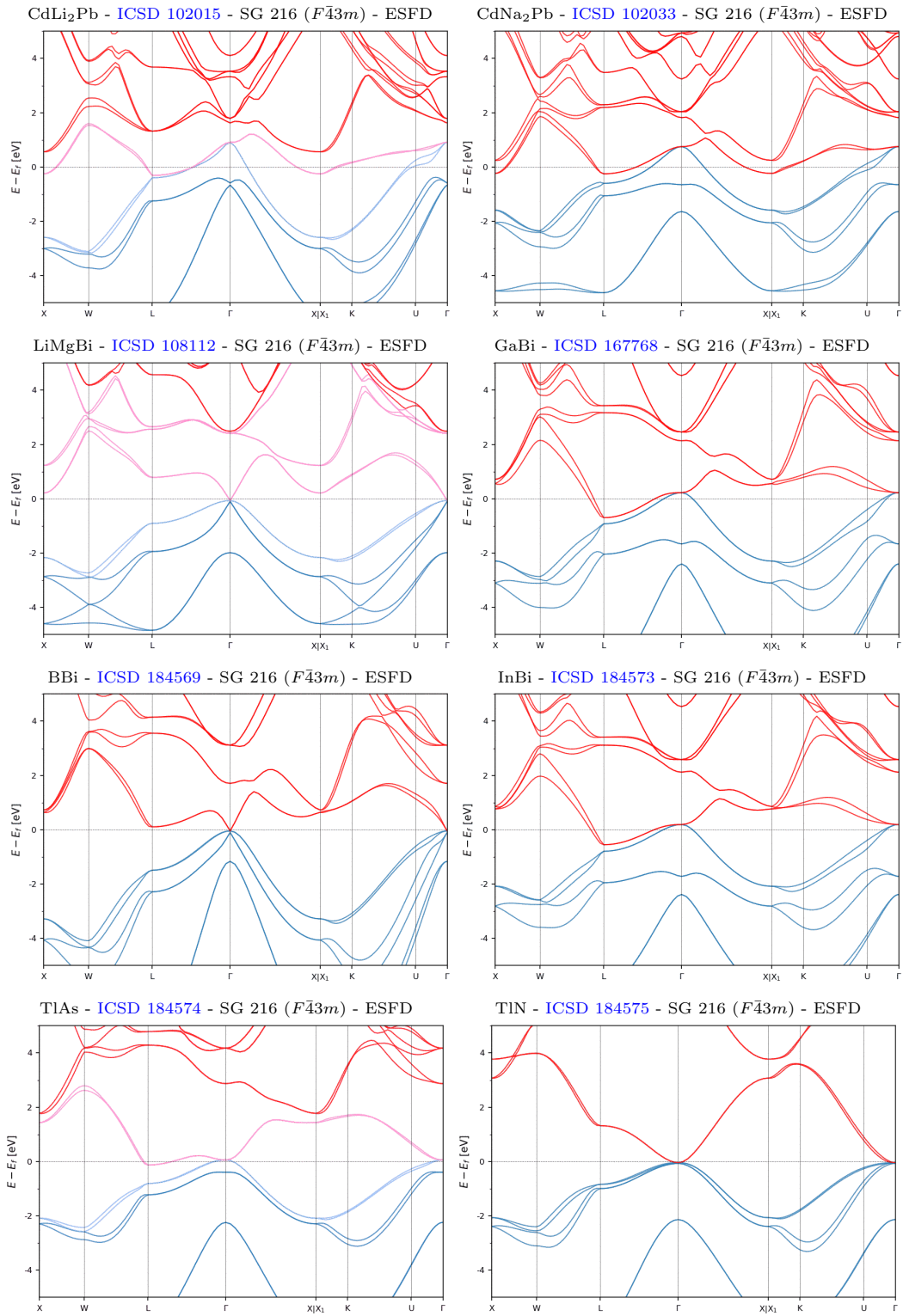


Figure S68. The ESFD-classified topological semimetals with the simplest bulk Fermi surfaces and fourfold-degenerate, achiral spin-3/2 fermions close to E_F . (part 4/10)

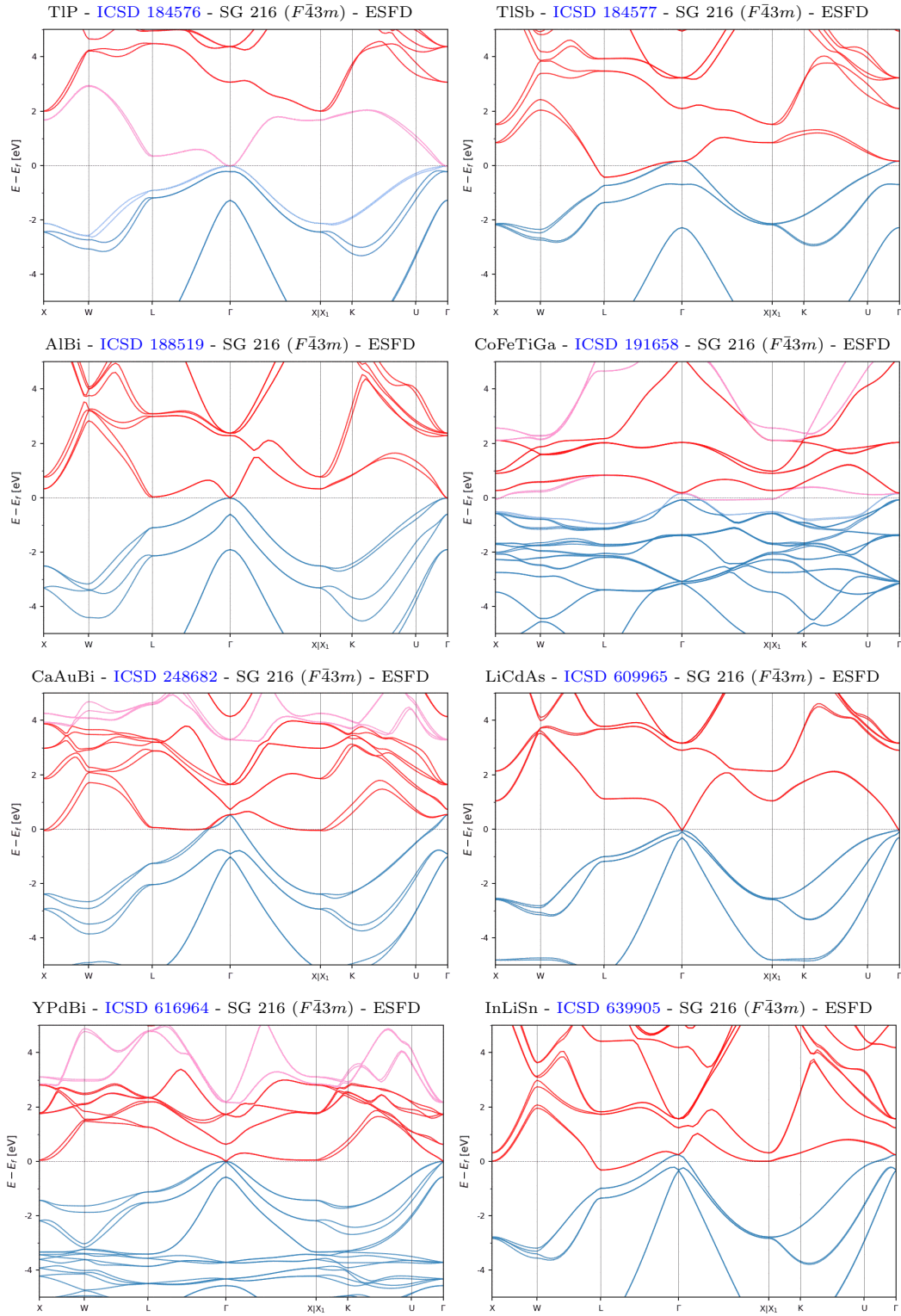


Figure S69. The ESFD-classified topological semimetals with the simplest bulk Fermi surfaces and fourfold-degenerate, achiral spin-3/2 fermions close to E_F . (part 5/10)

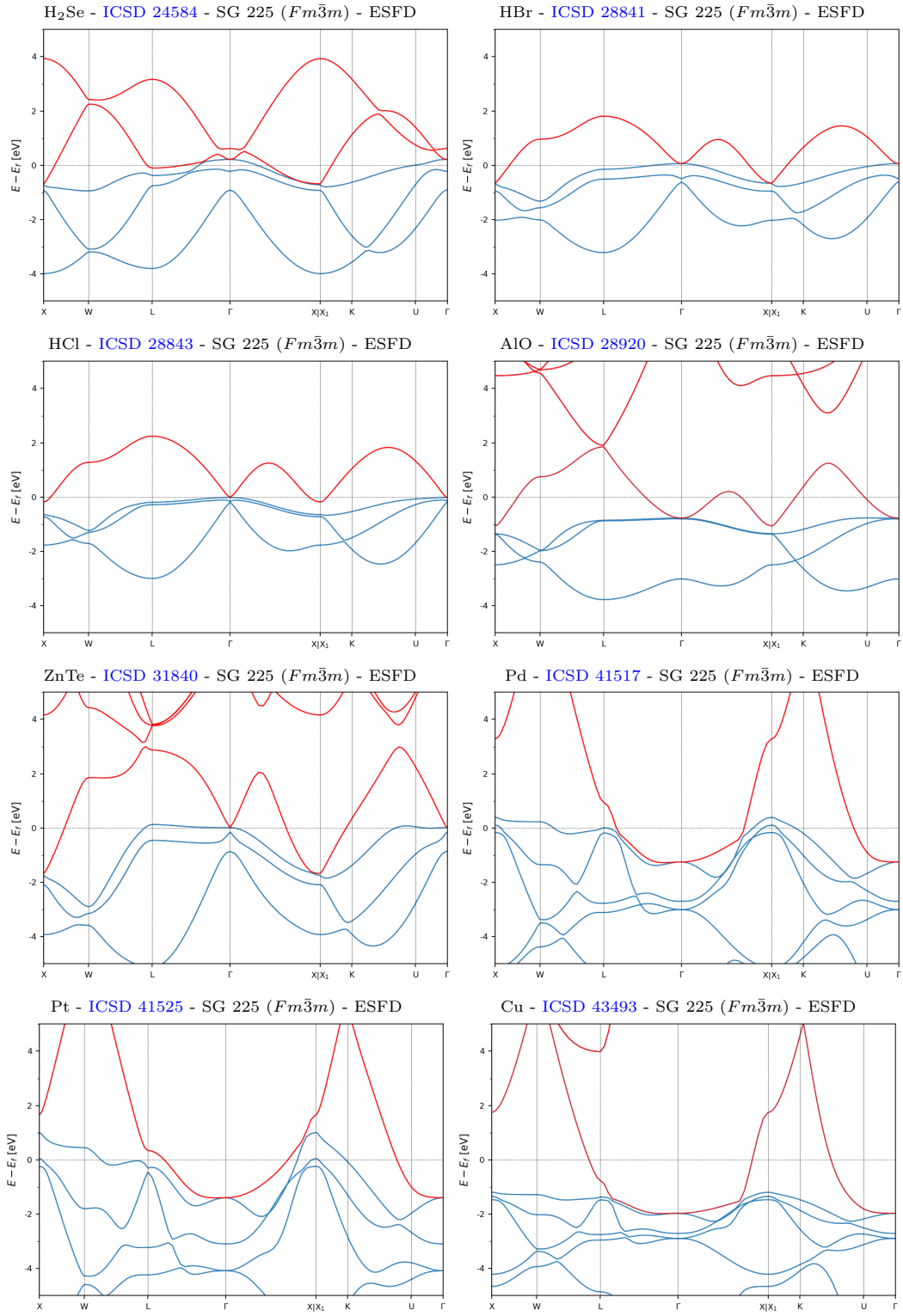


Figure S70. The ESFD-classified topological semimetals with the simplest bulk Fermi surfaces and fourfold-degenerate, achiral spin-3/2 fermions close to E_F . (part 6/10)

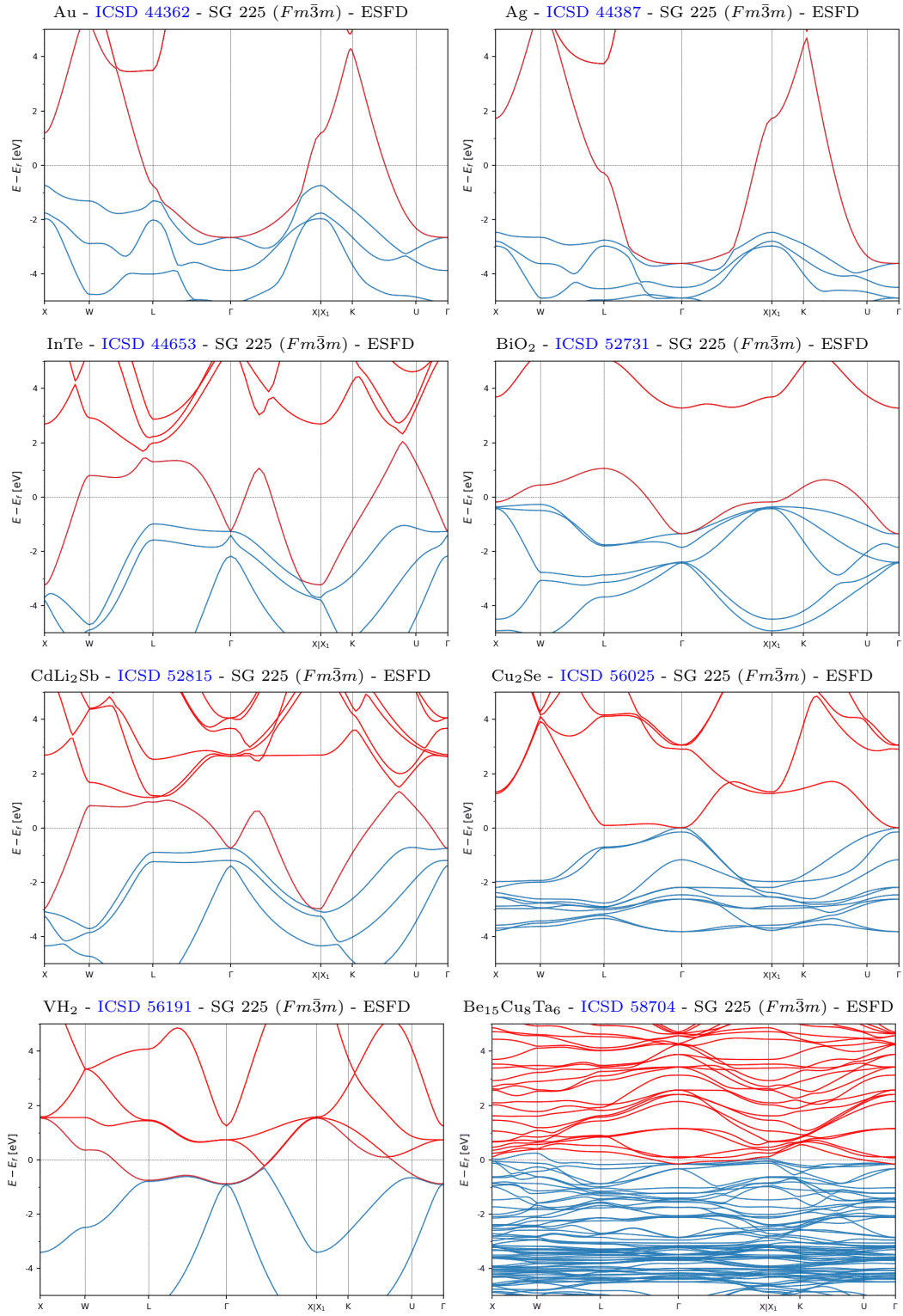


Figure S71. The ESFD-classified topological semimetals with the simplest bulk Fermi surfaces and fourfold-degenerate, achiral spin-3/2 fermions close to E_F . (part 7/10)

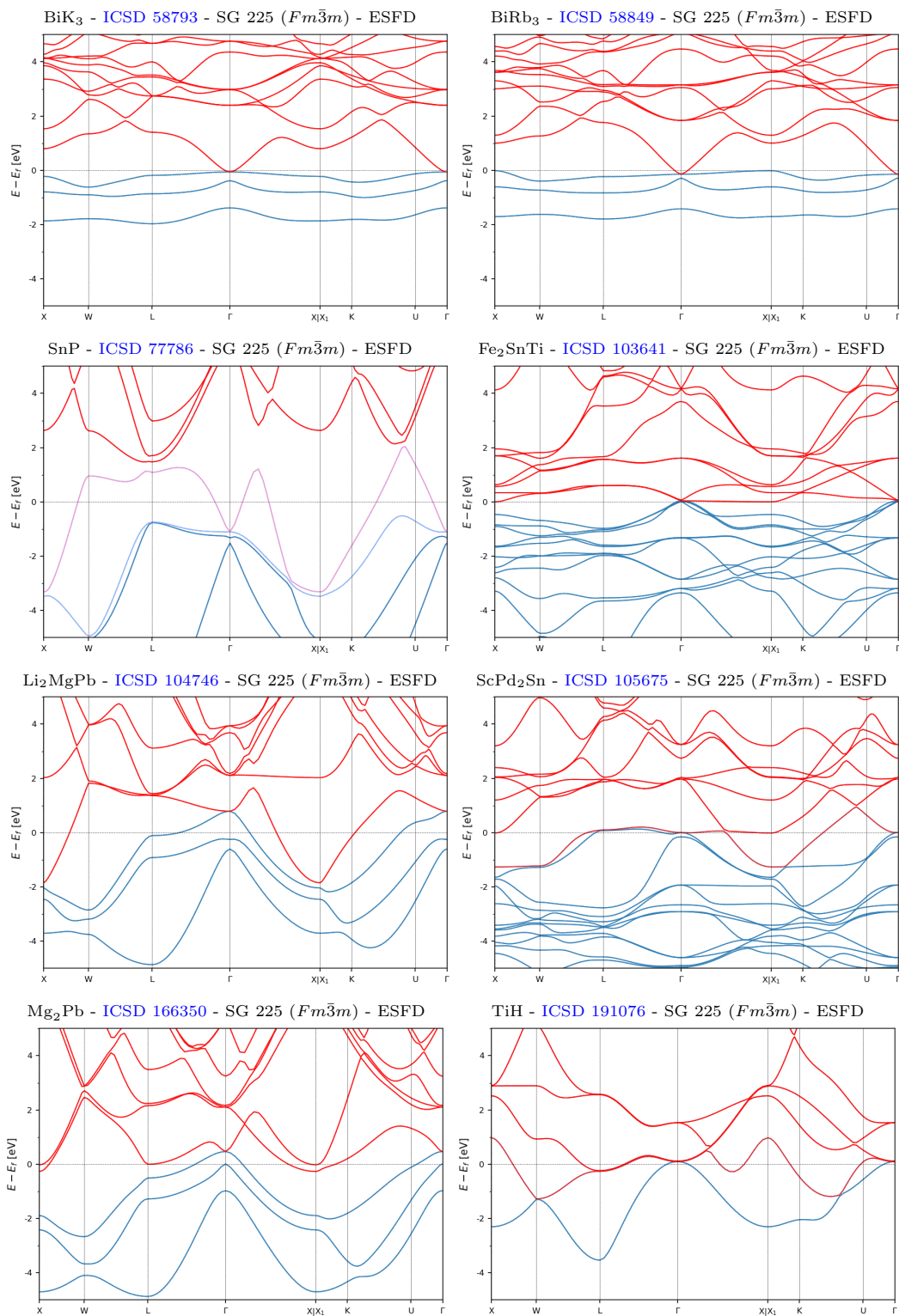


Figure S72. The ESFD-classified topological semimetals with the simplest bulk Fermi surfaces and fourfold-degenerate, achiral spin-3/2 fermions close to E_F . (part 8/10)

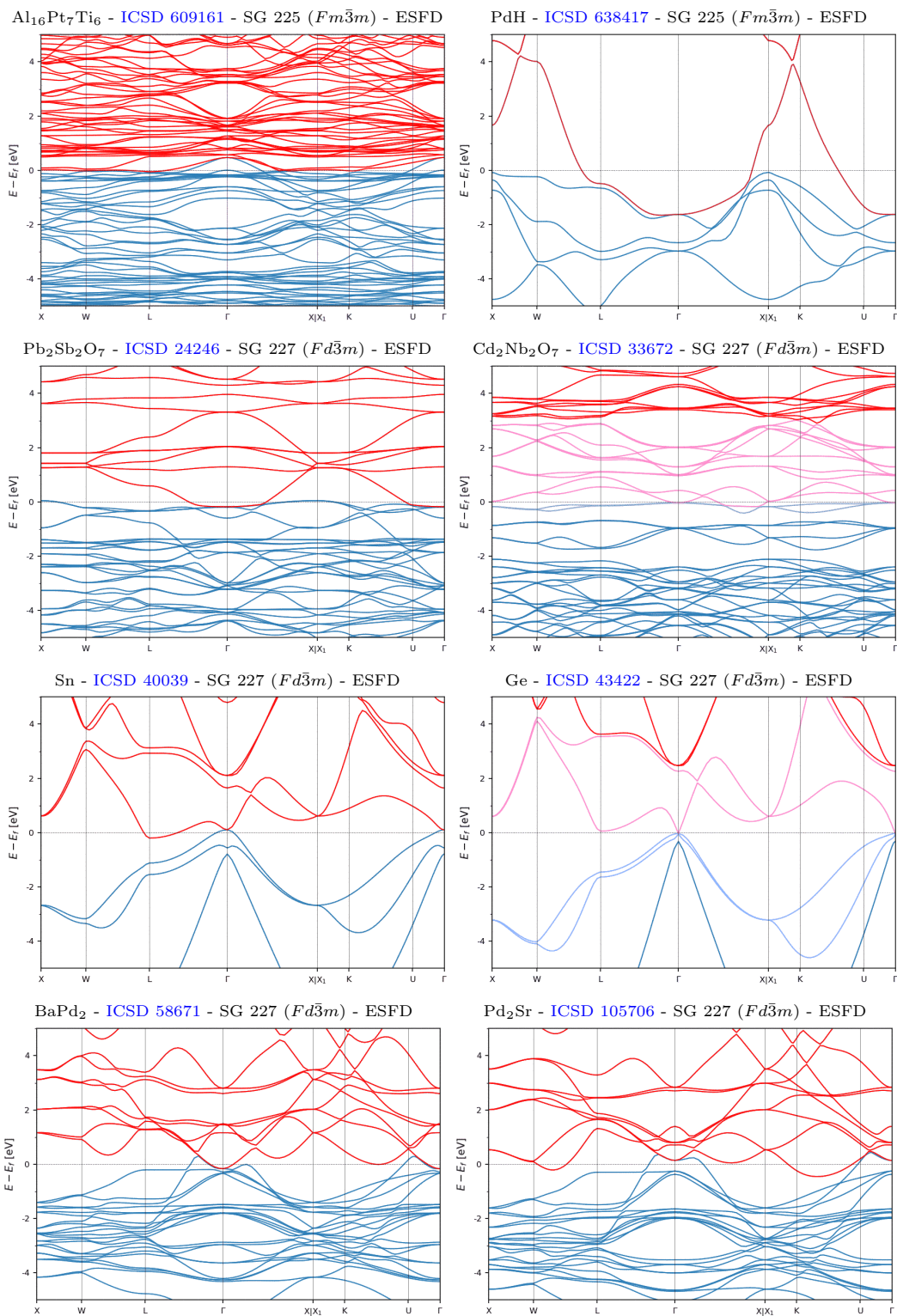


Figure S73. The ESFD-classified topological semimetals with the simplest bulk Fermi surfaces and fourfold-degenerate, achiral spin-3/2 fermions close to E_F . (part 9/10)

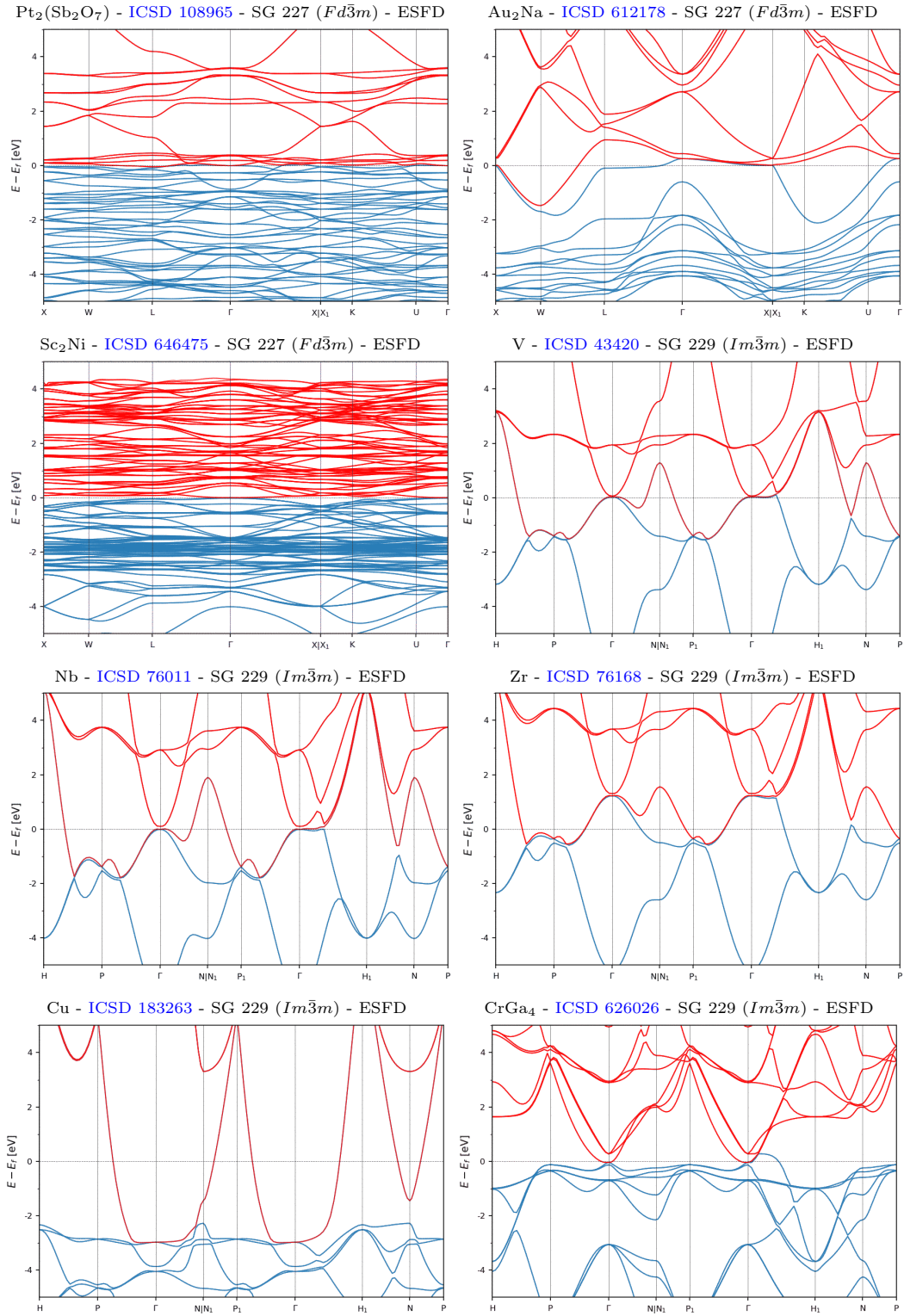


Figure S74. The ESFD-classified topological semimetals with the simplest bulk Fermi surfaces and fourfold-degenerate, achiral spin-3/2 fermions close to E_F . (part 10/10)

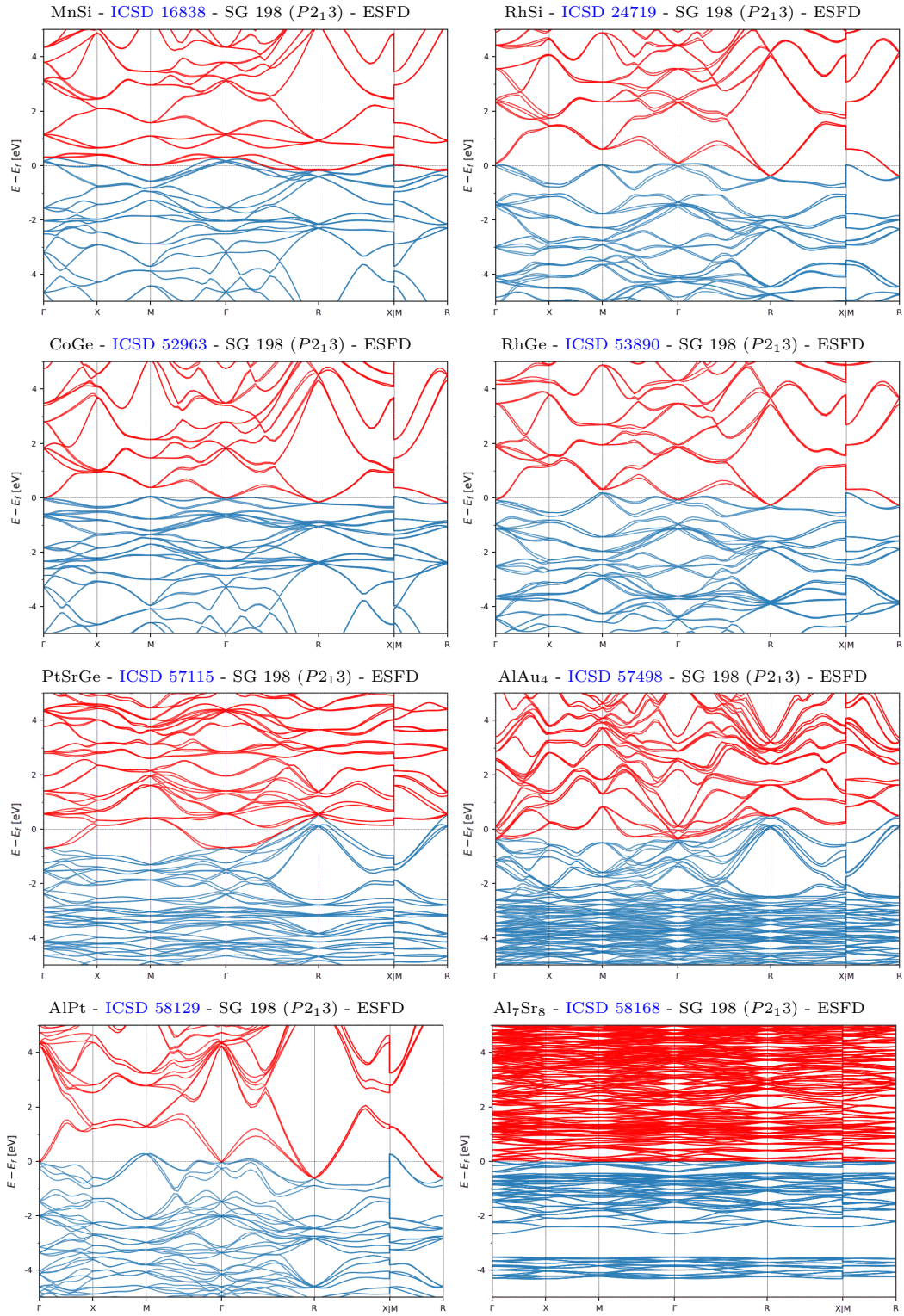


Figure S75. The ESFD-classified topological semimetals in chiral space groups with the simplest bulk Fermi surfaces and enforced chiral fermions close to E_F . (part 1/6)

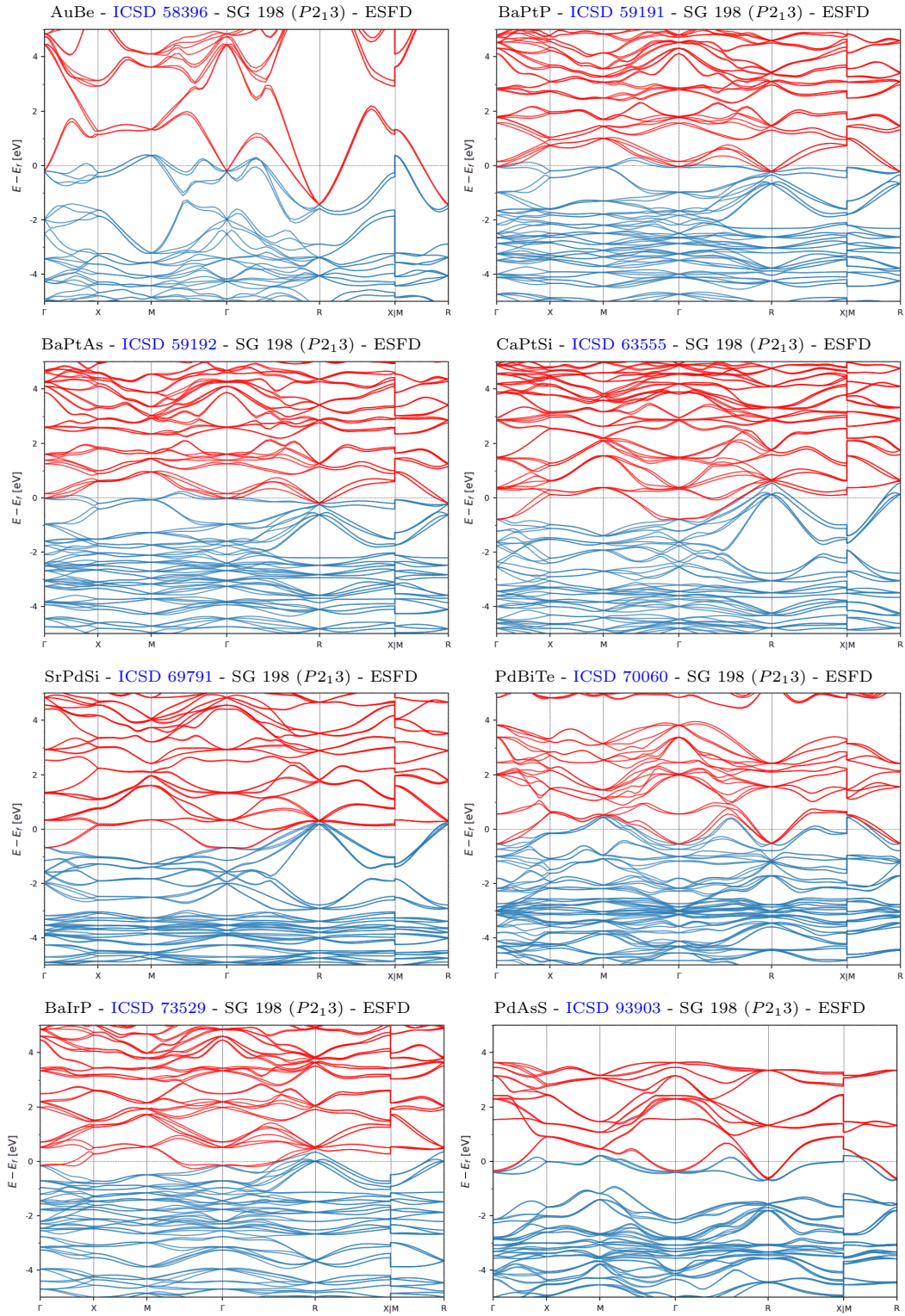


Figure S76. The ESFD-classified topological semimetals in chiral space groups with the simplest bulk Fermi surfaces and enforced chiral fermions close to E_F . (part 2/6)

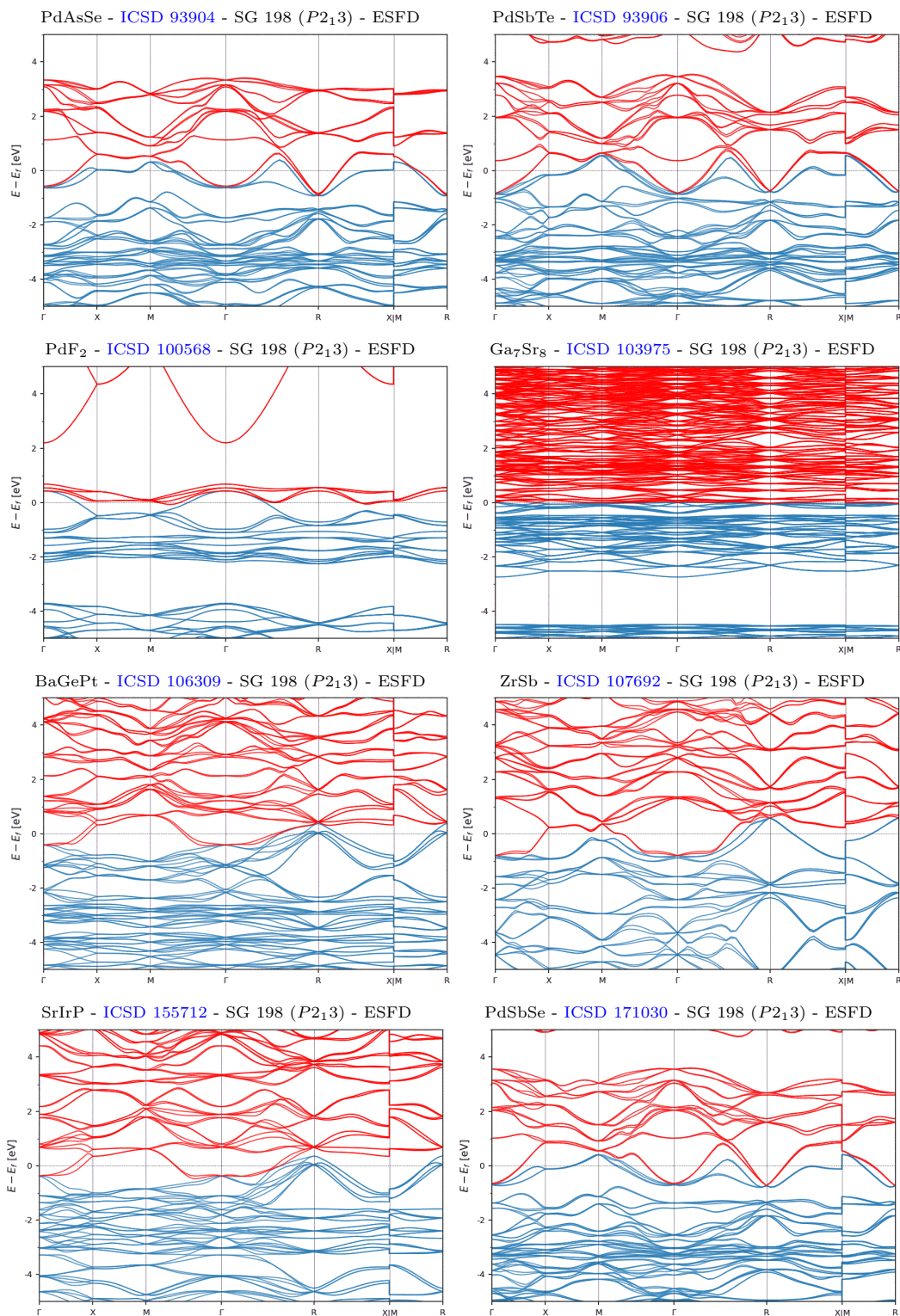


Figure S77. The ESFD-classified topological semimetals in chiral space groups with the simplest bulk Fermi surfaces and enforced chiral fermions close to E_F . (part 3/6)

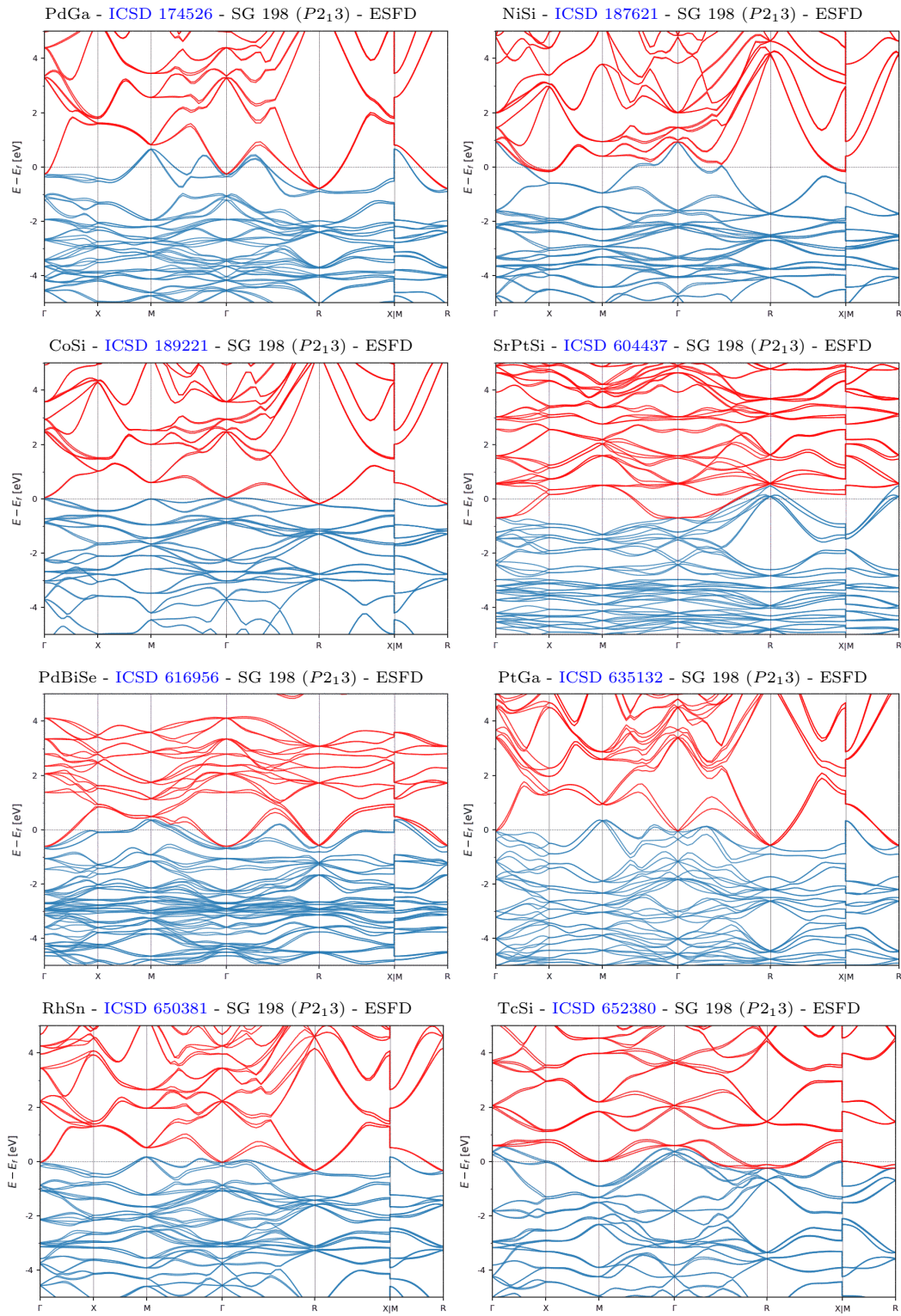


Figure S78. The ESFD-classified topological semimetals in chiral space groups with the simplest bulk Fermi surfaces and enforced chiral fermions close to E_F . (part 4/6)

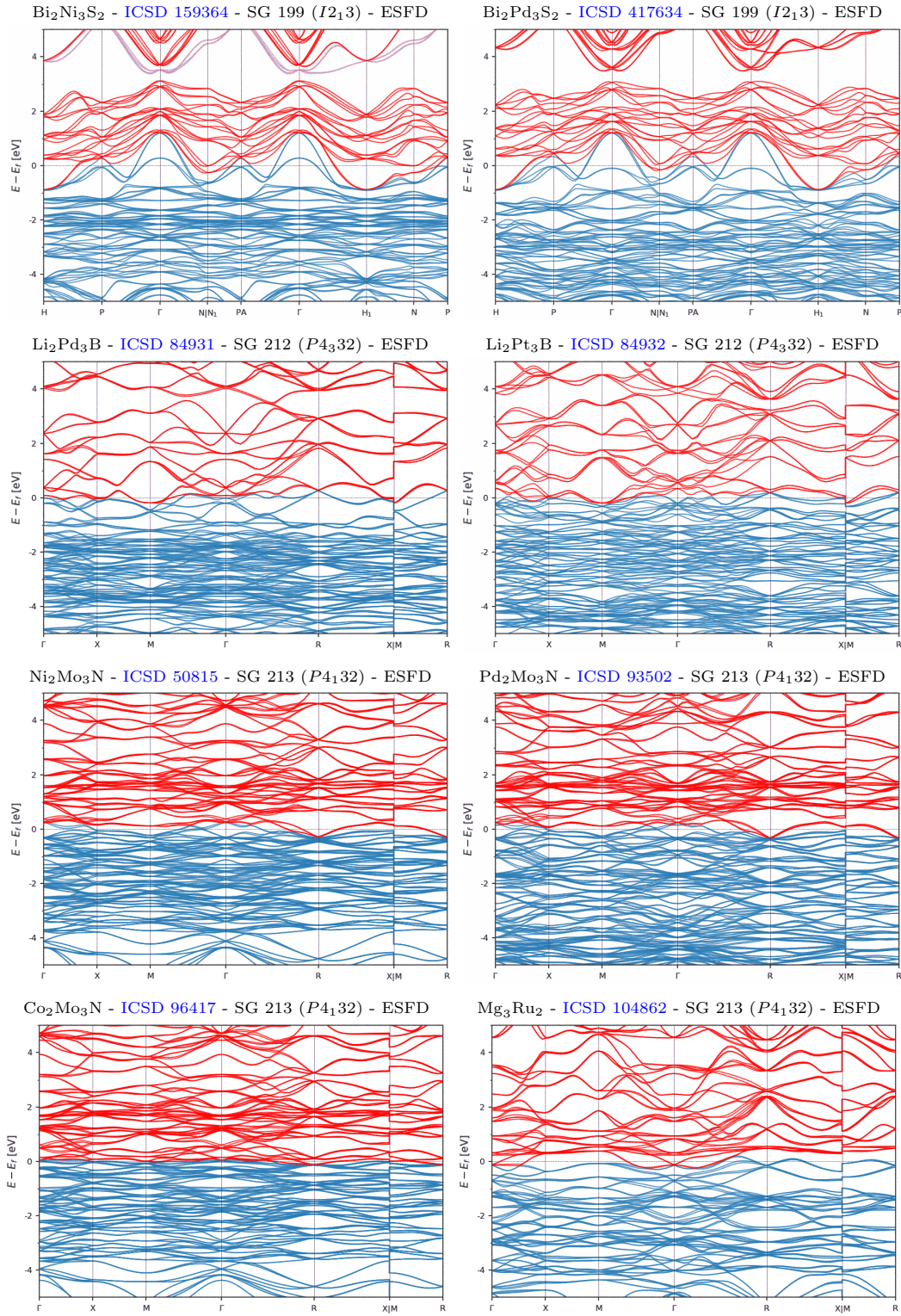


Figure S79. The ESFD-classified topological semimetals in chiral space groups with the simplest bulk Fermi surfaces and enforced chiral fermions close to E_F . (part 5/6)

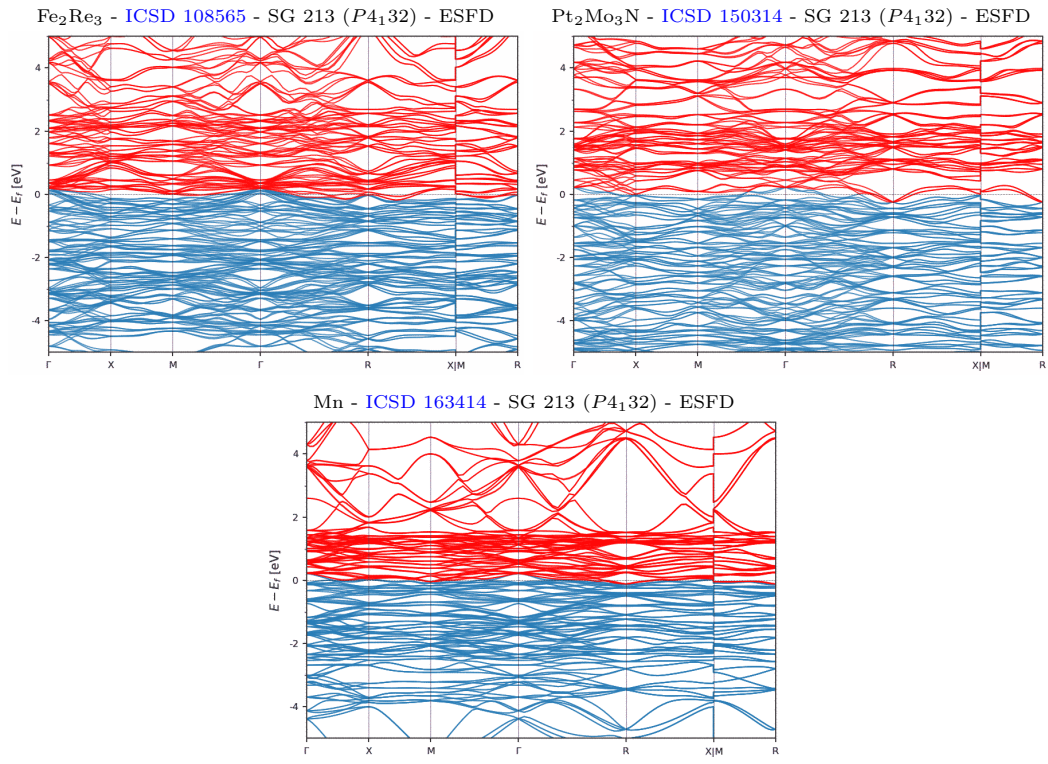


Figure S80. The ESFD-classified topological semimetals in chiral space groups with the simplest bulk Fermi surfaces and enforced chiral fermions close to E_F . (part 6/6)

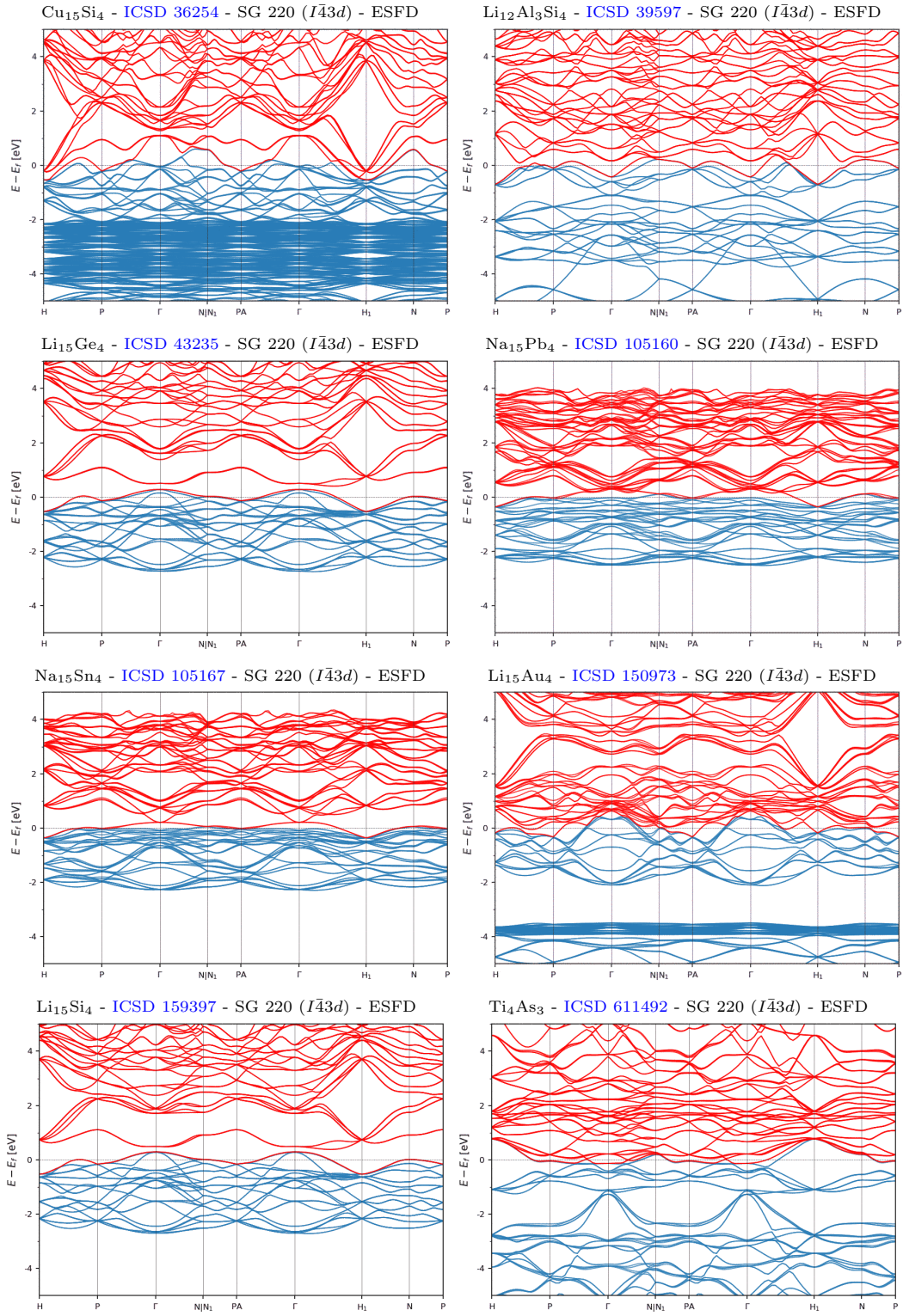


Figure S81. The ESFD-classified topological semimetals with the simplest bulk Fermi surfaces and eightfold-degenerate double Dirac fermions close to E_F . (part 1/3)

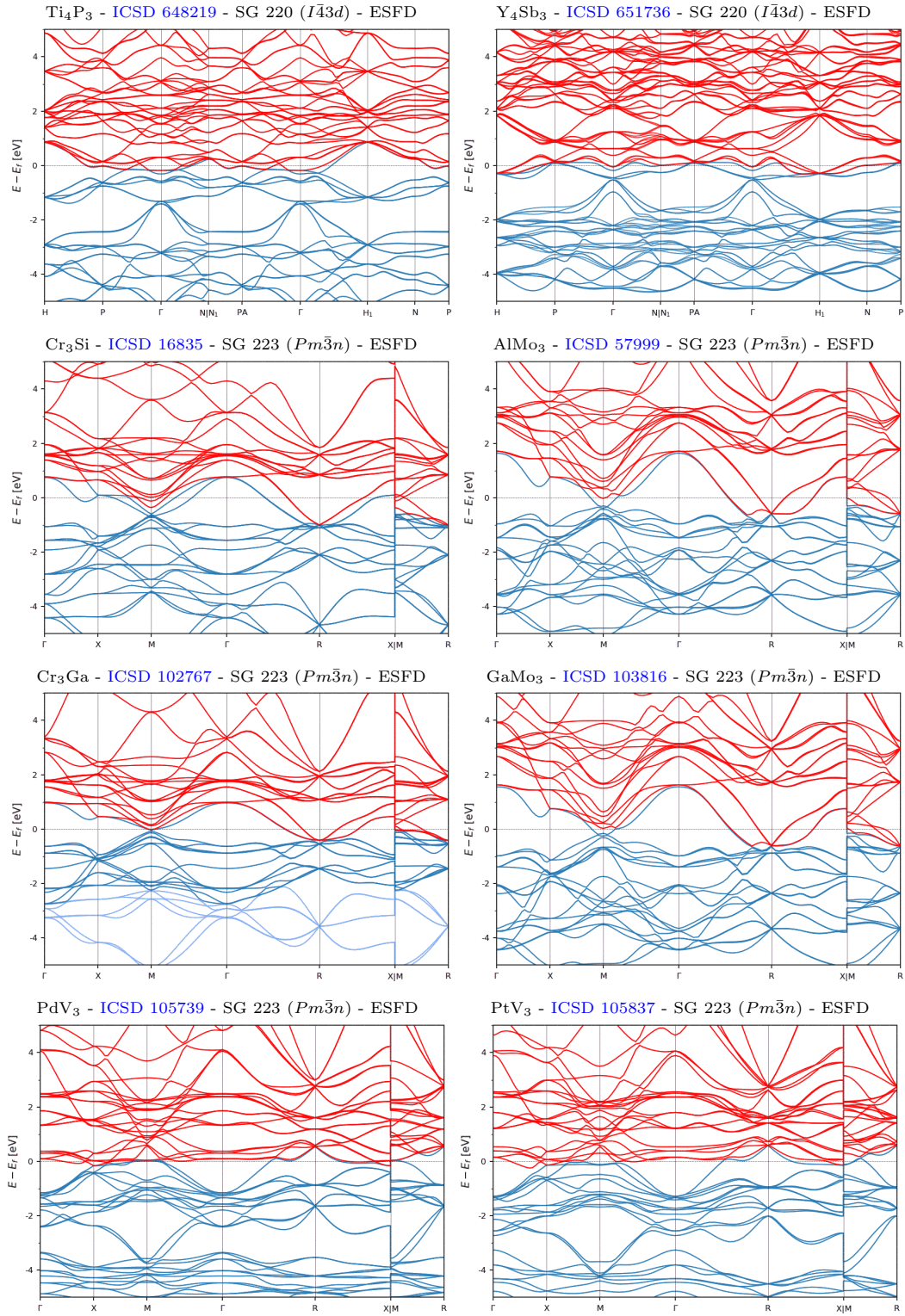


Figure S82. The ESFD-classified topological semimetals with the simplest bulk Fermi surfaces and eightfold-degenerate double Dirac fermions close to E_F . (part 2/3)

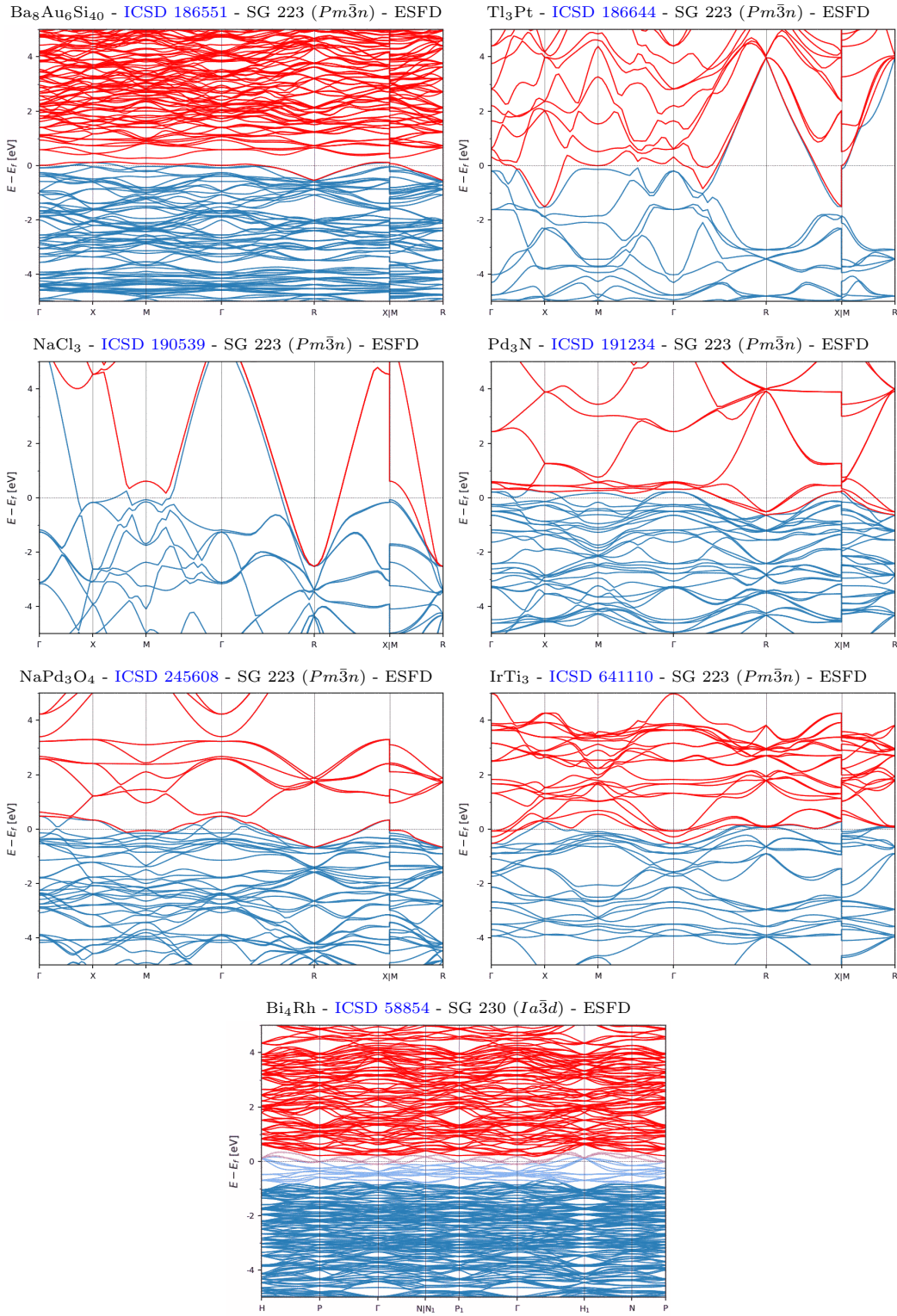


Figure S83. The ESFD-classified topological semimetals with the simplest bulk Fermi surfaces and eightfold-degenerate double Dirac fermions close to E_F . (part 3/3)

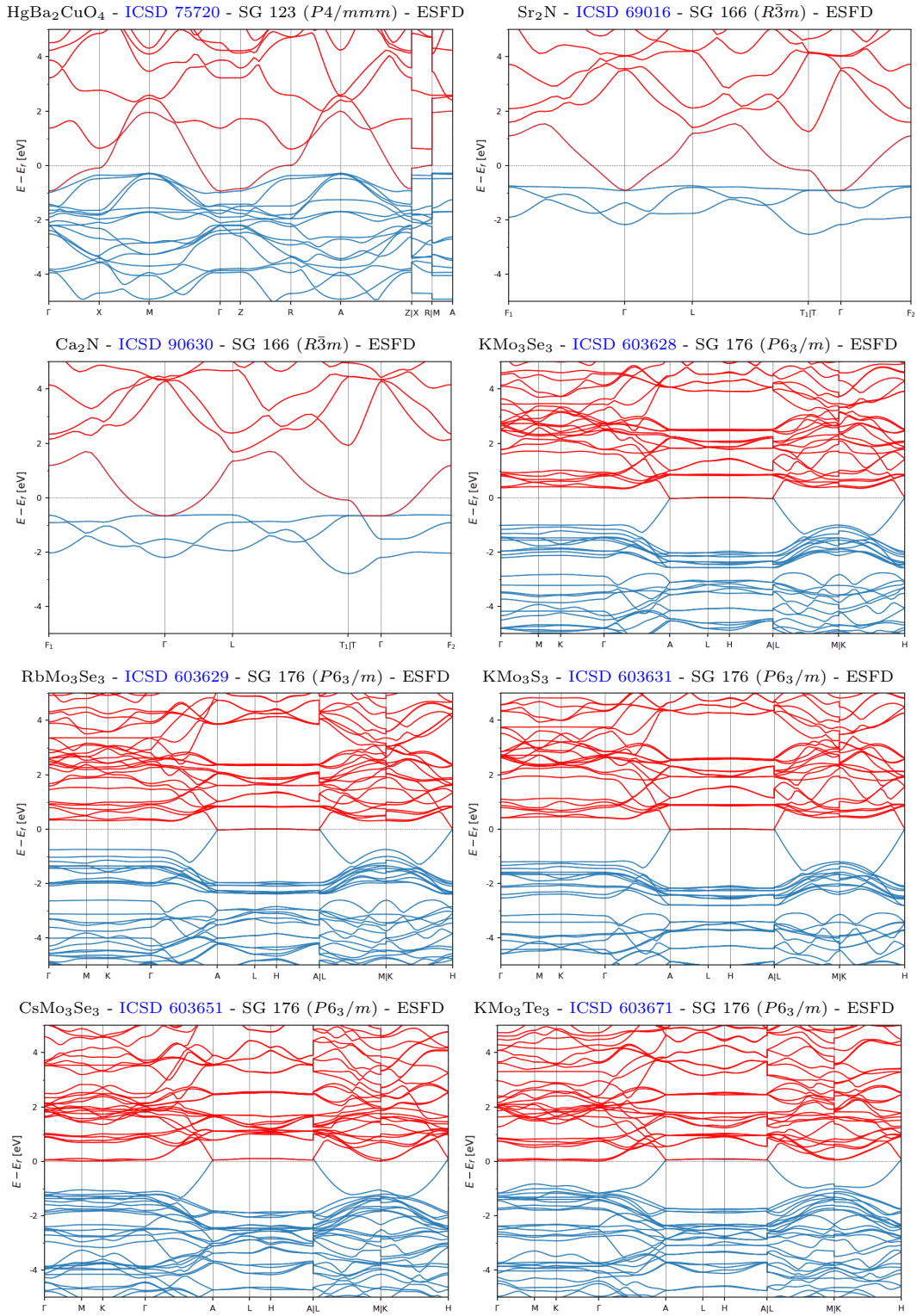


Figure S84. The ESFD-classified topological semimetals with the simplest bulk Fermi surfaces beyond those shown in Figs. S64 through S83. (part 1/2)

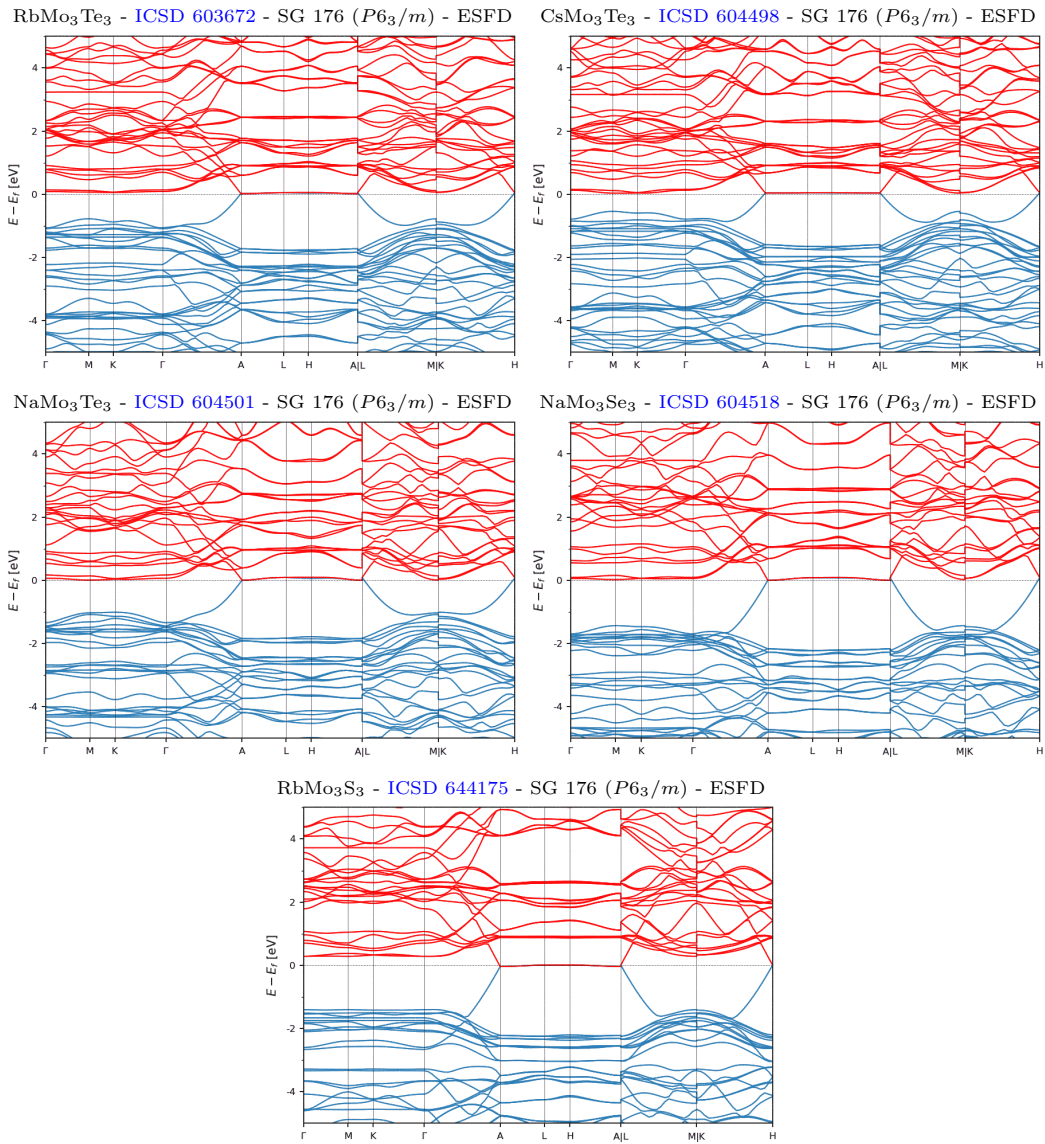


Figure S85. The ESFD-classified topological semimetals with the simplest bulk Fermi surfaces beyond those shown in Figs. S64 through S83. (part 2/2)

2. ES-Classified Semimetals

In this section, we list in Figs. S86, S87, S88, S89, S90, and S91 the enforced semimetals with the simplest bulk Fermi surfaces whose nodal degeneracies lie along high-symmetry BZ lines (ES in the nomenclature established in Ref. 38). Typically, the bulk Fermi pockets of ES materials are characterized by fourfold-degenerate, linearly dispersing Dirac fermions [6, 167, 207, 208]. However, it is also possible for ES materials to host chiral fermions with larger Chern numbers [209–213], threefold-degenerate “nexus” fermions [214–219], or more exotic mixtures of chiral and achiral fermions [220]. Almost all of the materials shown in Figs. S86, S87, S88, S89, S90, and S91 are conventional Dirac semimetals, with two exceptions. First, In_2ZnS_4 [ICSD 15636 and ICSD 65725, SG 160 ($R3m$)] in Fig. S87 is a nexus fermion semimetal with narrowly separated threefold degeneracies. Second, Ta_2ISe_8 [ICSD 35190, SG 97 ($I422$)] in Fig. S86 is a structurally chiral, quasi-1D Weyl semimetal that, as demonstrated in recent theoretical and experimental investigations, becomes gapped by a topological (axionic) charge-density wave when cooled just below room temperature [26, 27, 69, 221–223]. Most notably, Figs. S86 and S90 respectively include the archetypal, experimentally confirmed Dirac semimetals Cd_3As_2 [ICSD 107918, SG 137 ($P4_2/nmc$)] [6, 19, 114, 115] and Na_3Bi [ICSD 26881, SG 194 $P6_3/mmc$] [167, 171, 172]. As recently shown in Ref. 58, Dirac points with $4mm$ or higher symmetry also exhibit topological hinge states; because a significant number of the Dirac semimetals in Figs. S86, S87, S88, S89, S90, and S91 have SGs whose point groups contain $4mm$, then the listed Dirac semimetals may also be classified as higher-order topological semimetals. Finally, the results of Refs. 34, 58, 95, 224–230 also imply the presence of hinge states in additional ES materials without fourfold symmetry, including the materials shown in Figs. S86, S87, S88, S89, S90, and S91 with threefold or sixfold rotational symmetries.

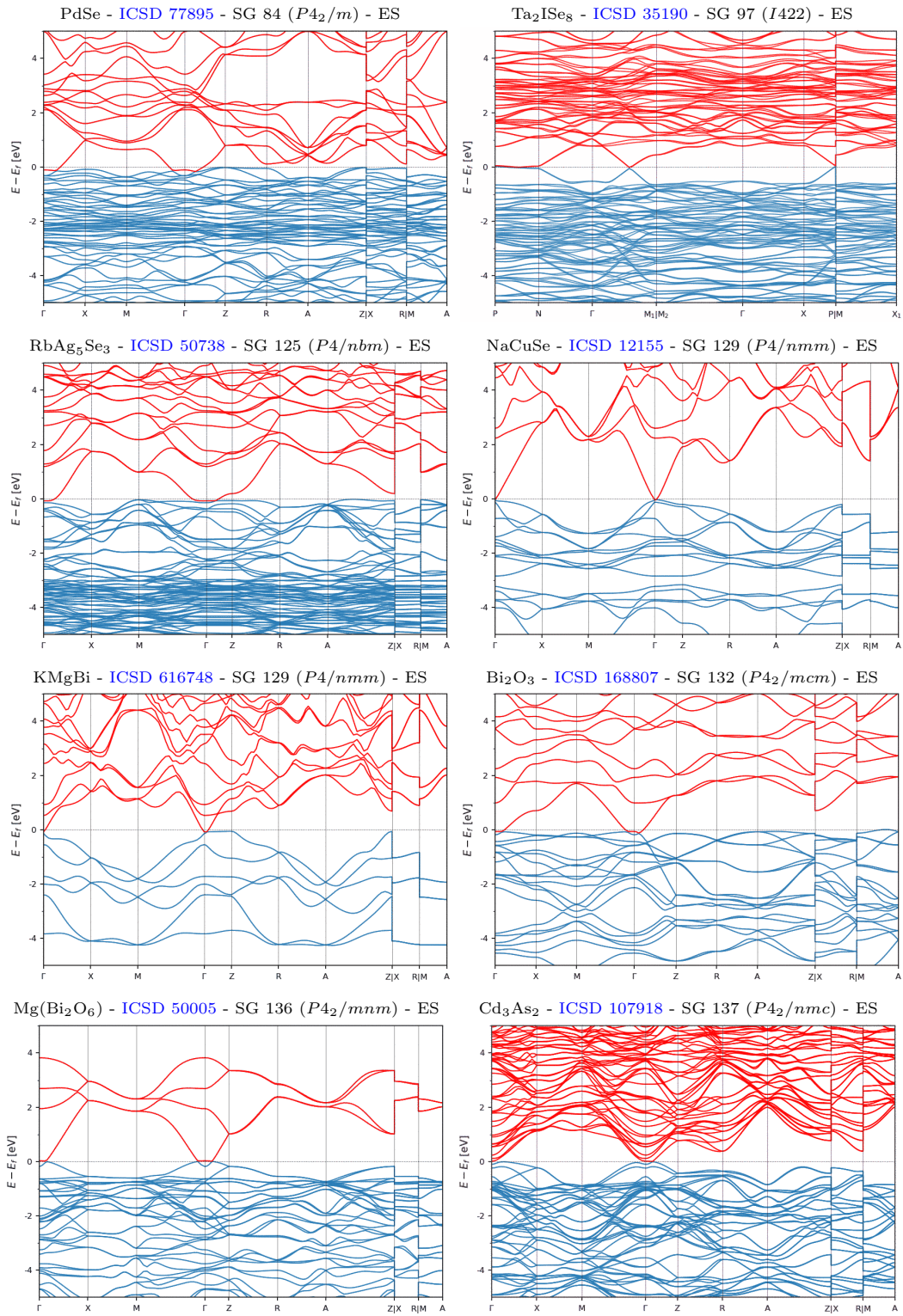


Figure S86. The ES-classified topological semimetals with the simplest bulk Fermi surfaces. (part 1/6)

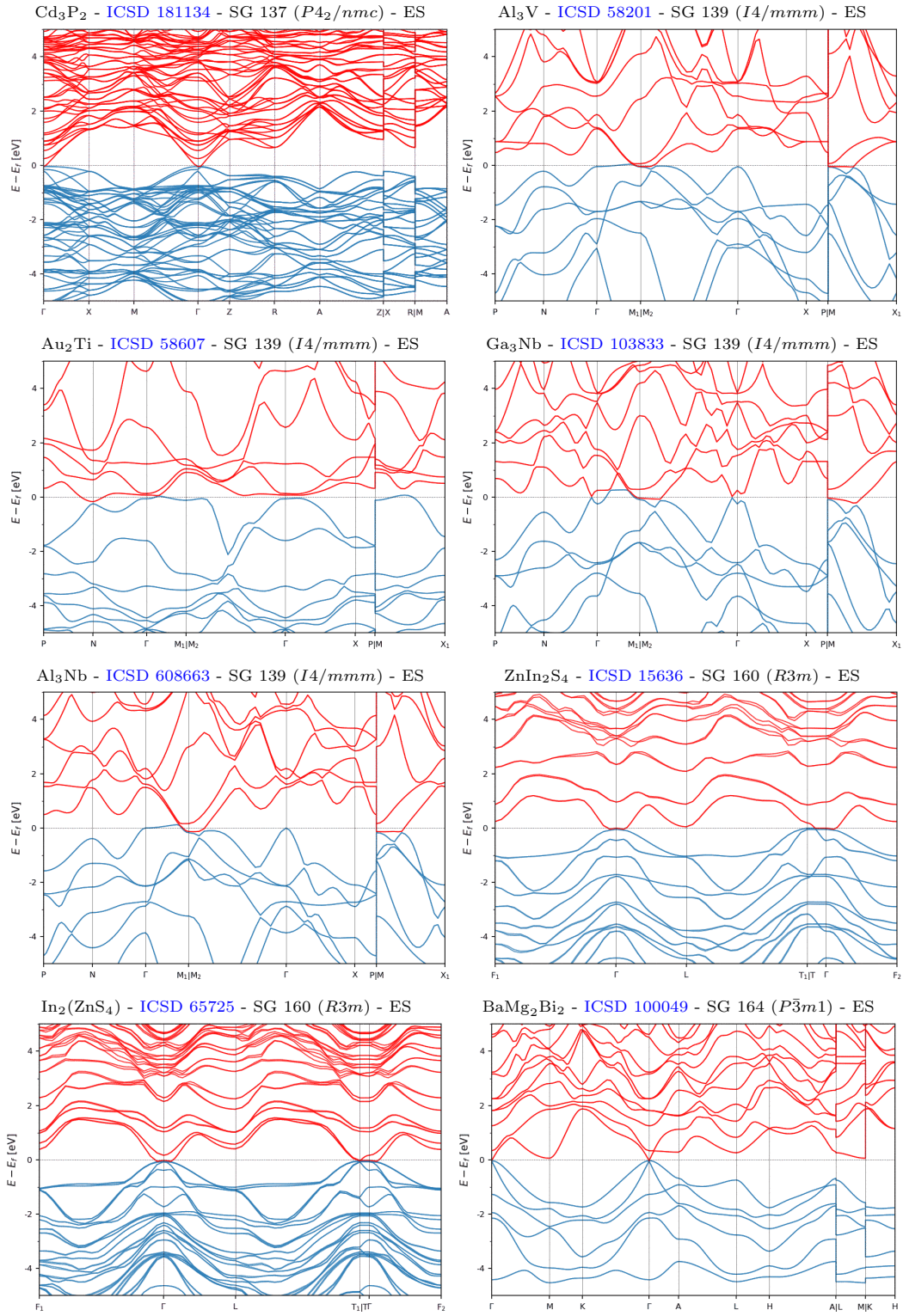


Figure S87. The ES-classified topological semimetals with the simplest bulk Fermi surfaces. (part 2/6)

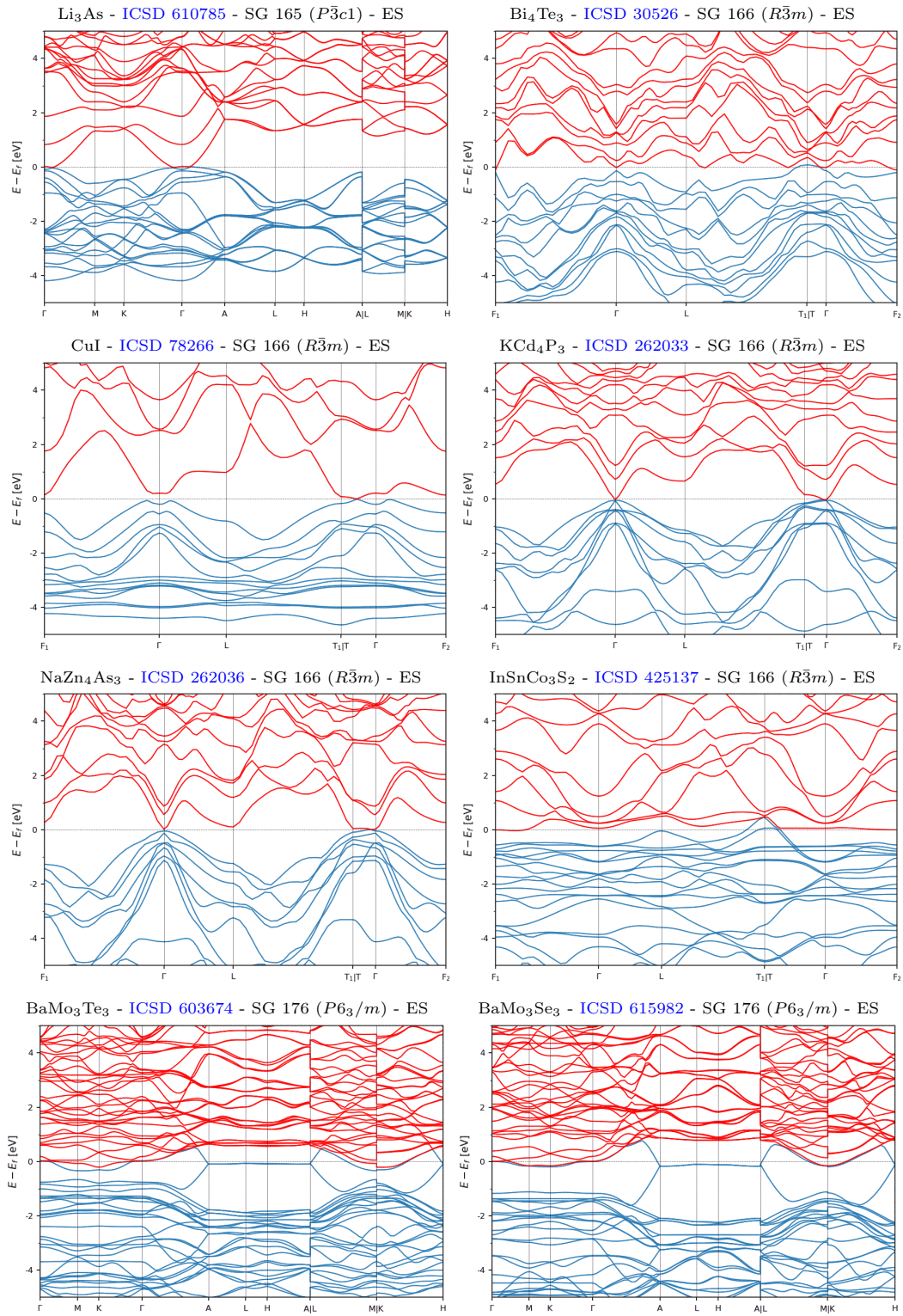


Figure S88. The ES-classified topological semimetals with the simplest bulk Fermi surfaces. (part 3/6)

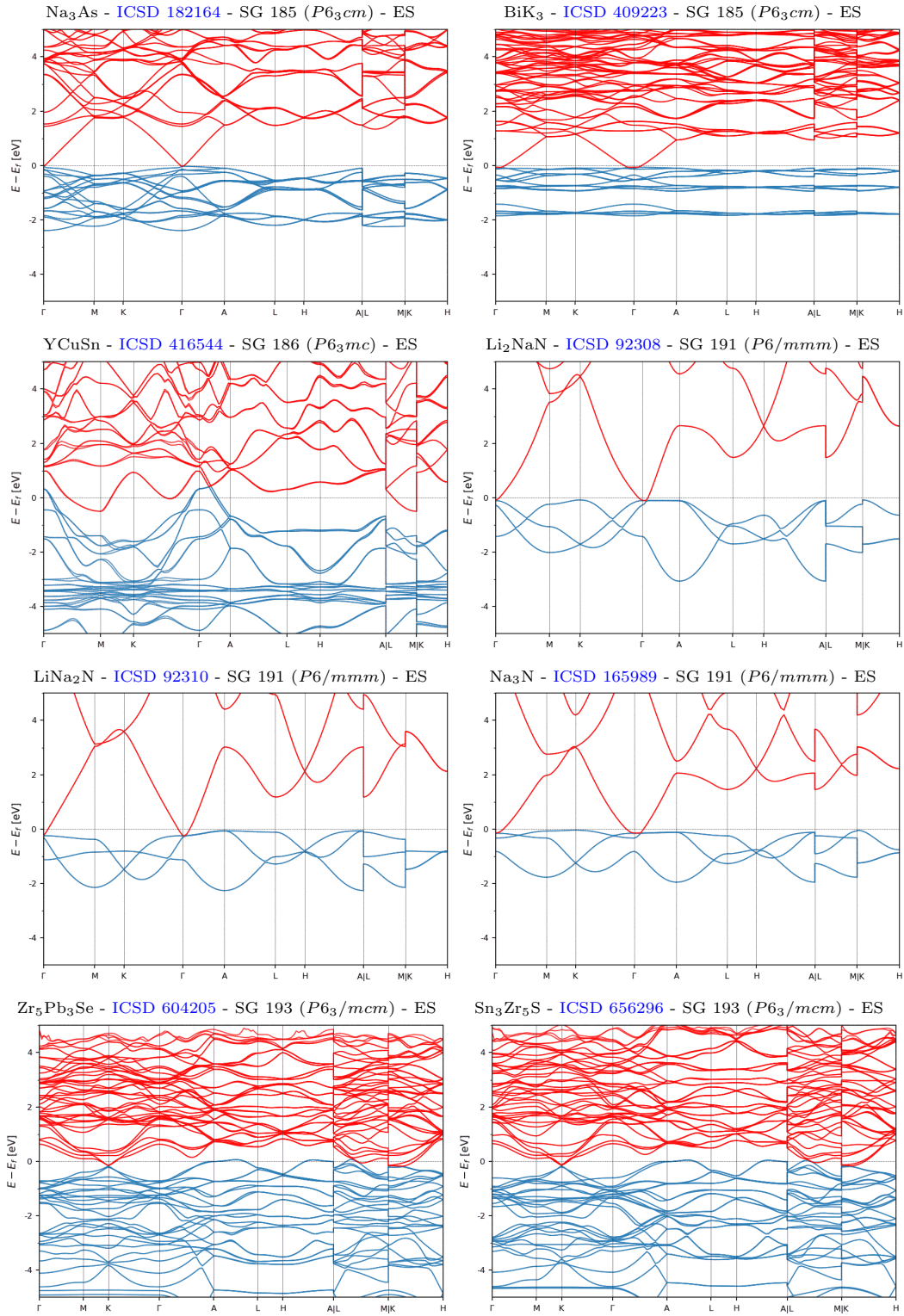


Figure S89. The ES-classified topological semimetals with the simplest bulk Fermi surfaces. (part 4/6)

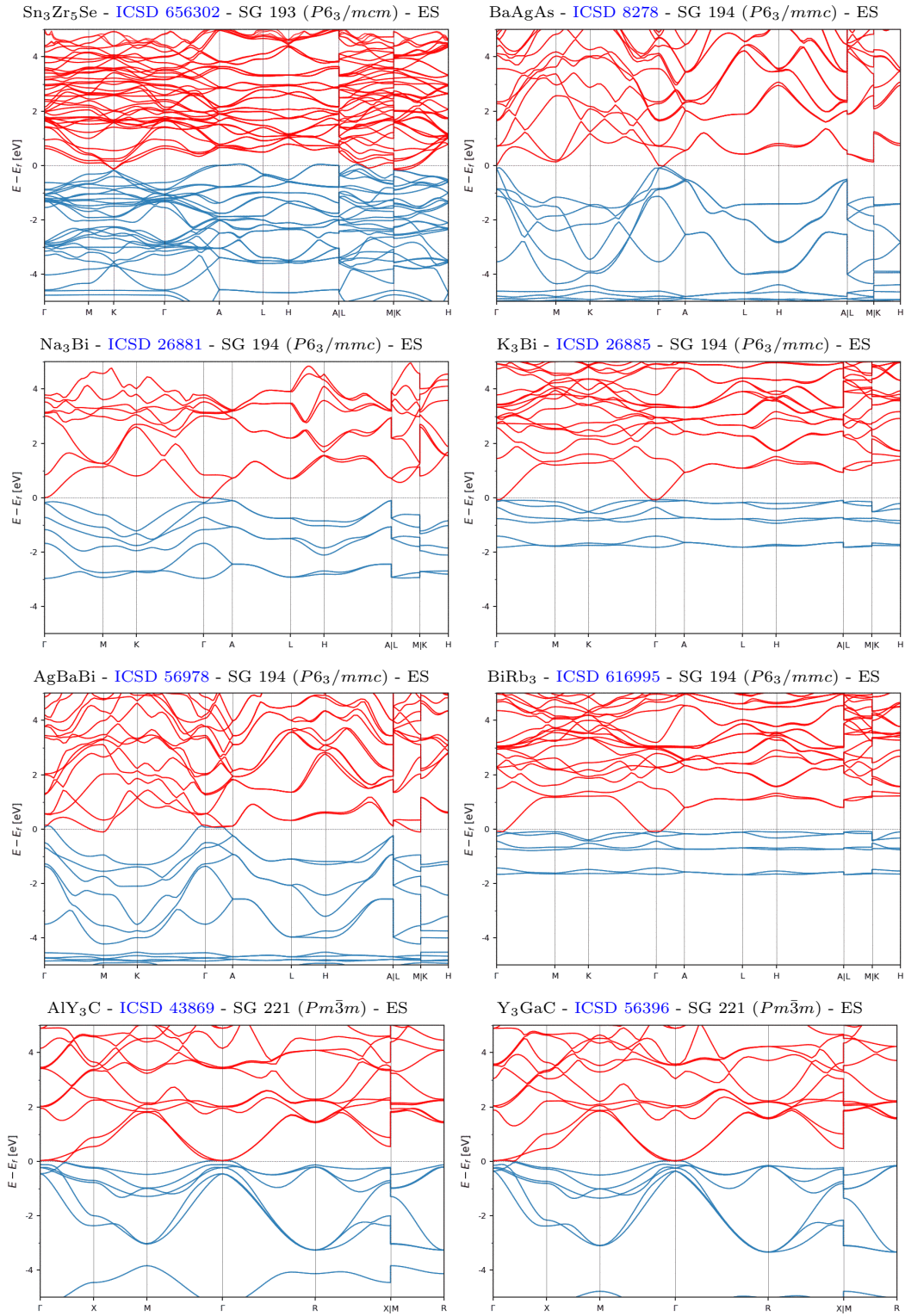


Figure S90. The ES-classified topological semimetals with the simplest bulk Fermi surfaces. (part 5/6)

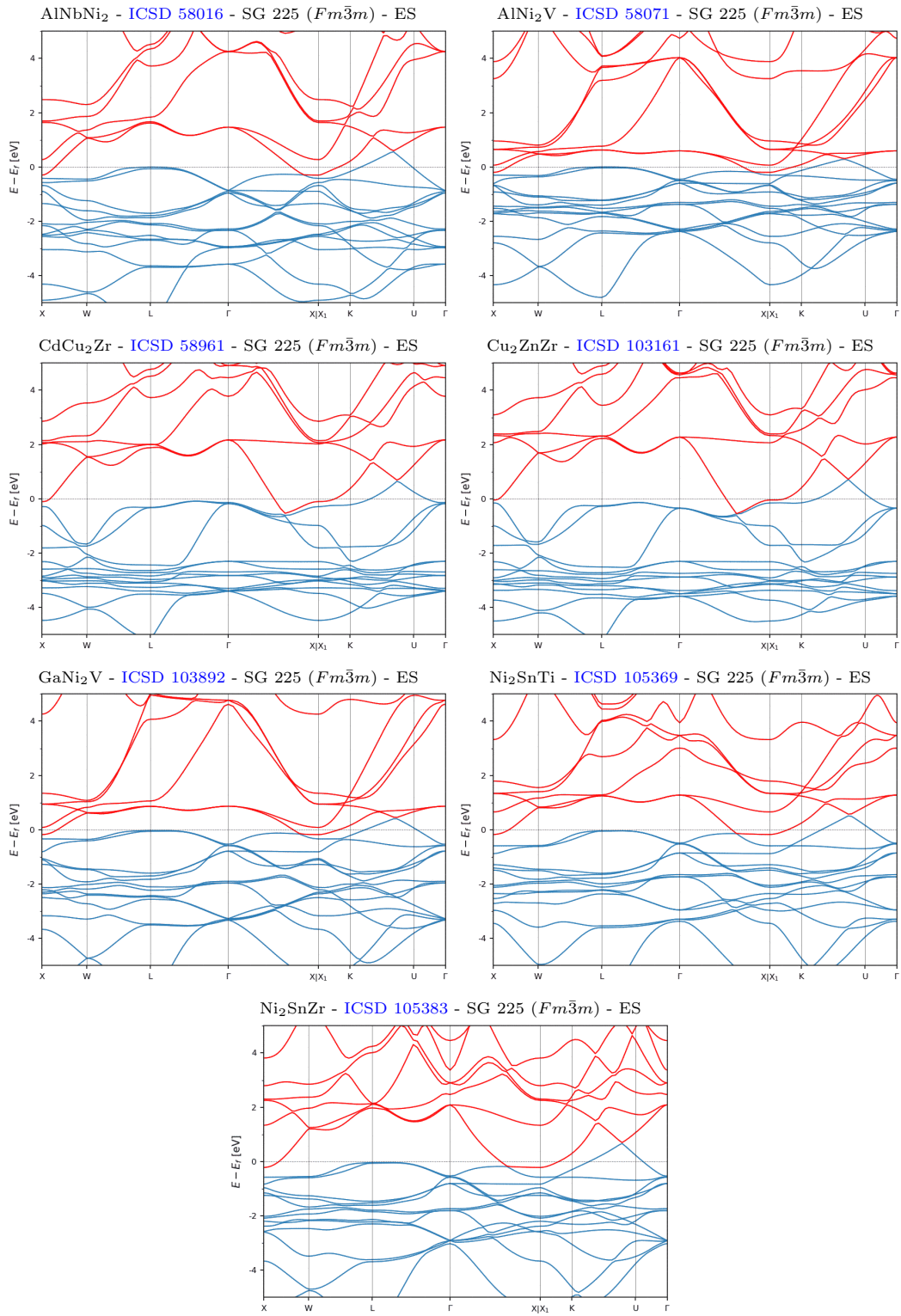


Figure S91. The ES-classified topological semimetals with the simplest bulk Fermi surfaces. (part 6/6)

D. Semimetal-Insulator Transitions Driven by Spin-Orbit Coupling

In this section, we show the materials with the largest gaps at E_F or the fewest and smallest bulk Fermi pockets that are topological insulating in the presence of SOC and enforced or symmetry-indicated semimetals when the effects of SOC are neglected. Specifically, when the strength of SOC is artificially tuned to zero without (un)inverting bands (*i.e.* without changing the bulk band ordering), the bulk gaps of spinful TI, TCI, and HOTI phases necessarily close and the bulk transitions into a spinless (spin-degenerate) topological semimetal phase [31, 34, 36]. The prototypical example of an SOC-driven transition between a spinless topological semimetal phase without SOC and a TI phase with SOC occurs in graphene, which is an ESFD semimetal in the absence of SOC [28, 31, 159], and a 2D TI when the (weak) effects of SOC are taken into consideration [3, 126] (see SM 10). In Figs. S92, S93, S94, S95, S96, and S97, we respectively show the spinful topological (crystalline) insulators that originate from weak-SOC ESFD, ES, NLC-symmetry-indicated (NLC-SM), and SEBR-symmetry-indicated (SEBR-SM) topological semimetals. For concision, in Figs. S92, S93, S94, S95, S96, and S97, we only show material band structures calculated incorporating the effects of SOC; the corresponding band structures and topological information calculated without SOC can be accessed for each material by clicking on the ICSD number listed above each plot.

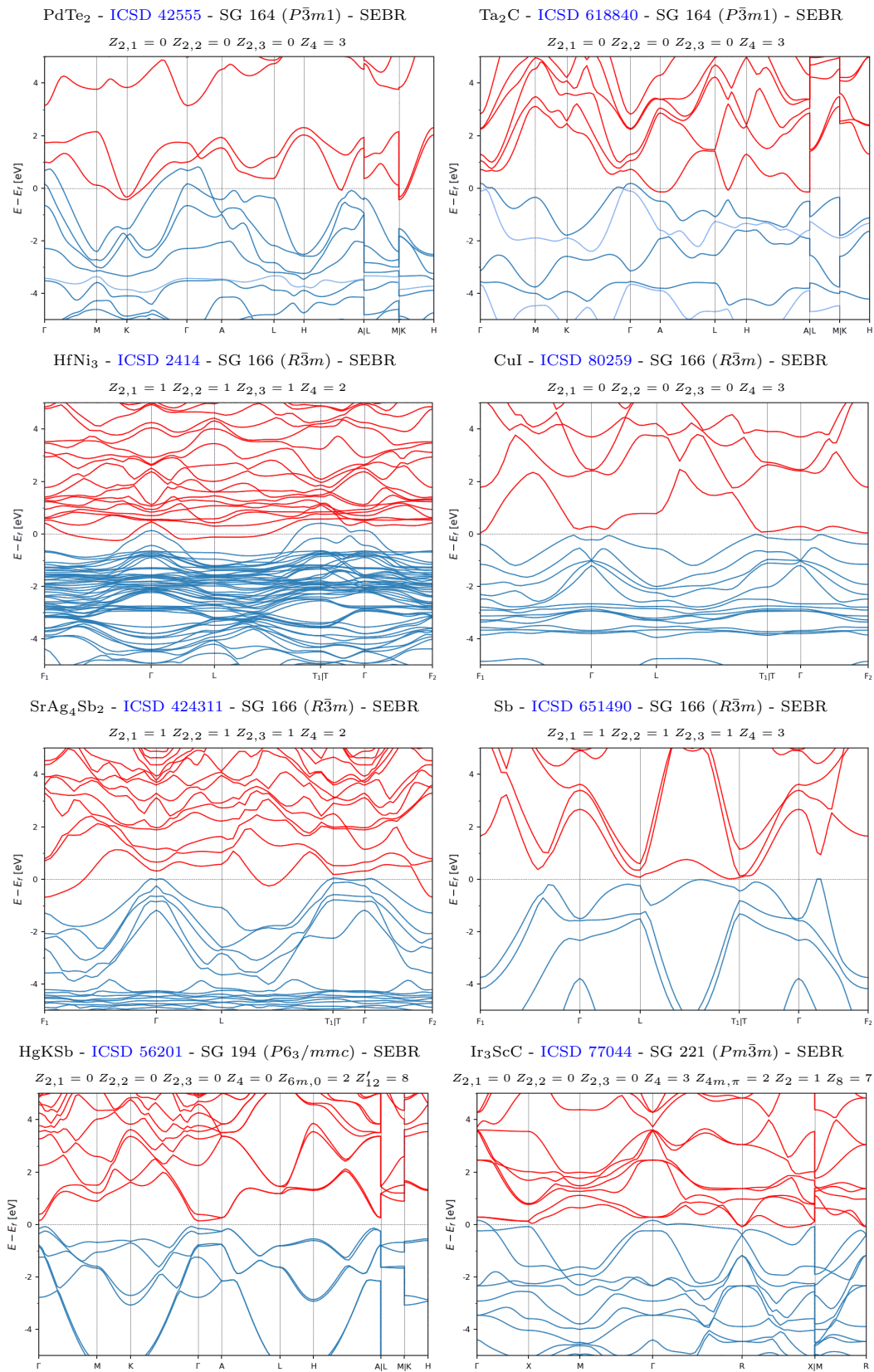


Figure S92. The spinful topological (crystalline) insulators with the largest bulk gaps or the fewest Fermi pockets that are classified as ESFD topological semimetals when the effects of SOC are neglected. (part 1/2)

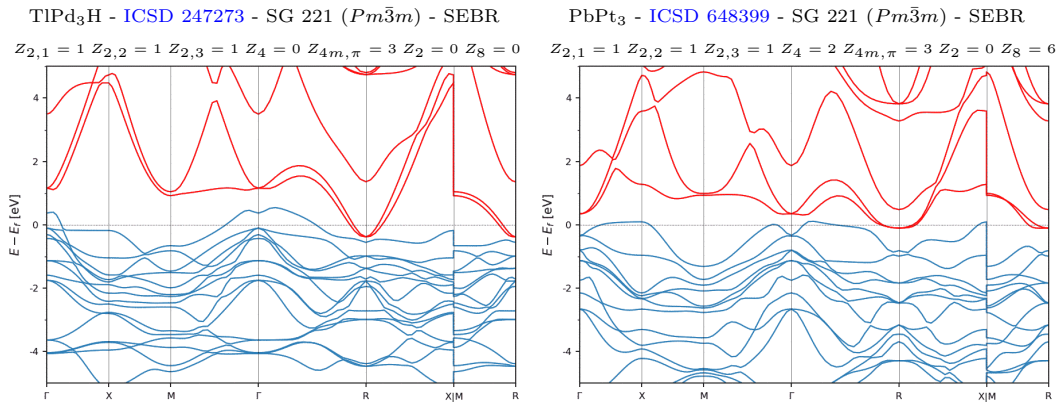


Figure S93. The spinful topological (crystalline) insulators with the largest bulk gaps or the fewest Fermi pockets that are classified as ESFD topological semimetals when the effects of SOC are neglected. (part 2/2)

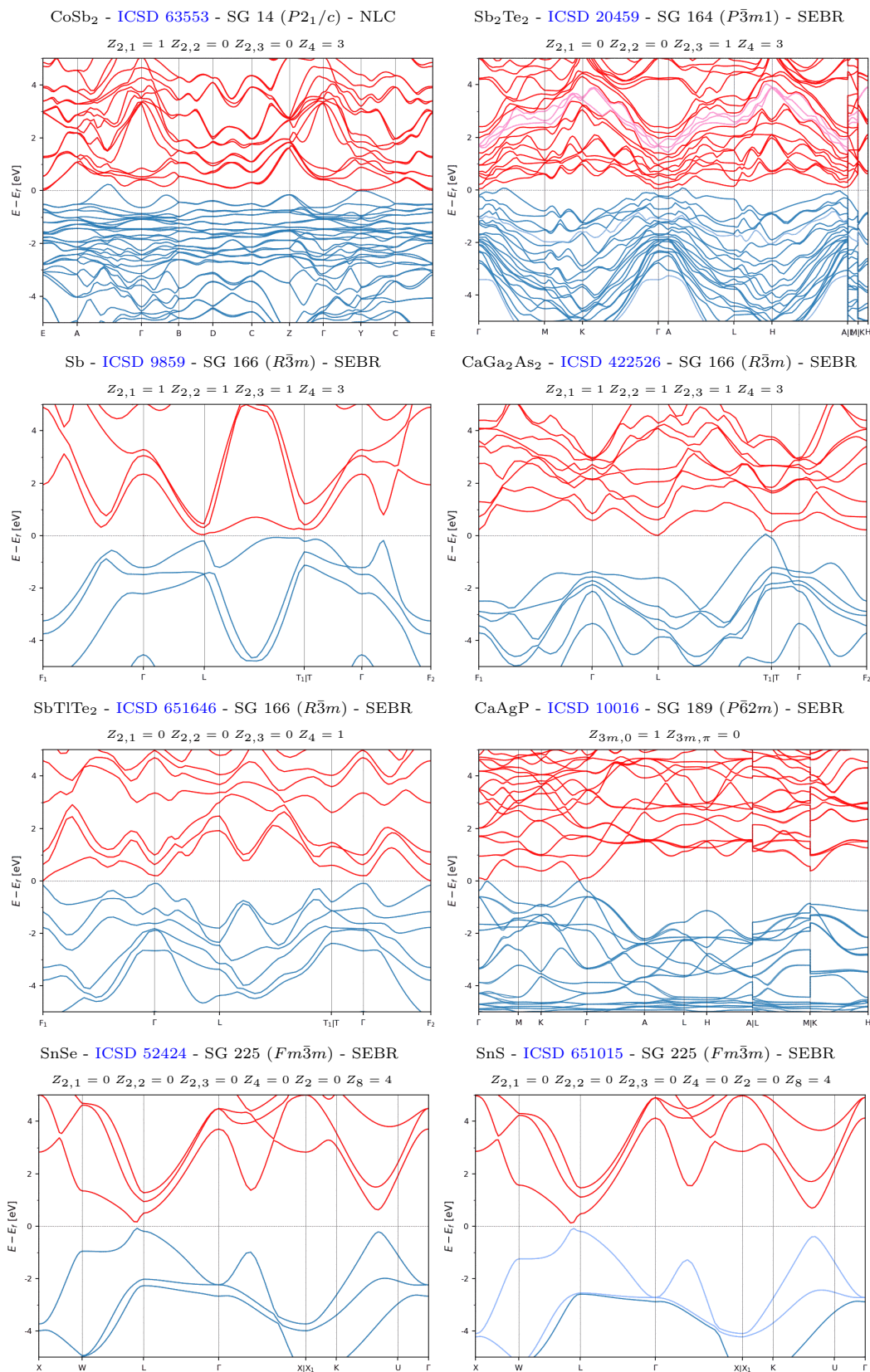


Figure S94. The spinful topological (crystalline) insulators with the largest bulk gaps or the fewest Fermi pockets that are classified as ES topological semimetals when the effects of SOC are neglected. (part 1/2)

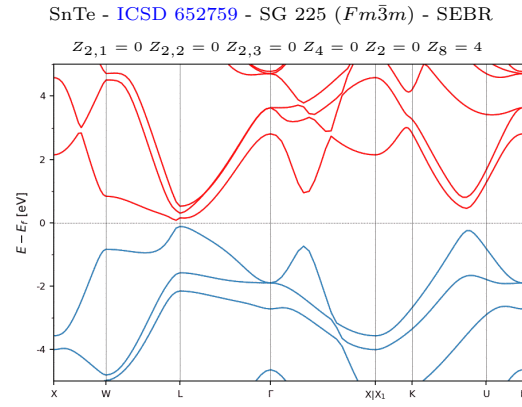


Figure S95. The spinful topological (crystalline) insulators with the largest bulk gaps or the fewest Fermi pockets that are classified as ES topological semimetals when the effects of SOC are neglected. (part 2/2)

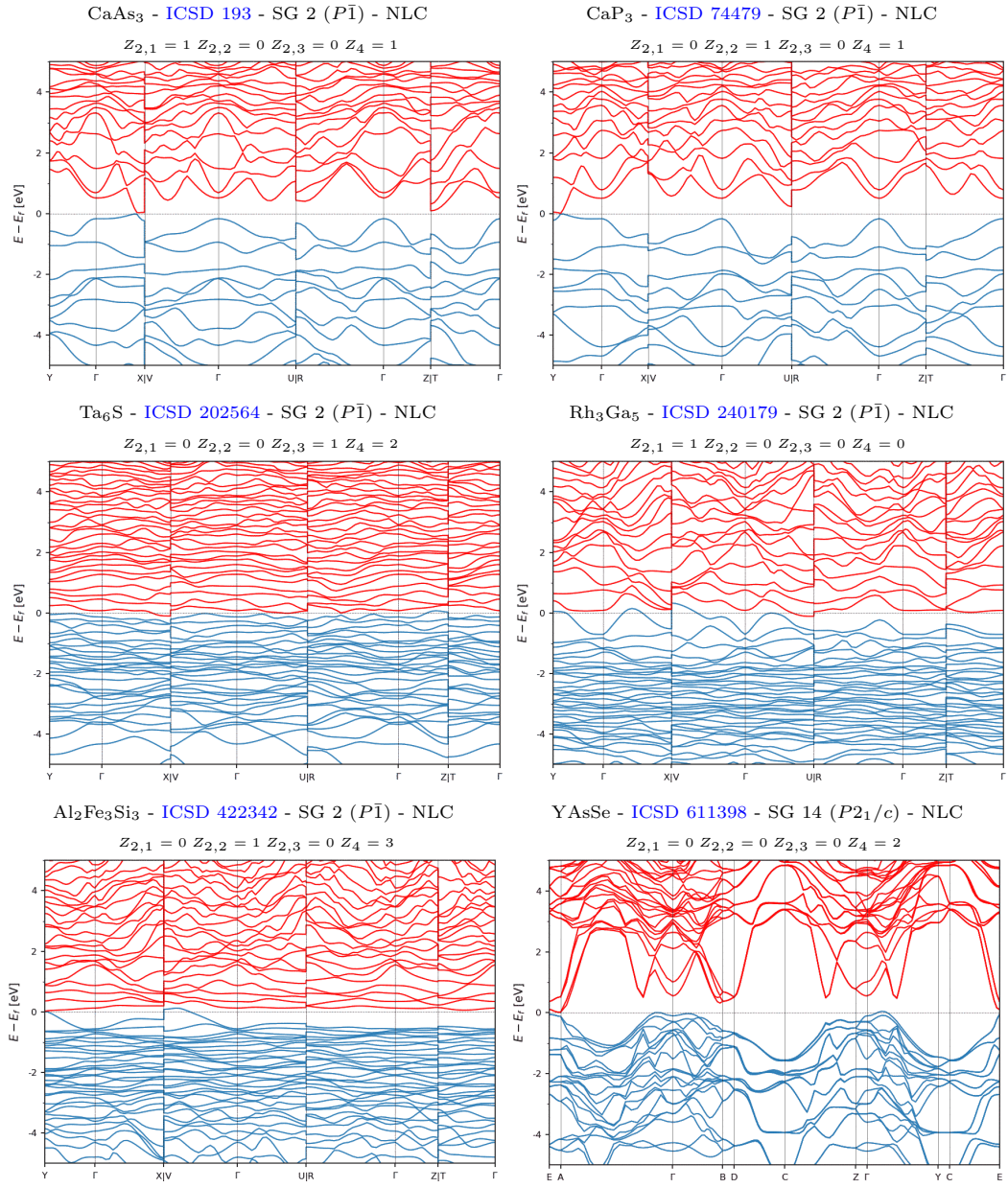


Figure S96. The spinful topological (crystalline) insulators with the largest bulk gaps or the fewest Fermi pockets that are classified as NLC-SM topological semimetals when the effects of SOC are neglected.

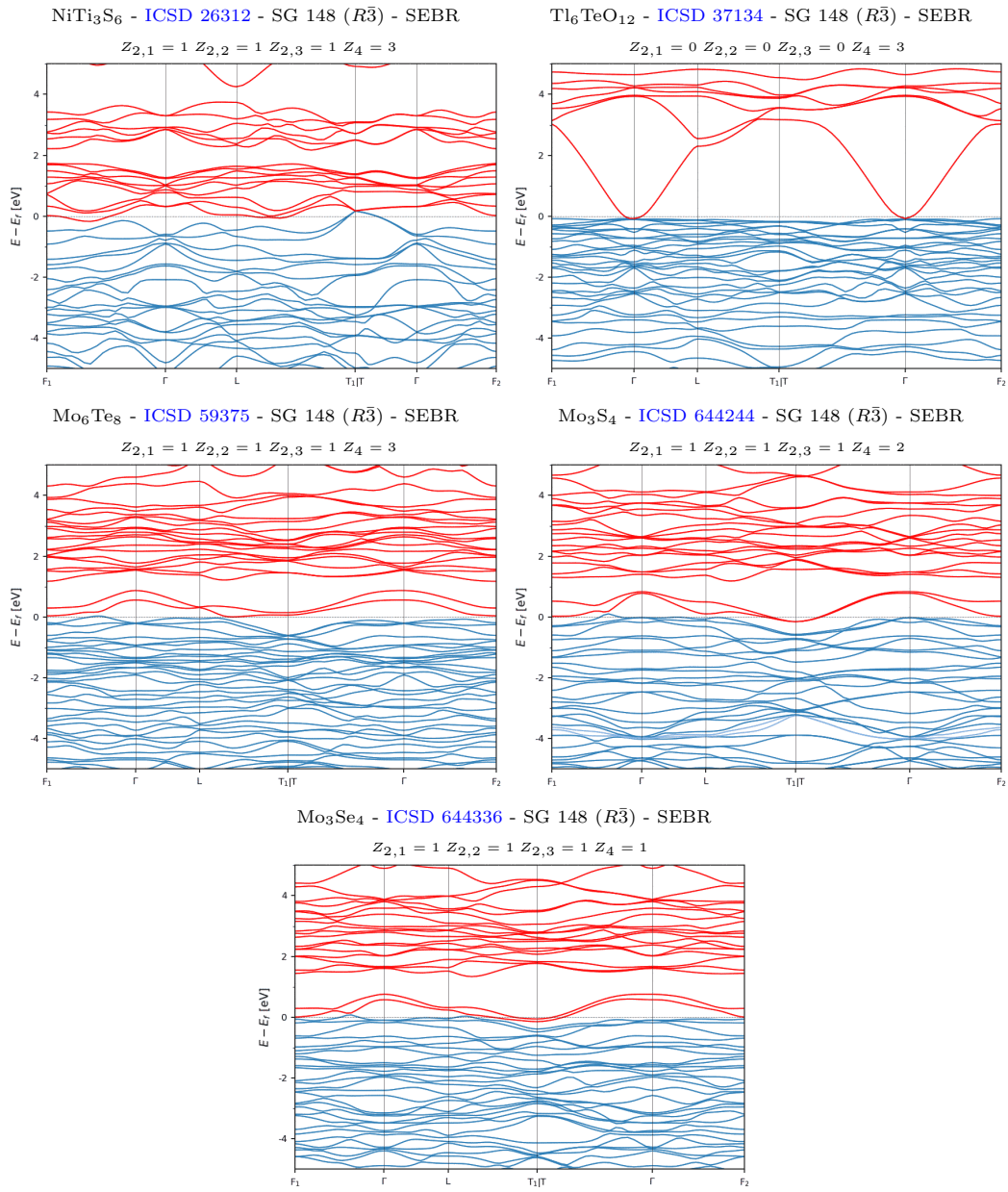


Figure S97. The spinful topological (crystalline) insulators with the largest bulk gaps or the fewest Fermi pockets that are classified as SEBR-SM topological semimetals when the effects of SOC are neglected.

E. Materials with Fragile Topological Bands at or Close to E_F

In this section, we show the materials with the largest gaps at E_F or the fewest and smallest bulk Fermi pockets that host groups of well-isolated bands at or near E_F with symmetry-indicated fragile topology [42–47, 95–100, 173]. Specifically, as derived in Refs. 42, 44, and 45, in some cases, isolated groups of bands within the spectrum can be diagnosed as fragile topological, even if the entire valence (or conduction) manifold does not exhibit fragile topology. In Figs. S98, S99, S100, S101, S102, and S103, we respectively show representative examples of SEBR-, ESFD-, ES-, and LCEBR-classified materials with well-isolated fragile bands close to E_F [we do not find any examples of NLC-classified topological (crystalline) insulators with few bulk Fermi pockets and well-isolated fragile bands close to E_F]. Though just over half of the materials listed in Figs. S98, S99, S100, S101, S102, and S103 were previously identified in Ref. 44 as hosting fragile bands, the remaining materials in this section have not been previously highlighted for hosting fragile topology. The materials with well-isolated fragile bands not previously listed in Ref. 44 are Sb_2Te_2 [ICSD 20459, SG 164 ($P\bar{3}m1$)], $\text{Ta}_2\text{S}_2\text{C}$ [ICSD 23790, SG 164 ($P\bar{3}m1$)], $\text{Pb}_2\text{Bi}_2\text{Se}_5$ [ICSD 30372, SG 164 ($P\bar{3}m1$)], BiTe [ICSD 30525, SG 164 ($P\bar{3}m1$)], $\text{As}_2\text{Ge}_5\text{Te}_8$ [ICSD 63174, SG 164 ($P\bar{3}m1$)], Ta_2C [ICSD 409555, SG 164 ($P\bar{3}m1$)], BiSe [ICSD 617073, SG 164 ($P\bar{3}m1$)], and TiS_2 [ICSD 72042, SG 227 ($Fd\bar{3}m$)] in Figs. S98 and S99; TaSe_2 [ICSD 24313, SG 164 ($P\bar{3}m1$)], BiTe [ICSD 44984, SG 225 ($Fm\bar{3}m$)], and Bi_4Rh [ICSD 58854, SG 230 ($Ia\bar{3}d$)] in Figs. S100 and S101; SrZn_2Sb_2 [ICSD 12152, SG 164 ($P\bar{3}m1$)], Sc_2C [ICSD 280743, SG 164 ($P\bar{3}m1$)], and TaN [ICSD 105123, SG 194 ($P6_3/mmc$)] in Fig. S102; and TiS_2 [ICSD 91579, SG 164 ($P\bar{3}m1$)] and $\text{Al}_5\text{C}_3\text{N}$ [ICSD 36303, SG 186 ($P6_3mc$)] in Fig. S103.

Finally, because recent works have demonstrated that insulators with fragile topological bands can exhibit anomalous corner modes [34, 45, 58, 95, 98, 101] and nontrivial twisted-boundary [46, 99] and topological defect responses [106], then the materials highlighted in this section represent new avenues for experimentally investigating novel topological response effects in solid-state systems.

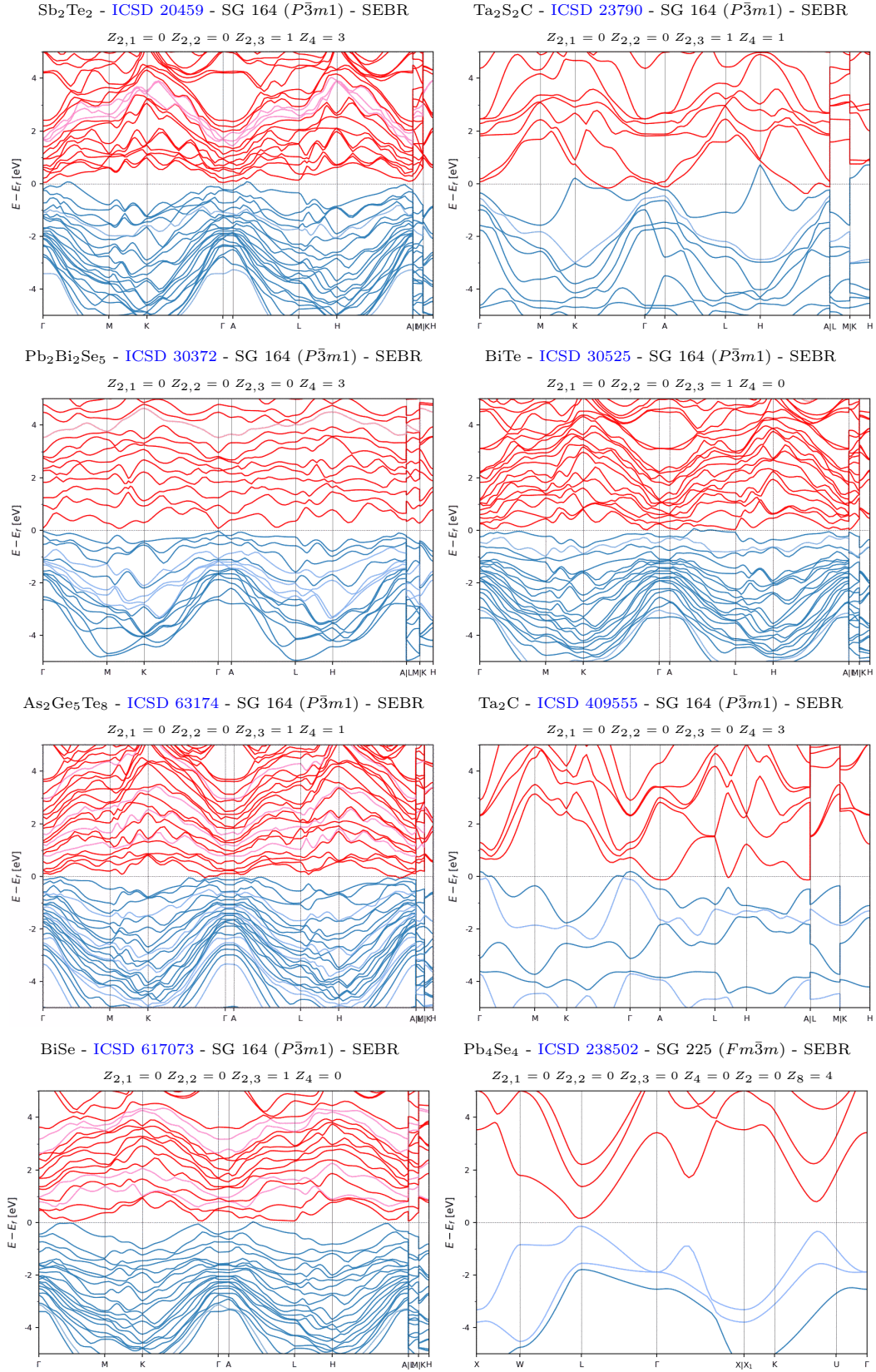


Figure S98. The SEBR-classified topological (crystalline) insulators with the largest bulk gaps or the fewest and smallest bulk Fermi pockets that host well-isolated fragile bands at or close to E_F . (part 1/2)

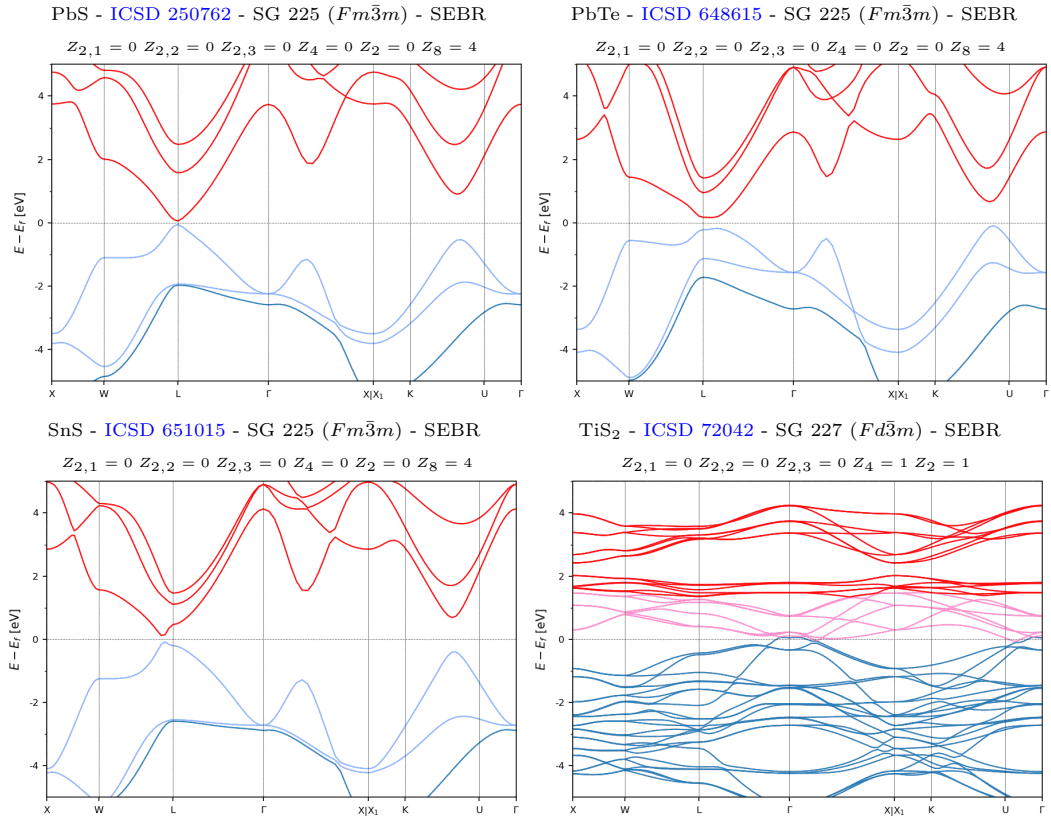


Figure S99. The SEBR-classified topological (crystalline) insulators with the largest bulk gaps or the fewest and smallest bulk Fermi pockets that host well-isolated fragile bands at or close to E_F . (part 2/2)

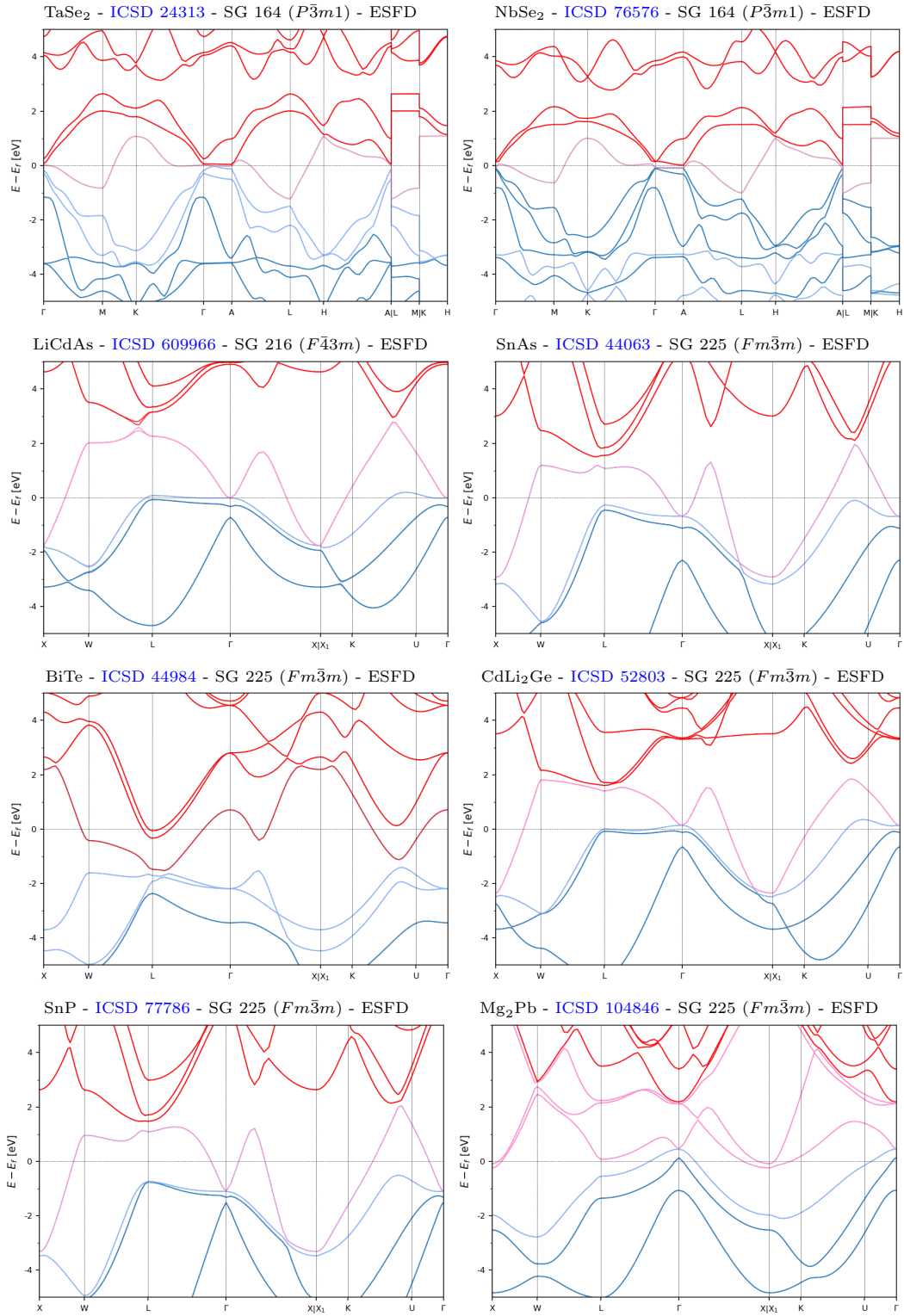


Figure S100. The ESFD-classified topological semimetals with the simplest bulk Fermi surfaces and well-isolated fragile bands at or close to E_F . (part 1/2)

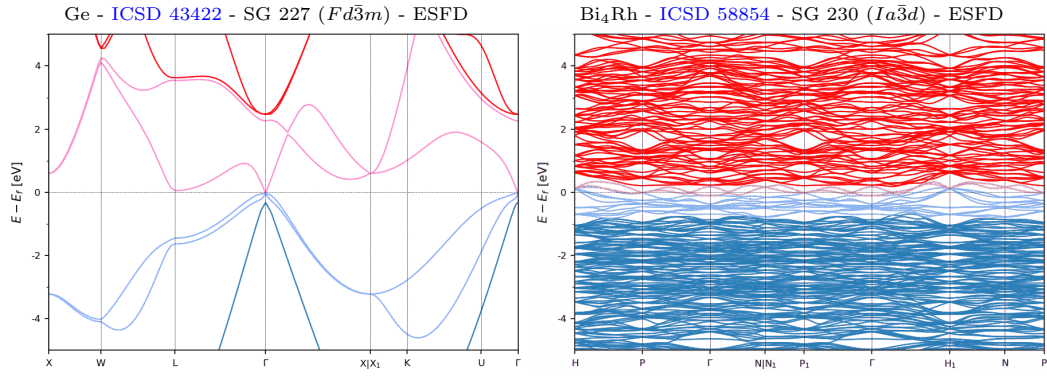


Figure S101. The ESFD-classified topological semimetals with the simplest bulk Fermi surfaces and well-isolated fragile bands at or close to E_F . (part 2/2)

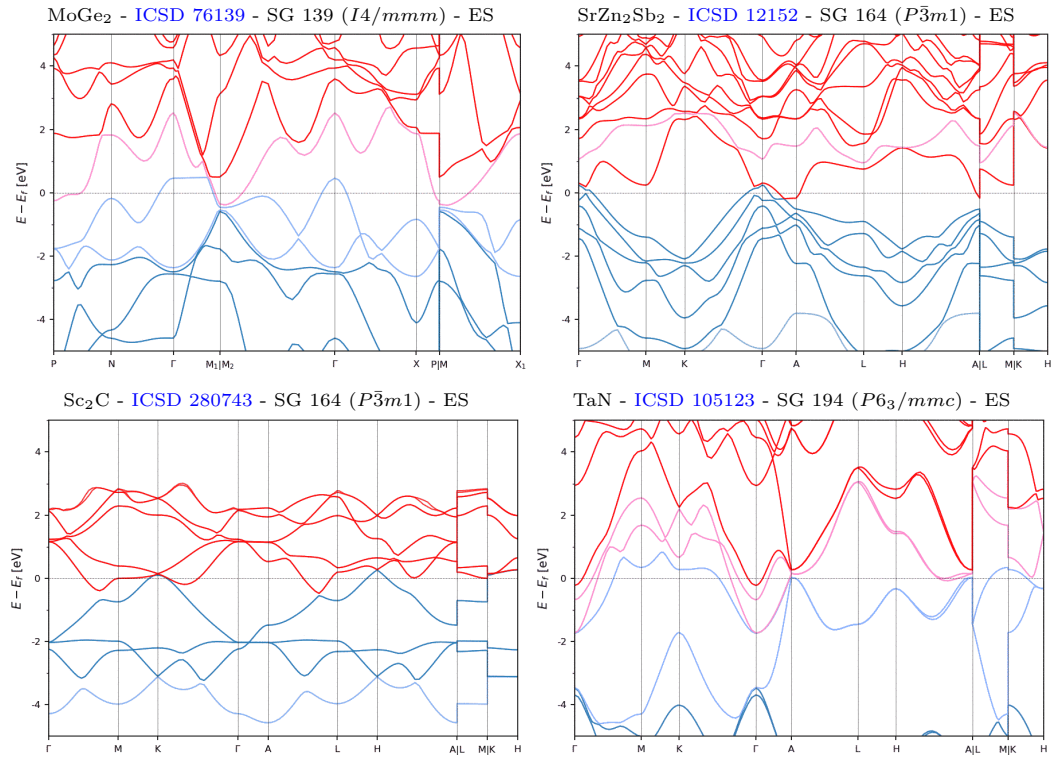


Figure S102. The ES-classified topological semimetals with the simplest bulk Fermi surfaces and well-isolated fragile bands at or close to E_F .

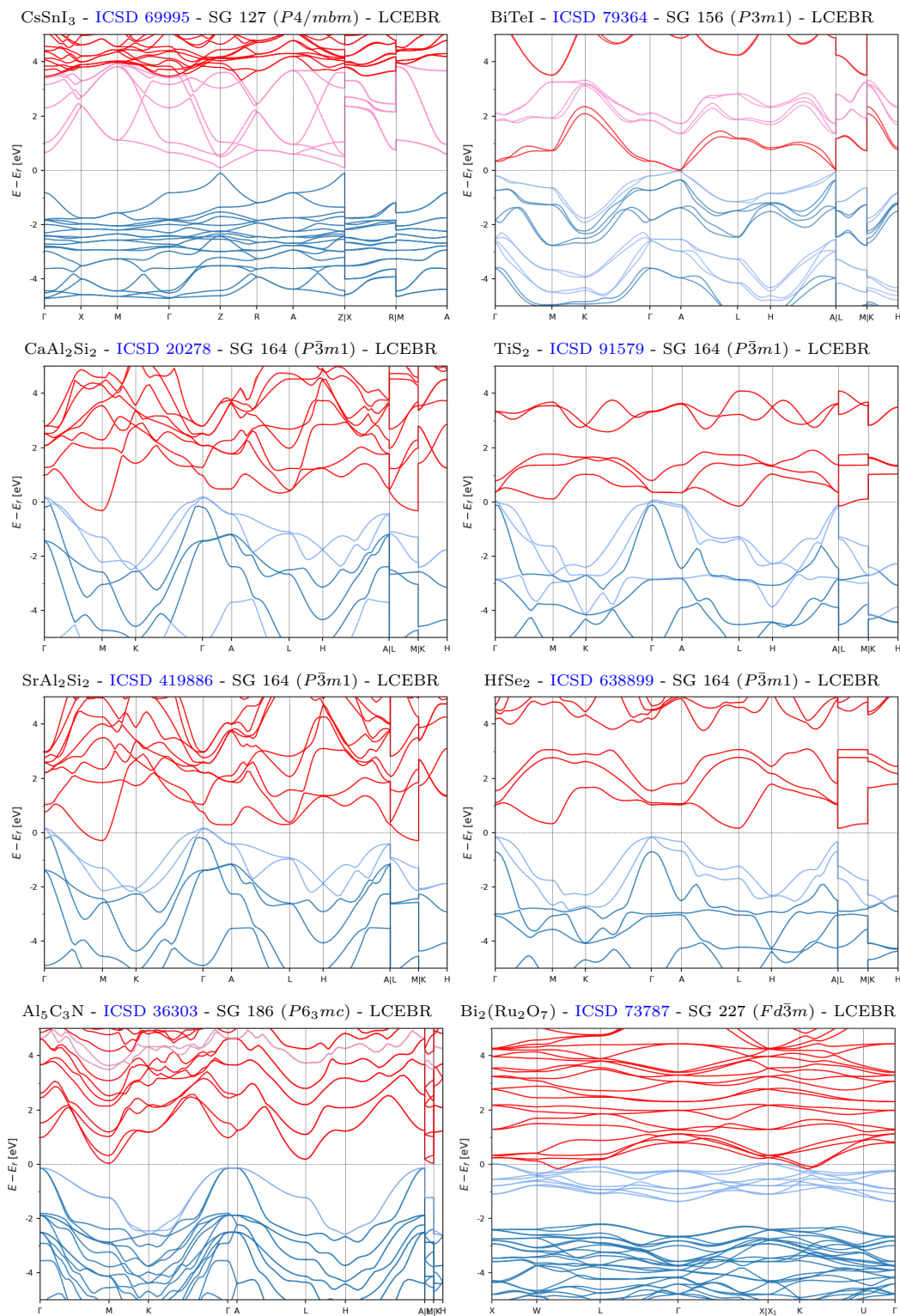


Figure S103. Representative examples of LCEBR-classified insulators with trivial symmetry-indicated strong topology and well-isolated fragile bands at or close to E_F .